SOVIET PHYSICS

JETP

A translation of the Zhurnal Éksperimental'noĭ i Teoreticheskoĭ Fiziki.

Vol. 13, No. 6, pp. 1081-1346 (Russ. orig. Vol. 40, No. 6, pp. 1541-1908, June, 1961) December, 1961

INVESTIGATION OF THE $V^{51}(C^{12}, 2n)Cu^{61}$ *REACTION*

A. S. KARAMYAN* and A. A. PLEVE

Joint Institute for Nuclear Research

Submitted to JETP editor December 3, 1960

J. Exptl. Theoret. Phys. (U.S.S.R.) **40**, 1541-1542 (June, 1961)

In a study of the reaction $V^{51}(C^{12}, 2n)Cu^{61}$ it was discovered that previously published results may be inaccurate, owing to the presence of Mn^{56} among the reaction products. This isotope emits radiation similar to that of Cu^{61}. The quantitative side of the problem requires further, more detailed investigation.

THE reaction $V^{51}(C^{12}, 2n)Cu^{61}$ was investigated previously, using the stacked foil method. The copper was chemically separated from the samples. The excitation curve for this reaction has a characteristic evaporation maximum at small energies. As the energy of the C^{12} ions increases, however, the cross section does not fall off to zero but remains roughly constant at 10 mb in the energy range of 55 to 75 Mev. This was somewhat unexpected for a heavy-ion reaction, since such an excitation curve shape is typical of direct knock-on processes. These are observed in reactions involving fast light particles whose energy is substantially greater than the binding energy of the nucleon in the nucleus. In the experiments described, the energy of the heavy ions did not exceed 6.3 Mev/nucleon. Therefore another investigation of the products of the $V^{51} + C^{12}$ reaction has been undertaken. The isotope Cu^{61}, which is obtained when two neutrons are emitted from the compound system, was studied first. As in reference 1, the method of stacked foils was employed. The induced activity was measured in an end-window beta counter. The reaction products were identified by their half-lives and by the end-point energies of the beta spectra. These latter were measured by absorption.

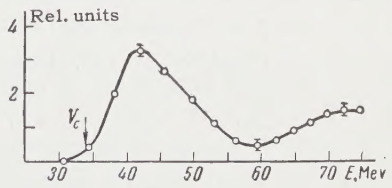

The figure presents the yield curve of the product with $T_{1/2} \sim 3$ hours, formerly ascribed completely to Cu^{61} (V_C is the Coulomb barrier of the reaction). It is seen that the curve rises to a certain extent at large energies. In this connection, a careful analysis was made of the experimental data. It was found that the half-lives and energies of beta particles on the right and left portions of the yield curve were somewhat different. This difference, although small, is distinctly apparent. It is probable that we are dealing with two different products here.

The respective periods and energies are presented in the table, where the letter X designates the product responsible for the rise of the yield curve at $E^* \sim 60$ Mev (E^* is the excitation energy of the compound nucleus).

Thus, at large energies, it is apparently impossible to attribute the yield of the product with $T_{1/2} \sim 3$ hours entirely to the reaction $V^{51}(C^{12}, 2n)Cu^{61}$. If this reaction continues to take place, its yield is

*Deceased.

Product	Half-life, hours [1]		Particle energy, Mev	
	Data of present work	Literature data[2]	Data of present work	Literature data[2]
Cu^{61}	3.3±0.05	3.33	1.2±0.2	1.22
X	2.8±0.05		2.0±0.4 (60%) 0.5±0.2 (40%)	

masked by another activity with a larger yield and similar characteristics. According to reference 2, only Mn^{56} among the possible products of the $V^{51} + C^{12}$ reaction has similar characteristics: $T_{1/2} = 2.6$ hours, $E_\beta = 2.8$, 1.0 and 0.6 Mev. It can be formed when an alpha particle, a neutron, and two protons are emitted from the compound system. The energy threshold for this reaction is approximately 55 Mev, which is not in disagreement with estimates made from the excitation curve in the figure (computations of the threshold energy value were based on Cameron's data (private communication) on nuclear masses with different assumptions as to the mechanism of the reaction). But in such an event, the source of error in the chemical separation[1] remains obscure.

Dorofeev and others[3] tried to detect neutrons produced in reactions involving heavy ions. The authors made use of secondary reactions caused by neutrons in threshold detectors, in particular the reaction $C^{12}(n, 2n)C^{11}$, where $Q = -18.5$ Mev. If the excitation energy is on the order of 70 Mev and only two neutrons are emitted as a result of the reaction $V^{51} + C^{12}$, they can have an energy of 20 Mev or even more. With a cross section of ~ 10 mb for the reaction $V^{51}(C^{12}, 2n)Cu^{61}$, it can be expected that neutrons with $E \geq 18.5$ Mev will induce a marked activity in the carbon. Measurements have shown[3] that this activity is considerably smaller than anticipated.

Reactions involving heavy ions, which at large excitation energies lead to emission of two neutrons, require further and more detailed investigation. It can only be said that the cross section for such a reaction on vanadium is known to be less than 10 mb.

It was reported earlier[4] that the cross section for the reaction $Nb^{93}(C^{12}, 2n)Ag^{103}$ is also constant in the energy inverval 55 — 70 Mev and is approximately 10 mb. This result is obviously also in need of verification.

The authors are grateful to Professor G. N. Flerov for his valuable guidance and advice when discussing the results.

[1] Karamyan, Gerlit, and Myasoedov, JETP **36**, 621 (1959), Soviet Phys. JETP **9**, 431 (1959).

[2] Strominger, Hollander, and Seaborg, Revs. Modern Phys. **30**, 585 (1958).

[3] Karamyan, Dorofeev, and Klochkov, JETP **40**, 1004 (1961), Soviet Phys. JETP **13**, 705 (1961).

[4] A. S. Karamyan and A. A. Pleve, JETP **37**, 654 (1959), Soviet Phys. JETP **10**, 467 (1960).

Translated by Mrs. Jack D. Ullman
266

DESTRUCTION OF SUPERCONDUCTIVITY IN THIN TIN FILMS

A. M. KOLCHIN, Yu. G. MIKHAĬLOV, N. M. REĬNOV, A. V. RUMYANTSEVA, A. P. SMIRNOV, and V. N. TOTUBALIN

Leningrad Physico-Technical Institute, Academy of Sciences, U.S.S.R.

Submitted to JETP editor December 3, 1960; resubmitted December 27, 1960

J. Exptl. Theoret. Phys. (U.S.S.R.) 40, 1543-1550 (June, 1961)

It is shown that the destruction of superconductivity in thin tin films [of order $(1-8)\times 10^{-5}$ cm] by current pulses of different shape and duration is not isothermal because of heating of the sample by the measuring current and eddy currents. The destruction time of the superconducting state depends on the current pulse amplitude and at sufficiently large currents it is of the order of 5×10^{-9} sec. The first traces of resistance appear for currents which are much smaller than the values at which the resistance increases rapidly. Hysteresis, both of a thermal and nonthermal nature, has been detected in the transition from the normal to the superconducting state.

1. INTRODUCTION

IN line with the possibility of the use of superconducting phenomena for practical purposes,[1,2] the study of the destruction of superconductivity of thin films of superconducting metals by a current is of interest. In references 3 and 4, the values of the critical field and the currents were determined for films of tin in the form of discs and cylinders in measurements with direct current or with pulses of comparatively long duration. The effect of heat on the values of the critical currents was noted by the authors. This effect can be decreased considerably if the measurements are carried out with pulses of very short duration. Only recently have the first reports appeared in the literature[1,2,5,6] on a detailed study of the transition from the superconducting to the normal state with the use of short pulses.

The present research was undertaken with the purpose of making clear the laws of destruction of superconductivity by a magnetic field and by a current passing through a film, and also the study of the laws of return of the film to the superconducting state on removal of the field (current) over a wide range of temperatures for films of different thicknesses. The paper is limited to a statement of the results of investigation of the character of the destruction of superconductivity of tin films in the form of strips of thickness $(1-8)\times 10^{-5}$ cm under the action of current pulses of various shapes and duration, at temperatures close to the critical.*

2. SPECIMENS, APPARATUS, AND METHODS OF INVESTIGATION

Films for the investigation were prepared by the method of vacuum evaporation, for which a special apparatus was constructed. Eighteen films of different thickness and width could be obtained simultaneously in a vacuum chamber at a pressure of 10^{-6} mm Hg by use of nitrogen traps for the oil vapor.[7] The tin was evaporated from a long tantalum vessel, which guaranteed identical film thickness over the whole sample. The specimens were sputtered on the substrate through masks and had the shape shown in Fig. 1. Silver contacts were first imbedded in the substrate; lead conductors were later soldered to these. To make a satisfactory superconducting contact between the film and the leads at the silver contacts, a lead film was evaporated in a vacuum after application of the tin specimen. Glass or mica, was used as the substrate. It was first chemically cleaned, and was heated for a long time in the vacuum before evaporation.

The thickness of the film was estimated by weighing control glasses, evaporation on which was carried out simultaneously with obtaining of

*The results of the research were reported at the Seventh All-Union Conference on Low Temperature Physics at Kharkov in June, 1960.

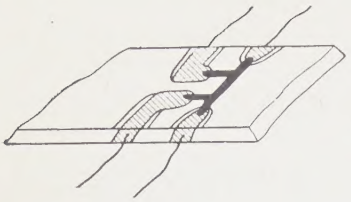

FIG. 1. Specimen with current and voltage contacts.

the specimens. The results given below were obtained on films of thickness $(1-8)\times 10^{-5}$ cm and width 0.10 — 0.25 mm. During the time of evaporation, which lasted from several tens of seconds to several minutes, the temperature of the base layers did not exceed 45° C. The films obtained under such conditions had a resistance of 30 — 130 ohm at room temperature.

The study at direct current at comparatively low currents through the specimen was carried out by means of a potentiometric system with a galvanometer or with a slide-wire resistor, which gradually changed the current in the circuit of the specimen. The values of the current through the specimen and the voltage on it were recorded by automatic potentiometer recorders of the type ÉPP-09M or ÉPP-11M.

The transition of the specimens from the superconducting state to the normal one and back was also studied with the aid of an oscillographic apparatus which made it possible to observe visually and photograph the volt-ampere characteristics of the specimen. Two ÉNO-1 oscillographs were used, so connected that the vertical-deflection amplifier of one played the role of the horizontal-deflection amplifier of the other. Both sinusoidal current and triangular pulses with different rise times and repetition frequencies from several to hundreds of cycles per second, could be applied to the specimen. The minimum length of the rise time of the pulse in these experiments was 0.1 millisecond. The block diagram of this apparatus is shown in Fig. 2.

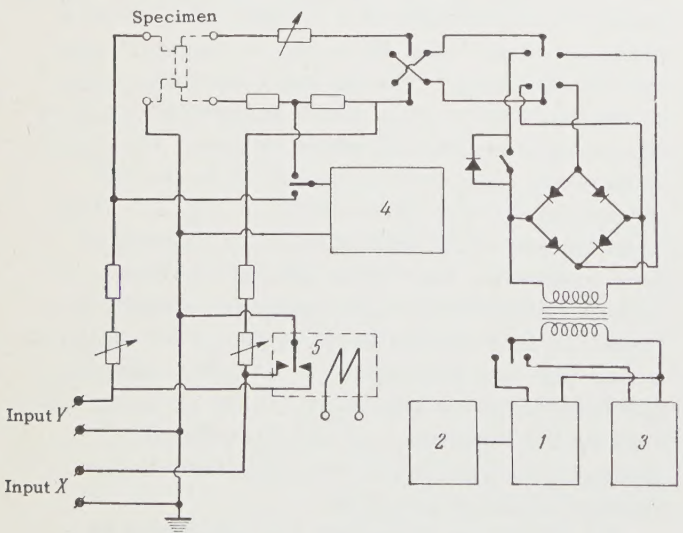

FIG. 2. Circuit for observation of volt-ampere characteristics: 1 — generator of triangular pulses, 2 — triggering generator, 3 — audio oscillator, 4 — millivoltmeter or oscilloscope for control of pulse amplitudes, 5 — polarized relay which serves to produce the coordinate axes on the screen of the oscilloscope.

For a study of destruction of superconductivity with much shorter pulses, generators of the type GIS-2 and GI-3M were used with a rise time of 0.15 and 0.05 microsecond, respectively. The lengths of the pulses were varied from 0.1 to 10 microseconds. The current through the specimen and the voltage across it could be recorded simultaneously by means of a two-beam oscillograph of the type DÉSO-1. To observe small signals, amplifiers of the type UR-1 were used. Studies on short pulses were carried out in a special cryostat with coaxial leads. The specimen on the substrate was mounted at the end of the coaxial lead so that together with the matching impedance it served as a continuation of the central conductor. Use of a superconducting lead screen located near the specimen made it possible to observe an undistorted picture of the transition of the specimen from the superconducting state to the normal one, since the lead screen decreased the inductance of the specimen (in our case, by a factor of 10).

3. RESULTS OF INVESTIGATIONS AND THEIR DISCUSSION

a) Direct current. At a temperature of 4.2° K, the resistance of the film studied amounted to 1 — 6 ohms, and the specific resistance to 0.4 — 1 microhm-cm. The transition temperature of the specimens from the normal to the superconducting state for a measurement current of 40 μa was in the region of 3.75 — 3.85° K, i.e., it was displaced in the direction of higher temperatures in comparison with the critical temperature for bulk specimens.

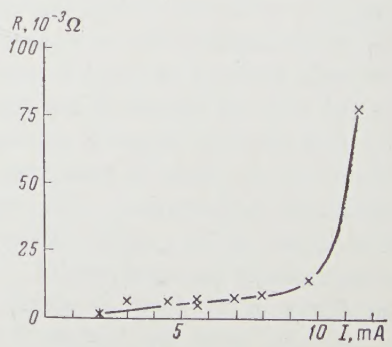

FIG. 3. Initial portions of the specimen resistance vs. current curve (direct current).

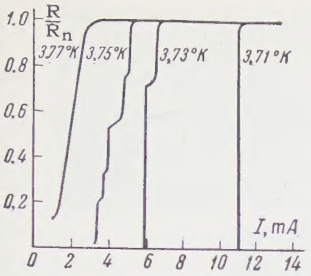

FIG. 4. Dependence of the resistance on the current in the transition of the specimen from the superconducting state to the normal (direct current).

FIG. 6. Volt-ampere characteristic of a specimen for large current amplitude. The resistance of the specimen in the normal state changes as the result of heating.

The temperature interval of the transition was in the range 0.02 — 0.05° K.

Measurements have shown that with increase in the current in the specimen a very slow increase takes place in the resistance, up to a value of the order of 10^{-2} of the total resistance of the specimen (Fig. 3). A region of faster growth of the resistance with increase in temperature follows thereafter. A similar character of the initial stage of the transition was observed by Bremer and Newhouse.[5] At temperatures close to critical, and consequently at low currents, a non-monotonic increase in the potential on the specimen is observed, and consequently a similar increase appears in the resistance for a relatively large range of currents. A similar phenomenon was observed for thin tin wires by Galkin and others.[8]

For very low temperatures and, correspondingly, higher currents, the transition picture changes. The increase in current leads to a rapid appearance of a certain fraction of the resistance. Upon further increase of the current, the resistance is almost unchanged; thereafter, a second jump in the resistance takes place, etc. Sometimes, after a stage of smooth increase in the resistance, only one sharp jump is observed in the resistance, up to 0.95 of the full value; afterwards, a gradual increase to the total value occurs (Fig. 4).

A similar character for the change in the resistance can be explained by the inhomogeneity of the specimens. First traces of the resistance appear upon destruction of the superconductivity of the "weak points" of the specimen, which have a low value of critical current. Upon further increase in the current, resistance appears in regions which have a high critical current while the principal effect on the velocity and character of the transition is produced by the generation of heat in the normal parts of the specimen. The heating can be very pronounced and can lead to burning of the specimen.

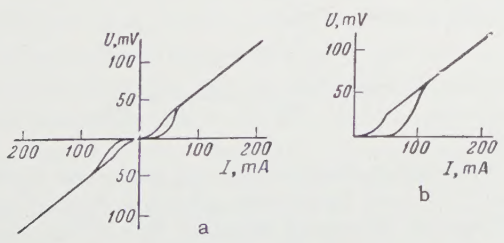

FIG. 5. Volt-ampere characteristics of the specimens: a — current of sinusoidal shape, b — current obtained as the results of half-wave rectification.

b) Pulses of triangular shape. The volt-ampere characteristics of specimens taken with the help of the apparatus whose circuit is shown in Fig. 2 make it possible to study in detail the character of the transition from the superconducting to the normal state upon increase of current through the specimen. The possibility of change within wide limits of the pulse repetition frequency, and of the rise times of the pulse and its amplitude allow one to elucidate the effects of thermal action on the character of the superconducting transition. The volt-ampere characteristics of a specimen obtained by passage of current of sinusoidal shape (Fig. 5a), and a current obtained as the result of half-wave rectification (Fig. 5b) show that the specimen has a much higher temperature in the first case, although the bath temperature was the same in both cases. Heating of the specimens by the current can be so great that a significant increase is observed in the resistance of the specimen in the normal state (Fig. 6).

To decrease the effect of heating, experiments were carried out on current pulses of triangular shape with the length of the leading front of 0.1 to 2 milliseconds. The repetition frequency of the pulses was set so that the specimen which was heated by the previous pulse managed to take on the temperature of the bath before the arrival of the following pulse. Thus the transition from the superconducting state to the normal can in first approximation be regarded as isothermal.[5] Even for the case of very short pulses (rise time 0.1 millisecond and decay time 0.1 millisecond) the specimen is heated during the time of transition from the superconducting to the normal state. Films mounted on a mica substrate made it possible to reduce the repetition frequency of the

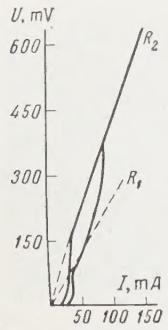

FIG. 7. Volt-ampere characteristics of a specimen. The stepwise character of the transition is seen.

pulses without change in the character of the transition to higher values, which is explained by the better thermal conductivity of the mica. In a number of specimens, a stepwise increase in resistance was also observed here (Fig. 7).

The existence of hysteresis in the transition from the normal state to the superconducting state is partly due to the heating of the specimen;* moreover, the existence of hysteresis of a non-thermal origin was observed. The character of the transition of the film from a normal state to the superconducting state upon decrease in current through the specimen depends essentially on whether the specimen was completely transformed to the normal state. If only a part of the specimen is transformed to the normal state under the action of the current in the pulse, then the intermediate state which is formed is so stable that in the action of the next pulse the film still preserves the value of the resistance which appeared under the action of the previous pulse (Fig. 8a).

Only upon increase of the current pulse amplitude to a value sufficient for transition of the entire sample to the normal state does the specimen become superconducting before the start of the next pulse (Fig. 8b). The existence of hysteresis can even be due to the small content of superconducting phase in the layer when the resistance of the specimen differs slightly from the total value of the resistance in the normal state. This manifests itself on the branch of the volt-ampere characteristic (corresponding to the transition from the normal state to the superconducting state) in a decrease in the duration of existence of the normal phase with increase in the current amplitude of the pulse (Figs. 8b, c).

The rate of increase of current in the pulse has a significant effect on the character of the development of the intermediate state in the film. Upon decrease of the rise time from 2 to 0.5 milliseconds, the initially more rapid growth of the resistance shifted in the direction of higher currents as in the research of Alekseevskii and Mikheeva,[3] but upon further increase in the growth rate—for a change of the growth time of the current from 0.5 to 0.1 millisecond—the initially faster growth rate of the resistance shifts in the direction of smaller currents (Fig. 9).

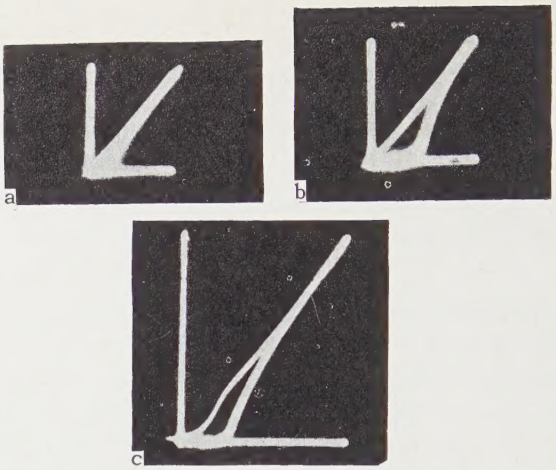

FIG. 8. Volt-ampere characteristics obtained by triangular pulses for different current amplitudes in the pulse. The rise time of the current in the pulse was 0.5 millisecond, the decay time was 0.1 millisecond, the repetition frequency of the pulses was 50 cps. a – I_{max} = 85 ma, b – I_{max} = 105 ma, c – I_{max} = 150 ma.

The character of this change makes it possible to assume the existence of two different mechanisms of propagation of the normal phase, depending on the growth rate of the current in the pulse. For a sufficiently slow growth of the current, the propagation of the normal phase is essentially determined by the motion of the heat front from the normal regions, which are heated by Joule heat.[6]

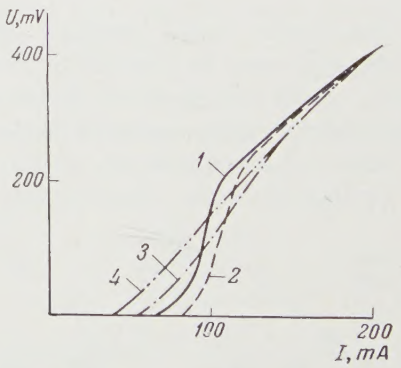

FIG. 9. Volt-ampere characteristics of specimens for different current rise times for constant amplitude (current pulses of triangular shape). Repetition frequency 50 cps. The curves correspond to the following rise times of current: 1 – 1 millisecond; 2 – 0.5 millisecond; 3 – 0.2 millisecond; 4 – 0.1 millisecond.

*A work recently appeared[9] which confirms these results.

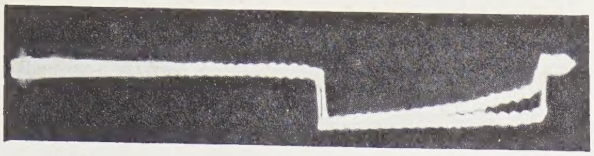

FIG. 10. Oscillogram of the transition of the specimen from the superconducting state to the normal under the action of rectangular pulse of 2 milliseconds duration. The upper curve is the current pulse, the lower is the voltage across the specimen.

Beginning with a certain rate of change of the current in the pulse, the process of propagation of the normal phase takes place chiefly under the action of the magnetic field of the increasing current and the heat which is generated in the normal regions by the eddy currents due to the appearance of a field in this region.

The overheating of the specimen and the rate of its cooling are essentially determined by the thermal conductivity of the substrate which, in this case, is a heat radiator, since the heat removal through the helium is very small. It was shown in reference 1 that even putting the film specimens in He II has no significant effect on the dissipation of the heat released in the specimen during the action of the pulse.

c) Pulses of rectangular shape. Investigations with current pulses of rectangular shape of duration from 0.1 to 10 microseconds, with rise times of 0.05 and 0.15 microsecond, have made it possible to disclose new laws in the character of the transition from the superconducting to the normal state. On passage of the current pulse through the specimen, the change in the resistance during the time of action of the pulse takes place in double fashion. Initially, a sharp rise in resistance was observed in our specimens during the rise time of the current in the pulse. Analysis of the oscillograms shows that, for a given temperature, a definite value of resistance of the specimen corresponds to each particular value of the current amplitude in the pulse. With increase in the growth rate of the current, the start of the more rapid growth of resistance continues to be displaced in the direction of lower currents, which indicates the very large effect of the eddy currents. Moreover, although the current through the specimens is not changed, the resistance of the specimen continues to grow. Increase of the resistance of the film with time in this case takes place as a result of current heating of the part of the specimen, which is already in the normal state, and goes more slowly than according to a linear law (Fig. 10).

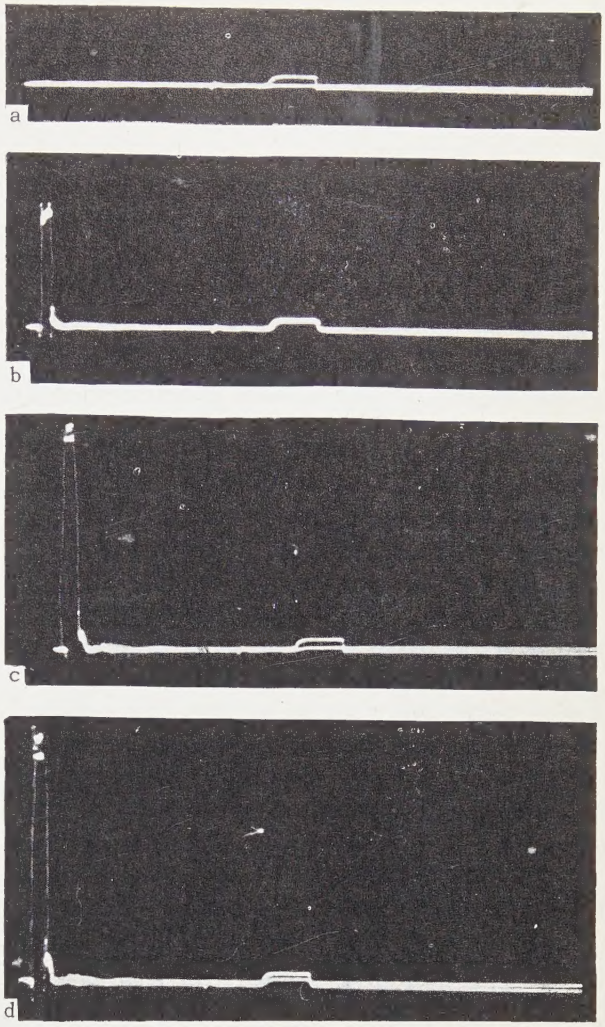

FIG. 11. Effect of the amplitude of the current in the pulse on the transition of the specimen from the normal state to the superconducting. The length of the pulses was 0.5 and 1.5 microseconds, respectively. a – I_1 = 0, b – I_2 = 100 ma, c – I_3 = 190 ma, d – I_4 = 200 ma.

The existence of phase delays of the normal state was again confirmed with the help of two successive current pulses also with short pulses in the case of a decrease in the current. Upon passage of two pulses through the specimen, the amplitude of the second pulse was so set that this pulse did not transform the specimen to the normal state in the absence of the first pulse (Fig. 11a). The presence of resistance in the film in the case of the second pulse was detected when the amplitude of the current of the first pulse only was increased (Fig. 11b). If now the amplitude of the first pulse is increased so that the specimen goes over entirely into the normal state during the time of action of the pulse, then the normal phase is not observed in the specimen in the second pulse and the specimen continues to remain superconducting

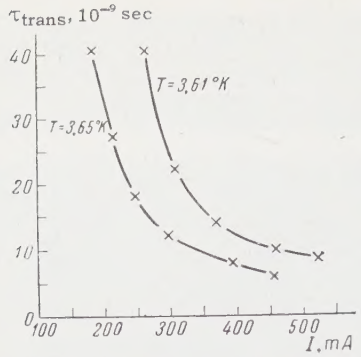

FIG. 12. Dependence of the times of transition from the superconducting state to the normal on the amplitude of the current in the pulse at different temperatures of the helium bath.

(Fig. 11c). Upon further increase in the amplitude of the first pulse, the amplitude of the second pulse is shown to be sufficient for transformation of the specimen to the normal state (Fig. 11d).

Analysis of the oscillograms shows that the reasons for the appearance of the normal phase during the time of action of the second pulse are different in the cases shown in Figs. 11b and d. In the first case (Fig. 11b), this is brought about by retardation of the normal phase in the specimen after cessation of the action of the first pulse. The time of existence of the normal phase is shown to be appreciable and reaches tens of microseconds. If the same specimen were completely transformed to the normal state, then the transition to the superconducting state is completed in a time less than the decay time of the current, i.e., 0.05 microsecond. In the second case (Fig. 11d), the increase of amplitude of the first pulse led to heating of the specimen to a temperature at which the amplitude of the second pulse was sufficient for appearance of the normal phase in the specimen. It then followed that the structure of the intermediate state, which is formed upon destruction of the superconductivity by the current, differs essentially from the structure of the intermediate state in the spontaneous formation of the superconducting phase.

Measurements of the transition times of the specimen from the superconducting state to the normal state were carried out with these same pulses as a function of the amplitude of the current in the pulse. The transition time was determined as the time between the instants of achieving half-maximum by the current through the specimen and the voltage across it. The character of the dependence of the transition time on the current amplitude (Fig. 12) is the same as in references 1 and 10. The time of transition for the specimens from the superconducting to the normal state for sufficiently high current amplitudes in the pulse was $\tau < 5 \times 10^{-9}$ sec.

4. CONCLUSION

The results set forth above were obtained on films of such thickness for which the values of the currents which destroy superconductivity depend weakly on the thickness of the specimens. For thinner films, one can expect other laws[1] both for destruction of superconductivity by the current and for the transition of specimens from the normal to the superconducting state.

Recording of the first traces of resistance upon increase in the current depends significantly on the sensitivity of the measuring apparatus.

In the action of very short current pulses, the principal effect on the character of the transition is supplied by Joule heat and the heat generated by eddy currents.

In addition to hysteresis of a thermal character, which is brought about in the transition from the normal to the superconducting state, a hysteresis was observed which was brought about by the existence of superconducting regions in the normal phase. The time for spontaneous transition to the superconducting phase is appreciably less than the time for destruction of the intermediate state formed in the destruction of the superconductivity by the current.

For films of the thickness investigated, the transition time from superconducting to normal state depends materially on the current amplitude in the pulse. For sufficiently large current amplitudes in the pulse, the transition time is $\tau < 5 \times 10^{-9}$ sec.

[1] Crittenden, Cooper, and Schmidline, Proc. IRE **48**, 1233 (1960).

[2] Newhouse, Bremer, and Edwards, Proc. IRE **48**, 1395 (1960).

[3] N. E. Alekseevskii and M. N. Mikheeva, JETP **38**, 292 (1960), Soviet Phys. JETP **11**, 211 (1960).

[4] N. I. Ginzburg and A. I. Shal'nikov, JETP **37**, 399 (1959), Soviet Phys. JETP **10**, 285 (1960).

[5] J. W. Bremer and V. L. Newhouse, Phys. Rev. **116**, 309 (1959).

[6] J. W. Bremer and V. L. Newhouse, Phys. Rev. Lett. **1**, 282 (1958).

[7] Borovik, Lazarev, and Fedorova, Ukr. Phys. J. **2**, 182 (1957).

[8] Galkin, Kan, and Lazarev, JETP **20**, 865 (1950).

[9] Smallman, Slade, and Cohen, Proc. IRE **48**, 1562 (1960).

[10] F. W. Schmidlin and E. C. Crittenden, Proceedings of the 5th International Conference on Low Temperature Physics and Chemistry, p. 234 (Madison, 1958).

Translated by R. T. Beyer
267

INVESTIGATION OF LARGE IONIZATION BURSTS PRODUCED BY COSMIC RAY PARTICLES AT SEA LEVEL

J. BABECKI, Z. BUJA, N. L. GRIGOROV, J. LOSKIEWICZ, J. MASSALSKI, A. OLES, and V. Ya. SHESTOPEROV

Institute of Nuclear Physics, Moscow State University

Submitted to JETP editor December 20, 1960

J. Exptl. Theoret. Phys. (U.S.S.R.) 40, 1551-1561 (June, 1961)

An array consisting of 128 ionization chambers with total area 10 m^2 was employed to study ionization bursts equivalent to the traversal of 1000 or more relativistic particles through the chambers. The exponent of the integral spectrum of bursts recorded by the large-area array $\gamma = 1.71 \pm 0.04$. For the individual particles the spectral exponent is $\gamma = 1.96 \pm 0.03$. The causes of this disparity and the nature of the large ionization bursts are discussed.

INTRODUCTION

INTERACTION processes in the $10^{12} - 10^{13}$ ev region have been studied during the last few years mainly by two methods, exposure of emulsion stacks to cosmic rays at great altitudes and by means of ionization chambers. A sharp disparity in the results of investigations by these methods has been observed. This disparity involves the following.

The emulsion method indicates that γ quanta (and consequently, π^0 mesons, too) are produced in air with a rapidly dropping spectrum [integral spectrum exponent ~ 3 (see reference 1) in the region of energy $\geq 10^{12}$ ev]. At the same time, it follows from the ionization method that the spectrum of ionization bursts, which should coincide with the spectrum of nuclear-active particles incident on the apparatus from the air, has an exponent of $1.5 - 1.6$ (see references 2 and 8).

In our opinion, the experimental results presented below can explain the reason for this disparity.

The present work was performed on an array designed for the study of interaction processes involving particles of energy $10^{12} - 10^{13}$ ev with the aid of photographic emulsion.[3] A large number of ionization chambers in this array, along with a combination of lead-graphite filters, acted as an ionization calorimeter,[4] and at the same time was designed to determine the coordinates of the shower passing through the emulsion.

This array was recently assembled at an altitude of 3200 m above sea level on Mount Aragats. Before its installation on the mountain, a simplified version of this array was used in experiments in Moscow at a height of 50 m above sea level. In the experiments at sea level, data was obtained on the character of the ionization bursts produced by high-energy particles, on air showers associated with high-energy particles, and on the energy of the nuclear-active components in extensive air showers.

Comparison of the results of the measurements at sea level with the analogous results obtained at mountain altitudes with the same equipment is undoubtedly of interest, since later on in the analysis of the experimental data, it is possible to eliminate effects due to apparatus factors, which sometimes cannot be taken into account correctly when a comparison is to be made of data obtained at different altitudes on nonidentical arrays.

1. APPARATUS

The array used in Moscow is shown schematically in Fig. 1.

It consisted of four rows of ionization chambers I-IV (32 chambers in each row) between which were lead and graphite filters (the filter thicknesses are shown in Fig. 1). Each chamber consisted of a brass cylinder 330 cm long, 10 cm diam, and 2 mm wall thickness. The collecting electrode was made from a brass tube of 4 mm diam.[3] The chambers were filled with pure argon

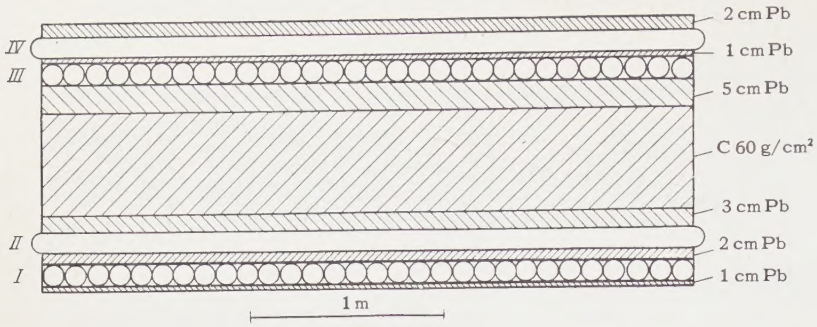

FIG. 1. Schematic diagrams of the arrangement employed. I–IV cylindrical ionization chambers.

to a pressure of 5 atm and operated with a potential difference of 1000 volts between electrodes. Special control measurements showed that saturation in the collection of electrons in the chamber occurred at a potential difference of 200 — 300 volts. During operation, the volt-ampere characteristics of all the chambers were taken periodically, and when contamination of the gas was detected (manifested by an increase in the potential at which the saturation of the ionization current occurs), the chambers were refilled with pure argon. Over the entire 7 months of operation, 26 of the 128 chambers in the apparatus were refilled.

The chambers of rows I and II, as well as the chambers of rows III and IV, were placed perpendicularly to one another. This arrangement of the chambers made it possible to determine the coordinate of the shower produced by the recorded bursts.

Each chamber was connected to an amplifier which permitted the measurement of the pulse amplitude for the individual chambers over a 300- to 400-fold range.

For rows I and II, the minimum registrable ionization pulse corresponded to the traversal of 200 relativistic particles. For the chambers of rows III and IV, the minimum pulse corresponded to 50 relativistic particles.* The pulse amplitudes were recorded on photographs of the screens of four single-sweep oscillographs to which each amplifier was connected, in turn, by means of mechanical commutators.[5]

The oscillograph was triggered by a special circuit which was actuated only if the total ionization exceeded a given threshold value simultaneously in each of any two rows.

These threshold values corresponded to a total ionization of 1200 relativistic particles for rows I and II and 2400 relativistic particles for rows III and IV.

To sum up the ionization pulses within each row, the pulses from each amplifier were fed to a summation unit and then to a summation amplifier. The pulses from the summation amplifer were fed to the control circuit of the apparatus and, at the same time, their amplitudes were recorded along with the pulses from the individual amplifiers.

The apparatus was installed in a special location with ~ 2 g/cm^2 of material of low atomic weight above it. A total of about 3 g/cm^2 of material, including counter units, was located above the apparatus.

During the operation of the apparatus, all amplifiers were calibrated electronically twice daily. Experience showed that the amplification of the great majority of amplifiers ($\geq 90\%$) changed by less than 2 — 3% during one day.

To check the stability of the apparatus, the operating frequency distribution for each chamber was plotted during the entire period of measurements. It turned out that, within the limits of statistical accuracy, all chambers of a given row operated the same number of times.

The operating rate of the apparatus during the entire period of the experiment also remained constant. During the first half of the entire period of measurement, the frequency of bursts of size $J_1 \geq 1200$ relativistic particles in row I was $(1.27 \pm 0.03) \times 10^{-1}$ hr^{-1} m^{-2} and during the second half of the period, the frequency of such bursts was $(1.25 \pm 0.03) \times 10^{-1}$ hr^{-1} m^{-2}.

2. RESULTS

a) Nature of ionization bursts in chambers under 60 g/cm^2 of graphite. Data on the ionization bursts in chambers under 60 g/cm^2 of graphite (chambers of rows I and II) were obtained during 2640 hours of operation of the apparatus.

The system of recording the ionization bursts (it was required that pulses from two rows of

*Here and in what follows the magnitude of the ionization pulse J is expressed in terms of the corresponding number of relativistic particles traversing simultaneously a path of length equal to the chamber diameter.

chambers be in coincidence and exceed 1200 relativistic particles in each row) practically excluded the recording of bursts from nuclear disintegrations in which the ionization in the chambers is produced by strongly ionizing particles of small range.

The recorded bursts could be produced only by cascade showers developing in the lead filters located over the chambers and between the chambers of rows I and II. One of the characteristic signs of electron-photon showers is the shift in the maximum of the showers to the region of larger thickness with an increase in the energy of the "primary" photons (electrons) producing these showers, i.e., with an increase in the size of the burst. Three centimeters of lead (~ 6 shower units) was above the second row of chambers and five centimeters of lead (~ 10 shower units) was above the first row; it should therefore be expected, firstly, that for the selected bursts with 1200 or more relativistic particles (which corresponds to an energy of $\geq 2 \times 10^{11}$ ev for the electron-photon component of the shower) the size of the burst in the first row will be bigger on the average than in the second row ($J_1 > J_2$), and, secondly, that the mean value of the ratio $(\overline{J_1/J_2})$ will increase with the size of the recorded bursts.

The experimental data obtained actually give $(\overline{J_1/J_2}) = 1.5 \pm 0.1$ for showers with 1200 to 2400 relativistic particles and $(\overline{J_1/J_2}) = 3.4 \pm 0.8$ for showers with more than 12 000 particles.

The same data indicate that the electron-photon component responsible for the bursts in the first and second rows of chambers is generated inside the apparatus and, in any case, does not come from the air. In the latter case, rows I and II would record showers far from the maximum of their development (a total thickness of ~ 22 shower units of lead was placed above the second row from the upper boundary of the apparatus) and the ratio $(\overline{J_1/J_2})$ would be ~ 0.5.

At sea level, the following two processes can lead to the production of an electron-photon component in the apparatus.

1. Interaction of high-energy nuclear-active particles in the graphite block (partially in the lead filters) of thickness $\sim 0.8 - 0.9$ of the interaction mean free path. Produced as a result of such an interaction are π^0 mesons whose decay gives γ quanta responsible for electron-photon showers in the lead.

2. Electromagnetic interactions of high-energy μ mesons in the filters of the apparatus (bremsstrahlung and high-energy δ electrons) can also lead to the production of showers containing a large number of particles.

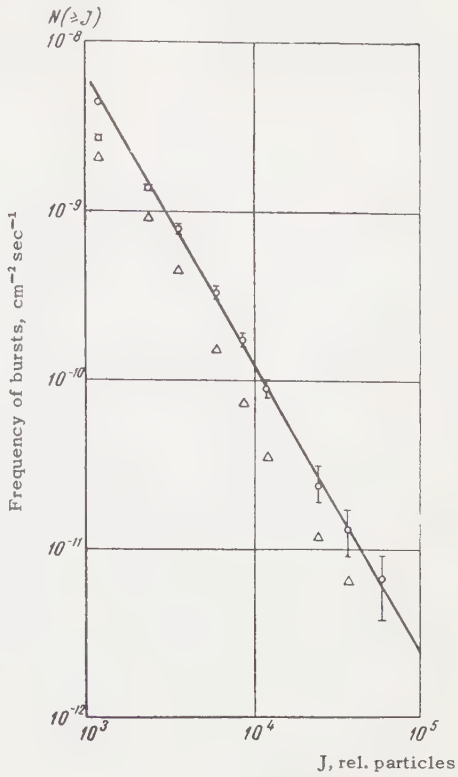

FIG. 2. Integral spectra of ionization bursts recorded in the lower rows of chambers: circles with errors – in row I with the control system operating at a threshold ≥ 1200 particles and o – at a threshold ≥ 600 particles; $\triangle$ – in row II with a threshold ≥ 1200 particles. The quantity J for the measured burst is laid off on the abscissa axis (without corrections); the number of bursts of size $\geq J$ is laid off on the ordinate axis.

Despite the small probability of the latter processes, a considerable excess of high-energy μ-meson flux over the flux of nuclear-active particles at sea level leads to a considerable contribution from μ mesons to the recorded bursts. However, some conclusions on the properties of the interaction of high-energy nuclear-active particles can also be drawn from an analysis of the experimental data obtained by us.

b) Spectrum of bursts recorded by arrays with large area and spectrum of individual particles. To construct the spectrum of ionization bursts, we took the total ionization recorded by all chambers in a given burst for the first and second rows, separately.

Figure 2 shows the integral spectra of the bursts recorded in the first and second rows of chambers.

If the obtained distribution is represented in the form of an exponential law of the type $N(\geq J) = AJ^{-\gamma}$, then we obtain for the exponent γ, by the

method of least squares, the values: $\gamma_I = 1.71 \pm 0.04$ for the first row and $\gamma_{II} = 2.00 \pm 0.04$ for the second row. The steeper spectrum for the second row of chambers reflects the fact that with an increase in the size of the burst the electron-photon showers do not have time to attain their maximum development in the filter of 3 cm Pb above the second row of chambers.

A deviation of the spectrum of bursts from the exponential law in the region of $J \sim 10^3$ relativistic particles is an apparatus effect associated with the recording threshold of 1200 particles in both rows I and II. The apparatus operated with a recording threshold of 600 relativistic particles in rows I and II for 600 hours. The intensity of bursts with 1200 or more particles obtained during this period is denoted by the circles (without the errors) in Fig. 2.

Using the cascade curves for lead,[6] one can establish that, for a wide energy interval of electron-photon cascades, the showers recorded by the first row of chambers will be close to their maximum development. Therefore the further analysis of the bursts will refer to the first row of chambers.

The exponent of the spectrum obtained by us for the first row of chambers $\gamma_I = 1.71 \pm 0.04$ is in good agreement with the results of other authors,[2] despite an important difference in the areas of the apparatus employed. It should be noted that the data obtained by us do not confirm the change in the exponent in the region of large bursts which was observed by Murzina, Nikol'skii, and Yakovlev.[7]

Usually, the spectrum of ionization bursts is identified with the spectrum of nuclear-active particles at the level of observation (if the contribution from μ mesons in the recorded bursts is small). But the correctness of this identification essentially depends on the type of array employed. If the area of the array is so small that the nuclear-active particles recorded by it never arrive in groups, then in this case the spectrum of the bursts will correspond to the spectrum of the particles.

If the array has a large area, groups of nuclear-active particles will pass through it quite frequently and produce "bursts with a structure;"[8] in this case the spectrum of the bursts will no longer reflect the spectrum of the individual nuclear-active particles. Then, with an increase in the energy, the distance between particles in such a group diminishes,[8] and, consequently, the probability that the apparatus is recording several particles or an entire group of particles and not the individual particles of the group increases.

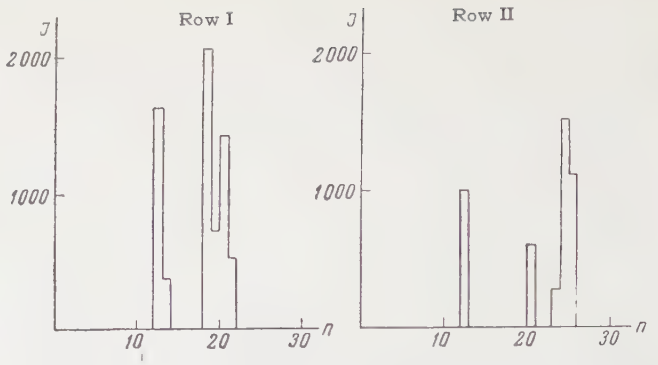

FIG. 3. Distribution of the ionization in chambers of rows I and II in one of the cases of a burst with "structure." The number of the chamber is laid off on the abscissa axis and the amount of ionization in the chambers, on the ordinate axis.

Owing to the large number of chambers in our array and independent recording of the ionization in each chamber, we were able to obtain experimental data on the influence of groups of nuclear-active particles on the shape of the spectrum of the bursts.

When ionization occurred in several chambers of row I or II, and was absent in chambers between them or was significantly less than in the neighboring chambers, we assumed that in these cases several nuclear-active particles were incident on the apparatus. Since these cases differed by a non-monotonic distribution of the amount of ionization in the chambers, we say that such bursts have a "structure." A typical example of one such burst is shown in Fig. 3.

The contribution of bursts with structure to the total number of bursts of different size is shown in Table I (the data refer to the first row of chambers).

A similar picture occurs for bursts recorded by the second row of chambers.

In order to see how the mean distance between particles of a group varies with their energy, we determined the mean distance $\bar{l}$ between chambers recording the maximum bursts due to the individual "structures" in the bursts with structure. Here

Table I

Burst size (in number of rel. particles)	Total number of bursts	Number of bursts with structure	Percentage of bursts with structure
$1.2 \cdot 10^3 \leqslant J < 2.4 \cdot 10^3$	1177	79	7
$2.4 \cdot 10^3 \leqslant J < 3.6 \cdot 10^3$	526	70	13
$3.6 \cdot 10^3 \leqslant J < 6.0 \cdot 10^3$	408	83	20
$6.0 \cdot 10^3 \leqslant J < 8.4 \cdot 10^3$	144	39	27
$8.4 \cdot 10^3 \leqslant J < 1.2 \cdot 10^4$	80	17	21
$1.2 \cdot 10^4 \leqslant J < 2.4 \cdot 10^4$	62	19	32
$2.4 \cdot 10^4 \leqslant J < 3.6 \cdot 10^4$	11	6	55
$3.6 \cdot 10^4 \leqslant J < 6.0 \cdot 10^4$	6	5	84
$J \geqslant 6.0 \cdot 10^4$	6	5	84

Table II

Burst size	$\bar{l}$, cm	Burst size	$\bar{l}$, cm
$1.2 \cdot 10^3 \leqslant J < 2.4 \cdot 10^3$	97	$1.2 \cdot 10^4 \leqslant J < 2.4 \cdot 10^4$	56
$2.4 \cdot 10^3 \leqslant J < 3.6 \cdot 10^3$	105	$2.4 \cdot 10^4 \leqslant J < 3.6 \cdot 10^4$	49
$3.6 \cdot 10^3 \leqslant J < 6.0 \cdot 10^3$	93	$3.6 \cdot 10^4 \leqslant J < 6.0 \cdot 10^4$	42
$6.0 \cdot 10^3 \leqslant J < 8.4 \cdot 10^3$	72	$J \geqslant 6.0 \cdot 10^4$	36
$8.4 \cdot 10^3 \leqslant J < 1.2 \cdot 10^4$	58		

we considered the two largest structures under the condition that the amount of ionization of one was less than twice the other.

The dependence of $\bar{l}$ on the size of the total burst with structure is shown in Table II (the data refer to the first row).

A similar dependence of the distance $\bar{l}$ on J also occurs for bursts recorded by the second row of chambers.

Since with an increase in the size of the burst, the transverse dimensions of a shower of nuclear-active particles decreases (see Table II), i.e., an increasing fraction of the energy of such a shower is incident on the apparatus, then the spectrum of the bursts is gradually transformed (with an increase in J) from the energy spectrum of particles into the energy spectrum of nuclear showers (showers of nuclear-active particles).

In order to obtain the spectrum of bursts produced by individual particles, we proceeded as follows. Each burst with structure was subdivided into the individual bursts of which it was composed ("structures"). These individual bursts were added to the single bursts (without structure) of corresponding size.

The spectrum of bursts from individual particles obtained in this way is shown in Fig. 4 (for the first row). As is seen, it also can be described by the law

$$N(\geqslant J) = BJ^{-\gamma}$$

with $\gamma = 1.96 \pm 0.03$ (the value of γ and its error were obtained by the method of least squares).

As is seen from the obtained data, the spectrum of the bursts ($\gamma = 1.71 \pm 0.04$) measured by an apparatus with a large area differs significantly from the spectrum of individual particles ($\gamma = 1.96 \pm 0.03$) observed at a given level in the atmosphere. The obtained exponent of the integral spectrum of bursts from individual particles may be somewhat lowered, since owing to the finite diameter of the ionization chambers (10 cm) it was possible to record a large burst as one without structure, although it was produced by a group of nuclear-active particles traveling at distances of $\lesssim 10$ cm from one another.

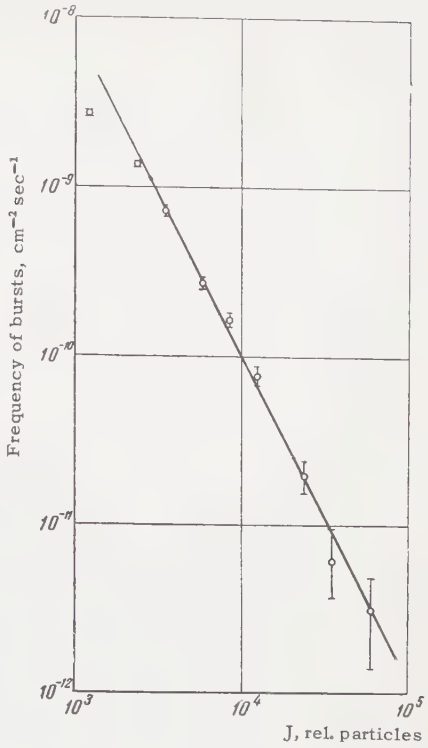

FIG. 4. Integral spectrum of bursts from individual particles. Axis of abscissas – size of burst J; ordinate axis – number of bursts of size $\geq$ J.

3. DISCUSSION OF RESULTS

As we have shown, the spectrum of the ionization bursts measured by an array with a large area does not reflect the true spectrum of the individual particles at a given level in the atmosphere. This is connected with the fact that if the ionization burst is of a sufficiently large size, the recorded burst is produced by a group of nuclear-active particles incident on the apparatus simultaneously. The size of the burst is then proportional to the total energy of the particles in the group.

The experimental data shown in Table I indicate that the large bursts (under conditions of an apparatus with an area of the order of several square meters) are produced by several nuclear-active particles, i.e, by a shower of nuclear-active particles. Of course, for a burst of sufficiently large size, practically the entire energy of such a shower will fall on the apparatus. Consequently, in this case, the size of the burst J will be proportional to the energy of the nuclear shower reaching the level of observation, i.e., the depth X g/cm^2 in the atmosphere. The altitude curve of such large bursts will now be determined by the altitude curve of the showers of nuclear-active particles with a given total energy and not at all by the altitude curve of the

individual nuclear-active particles. What will be the altitude curve of the bursts in this case?

We assume that 1) the primary particles incident on the boundary of the atmosphere expend all their energy on the production of π mesons in a single interaction with the nuclei of the air atoms; 2) in each interaction, $\pi^{\pm}$ mesons give up an average of $\frac{1}{3}$ of their energy to π^0 mesons; 3) the interaction mean free paths of the primary particles and π mesons are the same and are equal to L; 4) the spectrum of the primary particles is exponential:

$$F(\geqslant E_0) = A/E_0^{\gamma}.$$

We denote the energy flux of all nuclear-active particles reaching the level X g/cm^2 by S(E;X). This energy flux will consist of the energy flux of the primary particles $S_n(E_0; X)$ not experiencing any interactions in a layer of X g/cm^2 of the atmosphere and of the π-meson energy flux $S_{\pi}(X)$.

Let N_0 particles of energy E_0 be incident on the boundary of the atmosphere. An average of N(X) particles reach the layer X, where $N(X) = N_0 e^{-X/L}$ (since their inelasticity coefficient can be taken equal to unity).

Since

$$S_n(E_0; X) = N(X)E_0 = N_0 E_0 e^{-X/L}, \quad (1)$$

then

$$S_n(E_0; X) = S_n(E_0; 0)\, e^{-X/L}. \quad (2)$$

The change in the π-meson energy flux in the layer dX will be (we neglect decays)

$$dS_{\pi}(X) = -\frac{1}{3} S_{\pi}(X) \frac{dX}{L} + \frac{2}{3} S_n(X) \frac{dX}{L}, \quad (3)$$

from which we have

$$S_{\pi}(X) = S_n(E_0; 0)\,(e^{-X/3L} - e^{-X/L}). \quad (4)$$

Hence the total energy flux of nuclear-active particles resulting from primary particles of energy E_0 will on the average vary with the depth X according to the law

$$S(X) = S_n(E_0; X) + S_{\pi}(X) = S_n(E_0; 0)\, e^{-X/3L}, \quad (5)$$

or

$$S(X) = N_0 E_0 e^{-X/L_E} = S_0 e^{-X/L_E}, \quad (6)$$

where L_E is the mean free path for the absorption of the energy flux in a nuclear shower and is equal to 3L.[9]

If it is assumed that, at a depth of X g/cm^2 in the atmosphere, the number of showers with a total nuclear-component energy $\geq E$ is equal to $N(\geq E; X)$, then, since these showers were produced by primary particles of energy $\geq Ee^{X/LE}$, we have

$$N(\geqslant E; X) = F(\geqslant Ee^{X/L_E}) = A/(Ee^{X/L_E})^{\gamma} = (A/E^{\gamma})\, e^{-X\gamma/L}. \quad (7)$$

From this expression it follows, first, that the shape of the spectrum of larger bursts resulting from the recording of showers of nuclear-active particles coincides with the shape of the spectrum of primary particles incident on the boundary of the atmosphere. Second, the number of bursts with total energy $\geq E$ decreases with an increase in the depth of the atmosphere as e^{-X/L_a}, where the absorption mean free path $L_a = L_E/\gamma = 3L/\gamma$ does not depend on the energy of the burst if this energy is sufficiently large. Thirdly, we have the numerical value $L_a = 3L/\gamma \approx 200/1.7 \approx 120$ g/cm^2, i.e., the same as in the region of low-energy bursts when the bursts are produced by individual particles hitting the apparatus.

Hence, in the regions of small and sufficiently large ionization bursts, all the characteristics of these bursts are the same: the spectrum is exponential with the same exponent as for the primary particles and the variation of the number of bursts with altitude also does not depend on the size of the burst (at least, for the two extreme groups of bursts: very small and very large). This fact led some authors[10,11] to conclude that the elementary act of interaction of primary cosmic particles in the energy range from 10^{10} to 10^{13} ev is invariant.

However, as was shown above, the fact that the shape of the spectrum and the absorption mean free path L_a are independent of the size of the bursts can be explained even with the basic change in the character of the elementary act: a low inelasticity at energies of $\sim 10^{10}$ ev and complete inelasticity at energies of $\sim 10^{13}$ ev.

It thus follows that the conclusion[10,11] on the invariance of the elementary act over a wide range of energies based on an analysis of bursts without taking into account the above-mentioned properties of large bursts is, at least, ambiguous.

As is indicated by the data of Table II, the average distance between particles in a group decreases with an increase in the total energy of the particles of the group (size of the burst), and, consequently, the effect of recording groups of particles arriving from the air will be inherent in apparatus of any size. The difference between different arrays reduces only to the value of the "critical" energy of the group of particles E_c beginning with which a given energy release in π^0 mesons within the apparatus (for a burst of given size) involves, with a probability close

to unity, a group of particles and not a single particle.

If bursts with structure are recorded and the nuclear-active particles are $\pi^{\pm}$ mesons, then the entire discussion above should also refer to π^0 mesons, i.e., to γ quanta reaching the apparatus from the air; hence both the spectrum of nuclear-active particles and the spectrum of γ quanta will reflect not only the spectrum of primary particles, but also the conditions of production of these particles in the shower.

Under certain assumptions, which seem to us to be natural ones, it is found that, only owing to the increase in the multiplicity of the secondary particles in the shower with the energy of the primary particles, the spectrum of individual particles will be softer than the primary particle spectrum for a constant inelasticity coefficient.

In fact, we assume that the mean number of particles $\bar{n}$ of energy ϵ in a shower whose total energy is E depends on E in the following way: $\bar{n} \sim E^m$, where $\epsilon = E/\bar{n}$.

The spectrum of showers at a given depth in the atmosphere has the form

$$F(E)\,dE = BE^{-(\gamma+1)}\,dE.$$

From this we readily find that the observed spectrum of individual nuclear-active particles has the form

$$N(\varepsilon)\,d\varepsilon \sim \varepsilon^{-\beta}d\varepsilon, \qquad \beta = (\gamma + 1 - 2m)/(1 - m). \quad (8)$$

The exponent of the integral spectrum of the particles is

$$\gamma^* = \beta - 1 = (\gamma - m)/(1 - m), \quad (9)$$

where γ is the exponent of the integral spectrum of the showers, or, what is the same thing, of the primary particles. Therefore

$$m = (\gamma^* - \gamma)/(\gamma^* - 1). \quad (10)$$

The data obtained by us indicates that the spectrum of individual nuclear-active particles is steeper than the shower spectrum. Unfortunately, we cannot make a quantitative estimate of the value of m from our measurements, since at sea level the main contribution to the number of recorded bursts comes from μ mesons. Owing to this, the exponent γ does not coincide with the spectrum of nuclear showers. But if we draw upon the mountain altitude data obtained by the Japanese group,[12] and assume that the integral spectrum of the showers at mountain altitudes has the exponent $\gamma \approx 1.7$ (in the energy region $\geq 10^{12}$ ev), then one would have to take m = 0.5 to explain the softness of the spectrum of individual nuclear-active particles.

It should be emphasized that m is not the mean multiplicity of particles produced in an elementary act, but associates the particle multiplicity in a shower with the shower energy at a given depth (the inappropriateness of the value m = 0.5 can be seen only after accurate calculation of the particle spectrum for a nuclear shower at various depths).

The authors thank V. Trush for his great help in the reduction of the experimental data.

[1] Duthie, Fisher, Fowler, Kaddoura, Perkins, and Pinkau, Proceedings of the Moscow Cosmic Ray Conference, VINITI Moscow, 1960, Vol. 1.

[2] Dovzhenko, Zatsepin, Murzina, Nikol'skii, and Yakovlev, ibid., Vol. 2; Dmitriev, Kulikov, and Khristiansen, JETP **37**, 893 (1959), Soviet Phys. JETP **10**, 637 (1960).

[3] Grigorov, Kondrat'eva, Savel'eva, Sobinyakov, Podgurskaya, and Shestoperov, op. cit. ref. 1, Vol. 1.

[4] Grigorov, Murzin, Rapoport, JETP **34**, 506 (1958), Soviet Phys. JETP **7**, 348 (1958).

[5] Grigorov, Shestoperov, and Sobinyakov, Приборы и техника эксперимента (Instrument and Measurement Techniques) No 6, 67 (1959).

[6] K. Ott, Z. Naturforsch **9a**, 488 (1954).

[7] Murzina, Nikol'skii, and Yakovlev, JETP **35**, 1298 (1958), Soviet Phys. JETP **8**, 906 (1959).

[8] Grigorov, Shestoperov, Sobinyakov, and Podgurskaya, JETP **33**, 1099 (1957), Soviet Phys. JETP **6**, 848 (1958).

[9] Grigorov, Murzin, and Rapoport **36**, 1068 (1959), Soviet Phys. JETP **9**, 759 (1959).

[10] Dmitriev, Kulikov, Khristiansen, JETP **37**, 893 (1959), Soviet Phys. **10**, 637 (1960).

[11] Baradzeĭ, Rubtsov, Smorodin, Solov'ev, and Tolkachev, op. cit. ref. 1.

[12] Fujimoto, Hasegawa, Kazuno, Nishimura, Niu, and Ogita, op. cit. ref. 1, 1960.

Translated by E. Marquit
268

MAGNETIC AND MAGNETOELASTIC PROPERTIES OF DYSPROSIUM AND GADOLINIUM

K. P. BELOV, R. Z. LEVITIN, S. A. NIKITIN, and A. V. PED'KO

Moscow State University

Submitted to JETP editor December 27, 1960

J. Exptl. Theoret. Phys. (U.S.S.R.) 40, 1562-1569 (June, 1961)

The temperature dependences of the magnetization, magnetostriction, modulus of elasticity and internal friction of dysprosium and gadolinium have been measured.

Large anomalies, which are strongly affected by a magnetic field, have been detected in the modulus of elasticity and internal friction of dysprosium in the region of the ferromagnetism-antiferromagnetism transition ($\Theta_1 = 85 - 88°$ K). In the same temperature region dysprosium possesses a very large magnetostriction ($\lambda \approx 1000 \times 10^{-6}$) which is of an isotropic nature ($\lambda_{\parallel}$ and $\lambda_{\perp}$ are of opposite sign). It was established that in distinction to the antiferromagnetism-paramagnetism transition ($\Theta_2 = 178°$ K), the transition at 88° K is connected with a change in the nature of the magnetic interaction between the magnetic sublattices in dysprosium.

In gadolinium a maximum magnetization and minimum coercive force and residual magnetization are observed near the temperature 210° K. Magnetostriction vanishes at the same temperature. An anomalous behavior of gadolinium (compared with Ni and Fe) is observed near the Curie point (290.5° K). It is suggested that in the interval 210 — 290.5° K an antiferromagnetic state exists in gadolinium which is, however, destroyed by a weak field.

GREAT interest has arisen recently in studying the magnetic properties of the rare earth metals and alloys. This interest is aroused by the two following reasons:

a) A complicated ferromagnetism-antiferromagnetism-paramagnetism transition is observed in a number of rare-earth metals (Dy, Ho, Er, Tb and Tu). A study of such a complicated magnetic transition is of interest from the point of view both of magnetic theory and of the theory of phase transitions.

b) In the rare earth elements, as distinct from the elements of the iron group, the uncompensated electron spins are in a shell which is screened by the higher lying 5s and 5p electron shells. Because of this, direct exchange interaction between the 4f-electrons of neighboring atoms is evidently made very difficult or completely prevented.

It is assumed that indirect exchange via the free electrons takes place in rare earth metals. In addition, Vonsovskii and Izyumov[1] consider that the 5s and 5p electrons may take an active part in this exchange.

These circumstances must influence the magnetic behavior of rare-earth ferromagnets. In fact, their magnetic behavior is very varied. However, so far we still have very scanty information about the properties of these interesting substances.

It is especially important to study in detail the magnetic and nonmagnetic properties of the rare earth metals in the temperature regions of the ferromagnetic-antiferromagnetic transition (the point Θ_1), antiferromagnetic-paramagnetic transition (Θ_2) and in the intervening temperature range from Θ_1 to Θ_2.

At present we have fairly detailed data on the magnetic properties of Dy, so that it is appropriate to start our consideration with this metal. Trombe[2] and Elliott, Legvold and Spedding[3] have studied the magnetic properties of Dy. These authors established that for dysprosium $\Theta_1 = 85 - 90°$ K and $\Theta_2 = 178°$ K, i.e., Dy is in the ferromagnetic state below 85° K, in the paramagnetic state above 178° K, and in the intermediate region from 85 to 178° K dysprosium shows antiferromagnetic behavior, which is strongly influenced by an external magnetic field. In strong magnetic fields the magnetization curve I(T) has the usual Weiss form. However, in weaker fields a rapid fall in magnetization is found on heating to a certain temperature (in zero field this fall in magnetization takes place at $\Theta_1 = 85°$ K). Further, at $\Theta_2 = 178°$ K a small increase in magnetization is found and a final decrease, as is usual at the Néel point of antiferromagnets.

Néel[4] has proposed the following hypothesis to explain the properties of Dy. The hexagonal lat-

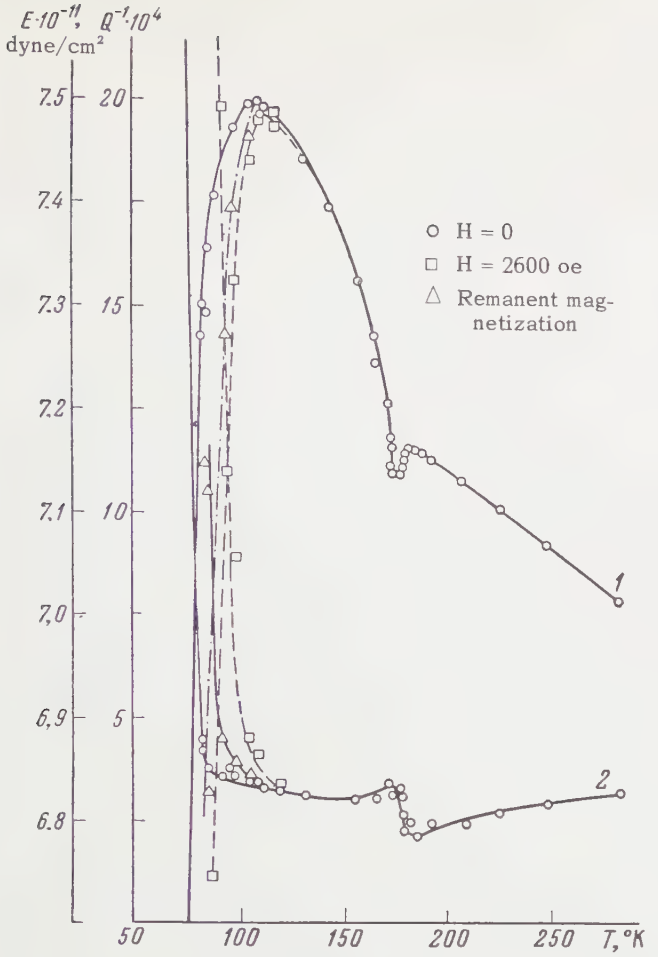

FIG. 1. Temperature dependence of Young's modulus (curve 1) and of internal friction (2) for dysprosium.

tice of Dy is subdivided into two magnetic sublattices. In each of these there is a strong positive exchange interaction i.e., both sublattices are ferromagnetic. However, there is a weak negative interaction between the sublattices on which the influence of magnetic interaction forces can act (magnetocrystalline energy). As a result of this, a parallel or antiparallel configuration of the magnetic moments of the sublattices may be set up. According to Néel, a change in this configuration of the magnetic moments depends on the nature of the temperature variation of the anisotropy constant K_2 at the point Θ_1.

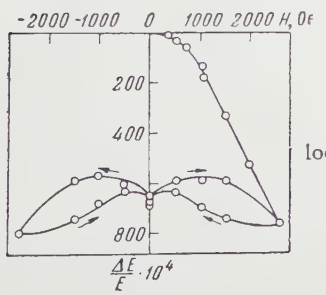

FIG. 2. ΔE-effect hysteresis loop for dysprosium at 85°K.

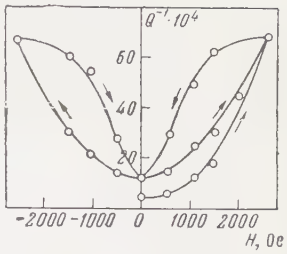

FIG. 3. Internal friction, Q^{-1}, hysteresis loop for dysprosium at 85°K.

On the basis of the suggested hypothesis, Néel has given a qualitative explanation of the magnetization curves between Θ_1 and Θ_2. Enz[5] has recently suggested that in the Dy crystal the spins situated in neighboring basal planes are turned at some angle relative to one another. According to Enz, this arrangement of spins in Dy is explained by the 'competition' between the positive exchange interaction between the spins in neighboring planes and the negative exchange interaction between spins lying in next nearest neighbor planes. The existing experimental material on its magnetic properties is insufficient to verify these suggestions about the structure and the nature of the magnetic transformations in Dy. Additional experimental data are essential for this.

1. THE MAGNETOELASTIC PROPERTIES OF DYSPROSIUM

For a more detailed investigation of the properties of dysprosium we undertook measurements of its magnetoelastic characteristics: the magnetostriction λ, the modulus of elasticity E and the internal friction Q^{-1} (a quantity proportional to the damping decrement of oscillations) near the points Θ_1 and Θ_2 and in the temperature interval between them.

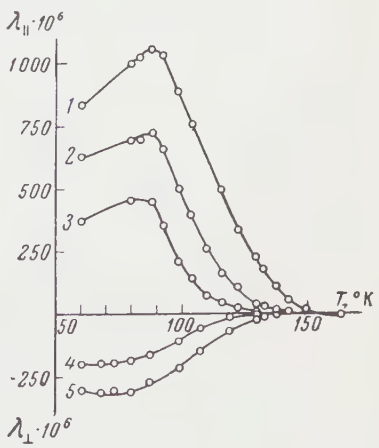

FIG. 4. Temperature dependence of the magnetostriction of dysprosium in constant magnetic field: curve 1 — longitudinal magnetostriction $\lambda_\parallel$ in a field H = 15,000 oe; 2 — $\lambda_\parallel$ in a field H = 9,500 oe; 3 — $\lambda_\parallel$ in a field H = 6,500 oe; 4 — transverse magnetostriction $\lambda_\perp$ in a field H = 15,000 oe; 5 — $\lambda_\perp$ in a field H = 9,500 oe.

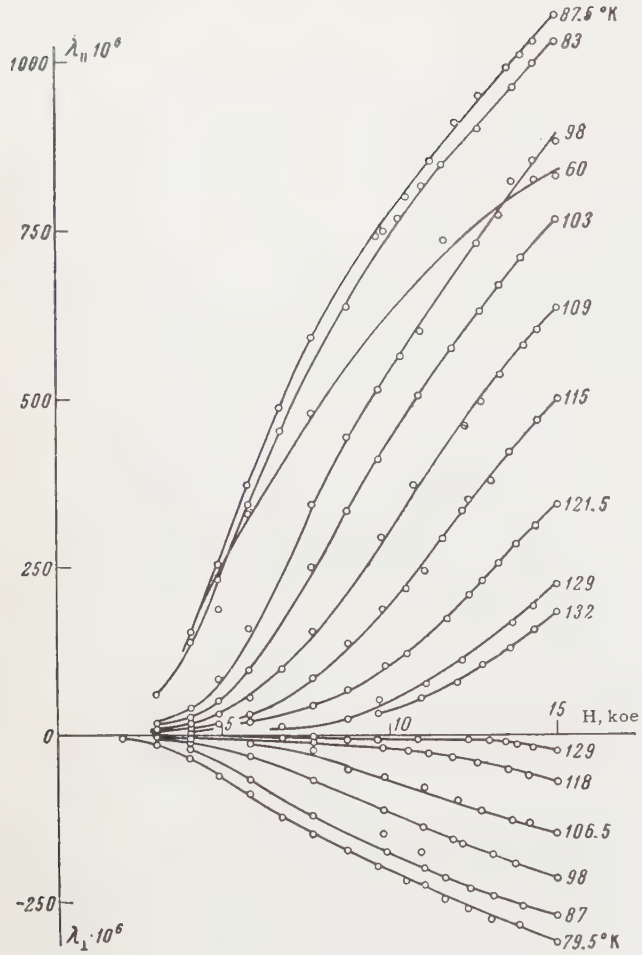

FIG. 5. Isotherms of longitudinal, $\lambda_{\parallel}$, and transverse, $\lambda_{\perp}$, magnetostriction for dysprosium.

Figure 1 shows the results of measurements of the temperature dependence of the modulus E and of Q^{-1} in a polycrystalline specimen of Dy, made by a radio-frequency method (at 128 kc/sec).[6] Similar dependences are obtained for the shear modulus and internal friction for torsional oscillations. The curves of Fig. 1 confirm the existence of two points Θ_1 and Θ_2 for Dy. In our case these are $\Theta_2 = 175°$ K and $\Theta_1 = 88°$ K.

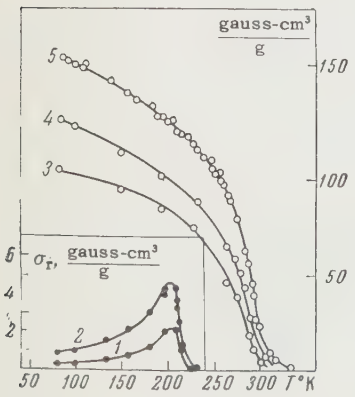

FIG. 6. Temperature dependence of the magnetization of gadolinium in different fields: curve 1 – H = 0.32 oe, 2 – H = 0.64 oe, 3 – H = 400 oe, 4 – H = 1,000 oe, 5 – H = 2,000 oe.

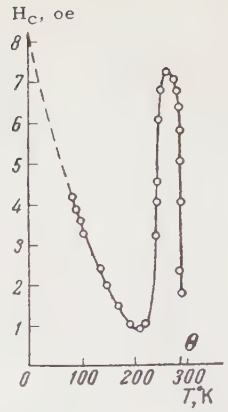

FIG. 7. Temperature dependence of the coercive force of gadolinium.

It can be seen from Fig. 1 that the nature of the anomalies in E and Q^{-1} in Dy at Θ_2 are the same as in the antiferromagnetic compound Cr_2O_3,[7,9] i.e., Θ_2 is a Néel point. The anomalies in E and Q^{-1} at the point Θ_1 are of quite a different nature. From Fig. 1 it is seen that the anomalies in E and Q^{-1} at Θ_1 are very great, much larger than at Θ_2. In addition, as distinct from the point Θ_2, a magnetic field has a strong influence on the modulus E (ΔE effect) and on the magnitude of Q^{-1}.

Further, irreversible changes in the magnitudes of E and Q^{-1} are observed on applying and removing the magnetic field. Figure 2 shows the hysteresis loop of the ΔE effect, measured for dysprosium in the region of Θ_1. An analogous loop is also found for the internal friction (Fig. 3). All this points to Θ_1 not being a second-order phase transition; rather it recalls a first-order magnetic transition. This transition is not related to any structural transformation, since x-ray studies[8] established the absence of changes in the crystallographic symmetry and lattice parameters of Dy in this temperature interval.

The results of measurements of magnetostriction are shown in Fig. 4. We must consider the

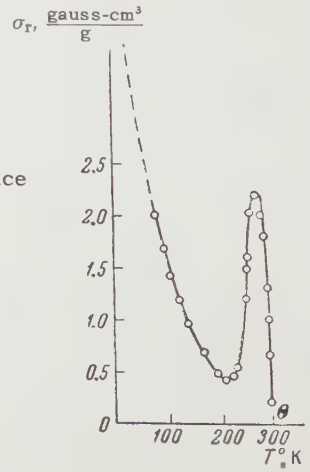

FIG. 8. Temperature dependence of the remanent magnetization of gadolinium.

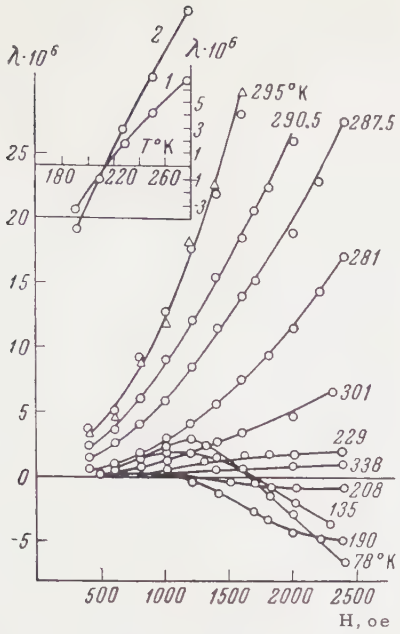

FIG. 9. Isotherms of the longitudinal magnetostriction, $\lambda_{\parallel}$, for gadolinium. Inset – temperature dependence of $\lambda_{\parallel}$ in fields: curve 1 – H = 1,700 oe, 2 – H = 2,500 oe.

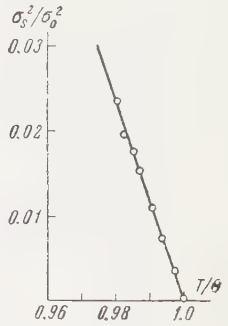

FIG. 10. Relative spontaneous magnetization of gadolinium near the Curie temperature.

following facts in this respect: a) the magnetostriction in the neighborhood of Θ_2 reaches a record high value (greater than 1000×10^{-6}) and is still not saturated in a field of 15,000 oe. The magnetostriction decreases on departing from Θ_2 into both the ferromagnetic and antiferromagnetic regions; b) the magnetostriction at Θ_1 is anisotropic; $\lambda_{\parallel}$ and $\lambda_{\perp}$ have different signs and are different in magnitude; c) from the form of the magnetostriction isotherms taken in the temperature interval from Θ_1 to Θ_2 (Fig. 5), it follows that at every given temperature there exists some critical field H_C at which λ starts to increase rapidly. The value of H_C increases as Θ_2 is approached; d) there are no signs of the existence of volume magnetostriction near Θ_1, which usually accompanies the ferromagnetic Curie point.

It thus follows from the data presented on magnetostriction (and also from the data on E and Q^{-1}) that Θ_1 is not a ferromagnetic Curie point in the usual meaning of that phrase. The spontaneous magnetization of dysprosium is not destroyed there. Since the magnetostriction is anisotropic at Θ_1, it follows that magnetic interaction forces play an important part and in this way confirm Néel's hypothesis. However, the question of the role of the temperature variation of the anisotropy constant K_1 at Θ_1 remains uncertain (the measurement of the temperature dependence of K_1 has not yet been carried out for dysprosium).

On the other hand, our data show that the maximum value of magnetostriction occurs at Θ_1. The question arises as to whether a change in the temperature variation of the magnetostriction constant does not play an important part in this transition. This question can be resolved after measuring the temperature dependence of the constant K_1 in Dy.

2. MAGNETIC AND MAGNETOELASTIC PROPERTIES OF GADOLINIUM

Although the ferromagnetism of gadolinium was found earlier than that of the other rare earth elements, less attention has been paid to its properties, evidently because a transition point Θ_1 was not found for it. Gadolinium is considered a "normal" ferromagnet. In fact, in fields from hundreds of oersteds upwards, the temperature dependence of magnetization shows the usual "Weiss" curve (Fig. 6).

However, we found anomalies in the temperature variation of magnetization in weak fields (measured on a toroid, Fig. 6) also a coercive

	σ_0, gauss-cm³/g	μD	Θ°, K	ξ	$\sigma_0/\Theta^{1/3}$	$\Theta^{-1/3}$	ΔT at 5000 oe	ΔC_p cal/g-deg	$\Theta_p - \Theta_f$
Gd	235.5	7.12	290.5	1.17	33.0	0.15	1.0	0.045	11.5
Ni	56.8	0.6	631	6.75	6.6	0.12	0.45	0.032	14.0
Fe	221.8	2.22	1036	6.8	22.1	0.10	1.4	0.16	22.0
Alloy { 36% Ni, 64% Fe }	184.4		565	1.44	22.0	0.12		0.0042	37.0
$3Gd_2O_3 \cdot 5Fe_2O_3$	84	29	570	0.06					
Ferrite { 35% MnO, 15% ZnO, 49.5% Fe_2O_3 }	152		467	0.1—0.7					

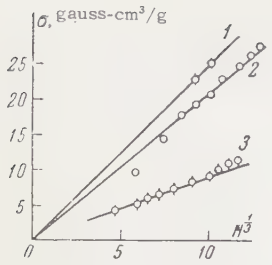

FIG. 11. The dependence of magnetization on $H^{1/3}$ at the Curie temperature: curve 1 – Fe, 2 – Gd, 3 – Ni.

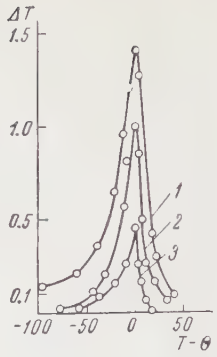

FIG. 12. Magnetocaloric effect near the Curie temperature: curve 1 – Fe, 2 – G, 3 – Ni.

force H_c (Fig. 7) and remanent magnetization σ_r (Fig. 8). The minimum values of H_c and σ_r and the maximum magnetization in weak fields occur at a temperature of 210° K. Above this temperature the magnetization falls rapidly, and the values of H_c and σ_r increase sharply up to the Curie point (Θ = 290.5° K). We should remark that the existence of these anomalies is not connected with the presence of impurities in the Gd specimens and with their thermal treatment. Our experiments were carried out on Gd specimens of 99.5 and 99.8% purity with different thermal treatment, and the anomalies were invariably found at 210° K.

There is also a magnetostriction minimum at 210° K which here changes sign (see Fig. 9).

In considering all these experimental facts one could limit oneself to the statement that a temperature is found in Gd (similar to the 217° point for Ni and 294° C for Co) at which there are temperature anomalies in the permeability μ and in H_c, and that these anomalies are apparently brought about by an anomalous temperature variation of the magneto-crystalline anisotropy constant K_1 (the temperature variation of K_1 in Gd has not yet been measured). We should note straight away that in Gd, as distinct from Ni and Co, there are two singularities in the behavior of the magnetic properties in the region of the Curie point Θ.

First, the magnetic transformation for Gd near the point Θ has an exceptionally "spread-out" nature. The slope of the decrease of spontaneous magnetization with temperature is very small. This slope can be measured[10] by the value of the coefficient ξ in the formula

$$(\sigma_s/\sigma_0)^2 = \xi(1 - T/\Theta).$$

While $\xi = 6 - 7$ for Ni and Fe, it is 1.17 in Gd (see Fig. 10 and the table). Such a small value of ξ usually occurs in ferrites[10] and in some alloys.

Second, one would expect that the paraprocess at Θ should be very large in Gd, since the magnetization is especially high and the Curie temperature low. One can estimate the magnitude of the paraprocess from the slope of the true magnetization curve σ_i right at the Curie point: $\sigma_i = aH^{1/3}$. From theory[10] it follows that the value of $a \sim \sigma_0/\Theta^{1/3}$, i.e., the greater σ_0 and the smaller Θ, the greater is the slope of the straight line $\sigma_i(H^{1/3})$ at the point Θ.

Table I shows the calculated values of $\sigma_0/\Theta^{1/3}$ for Gd, Fe and Ni. It can be seen that this ratio is considerably larger for Gd than for Ni and Fe. However, experiment gives other values for a. It can be seen from Fig. 11 that the value of a for Gd is less than for Fe and slightly larger than for Ni. In Gd we thus have a sort of "depressed" paraprocess.

This is confirmed by the results of measuring the magnetocaloric effect, ΔT, near the Curie point, shown in Fig. 12 for a field H = 5000 oe for Gd (our data), for Ni (data of Weiss and Forrer[11]) and for Fe (data of Potter[12]). For Gd the magnetocaloric effect at Θ is smaller than for Fe and slightly greater than in Ni (see Table I).

We are at present not clear about the nature of the magnetic anomalies of Gd at 210° K and of the unusual behavior of its magnetic properties in the temperature interval from 210° to Θ.

It is possible that it is to be explained by Gd, like Dy, being in the antiferromagnetic state between 210 and 290.5° K which is destroyed by a weak field.

We express our indebtedness to Professor E. M. Savitskii, V. F. Terekhova, and I. V. Burov for providing the gadolinium specimens for our experiments, and to A. S. Borovik-Romanov for his participation in the discussion of the results.

[1] S. V. Vonsovskii and Yu. A. Izyumov, Физика металлов и металловедение (Phys. of Metals and Metallography) **10**, 321 (1960).

[2] F. Trombe, Compt. rend. **221**, 19 (1945); J. Phys. Radium **12**, 222 (1951); Compt. rend. **236**, 591 (1953).

[3] Elliott, Legvold, and Spedding, Phys. Rev. **94**, 1143 (1954); Behrendt, Legvold, and Spedding, Phys. Rev. **109**, 1544 (1958).
[4] L. Néel, Compt. rend. **242**, 1549, 1824 (1956).
[5] U. Enz, Physica **26**, 698 (1960).
[6] J. Zacharias, Phys. Rev. **44**, 116 (1953).
[7] K. P. Belov and R. Z. Levitin, Ферриты (Ferrites), Minsk, 1960, p. 87.
[8] Banister, Legvold, and Spedding, Phys. Rev. **94**, 1140 (1954).
[9] K. P. Belov and R. Z. Levitin, JETP **37**, 565 (1959), Soviet Phys. JETP **10**, 400 (1960).
[10] K. P. Belov, Магнитные превращения (Magnetic Transformations), Fizmatgiz, 1959.
[11] P. Weiss and R. Forrer, Ann. de Phys. **5**, 153 (1926).
[12] H. H. Potter, Proc. Roy. Soc. **146A**, 362 (1934).

Translated by R. Berman
269

NEUTRON POLARIZATION IN THE REACTION C^{12} (d, n) N^{13}

I. I. LEVINTOV and I. S. TROSTIN

Submitted to JETP editor December 28, 1960

J. Exptl. Theoret. Phys. (U.S.S.R.) **40**, 1570-1571 (June, 1961)

The azimuthal asymmetry of neutrons from the reaction $C^{12}(d, n)N^{13}$ scattered on helium was measured. The measurements were carried out on the neutron group corresponding to the formation of N^{13} in the ground state. The deuteron energy was 11.8 ± 0.8 Mev. The polarization values of neutrons emitted at various angles from the carbon target are calculated with the Seagrave phase shifts for the scattering of neutrons on He^4.

WITH the aid of a helium analyzer, described earlier in detail in reference 1, we measured the azimuthal asymmetry in the scattering of neutrons from the reaction $C^{12}(d, n)N^{13}$. The measurements were carried out on the neutron group corresponding to the formation of N^{13} in the ground state.

A 12.3-Mev deuteron beam from the cyclotron at the Institute of Theoretical and Experimental Physics, Academy of Sciences, U.S.S.R. was focused by a system of magnetic quadrupole lenses onto a graphite target obtained by depositing an ammonia solution of aquadag on a gold base. The thickness of the graphite layer corresponded to the range of 1.6-Mev deuterons; the beam cross section at the target was 3 × 5 mm; the average beam current was 1.5 μa. The proportional helium counters of the analyzer operated under a pressure of 6.26 atm. The pressure was maintained constant to an accuracy of ± 0.5 mm Hg. A stream of commercial helium (99.8%) flowed continuously through the counters at a rate of 40 cc/sec.

The helium analyzer consisted of a battery of three counters (7 mm diam and 66 mm long) lying in a plane perpendicular to the rocking plane (plane of the reaction). The distance from the target to the rocking axis was 150 mm. The rocking axis passed through the center of the effective volume of the counters, whose length varied with the angle of emission of the neutrons in the limits of 15 — 25 mm. For a counter rocking angle of ± 19°, the size of the angle within which the neutrons from the target entered the effective volume of the counters was 3°, and the angular spread of the helium recoil nuclei recorded by the analyzer did not exceed 10°. Therefore, the correction to the observed asymmetry due to the anisotropy in the distribution of neutrons from the reaction was small (~ 2 — 3%), and instead of integrating over the effective volume in the calculation of the polarization of the analyzer, it was possible to limit the calculation to one point at the center of rocking. Hence the parameters of the arrangement ensured (in contrast to the experiment of reference 1) that the measurements were made under conditions of "good geometry."

The recorded helium recoil nuclei corresponded to neutrons of energy $\gtrsim 0.8\ E_{max}$ (E_{max} is the maximum energy for a given angle of observation). In this interval, there were no neutrons associated with the production of N^{13} in the excited state. We thus actually measured the asymmetry for the group of neutrons corresponding to the formation of N^{13} in the ground state in a deuteron energy interval determined by the target thickness (~ 1.6 Mev). The background of spurious pulses in the analyzer channel from neutrons produced in the base, diaphragms, etc. did not exceed 10 — 15% and was eliminated by special measurements.

The counters were calibrated in the same way as in reference 1, i.e., on neutrons from the reaction under study emitted at an angle $\theta_n = 60°$. We obtained the following values for the ratio R

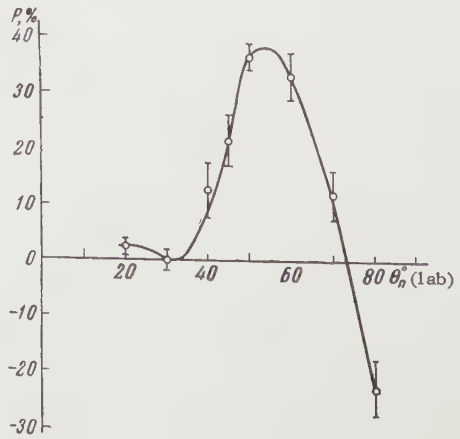

of counts at a rocking angle $\varphi_\alpha = +19°$ to counts at a rocking angle $\varphi_\alpha = -19°$ for various angles of emission of neutrons from the carbon target (only the statistical errors of measurement are shown):

θ_n (lab), deg	10	30	40	45	50	60	70	80
R	1.05±0.03	1.00±0.03	1.21±0.11	1.45±0.12	1.94±0.08	1.79±0.13	1.23±0.09	0.66±0.06

The calculation of the polarization of the reaction from the asymmetry data was carried out by means of Seagrave phase shifts for the scattering of neutrons on He^4 (see reference 2). The values obtained for the neutron polarization are given in the table and in the figure (for $E_d = 11.8 \pm 0.8$ Mev). The positive value of the polarization was taken in the direction $\mathbf{n} = \mathbf{k}_n \times \mathbf{k}_d$.

θ_n (lab), deg	20	30	40	45	50	60	70	80
E_n (lab), Mev	11.4	11.2	10.9	10.8	10,6	10,3	9.92	9,54
P_n, %	2.6±1,5	0±1.7	12.8±5.2	21.6±4.6	36.4±2.1	33.1±3.9	11.7±4.2	−22.6±4.9

The authors express their deep gratitude to the cyclotron crew of the Institute of Experimental and Theoretical Physics, Academy of Sciences, U.S.S.R. for the smooth operation of the accelerator, to F. A. Pavlovskii for aid in the preparation and adjustment of the electronic equipment, and to V. A. Smotryaev for aid in the reduction of the experimental data.

[1] Levintov, Miller, and Shamshev, JETP **32**, 274 (1957), Soviet Phys. JETP **5**, 258 (1957).

[2] J. D. Seagrave, Phys. Rev. **92**, 1222 (1953).

Translated by E. Marquit
270

ISOTOPE MASSES AND BINDING ENERGY OF NUCLEI IN THE REGION FROM STRONTIUM TO RUTHENIUM

R. A. DEMIRKHANOV, V. V. DOROKHOV, and M. I. DZKUYA

Submitted to JETP editor December 28, 1960

J. Exptl. Theoret. Phys. (U.S.S.R.) 40, 1572-1582 (June, 1961)

A double focusing mass spectrograph was employed to measure the masses of stable isotopes in the region $84 \leq A \leq 104$. The average resolving power of the instrument was 50 000 — 60 000. Twenty-five isotope masses were measured. The measurements were performed by checking the "internal consistency" of the results. For this purpose, 60 mass doublets were measured. Most of the isotope masses were determined from measurements of 3 — 4 doublets of different organic composition. Besides the 25 stable isotopes, the masses of 59 radioactive isotopes were determined. The binding energy per nucleon, binding energy of the last neutron (B_n) and proton (B_p), and the neutron (P_n) and proton (P_p) pairing energies were calculated on the basis of these data. The sharp break in the nucleon binding energy curve and the discontinuities in the energies B_n and P_n in nuclei containing 50 neutrons definitely confirm the existence of the "magic" number $N = 50$. Furthermore, anomalously large values of B_n and P_n have been found in nuclei with $N = 48$. On the other hand, no nonmonotonic variation of the above-mentioned parameters has been observed for $Z = 40$, which signifies that no subshell exists for $Z = 40$.

THE measurement of the masses of nuclei in the region from strontium to ruthenium is of interest from the viewpoint of elucidating the variation of the nuclear binding energy close to the magic number $N = 50$. To measure the masses of the isotopes of strontium, yttrium, zirconium, niobium, molybdenum, and ruthenium, we used a double focusing mass-spectrograph. The average resolving power of the intrument was 50 000 — 60 000.

We measured the doublets formed by an organic compound and the isotope under study. We calculated the instrument dispersion in each separate case by using fragments of the organic compounds with a mass difference of one mass of hydrogen. The use of this method made it possible to improve the accuracy of the measurements in this mass region by a factor of about 10 — 15 times, i.e., to obtain $\Delta M/M \approx (2-5) \times 10^{-7}$. A considerable part of the isotope masses in this region has not been measured on a mass spectroscope (Zr^{91}, Zr^{92}, Mo^{95}, Ru^{98}, and others); the values of the masses of the isotopes Ru^{100} and Ru^{101} were measured for the first time.

It is of interest to study the energy variation in the region $Z = 40$, which, in the opinion of several authors, is a "semi-magic" number.[1-4] Conclusions based on the values of six isobaric pairs and one isobaric triplet can be compared with those based on the region of heavier masses ($A \approx 200$).

MASS MEASUREMENTS

1. Strontium. We measured the masses of the strontium isotopes by comparing the masses of strontium evaporated in a tungsten vessel with the organic compounds toluene (C_7H_8, $M = 92$) and isoamyl alcohol ($C_5H_{12}O$, $M = 88$) and their fragments. In the first case, the vapor pressure of the toluene was sufficient to maintain the arc of the ion source. In the case of isoamyl alcohol, the ion-source arc was maintained on helium, and the standard organic compound $C_5H_{12}O$ was introduced additionally into the ion source. The values of the doublets and the isotope masses of strontium were calculated with the "weights" for the measurements shown in Table I.

2. Yttrium. The yttrium ions were obtained by evaporation of a metallic powder of yttrium in a tungsten vessel. The discharge in the ion source was maintained on toluene vapors (C_7H_8, $M = 92$). A toluene fragment (C_7H_5, $M = 89$) was used to measure the mass of the yttrium isotope. The values of the doublet and mass of yttrium are shown in Table I.

3. Zirconium. To obtain the zirconium ions, we evaporated zirconium chloride in a crucible and introduced the vapors into the discharge arc. We measured the zirconium masses by comparison with organic compounds of aniline (C_6H_7N,

Table I

Doublet	ΔM, 10^{-3} amu	Isotope mass, amu	Mean value of mass, amu	Isotope mass from mass-spectroscopic data, amu	Isotope mass from Wapstra's data,[5] amu
$C_7H_5O - Sr^{84}$	144.148±0.017	83.940088±24			
$C_6H_{12} - Sr^{84}$	180.583±0.023	83.940041±26	83.940070±17	83.939924±150* [6]	83.939860±250
$C_5H_{11}O - Sr^{86}$	164.039±0.024	85.936481±26		85.936658±110* [6]	
$C_7H_2 - Sr^{86}$	106.482±0.042	85.936542±44	85.936497±23	85.935330±430 [7]	85.936620±200
				85.93670± 50 [8]	
$C_6H_{11}O - Sr^{87}$	172.251±0.021	86.936411±24			
$C_7H_3 - Sr^{87}$	114.628±0.021	86.936538±25	86.936472±42	86.936612± 80* [6]	86.936576±150
$C_7H_4 - Sr^{88}$	125.862±0.038	87.933456±40		87.933956±110* [6]	
$C_7H_5 - Sr^{88}H$	125.822±0.080	87.933381±81	87.933454±16	87.933740±530 [7]	87.933750±200
				87.933634± 18 [8]	
$C_7H_5 - Y^{89}$	133.303±0.007	88.934147±15	88.934147±15	88.933998±110* [6]	88.934080±200
$C_7H_6 - Zr^{90}$	142.323±0.021	89.932694±25		89.932932±250* [6]	
$C_6C^{13}H_6 - Zr^{90}$	137.832±0.036	89.932826±40	89.932771±20	89.931780±630 [8]	89.932840±200
$C_6H_4N - Zr^{90}$	129.768±0.050	89.932747±52		89.933500±200 [8]	
$C_7H_7 - Zr^{91}$	149.184±0.028	90.934550±30			
$C_6H_5N - Zr^{91}$	136.626±0.037	90.934531±40	90.934543±20	—	90.934140±200
$C_7H_8 - Zr^{92}$	157.539±0.019	91.934837±25			
$C_6C^{13}H_7 - Zr^{92}$	153.078±0.025	91.934827±30	91.933832±22	-	91.933820±210
$C_6H_6N - Zr^{92}$	145.006±0.029	91.932824±33			
$C_7H_{10} - Zr^{94}$	172.074±0.063	93.936080±65			
$C_6C^{13}H_9 - Zr^{94}$	167.608±0.036	93.936081±40			
$C_6H_6O - Zr^{94}$	135.626±0.022	93.936146±25	93.936126±25	—	93.935800±350
$C_5C^{13}H_7N - Zr^{94}$	154.877±0.028	93.936236±31			
$C_7H_{12} - Zr^{96}$	185.576±0.044	95.938858±46	95.938838±46		95.938530±500
$C_6H_7N - Nb^{93}$	141.570±0.020	92.935862±25	92.935862±25	92.935208± 90* [6]	93.935260±240
$C_7H_8 - Mo^{92}$	153.539±0.024	91.936152±30			
$C_6C^{13}H_7 - Mo^{92}$	149.078±0.029	91.936076±35	91.936098±42	-	91.935210±290
$C_4H_6O_2 - Nb^{93}$	113.977±0.054	91.936094±66			
$C_7H_{13} - Mo^{94}$	173.205±0.046	93.934955±50			
$C_6H_9O - Mo^{94}$	136.572±0.070	93.935200±75	93.935024±52	93.934300±800 [8]	93.934330±270
$C_5C^{13}H_9N - Mo^{94}$	168.088±0.088	93.935003±90			
$C_7H_{11} - Mo^{95}$	159.271±0.030	94.936031±35			
$C_6H_7O - Mo^{95}$	122.920±0.040	94.935988±45	94.936015±15	—	94.935700±400
$C_7H_{12} - Mo^{96}$	160.462±0.022	95.935112±30			
$C_6H_8O - Mo^{96}$	122.995±0.070	95.935061±75	95.935173±44	95.935970±390 [8]	95.934900±430
$C_5C^{13}H_{11} - Mo^{96}$	184.721±0.023	95.935252±30			
$C_7H_{13} - Mo^{97}$	195.804±0.040	96.936782±45			
$C_6H_9O - Mo^{97}$	159.502±0.060	96.936696±65	96.936755±30	—	96.936470±500
$C_7H_{14} - Mo^{98}$	204.220±0.041	97.936508±45			
$C_6H_{10}O - Mo^{98}$	167.758±0.070	97.936581±75	97.936543±16	97.936100±400 [7]	97.936560±500
$C_6C^{13}H_{13} - Mo^{98}$	190.685±0.046	97.936572±50			
$C_7H_{15} - Mo^{100}$	217.721±0.031	99.939291±35	99.939291±35	99.938600±400 [9]	99.938280±500
$C_7H_{12} - Ru^{96}$	186.574±0.062	95.937870±64			
$C_6H_8O - Ru^{96}$	150.217±0.124	95.937839±125	95.937865±15	—	95.937920±500
$C_6H_{10}N - Ru^{96}$	173.998±0.094	95.937860±95			
$C_7H_{14} - Ru^{98}$	204.751±0.301	97.935077±301			
$C_6H_{10}O - Ru^{98}$	168.659±0.422	97.935681±422			
$C_6H_{12}N - Ru^{98}$	192.071±0.402	97.936080±402	97.935871±60	—	97.937130±650
$C_8H_2 - Ru^{98}$	111.041±0.220	97.935803±220			
$C_7H_{15} - Ru^{99}$	211.593±0.165	98.937277±165			
$C_8H_{11}O - Ru^{99}$	175.413±0.068	98.937069±70	98.937100±50	—	98.938200±900
$^1/_2$ $Hg^{198} - Ru^{99}$	77.765±0.302	98.937091±302			
$C_7H_{16} - Ru^{100}$	220.964±0.094	99.936048±95			
$C_6H_{14}N - Ru^{100}$	208.264±0.234	99.936171±234			
$C_8H_4 - Ru^{100}$	127.275±0.258	99.935853±258	99.935932±74	—	—
$^1/_2$ $Hg^{200} - Ru^{100}$	80.298±0.129	99.935658±130			
$C_8H_5 - Ru^{101}$	134.076±0.104	100.937194±105			
$C_6H_{13}O - Ru^{101}$	191.356±0.150	100.937410±150	100.937271±44	—	—
$^1/_2$ $Hg^{202} - Ru^{101}$	80.182±0.088	100.937294±90			
$C_8H_6 - Ru^{102}$	142.973±0.070	101.936439±72	101.936439±72	101.935900±600 [10]	101.936410±500
$C_8H_4 - Ru^{104}$	157.576±0.082	103.938120±84	103.938132±23	103.938000±500 [10]	103.937800±700
$C_7H_6N - Ru^{104}$	144.939±0.167	103.938180±167			

*The mass values were recalculated for the auxiliary standard values H = 1.008142 ± 1, C = 12.003820 ± 5. The value of the error remains unchanged.

M = 93), cumene (C_9H_{12}, M = 120), and their fragments. In a number of cases, it was possible to use ions containing the carbon isotope C^{13} for the mass measurements.

The measured doublets, the zirconium isotope masses obtained from each individual doublet, and the mean values of the masses calculated with a "weight" for the measurements are listed in Table I.

4. Niobium. The niobium ions were obtained by evaporation of metallic niobium in a tungsten vessel and subsequent introduction of the vapor into the discharge arc of the ion source. We used aniline (C_6H_7N, M = 93) to measure the mass of Nb^{93}. The instrument dispersion was determined from the aniline fragments. The values of the doublets and the niobium mass are given in Table I.

5. Molybdenum. We used molybdenum chloride to obtain molybdenum ions. This compound is unstable and decomposes in air. We had to use it, however, since it was the only volatile molybdenum compound at our disposal. We determined the molybdenum isotope masses by checking the "internal consistency" of the measurements, i.e., the masses of the six molybenum isotopes were measured by comparison with organic compounds of different composition. We employed heptane (C_7H_{16}, M = 100), cyclohexane ($H_6H_{10}O$, M = 98), and their fragments.

The data on measurements of the isotope masses of molybdenum are shown in Table I.

6. Ruthenium. The ruthenium ions were obtained by evaporation in a tungsten vessel (M = 101, 102, and 104) and from ruthenium chloride. Owing to the fact that the melting point of ruthenium is high (~ 2000° C), only the most abundant isotopes (M = 101, 102, and 104) could be obtained from the evaporation in a tungsten crucible. The masses of these isotopes were measured with the aid of the organic compound sytrene (C_8H_8, M = 104). To obtain the less abundant ruthenium isotopes, we used ruthenium chloride and organic compound heptane (C_7H_{16}, M = 100). With heptane it is possible to obtain doublets for the masses 100, 99, 98, and 96; also, one may use the compound $C_6C^{13}H_{16}$ to obtain a doublet for the mass 101.

Admixtures of organic fragments containing C^{13}, and, consequently, producing the doublets $CH—C^{13}$ require a resolution of 45 000 for a mass of 100. Owing to the fact that the resolving power of the mass spectrograph was equal to 50 000 — 60 000, it was not necessary to correct for the C^{13}, since the doublet, for example, $C_7H_8—C_6C^{13}H_7$, is fully resolved. Hence there is no error associated with an unresolved admixture of C^{13} in a standard base.

Most of the measured isotopes were obtained from 2 — 4 different doublets (organic compounds of different composition). The masses of three ruthenium isotopes, Ru^{99}, Ru^{100}, and Ru^{101} were also measured by means of the doublets formed by doubly ionized ions of mercury, $\frac{1}{2}Hg^{198}$, $\frac{1}{2}Hg^{200}$, and $\frac{1}{2}Hg^{202}$, respectively. In this case, as well as in the case in which organic compounds were used to obtain the doublet, the base was computed from fragments of organic compounds with a difference of one unit mass (H^1).

The relatively good agreement of the results makes it possible to state that the measurements are "internally" consistent, i.e., there are no systematic errors within the limits of the experimental accuracy. The errors in the values of the doublets were calculated in the standard way as the weighted mean square error. The mean value of the error over the entire range of measured masses is $\approx 30\ \mu m$, which corresponds to a relative accuracy of $\Delta M/M \approx 3 \times 10^{-7}$.

For the determination of 25 isotope masses we measured 60 doublets. Moreover, we made a qualitative check of the measurements by measuring the doublets $CH—C^{13}$, $CH_2—N$, $CH_4—O$, and $OH_8—C_2$ for masses of 92 to 104. The results of the measurements of these doublets are shown in Table II. Comparison of the mean values of these mass differences with similar differences measured for masses 13, 14, and 16[11,12] show that the data are in fully satisfactory agreement. This con-

Table II

Mass		Value of doublet, mmu				
		$CH—C^{13}$	$CH_2—N$	$NH_2—O$	$CH_4—O$	$C_2—OH_4$
$_{38}Sr$	84					57.557±0.050
	86					57.504±0.029
	87				36.427±0.017	
$_{40}Zr$	90	4.459±0.035	12.565±0.054			
	91		12.558±0.042			
	92	4.466±0.012	12.533±0.035			
	94	4.466±0.073			36.434±0.061	
$_{42}Mo$	92	4.517±0.032				
	94	4.519±0.100			36.428±0.140	
	95				36.355±0.060	
	96	4.528±0.013			36.337±0.075	
	97				36.348±0.047	
	98	4.463±0.031			36.461±0.080	
$_{44}Ru$	96		12.613±0.046	23.876±0.168	36.354±0.111	
	98		12.598±0.031	23.723±0.043	36.430±0.315	
	99				36.320±0.092	
	100		12.578±0.070			
	104		12.551±0.068			
Mean with "weight"		4.488±0.008	12.572±0.007	23.762±0.068	36.414±0.022	57.517±0.019
Data from ref. 11, 12		4.471±0.003	12.578±0.004	23.808±0.008	36.388±0.004	57.496±0.006*

*Calculated.

Table III

Isotope	Z	N	Isotope mass, amu	Binding energy, Mev	B_n, Mev	B_p, Mev	P_n, Mev	P_p, Mev
Rb^{84}		47	83.941090±25	728.583	—	—	—	—
Rb^{85}		48	84.940175±165	737.801	9.218	—	—	—
Rb^{86}		49	85.938387±25	747.832	10.031	—	—	—
Rb^{87}		50	86.936522±170	757.935	10.103	—	—	—
Rb^{88}	37	51	87.939034±80	763.962	6.253	—	0.072	—
Rb^{89}		52	88.939887±115	771.535	7.573	—	—	—
Rb^{90}		53	89.942510±340	777.458±0.316	5.923	—	1.320	—
Rb^{91}		54	90.943120	785.257	7.799	—	—	—
Sr^{84}*		46	83.940070±17	728.748	—	—	—	—
Sr^{85}		47	84.940428±400	736.780±0.372	8.033	8.197	—	—
Sr^{86}*		48	85.936497±23	748.807	12.027	11.006	3.994	—
Sr^{87}*		49	86.936472±42	757.197	8.390	9.365	—	—
Sr^{88}*	38	50	87.933454±16	768.373	11.176	10.603	2.786	—
Sr^{89}		51	88.935717±20	774.632	6.259	10.670	—	—
Sr^{90}		52	89.936410±100	782.354	7.721	10.819	1.462	—
Sr^{91}		53	90.939053±20	788.259	5.905	10.801	—	—
Sr^{92}		54	91.940232±80	795.527	7.268	10.270	1.363	—
Y^{86}		47	85.942947±65	742.016	—	5.236	—	—
Y^{87}		48	86.938490±220	754.533±0.205	12.516	5.726	—	—
Y^{88}		49	87.937400±300	763.914±0.280	9.381	6.717	—	—
Y^{89}*		50	88.934147±15	775.310	11.395	6.936	2.014	—
Y^{90}	39	51	89.935840±100	782.099	6.790	7.467	—	—
Y^{91}		52	90.936193±12	790.137	8.038	7.783	1.248	—
Y^{92}		53	91.938172±65	796.661	6.524	8.402	—	—
Y^{93}		54	92.939586±280	803.710±0.260	7.050	8.183	0.526	—
Y^{94}		55	93.941896±320	809.926±0.298	6.215	—	—	—
Zr^{87}		47	86.942250±260	750.247±0.242	—	8.230	—	2.994
Zr^{88}		48	87.937835±300	762.724±0.280	12.477	8.191	—	2.465
Zr^{89}		49	88.937136±150	771.741	9.017	7.827	—	1.110
Zr^{90}*		50	89.933271±20	783.706	11.965	8.397	2.948	1.461
Zr^{91}*		51	90.934543±10	790.888	7.182	8.789	—	1.322
Zr^{92}*		52	91.934322±22	799.460	8.572	9.324	1.390	1.540
Zr^{93}	40	53	92.936266±120	806.017	6.556	9.356	—	0.954
Zr^{94}*		54	93.936126±25	814.514	8.497	10.803	1.941	2.620
Zr^{95}		55	94.939208±25	820.010	5.496	10.084	—	—
Zr^{96}*		56	95.938868±46	828.690	8.680	—	3.184	—
Zr^{97}		57	96.940635±70	835.414	6.724	—	—	—
Nb^{89}		48	88.941286±200	767.092	—	4.368	—	—
Nb^{90}		49	89.939891	776.757	9.665	5.016	—	—
Nb^{91}		50	90.936063±50	788.688	11.931	4.982	2.266	—
Nb^{92}		51	91.936046±50	797.070	8.382	6.182	—	—
Nb^{93}*	41	52	92.935862±25	805.608	8.538	6.147	0.156	—
Nb^{94}		53	93.937182±80	812.745	7.137	6.728	—	—
Nb^{95}		54	94.937008±20	821.274	8.528	6.760	1.391	—
Nb^{96}		55	95.938523±50	828.229	6.956	8.219	—	—
Nb^{97}		56	96.938795±60	836.342	8.113	7.652	1.157	—
Mo^{90}		48	89.942611	773.440	—	6.348	—	1.980
Mo^{91}		49	90.940813±200	783.480	10.041	6.723	—	1.707
Mo^{92}*		50	91.936098±42	796.237	12.757	7.549	2.716	2.567
Mo^{93}		51	92.936520±100	804.210	7.973	7.140	—	0.958
Mo^{94}*		52	93.935024±52	813.970	9.759	8.362	1.786	2.215
Mo^{95}*		53	94.936015±15	821.413	7.443	8.668	—	1.940
Mo^{96}*	42	54	95.935173±44	830.564	9.150	9.290	1.707	2.530
Mo^{97}*		55	96.936755±30	837.457	6.893	9.228	—	1.009
Mo^{98}*		56	97.936543±16	846.021	8.564	9.678	1.671	2.026
Mo^{99}		57	98.938884±55	852.207	6.186	—	—	—
Mo^{100}*		58	99.939291±35	860.194	7.987	—	1.801	—
Mo^{101}		59	100.942031±80	866.010	5.815	—	—	—
Tc^{94}		51	93.939601±130	808.923	—	4.713	—	—
Tc^{95}		52	94.938000±150	818.780	9.857	4.810	0.097	—
Tc^{96}		53	95.938333±325	826.836±0.303	8.056	5.423	—	—
Tc^{97}		54	96.936800	836.630	9.794	6.066	1.738	—
Tc^{98}		55	97.937691±85	844.167	7.537	6.710	—	—
Tc^{99}	43	56	98.937414±50	852.791	8.624	6.770	1.087	—
Tc^{100}		57	99.938812±250	859.856±0.233	7.065	7.648	—	—
Tc^{101}		58	100.939021±60	868.027	8.172	7.833	1.107	—
Tc^{102}		59	101.940719±350	874.812±0.325	6.785	8.803	—	—
Ru^{95}		51	94.940570±300	815.602±0.280	—	6.679	—	1.966
Ru^{96}*		52	95.937865±15	826.487	10.885	7.707	—	2.897
Ru^{97}		53	96.937238	835.437	8.950	8.601	—	3.178
Ru^{98}*		54	97.935871±60	845.076	9.639	8.446	0.689	2.389
Ru^{99}*		55	98.937100±50	852.298	7.222	8.132	—	1.422
Ru^{100}*	44	56	99.935932±74	861.752	9.454	8.961	2.232	2.191
Ru^{101}*		57	100.937271±44	868.872	7.120	9.016	—	1.368
Ru^{102}*		58	101.936439±72	878.013	9.141	9.986	2.021	2.153
Ru^{103}		59	102.937921	884.999	6.986	10.187	—	1.384
Ru^{104}*		60	103.938132±23	893.169	8.170	—	1.184	—
Rh^{98}		53	97.940531±180	839.952	—	4.515	—	—
Rh^{99}		54	98.939330±70	849.437	9.485	4.361	—	—
Rh^{100}	45	55	99.939700±250	857.459±0.233	8.022	5.160	—	—
Rh^{101}		56	100.939188±350	866.302±0.325	8.845	4.550	0.821	—
Rh^{102}		57	101.938560±300	875.253±0.280	8.951	6.381	—	—
Rh^{103}		58	102.937121	881.959	6.706	6.946	0.755	—
Rh^{104}		59	103.938320	892.266	7.250	7.210	—	—

*Isotopes measured in the present experiment.

clusion also applies to the calculated doublet OH_8-C_2.

As is seen from Table I, half of the isotope masses reported in the present article have not been measured with a mass spectroscope. The masses of the isotopes Ru^{100} and Ru^{101} were measured for the first time.

Comparison of the values of the masses obtained in the present experiment with the mass spectroscopic data and the data of Wapstra[5] (col-

umns 5 and 6 of Table I) indicates that there is no systematic deviation of one group of measurements with respect to the other. In most cases, the differences fall within the combined error of measurement. The exceptions are the isotopes Nb^{93}, Zr^{90}, and Zr^{92}. The best agreement occurs for the results of Isenor et al.[8] (1960). There is satisfactory agreement on the masses of molybdenum and ruthenium with the data of Duckworth et al., but the errors in the measured masses are large (0.4 — 0.8 mmu).[4,7,9,10]

BINDING ENERGY OF NUCLEONS IN THE NUCLEUS

The mass values of the nuclei obtained in the present experiment make it possible to determine with better accuracy the binding energy of nucleons in the nucleus, the binding energy of the last neutron and proton, and the pairing energy of neutrons and protons.

Besides measuring the masses of 25 stable isotopes of Sr, Y, Zr, Nb, Mo, and Ru, we calculated the masses and binding energies of 59 radioactive isotopes. The calculation was made by means of the Q values measured in nuclear reactions and α and β transitions.[13,14] The isotope masses measured in the present experiment served as reference values. The masses were calculated from all the data available in the sources already referred to. Wherever possible, we calulated the masses by several independent methods. The final value was obtained by averaging the results with a "weight" for the measurement. In all, 86 Q values were used. In six cases, the Q values were discarded as incompatible with the results of other reactions and mass-spectroscopic measurements.

From these data, we calculated the binding energies of the nuclei, the binding energies per nucleon (E/A), the binding energies of the last neutron B_n and of the last proton B_p, and the pairing energies of neutrons P_n and protons P_p. The results of the calculations are listed in Table III. Column 4 of this table gives the masses of the measured and calculated isotopes with the corresponding errors of measurement. Where the errors are not shown (eight cases), only the upper or lower limit of the Q value for the given reaction was known. The errors in the binding energies of the nuclei (column 5) are given only if they exceed 200 kev. The values of B_n and B_p, in most cases, have errors not exceeding 0.3 Mev. Correspondingly, errors in the values of P_n and P_p do not exceed 0.4 Mev. As auxiliary standards,

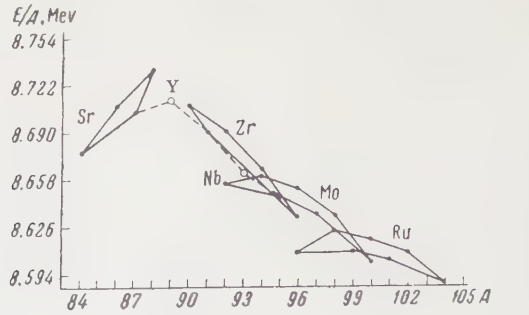

FIG. 1. Binding energy per nucleon in the range $84 \leq A \leq 104$.

we used the following masses:[11,12] $n_0 = 1.008985 \pm 1$; $H^1 = 1.008142 \pm 1$; $C^{12} = 12.003820 \pm 5$; $C^{13} = 13.007491 \pm 3$; $N^{14} = 14.007527 \pm 4$. For the conversion from atomic mass units to energy units, we used the relation: 1 amu = 931.145 ± 0.010 Mev. The symbols H, C, N, and O everywhere denote the isotopes occurring with greatest abundance, i.e., H^1, C^{12}, N^{14}, and O^{16}.

The binding energy per nucleon gives a general characteristic of the binding energy of nucleons in the nucleus. A graphical picture of the average binding energy per nucleon for stable nuclei in the region $84 \leq A \leq 104$ is shown as a function of A in Fig. 1. Binding energies of isotopes with the same Z are joined by solid lines. The binding energies of nuclei with odd Z (Y, Nb) are denoted by circles and are joined by broken lines to elements with odd A and even Z. The maximum errors in the values of E/A are 0.6 — 0.8 kev, i.e., they were too small to show in the figure (on the corresponding scale).

The mass region $84 \leq A \leq 104$ is of interest in connection with the fact that it includes the "magic" number N = 50. There should be a break in the curve of binding energy per nucleon in the region of the "magic" number. As seen in Fig. 1, a sharp break in the curve of binding energy per nucleon is observed at N = 50 for both even and odd Z (nuclei $_{38}Sr^{88}_{50}$, $_{39}Y^{89}_{50}$, and $_{40}Zr^{90}_{50}$). In this connection, it should be stressed that certain patterns of variation in the curve of binding energy per nucleon noted in previous studies[15,16] are observed in the nuclear range under consideration. Thus, in particular, there is a marked difference in the binding energies of the nucleons between nuclei with even and odd mass numbers. The curve of binding energy per nucleon for odd A and Z = const nowhere intersects the curve for even A.

A jump of about 3 — 3.5 Mev in the binding energy of the (N+1)th neutron after the neutron shells are filled (N = 50) is clearly observed. This is 30 — 40% (depending on the nucleus) of

Table IV

Isobar	Value and error, mmu	
	Geiger et. al.[17]	Present experiment
$_{42}Mo^{92}_{50} - {}_{40}Zr^{92}_{50}$	1.340±0.260	1.776±0.048
$_{40}Zr^{94}_{54} - {}_{42}Mo^{94}_{52}$	1.220±0.200	1.102±0.058
$_{40}Zr^{96}_{56} - {}_{42}Mo^{96}_{54}$	3.630±0.280	3.695±0.064
$_{44}Ru^{96}_{52} - {}_{42}Mo^{96}_{54}$	3.020±0.220	2.692±0.050
$_{40}Zr^{96}_{56} - {}_{44}Ru^{96}_{52}$	0.610±0.360	1.003±0.050
$_{42}Mo^{98}_{56} - {}_{44}Ru^{98}_{54}$	—	0.672±0.065
$_{42}Mo^{100}_{58} - {}_{44}Ru^{100}_{56}$	—	3.359±0.080

the value of the binding energy of the nearest even neutron. It is of interest to analyze the numerical data for the values of B_n, B_p, P_n, and P_p in this mass region. Over the entire range of measured and calculated masses, the average binding energy is 8.470 Mev for the last neutron and 7.670 Mev for the last proton. Consequently, the observation[15] that the binding energy of the last neutron is greater than the binding energy of the last proton is valid for this mass region, too. The average binding energy of the last neutron B_n is 8.480 Mev for even Z and 8.440 Mev for odd Z, i.e., equal within the limits of measurement error. The picture for the average binding energy of the last proton is quite different: B_p is equal to 8.960 Mev for even Z and 6.380 Mev for odd Z. As we see, the difference (~2.580 Mev) is far beyond the limits of experimental error.

The average pairing energy is $P_n = 1.580$ Mev for neutrons and $P_p = 1.930$ Mev for protons. Although the difference lies within the limits of experimental error, it is nevertheless seen that the average proton pairing energy is higher than the average neutron pairing energy.

The obtained experimental data permit one to calculate the mass difference for seven isobaric pairs. In Table IV, the resulting values of the mass differences are compared with those available in the literature. The binding energies of the isobars in which two protons are replaced by two neutrons are not always large, as was noted earlier.[16] In the region under study, the following two isobars are exceptions:

$$_{40}Zr^{96}_{56} - {}_{42}Mo^{96}_{54} \text{ and } {}_{42}Mo^{100}_{58} - {}_{44}Ru^{100}_{56}.$$

This result can be explained qualitatively by considering the parabolic curves of the binding energies of the isobars constructed for mass numbers A = 92, 94, 96, 98, and 100 (see Fig. 2). A group of parabolas corresponding to isobaric pairs is shown in the figure. The value of the symmetric

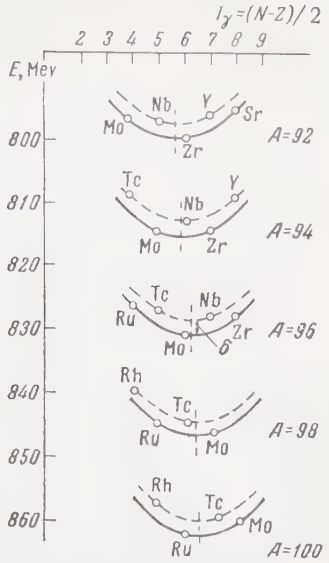

FIG. 2. Binding energy of nucleus as a function of the neutron excess T_γ.

term T_γ is laid off along the abscissa axis and the value of the binding energy of the nucleus in Mev is laid off along the ordinate axis.

In addition to the parabolas for even-even nuclei (solid lines), we constructed parabolas corresponding to radioactive odd-odd nuclei (dotted lines). For the construction of the parabolas, we used the experimental data for the binding energies of nuclei measured in the present work. Moreover, we used an expression for the calculation of the symmetry energy $T_\gamma = (N-Z)/2$ in the semiempirical formula for the binding energy[18] at

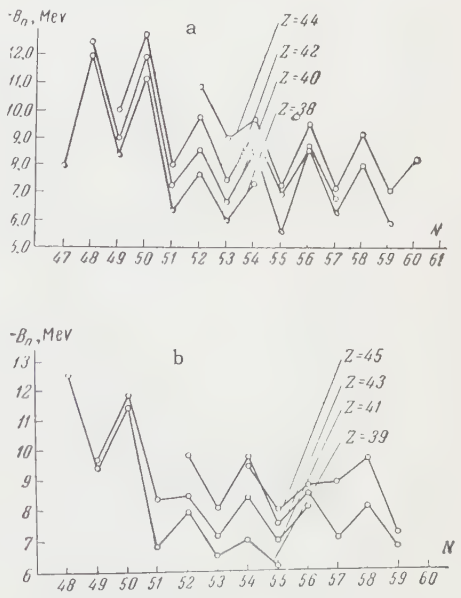

FIG. 3. Binding energy of the last neutron as a function of the number of neutrons N: a – for even Z; b – for odd Z.

Table V

Isotope	$A=92$; $T_{\gamma\,min}=5.71$					$A=94$; $T_{\gamma\,min}=5.88$				
	Sr	Y	Zr	Nb	Mo	Y	Zr	Nb	Mo	Tc
T_γ	8	7	6	5	4	8	7	6	5	4
E, Mev	795,7	796.7	799.5	797.1	796,2	809.9	814.5	812.7	814.0	808.9

Isotope	$A=96$; $T_{\gamma\,min}=6.08$					$A=98$; $T_{\gamma\,min}=6.36$				$A=100$; $T_{\gamma\,min}=6.50$			
	Zr	Nb	Mo	Tc	Ru	Mo	Tc	Ru	Rh	Mo	Tc	Ru	Rh
T_γ	8	7	6	5	4	7	6	5	4	8	7	6	5
E, Mev	828.7	828.2	830.6	826.8	826.5	846.0	844.2	845.1	840.0	860.2	859,9	861.8	875.5

which the binding energy is at a minimum for a given mass number A. Following reference 18, we use the expression

$$T_{\gamma min}=\frac{U_c(A-1)\,A^{-1/3}-1/4\,(M_nc^2-M_pc^2)}{2\,(U_\tau A^{-1}+U_cA^{-1/2})},$$

to obtain the value of T_γ for the isobar. The values of the binding energies T_γ and $T_{\gamma min}$ are listed in Table V. The values of the parameters $U_c = 0.177$ Mev and $U_\tau = 23.7$ Mev were taken from reference 19. As is seen from Fig. 2, the position of the isobaric pairs relative to the vertex of the parabola (T_γ = min) changes with A. Thus, for example, molybdenum shifts from the left branch of the parabola (A = 92; excess of protons with respect to neutrons) through the center of the parabola (A = 96) to the right branch (A = 100; excess of neutrons with respect to protons). Similar variations occur for zirconium and ruthenium.

All comparisons of isobaric pairs made in earlier studies[15,16] were based on the left branch of the parabolas, since in the region of heavier masses ($A \approx 200$) there are no stable isotopes corresponding to the right branch of a similar parabola, owing to the instability of the nuclei as regards β decay.

From an analysis of Fig. 2, it is readily seen that there is a difference δ equal to the difference in the binding energy for even-even and odd-odd nuclei. The mean value of $\frac{1}{2}\delta$ for this mass region (A = 92 — 100) is 1.05 Mev. This value is in very good agreement with the value of the term taking into account the pairing effect in the semiempirical formula for the nuclear binding energy. This term, according to reference 19, is expressed in the form: $C_{pair}A^{-3/4}\,\delta$, where C_{pair} = 34 Mev and $\delta = +1$ or -1, depending on the parity of the nucleus. The mean value of this expression for the given mass region is 1.11 Mev. The difference between the experimental and theoretical values is equal to 0.06 Mev, which lies within the limits of experimental error.

Figure 3 shows the values of B_n as functions of N for Z = const for even and odd Z. As seen from Fig. 3, the value of B_n is a maximum at N = 48, and not at N = 50. The difference is rather considerable (~ 1.0 mmu) and exceeds the measurement error. Nuclei with N = 50 have somewhat smaller values of B_n, but these values are significantly larger than any even or odd number of neutrons for N > 50. There is good agreement with the parity rule: the binding energy of

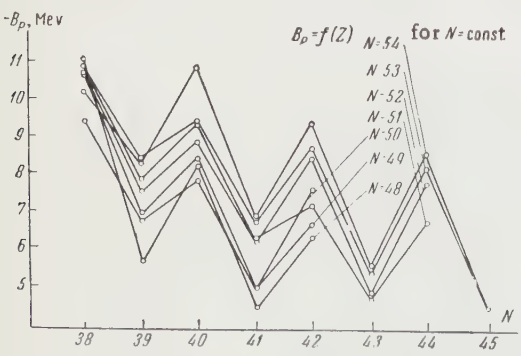

FIG. 4. Binding energy of the last proton as a function of the number of protons Z (N = const).

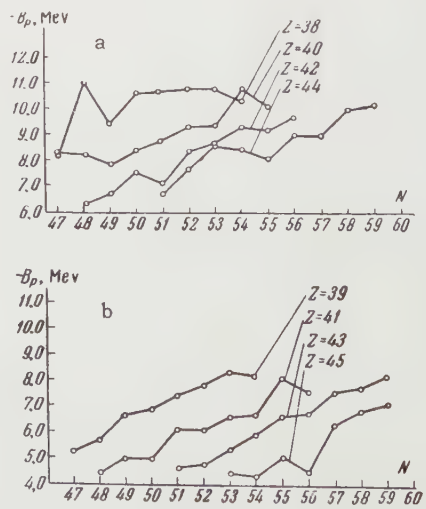

FIG. 5. Binding energy of the last proton as a function of the number of neutrons N: a — for even Z; b — for odd Z.

the last neutron is always greater for nuclei with even N than for neighboring nuclei with odd N. With an increase in the number of neutrons in the nucleus, the values of B_n decrease for both even and odd Z. The values of B_n increase with Z.

Figure 4 gives the dependence of the binding energy of the last proton on the number of protons for N = const. In this case, too, the parity rule is strictly fulfilled. The character of the curves shows no change whatsoever as a function of the number of neutrons. There are no visible changes as one goes from the region with unfilled neutron shells (N = 48, 49) to the region of filled shells (N = 51, 52). Figure 5 shows the dependence of B_p on the number of neutrons for Z = const. There is a visible monotonic decrease in B_p (for both even and odd N) with an increase in Z. The values of $B_p(N)$ for even and odd Z increase with the number of neutrons. This increase, however, is not always monotonic (Z = 42, 44).

The neutron pairing energies for the "magic" number N = 50 have a maximum for Z = 39, 41, and 42. At the same time, the value of P_n for N = 48 attains values higher than the maximum for N = 50.

In some nuclei with N = 50 ($_{40}Zr^{90}_{50}$, $_{41}Nb^{91}_{50}$, $_{42}Mo^{92}_{50}$), the values of B_n and P_n are the maximum values as compared to nuclei which do not have a "magic" number of neutrons. It is of interest to note, however, that nuclei with 48 neutrons have anomalously high values of B_n and P_n ($_{38}Sr^{86}_{48}$, $_{39}Y^{87}_{48}$, $_{40}Zr^{88}_{48}$), higher than for nuclei with the magic number of neutrons N = 50.

The proton pairing energies, in the great majority of cases, are greater in the case of even-even nuclei, but there are two exceptions ($_{40}Zr^{87}_{47}$ and $_{44}Ru^{97}_{53}$). It is possible that these exceptions are connected with the fact that the calculation of the proton pairing energy for even-odd nuclei is not entirely valid, since in this case, owing to the presence of an odd nucleon of a different type in the nucleus, a so-called residual np interaction occurs. It is not appropriate to identify this interaction with pairing energy.[20]

Analysis of the data in Table III and Figs. 3, 4, and 5 for the binding energies of the last neutron and proton and the values of the pairing energies makes it possible to state that there are no appreciable changes of these parameters for Z = 40. Consequently, the suggested existence of a "subshell" or "semi-magic" number at Z = 40 is not confirmed by the experimental data. A similar conclusion was already made in a number of papers of a statistical character.[20,21]

In conclusion, the authors consider it their obligation to express their gratitude to E. E. Baroni and V. M. Soĭfer for the preparation of the chloride compounds of a number of elements used in the present work and to G. A. Dorokhova for aid in the work.

[1] E. Segrè, Experimental Nuclear Physics, John Wiley and Sons, 1953, Chap. 5.

[2] V. A. Kravstov, JETP **30**, 408 (1956), Soviet Phys. JETP **3**, 297 (1956).

[3] A. V. Savich, JETP **30**, 501 (1956), Soviet Phys. JETP **3**, 400 (1956).

[4] Duckworth, Kegley, Olson, and Stanford, Phys. Rev. **83**, 1114 (1951).

[5] A. H. Wapstra, Physica **21**, 385 (1955).

[6] Collins, Johnson, and Nier, Phys. Rev. **94**, 398 (1954).

[7] H. E. Duckworth and R. S. Preston, Phys. Rev. **82**, 468 (1951).

[8] Isenor, Barber, and Duckworth, Can. J. Phys. **38**, 819 (1960).

[9] Duckworth, Preston, and Woodcock, Phys. Rev. **79**, 188 (1950).

[10] B. G. Hogg and H. E. Duckworth, Can. J. Phys. **30**, 637 (1952).

[11] Demirkhanov, Gutkin, Dorokhov, and Rudenko, Атомная энергия (Atomic Energy) **1**, 21 (1956).

[12] Demirkhanov, Gutkin, and Dorokhov, ibid. **2**, 544 (1957).

[13] R. W. King, Revs. Modern Phys. **26**, 327 (1954); D. M. Van Patter and W. Whaling, ibid. **26**, 402 (1954).

[14] D. M. Van Patter and W. Whaling, Revs. Modern Phys. **29**, 757 (1957); H. E. Duckworth, ibid. **29**, 767 (1957); L. J. Lidofski, ibid. **29**, 773 (1957).

[15] Demirkhanov, Gutkin, and Dorokhov, JETP **35**, 917 (1958), Soviet Phys. JETP **8**, 639 (1959).

[16] Demirkhanov, Gutkin, and Dorokhov, JETP **37**, 1217 (1959), Soviet Phys. JETP **10**, 866 (1960).

[17] Geiger, Hogg, Duckworth, and Dewdney, Phys. Rev. **89**, 621 (1953).

[18] J. M. Blatt and V. F. Weisskopf, Theoretical Nuclear Physics, John Wiley and Sons, 1953.

[19] A. Moszkowski, In collection: Строение атомного ядра (Structure of the Atomic Nucleus), IIL, 1959, p. 471).

[20] V. A. Kravtsov, JETP **36**, 1224 (1959), Soviet Phys. **9**, 871 (1959).

[21] N. Zeldes, Nuclear Phys. **7**, 27 (1958).

Translated by E. Marquit
271

THERMAL CONDUCTIVITY AND DIFFUSION IN WEAK He^3—He^4 *SOLUTIONS IN THE TEMPERATURE RANGE FROM THE* λ *POINT TO 0.6°K*

T. P. PTUKHA

Institute for Physics Problems, Academy of Sciences, U.S.S.R.

Submitted to JETP editor December 29, 1960

J. Exptl. Theoret. Phys. (U.S.S.R.) **40**, 1583-1593 (June, 1961)

Using a thermal flow method, measurements have been made of the effective thermal conductivity coefficient κ_{eff} for He^3-He^4 solutions over a range in He^3 molar concentration from 10^{-4} to 10^{-2}. The thermal conductivity coefficients κ and diffusion coefficients D have been derived from these values of κ_{eff}. The thermal conductivity coefficient increases as the temperature is decreased; for any given temperature, κ becomes smaller as the solution concentration increases. Various quantities characterizing the interaction of the impurity and thermal excitations have been computed on the basis of the data obtained. The results are found to be in satisfactory agreement with the Khalatnikov-Zharkov theory.

Landau and Pomeranchuk have shown[1] that impurities (He^3 atoms) dissolved in liquid helium below the λ point do not take part in superfluid motion, but enter into the normal component of the solution. For weak solutions, in which the interaction of the impurity particles with one another is negligibly small, the solution can be treated as a mixture of three gases of elementary excitations: a roton gas, a phonon gas, and a gas of impurity excitations. The thermal (rotons and phonons) and impurity excitations, which transfer energy and momentum upon colliding with one another, are responsible for the kinetic processes in the solution.

In the present work a thermal flow method was used to investigate the phenomena of diffusion and thermal conductivity in weak He^3-He^4 isotopic mixtures. From the results of experiments to study these processes one can compute certain quantities characterizing the interaction and scattering laws for the impurity and thermal excitations.

The processes of heat transfer and diffusion of He^3 in He^4 below the λ point may be represented in the following form: at the initial moment, when the heat flux is zero, the impurities have a uniform distribution throughout the thermal excitation gas; the partial pressures of the impurity and thermal excitation gases are everywhere the same. When power is applied to the heater, the thermal and impurity excitations will move to the cold end of the reservoir. The heat carried by them is

$$\mathbf{q} = \rho\sigma T\mathbf{v}_n, \tag{1}$$

where ρ is the density and σ the entropy per unit mass of the mixture, and $\mathbf{v}_n$ is the velocity of the normal component of the liquid. As a result of this process there is developed a concentration gradient ∇c. In the steady-state condition it is necessary that the osmotic pressure arising as a result of the presence of a concentration gradient be balanced by the thermomechanical pressure (thermo-osmosis):

$$(kT/m_3)\nabla c = -\sigma_0\nabla T, \tag{2}$$

where m_3 is the mass of the He^3 atom, σ_0 is the entropy per unit mass of pure He^4, k is the Boltzmann constant, and $c = N_3m_3/(N_3m_3 + N_4m_4)$ is the concentration (m_4 is the mass of the He^4 atom; N_3 and N_4 are the numbers of He^3 and He^4 atoms per unit volume); for weak mixtures, $c = N_3m_3/N_4m_4 = \epsilon m_3/m_4$, where ϵ is the molar concentration.

The phenomenon of thermo-osmosis has been observed experimentally. The most complete quantitative measurements have been made by Wansink and Taconis.[2]

Thus, in the presence of a thermal current there appear in the reservoir that contains the mixture a concentration gradient ∇c directed from the cold to the warm end, and a temperature gradient ∇T in the opposite direction, which give rise to inverse processes — diffusion of the impurities and of the thermal excitations. The additional thermal flow arising from the transfer of heat by the diffu-

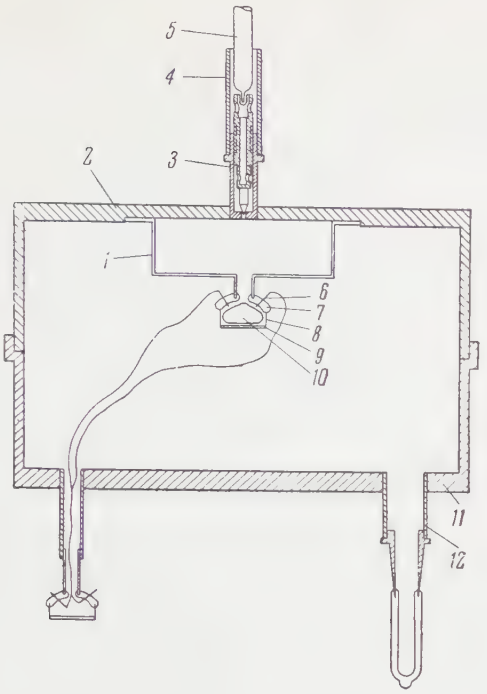

FIG. 1. Diagram of apparatus for thermal conductivity and diffusion measurements in He^3-He^4 solutions.

sion of the thermal excitations is characterized by a thermal conductivity coefficient κ.

A theory of diffusion and thermal conductivity for weak He^3-He^4 solutions has been developed by Khalatnikov and Zharkov.[3] In the general case, the total heat flux **Q** is related to the temperature gradient by the following expression:

$$\mathbf{Q} = -[(\rho D m_3 \sigma_0^2/kc)(\rho_n/\rho_{n0})^2 + \varkappa]\nabla T, \qquad (3)$$

where D is the impurity diffusion coefficient, and ρ_{n0} is the fraction of the solution normal component density (ρ_n) contributed by the rotons and phonons.

The proportionality coefficient between the heat flux **Q** and ∇T is the effective thermal conductivity coefficient of the mixture

$$\varkappa_{\text{eff}} = \frac{\rho D m_3 \sigma_0^2}{kc}\left(\frac{\rho_n}{\rho_{n0}}\right)^2 + \varkappa = \varkappa_M + \varkappa. \qquad (4)$$

In this expression, the first term, κ_M, characterizes the heat transfer due to motion of the elementary excitations as a whole (i.e., motion of the normal component of the solution), and the second term, κ, is associated with the heat flow arising, as in the case of ordinary condensed bodies, from diffusion of the thermal excitations (the thermal conduction process).

Under stationary conditions, it is the effective thermal conductivity coefficient κ_{eff} which is determined experimentally. Only in the limiting case

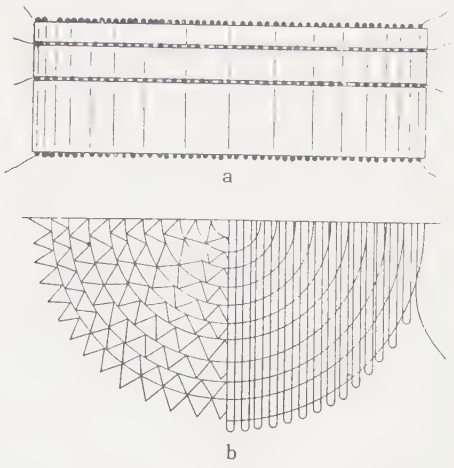

FIG. 2. Interior portion of apparatus: a – side view; b – top view.

$\kappa \gg \kappa_M$ is it possible to find separately the thermal conductivity coefficient κ, while under conditions for which $\kappa_M \gg \kappa$ the diffusion coefficient D can be determined.

METHOD OF MEASUREMENT

Several kinds of apparatus were tried out in the course of the present studies; two of these are represented in the results given here. Figure 1 illustrates the apparatus with which the preliminary experiments were conducted, and results obtained in the temperature region from the λ point to 1.5°K. In this case, low temperatures were attained by pumping He^4 vapor (a second system was used to produce ultra-low temperatures, with the aid of He^3).

The reservoir 1, in which the mixture under study was held (inside diameter 19.52 mm, height 6.57 mm), was turned from a single piece of stainless steel and had a wall thickness of 0.2 mm. In order to provide good thermal contact with the helium bath, the cover 2 of the reservoir was made of copper. To the cover was soldered a small valve 3, communicating with a tube 4 through which the mixture was introduced into the volume 1. The valve was operated within the Dewar by means of a Stay-bright rod 5; the latter could be decoupled from the valve and raised, in order to prevent heat conduction along it to the reservoir.

Four resistance thermometers were assembled for measuring the temperature gradient. The support for the thermometers consisted of three flat disks (shown in cross-section in Fig. 2a) consisting of smooth and corrugated ribbons coiled together. Parchment was used as the material for the ribbons; in addition to its poor thermal conduc-

tivity, this substance possesses another essential property — its linear dimensions change little with temperature. Inasmuch as the thickness of each disk determines the distance between thermometers, which must be accurately known, the preparation of the disks presented certain difficulties. However, since the disks were prepared in precision-made forms, their dimensions can be guaranteed to an accuracy of 0.01 mm. The thermometers were made of 35-micron phosphor bronze wire, laid out in a flat zig-zag pattern across the surfaces of the disks, and fixed in place with BF cement (Fig. 2b).

After preparation of the thermometers the maximum error in the value of Δx (the distance between thermometers) was found to be 0.05 mm.

Current and voltage leads for the electrical circuit were carried out of the reservoir by means of a platinum glass seal 7 with platinum wires 6 bonded into the glass. The seal terminated in a platinum ring 8 and was closed off by a copper plate 9. A glass block 10 ground to match its interior dimensions was placed within the seal, making its volume negligibly small (it amounted to 1% of the reservoir volume).

The heat flow in the mixture under study was generated by a plane constantan heater. To avoid convection, the heater was placed at the bottom of the reservoir.

The experimental volume 1 was surrounded by a vacuum jacket formed by the cover 2 in conjunction with a cylindrical copper vessel 11. The tube 12 served for evacuating the jacket.

The experiment was carried out in the following manner. With the aid of a Toepler pump a known quantity of the He^3-He^4 mixture was condensed into the reservoir 1 through a small charcoal trap cooled by liquid nitrogen. Condensation proceeded at a temperature somewhat below that of the λ point. When the necessary quantity of the mixture had been condensed, the valve 3 was immediately closed. Thus any danger of variation in the concentration in the liquid due to He^3 enrichment of the gaseous phase was completely avoided. Any surplus of the mixture above the valve was then pumped off with the Toepler pump; the presence of a vacuum in the tube 4 was regulated by a thermometer lamp. The inner helium bath was brought to the specified temperature, which could be maintained constant to an accuracy of 10^{-5} °K with the aid of the stabilizing apparatus developed by Vetchinkin.[4] Temperature measurements were then carried out for various thermal fluxes from the heater.

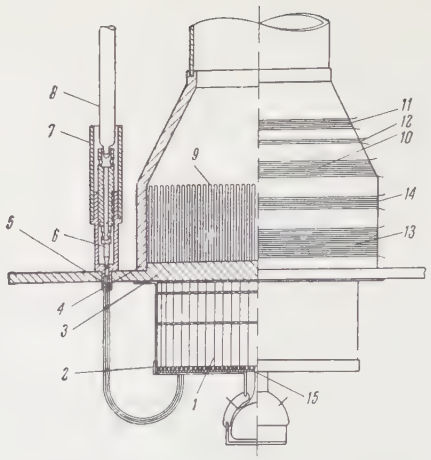

FIG. 3. Apparatus for ultra-low temperatures.

The magnitude of the thermal flux was determined from the known resistance of the heater and the current flowing through it. Since the reservoir 1 had thin stainless-steel walls, heat leakage along its walls was negligibly small, amounting to 0.5% of the total power supplied to the heater.

The thermometer resistances were measured with an ordinary potentiometer. For convenience in measuring the resistance, a high degree of stability in the currents (to 10^{-5} of their net value) in both the potentiometer and measuring circuits was insured by use of the weak-current stabilizer described by Vetchinkin.[5]

So far, we have described the apparatus used to obtain data in the temperature region from the λ point down to 1.15° K. Temperatures below 1.15° K were attained by pumping He^3 vapor. All experiments with He^3 were carried out in an ultra-low temperature cryogenic system constructed under the supervision of Peshkov.[6]

The apparatus employed for the measurements in this temperature range is illustrated schematically in Fig. 3. The chamber for the mixture to be studied was a thin-walled stainless steel reservoir having an inside diameter of 20 mm and a height of 6.67 mm. The copper cap 2 served as the bottom of the chamber. The reservoir was in contact with the He^3 bath 4 through the copper cover 3. The volume was filled with the mixture by means of the capillary 5 (of 0.4 mm i.d.), the valve 6, and the thin-walled tube 7. The rod 8 by which the valve was operated could be disengaged. Since liquid He^3 has extremely poor thermal conductivity, an additional copper latticework 9 was silver-soldered to the bottom of the copper-walled bath 4. This significantly improved the thermal contact between the warm lower and cooler upper layers of the liquid.

The temperature of the cold surface 3 was held constant with the aid of the electronic stabilizer mentioned above.[4] The phosphor bronze thermometer 10, the signals from which, amplified and transformed, were applied to the heater 11, served as a temperature sensing device. The thermometer 10 was incorporated into a bridge circuit; the ballast resistance 12, placed in helium, served as its other branch. This arrangement made it possible to maintain the temperature of the He^3 bath constant to an accuracy of 10^{-4}°K. The He^3 bath, together with the mixture reservoir, was surrounded by a vacuum jacket.

Four resistance thermometers of 35-micron phosphor bronze wire (such thermometers possess a linear characteristic from 2° K to 0.7° K) were prepared, in the manner described above (Fig. 2), for measurement of the temperature gradient in this apparatus. The thermometers were calibrated against the He^3 vapor pressure, which was measured with a MacLeod gauge. In addition, to provide standardization of the calibration curves, two resistance thermometers, made of 50-micron aluminum (13) and 53-micron cadmium wire (14) were wound onto the outside of the He^3 bath. The temperatures of the transitions of aluminum and cadmium into the superconducting state served as reference points.

The heat flow was generated by the heater 15.

In the work described here, measurements were carried out for solutions having three different concentrations. The purity of the He^3 used in preparation of the mixtures was determined mass-spectrometrically,* and was not less than 99.9995%. The relative error in concentration of a mixture was 1% for the lowest concentration and 0.5% for the higher ones.

Before passing on to a consideration of the results obtained with the systems thus described, it is necessary to explain why it was required that the interior volume of the reservoir containing the mixture be divided into the cells formed by coiling the corrugated ribbons into flat disks. In the initial experiments the thermometers were wound onto flat rings of ivory. The coils in each of them were strung through specially-cut notches in the rings in such a manner that they lay in one plane. Joined together, the rings formed a cylinder 18.2 mm in inside diameter. The thermal current was generated by a plane heater. The framework containing the thermometers and the heater was placed within the apparatus illustrated in Fig. 1, with the heater, to avoid convection, situated at the bottom of the reservoir 1. The experiment was carried out in the same fashion as that described above.

The results achieved in the measurements with thermometers of this construction were, briefly, as follows. With no power applied to the heater, no temperature differences were observed in the experimental volume. With heat flow present, a temperature gradient ∇T did appear, but this temperature distribution varied from experiment to experiment in such a way that for a given initial bath temperature and heat-flux the results varied by a factor of ten. The results of the measurements were so chaotic that it was difficult to distinguish any regularity in them, save only that a dependence of ∇T on power was observed; the greater the power supplied to the heater, the smaller the temperature difference as compared with that to be expected for the given heat-flux. The impression was formed that some sort of secondary convection currents were established in the reservoir, which led to a reduction in the concentration and temperature gradients. Inasmuch as for the solutions under investigation, below the λ point, the density falls with decreasing temperature[7] — i.e., the denser layers of the liquid were located further down in the reservoir — these could not be currents due to natural convection. To avoid these secondary convection currents, therefore, the volume of the reservoir was divided into cells, of average cross-section area 0.6 mm^2.

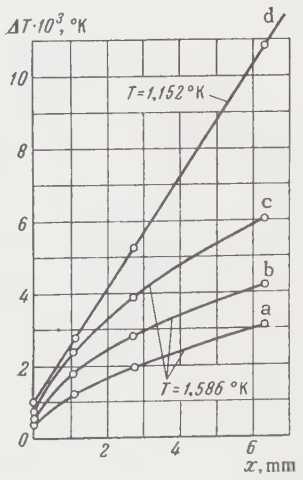

FIG. 4. Temperature distribution in reservoir for solutions of concentration $\varepsilon = 1.32 \times 10^{-3}$ of He^3 in He^4: a — for Q = 147.2; b — for Q = 212.1; c, d — for Q = 289.2 erg/cm^2 sec.

*The He^3 mass-spectrometer analysis was carried out in the laboratory of N. E. Alekseevskiĭ (Institute for Physics Problems, Academy of Sciences, U.S.S.R.).

$\varepsilon = 1.39 \cdot 10^{-4}$					$\varepsilon = 1.32 \cdot 10^{-3}$					$\varepsilon = 1.36 \cdot 10^{-2}$		
T, °K	$10^{-4}\,\varkappa_{eff}$, ergs/cm-sec-degree	$10^{-4}\,\varkappa$, ergs/cm-sec-degree	K(T), ergs/cm-sec-degree	10^4D, cm²/sec	T, °K	$10^{-4}\,\varkappa_{eff}$, ergs/cm-sec-degree	$10^{-4}\,\varkappa$, ergs/cm-sec-degree	K(T), ergs/cm-sec-degree	10^4D, cm²/sec	T, °K	$10^{-4}\,\varkappa_{eff}$, ergs/cm-sec-degree	$10^{-4}\,\varkappa$, ergs/cm-sec-degree
1.918	0.58	—	60	2.1	2.150	9.4	—	93	0.94	2.061	115	—
1.65	0.42	—	44	6.8	2.060	8.6	—	85	1.16	1.960	105	—
1.501	0.21	—	22	10.4	1.951	7.1	—	70	1.84	1.815	91	—
1.360	0.126	—	13	22.0	1.920	6.8	—	67	2.3	1.664	77	—
1.296	0.097	—	10.8	27.0	1.804	5.8	—	57	3.4	1.615	72	—
1.245	0.070	—	7.3	35.0	1.694	4.7	—	47	5.7	1.484	65	—
1.145	0.058	—	6.0	—	1.615	3.8	—	37	7.7	1.354	68	68
1.055	0.078	0.078	—	—	1.586	3.4	—	33	9.8	1.330	66	66
1.022	0.074	0.074	—	—	1.501	2.7	—	—	—	1.265	72	72
0.901	0.130	0.130	—	—	1.483	2.7	—	—	—	1.222	75	75
0.896	0.121	0.121	—	—	1.465	2.6	—	—	—	1.202	81	81
0.850	0.180	0.180	—	—	1.374	2.3	—	—	—	1.165	78	78
0.773	0.31	0.31	—	—	1.314	2.1	—	—	—	1.160	78	78
0.761	0.35	0.35	—	—	1.265	2.1	1.15	—	—	1.129	91	91
0.670	0.59	0.59	—	—	1.152	1.94	1.94	—	—	0.890	122	122
					1.141	1.87	1.87	—	—	0.794	145	145
					1.090	2.1	2.1	—	—	0.667	163	163
					1.073	2.4	2.4	—	—			
					0.948	4.2	4.2	—	—			
					0.826	7.9	7.9	—	—			
					0.773	9.8	9.8	—	—			
					0.662	14.7	14.7	—	—			
					0.607	17.7	17.7	—	—			

RESULTS OF THE MEASUREMENTS

Preliminary results of the present work have already been published.[8] In this article a more detailed treatment of these results will be carried out, and data obtained for a new mixture of concentration $\epsilon = 1.39 \times 10^{-4}$ He will also be presented.

As already mentioned, several thermometers were prepared for measurements of the temperature in the experimental volume. This made it possible to clarify the nature of the temperature distribution along the direction of the heat flow. At high temperatures, for which heat transport takes place principally through the motion of the normal component of the liquid ($\varkappa_M > \varkappa$), the temperature varies along the direction of the heat flow in accordance with the formula[3]

$$T - T_0 = \frac{c_0 dkT}{x_0 m_3 \mathfrak{s}_0} \frac{e^{-x/x_0} - 1}{1 - e^{d/x_0}}, \qquad x_0 = \frac{kTK(T)}{m_3 Q \mathfrak{s}_0}, \tag{5}$$

where d is the height, T_0 the temperature of the cold wall of the reservoir (at which x = 0), and K(T) is a function independent of concentration for which

$$\varkappa_M = K(T)/c. \tag{6}$$

Figure 4 shows several typical curves (a,b,c) obtained in this temperature region for various values of the power supplied to the heater (the y coordinate is the temperature difference ΔT indicated by the thermometers with and without the thermal current present, while the x coordinate is the distance of the thermometers from the cold wall). For comparison, curve d in the same figure shows the function $\Delta T(x)$ characteristic of the opposite limiting case, in which heat is transported chiefly by a mechanism analogous to ordinary thermal conductivity: for a power input the same as that for which curve c was obtained, a linear variation of ΔT with x is now observed.

For control purposes, several experiments with pure He^4 were carried out using each apparatus. In these cases no temperature gradient was observed when the power was turned on: the thermometers all indicated a uniform rise in the temperature of the helium within the reservoir. This temperature rise resulted from the Kapitza discontinuity at the boundary between the liquid helium and the reservoir cover. For a given thermal flux the difference between the final and initial (power-off) temperature of the helium in the reservoir increased as the bath temperature was lowered.

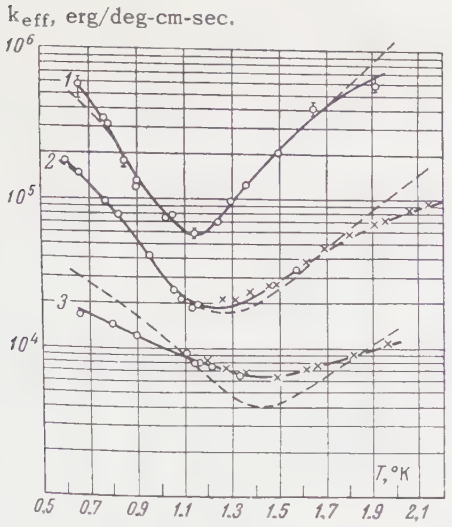

FIG. 5. Variation of the effective thermal conductivity of solutions of He^3 in He^4 with temperature and concentration: curves 1 – $\varepsilon = 1.39 \times 10^{-4}$; curves 2 – $\varepsilon = 1.32 \times 10^{-3}$; curves 3 – $\varepsilon = 1.36 \times 10^{-2}$; dashed curves are theoretical.

The time required for establishment of the steady-state condition never exceeded 10 — 12 minutes for any of the temperatures and concentrations employed in the experiments. For a given mixture concentration and thermal flux this time decreased as the initial temperature in the reservoir was lowered. Below 1° K, equilibrium was reached, practically speaking, in 1 — 2 min. For a given temperature, the equilibrium time also decreased with decreasing solution concentration.

Knowing the temperature gradient and thermal flux, one can obtain the effective solution thermal conductivity coefficient κ_{eff}. Values of κ_{eff} for various temperatures and concentrations are given in the table.*

The computations of κ_{eff} were carried out in the following manner: at high temperatures, for which, with power applied to the heater, the steady state temperature distribution along the x coordinate had an exponential form (for example, Fig. 4 a, b, c), use was made of Eq. (5). In this case, the experimentally-determined temperature differences and thermal fluxes were used to derive values of the function K(T), from which it was then possible to compute the value of κ_{eff} for each given solution concentration. The values of the function K(T) are given in the table.

For the case of a linear dependence of ΔT upon x (Fig. 4, d) the usual relation

$$Q = -\varkappa_{eff}\, \Delta T/d \qquad (7)$$

was employed.

*All data presented in the table are referred to the 1958 temperature scale.[9]

The variation of the effective thermal conductivity coefficient κ_{eff} with temperature is shown in Fig. 5. The values of κ_{eff} presented in the table and shown in the figure are averages of the values of κ_{eff} computed for various heater input powers. The coefficients κ_{eff} were independent of the magnitude of the thermal flux. The statistical scatter in the values of κ_{eff} computed for various powers at a given temperature did not exceed 10%.

For control, the measurements were performed using both types of apparatus described above and illustrated in Figs. 1 and 2. The results obtained from each (represented by the circles and crosses) agreed well with one another.

It is evident from Fig. 5 that the $\kappa_{eff}(T)$ curves possess a minimum which, as the solution concentration is reduced, shifts toward lower temperatures. This behavior in the curves confirms the hypothesis of the dual nature of heat transfer in a weak He^3-He^4 solution. Specifically, in the high temperature region lying to the right of the temperature of the minimum (T_{min}) the effective thermal conductivity coefficient κ_{eff} falls with decreasing temperature. This implies that in this region the predominant heat transport mechanism is that of motion of the normal component of the solution as a whole toward the cold end of the reservoir (i.e., the case $\kappa_M \gg \kappa$).

At temperatures to the left of T_{min}, the coefficient increases with decreasing temperature. This means that the further the temperature lies below T_{min}, the greater is the part played in the process of heat transfer from the heated to the cold end by a mechanism analogous to ordinary heat conduction (in which the thermal energy is transferred by the diffusion of thermal excitations), and, since the number of thermal excitations falls with decreasing temperature — i.e., their mean free path increases — the thermal conductivity coefficient and, in consequence, the effective thermal conductivity coefficient ($\kappa_{eff} = \kappa$) must grow (the case for which $\kappa \gg \kappa_M$).

In the vicinity of the minimum, clearly, both mechanisms make equal contributions to the heat transfer process in the solution ($\kappa_M \sim \kappa$).

Values of the thermal conductivity coefficient for the case $\kappa = \kappa_{eff}$ are given in the table. From comparison of the κ's obtained for various concentrations it is evident that at low temperatures the impurities cause a fundamental change in the magnitude of κ: for a given temperature the value of the coefficient κ becomes smaller as the He^3 concentration of the solution increases. At temperatures below 1.1° K the principal role in the

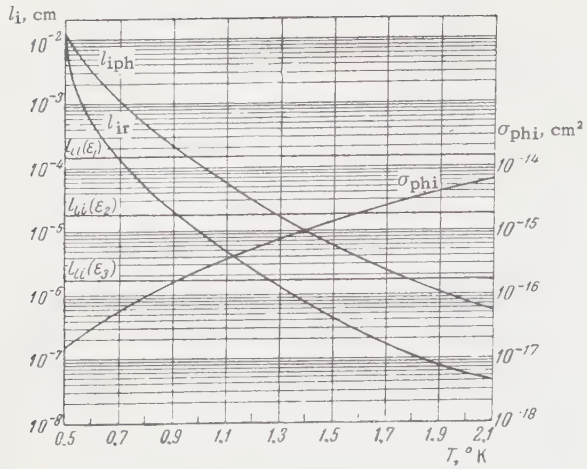

FIG. 6. Impurity mean free paths ($\varepsilon_1 = 1.39 \times 10^{-4}$; $\varepsilon_2 = 1.32 \times 10^{-3}$; $\varepsilon_3 = 1.36 \times 10^{-2}$). Cross section for scattering of phonons by impurities as a function of temperature.

heat conduction process is played by the scattering of phonons by impurities, which leads to a reduction in the phonon mean free path.

In the table are also given the values of the diffusion coefficients D, derived from the κ_{eff} in the alternative limiting case $\kappa_M \gg \kappa$. For the mixtures having He^3 concentrations ϵ equal to 1.32×10^{-3} and 1.39×10^{-4}, it was found possible to determine the coefficients D over the temperature interval from 2.15 down to 1.2° K. In this region diffusion is governed by the scattering of impurities by rotons, and here the diffusion coefficient increases exponentially with decreasing temperature. Inasmuch as the values of the coefficient D obtained for solutions of differing concentration agree well with one another, one may conclude that for weak solutions the diffusion coefficients are independent of concentration. The absolute values of D are in good agreement with the data of Beenakker et al.[10] as well as with the results of Garvin and Reich,[11] who used a spin-echo method for determination of D.

The results of these experiments on the processes of heat conduction and diffusion permit the calculation of several quantities characterizing the interaction and scattering laws for elementary excitations. The following values were used here for the parameters of the roton energy spectrum: $\Delta_r/k = 8.65°$ K, $p_0/\hbar = 1.92 \times 10^8$ cm^{-1}, and $\mu_r = 1.08 \times 10^{-24}$ g.

The value $\mu = 8.5\ m_1$ (m_1 is the mass of the proton) was used for the effective mass of an impurity. The cross section σ_{ir} for scattering of impurities by rotons was calculated. The characteristic time for impurity-roton scattering, required for this purpose, was computed from the experimental value of κ_{eff}, taken at T = 1.5° K for a mixture of concentration $\epsilon = 1.39 \times 10^{-4}$. The absolute value of σ_{ir} is 2.2×10^{-14} cm^2.

According to the theory of Khalatnikov and Zharkov[3] the thermal conductivity coefficient κ is made up of roton, phonon and impurity components: $\kappa = \kappa_r + \kappa_{ph} + \kappa_i$. For the solutions used in these experiments below 1.1° K, the phonon component of the thermal conductivity is much greater than the sum of the roton and impurity components of κ. From the values of the thermal conductivity coefficient κ in this temperature region one can compute the effective cross section $\sigma_{ph\,i}$ for scattering of a phonon by an impurity. In the present work the value

$$\sigma_{phi} = 2.7 \cdot 10^{-17}\, \delta T^5 \text{ cm}^2$$

is obtained for $\sigma_{ph\,i}$, where δ is a certain function of the parameters characterizing the impurity energy spectrum which, as follows from reference 3, has the form $\delta = A + B/T$. Inasmuch as the function $\partial\Delta_i/\partial\rho$ (Δ_i is the zero-point energy of an impurity excitation) was not known, Khalatnikov and Zharkov[3] assumed δ to be of order unity. For the function δ, however, as determined from the experimental values obtained in the present work for the phonon contribution to the thermal conductivity, it is necessary to have $\delta = 10/T$ ($A \ll B$).

An article has just appeared, by Staas, Taconis and Fokkens,[12] in which data are presented on the viscosity of solutions. They have found for a certain quantity $\bar{\delta}$ the value 1.86. As follows from Zharkov's theory of viscosity,[13] $\bar{\delta}$ is a function of the temperature and of the parameters determining the impurity energy spectrum. Since, however, the dependence of Δ_i upon ρ was unknown, it was assumed in this theory that $\bar{\delta} = 1$. It was pointed out in reference 13 that the δ in the thermal conductivity theory should differ slightly from the $\bar{\delta}$ appearing in the viscosity theory. It is difficult, however, to make a comparison of these quantities, as calculated from the experimental data on viscosity and thermal conductivity, since in the paper by Staas, et al.[12] it is not stated at what temperatures $\bar{\delta}$ was determined, nor what values were assumed for the theoretical parameters.

The temperature dependence of the phonon-impurity scattering cross section under the condition $\delta = 10/T$ is shown graphically in Fig. 6. Using this expression for δ, we obtain for the derivative $\partial\Delta_i/\partial\rho$

$$\partial\Delta_i/\partial\rho = 4.6\, k/\rho$$

(k is the Boltzmann constant).

Using the cross section σ_{iph} obtained from the experimental results and the value $\delta = 10/T$, and making use of the relations (6.7) and (7.9) of Khalatnikov and Zharkov's paper,[3] one may compute theoretical curves for the temperature dependence of the effective solution thermal conductivity. These curves are shown dashed in Fig. 5 over the regions where they deviate from the experimental curves. It is evident from Fig. 5 that for curves 1 and 2 the experimental and theoretical values agree well, within their limits of accuracy, except in the temperature range above 1.7°K. Above 1.7°K the curves begin to diverge. It should be remarked that the theory developed in reference 3 is correct only for the case in which the rotons constitute an ideal gas. At temperatures above 1.7°K it is possible to make only a qualitative comparison with the theory. A greater divergence between the experimental and theoretical values is found for the mixture of concentration $\epsilon = 1.36 \times 10^{-2}$ He^3. The experimental curve has a less pronounced minimum than would be expected, and deviates from the theoretical curve over the whole temperature range (except at the points of intersection). This solution can evidently no longer be regarded as a weak one.

The impurity mean free paths were calculated from the cross sections for the scattering of the impurities by phonons and rotons obtained from the experimental data. The temperature dependence of the mean free paths for collisions of impurities with rotons (l_{ir}) and with phonons (l_{iph}) is shown in Fig. 6. For comparison, the same figure also shows the path lengths for impurity-impurity scattering (l_{ii}). It is clear from the figure that in the low temperature limit the mean free paths exceed by hundreds of thousands of times the mean interatomic distances. Such large values for the mean free paths cannot of course be explained, if helium is regarded as an ordinary liquid, since if it is assumed that the He^3 atoms are scattered by atoms of He^4, such path lengths could be obtained only for a He^4 density of 8×10^{-6} g/cm^3. These results again bear out the Landau-Pomeranchuk viewpoint that impurities in liquid helium below the λ point interact with the excitation quanta — the rotons and phonons.

I take this opportunity to express my deep gratitude to Professor V. P. Peshkov for his constant assistance in this work, and for his valued advice; to Professor I. M. Khalatnikov and R. G. Arkhipov for valuable discussions; to V. N. Zharkov and A. Andreev for their aid in considering the results of the present article; to A. I. Filimonov and Yu. N. Ippolitov for their assistance in assembling the apparatus; and also to B. D. Yurasov, who prepared the intricate glass parts of the apparatus.

[1] L. D. Landau and I. Ya. Pomeranchuk, Doklady Akad. Nauk SSSR **69**, 165 (1949).

[2] D. H. N. Wansink and K. W. Taconis, Physica **23**, 125 (1957).

[3] I. M. Khalatnikov and V. N. Zharkov, JETP **32**, 1108 (1957), Soviet Phys. JETP **5**, 905 (1957).

[4] A. N. Vetchinkin, Приборы и техника эксперимента (Instrum. and Exptl. Techniques) **1** (1961).

[5] A. N. Vetchinkin, ibid. **3**, 97 (1960).

[6] Peshkov, Zinov'eva, and Filimonov, JETP **36**, 1034 (1959).

[7] T. P. Ptukha, JETP **34**, 33 (1958), Soviet Phys. JETP **34**, 22 (1958).

[8] T. P. Ptukha, JETP **39**, 896 (1960), Soviet Phys. JETP **12**, 621 (1961).

[9] H. van Dijk and M. Durieux, Physica **24**, 920 (1958).

[10] Beenakker, Taconis, Lynton, Dokoupil, and Soest, Physica **18**, 433 (1952).

[11] R. L. Garvin and H. A. Reich, Phys. Rev. **115**, 1478 (1959).

[12] Staas, Taconis, and Fokkens, Physica **26**, 669 (1960).

[13] V. N. Zharkov, JETP **33**, 929 (1957), Soviet Phys. JETP **6**, 714 (1958).

Translated by S. D. Elliott
272

ELECTRONIC PARAMAGNETIC RESONANCE OF THE Fe^{3+} ION IN CORUNDUM

L. S. KORNIENKO and A. M. PROKHOROV

Institute of Nuclear Physics, Moscow State University

Submitted to JETP editor January 4, 1961

J. Exptl. Theoret. Phys. (U.S.S.R.) 40, 1594-1601 (June, 1961)

Results are presented of an experimental study at various temperatures (290, 77, and 4.2°K) of the electronic paramagnetic resonance of the Fe^{3+} ion in corundum. Spin lattice relaxation times were measured at 4.2°K. The constants of the spin Hamiltonian and their temperature variation were determined.

THE electronic paramagnetic resonance (e.p.r.) spectrum of the Fe^{3+} ion in corundum was first studied by the authors in 1957.[1] It was shown subsequently[2] that this material can be used to make a paramagnetic amplifier. This served as one of the reasons for a more detailed study of the Fe^{3+} ion e.p.r. in corundum.

As is well known, the ground state of the Fe^{3+} ion is a ^6S-state with electronic configuration of the unfilled shell $3d^5$. Since the orbital momentum is zero in this case, to explain the existence of fine structure in the e.p.r. spectrum we must consider, apart from the ground state, higher impurity energy states, corresponding to other electronic configurations. The mechanism that gives rise to the splitting of the ^6S ground state has been discussed theoretically by a number of authors,[3-7] who have analyzed the various types of high-order perturbations, taking into account the effect of the electrostatic field of the crystal, spin-orbit coupling, and magnetic spin-spin interaction.

The investigations we previously made[1] in the frequency range 25 — 40 kMc enabled the form of the spin Hamiltonian and the values of its constants to be determined at room temperature (290°K) for a paramagnetic ion concentration (Fe:Al) of 0.01 — 0.02% (and not 0.1%, as was erroneously stated in reference 1). We have also reported[2] that the constant D is positive. This was established by comparing the relative intensities of the e.p.r. lines at 290 and 4.2°K. The experiments referred to were made at a wavelength of about 0.8 cm. From the fact that the sign of the constant a — F is the same as that of the constant D, it follows that it, too, is positive.

In the present paper the results are given of more accurate measurements of the e.p.r. spectra for the cases when the trigonal axis of the crystal is parallel or perpendicular to the direction of the external magnetic field (for brevity we will call these the parallel and perpendicular orientations); the measurements were made at frequencies in the range 9 — 10 kMc at temperatures of 290, 77, 4.2 and 2°K. From these measurements the values of the spin Hamiltonian constants were found at the various temperatures. Direct measurements were also undertaken of the initial splitting of the ground state energy levels (in zero magnetic field) at temperatures of 290 and 4.2°K, and of the spin-lattice relaxation time τ_1 at 4.2°K. The paramagnetic ion concentration in the specimens studied was 0.02 and 0.002%.

As was shown in reference 1, the e.p.r. spectrum of the Fe^{3+} ion in corundum can be interpreted with the aid of the spin Hamiltonian:[8]

$$\begin{aligned}\hat{\mathcal{H}} = {} & g\beta\mathbf{H}\hat{\mathbf{S}} + D\left[\hat{S}_z^2 - \tfrac{1}{3}S(S+1)\right] + \tfrac{1}{6}a\left[\hat{S}_\xi^4 + \hat{S}_\eta^4 + \hat{S}_\zeta^4 \right. \\ & \left. - \tfrac{1}{5}S(S+1)(3S^2+3S-1)\right] \\ & + \tfrac{1}{180}F\left[35\hat{S}_z^4 - 30S(S+1)\hat{S}_z^2 + 25\hat{S}_z^2 - 6S(S+1)\right. \\ & \left. + 3S^2(S+1)^2\right], \end{aligned} \tag{1}$$

where g is the spectroscopic splitting factor, assumed isotropic, β is the Bohr magneton, $\mathbf{H}$ is the vector magnetic field strength, $\hat{\mathbf{S}}$ is the electronic spin operator ($\hat{S}_i$ is the operator projecting it on the corresponding axis) with eigenvalue $S = 5/2$, a is the constant of the cubic crystal field, D and F are the constants of the trigonal crystal field of the second and fourth order, respectively. The coordinate system $\xi\eta\zeta$ lies along the cubic axes of the crystal field, and the z axis is directed along the trigonal axis of the crystal, which is also the [111] axis of the system $\xi\eta\zeta$.

When the Fe^{3+} ion replaces the Al^{3+} ion isomorphously in the crystalline lattice of corundum, there are two nonequivalent cases, differing in the directions of the cubic axes of the crystal field. The three cubic axes of one type of ion can be ob-

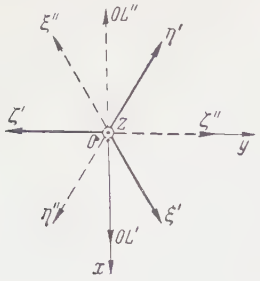

FIG. 1. The coordinate axes used in the expressions for the spin Hamiltonian of the Fe^{3+} ion in corundum. $\xi'\eta'\zeta'$ and $\xi''\eta''\zeta''$ are the projections of the mutually perpendicular axes of the cubic crystal field for the first and second systems of non-equivalent ions, respectively. (The axes themselves are inclined upwards.) z is the axis of the trigonal crystal field (directed vertically upwards). The x axis bisects the angle between the projections of the cubic axes ξ' and η''. OL′ and OL″ are lines used for calculating the Euler angles φ_1 and φ_2 for the first and second system of ions, respectively.

tained by reflecting the corresponding three axes of the other type of ion in the plane perpendicular to the trigonal axis (xy), or by rotating it through 60°. When the axes are labelled as in Fig. 1, the Euler angles for transforming from the coordinates xyz to the coordinates $\xi\eta\zeta$ are, for the first system $(\xi'\eta'\zeta')$,

$$\varphi_1 = 0,\ \theta = 54°44',\ \varphi_2 = 45°,$$

and for the second system $(\xi''\eta''\zeta'')$

$$\varphi_1 = 180°,\ \theta = 54°44',\ \varphi_2 = 45°.$$

After introducing the dimensionless coefficients

$$h_i = g\beta H_i/D \quad (i = x, y, z),$$
$$\alpha = a/D,$$
$$f = F/D, \tag{2}$$

substituting $S = 5/2$ in (1), and, for simplicity, changing $S(S+1)/3 = 35/12$ into $5/4$ (this changes the Hamiltonian trivially by a constant), and after the necessary transformations, we obtain, in the representation that makes the matrix operator $\hat{S}_z$ diagonal, the Hamiltonian matrix for the Fe^{3+} ion in corundum in the following form:

$$\begin{vmatrix}
-\frac{5}{2}h_z+5-\frac{\gamma}{3} & \frac{\sqrt{5}}{2}h^+ & 0 & \pm ip & 0 & 0 \\
\frac{\sqrt{5}}{2}h^- & -\frac{3}{2}h_z+1+\gamma & \sqrt{2}\,h^+ & 0 & 0 & 0 \\
0 & \sqrt{2}\,h^- & -\frac{1}{2}h_z-1-\frac{2\gamma}{3} & \frac{3}{2}h^+ & 0 & \mp ip \\
\mp ip & 0 & \frac{3}{2}h^- & \frac{1}{2}h_z-1-\frac{2\gamma}{3} & \sqrt{2}\,h^+ & 0 \\
0 & 0 & 0 & \sqrt{2}\,h^- & \frac{3}{2}h_z+1+\gamma & \frac{\sqrt{5}}{2}h^+ \\
0 & 0 & \pm ip & 0 & \frac{\sqrt{5}}{3}h^- & \frac{5}{2}h_z+5-\frac{\gamma}{3}
\end{vmatrix} \tag{3}$$

$$h^{\pm} = h_x \pm ih_y, \qquad \gamma = \alpha - f, \qquad p = (2\sqrt{5}/3)\alpha.$$

For the matrix elements with plus-or-minus sign, the upper sign corresponds to the first, and the lower sign to the second system of non-equivalent ions. Inspection of the matrix (3) shows that the constant f is present only in the combination $(\alpha - f)$ with the constant α. The constant α also appears in terms with plus-or-minus signs, and, on changing the sign of α, the Hamiltonian matrix for one system of ions transforms into the matrix for the other system. Since it is impossible to establish which of the two experimentally observed spectra corresponds to which system of ions, it follows that by measuring the positions of the e.p.r. lines it is impossible to determine either the value of the constant f (except in the combination $\alpha - f$), or the sign of the constant α.

For the parallel orientation ($h_Z = h$, $h_X = h_Y = 0$), the sixth-degree secular equations for both systems of ions are equivalent, and can be factored into two linear and two quadratic equations. In this case the energy levels depend on the value of the external magnetic field h as follows:

$$\varepsilon_{6,3} = +h+2-\tfrac{1}{2}(\alpha-f) \pm \tfrac{1}{6}\sqrt{\{9h+[18+(\alpha-f)]\}^2+80\alpha^2},$$
$$\varepsilon_{5,2} = \pm\tfrac{3}{2}h+1+(\alpha-f),$$
$$\varepsilon_{4,1} = -h+2-\tfrac{1}{2}(\alpha-f) \pm \tfrac{1}{6}\sqrt{\{9h-[18+(\alpha-f)]\}^2+80\alpha^2}. \tag{4}$$

The energy levels are numbered in order of increasing energy in strong magnetic fields. The

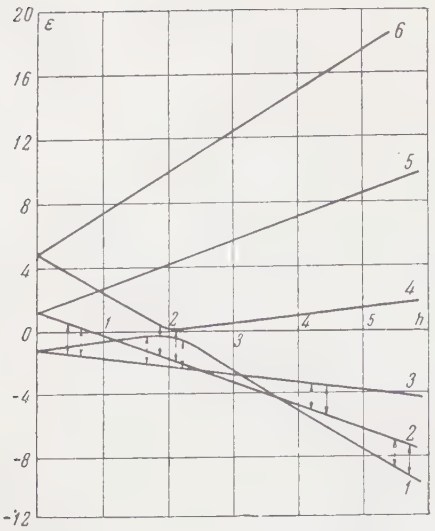

FIG. 2. The variation of the energy levels of the Fe^{3+} ion in corundum with the magnetic field for the parallel orientation ($\theta = 0°$). The arrows indicate the resonance transitions when radiation with frequencies in the range 9 – 10 kMc is used (full arrows for the case $\nu > \nu''$, broken arrows for the case $\nu < \nu'$). The numbers on the curves give the numbers of the levels in order of increasing energy in strong magnetic fields. The axes are marked in dimensionless units: $\varepsilon = E/D$, where E is the energy of the level; $h = g\beta H/D$.

variation of the position of the energy levels with the magnetic field h is shown in Fig. 2.*

The wave functions φ_i of the corresponding energy levels ϵ_i can be expanded in terms of the eigenfunctions ψ_k of the operator $\hat{S}_z$, where k = 1, 2, ... 6 corresponds to its eigenvalues with M $= -5/2, -3/2, \ldots, +5/2$:

$$\varphi_1 = \alpha_1\psi_1 + i\alpha_2\psi_4, \quad \varphi_2 = \psi_2, \quad \varphi_3 = \beta_1\psi_3 + i\beta_2\psi_6,$$
$$\varphi_4 = i\alpha_2\psi_1 - \alpha_1\psi_4, \quad \varphi_5 = \psi_5, \quad \varphi_6 = i\beta_2\psi_3 - \beta_1\psi_6. \quad (5)$$

Here

$$\alpha_1 = (a_{44} - \varepsilon_1)/\sqrt{(a_{44} - \varepsilon_1)^2 - p^2},$$
$$\alpha_2 = p/\sqrt{(a_{44} - \varepsilon_1)^2 - p^2},$$
$$\beta_1 = (a_{66} - \varepsilon_3)/\sqrt{(a_{66} - \varepsilon_3)^2 - p^2},$$
$$\beta_2 = p/\sqrt{(a_{66} - \varepsilon_3)^2 - p^2};$$

a_{ii} are the corresponding diagonal terms in (3), and $p = (2\sqrt{5}/3)|\alpha|$.

When radiation with a frequency in the range 9 – 10 kMc is used, five e.p.r. lines can be observed. The first, fourth, and fifth (in order of increasing value of the magnetic field at resonance) correspond to transitions $3 \longleftrightarrow 2$, $2 \longleftrightarrow 3$ and $1 \longleftrightarrow 2$ (the first number is the number of the lower level, and the second, the number of the upper level). For frequencies $\nu < \nu'$ the second and third lines correspond to the transition $3 \longleftrightarrow 1$, but for frequencies $\nu > \nu''$ they correspond to the transition $2 \longleftrightarrow 4$. The frequencies ν' and ν'' are certain critical frequencies, the values of which depend on temperature, as do the values of the spin Hamiltonian constants. If $\nu' < \nu < \nu''$, the second and third lines are generally not observed. The values of ν' and ν'' can be calculated, if the values of the spin Hamiltonian constants are known, from the condition $\partial(\Delta\epsilon)/\partial h = 0$, where $\Delta\epsilon$ is the energy difference between the first and third, or fourth and second levels. These conditions result in the expressions

$$h\nu' \approx 2D + \tfrac{1}{9}(a - F) - \tfrac{4}{9}\sqrt{10}|a| + \tfrac{5}{27}|a|^2/D, \quad (6)$$

$$h\nu'' = 2D - \tfrac{13}{9}(a - F) + \tfrac{4}{9}\sqrt{10}|a|. \quad (7)$$

As can be seen from (6) and (7), if frequencies are used which are close to ν' or ν'' (but do not lie between them), it is possible to determine the value of $|a|$ from terms of the same order of magnitude as the terms which contain $a - F$ (we recall that in reference 1 the value of $|a|$ was found from terms which were second order perturbations, and this led to a lower accuracy). This fact was taken into account when the frequencies used in the study of the e.p.r. spectrum were chosen.

The e.p.r. lines were observed with the aid of a reflection type radiospectrometer. Accurate orientation of the crystal relative to the direction of the external magnetic field was obtained with a resonator of special construction, which allowed the crystal to be rotated about two mutually perpendicular axes in the course of the experiment. The frequency of the microwave source was stabilized with respect to the spectrometer resonator; the absolute frequency error was continuously controlled, and did not exceed 0.2 – 0.3 Mc. To measure the magnetic field strength proton nuclear magnetic resonance was used. The diameter of the pole pieces of the electromagnet used in the experiments was 260 mm, and the distance between the pole pieces was 30 – 65 mm. To increase the accuracy of measurement, the distribution of the magnetic field in the gap between the poles was explored, and the paramagnetic crystal and proton transducer of the field measuring device were placed at points whose field values differed by less than 0.005%.

It was established in the course of the experiments that, when working at frequencies such that $\nu > \nu''$, an operating frequency could be chosen closer to the critical frequency than when working

*The solution of the secular equation in this case has also been considered by Vinokurov, Zaripov, and Yafaev.[9]

Table I

Temperature, °K	Frequencies Mc	Resonance magnetic field values (oe) corresponding to various transitions				
		3 ⟷ 2	2 ⟷ 4	2 ⟷ 4	2 ⟷ 3	1 ⟷ 2
290	9641.7	752.5	3489.3	3595.6	7624.8	10147.2
		(752.5)*	(3490.5)	(3595.3)	(7624.6)	(10146.8)
77	9838.4	778.8	3589.3	3658.5	7789.9	10363.1
		(778.7)	(3587.7)	(3657.6)	(7789.7)	(10363.0)
4.2	9846.8	779.4	3592.8	3663.0	7798.0	10375.5
		(779.8)	(3592.5)	(3662.5)	(7798.0)	(10375.7)

*In brackets are given the values calculated from the spin Hamiltonian constants given in Table II.

Table II

Constants	Values of the spin Hamiltonian constants for the Fe^{3+} ion* in corundum		
	at 290°K	at 77°K	at 4.2°K
g	2.0030 ± 0.0006	2.0032 ± 0.0007	2.0029 ± 0.0007
D, Oe	$+1796.4 \pm 0.4$	$+1836.2 \pm 0.6$	$+1838.5 \pm 0.6$
$a - F$, Oe	$+ 353.2 \pm 0.4$	$+362.6 \pm 0.5$	$+ 362.7 \pm 0.5$
$\lvert a \rvert$, Oe	248.7 ± 1.0	254.1 ± 1.3	253.5 ± 1.3

*Fe^{3+} ion concentration $\leq 0.02\%$.

at frequencies such that $\nu < \nu'$. When the frequency approached the critical value ν', the e.p.r. lines corresponding to the transition $1 \longleftrightarrow 3$ smeared out more rapidly than the lines corresponding to the transition $4 \longleftrightarrow 2$ when the other critical frequency ν'' was approached. Since the values of the spin-Hamiltonian constants, and, consequently, the quantities ν' and ν'', depended on temperature, the radiation frequency used in the experiments at various temperatures also varied. The frequencies lay in the range 9000 — 9200 Mc ($\nu < \nu'$), and 9600 — 9850 Mc ($\nu > \nu''$).

In Table I a summary is presented of the experimental data on the positions of the e.p.r. line peaks in the magnetic field for the parallel orientation, measured at frequencies $\nu > \nu''$ and at different temperatures, for specimens with 0.02% Fe^{3+} ion concentration. For comparison, the brackets contain the values of the resonance fields calculated on the basis of the spin-Hamiltonian constants found from these measurements and given in Table II. Measurements made at frequencies $\nu < \nu'$ gave results in agreement with measurements at $\nu > \nu''$.

The width of the first, fourth and fifth lines, measured between the half-intensity points, was 10 ± 2 oe for the specified paramagnetic ion concentration, and did not depend on temperature. The widths of the second and third lines depend greatly on the radiation frequency chosen, since the corresponding transitions occur in a region where the derivative $\partial\epsilon/\partial h$ for the fourth or third levels changes sign. Usually the quantity $\Delta\nu = \nu - \nu''$ ($\nu' - \nu$) was chosen, so that the width of these lines was 20 — 30 oe.

Measurements at a temperature of about 2°K showed that the values of the spin-Hamiltonian constants at this temperature did not differ from the values at 4.2°K.

At 290°K measurements were also made of the e.p.r. spectra for the parallel orientation on specimens with paramagnetic ion concentrations of 0.002%. These measurements showed that the possible deviation of the constants from the values given in Table II does not exceed the limits of experimental error. The line width in this case is 10 — 20% smaller than when the concentration is 0.02%. This shows that magnetic dipole-dipole interaction of the paramagnetic ions is already starting to have a significant effect in the range of concentrations considered.

The shape of the lines is intermediate between Gaussian and Lorentzian, and its character does not change in this concentration range. When the concentration of the Fe^{3+} ions is further diminished, the widths of the e.p.r. lines remain practically unchanged.

It is seen from our results that the values of the constants D, a — F, and |a|, all increase as the temperature is lowered, but that the value of the constant g is practically unchanged. The values obtained for the constants agree with the results of Bogle and Simmons,[10] with the exception of the constant |a|, which they found to get

Table III

Temperature, °K	Experimental value of $h\nu/D$	Resonance magnetic field value (oe)	Calculated value of $h\nu/D$	$\left\|\frac{h\nu_{exp.}-h\nu_{calc.}}{h\nu_{exp.}}\right\|$, %
290	1.9138 (ν=9640.5 Mc)	1355.4	1.9138	—
		3394.9	1.9139	0.005
		7294.0	1.9168	0.15
77	1.9109 (ν=9838.5 Mc)	1381.1	1.9097	0.06
		3467.6	1.9107	0.01
		7445.6	1.9115	0.03
4.2	1.9105 (ν=9846.6 Mc)	1383.8	1.9106	0.005
		3470.2	1.9099	0.03
		7456.3	1.9126	0.1

smaller as the temperature was decreased. They obtained this result, apparently, because the crystal was not oriented sufficiently accurately.

For the perpendicular orientation of the crystal ($h_X = h$, $h_Z = h_Y = 0$), the sixth order secular determinant for the energy levels can be written as the product of two third order determinants: $\Delta = \Delta_+\Delta_- = 0$, where

$$\Delta_- = \begin{vmatrix} 5-\frac{1}{3}(\alpha-f)-\varepsilon & \frac{\sqrt{5}}{2}h & +i\frac{2\sqrt{5}}{3}|\alpha| \\ \frac{\sqrt{5}}{2}h & 1+(\alpha-f)-\varepsilon & \sqrt{2}h \\ -i\frac{2\sqrt{5}}{3}|\alpha| & \sqrt{2}h & -1-\frac{2}{3}(\alpha-f)\pm\frac{3}{2}h-\varepsilon \end{vmatrix}. \quad (8)$$

Analysis of the secular equation shows that the energy spectrum does not change when the crystal is rotated about the trigonal axis while this remains perpendicular to the direction of the magnetic field. This prediction agrees with experiment.

The behavior of the energy levels for the perpendicular orientation is shown in Fig. 3. Three

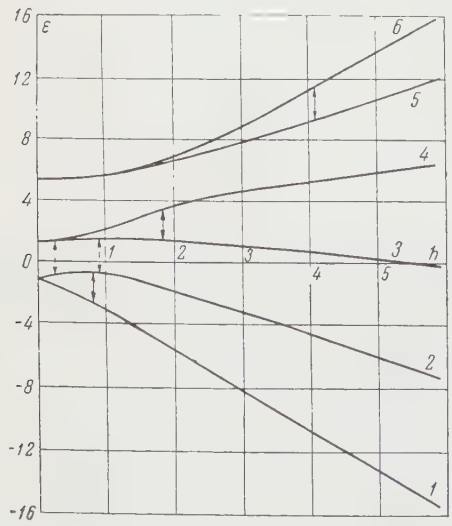

FIG. 3. Variation of the energy levels of the Fe^{3+} ion in corundum with the magnetic field for the perpendicular orientation ($\theta = 90°$).

e.p.r. lines are observed in this case, to which are added two other lines for some radiation frequency values; the latter two lines correspond to transitions between levels 2 and 3 (they are shown in Fig. 3 by broken arrows). It was ascertained how well the spectrum for the perpendicular orientation could be described by the spin Hamiltonian (1) with the values of the constants found from the spectrum in the parallel orientation. To do this, the energy difference of the levels between which the corresponding resonance transition occurs was calculated, using the values for the constants from Table II, for each of the experimental values of the resonance magnetic field. The value obtained was compared with the quantum of radiation used. The results of this comparison are given in Table III.

Direct measurements were also made on the initial splitting (in the absence of magnetic field) between the neighbors of the spin doublets in the ^6S ground state at 290 and 4.2°K. The following results were obtained:

	$T = 290°$ K	$T = 4.2°$ K
Δ_1, Mc:	11768±4 (11759 ±6)	12046±13 (12044±6)
Δ_2, Mc:	18873±11 (18866±6)	19298± 3 (19291±6),

where Δ_1 is the energy difference between the middle and lower doublets, and Δ_2 is the energy difference between the middle and upper doublets. For comparison are given in brackets the values of Δ_1 and Δ_2 calculated from the spin Hamiltonian constants (see Table II) by the formula obtained from (6) when h = 0:

$$\Delta_{2,1} = \sqrt{[3D+\tfrac{1}{6}(a-F)]^2+\tfrac{20}{9}a^2} \pm [D-\tfrac{3}{2}(a-F)]. \quad (9)$$

The agreement between the experimental and calculated values indicates that the spin Hamiltonian (1) also describes well the energy levels of the Fe^{3+} ion in corundum when the value of the external magnetic field tends to zero.

Preliminary experiments made at 290°K on specimens with Fe^{3+} ion concentrations of about

0.2 and 0.5% showed that in this case a marked dependence is observed of the spin-Hamiltonian constants on the paramagnetic ion concentration.

The method of pulse saturation was used to measure the values of the spin-lattice relaxation times τ_1 at 4.2° K. The measurements were made at a wavelength of 3.2 cm. The transition corresponding to the first e.p.r. line in the parallel orientation was studied. The time τ_1 was $(12 \pm 1) \times 10^{-3}$ sec for an Fe^{3+} ion concentration of 0.002%, and $(8 \pm 1) \times 10^{-3}$ sec for a concentration of 0.02%. The relaxation process in both cases was described by a single exponential.

The authors thank R. P. Bashuk and A. S. Bebchuk for providing the specimens for the studies, the late G. A. Feshchenko for fruitful discussions, and V. A. Kozlov and N. G. Slovetskaya for help with the measurements.

[1] L. S. Kornienko and A. M. Prokhorov, JETP **33**, 805 (1957), Soviet Physics JETP **6**, 620 (1958).

[2] L. S. Kornienko and A. M. Prokhorov, JETP **36**, 919 (1959), Soviet Phys. JETP **9**, 649 (1959).

[3] J. H. Van Vleck and W. G. Penney, Phil. Mag. **17**, 961 (1934).

[4] M. H. L. Pryce, Phys. Rev. **80**, 1107 (1950).

[5] Nagamija, Yosida, and Kubo, Phil. Mag. Suppl. **4**, 1 (1955).

[6] H. Watanabe, Progr. Theor. Phys. Japan **18**, 405 (1957).

[7] Powell, Gabriel, and Johnston, Phys. Rev. Letters **5**, 145 (1960).

[8] B. Bleaney and R. S. Trenam, Proc. Roy. Soc. **A223**, 1 (1954).

[9] Vinokurov, Zaripov, and Yafaev, JETP **37**, 312 (1959), Soviet Phys. JETP **10**, 220 (1960).

[10] G. S. Bogle and H. F. Symmons, Proc. Phys. Soc. **73**, 531 (1959).

Translated by K. F. Hulme
273

ENERGY SPECTRUM AND TOTAL NUMBER OF LOW-ENERGY COSMIC-RAY PHOTONS IN THE STRATOSPHERE

A. N. CHARAKHCH'YAN and T. N. CHARAKHCH'YAN

P. N. Lebedev Physics Institute, Academy of Sciences U.S.S.R.; Institute of Nuclear Physics, Moscow State University

Submitted to JETP editor January 4, 1961

J. Exptl. Theoret. Phys. (U.S.S.R.) 40, 1602-1605 (June, 1961)

Results of calculations and experiments on the energy spectrum of cosmic-ray photons in the stratosphere (in the energy range from 50 to 3000 kev) are presented.

It is customarily assumed that the main source of low-energy photons (tens of kev and more) in the cosmic rays of the stratosphere is electron bremsstrahlung. It is of interest to verify this premise by calculation and experiment. We propose that the following calculations indicate that this assumption is not justified for the softest part of the spectrum of the stratosphere photons.

At not too high altitudes in the stratosphere, owing to electromagnetic cascade multiplication, the energy spectrum of the electrons or photons is the average of a large number of superimposed cascades from different generations. The photon spectrum in the stratosphere will therefore be close in form to the equilibrium spectrum (integrated over the depth) obtained in the theory of cascade showers.[1] In addition, the energy spectrum for the photons of energy many times smaller than the energy of the electrons or photons which give rise to avalanches, will be independent of the initial energy of the photons and the electrons. As shown by us earlier,[2] such a theoretical interpretation is well justified experimentally when it comes to the low-energy electrons in the stratosphere.

Belen'kii[1] gives for the equilibrium spectrum of the photons the following integral equation

$$\int_E^\infty P(E')\,W_e(E'E)\,dE' - \sigma(E)\,\Gamma(E) + \int_E^\infty \Gamma(E')\,W_k(E'E)\,dE' = 0, \qquad (1)$$

where $\Gamma(E)$ is the sought photon distribution function, $P(E')$ is the electron distribution function,

$$\sigma(E) = \int_0^E [W_p(EE') + W_k(EE')]dE'$$

is the total photon absorption cross section along a unit cascade path, and W_e, W_p, and W_k are the cross sections on a cascade unit path of the electron bremsstrahlung, pair production by photons, and Compton scattering of photons, respectively.

The first term of Eq. (1) is the number of bremsstrahlung photons of energy E generated on a unit path. As a good approximation, $W_e(E'E) = A/E$ (case of total screening), and

$$\int_E^\infty P(E')\,dE' = N(E)$$

is the equilibrium electron integral spectrum, the expression for which was given in reference 1. The second term of the equation is the number of photons of energy E absorbed on a unit path. The third term of the equation takes into account photons with energy E, obtained by Compton scattering from photons with energy $E' > E$.

The complexity of the expression for W_k in (1) makes it difficult to solve the equation in general form. Solutions were obtained for the simplified formulas $W_k = g/E'E$ (Belen'kii[1]) and $W_k = (g/E'E)[1 + (E/E')^2]$ (Isaev[3]). The exact expression for W_k in (1), given by the well known Klein-Nishina and Tamm formula, has the form

$$W_k(E'E) = \frac{g}{E'E}\left[1 + \left(\frac{E}{E'}\right)^2 - \frac{2mc^2}{E'^2}(E' - E) + \frac{(mc^2)^2}{E'^3}\frac{(E-E)^2}{E}\right]. \qquad (2)$$

Here E' and E are the energies of the primary and secondary photons, in Mev, mc^2 is the electron rest-mass energy, and g = 1.32 Mev.

The foregoing approximations are not good enough for photons with energies less than 4 — 5 Mev. We have attempted to obtain a solution of (1) by using the exact expression for $W_k(E'E)$ in (2).

Let us introduce

$$\Gamma(E) = \frac{N(E)}{E}\,\frac{Z(E)}{\sigma(E)}. \qquad (3)$$

After substituting $\Gamma(E)$ in (1) we obtain for $Z(E)$ the expression

$$A - Z(E) + \frac{E}{N(E)} \int_{E}^{E_1} \frac{W_k(E'E)}{E'\sigma(E')} N(E') Z(E') dE' = 0. \quad (4)$$

Unlike the methods of references 1 and 3, in which the photons involved have relatively high energies, the upper limit of the integral in (4) is in general not infinite, for E_1 becomes infinite only when $E \geq 0.25$ Mev. For smaller values of E, the upper limit of E_1 is determined from the well known relation $E = mc^2E_1/(mc^2 + 2E_1)$, obtained from the energy and momentum conservation laws in the Compton scattering of photons.

The solution of (4) is sought in the form of a series in powers of $\mu \leq 1$, a parameter introduced as a factor in the third term of (4):

$$Z(E) = \sum \mu^n Z_n(E). \quad (5)$$

Naturally, such a solution will correspond to our problem when $\mu = 1$. Substituting the series (5) into (4) and equating the terms of like powers of μ to zero, we obtain the terms of the series

$$Z_0 = A, \qquad Z_1 = \frac{E}{N(E)} \int_{E}^{E_1} \frac{W_k(E'E)}{E'\sigma(E')} N(E') Z_0(E') dE',$$
$$Z_2 = \frac{E}{N(E)} \int_{E}^{E_1} \frac{W_k(E'E)}{E'\sigma(E')} N(E') Z_1(E') dE' \ldots. \quad (6)$$

For sufficiently small values of E we have $A = 1.3$ (see reference 1).

In view of the complexity of the integrand, the integrals were evaluated numerically. The series (5) converges rather rapidly also when $\mu = 1$. The remainder of the series amounts to not more than 1% of the sum of the first five or six terms. For low energies, from 0.02 to 0.1 Mev, the values of $\delta(E)$ in (3) and (6) were taken with account of the photoabsorption effect. The calculated differential spectrum of the photons is shown for the case of air in the figure, curve 1. The ordinates show the ratio of the number of photons with energy E in a 1-Mev interval to the total number of equilibrium electrons, $N_e = E_0/\beta$, and the abscissas represent the photon energy. Curve 2 is for the integral spectrum.

The experimental data on the intensity of low-energy photons in the stratosphere have been obtained by measurements with the aid of a scintillation counter. The apparatus consisted of a cylindrical 40 × 40 mm NaI(Tl) scintillator with FÉU-1S photomultiplier. Connected to the output of the photomultiplier was a two-stage amplifier and the electronic portion of the circuit, used to broadcast the number of flashes in the scintillator.

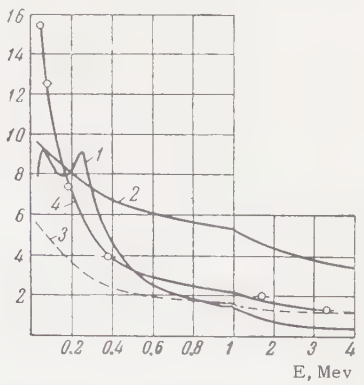

Curve 1 – differential spectrum of photons in air: ordinates – ratio of equilibrium number of photons with energy E in a 1-Mev interval to the total number of cascade electrons; abscissas – photon energy E; 2 – corresponding integral spectrum of the photons; 3 – calculated ratio of the frequency of flashes in the crystal to the total number of electrons, as a function of E_{thr}; 4 – experimental ratio of frequency of flashes in the crystal to the total number of electrons, as a function of E_{thr}.

A voltage divider was inserted between the output of the photomultiplier and the amplifier in order to set the threshold for the registration of a specified pulse amplitude, corresponding to an energy release in the crystal, Ethr, greater than 50, 85, 170, 480, 1700, and 3200 kev. The measurements have been carried out at geomagnetic latitude 51° and altitudes up to 33 – 35 km. The results of the experiment, pertaining to the altitude at which the photons had maximum intensity (100 g-cm^{-2}) are shown dotted in the figure. The ordinates represent the ratio of the frequency of the scintillations in the crystal, after subtracting the scintillations corresponding to charged particles, to the total number of electrons at the same altitude. The abscissas represent the value of E_{thr} (to obtain the number of scintillations per second produced in the crystal by the photons, it is necessary to multiply the ordinates of curve 4 by 18).

The experimental data obtained are comparable with the expected integral spectrum of the recoil electrons in the crystal due to photons. The integral spectrum of the recoil electrons in the scintillator was determined by first calculating the equilibrium spectrum of the photons and using the data on the cross section of the absorption of the photons in the NaI(Tl) crystal as a function of their energy.[4] The results of these calculations are represented by curve 3. As can be seen from the figure, the total flux of registered photons is practically three times greater than expected. The discrepancy is less significant for photons with energies greater than several Mev. There is little likelihood that this disparity in the spectrum can

be attributed to inaccuracy in the measurements. This inaccuracy is less than 10 or 15%, and the accuracy of the numerical calculations is approximately 10%.

It should be noted that the experimental data on the spectrum of the photons obtained at other altitudes, both before and after the maximum of the intensity curve, practically coincide with the data at the maximum. In addition, the ratio of the total number of registered photons to the total number of electrons also depends little on the altitude. These features of the altitude dependence speak in favor of a cascade origin of the low-energy photons in the stratosphere. It is difficult at present, however, to draw any final conclusion concerning the causes of disparity between the experimental and calculated data.

The authors are most grateful to I. P. Ivanenko for a discussion of the results.

[1]S. Z. Belen'kii, Лавинные процессы в космических лучах (Cascade Processes in Cosmic Rays), Gostekhizdat, 1948, pp. 79, 106, 20.

[2]A. N. Charakhch'yan and T. N. Charakhch'yan, JETP **35**, 1088 (1958), Soviet Phys. JETP **8**, 761 (1959).

[3]P. S. Isaev, JETP **24**, 78 (1953).

[4]Chechik, Faĭnshteĭn, and Lifshitz, Электронные умножители (Electron Multipliers), Gostekhizdat 1957, p. 514.

Translated by J. G. Adashko
274

PARAMAGNETIC RESONANCE OF Mn^{2+} *IN SrS*

A. A. MANENKOV and A. M. PROKHOROV

P. N. Lebedev Physics Institute, Academy of Sciences, U.S.S.R.

Submitted to JETP editor January 4, 1961

J. Exptl. Theoret. Phys. (U.S.S.R.) **40**, 1606-1609 (June, 1961)

The electron paramagnetic resonance spectrum of Mn^{2+} in the SrS crystal lattice is investigated. The constants of the spin Hamiltonian describing the observed spectrum are determined. The cubic field constant a is estimated from the anisotropic line broadening for the transitions $M = \pm 3/2 \rightarrow \pm 1/2$ in powder. The spin-lattice relaxation time at room temperature, $T_1 = 5 \times 10^{-8}$ sec, is determined from the difference in the width of the $M = 1/2 \rightarrow -1/2$ transition lines at 300 and at 77° K. The low value of the hyperfine-structure constant A indicates that the coupling between the Mn^{2+} ions and the surrounding ions of the crystal lattice is of a covalent nature.

MANY investigators have studied in detail the paramagnetic resonance of Mn^{2+} ions in various crystals (see, for example, references 1 — 4). The ground state of Mn^{2+}, ^6S, has zero orbital momentum and to a first approximation is not split by a crystalline electric field. However, significant splittings of the energy levels by a crystalline field have been found in many crystals. These splittings are due to admixture of higher states, with non-zero orbital momentum, to the ^6S state. The degree of admixture of states depends appreciably on the symmetry and magnitude of the crystal field.

The case of a cubic field is of considerable interest. Watanabe[5] has analyzed the splitting of the ^6S state by a cubic field in detail theoretically, and has also compared his calculation with the existing experimental results for Mn^{2+} and Fe^{3+}. We should note, however, that although Watanabe's calculations agree qualitatively with the experimental data, there are in some cases considerable quantitative disagreements between the theoretical calculations and the experimental data.

We have investigated the paramagnetic resonance of Mn^{2+} in the SrS crystal lattice, which has cubic symmetry. The specimens studied were polycrystalline and contained about 0.05% of Mn^{2+} ions. The measurements were made at room temperature and at liquid nitrogen temperature at a frequency $\nu = 9{,}300$ Mc/sec. At both temperatures spectra consisting of six groups of lines with hyperfine structure (hfs) corresponding to the nuclear spin of Mn^{55}, $I = 5/2$, were observed. Although the general nature of the spectrum did not differ appreciably at 300 and at 77° K, a narrowing of the lines and a small increase in the hfs constant were found on going from 300 to 77° K. Figure 1 shows the composition of the full spectrum, made up from oscillograms of the separate groups of hfs lines, photographed at 77° K.

The observed spectrum is described by the spin Hamiltonian

$$\hat{\mathcal{H}} = g\beta \mathbf{H}\hat{\mathbf{S}} + A\hat{\mathbf{S}}\hat{\mathbf{I}} + \frac{1}{6}a\left[\hat{S}_x^4 + \hat{S}_y^4 + \hat{S}_z^4 - \frac{1}{5}S(S+1)(3S^2-1)\right], \quad (1)$$

where the first term describes the interaction between an electron spin **S** and the external magnetic field **H**, the second — the interaction of an electron spin with the nuclear spin **I** of Mn^{55}, and the third the interaction of an electron spin with the crystal field of cubic symmetry. Calculation by perturbation theory, taking into account third order terms in the hyperfine interaction and first order in the cubic field constant, leads to the following formula for the magnitude of the magnetic field strength at which absorption lines corresponding to the electron transitions $M \rightarrow M-1$ would be observed:

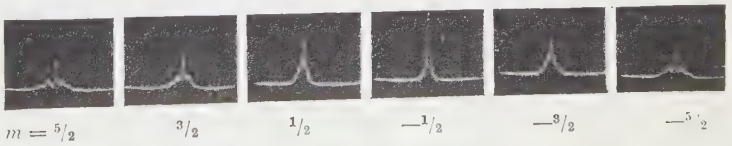

FIG. 1. Paramagnetic resonance spectrum of Mn^{2+} in SrS, observed at 77°K. The magnetic field increases to the right.

$$H - H_0 = Am - \frac{A^2}{2H_0}\{I(I+1) - m^2 + m(2M-1)\}$$
$$+ \frac{A^3}{4H_0}\{[S(S+1) - M(M+1)$$
$$+ 2M(m-M)][I(I+1) - m(m-1)]$$
$$- [S(S+1) - M(M-1) + 2(M-1)(m-M+2)]$$
$$\times [I(I+1) - m(m+1)]\} + F(a, M), \qquad (2)$$

where

$$H_0 = h\nu/g\beta,$$

$$F(a, M) = \begin{cases} 0 \text{ for the transition } M = 1/2 \to -1/2, \\ \pm 5/2\, pa \text{ for the transitions } M = \pm 3/2 \to \pm 1/2, \\ \mp 2pa \text{ for the transitions } M = \pm 5/2 \to \pm 3/2, \end{cases}$$

$$p = 1 - 5\Phi, \qquad \Phi = l^2m^2 + l^2n^2 + m^2n^2$$

(l, m and n are the direction cosines of the angles which the external magnetic field makes with the cubic axes of the crystals).

As can be seen from (2), the second- and third-order shifts in the hyperfine structure are not the same for different electron transitions, as they depend on the magnetic quantum number M. The shifts produce splittings of every component of the hyperfine structure with a given nuclear magnetic quantum number into 2S = 5 (S is the electronic spin of Mn^{2+}) lines, corresponding to different electronic transitions. From (2) it is seen that the magnitude of these splittings increases with increasing |m|.

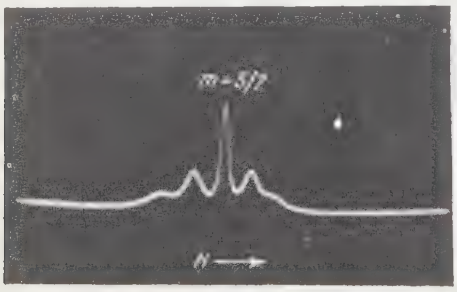

FIG. 2. The group of lines in the paramagnetic resonance spectrum of Mn^{2+} in SrS, corresponding to the nuclear magnetic quantum number m = 5/2. The central line of this group belongs to the electronic transition M = 1/2 → −1/2. The arrow shows the direction of increasing magnetic field.

For the two extreme groups of lines corresponding to $m = \pm 5/2$ (see Fig. 1), all five lines are well resolved. To show this more easily, the oscillogram of the group of lines with $m = 5/2$ is reproduced in greater enlargement in Fig. 2. We notice that the splittings produced by the second order hfs shifts increase symmetrically from the center to the edges of the spectrum, while the third order shift leads to asymmetries of these splittings, as is seen in Fig. 1 especially clearly for the lines $m = \pm 1/2$ and $m = \pm 3/2$.

Comparison of the observed spectrum with Eq. (2) gives the following values for the constants of the Hamiltonian:

$$g = 2.0009 \pm 0.0005, \qquad A = (75.4 \pm 0.2)\cdot 10^{-4}\,\text{cm}^{-1},$$
$$a < 1.4\cdot 10^{-4}\,\text{cm}^{-1} \qquad \text{at } T = 300^\circ\text{ K};$$

$$g = 2.0010 \pm 0.0005, \qquad A = (77.0 \pm 0.2)\cdot 10^{-4}\,\text{cm}^{-1},$$
$$a < 1.2\cdot 10^{-4}\,\text{cm}^{-1} \qquad \text{at } T = 77^\circ\text{ K}.$$

The signs of the constants A and a remain indeterminate. The identification of the lines in Fig. 1 with the quantum numbers m corresponds to a positive sign for A. The constants g and A were determined by comparing the positions of the lines $M = 1/2 \to -1/2$, which have the smallest width, with (2). In the best resolved group with $m = 5/2$ the line width for $M = 1/2 \to -1/2$ is 2.8 and 1.9 gauss at 300 and 77° K respectively, while the width for the lines $M = \pm 3/2 \to \pm 1/2$ and $M = \pm 5/2 \to \pm 3/2$ is 5.6 gauss at 300° K and 4.3 gauss at 77° K. The differences between the line widths for $M = 1/2 \to -1/2$, $M = \pm 3/2 \to \pm 1/2$ and $M = \pm 5/2 \to \pm 3/2$ is connected with the anisotropic broadening produced by the random spread of the crystal field axes in the powder, and it follows from (2) that this is negligible for the lines $M = 1/2 \to -1/2$.

The cubic field constant a was determined from the anisotropic broadening of the lines $M = \pm 3/2 \to \pm 1/2$, $\Delta H_a \sim 5/2\,\Delta pa$, using for the maximum dispersion of p in the powder the value $|\Delta p| = 1.25$ and estimating ΔH_a from the difference in width of the lines $M = \pm 3/2 \to \pm 1/2$ and $M = 1/2 \to -1/2$.

The lines $M = \pm 5/2 \to \pm 3/2$ have roughly the same width as the lines $M = \pm 3/2 \to \pm 1/2$. This indicates that the crystal field in SrS has cubic symmetry, since is the case of a cubic field the anisotropic broadening for the lines $M = \pm 5/2 \to \pm 3/2$ and $M = \pm 3/2 \to \pm 1/2$ should be approximately the same, in that the frequency shifts, produced by a cubic crystal field, differ for these lines only by the factor $(5/2\,pa)/(2pa) = 5/4$. The larger width of the lines $M = 1/2 \to -1/2$ at room temperature than at 77° K is due to the contribution from the spin-lattice interaction. The spin-lattice relaxation time at room temperature, calculated from the difference between the widths of the lines $M = 1/2 \to -1/2$ at room temperature and at liquid nitrogen temperature is $T_1 = 5 \times 10^{-8}$ sec. As direct measurement of the spin-lattice relaxation time shows, the contribution from spin-lattice interaction to the line width at liquid nitrogen temperature is negligible.

The relative intensities of the lines $M = \pm 5/2 \to \pm 3/2$, $M = \pm 3/2 \to \pm 1/2$ and $M = 1/2 \to -1/2$, taking

their widths into account, agree with the theoretical ratio 5 : 8 : 9 : 8 : 5.

It is interesting to note that the magnitude of the hyperfine structure constant A for Mn^{2+} in SrS is considerably less than for Mn^{2+} in CaF_2.[2] This probably indicates the covalent character of the bonding of Mn^{2+} in SrS.

[1] B. Bleaney and D. J. E. Ingram, Proc. Roy. Soc. **A205**, 336 (1951).

[2] W. Low, Phys. Rev. **105**, 793 (1957).

[3] R. Stahl-Brada and W. Low, Phys. Rev. **116**, 561 (1959).

[4] W. Low and U. Rosenberger, Phys. Rev. **116**, 621 (1959).

[5] H. Watanabe, Prog. Theoret. Phys. (Kyoto) **18**, 405 (1957).

Translated by R. Berman
275

THE Cl^{35} (n, p) REACTION AND NEUTRON RESONANCE PARAMETERS OF CHLORINE

Yu. P. POPOV and F. L. SHAPIRO

P. N. Lebedev Physics Institute, Academy of Sciences, U.S.S.R.

Submitted to JETP editor January 4, 1961

J. Exptl. Theoret. Phys. (U.S.S.R.) 40, 1610-1614 (June, 1961)

The cross section for the Cl^{35} (n, p) reaction has been measured as a function of energy for neutrons having energies up to 20 kev. Parameters are given for resonances at −0.21, 0.405 and 4.3 kev. The results are discussed together with the data previously obtained on the cross section for the radiative capture of neutrons by chlorine.[1]

INTRODUCTION

FOR slow neutrons, the (n, p) reaction with chlorine is energetically possible only for the isotope Cl^{35}, whose abundance is 75.4%. For thermal neutrons, the cross section for the reaction Cl^{35} (n, p) is about 0.2 barns;[2-5] protons are emitted with an energy of 600 kev. We have measured the cross section for this reaction as a function of energy for neutrons having energies up to 20 kev. In this energy range, the total cross section for the interaction of neutrons with chlorine has been investigated in references 6 — 8; the cross section for radiative capture has been reported in reference 1.*

METHOD

The measurements were made with a spectrometer based on the slowing down of neutrons in lead.[10-11] The energy resolution of the spectrometer (half-width of an isolated resonance) was ~ 70% for E = 15 kev and ~ 35% for E ≲ 1 kev. The procedure for measuring a cross section using this method has been described earlier.[1,9]

Attempts were made to detect the protons with gas discharge counters filled with CCl_4. The counters were warmed to 50° C (vapor pressure of CCl_4 ~ 300 mm Hg) and operated as proportional counters. Preliminary measurements showed that the reaction Cl^{35} (n, p) has resonances at 405 ev and 4.3 kev. However, the poor response time of the counters made quantitative measurements impractical.

The proportional counters were replaced by scintillation detectors. The phosphor was a fine powder of ZnS(Ag), which was poured into a container filled with CCl_4 or C_3Cl_6. The latter are transparent liquids which served as both samples and light pipes.* The effective sample thickness was about 2×10^{21} chlorine nuclei per cm^2.

The electronic circuitry was set to record protons, but not γ rays, the adjustment being monitored by a strong Co^{60} source (E_γ = 1.3 Mev). Gamma rays could arise from neutron capture in lead (E_γ = 7.4 Mev). Other spurious reactions which could have been observed are Zn(n, α) and S(n, α). The possible contributions of such spurious reactions are indicated by the results shown in Fig. 1.

Even if the extreme assumption were made that the counting rate of the CCl_4 + ZnS detector at 30

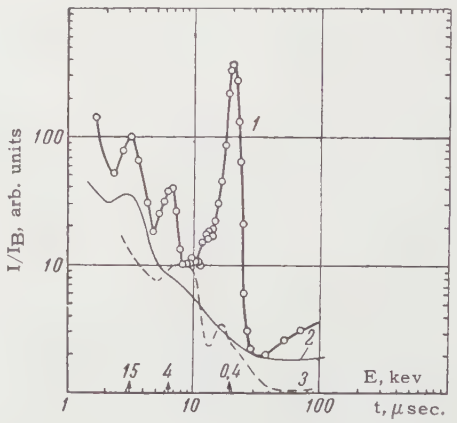

FIG. 1. This figure shows the relative detector counting rate as a function of slowing down time (t). I is the detector counting rate, I_B is the counting rate of a boron counter and is proportional to the neutron density. Curve 1 was taken with a CCl_4 + ZnS(Ag) detector, Curve 2 with a CS_2 + ZnS(Ag) detector, and curve 3 with a γ ray detector. Curve 3 gives the γ ray background of the spectrometer. Curve 2 is normalized to agree with curve 1 at t = 30 μsec, curve 3 is normalized to agree with curve 1 at t = 9 μsec.

*Preliminary results from reference 1 are quoted in reference 9.

*Other mixtures were tried, such as ZnS(Ag) + NaCl, CsI(Tl) + CCl_4, or terphenyl and toluene + NaCl. These were considerably worse from the point of view of efficiency compared to discrimination against γ rays.

μsec were entirely due to the ZnS reaction, while the counting rate at 9 μsec were entirely due to the γ background from radiative neutron capture in lead,* then the contributions of these factors to the counting rate represented by curve 1 at other energies would be negligible.

RESULTS

Figure 2 shows the cross section for the reaction $Cl^{35}(n,p)$, measured as a function of energy. The curve is normalized to the thermal cross section $\sigma_{np} = 0.19 \pm 0.05$ barn.[12] The uncertainty in the absolute cross section is essentially due to the uncertainty in the thermal cross section, which is $\pm 26\%$. Figure 2 also shows the cross section for the (n,γ) reaction in chlorine.[1]

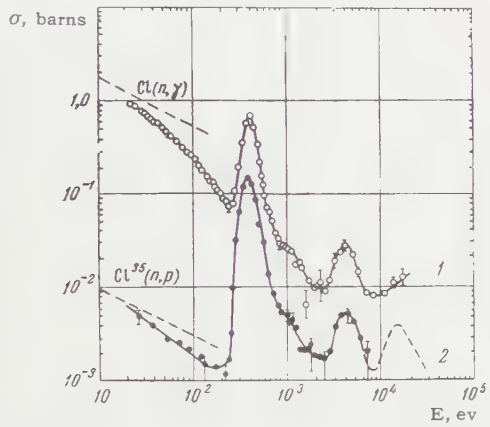

FIG. 2. Energy dependence of the cross sections for neutron capture in chlorine. Curve 1: cross section for the reaction $Cl(n,\gamma)$, measured with the naturally occurring mixture of isotopes and normalized to a cross section $\sigma_\gamma = 33.8$ barns at $E = 0.025$ ev.[12] Curve 2: cross section for the reaction $Cl^{35}(n,p)S^{35}$, normalized so that $\sigma(n,p) = 0.19 \pm 0.05$ barns at $E = 0.025$ ev.[12] The errors shown on the curve are statistical; an error also arises because the normalization is uncertain. Taking errors associated with the background also into account, this amounts to ~30%. At energies near 2 kev, the cross section might be a factor 2 less than that shown (because of inadequate corrections for background).

DISCUSSION OF THE RESULTS

1. Negative energy resonance. The dotted straight lines on Fig. 2 represent extrapolations of the thermal (n,γ) and (n,p) cross sections according to the 1/v law. The observed cross section falls off faster than this extrapolation, and this indicates a resonance at negative energies. This resonance occurs at $E_0 = -140$ ev according to an analysis of the total cross section[8] and at $E_0 = -210$ ev from an analysis of the capture cross section.[1] In the latter analysis, the relation $(\sigma_\gamma v)^{-1/2} = f(E)$ was assumed, where according to the Breit-Wigner formula for a narrow resonance ($\Gamma \ll |E_0|$) the function f should be given by

$$(\sigma_\gamma v)^{-1/2} = c(E - E_0). \qquad (1)$$

In the work being reported upon here, the analysis of reference 1 was improved in two ways. In the first place, the experimental values of $\sigma_\gamma v$ were corrected for the presence of the resonance at 405 ev, taking the instrumental resolution into account. The resolution of the apparatus was obtained from measurements of the (n,p) reaction, which showed that the baseline of the peak at 405 ev was very small. In the second place, the capture cross section was corrected for, assuming a 1/v law — i.e., (1) was replaced by the relation

$$[\sigma_\gamma v - \alpha(\sigma_\gamma v)_0]^{-1/2} = c(E - E_0), \qquad (2)$$

where $(\sigma_\gamma v)_0$ is the value of $\sigma_\gamma v$ at $E = 0$.

The experimental data are fitted best by $\alpha = 0$ and $E_0 = -210$ ev, although experimental errors are such that α could be less than 4×10^{-2}, which corresponds to $|E_0| > 175$ ev.* The (n,p) results do not contradict the resonance energy obtained from analysis of the (n,γ) data. However, the value of E_0 obtained from the (n,p) data is unreliable, since it is strongly dependent on the assumptions made about the background due to (n,α) and (n,γ) reactions.

2. Positive energy resonances. Both curves of Fig. 2 clearly show resonances at 405 ev and at 4.3 ± 0.3 kev. There is also a bump near 1 kev which may be due to a resonance at 1.1 ± 0.2 kev. The cross section for the (n,p) reaction showed a peak at ~ 15 kev; in this energy range, measurements are not reliable because of the large background due to the zinc and sulphur reactions. Since the (n,p) reaction is possible only for Cl^{35}, as was noted above, all the resonances refer to this isotope. In the total cross section measurements, Cl^{35} resonances have been observed at 405 ev,[8] 15 kev and 17 kev.[14]

Tables I and II show the level parameters calculated from the data on the (n,γ) and (n,p) re-

*The γ background due to capture of neutrons in the chlorine sample was small compared to γ-background from neutron capture in lead.

*Capture by the Cl^{37} isotope gives $\alpha = 0.5 \times 10^{-2}$, while resonances with positive energy give $\alpha < 0.1 \times 10^{-2}$. The direct capture of neutrons must follow the 1/v law,[13] but there are no data on the magnitude of direct capture for chlorine.

Table I. Parameters of neutron resonances in Cl^{35}

Parameter	E_0, ev				
	−210±10	405	1100±200	4300±300	(15 and 17)×10³
Γ_γ, ev	0.50±0.01	0.5*	0.5*	0.5*	
$\sigma_0\Gamma_\gamma$, barn-ev		120±10	~8	80±27	
$\sigma_0\Gamma_p$, barn-ev		16±5	~0.8	5.6±2.0	~10
$10^3\Gamma_p$, ev	2.4±0.8	70±22	~50	35±15	~100
γ^2_{0p}, ev**	70	[2.10³]	[~10³]	[8.10²]	~2·10³
γ^2_{1p}, ev**		9·10³	~6·10³	3.8.10³	
$10^3\Gamma_n$, ev***		26–65	4–30	250–700	(30+35)·10³[14]
γ^2_{0n}, ev**	7.4·10²	[1.0–1.7]	[0.1–0.2]	[3.3–5.8]	(1.2+1.4)·10²
γ^2_{1n}, ev**		(2–4.9).10³	(1–5)·10²	(5.6–16)·10²	
l	0 ($g=^5/_8$)	1	1	1	0

*The radiation widths are taken to be equal to the radiation width of the level at $E_0 = -210$ ev.

**γ^2_{0p} and γ^2_{0n} are the reduced proton and neutron widths calculated on the assumption that the resonance corresponds to orbital angular momentum $l = 0$; similarly, γ^2_{1p} and γ^2_{1n} correspond to the assumption $l = 1$.

***The magnitude of Γ_n depends on the assumption made about the spin of the compound nucleus Cl^{36} (see Table II).

Table II. Parameters of the resonances at 405 ev and 4.3 kev in Cl^{35} as a function of the statistical factor $g = (2J+1)/2(2l+1)$

E_0	g*	$10^3\Gamma_n$, ev	$10^3g\Gamma_n$, ev	Γ, ev	$\sigma_0\Gamma$, barn-ev	σ_0, бн
405 ev	$^3/_8$	65±5	25±2	0,64	155±15	240±25
	$^5/_8$	38±3	24±2	0,61	147±15	240±25
	$^7/_8$	26±2	22±2	0,60	144±15	240±25
4,3 kev	$^3/_8$	>700	>260	>1,2	>160	~140
	$^5/_8$	410±150	260±80	0,95	155±40	164±40
	$^7/_8$	250± 50	220±50	0,78	130±27	167±40

*The value $g = 1/8$ for the 405 ev level is inconsistent with the measured cross section for absorption, while for the 4.3 kev level it does not accord with measurements of the (n, γ) cross section.

actions. In the calculations the radiation widths of the various levels were taken equal to the radiation width of the level at −210 ev, i.e., equal to 0.5 ev.[1] Supplementary measurements of self-absorption were carried out for the resonance at 405 ev. These gave a value for the strength $\sigma_0\Gamma$ of the level of 120 ± 30 barn-ev per Cl^{35} nucleus, which agrees with the data of reference 1 (see Table II).

3. The negative energy resonance in Cl^{35} determines the cross section for capture of thermal neutrons and hence must be an s-resonance, i.e., corresponds to capture of a neutron with orbital angular momentum $l = 0$. If the resonances at 405 ev, 1.1 kev and 4.3 kev were also taken to correspond to $l = 0$, then the reduced neutron widths of these resonances* would come out to be two to three orders of magnitude smaller than the reduced neutron widths for the resonances at −210 ev and 17 kev (the last is an s-resonance[14]). Hence the resonances at 405 ev, 1.1 kev and 4.3 kev must have $l = 1$. For the 405 ev resonance, this conclusion contradicts the data quoted in reference 14; the 1.1 kev and 4.3 kev resonances are not noted in reference 14.

It should be noted that the reduced proton width for the negative energy resonance is very small.

In the energy range 0.5 to 2×10^4 ev the resonance integral $R = \int_{E_1}^{E_2} \sigma dE/E$ for the $Cl^{35}(n,p)$ reaction is equal to $R_p = 0.074 \pm 0.025$. For the (n,γ) reaction this integral is $R_\gamma = 14.0 \pm 0.8$ b.[1] The total resonance integral for absorption is thus equal to 14.1 ± 0.8 b, which is in satisfactory agreement with results obtained by other authors (12 barns[17] and 12.7 ± 1.7 barns[18]).

*The reduced partial widths γ^2_{1i} were calculated by dividing the measured partial widths Γ_i by twice the penetrability P_l: $\gamma^2_{1i} = \Gamma_i/2P_l$, where $P_l = kR/F_l^2 + G_l^2$ (for further details, see reference 15). The calculations were carried out using the tables in reference 16 and the formula $R = 1.3\,A^{1/3} \times 10^{-13}$ cm.

The authors would like to thank Yan I-min, who was very helpful in the early stages of this work.

[1] Kashukeev, Popov, and Shapiro, Нейтронная физика (Coll., Neutron Physics) Atomizdat, in press; J. Nucl. Energy (to be published).

[2] Gilbert, Roggen, and Rossel, Helv. Phys. Acta **17**, 97 (1944).

[3] M. Maurer, Z. Naturforsch. **4**, 150 (1949).

[4] Seren, Friedlander, and Turkel, Phys. Rev. **72**, 888 (1947).

[5] H. Berthet and J. Rossel, Helv. Phys. Acta **27**, 159 (1954), Helv. Phys. Acta **28**, 265 (1955).

[6] C. T. Hibdon and C. O. Muehlhause, Phys. Rev. **79**, 44 (1950).

[7] Toller, Patterson, and Newson, Phys. Rev. **99**, 620 (1955).

[8] Brugger, Evans, Joki, and Shankland, Phys. Rev. **104**, 1054 (1957).

[9] Bergman, Isakov, Popov, and Shapiro, Ядерные реакции при низких и средних энергиях (Nuclear Reactions at Low and Medium Energies), Academy of Sciences, U.S.S.R., 1958 (p. 141).

[10] Lazareva, Feĭnberg, and Shapiro, JETP **29**, 381 (1955), Soviet Phys. JETP **2**, 351 (1956).

[11] Bergman, Isakov, Murin, Shapiro, Shtranikh, and Kazarnovskii, Proc. Geneva Conference **4**, 166 (1955).

[12] D. J. Hughes and R. B. Schwartz, Neutron Cross Sections, BNL-325 (second edition, 1958).

[13] A. M. Lane and J. E. Lynn, Nucl. Phys. **17**, 563 (1960).

[14] Hughes, Magurno, and Brussel, Neutron Cross Sections, BNL-325 (Suppl. 1 to second edition, 1960).

[15] A. M. Lane and R. G. Thomas, Rev. Modern Phys. **30**, 257 (1958).

[16] Bloch, Hull, Broyles, Bouricius, Freeman, and Breit, Revs. Modern Phys. **23**, 147 (1951).

[17] P. Macklin and H. Pomerance, Proc. Geneva Conference **5**, 96 (1955).

[18] V. B. Klimentov and V. M. Gryazev, Атомная энергия (Atomic Energy) **3**, 507 (1957).

Translated by R. Krotkov
276

EXCITATION OF THE He^4 *NUCLEUS BY 150 Mev PIONS*

Yu. A. BUDAGOV, P. F. ERMOLOV, E. A. KUSHNIRENKO, and V. I. MOSKALEV

Joint Institute for Nuclear Research

Submitted to JETP editor January 10, 1961

J. Exptl. Theoret. Phys. (U.S.S.R.) 40, 1615-1617 (June, 1961)

An upper limit of 3.8×10^{-27} cm^2 has been obtained for the He^4 excitation cross section in reactions (1) and (2) by investigating the interaction between 150-Mev π^- mesons and helium in a diffusion cloud chamber. The total cross section and the cross section for inelastic π^--He interaction and also the cross sections for reactions (1) and (2) are presented.

MANY experimental data (see, e.g. Ref. 1) indicate the possible existence of a virtual state of the He^4 nucleus at an excitation energy of ~ 22 Mev. The analysis of Baz' and Smorodinskii[2] has shown that one can fit the experimental data to the following level parameters: spin and parity 2^-, isospin $T = 0$. Since the energy of the level is higher than both the proton (19.8 Mev) and the neutron (20.6 Mev) binding energy, the lifetime of the level is very short (level width ~ 2 Mev) and it is rather difficult to observe the level.

In the present paper we tried to estimate the probability of exciting the He^4 nucleus in the reactions

$$\pi^- + He^4 \to \pi^- + He^3 + n, \qquad (1)$$

$$\pi^- + He^4 \to \pi^- + T + p \qquad (2)$$

for an energy of the incoming meson of around 150 Mev.

The reactions (1) and (2) were investigated by means of a diffusion chamber[3] filled with helium at a pressure of 18 atm and placed in a magnetic field of 12 000 oe. The chamber was exposed to the π^- beam of the proton synchrotron of the Joint Institute for Nuclear Research. About 30 000 stereoscopic pictures were taken. They were scanned twice and 1802 events of π^--He^4 interaction were found. The kinematics of these events were determined by reprojection and 304 events of reaction (1) and 87 events of reaction (2) were identified.

The total π^--He^4 interaction cross section, i.e., the sum of the inelastic π^--He^4 cross section and of the cross sections for reactions (1) and (2) was found by measuring the total π^- track length in the chamber. The following values were obtained: $\sigma_t = (254 \pm 16)$; $\sigma_{nuc} = (171 \pm 12)$, $\sigma_1 = (53 \pm 6)$ and $\sigma_2 = (11.3 \pm 2.3) \times 10^{-27}$ cm^2.

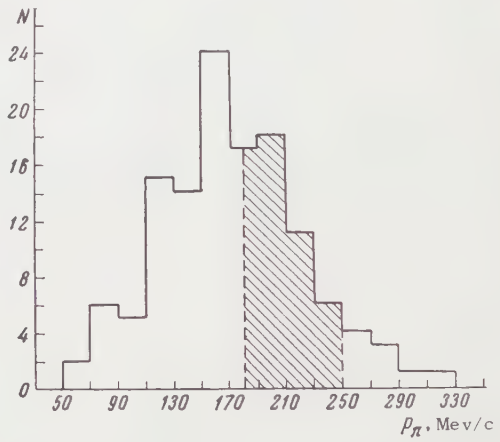

FIG. 1. Momentum distribution of π^- mesons from reaction (1) in the center-of-mass system.

If one assumes that the reactions that go through the excited state of He^4, namely

$$\pi^- + He^4 \to \pi^- + He^{4*} \to \pi^- + He^3 + n, \qquad (3)$$

$$\pi^- + He^4 \to \pi^- + He^{4*} \to \pi^- + H^3 + p \qquad (4)$$

happen with an appreciable probability, then one should observe in the center of mass system (c.m.s.) a peak at a momentum $p = 215$ Mev/c. It should have a width given by the energy uncertainty of the primary π meson beam and by the width of the level. It should be superimposed on the wide distribution originating from reactions (1) and (2).

The experimentally observed distribution of c.m.s. momenta of π^- mesons from reaction (1) is shown in Fig. 1. Only those events which allowed a determination of the π^- momentum to at least 10% by measurement of the radius of curvature (track length of the scattered π^- meson > 4 cm) were used. There were 127 such events. The analogous distributions from reaction (2) are plotted in Fig. 2: histogram (a) has been determined by

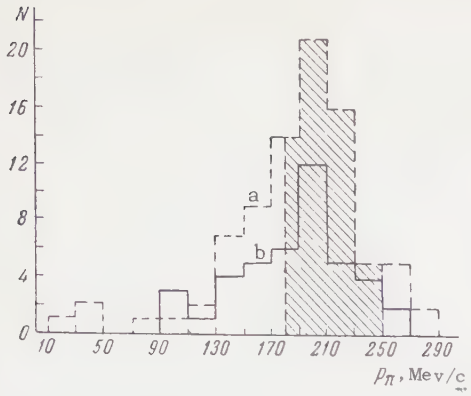

FIG. 2. Momentum distribution of π^- mesons from reaction (2) in the center-of-mass system.

measuring the angles of the outgoing particles and the momentum of the incoming π^- meson and contains 86 cases; histogram (b) contains 42 cases which allowed a determination of the momenta to at least 10% by measurement of the radius of curvature.

In order to estimate the cross section for excitation of a level at 22 Mev all events which had a π meson momentum in the interval 180 Mev/c $< p_\pi <$ 250 Mev/c (cross-hatched region in Figs. 1 and 2) were further analyzed. They were checked for kinematical consistency with reactions (3) and (4). These are: (i) The vectors of the momenta of He^{4*}, H^3, p, have to be coplanar. (ii) The emission angles of He^3, H^3 or p should not exceed the largest emission angle they could have in the laboratory system consistent with the supposed momentum of the He^{4*} particle if they would originate in the decay $He^{4*} \rightarrow He^3 + n$ or $He^{4*} \rightarrow H^3 + p$. (iii) The energy of the particles He^3, H^3 and p in the rest system of He^{4*} should lie in the interval consistent with the decay of He^{4*} with an excitation energy of 22 ± 1 Mev.

The above kinematical conditions were fulfilled within the accuracy of the measurements by 7 events of reaction (1) and by 7 events of reaction (2). This corresponds to an upper limit for the cross section for excitation of He^4 of 3.8×10^{-27} cm^2. Such a small contribution of reactions (3) and (4) to the total inelastic π^--He interaction (< 2.2%) is consistent with the experiments of Hofstadter et al.,[4] Tyren et al.,[5] and Selove and Teem.[6] There it was observed that the influence of the excited state in helium is very small indeed on the scattering of electrons of energy 400 Mev and of protons of 185 and 95 Mev.

The results of the present work also allow to conclude that the angular correlation observed by Kozodaev et al.[7] in the reaction $\pi^\pm + He^4 \rightarrow \pi^\pm + H^3 + p$ at an energy of 300 Mev can not be explained by an excited state of He^{4*}.

We express our gratitude to V. P. Dzhelepov, R. M. Sulyaev, and Yu. A. Shcherbakov for valuable discussions.

[1]Bogdanov, Vlasov, Kalinin, Rybakov, Samoĭlov, and Sidorov, Proc. of the All-Union Conf. on Nucl. React. at Low and Med. Energies, Moscow (1958).

[2]A. I. Baz' and Ya. A. Smorodinskii, JETP **27**, 382 (1954).

[3]Budagov, Viktor, Dzhelepov, Ermolov, and Moskalev, Synopsis of the Colloquium on Cloud Chambers, Diffusion Chambers and Bubble Chambers, Joint Inst. Nucl. Res., Dubna (1958).

[4]R. Hofstadter, Revs. Modern Phys. **28**, 214 (1956).

[5]Tyren, Tibell, and Marris, Nucl. Phys. **4**, 277 (1957); Hillman, Johansson, Tibell, and Tyren, Nucl. Phys. **12**, 596 (1959).

[6]W. Selove and J. M. Teem, Phys. Rev. **112**, 1658 (1958).

[7]Kozodaev, Kulyukin, Sulyaev, Fillippov, and Shcherbakov, JETP **38**, 409 (1960), Soviet Phys. JETP **11**, 300 (1960).

Translated by M. Danos
277

EXPERIMENTAL VERIFICATION OF THE $\Delta I = \frac{1}{2}$ SELECTION RULE IN THE LEPTONIC DECAY OF KAONS

D. V. NYAGU, É. O. OKONOV, N. I. PETROV, A. M. ROZANOVA, and V. A. RUSAKOV

Joint Institute for Nuclear Research

Submitted to JETP editor January 10, 1961

J. Exptl. Theoret. Phys. (U.S.S.R.) 40, 1618-1624 (June, 1961)

The relative probability for the decays $K_2^0 \to e^{\pm} + \pi^{\mp} + \nu$ has been measured with a cloud chamber containing a lead plate; these decays comprise 46 ± 11% of all decays with charged products. Four electron-positron pairs with large divergence angles were found and analyzed. It is shown that these events should be considered to be direct experimental evidence for the existence of the hitherto unobserved decay mode $K_2^0 \to 3\pi^0$. The value of the absolute probability for the decays $K_2^0 \to e^{\pm} + \pi^{\mp} + \nu$ determined from the mean life of the K_2^0 meson (with the $K_2^0 \to 3\pi^0$ mode taken into account) is consistent, within the experimental error, with twice the absolute probability for the decay $K^+ \to e^+ + \pi^0 + \nu$; this is evidence that the $\Delta I = \frac{1}{2}$ selection rule can be extended to leptonic K decays. An estimate of the absolute probability for $K_{\mu 3}^0$ decay is also consistent with the $\Delta I = \frac{1}{2}$ rule.

THE first isospin selection rule for hyperon and kaon decay processes was stated by Gell-Mann and Pais,[1] who proposed that the magnitude of the isospin could change by $\frac{1}{2}$ in non-leptonic decays. Further work showed that, within the experimental accuracies, all decays involving only strongly interacting particles are satisfactorily described by the $\Delta I = \frac{1}{2}$ selection rule (see, for example, the review article by Okonov[2]).

More recently Okun'[3] considered this rule within the framework of the composite model of elementary particles proposed by Sakata;[4] in this model the nucleon and Λ^0 are taken to be the fundamental particles. Okun' showed that if only four-Fermion interactions are considered, then the basic decay is $\Lambda^0 \to p + e^-(\mu^-) + \nu$, in which the isospin of the strongly interacting particles changes by $\frac{1}{2}$. In the framework of the Sakata model, all other leptonic decays of strange particles can be described as proceeding via this basic decay. It follows that the $\Delta I = \frac{1}{2}$ rule can be extended to K_{e3} and $K_{\mu 3}$ decays, with resultant expressions for the absolute decay probabilities

$$W(K_{e3}^0) = 2W(K_{e3}^+) \quad (1)$$

$$W(K_{\mu 3}^0) = 2W(K_{\mu 3}^+). \quad (2)$$

Marshak et al.[5] arrived at the same conclusion making the more general assumptions that the transformation properties in isospin space are the same for weak interactions of strange particles with and without lepton participation.

The first steps toward the verification of the $\Delta I = \frac{1}{2}$ rule for both leptonic and nonleptonic K decays were taken by Kobzarev and Okun'[6] and Okubo et al.,[7] who calculated the mean life of K_2^0 from experimental data on K^+ decay. The calculated value differed little from the experimental value.

However, a direct comparison of the absolute probabilities for leptonic decay of kaons [a check of the validity of Eqs. (1) and (2)] has not yet been made* for lack of experimental data on K_2^0 decay. In the cloud-chamber experiment of Bardon et al.,[9] several cases of K_{e3} and $K_{\mu 3}$ decay of K_2^0 were identified by the kinematics of the V^0 event and ionization measurements. However, as these authors themselves point out, they were not able to estimate with any accuracy the relative probabilities for these decays.

The present experiment is part of an investigation† of the properties of K_2^0 mesons with a cloud chamber and was performed with the proton synchrotron of the Joint Institute for Nuclear Research. Its purpose was the determination of the absolute probability for the decays $K_2^0 \to e^{\pm} + \pi^{\mp} + \nu$ and an estimate of the $K_{\mu 3}^0$ decay probability.

*An attempt at an experimental determination of the total probability for leptonic decay of K_2^0 was made by Crawford et al.[8]; in all, eight leptonic decays of K_1^0 and K_2^0 were observed.

†Partial results of this investigation have been published[10] and reported to the Rochester conference.[11] It should be mentioned that our communication was published in a strongly distorted form in the Proceedings of the Rochester Conference.

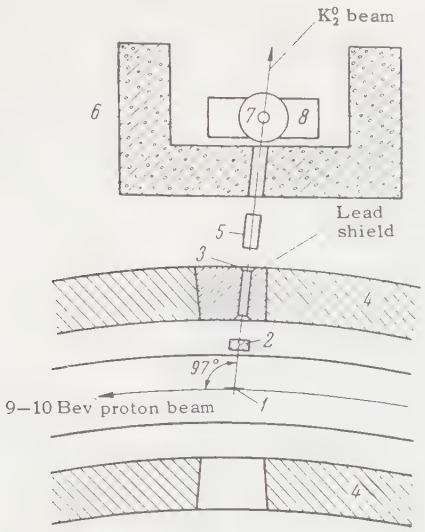

FIG. 1

In order to identify the decays, we placed in the chamber a 5.8 g/cm^2 lead plate perpendicular to the K_2^0 beam. The K_{e3}^0 decays were selected by measuring the momentum loss of the decay product on traversing the plate, since an electron has a high probability for a large energy loss by radiation in the plate. For example, the probability of loss by radiation of more than 30% of the electron's initial energy is 0.86.

The experimental arrangement is shown in Fig. 1. The source of the K_2^0 mesons was an internal 20 × 25 × 70 mm lead target placed in the beam of 9 — 10 Bev protons. The particles which come out of the target at an angle of 97° with the proton beam pass through a window in the wall of the accelerator vacuum chamber, through a 50 — 100 g/cm^2 lead converter, 2, and through a 30 × 120 mm lead collimator 1.5 m long, 3, set in an aperture, 4, in the iron yoke of the proton synchrotron magnet. Then the particle beam passes between the polepieces of a beam-purifying SP-63 magnet, 5, with a 10,000 oe field. Further on, the beam passes through a second lead collimator 1.5 m long with a 50 × 200 mm rectangular cross section set in the concrete shield, 6, and then into the cloud chamber, 7, which is in the field of an MS-4 electromagnet, 8.

The distance from the last collimator slit to the chamber was over 1 m, so that all K_1^0 particles produced in the collimator walls would decay on the way to the chamber. The cloud chamber was 8 m from the internal target. The chamber used has been described in detail in a previous paper.[12]

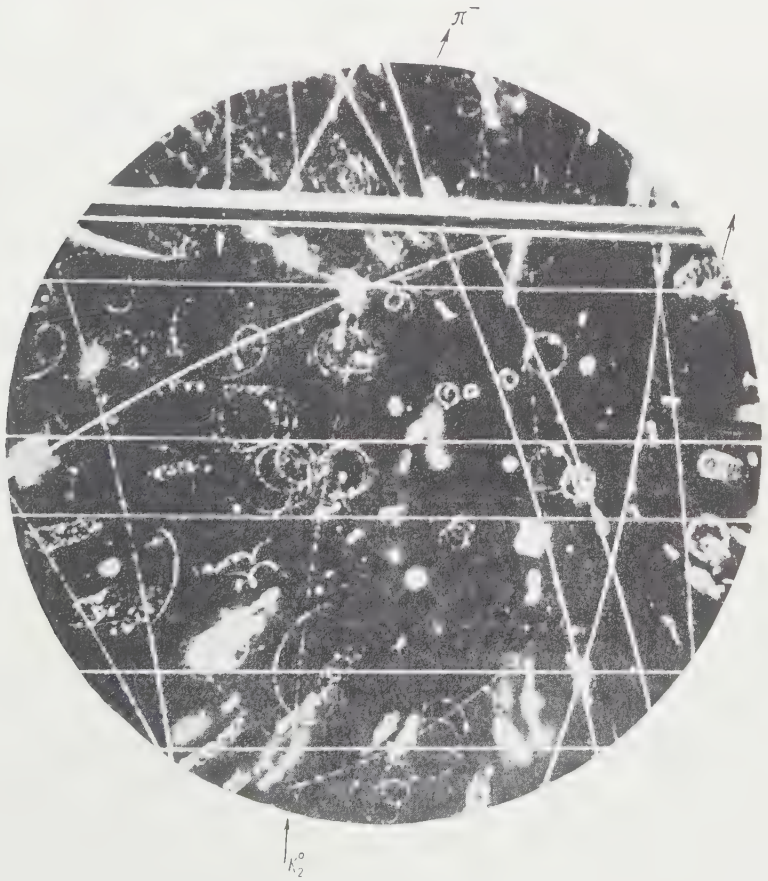

FIG. 2

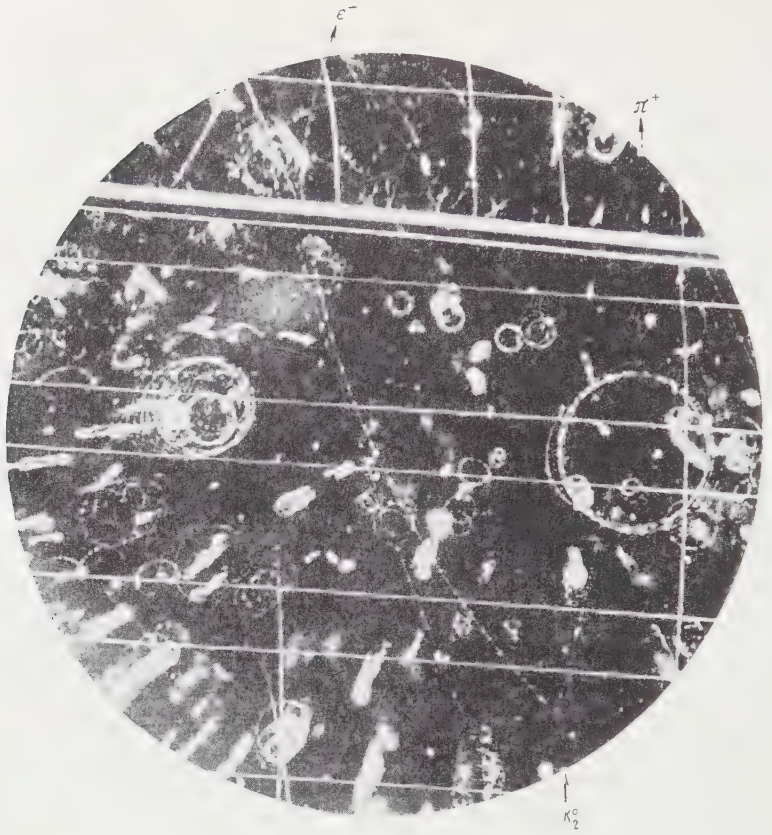

FIG. 3

In the present arrangement, the height of the illuminated region of the chamber was increased to 90 mm by enlarging the gap between the windings of the MS-4 magnet. The average magnetic field in the illuminated region was 15,000 oe with field inhomogeneity not exceeding 4%. The cylindrical glass wall of the chamber was 2 g/cm^2 thick.

EXPERIMENTAL RESULTS

In all, about 12,000 stereo pictures were made; they registered 670 V^0 decays and one four-prong event. About 40 events were identified as decays of Λ^0 particles produced by K_2^0 mesons in the lead plate and in the chamber walls. The remaining events were K_2^0 decays. With an average intensity of 5×10^8 accelerated protons per pulse, each picture showed about 10 protons knocked out of the chamber walls. The number of electron pairs detected was about a third of the number of V^0 events; only four pairs made large angles with the direction of the K_2^0 beam. The latter figure shows that the noise from uncollimated γ rays was very small in our apparatus; this allowed neutral $K_{3\pi}$ decays to be detected by their Dalitz pairs (pairs from the decay $\pi^0 \rightarrow \gamma + e^+ + e^-$).

Among the 440 K_2^0 decays detected in the chamber with the lead plate, 114 cases were observed in which charged decay products penetrated the plate; in each of these cases, because of the mode of illumination of the chamber, the particle would necessarily be observed after traversing the plate. Examples of cases in which such particles (π^- and e^-) traverse the plate are shown in Figs. 2 and 3. In all cases, the following were measured: momenta* of the decay product before and after passing through the lead plate, the angles at which the particle entered and left the plate, and also the momentum of the second decay product. In all, 24 cases of plate penetration were found in which the particle lost more than 30% of its momentum (18 cases) or stopped in the plate (5 cases) or made a star (1 case). In each case, as can be seen from Table I, the observed energy loss or stopping cannot be due to ionization loss.

In six cases of penetration, showers of two or three electrons were observed. For these, the average momentum of the shower particles is shown in the second column of the table. Clearly,

*The error of the momentum measurement did not exceed 10%.

Table I

Particle momentum, Mev/c		Momentum loss, %	Lead thickness g/cm²	Momentum of second particle, Mev/c
before penetration	after penetration			
279	Star	—	6.5	148
209	Stopped	—	7.1	68
225	137 shower	39	6.0	—
270	63 "	77	6.0	193
135	45 "	67	5.9	68
202	32	84	5.9	36
229	59 shower	74	5.8	301
290	144	51	6.1	99
126	27 shower	79	5.9	248
310	144	54	5.8	252
150	9	94	8.8	—
189	18	90	8.8	234
117	22	81	6.2	158
283	54	81	5.9	166
351	225	36	7.1	99
193	113	41	6.3	—
144	77	47	5.9	410
113	50	56	6.2	207
144	Stopped	—	8.4	148
148	16 shower	89	6.5	135
218	140	36	7.1	50
236	Stopped	—	5.9	92
180	"	—	10.0	—
—	"	—	6.0	270

all of the penetrations with momentum loss greater than 30% must be identified as electron penetrations. The five particles that stopped may be electrons or pions that produce prongless stars. In order to find the true number of electron plate penetrations it is necessary to correct first for the cases of penetration in which the momentum loss is less than 30% and then subtract the number of pions that produce prongless stars from the total number of stopped particles.

The first correction was found for each case of penetration by using the Eyges formulas[13] for the probability distribution of the total electron energy loss due to radiation and ionization. This method yielded an addition of three events. The second correction was taken to be equal to the number of nuclear interactions with the lead nuclei that would be produced by all the decay products that penetrated the plate (excluding electrons and muons) if the cross section were geometrical.* The correction was three events. Thus, the true number of electron penetrations is 24.

In order to determine the relative probability of K_{e3} decay, a correction must be made for the motion of the decaying K_2^0. It can easily be shown that the motion of the K_2^0 leads to an increase in the number of heavy decay products (pions and muons) penetrating the plate as compared to the number of penetrations of light decay products (electrons and neutrinos). Obviously, this correction is equal to the ratio of the solid angles (in the center-of-mass system of the K_2^0) within which the emitted pions or electrons penetrate the plate. In calculating this correction we used a value of about 120 Mev for the average energy of the decaying K_2^0 particles; this value was determined from the momentum measurements (Table I) with the assumption that the energy spectra of electrons and neutrinos are identical in K_{e3} decay. The result was that the number of electron penetrations of the plate should be multiplied by a factor of 1.1 to correct for the motion of the K_2^0 particles.

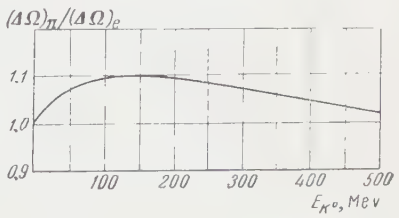

FIG. 4

Figure 4 shows the dependence of this correction on the K_2^0 energy. From the curve it is clear that we do not make a significant error by using an average energy of the K_2^0 particles* (100 Mev) to determine this correction

Our final result is that the corrected number of electron penetrations is 26. This corresponds to a K_{e3} decay probability $q = 0.46 \pm 0.11$ relative to all decays with charged products. The error is a mean square composed of the statistical error and the errors in the selection of events and in the corrections.

*The number of muons that penetrated the plate is roughly estimated at 25. The correction for possible stoppings of elastically scattered pions is negligibly small.

*Our estimate of the average K_2^0 energy is somewhat too high.

The four observed electron-positron pairs, interpreted as Dalitz pairs from the decay $K_2^0 \to 3\pi^0$ (and discussed below), make it possible to evaluate the relative probability for this decay mode (under our conditions, the calculated efficiency for detection of Dalitz pairs was about 75%). Our value for the relative probability is $w(K_2^0 \to 3\pi^0)/\Sigma w = 0.18 \pm 0.09$.* From this we can now determine the probability for the decay $K_2^0 \to e^{\pm} + \pi^{\mp} + \nu$ relative to all K_2^0 decays (0.38 ± 0.10), and, from the lifetime of the K_2^0

$$\tau(K_2^0) = \left(6.1 \begin{smallmatrix} +1.6 \\ -1.1 \end{smallmatrix}\right) 10^{-8} \text{ sec},$$

we can find the absolute probability for K_{e3}^0 decay; the latter is $w(K_{e3}^0) = (6.2 \pm 2.0) \times 10^6$ sec^{-1}.

The fraction of $K_2^0 \to 3\pi^0$ decays can also be estimated under the assumption that the $\Delta I = \frac{1}{2}$ rule holds for $K \to 3\pi$ decays; from this assumption it follows that the $K^+ \to 3\pi$ and $K_2^0 \to 3\pi$ absolute probabilities are equal and also that $K_2^0 \to \pi^+ + \pi^- + \pi^0$ and $K_2^0 \to 3\pi^0$ are related.[6,7] Using this assumption and the experimental values for the $K^+ \to 3\pi$ branching ratio $(7.7 \pm 0.7)\%$[14] and mean life $(1.21 \pm 0.01) \times 10^{-8}$ sec, we find the relative probability for $K_2^0 \to 3\pi^0$ to be 0.30 ± 0.03 and the absolute probability for $K_2^0 \to e^{\pm} + \pi^{\mp} + \nu$ to be $(5.8 \pm 1.8) \times 10^6$ sec^{-1}.

Both of the above absolute probabilities for K_{e3}^0 decay agree within experimental error with twice the probability of the corresponding K decay:[14,15] $2w(K_{e3}^+) = (8.4 \pm 1.2) \times 10^6$ sec^{-1}. This agreement is evidence that the $\Delta I = \frac{1}{2}$ rule may be extended to leptonic K decays. However, final confirmation of this rule awaits more accurate determinations of both the K_{e3} relative probability and the K_2^0 mean life.[7]

Table II

Case No.	Momentum, Mev/c		Angle with beam, deg	Divergence angle, deg
	+	−		
1	55	42	7 — 9	65
2	10	43	99	50
3	111	103	19	70
4	26	79	25	10

It should be noted that the detection of one four-prong decay and four electron pairs with large divergence angles allows a rough experimental determination of the fraction of K_2^0 particles that decay into three pions. If all four pairs, with parameters shown in Table II, are taken to be Dalitz pairs from $K_2^0 \to 3\pi^0$, then we find that the total number of $K_{3\pi}$ decays is about 30 per cent of the total number of K_2^0 decays. This is not in disagreement with the $\Delta I = \frac{1}{2}$ rule, which predicts equality of the absolute probabilities for $K^+ \to 3\pi$ and $K_2^0 \to 3\pi$. The absolute probability for $K_2^0 \to \mu^{\pm} + \pi^{\mp} + \nu$ determined from the experimental values of the K_{e3}^0 and $K_{3\pi}^0$ branching ratios is $(5.6 \pm 3.0) \times 10^6$ sec^{-1}, and agrees within experimental error with twice the $K_{\mu 3}^+$ probability $(6.8 \pm 0.8) \times 10^6$ sec^{-1}.

The analysis of the large-angle electron pairs is of interest as a proof of the existence of the $K_2^0 \to 3\pi^0$ decay mode. There is uncertainty in the identification of only the third of the four pairs shown in Table II; because of the background, sufficiently accurate ionization measurements could not be made on the decay products. In the remaining cases, the identification is beyond doubt.

What is the nature of these pairs? The fourth could be, in principle, the result of conversion of a "beam" γ ray by the chamber gas, since the probability that one of the electron pairs observed in the direction of the incident beam have a divergence angle greater than $20 - 25°$ is 0.6.* Because of their large angles with the incident beam, the first two pairs cannot be attributed to this process. Nor can they be attributed to conversion of non-collinear rays, since in that case several hundred pairs with smaller divergence angles would have been observed. The electron-positron pairs we detected cannot be Dalitz pairs from the decay of π^0's created by "beam" neutrons striking the nuclei in the chamber gas, since not a single star with an electron-positron pair was detected. Moreover, an estimate made on the basis of the observed production of charged pions shows that the probability of observation of a single Dalitz pair from the decay of a π^0 produced in a prongless star is less than 10^{-2}. At the same time, the decay of a K_2^0 into π^0 mesons accounts very well for all the features of the observed Dalitz pairs.

Since we did not detect a single decay of the long-lived K^0 into π^+ and π^-, the decay $K_2^0 \to 2\pi^0$ is extremely improbable. The probabilities of other K_2^0 decays involving π^0 mesons and other neutrals (for example, $K_2^0 \to 2\pi^0 + \gamma$) are also very small.

Thus, there is every reason to ascribe the observed Dalitz pairs to the decay $K_2^0 \to 3\pi^0$. Therefore, the very fact that they are observed must be considered as direct experimental evidence for

*As will be evident from the discussion of the properties of these pairs, this value may be too high.

*This probability was determined from the distribution calculated by Borsellino.[16]

this decay. The ratio of the number of single Dalitz pairs and the number of four-prong events due to the $K_2^0 \to \pi^+ + \pi^- + \pi^0$ decay with a Dalitz pair is also evidence in favor of this interpretation.[10*]

In conclusion, the authors express their gratitude to the proton synchrotron crew for making this experiment possible. The authors are also grateful to B. M. Pontecorvo for his constant interest in this work and for evaluation of the results, to V. P. Dzhelepov and V. I. Veksler for aid in performing the experiment, to L. B. Okun' and I. V. Chuvilo for useful comments, and to M. P. Anikina, V. A. Smirnov, and P. I. Zhabin for helping with the measurements.

[1] M. Gell-Mann and A. Pais, Proceedings of the Glasgow Conference, 1954.

[2] É. O. Okonov, Fortschr. Physik **8**, 42 (1960).

[3] L. B. Okun', JETP **34**, 469 (1958), Soviet Phys. JETP **7**, 322 (1958).

[4] S. Sakata, Progr. Theoret. Phys. **16**, 696 (1956).

[5] Okubo, Marshak, Sudarshan, Teutsch, and Weinberg, Phys. Rev. **112**, 665 (1958).

[6] Yu. I. Kobzarev and L. B. Okun', JETP **34**, 763 (1958), Soviet Phys. JETP **7**, 524 (1958).

[7] Okubo, Marshak, and Sudarshan, Phys. Rev. Lett. **2**, 12 (1959).

[8] Crawford, Cresti, Douglas, Good, Kalbfleisch, and Stevenson, Phys. Rev. Lett. **2**, 361 (1959).

[9] Bardon, Lande, Lederman, and Chinowsky, Ann. Phys. **5**, 156 (1958).

[10] Okonov, Petrov, Rozanova, and Rusakov, JETP **39**, 67 (1960), Soviet Phys. JETP **12**, 48 (1961).

[11] Nyagu, Okonov, Petrov, Rusakov, and Rozanova, Proceedings of the Rochester Conference, 1960, p. 603.

[12] Dzhelepov, Kozodaev, Osipenkov, Petrov, and Rusakov, Приборы и техника эксперимента (Instrum. and Exptl. Techniques) **3**, 3 (1956).

[13] L. Eyges, Phys. Rev. **76**, 264 (1949).

[14] C. O'Ceallaigh and G. Alexander, Proceedings of the Rochester Conference, 1957.

[15] Bruin, Halthnigen, and Jengejans, Nuovo cimento **9**, 422 (1957).

[16] A. Borsellino, Phys. Rev. **89**, 1023 (1953).

*The $\Delta I = \frac{1}{2}$ rule gives 2 for the ratio of $K_2^0 \to 3\pi^0$ to $K_2^0 \to \pi^+ + \pi^- + \pi^0$.

Translated by M. Bolsterli
278

EMULSION STUDY OF THE INTERACTION BETWEEN 8.7-Bev PROTONS AND QUASI-FREE NUCLEONS

K. I. ALEKSEEVA, G. B. ZHDANOV, E. A. ZAMCHALOVA, M. I. TRET'YAKOVA, and M. N. SHCHERBAKOVA

P. N. Lebedev Physics Institute, Academy of Sciences, U.S.S.R.

Submitted to JETP editor January 11, 1961

J. Exptl. Theoret. Phys. (U.S.S.R.) **40**, 1625-1637 (June, 1961)

The angular and momentum distributions of protons and π mesons from stars produced by 8.7-Bev protons in photographic emulsion and containing no more than one gray and one black track are investigated. It is shown that most stars of this type can be regarded as resulting from inelastic interactions between the proton and a free or quasi-free nucleon. Interactions of this type comprise ~ 25% of the total number of inelastic interactions with nuclei of the emulsion. The angular and momentum distributions of the protons and mesons (in the nucleon-nucleon c.m.s.) are compared with the predictions of the peripheral[12] and central[1,10,11] interaction theories. It is shown that part of the interactions with quasi-free nucleons (about 20%) cannot be ascribed to peripheral interactions, mainly because of the large emission angles and large transverse momenta of the secondary protons. Nevertheless, the characteristics of most of the cases agree with the properties expected for peripheral interactions.

In a previous experiment,[1] we studied the angular distributions of secondary particles in stars produced by the interactions between 8.7-Bev protons and emulsion nuclei. It was shown that an appreciable part of such stars (at least 15%) are characterized by a narrower angular distribution of the particles in comparison with the predictions of the theory of central interactions with one nucleon, and even more so with several nucleons. It was noted that these interactions are apparently peripheral nucleon-nucleon interactions. In the present study, we investigated the energy and angular characteristics of different kinds of particles emitted in interactions of the nucleon-nucleon type.

1. EXPERIMENTAL METHOD

In this work, we used part of an emulsion stack (stack No. 13, NIKFI-BR emulsion) of 10 × 10 cm pellicles exposed to the 8.7-Bev proton beam at the Joint Institute for Nuclear Research.

The basic problem of the experiment was to study the energy and angular distribution of secondary particles in interactions between the incident nucleon and a free or quasi-free nucleon. By interactions with a quasi-free nucleon we have in mind those in which only a very small part (< 2%) of the primary energy in the laboratory system is transferred to other nucleons of the same nucleus.*

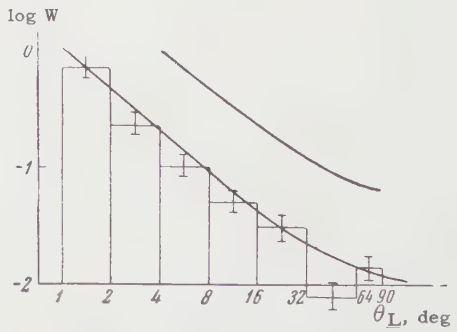

FIG. 1. Probability W of finding tracks with a minimum length L_{min} in one emulsion pellicle (histogram – experimental data; solid lines – calculated results; upper curve represents L_{min} = 2 mm, and lower curve L_{min} = 10 mm). Geometrical correction $k_g = W^{-1}$.

About 2000 stars were found as a result of the scanning of the emulsion pellicles (mainly by scanning along the tracks of the primary proton beam and only partially by area scanning). From these stars, we selected 330 stars of different types which contained tracks flat enough so as to permit accurate measurements of the particle momentum (p) and ionization (I).

*Such a definition practically excludes not only central collisions but also peripheral collisions with other nucleons.

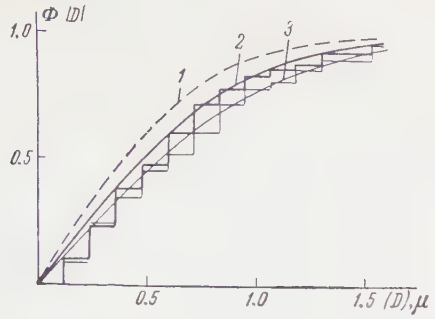

FIG. 2. Integral distribution of second differences of the coordinates from measurements of primary proton beam tracks (2) for a cell length of 2000 μ. Shown for comparison are the corresponding distributions for Coulomb scattering (1) at 9.2 Bev/c and for a group of secondary particles (3) of measured momentum greater than 6 Bev/c.

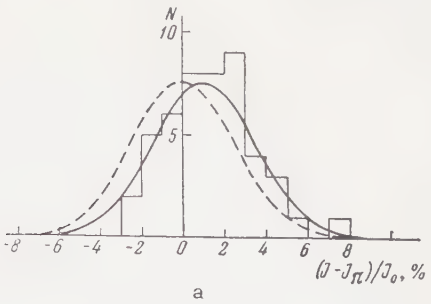

a

FIG. 3a. Results of measurements of relative ionization for π mesons in the region of the minimum of the ionization vs. momentum curve ($p\beta = 0.4 - 0.8$ Bev/c). Taken as the zero value of the axis of abscissas is the theoretical value of the ionization for π mesons at the position of the minimum.

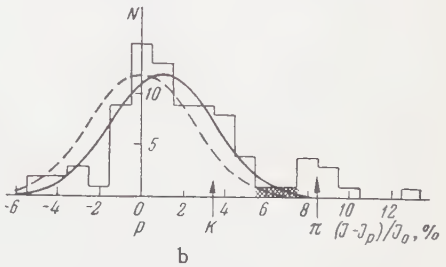

b

FIG. 3b. Results of measurements of the relative ionization for particles of momenta $p\beta > 2.5$ Bev/c. Taken as the zero value on the abscissa axis is the theoretical value of the ionization for a proton of this momentum (also shown are the positions of the maxima of the corresponding curves for K and π mesons).

We determined (as a function of the laboratory space angle θ_L) the geometrical correction k_g necessary for the analysis of all angular and momentum distributions (see Fig. 1). The corrections for fast and slow particles were different (curves 1 and 2, respectively). It should be mentioned that the very strict selection criteria as regards the dip angle δ of the fast tracks which were to be measured (length $L \geq 1$ cm in one pellicle, which corresponded, on the average, to angles $\delta \leq 1°$) were dictated by the very strong dependence of spurious scattering on the angle δ as was observed by us in some pellicles.

The statistical error of the momentum measurements was, as a rule, 25%; spurious scattering and "noise" were determined from measurements on primary proton tracks (in the same pellicle). The results of such measurements are shown in Fig. 2. In the region of the greatest momentum (≥ 6 Bev/c), where it was difficult to take into account spurious scattering in individual cases, we usually resorted to a statistical treatment of the data for a group of tracks; the mean value of the momentum of such particles was 7.5 Bev/c.

The total error in the measurement of the relative ionization I/I_0 on secondary particle tracks (with respect to primary beam tracks at the same place in the pellicle) was estimated as $\sim 2\%$, which is confirmed by the spread in the values of I/I_0 for π mesons in the region of the ionization curve minimum (Fig. 3a). In all cases the measurements were repeated. The particles were identified with the help of the curves of Barkas.[2]

In the region bordering on the point of intersection of the proton and π-meson curves ($p\beta = 1.5 - 2.5$ Bev/c), where it is not possible to identify the particles with the required accuracy, we made a statistical analysis of the sign of the charge of the particles based on the study of the magnetic deflection in the field of the accelerator.[3] We thus obtained the ratio $N_+ : N_- = 1.50 \pm 0.50$.

As additional information, we used data obtained by electronic methods at the Joint Institute for Nuclear Research* concerning the composition of a beam of positive charged secondary particles for the angle $\theta_L = 1°$, momentum p = 2.25 Bev/c, and a copper target, and for $\theta_L = 3°$, p = 2.9 Bev/c and a beryllium target; in both cases the ratio of the number of π^+ mesons to the number of protons was $N_{\pi^+} : N_p \approx 0.8 : 1$. If we take into account the values for $N_+ : N_-$ and $N_{\pi^+} : N_p$, we obtain for the ratio of the number of mesons of both signs to the number of protons $N_{\pi^\pm} : N_p = 3 : 1$.

Figure 3b shows the distribution of the relative ionization for secondary particles of momentum $p\beta > 2.5$ Bev/c. It is seen that in the great majority of cases, π mesons are well-separated from protons. (In the figure, the "zone of indetermi-

*The authors thank M. F. Likhachev, V. S. Stavinskiĭ, Hsu Yun-Ch'ang and Chan Nai-Sen for permission to use the results of their measurements prior to publication.

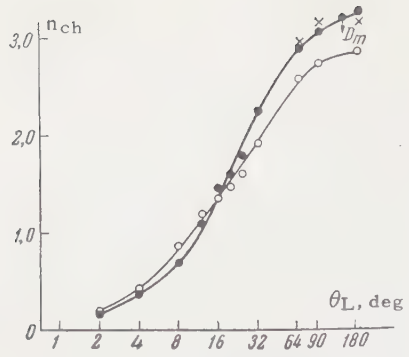

FIG. 4. Angular distribution of relativistic or gray tracks n_{ch} (in lab system) for stars of type $n_b \leq 1$, $n_g \leq 1$ (without elastic scatters): ● – pp interactions (69 stars with even values of $n_s + n_g$), ○ – pn interactions (58 stars with odd values of $n_s + n_g$). Points indicated by crosses were calculated from the requirement of symmetry in the c.m.s. distribution with respect to the angle 90° (for even values of $n_s + n_g$). Here, and in the figures which follow, the arrow indicates the allowable deviation for the 95% confidence level (D_m) according to the Kolmogorov test.

nacy'' in which the probabilities of identifying particles as protons and π mesons differ by a factor less than three, is shown cross-hatched.)

2. SEPARATION OF INTERACTIONS WITH QUASI-FREE NUCLEONS

The usual procedure for separating interactions with individual nucleons of the emulsion nuclei (see, for example, reference 4) involves the selection of events in which the nucleus as a whole does not experience any visible excitation (including β decay in the case of pp interactions). Usually, about 10% of all interactions observed in emulsion are selected in this way. An additional, although weak, ''sifting out'' of non-nucleon interactions is made by the application of the modified kinematical criterion of Birger and Smorodin[5] based on the laws of conservation of energy and momentum of all particles before and after the interaction. In individual cases, however, this criterion is a necessary condition, but is far from satisfactory, owing to the scanty information on the energy characteristics of all the interaction products.

On the other hand, whenever we have to do with a statistical analysis of data on a comparatively large number of interactions, it turns out to be possible to limit ourselves to the kinematical criterion, which, under some quite natural assumptions, changes, generally speaking, from a necessary into a necessary and sufficient condition. Actually, we assume that it is possible to find some characteristic, in particular, a small number of black and gray tracks, which distinguishes interactions with a ''target'' mass quite close to the mass of a nucleon. Since there are no targets with a mass smaller than that of a nucleon, one can then also calculate the upper limit of a possible ''contamination'' of interactions of a non-nucleon type in the group of interactions.

The method employed by us to determine the average mass of the ''target'' $\overline{M}_T$ from data on the angular and momentum distribution of the secondary mesons and protons was based on the relation

$$\overline{n_N (E_L - p_L^{\perp} c)} + k_0 \overline{n_{\pi^\pm} (E_L - p_L^{\parallel} c)_{\pi^\pm}} = 1.05\, M_N c^2, \quad \text{(1a)}$$

where n_N and $n_{\pi^\pm}$ are the numbers of secondary nucleons and charged π mesons having a given value of the quantity $E_L - p_L^{\parallel} c$, which is the difference between the total energy and the longitudinal momentum in the laboratory system; $k_0 = 1.5$* is a coefficient taking into account (on the average) neutral mesons; M_n is the nucleon mass. Here it was assumed that the average energies and the longitudinal momenta of the charged and neutral nucleons (or, correspondingly, mesons) are the same. The quantities $(\overline{E}_L - \overline{p}_L^{\parallel} c)_p$, $(\overline{E}_L - \overline{p}_L^{\parallel} c)_\pi$, and $\overline{n}_{\pi^\pm}$ can be determined from an analysis of the angular and energy characteristics of π mesons and protons. In order to obtain more accurate angular distributions, we made use of the data (see Fig. 4) obtained in a previous work[1] for 127 stars of the type $n_b \leq 1$ and $n_g \leq 1$ found without any bias and not including cases which can be regarded as elastic scattering of the primary proton (see below).

As seen in Fig. 4, the character of the angular distribution for 69 stars with an even number of shower (n_s) and gray (n_g) tracks is in agreement with the assumption that the angular and momentum distributions of protons and mesons are symmetric about the angle $\theta_0 = 90°$ in the nucleon-nucleon c.m.s. for pp interactions.† If it is assumed that there is full symmetry of the angular and momentum distributions for both protons and mesons (relative to the angle $\theta_0 = 90°$), then, after summation of symmetric particles by pairs, relation (1a) becomes equivalent to a c.m.s. energy balance:‡

*In particular, the closeness of k_0 to 1.5 is confirmed by the appropriate statistical-theory calculations made by V. M. Maksimenko for the case of central interactions.

†At the same time, for odd values of $n_s + n_g$ (pn interactions) there is a very marked asymmetry evidently connected with the asymmetry in emission of protons.[4]

‡Omitted from relation (2) is that small part of the energy which can be released in a nuclear disintegration in accordance with the foregoing definition of a quasi-free nucleon of the target.

$$\bar{n}_N \bar{E}_{0p} + k_0 \bar{n}_{\pi^\pm} \bar{\epsilon}_{0\pi} = 2\gamma_c M_N c^2. \quad (2)$$

Here $\bar{E}_{0p}$ and $\bar{\epsilon}_{0\pi}$ are the mean c.m.s. energies of the protons and mesons, respectively, which can be determined experimentally by means of the momentum and angular characteristics of the particles in the forward cone. As will be seen from what follows, the value of $\bar{n}_N$ obtained by us with the aid of relation (2) is 2.0 ± 0.2, which corresponds to a possible mixture of collisions with two nucleons ($n_N = 3$) of up to 20%.

Hence the selection of stars on the basis of a small number of black ($n_b \leq 1$) and gray ($n_g \leq 1$) tracks separates interactions characterized by an average "target" mass close to M_N. The total number of such interactions is then ~ 25% of all interactions with emulsion nuclei. On this basis, one can calculate that the ratio of interactions of type pp to pn in these stars should be ~ 1.2. It should be noted that for stars with $n_b = 2.3$ (with $n_g \leq 1$) the average mass of the target already turns out to be significantly greater than M_N, and, at the same time, the departure from symmetry relative to the angle $\theta_0 = 90°$ in the angular distribution is quite marked.

In the analysis of stars with a small number of particles, both slow and fast ($n_s + n_g$), a certain role can, generally speaking, be played by a mixture of cases of elastic scattering, whose cross section[6] is ~ 85% of the cross section for inelastic interactions of protons with light and heavy emulsion nuclei. However, only a small part of the cases of elastic scattering (< 2%) involves a deflection of the proton by an angle $\theta_L \geq 1.5°$ with respect to the primary particle, and therefore the discarding of all cases in which the proton is deflected by an angle $\theta_L \leq 1.5°$ ensures a practically complete elimination of cases of elastic scattering.

As regards weak excitation of the residual nucleus associated with the presence of one black track, and sometimes even a recoil nucleus, this can evidently be made to agree with the obtained target mass M_N (on the average) if one takes into account the presence of internal (Fermi) motion of the quasi-free nucleons involved in the interactions with the primary particles. Indeed, as a result of the interaction, the residual nucleus should acquire a recoil momentum equal in magnitude, but of opposite sign, to the momentum of the nucleon leaving the target. For light nuclei, the rms value of this momentum is ~ 350 Mev/c.

We compared the estimate obtained above for the fraction of collisions with quasi-free nucleons in emulsion nuclei (~ 25%) with existing information on the character of the proton distribution in nuclei.[8] To do this, we assumed that the distributions of neutrons and protons coincide. Furthermore, instead of the optical model usually employed for the calculation of the transparency of nuclei, we used the rougher model of successive collisions with nucleons encountered along a chord of length determined by the collision parameter (with a subsequent averaging over the collision parameters).

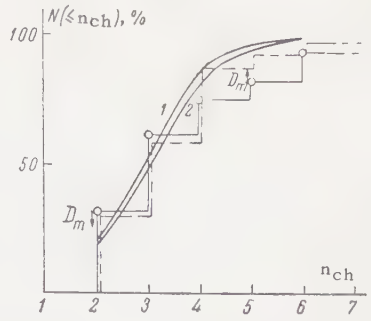

FIG. 5. Integral distributions of the number of charged products per star ($n_{ch} = n_s + n_g$). The solid-line histogram represents the experimental results of the present work; the dashed-line histogram represents the results obtained in reference 14. Curves 1 and 2 are the theoretical results for peripheral[12] and central[1,11,12] interactions, respectively.

On the basis of a similar model, we calculated the cross sections for inelastic interactions and the total cross sections for emulsion nuclei with the aid of the corresponding cross sections for the elementary processes: $\sigma_{inel} = 25$ and $\sigma_{tot} = 33$ mb.* The results of the calculations agree with good accuracy (5 — 7%) with the corresponding results of Barashenkov[9] obtained with the optical model of the nucleus.

Using the same model for the calculation of the number of collisions with one nucleon, we obtained estimates of 45 and 42%, respectively, of the cross sections σ_{inel} and σ_{tot} (interactions with two nucleons constitute ~ 20%). If we impose the additional condition that the secondary particles produced in the first interaction do not encounter any nucleons in their paths, we then estimate that 30% of the interactions take place with one nucleon.

3. ANGULAR AND MOMENTUM DISTRIBUTIONS OF PARTICLES IN INTERACTIONS WITH QUASI-FREE NUCLEONS

For the selected stars of type $n_b \leq 1$, $n_g \leq 1$ in which we identified and measured ~ 80 particles and which could be considered mainly as nucleon-

*Later measurements recently made at CERN (private communication) indicate that it is more correct to take the value $\sigma_{inel} = 30$ mb and $\sigma_{tot} = 38$ mb.

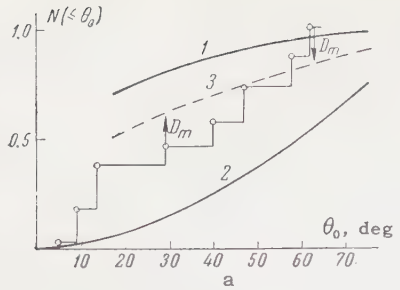

FIG. 6a. Integral c.m.s. angular distribution for protons. Curves 1 and 2 are the theoretical distributions for peripheral[12] and central[1,11,12] (isotropy) interactions; curve 3 is the distribution for a mixture of interactions of both types (70% N_{periph} + 30% N_{centr}).

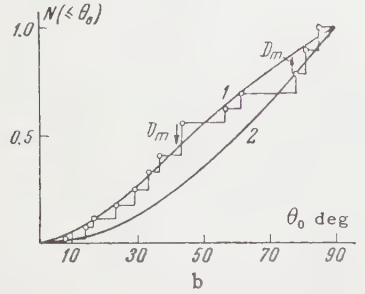

FIG. 6b. Integral c.m.s. angular distribution for π mesons. The notation is the same as in Fig. 6a.

nucleon interactions, the following characteristics were studied: 1) the distribution of the number of shower and gray tracks ($n_{ch} = n_s + n_g$) per star; 2) the c.m.s. angular distribution of protons and mesons; 3) c.m.s. total and transverse momentum and energy distributions for protons and mesons; 4) dependence of the mean momentum of the particles on the c.m.s. angle of emission. The greater part of these characteristics were compared with theoretical calculations based on two extreme assumptions as regards the interaction mechanism: a) central interaction of nucleons with the formation of a single excited system with zero angular momentum;[1,10,11] b) interaction of the peripheral type characterized by the exchange of one meson between the colliding nucleons.[12]

1. The integral distribution of the number of relativistic and gray tracks n_{ch} for $n_{ch} \geq 2$ is shown in Fig. 5.* As seen from the figure, the n_{ch} distribution is not a sufficiently sensitive characteristic for separating central and peripheral interactions. Along with the agreement of the experimental data ($\bar{n}_{ch} = 3.1 \pm 0.2$) with the mean multiplicity expected in the case of central and peripheral interactions (3.4 and 3.2, respectively), it should be noted that a considerable part of the stars with $n_{ch} > 6$ (constituting 5% of all cases) can in no way be explained by single collisions, and they should probably be ascribed chiefly to double inelastic interactions of nucleons in the nucleus. Moreover, the ratio of the number of stars with even n_{ch} to the number with odd n_{ch} 69:58 is in good agreement with the estimate given above for the relative numbers of pp and pn interactions.

2. The proton and meson angular c.m.s. distributions (in the forward hemisphere) are given in Figs. 6a and 6b, respectively. In the case of the former, the (π, p) particles, not identifiable directly, were not included because the angle θ_0 was not determined for them with sufficient accuracy.

It is seen from Fig. 6a that there is a considerable excess of protons in the small-angle region as compared to an isotropic distribution. If it is assumed that the observed interactions are a mixture of peripheral and central collisions with an isotropic distribution, then we can obtain satisfactory agreement with experiment for a "mixture" in which 50 to 70% are peripheral processes, where the "allowable" level of statistical fluctuations is estimated on the basis of the Kolmogorov test.* The meson angular distribution (Fig. 6b) agrees with the view of a purely peripheral character of all interactions, although the difference between peripheral and central collisions in this case is very weak. At the same time, the anisotropy in the proton angular distribution in this case proves to be distinctly less than in the case of the interactions studied (by other selection criteria for nucleon-nucleon interactions) in the experiment by the group at the Joint Institute for Nuclear Research.[14]

It should also be noted that under selection criteria permitting interactions with two and more black tracks in a star, which is a less strict condition than the criteria used by us, the extent to which the protons and mesons tend to be emitted forward (in the nucleon-nucleon system) again increases, despite the appreciably greater mass of the target as compared with the mass of a nucleon.

3. The integral c.m.s. momentum distributions for protons and π mesons (in the forward cone)

*The restriction $n_{ch} \geq 2$ is connected with the fact that a certain part of the stars with $n_{ch} = 1$ can be related to the process of diffraction production of π mesons.[13] However, in the determination of the mean value of n_{ch}, we also included cases with $n_{ch} = 1$.

*Formulas obtained by Gnedenko and Korolyuk[15] show that this test enhances the role of statistical fluctuations if the number of observed events is not sufficiently large.

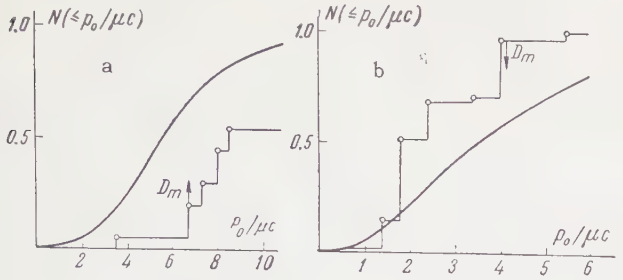

FIG. 7. Integral c.m.s. momentum distributions for protons (a) and π mesons (b) (in units of μc, where μ is the π-meson mass). Solid curve – theoretical distributions[11] for central interactions [the (π, p) particles are not included in case a].

are shown in Figs. 7a and 7b, respectively. Also shown there are the results of the statistical theory of central collisions. From a comparison of experiment with theory, one can conclude that, among the observed interactions, no more than 30 – 40% are central. The mean proton momentum is 1150 ± 110 Mev/c, which is practically no different from the data reported by Wang Shu-Fen et al;[14] the meson momentum (340 ± 55 Mev) proved to be approximately 25% lower. It should be borne in mind that the data of Wang Shu-Fen et al.[14] are based primarily on measurements of particles in the backward cone.

Finally, Figs. 8a and 8b give the integral distributions of the proton and meson c.m.s. transverse momentum $p_\perp$. Also given are the theoretical distributions obtained from the theory of central[1,10,11] and peripheral[12] interactions.* From a comparison of experiment with theory for the percentage of central collisions from the proton data, one obtains a lower limit of ~40% and from the π meson data one obtains an upper limit of ~40%. It should be borne in mind, however, that in this case the meson distribution provides a more sensitive criterion for estimating the percentage of central collisions, for the latter differs from peripheral collisions both in the larger momenta and larger angles of emission of the mesons, while for protons the higher momentum values can be offset by the narrower angular distribution of the particles in the case of peripheral interactions.

The latter characteristic of the proton distributions provides an additional possibility of estimating independently the percentage of peripheral interactions. In fact, according to the calculations of Chernavskii,[12] 70% of the recoil protons emitted backward in the c.m.s. should be gray tracks, while such tracks should be practically absent in the case of central interactions. Experiment shows that stars with $n_b \leq 1$, $n_g \leq 1$ have gray tracks at an angle $\theta_L \leq 90°$ in (25 ± 2.5)% of the cases; the overwhelming majority of these are proton tracks. If it is assumed that the number of slow recoil neutrons and protons is the same, one can then readily calculate an upper limit of ~80% for the frequency of peripheral interactions, while the lower limit is 60 – 65%.

4. The connection between the mean momentum of the particles p_0 and their c.m.s. angle of emission θ_0 has the following form:*

	θ_0	$\bar{p}_0/\mu c$	θ_0	$p_0/\mu c$
Protons†	0—20°	9.8 ± 1.8	30—90°	7.2 ± 0.7
π mesons	0—20°	3.9 ± 0.5	20—90°	2.1 ± 0.2

As seen from the data, there is a dependence of the momentum p_0 on the angle θ_0, which indicates that the degree of anisotropy of the c.m.s. angular distribution increases, especially for mesons, with an increase in the momentum. It turns out that for mesons such a dependence is more marked in the case of low multiplicity where $n_{ch} \leq 4$.‡

The mean values of the quantities considered above, with an estimate of their accuracy, and comparison with the corresponding theoretical results are given in the table.

The above-mentioned dependence of the momentum p_0 on the angle of emission of the particle θ_0, and, consequently, on θ_L is comparatively weak; for the other investigated quantities $p_\perp$ and θ_0 the dependence on θ_L is considerably stronger, especially for protons. This leads to a situation in which it is very important to introduce geometrical corrections in the distributions of $p_\perp$ and θ_0 and also in the calculation of the corresponding mean values and the errors involved in their determination, while for the distribution of p_0 the geometrical factor has no special significance.**

*It is assumed here that the angular distribution is isotropic for central interactions.

*We note that, for particles with c.m.s. velocities $\theta_0 \geq 0.8$, the same dependence will occur, to a good approximation, in the laboratory system.

†Without (π, p) particles.

‡A similar picture was observed[16] for secondary π mesons in a study of 7-Bev π-meson interactions with nucleons; the anisotropic part of the c.m.s. angular distribution was due almost entirely to the fastest mesons (c.m.s. energy ≥ 0.5 Bev); this group of particles was quite distinct mainly in stars with a small number of prongs.

**The influence of the geometrical corrections on the accuracy of the determination of the mean values was considered quantitatively by M. I. Podgoretskiĭ, to whom the authors express their gratitude for acquainting them with the appropriate formulas.

	Protons			π Mesons		
		theoretical			theoretical	
	exptl.	periph.	centr.	exptl.	periph.	centr.
Mean c.m.s. emission angle $\bar{\theta}_0$, deg	24 ± 5	–	57?	51 ± 11	46	57?
Mean c.m.s. momentum $\bar{p}_0/\mu c$	8.2 ± 0.8	–	5.6	2.4 ± 0.4	–	4.0
Mean total c.m.s. energy $\bar{\varepsilon}_0/\mu c$	10.8 ± 10%	–	–	2.6 ± 15%	–	–
Mean transverse momentum $\bar{p}_\perp/\mu c$	4.1 ± 0.6	2.3	5.3	1.5 ± 0.2	–	3.15

In the analysis of the experimental data for the mean values of momentum and energy shown in the table, it is necessary to bear in mind the following. First, if one carries out an averaging of the values of p_0 without recourse to the introduction of geometrical corrections in the limits of sufficiently wide angular intervals ($\theta_L = 0-4$, $4.5-11$, and $11.5-24°$), then the mean values of the meson and proton energies and momenta increase by only 2 and 1%, respectively, but the estimates of the statistical errors decrease to $\frac{2}{3}-\frac{1}{2}$ of their corrected value. Second, the same quantities can be averaged under the assumption (as was done in reference 15) that all (π, p) particles not identified directly are π mesons; in this case, the mean energy of the π mesons and protons increases by another 1.5 — 2%. Finally, if we also take into account the mean number of π mesons per interaction, namely 2.8, and use the energy balance (2), we can determine the mean number of secondary nucleons per star, and thus obtain the mean mass of the target $\bar{M}_T$ and the possible percentage of interactions with two nucleons inside a nucleus. One must only keep in mind the fact that relation (2) does not take into account the energy carried off by K mesons, which constitutes, according to rough estimates, about 10 —15% of the energy of the π mesons.

In the end, it turns out that the experimental data agree with a relative target mass of unity ($\bar{M}_t = M_N$), but the experimental error permits a value up to $1.2\,M_N$, which corresponds to a mixture in which 20% of the interactions involve two nucleons in a nucleus. Use of the earlier data on the number of stars of large multiplicity ($n_{ch} \geq 7$) gives approximately the same estimate of the upper limit for the number of inelastic interactions with two nucleons. However, both these estimates apparently give too high a value, since the mean multiplicity of the stars in which the secondary proton has a large transverse momentum ($p_\perp \geq 4\mu c$) does not differ by more than 15% from the multiplicity of the remaining stars.

Besides the value of $\bar{p}_0$ for nucleons and mesons, three quantities closely connected with it are of interest: the inelasticity of the interaction in the c.m.s. (K_0) and in the laboratory system (K_L), and the mean fraction of the initial energy carried away by one fast nucleon ($\bar{\alpha}$). For the stars of type $n_b \leq 1$, $n_g \leq 1$ studied by us $K_0 = 0.43 \pm 0.06$, $K_L = 0.31 \pm 0.04$,* $\bar{\alpha} = 0.55 \pm 0.05$.

The last quantity can be compared with the mean free path for the absorption of nucleons Λ_N, known

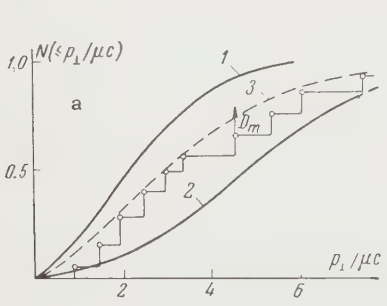

FIG. 8a. Integral distribution of proton transverse momentum. Curves 1 and 2 are the theoretical distributions for peripheral[12] and central[1,10,11] interactions; curve 3 is the distribution for a mixture of interactions of both (60% N_{periph} + 40% N_{centr}).

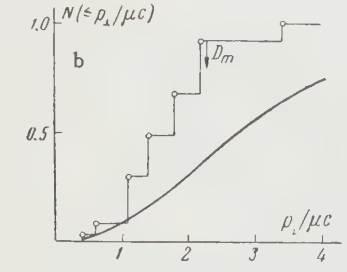

FIG. 8b. Integral distribution for π mesons. The curve represents the theoretical distribution for central interactions.[1,10,11]

*In the determination of K_0 and K_L we took into account only the energy carried off by π mesons.

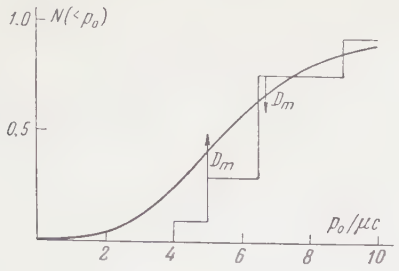

FIG. 9. Integral c.m.s. momentum distribution for protons with angles of emission $\theta_0 = 30 - 150°$. Solid line – theoretical distribution for central interactions.[11]

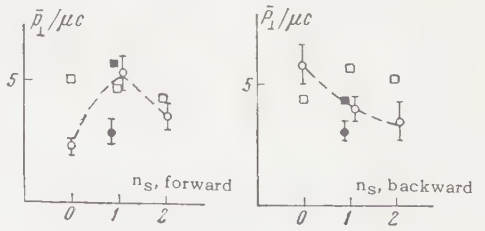

FIG. 10. Dependence of the mean transverse momentum of protons on the number n_s of other charged particles emitted in the forward and backward hemispheres in the c.m.s. (the circles indicate the experimental data and the squares, the theoretical data). Shown separately for $n_s = 1$ are cases with angles of emission $\theta_0 \leq 20°$ (● – experiment, ■ – theory) and angles of emission $\theta_0 > 20°$ (○ – experiment, □ – theory).

for light nuclei from cosmic-ray experiments,[17] namely $(\Lambda_N)_{air} = 125$ g/cm^2. If it is considered that for a nucleon energy spectrum of the form $E^{-\gamma}$ it is the values of α^γ and not the values of α that are averaged, while the mean free path for the interaction is $\Lambda_{air} = \Lambda_N(1 - \overline{\alpha^\gamma}) = 80$ g/cm^2. and also that approximately 35% of the collisions with light nuclei can have the character of two successive collisions with one nucleon, then the agreement between the value $(\Lambda_N)_{air}$ and the value we obtained for $\overline{\alpha}$ proves to be quite satisfactory.*

4. ANALYSIS OF SOME CORRELATIONS AND THE POSSIBILITY OF SEPARATING PERIPHERAL AND CENTRAL INTERACTIONS

For the separation of nucleon-nucleon interactions selected by one or another method into interactions of different types, it may prove highly advantageous to study various types of correlations.

First of all, from the statistical theory of central interactions it necessarily follows that there is a rather high probability that a momentum close to the value of the initial momentum of each of the colliding nucleons is transferred to the secondary particles. Such a transfer could lead to a situation in which one of the nucleons changes its direction of motion by more than 90° (in the c.m.s.) as a result of the collision and both appear in the same hemisphere. It should be kept in mind that the transfer of a large longitudinal momentum to one of the stationary nucleons of the nucleus cannot, generally speaking, take place in the case of two successive collisions of the peripheral type. Therefore the observation of two high-energy nucleons in one star can be an indication of the existence of central interactions even when there is no doubt as to the single-nucleon character of the collision. Among 140 stars of the type $n_s \leq 4$, $n_g \leq 1$ studied by us, we observed ten cases of simultaneous emission of two fast identified particles at angles $\theta_0 < 90°$ in the nucleon-nucleon c.m.s; in three of the cases, both particles were nucleons and in seven cases one of the particles was a nucleon and the other a π meson or (π, p) particle. Since K mesons constitute only ~ 10% of the number of π mesons, it is unlikely that in all three cases at least one of the particles considered to be a nucleon was a K meson.

Comparison of various correlations with the theoretical expectations can be carried out rather conveniently if the theoretical results are represented in the form of "artificial stars," i.e., a set of randomly selected characteristics of stars satisfying all the required conservation laws.[11] We studied one such correlation by analyzing the momentum distribution of protons emitted at angles $\theta_0 = 30 - 150°$, since in the case of peripheral collisions most of the nucleons (> 80%) are emitted at angles $\theta_0 \leq 30°$ (or $\theta_0 \geq 150°$); it can then be expected that, in the chosen angular interval, the momentum distribution will be determined only by central collisions. The experimental data (see Fig. 9) agrees with what is expected, although the large statistical fluctuations do not permit reliable conclusions on the relative number of central collisions.

On the other hand, one can consider the transverse momentum distribution for protons for eight stars with one gray track (with $n_b \leq 1$) among which there should be practically no central interactions. It turns out that only in one case does the value of $p_\perp$ exceed 2.5 μc, although among all the stars with $n_b \leq 1$, protons with $p_\perp > 2.5$ μc are encountered in 60% of the cases.

Furthermore, we considered the correlation between the proton transverse momentum $\overline{p}_\perp$ and

*In his calculations, Grigorov[17] took $\Lambda_{air} = 60$ g/cm^2, which, under additional assumptions on the character of the distribution of the quantity α, led to the value $\overline{\alpha} = 0.7$ for the interaction of a nucleon with an air nucleus.

the number (and also angles of emission) of other charged particles emitted either in the same hemisphere as the proton (in the c.m.s.) or in the opposite hemisphere (see Fig. 10). As seen from the analysis of Fig. 10, the correlation between $\overline{p}_\perp$ and the number of particles in one hemisphere proves to be considerably stronger than that obtained from the statistical theory of central collisions.

A visible correlation between the transverse or total momentum of the proton and the number of other charged particles (in a given angular interval) has a direct bearing on the asymmetric shower effect considered by Dobrotin et al.[18] for nuclear-active particles with a mean energy of the order of 300 Bev. Indeed, small values of the target masses for one of the colliding nucleons should inevitably be accompanied by a small momentum transfer to this nucleon, while the other nucleon, producing the basic part of the shower, can then considerably change its initial momentum, both longitudinal and transverse.

An asymmetry in the angular distribution of the produced particles was also observed in the emulsion stars studied by us: thus, for example, among 22 stars with $n_{ch} \geq 5$, there were six cases which were quite distinctly characterized by an asymmetric angular distribution of particles (no more than one particle was emitted at angles $\theta_L \leq 23°$ or $\theta_L > 23°$), while for artificial stars with six charged particles, such an asymmetry occurred only in two out of 21 cases, and in both cases the c.m.s. velocities of all charged particles were small.

Most of the correlations described above can be explained in a natural way within the framework of the concept of the peripheral character of the interactions. At the same time, some characteristics of the interactions, especially the presence of secondary protons with c.m.s. angles of emission $\theta_0 < 90°$ can be regarded as an indication of the existence of a certain percentage of collisions of a central type. For the final settlement of the question concerning the percentage of central collisions, it is necessary to conduct further experiments under cleaner conditions (for example, with a hydrogen bubble chamber).

Hence, as a whole, our data indicate that among interactions with emulsion nuclei a) a considerable portion of the events ($\sim 25\%$) have characteristics close to those of an interaction process involving the incident nucleon and only one (quasi-free) nucleon of the nucleus; b) interactions with quasi-free nucleons are mainly of a peripheral character, but there are indications of the existence of a small number of central collisions (about 20%).

In conclusion, the authors express their profound indebtedness to the administration of the Joint Institute for Nuclear Research for making available to them the emulsion exposed to the Institute's proton synchrotron, and also to D. S. Chernavskii, N. A. Dobrotin, G. T. Zatsepin, N. G. Birger, A. E. Chudakov, M. I. Podgoretskii, I. M. Gramenistskii, and G. I. Merzon for taking an active part in the discussion of the results of this work.

The authors thank the laboratory staff for taking part in the measurements.

[1] Zhdanov, Maksimenko, Tret'yakova, and Shcherbakova, JETP **37**, 620 (1959), Soviet Phys. JETP **10**, 442 (1960).

[2] W. H. Barkas and D. M. Young, UCRL-2579, Berkeley, 1954.

[3] I. Gramenitskii, Korbel, and Rob, Приборы и техника эксперимента (Instruments and Measurement Techniques) No. **1**, 42 (1961).

[4] Bogachev, Bunyatov, Gramenitskii, Lyubimov, Merekov, Podgoretskii, Sidorov, and Tuvdéndorzh, JETP **37**, 1225 (1959), Soviet Phys. JETP **10**, 872 (1960).

[5] N. G. Birger and Yu. A. Smorodin, JETP **36**, 1159 (1959), Soviet Phys. JETP **9**, 823 (1959).

[6] Bannik, Grishin, Danysz, Lyubimov, and Podgoretskii, JETP **37**, 1575 (1959), Soviet Phys. JETP **10**, 1118 (1960).

[7] Azhgireĭ, Vzorov, Zrelov, Meshcheryakov, Neganov, Ryndin, and Shabudin, JETP **36**, 1631 (1959), Soviet Phys. JETP **9**, 1163 (1959).

[8] Hahn, Ravenhall, and Hofstadter, Phys. Rev. **101**, 1131 (1956).

[9] V. S. Barashenkov, Preprint R-567, Joint Institute for Nuclear Research.

[10] Barashenkov, Wang Pei, and Mal'tsev, JETP **38**, 650 (1960), Soviet Phys. JETP **11**, 467 (1960).

[11] G. I. Kopylov, JETP **35**, 1426 (1958), Soviet Phys. **8**, 996 (1959).

[12] Gramenitskii, Dremin, Maksimenko, and Chernavskii, JETP **40**, 1093 (1961), Soviet Phys. **13**, 771 (1961).

[13] I. I. Ivanchik, JETP **36**, 617 (1959), Soviet Phys. JETP **9**, 427 (1959).

[14] Wang Shu-Gen, Visky, Gramenitskii, Grishin, Dalkhazhav, Lebedev, Nomofilov, Podgoretskii, and Strel'tsov, JETP **39**, 957 (1960), Soviet Phys. JETP **12**, 663 (1961).

[15] B. V. Gnedenko and V. S. Korolyuk, Doklady Akad. Nauk SSSR **80**, 525 (1951).

[16] Belyakov, Wang Shu-Fen, Glagolev, Dalkhazhav, Lebedev, Mel'nikova, Nikitin, Petržilka, Sviridov,

Suk, and Tolstov, JETP **39**, 937 (1960), Soviet Phys. JETP **12**, 650 (1961).

[17] N. L. Grigorov, Usp. Fiz. Nauk **58**, 599 (1956).

[18] Grigorov, Guseva, Dobrotin, Lebedev, Kotel'nikov, Murzin, Rapoport, Ryabikov, and Slavatinskii, Proceedings of the Moscow Cosmic Ray Conference, VINITI, Moscow, 1960, vol. 1.

Translated by E. Marquit
279

SPECIFIC HEAT OF NICKEL-ZINC SYSTEM FERRITES IN THE LOW-TEMPERATURE REGION

M. O. KOSTRYUKOVA

Moscow State University

Submitted to JETP editor January 11, 1961

J. Exptl. Theoret. Phys. (U.S.S.R.) 40, 1638-1643 (June, 1961)

The magnetic contribution to the specific heat for the ferrites $NiFe_2O_4$, $ZnFe_2O_4$ and the mixture $0.2\,Ni \cdot 0.8\,ZnFe_2O_4$ is determined from calorimetric data obtained between 1.8 and 20° K.

IN this work the specific heats of the ferrites $NiFe_2O_4$, $ZnFe_2O_4$ and of the mixture of $0.2\,Ni \cdot 0.8\,ZnFe_2O_4$ have been measured in the temperature range from 1.8 to 20° K. The measured specific heats have been applied in elucidating the details of the magnetic energy spectrum of these substances.

The ferrites of the nickel-zinc system are suitable substances for this investigation, since for some of them the Curie temperature is sufficiently low, and one can therefore conclude that in the low temperature region the magnetic specific heat appreciably exceeds the specific heat due to the lattice vibrations.

It follows from neutron-diffraction data[1] and from the results of magnetic measurements,[2] that the so-called ferrimagnetic spin ordering takes place at $T_C \sim 870°$ K in nickel ferrite ($NiFe_2O_4$) and is preserved down to 20° K. In mixed ferrites the temperature of the transition to the state of magnetic ordering decreases with the increase in the concentration of the nonmagnetic zinc ions; according to Pauthenet,[2] magnetic ordering in the ferrite $0.2\,Ni \cdot 0.8\,ZnFe_2O_4$ occurs in the temperature range between 70 and 292° K. Yafet and Kittel[3] have discussed the picture of ordering in mixed ferrites and have, in particular, indicated the possibility of triangular spin ordering occurring in them. The results of the latest studies of the properties of zinc ferrite ($ZnFe_2O_4$)[4,5] indicate the occurrence of an antiferromagnetic transition in it at $T_C \sim 9.5°$ K.

Until recently, low temperature specific heat measurements were only available for one substance of the ferrite class — magnetite ($FeFe_2O_4$),[6] in which ferrimagnetic ordering takes place at a high temperature ($T_C = 843°$ K).

The ferrite specimens studied in this work had the spinel x-ray pattern without extra lines, and the accuracy of their stoichiometric composition, according to the chemical data and x-ray analysis, amounted to several per cent.*

The method described earlier[7,8] was used in the specific heat measurements. The surface of the specimens was covered with a thin film of BF varnish to reduce the possibility of adsorption of the exchange gas.

The values of the heat capacity of the ferrites $NiFe_2O_4$, $ZnFe_2O_4$ and of the mixture $0.2\,Ni \cdot 0.8\,ZnFe_2O_4$ between 1.8 and 20° K are shown in Fig. 1 in C-T coordinates.

It follows from the data presented that the specific heat of nickel ferrite ($NiFe_2O_4$) does not show any marked indication of an anomaly in its temperature dependence. In addition, the molar heat capacity of nickel ferrite is considerably lower than that of zinc or of the mixed ferrite, for which the anomalous specific heat is large.

Since the magnetic ordering in nickel ferrite occurs at a high temperature, one might expect that the magnetic contribution to the specific heat of $NiFe_2O_4$ at low temperatures should be small compared with the lattice specific heat.

Calculations, made according to formulae obtained on the basis of a semi-classical theory of spin waves, for ferrites with strong AB coupling[9,6] (the electron spins of the ions of the A and B sublattices are then oriented corresponding to the +Z and −Z directions) lead to the following values of the magnetic specific heat:

$$C_{mag} \approx 0.113R\{2(2S_B - S_A)kT/11J_{AB}S_AS_B\}^{3/2}$$

$$\approx 0.16 \cdot 10^{-4}T^{3/2} \text{ cal/mole-deg.}$$

$$kT_c \approx 4\sqrt{2}\,J_{AB}\sigma_A\sigma_B = 36.7J_{AB},$$

$$J_{AB} \approx 24.5k, \qquad \sigma_N^2 = S_N(S_N+1).$$

*The ferrites were prepared by sintering in the Institute of Silicate Chemistry of the Academy of Sciences. The x-ray analysis of the specimens was kindly carried out by L. N. Rastorguev of the Steel Institute.

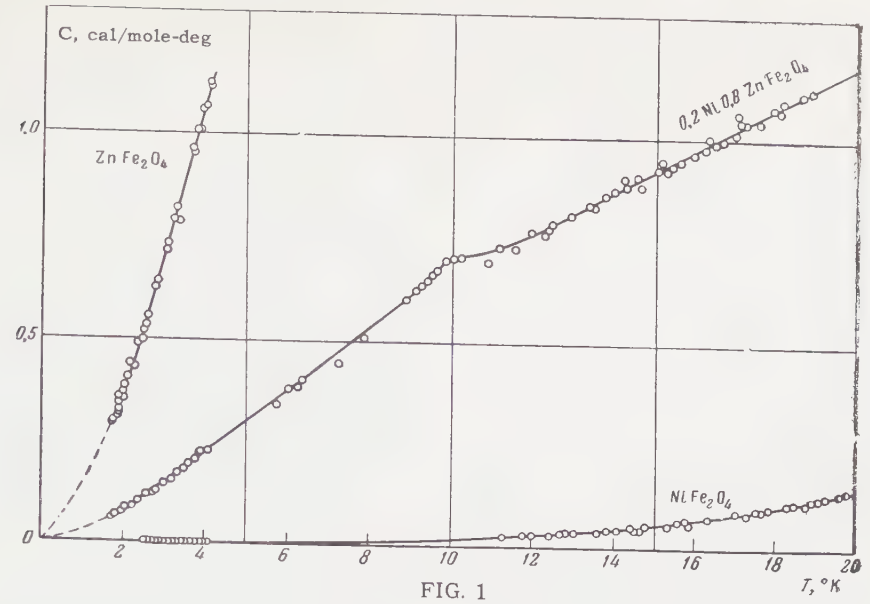

FIG. 1

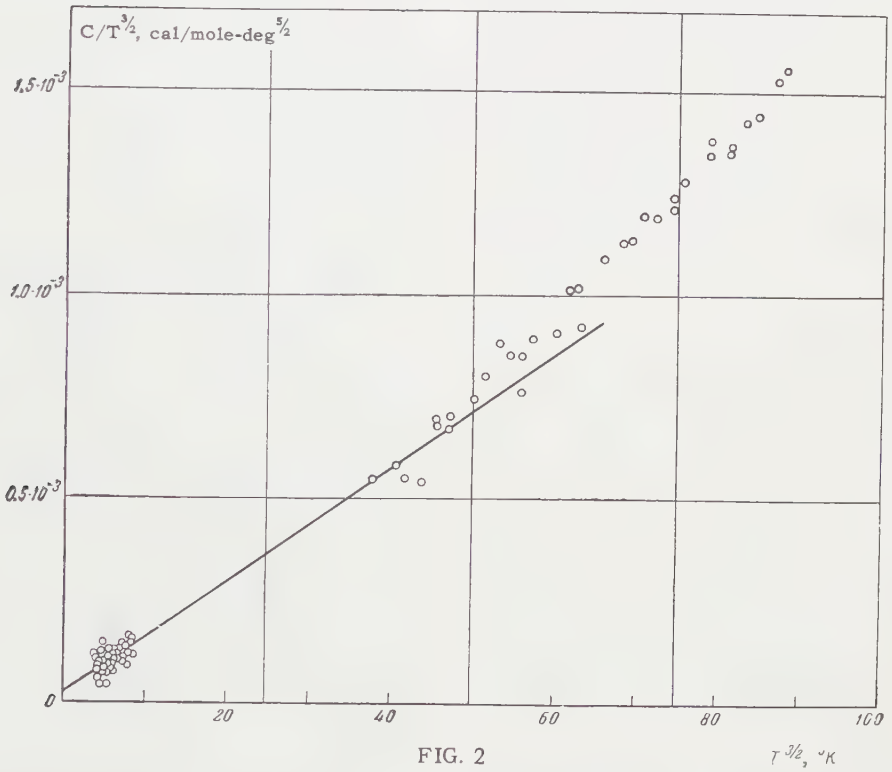

FIG. 2

Here S_A and S_B are the mean electron spins associated with the ionic moments of the tetrahedral and octahedral lattice sites, which for nickel ferrite are taken respectively as 1.75 and 2.5; J_{AB} is the negative exchange integral between nearest neighbor spins of the two sublattices. For the calculation, T_C is taken as 870° K.

In order to separate the magnetic specific heat from that due to the lattice vibrations, the results for nickel ferrite between 2 and 20° K are plotted in Fig. 2 as $C/T^{3/2}$ against $T^{3/2}$.* The straight line drawn through the experimental points corresponds to a specific heat between 2 and 12° K given by the expression

$$C[\text{cal/mole-deg.}] = 0.14\cdot10^{-4}T^3 + 0.16\cdot10^{-4}T^{7/2},$$

where the cubic term naturally describes the lattice specific heat ($\Theta_D = 321°$ K) and the term proportional to $T^{3/2}$ the magnetic specific heat.

We can thus consider that the experimental data for nickel ferrite do not contradict the results of the calculation, and the magnetic specific heat between 2 and 20° K represents a small fraction of the lattice specific heat. In what follows, the esti-

*More detailed data on the specific heat of $NiFe_2O_4$ are given elsewhere.[10]

mate of the specific heat corresponding to the lattice vibrations of zinc and of the mixed ferrites has been made according to the data obtained for nickel ferrite.

It should be noted that our data on the lattice specific heat of $NiFe_2O_4$ are close to the lattice specific heat of magnetite ($FeFe_2O_4$),[6] for which $C_{lattice} = 0.112 \times 10^{-4} T^3$ cal/mole-deg. However, the magnetic specific heat of magnetite, proportional to $T^{3/2}$ (see reference 6), is roughly 20 times greater than the magnetic contribution to the specific heat of $NiFe_2O_4$. It is possible that this is connected with the existence of the α-β transition in magnetite at 113° K.[11]

An anomaly was found in the C-T curve (Fig. 1) for the mixed nickel-zinc ferrite $0.2\,Ni \cdot 0.8\,ZnFe_2O_4$, with a maximum at a temperature ~ 9.7° K. An analogous anomaly in specific heat was found in mixed nickel-zinc ferrites by Westrum and Grimes,[12] and is probably connected with the antiferromagnetic transition in zinc ferrite at ~ 9.5° K.[4,5]

From the data shown in Fig. 3, where the coordinates are $C/T^{3/2}$ and $T^{3/2}$, it follows that the specific heat of the ferrite $0.2\,Ni \cdot 0.8\,ZnFe_2O_4$ can be represented by the following formula between 1.8 and 4° K:

$$C[\text{cal/mole-deg.}] = 4.5 \cdot 10^{-4} T^3 + 2.5 \cdot 10^{-2} T^{3/2}.$$

The cubic term separated out in this way cannot, however, be ascribed solely to the lattice specific heat, since for nickel ferrite the lattice specific heat is 32 times smaller than the cubic term in the specific heat of the mixed nickel-zinc ferrite.

The term in the heat capacity of the ferrite $0.2\,Ni \cdot 0.8\,ZnFe_2O_4$ which is proportional to $T^{3/2}$ exceeds the cubic term over a large part of the range of measurements (up to 14° K). Between 4 and 9.7° K the experimental data are close to the value of the term proportional to $T^{3/2}$, while above 9.7° K the growth in specific heat is considerably slowed down.

We can, therefore, consider that an appreciable part of the magnetic specific heat between 1.8 and 4° K is connected with the ordering which takes place below 9.7° K in the mixed nickel-zinc ferrite.

It is also seen from the data that the magnetic specific heat of the mixed nickel-zinc ferrite continues to increase with increasing temperature between 9.7 and 20° K (Fig. 1). This indicates that magnetic ordering in the mixed ferrite is preserved at higher temperatures and that the specific heat has a maximum lying above 20° K.

The maximum in the specific heat of the zinc ferrite we measured was found at 9.5° K; at this temperature the value is of the order of 3.5 cal/mole-deg. The experimental data shown in Fig. 4 for temperatures between 1.8 and 4° K, in $C/T^{3/2}$ and $T^{3/2}$ coordinates, enable one to express the specific heat by the relation

$$C[\text{cal/mole-deg.}] = 1.8 \cdot 10^{-3} T^3 + 12.1 \cdot 10^{-2} T^{3/2}.$$

The cubic term in the specific heat of zinc ferrite exceeds appreciably both the lattice specific heat of nickel ferrite (by 130 times) and the cubic contribution to the specific heat of the mixed nickel-zinc ferrite (by 4 times).

The $T^{3/2}$ term in the specific heat of nickel ferrite is 4.8 times greater than the $T^{3/2}$ term in the mixed ferrite.

The absence of a complete theory describing the state of magnetic ordering in zinc ferrite and in mixed nickel-zinc ferrites makes a comparison of the experimental data with theory difficult. The energy spectrum of antiferromagnets predicted by theory leads to a cubic temperature dependence of the magnetic specific heat in the region of not too low temperatures[13] (for temperatures greater than the gap in the energy spectrum of the antiferromagnet) and cannot explain the $T^{3/2}$ law.

At the same time, bearing in mind the fact that the $T^{3/2}$ term in the magnetic specific heat is large in zinc ferrite, we might think that both the cubic term and the $T^{3/2}$ term in the magnetic specific heat are due to antiferromagnetic ordering in $ZnFe_2O_4$.

In the process of preparation, zinc ferrite is always partly inverted.[2,14] A certain fraction of

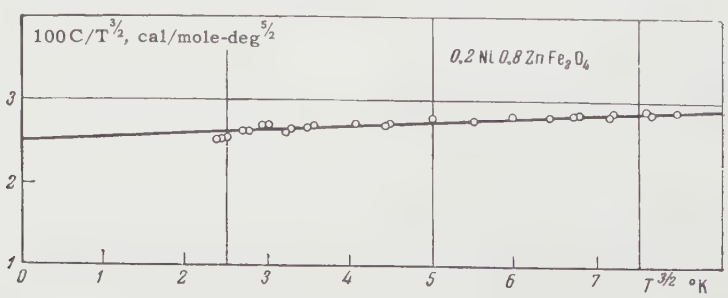

FIG. 3

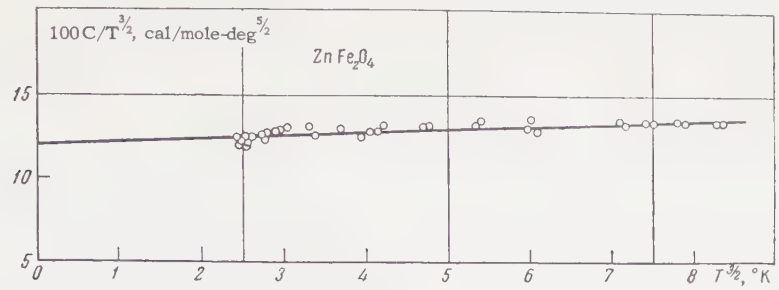

FIG. 4

the Zn ions of the A sublattice then changes place with the Fe ions of the B sublattice. The magnetic ordering may then be more complicated than, for example, the triangular type suggested by Yafet and Kittel[3] for mixed nickel-zinc ferrites with small Ni concentration.

It is highly likely that a considerable part of the $T^{3/2}$ specific heat is connected with this more complicated form of magnetic ordering, which takes place at low temperatures in different regions of a zinc ferrite specimen. The maximum specific heat at ~ 9.7° K in the mixed nickel-ferrite $0.2\,Ni \cdot 0.8\,ZnFe_2O_4$ is possibly produced by inclusions of the zinc ferrite type.

In conclusion, I express my sincere thanks to A. I. Shal'nikov for his constant interest in the work, to A. S. Borovik-Romanov, who took part in the discussion of the results, and to E. F. Gippius for help with the experiments.

[1] J. M. Hastings and L. M. Corliss, Revs. Modern Phys. **25**, 114 (1953).

[2] R. Pauthenet, Ann. de Phys. **7**, 710 (1952).

[3] Y. Yafet and C. Kittel, Phys. Rev. **87**, 290 (1952).

[4] J. M. Hastings and L. M. Corliss, Phys. Rev. **102**, 1460 (1956).

[5] E. F. Westrum, Jr. and D. M. Grimes, J. Phys. Chem. Solids **3**, 44 (1957).

[6] J. S. Kouvel, Phys. Rev. **102**, 1489 (1956).

[7] M. O. Kostryukova, Doklady Akad. Nauk SSSR **96**, 959 (1954).

[8] M. O. Kostryukova, JETP **30**, 1162 (1956), Soviet Phys. JETP **3**, 771 (1956).

[9] H. Kaplan, Phys. Rev. **86**, 121 (1952).

[10] M. O. Kostryukova and T. A. Leĭstner Вестник МГУ (Moscow State University Bulletin) **4** (1961).

[11] S. V. Vonsovskii, Современное учение о магнетизме (Modern Theories of Magnetism) part III, Gostekhizdat, 1953, Sec. 13.

[12] E. F. Westrum Jr. and D. M. Grimes, J. Phys. Chem. **61**, 761 (1957).

[13] Akhiezer, Bar'yakhtar, and Kaganov, Usp. Fiz. Nauk **71**, 533 (1960), Soviet Phys. Uspekhi **3**, 567 (1961).

[14] E. F. Westrum Jr. and D. M. Grimes, J. Phys. Chem. Solids **6**, 280 (1958).

Translated by R. Berman
280

VARIATION OF THE AXIAL AND RADIAL DIMENSIONS OF AN ELECTRON CLUSTER DURING SYNCHROTRON ACCELERATION

F. A. KOROLEV, A. G. ERSHOV, and O. F. KULIKOV

Moscow State University

Submitted to JETP editor January 17, 1961

J. Exptl. Theoret. Phys. (U.S.S.R.) 40, 1644-1652 (June, 1961)

A high-speed moving film was made of a cluster of glowing electrons accelerated in the 660-Mev synchrotron of the Physics Institute of the Academy of Sciences. The law of variation of the axial and radial dimensions of the electron cluster was determined by measuring the film density. The results of the measurements are in good agreement with the theory in which radiative damping of the electron oscillations is taken into account. An increase of the radial dimensions of the cluster has been observed and can be explained by quantum effects in the electron radiation.

In order to design large cyclic electron accelerators and accumulating systems, it is very important to know the law of variation of the axial and radial dimensions of the accelerated electron cluster. The axial, radial, and azimuthal dimensions of the cluster are determined by the distribution of the electrons relative to the amplitudes of the betatron and synchrotron oscillations. The existing theories describe the variation of the amplitudes of these oscillations during the acceleration process. The theory predicts the presence of radiation damping of the oscillations, as demonstrated first by Kolomenskii and Lebedev,[1] and also the possibility of excitation of oscillations under the influence of quantum fluctuations of the electron radiation, first pointed out by Sokolov and Ternov.[2]

It should be noted that to date there have been practically no experimental investigations devoted to a verification of the existing theories. The only known experimental work was performed by Sands,[3] who investigated the quantum excitation of synchrotron oscillations. The present investigation was undertaken to check the basic premises of the existing theories. To investigate the quantum excitation and radiation damping of oscillations it is necessary to have on hand a cyclic electron accelerator with sufficiently high maximum energy and a long electron acceleration time. Both requirements are well satisfied by the recently constructed S-60 synchrotron of the P. N. Lebedev Physics Institute of the U.S.S.R. Academy of Sciences.[4]

This "race track" synchrotron, with four straight sections, can accelerate electrons to 660 Mev in 0.6 sec. The radius of the electron equilibrium orbit is $R_S = 198$ cm, the fall-off exponent of the magnetic field is $n = 0.655$. The synchrotron has two resonators. The first operates as the electrons are accelerated to approximately 200 Mev, and the second—from the energy at which the first resonator is switched off to maximum. The instant of the transition from the first resonator to the second, called "interception," lies in the interval $t = 0.12 - 0.16$ sec, depending on the operating conditions of the accelerator (the time is reckoned from the instant of injection). The accelerating cycles are repeated every six seconds.

The investigation was carried out by taking high-speed motion-picture photographs of the glow of the electron cluster accelerated in the synchrotron. It should be noted that photography of the glow of the electron cluster was used earlier,[5,6] but without photometric processing of the resultant photographs.

The apparatus used in this investigation is illustrated in Fig. 1. A mirror placed inside the vacuum chamber of the accelerator brought the electrons radiated from a segment of the orbit approximately 40 mm long out through a window in the flange of the radial tube. A lens located outside the accelerator chamber produced an intermediate image of the cluster, which was photographed with the high-speed motion-picture camera. An SKS-1 motion picture camera was used, capable of operating up to 4500 frames per second. The pictures were taken at 500 frames per second. A neon bulb fed by a 250 or 500 cps ZG-10 audio generator was used to produce the time markers on the film. A reticle graduated in millimeters was placed in

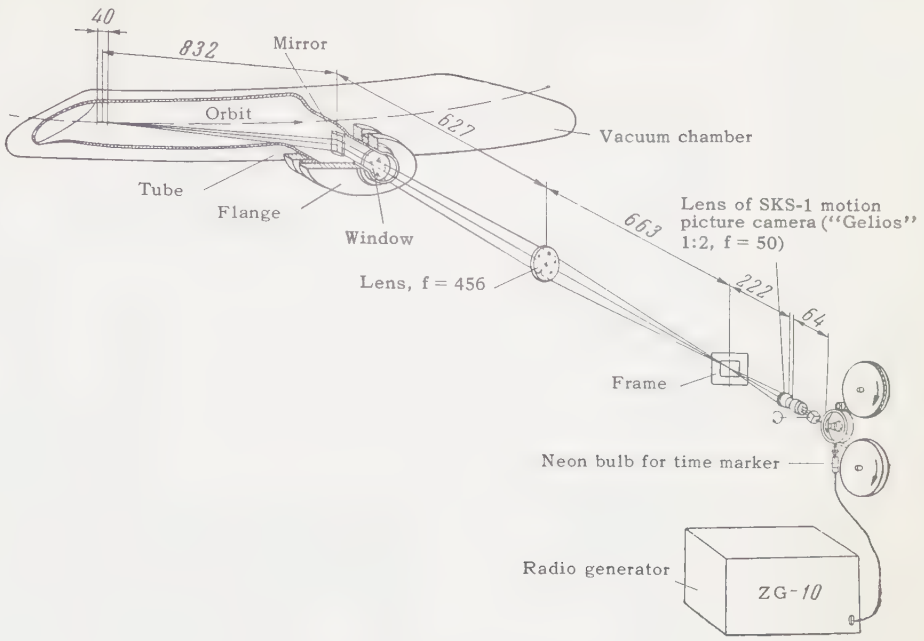

FIG. 1. Optical system of the apparatus.

the plane of the intermediate image produced by the lens, to measure the displacement of the picture of the cluster. The magnification of the optical system was 0.132. Standard MZ-2 16-mm film was used, rated 45 GOST sensitivity units. The number of electrons in the cluster, determined during the photography with a special electronic circuit, was approximately 10^7.

To interpret the resultant cluster photographs, we must have the characteristic curve of the film so as to convert the photographic density into radiation intensity. To obtain the characteristic curve, a step wedge was placed in the plane of the intermediate image and photographed by the light of the electrons. In addition, the radiation spot incident on the wedge was photographed, to monitor any irregularities in the illumination of the wedge steps. All this made it possible to determine the characteristic curve of the film for the wide range of variation of density prevalent in the photography of electron clusters.

It took about 200 frames to photograph the cluster in a single acceleration cycle. Each frame is an image of the cross section of the electron cluster, averaged over the exposure time of the frame, equal to approximately 4×10^{-4} sec. The illumination of any portion of the image on the film is directly proportional to the number of electrons passing during the exposure time through a unit surface of the conjugate area in the cluster cross section. Thus, by measuring the distribution of the illumination in the image of the cluster, we find the distribution of the electrons over the coordinates in the cross section of the cluster, and are able to determine the width of this distribution.

A series of successive photographs of a cluster during one acceleration cycle is shown in Fig. 2, from which we can see the general character of variation of the form and dimensions of the cross section of the cluster. The same figures shows the experimental plots of the distribution of the radiation intensity over the width (radial direction of the accelerator) in height (direction of the synchrotron magnetic field).

The threshold of registration on the film amounts in our case to only ~ 100 Mev (photograph No. 1). The cluster is oval in section, slightly elongated in the radial direction, and the photographic density is low because the intensity of radiation is still low. With increasing energy, up to the instant of interception, the form of the cluster changes insignificantly, and the intensity increases. It can be assumed that directly prior to interception the form of the cross section of the cluster is determined only by the betatron oscillations (photograph No. 2). At the instant $t = 0.147$ interception takes place and causes a strong radial broadening of the cluster, owing to the occurrence of synchrotron oscillations of large amplitude (photograph No. 3). The reduction in the density of the cluster image directly after interception, compared with the photograph prior to interception, is explained by the fact that in practice the same amount of radiation is distributed over a greater image area. The initial cluster begins to fluctuate in this case as a whole, and this leads, owing to the averaging of the position of the cluster during the exposure time, to a typical picture in the form of a "dumbbell" (photographs 4 and 5). The thicker parts of the dumbbell correspond to the "turning points" of the

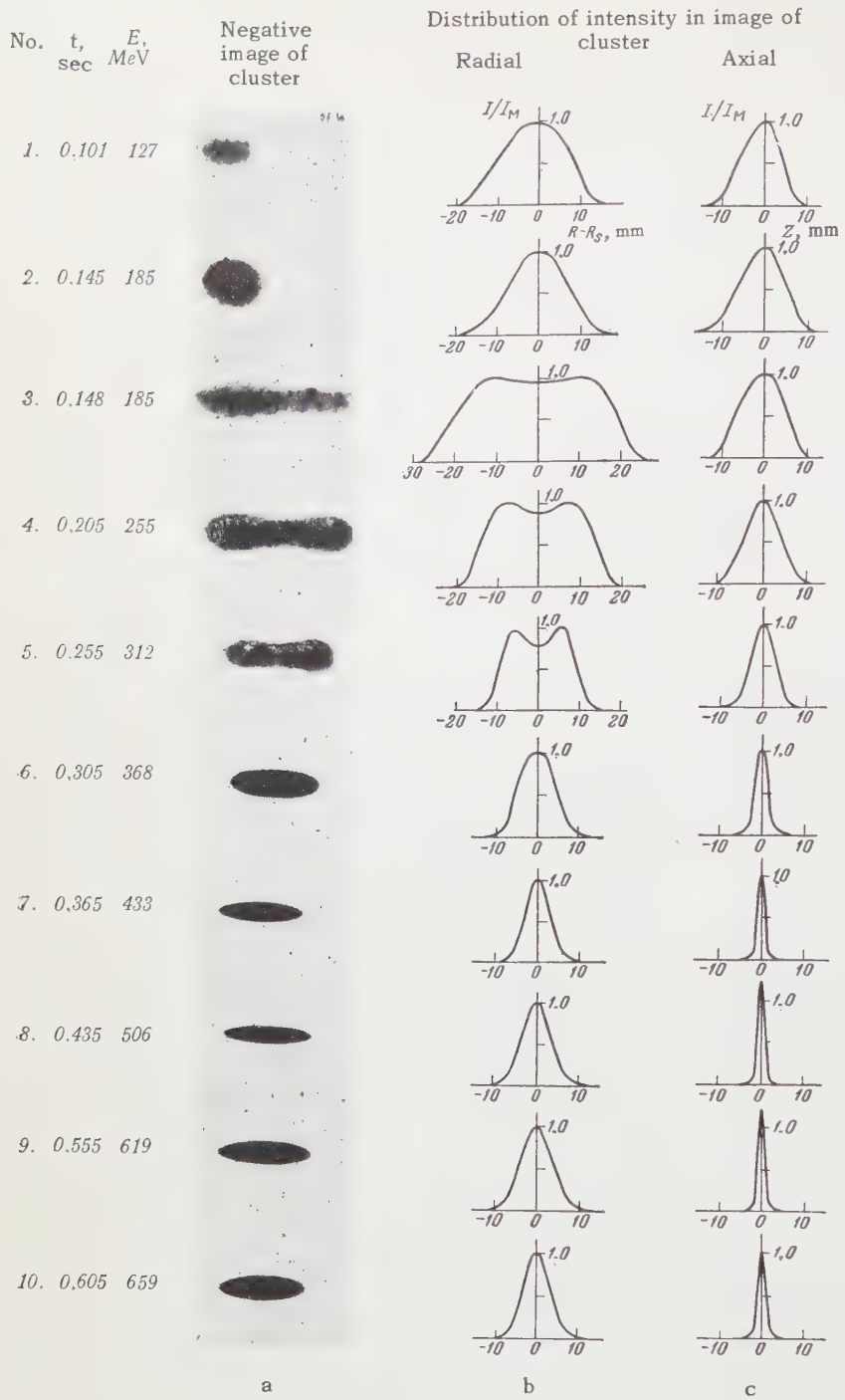

FIG. 2. Photographs of electron clusters at different instants of time in one cycle of acceleration, and corresponding distributions of radiation intensity. The ordinates represent the relative intensities.

vibrating cluster. The dimension of the cluster along the vertical direction (the z axis) remain practically unchanged during the instant of interception.

Later on, owing to the attenuation of the synchrotron and betatron oscillations, the cluster becomes compressed (picture No. 6). At the instant 0.365 sec and at an energy 433 Mev, the radial dimensions of the cluster are minimal (photograph No. 7). The cross section is similar in form at that instant to an elongated ellipse with sharpened ends and a semi-axis ratio 1 : 5. The vertical dimension of the cluster reaches a minimum at the instant 0.435 when the electron energy is 506 Mev (photograph No. 8). At the end of the acceleration cycle the cluster again broadens, both radially and vertically. However, the radial broadening of the cluster reaches a limit in this case at 619 Mev and 0.555 sec (photograph No. 9), followed again by a slight radial compression of the cluster. At the

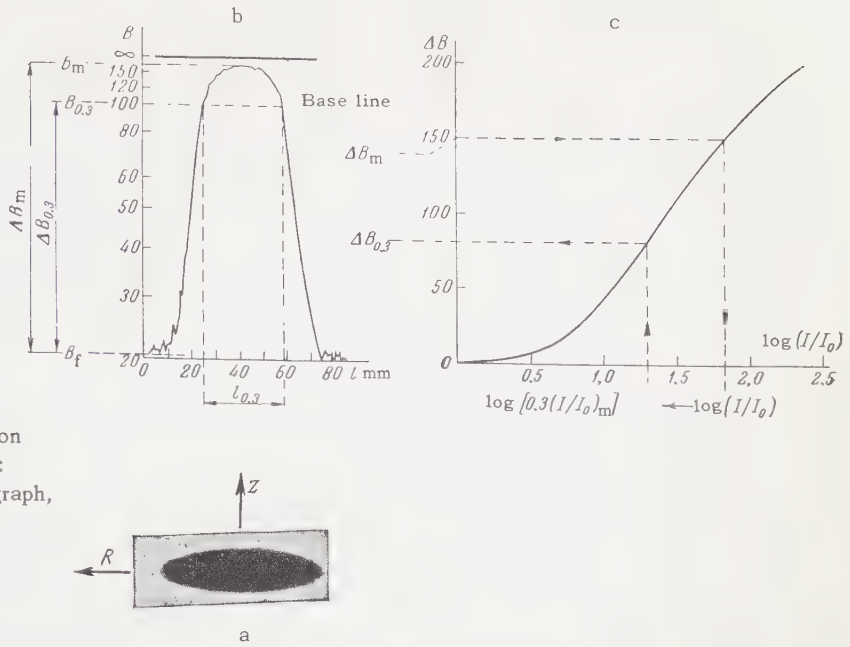

FIG. 3. Measurement of dimensions of electron clusters from the microphotograph of the picture: a – negative image of cluster, b – radial micrograph, c – characteristic curve of film.

instant when the electrons strike the target, the cluster has a form shown in photograph No. 10. The radial dimensions of the cluster become stabilized or even increase slightly apparently because of quantum build-up of the oscillations, while the stabilization and subsequent increase in the axial dimensions are still unexplained.

In order to refer the time of each frame of a given cycle to the instant of injection, the last photographed frame of the acceleration cycle was timed. On the basis of known data on the value of the electron energy in the target, the target radius, and the time necessary for the electrons to swing from the equilibrium orbit to the target, it was easy to calculate the instant of time corresponding to the start of the drift of the electron from the equilibrium orbit to the target. The error in the time correlation amounted to ± 0.01 sec. This was followed by a recalculation of the time markers produced by the neon bulb, fed from a ZG-10 generator of known frequency, so that the time corresponding to any frame of the film could be readily determined.

The electron-cluster photographs obtained were processed photometrically. An MF-4 microphotometer was used to record microphotographs of the distribution of the density in the cluster picture in two mutually perpendicular directions, corresponding to the direction of the accelerator radius R and the direction of the magnetic field z. Both directions intersected at the point of the image having the maximum photographic density. In addition, the base line, i.e., the line corresponding to infinite photographic density ($B = \infty$), was also recorded on the microphotograph.

Figure 3 illustrates the procedure used for the subsequent processing of the resultant microphotographs. The microphotographs for each frame chosen for processing were placed on a prepared density scale in such a way that the base lines of the microphotographs and of the scale coincided. The values of the density for the background (B_b) and for the maximum (B_m) were determined. The absolute value of the density at the maximum, $\Delta B_m = B_m - B_b$, was found.

From the characteristic curve of the photographic film we determined the logarithm of the intensity of radiation $\log (I/I_0)_m$,* corresponding to the absolute density at the maximum. To investigate the change in the radial and axial dimensions of the cluster, we measured the width of the microphotogram at a level corresponding to 0.3 of the maximum intensity, for which the logarithm of this value was determined from the formula $\log [0.3 (I/I_0)_m] = \log (I/I_0)_m + \log 0.3$. The characteristic curve was then used to find the absolute value of the density for this radiation intensity level ($\Delta B_{0.3}$). Adding the value of the background, we obtained for the microphotograph the density corresponding to this level of intensity ($B_{0.3}$). The width of the microphotograph of the cluster ($l_{0.3}$) was then measured at this density level.

*I_0 is the intensity of radiation incident on a certain step of the attenuator, I is the intensity of the radiation transmitted through this step.

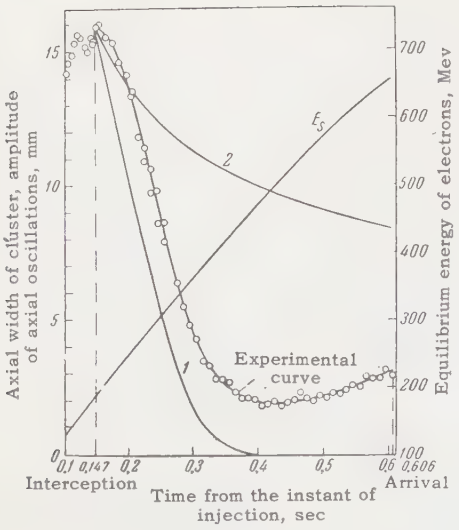

FIG. 4

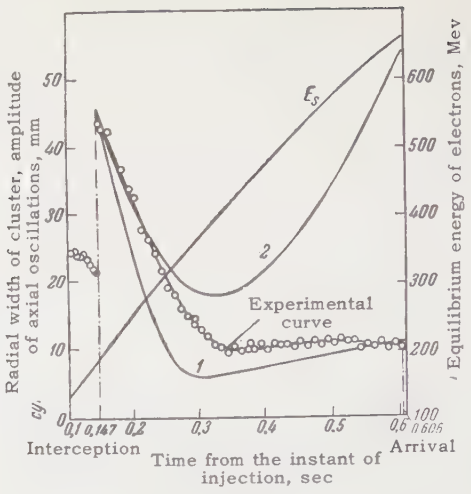

FIG. 5

Multiplying the resultant value of the width by the scale factor 0.331, we obtain the absolute value of the width of the electron distribution in the cross section of the cluster at a given level from the maximum of its distribution. Approximately 40 frames, spaced 0.01 sec apart, were processed in the series of photographs for a single acceleration cycle.

This method was used to process four frames with different electron acceleration cycles. Not one of the films enabled us to process completely the acceleration cycle, since the range of density variation from the start of acceleration until the electrons dropped on the target was so large, that it was impossible to carry out reliable photographic measurements on all the frames of the cycle. We therefore choose two films, on which part of the frames, corresponding to acceleration time from 0.1 to 0.3 sec, was reliably measured, as well as two films with reliably measured frames corresponding to the time from 0.25 to 0.6 sec.

The resultant experimental data on the variations of the axial and radial widths of the cluster at the 0.3 level for the two films, and their comparison with the theoretical variation of the summary oscillation amplitudes, are shown in Figs. 4 and 5 respectively. The choice of the width at the 0.3 level for the comparison with theory is dictated by the fact that in the photometry this width was measured most reliably. The plots for the widths at the levels corresponding to intensity values amounting to 0.2, 0.4, 0.5, and 0.6 of maximum, duplicate almost exactly the course of the given experimental curves.

In plotting the theoretical variation of the axial amplitude of the oscillations, we chose as the initial amplitude half the width of the cluster at the instant of interception, equal to 16 mm. The initial amplitudes of the radial betatron and synchrotron oscillations were determined in the following fashion. As follows from the measurements, the radial width of the cluster prior to interception amounts to 21 mm and, apparently, is due only to betatron oscillations. At the instant of interception, the radial dimensions of the cluster increase sharply and its width becomes equal to 45.4 mm, owing to the occurrence of synchrotron oscillations. We therefore took for the initial amplitude of the radial betatron oscillations half the width of the cluster prior to interception, equal to 21 mm, and for the initial amplitude of the radial synchrotron oscillations we took half the value of the differences of the widths before and after interception, amounting to 24.4 mm. To calculate the amplitudes we make use of the Kolomenskii and Lebedev formulas[7] in which account is taken of the radiation damping of the oscillations. The amplitude of the axial oscillations can be written here as

$$a_z = \left[a_{z_0}^2 \frac{E_{s_0}}{E_s} \exp\left(-\int_{t_0}^{t} \frac{W_s}{E_s}\, dt' \right) + \frac{13}{24\sqrt{3}} \frac{r_0 \Lambda c}{R_s n \gamma} \int_0^t \exp\left(-\int_{t''}^{t} \frac{W_s}{E_s}\, dt' \right) \gamma^4\, dt'' \right]^{1/2}, \qquad (1)$$

and the summary amplitude of the radial oscillations can be written

$$a_r = \left\{ \left[a_{rb_0} \left(\frac{E_{s_0}}{E_s} \right)^{1/2} \exp\left(-\frac{1}{2} \frac{n}{1-n} \int_{t_0}^{t} \frac{W_s}{E_s}\, dt' \right) + a_{rs_0} \left(\frac{V}{V_0} \right)^{1/4} \times \left(\frac{E_{s_0}}{E_s} \right)^{3/4} \exp\left(-\frac{1}{2} \frac{3-4n}{1-n} \int_{t_0}^{t} \frac{W_s}{E_s}\, dt \right) \right]^2 \frac{55}{24\sqrt{3}} \frac{r_0 \Lambda c}{R_s (1-n)^2 \gamma} \times \int_0^t \exp\left(-\frac{n}{1-n} \int_{t''}^{t} \frac{W_s}{E_s}\, dt' \right) \gamma^6\, dt'' \frac{55}{24\sqrt{3}} \frac{r_0 \Lambda c V^{0.5}}{R_s (1-n)^2 \gamma^{1.5}} \times \int_0^t \exp\left(-\frac{3-4n}{1-n} \int_{t''}^{t} \frac{W_s}{E_s}\, dt' \right) \gamma^{6.5} V^{-0.5}\, dt'' \right\}^{1/2}. \qquad (2)$$

The theoretical curves plotted from these formulas are denoted on both figures by the number 1. The theoretical curves, based on the Sokolov formulas in which radiation damping is not taken into account, are denoted on the same graphs by the number 2. According to theory[8] and the law assumed for the addition of the oscillation amplitudes, the formulas for the amplitudes will have the following form: for axial oscillations

$$a_z = \left[a_{z_0}^2 \frac{E_{s_0}}{E_s} + \frac{13}{24\sqrt{3}} \frac{r_0 \Lambda c}{R_s n \gamma} \int_0^t \gamma^4 dt' \right]^{1/2}, \qquad (3)$$

and for radial oscillations

$$a_r = \left\{ \left[a_{rb_0} \frac{E_{s_0}}{E_s} + a_{rs_0} \left(\frac{V}{V_0} \right)^{1/4} \left(\frac{E_{s_0}}{E_s} \right)^{3/4} \times \exp\left(-\frac{1}{2} \frac{3-4n}{1-n} \int_{t_0}^{t} \frac{W_s}{E_s} dt' \right) \right]^2 + \frac{55}{24\sqrt{3}} \frac{r_0 \Lambda c}{R_s (1-n)^2 \gamma} \int_0^t \gamma^6 dt' \right\}^{1/2}. \qquad (4)$$

In all these formulas, a_z, a_{rb}, and a_{rs} are the amplitudes of the axial betatron, radial betatron, and radial synchrotron oscillations, respectively, E_s is the equilibrium energy of the electron, W_s is the power of the radiation emitted by the electron, r_0 is the classical electron radius, Λ is the Compton length, R_s is the radius of the equilibrium orbit, n is the exponent of the fall-off of the magnetic field, γ is the ratio of the total energy of the electron to its rest energy, and V is the high frequency voltage on the resonator. The subscript zero denotes that the corresponding quantities are taken at the instant of time k_0. In our case $t_0 = 0.147$ sec. In addition, both plots show the build-up of the energy of the accelerated electrons, E_s.

Analyzing the experimental curves and comparing them with the theoretical ones, we can draw the following conclusions: 1) the theory that takes radiative damping into account, first developed by Kolomenskii and Lebedev,[1] gives sufficiently good albeit incomplete agreement with experiment; 2) in the energy region above 400 Mev, considerable radial oscillations are excited in the S-60 synchrotron of the Academy of Sciences Physics Institute by quantum oscillations, as first predicted by Sokolov and Ternov[2] and as developed in the macroatom theory of the same authors and Ivanenko[9]; 3) undamped axial oscillations exist, the presence of which does not follow from the theory; 4) in the energy region above 550 Mev a certain increase in the axial dimensions and a small decrease in the radial dimensions of the cluster are observed in the same synchrotron, which also cannot be explained theoretically.

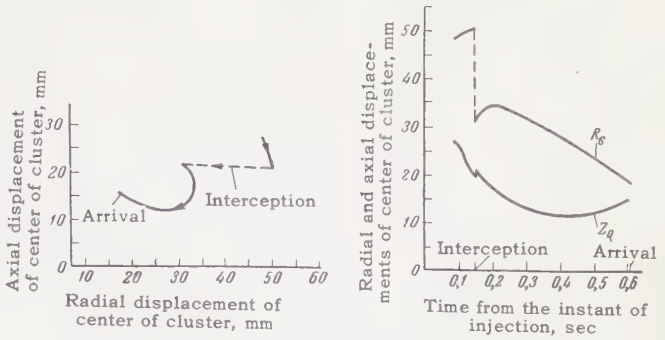

FIG. 6

In the study of the variation of the axial and radial widths of the cluster at different levels away from maximum, it was observed that from the time of interception to the instant 0.32 sec (E_s = 380 Mev) the central part of the cluster (corresponding to the level 0.6 of maximum) is compressed more rapidly than the peripheral parts, and then the widths change at approximately the same rate. The experimental plots show also that in the time interval from the interception (t = 0.147 sec) to t = 0.3 sec, i.e., in the portion where the cluster is intensely compressed, the speed of the radial compression is approximately twice the speed of the axial compression.

By measuring the position of the center of the image of the cluster of glowing electrons relative to the edges of the image of the frame (see Fig. 1) it was possible to trace the motion of the center of the cluster in the (R, z) plane, where R is the direction of the accelerator radius and z is the direction of the magnetic field. The results of the measurements are shown in Fig. 6, from which it is seen that the cluster experiences a considerable displacement in the chamber, and that at the instant of interception a sharp change takes place in the position of the center of the cluster. These displacements are evidently due to a change in the value of the equilibrium radius and a displacement of the null z plane. The point of reference was chosen on this figure arbitrarily. The total displacement of the entire beam amounts to approximately 30 mm in the radial direction and 20 mm in the vertical direction. All these measurements pertain to a definite point of observation of the cluster in one of the quadrants of the accelerator magnet.

Thus, the optical method of observing the cluster, employed in the present work, makes it possible not only to study the change in the dimen-

sions of the cluster during the acceleration process, but also to investigate the motion of an electron beam over the cross section of the accelerator chamber.

In conclusion, the authors consider it their duty to express their gratitude to Professor M. S. Rabinovich, Professor V. A. Petukhov, and V. E. Pisarev for graciously enabling us to carry out the experiment on the S-60 synchrotron, and also to the staff members of the Physics Institute Laboratory, Yu. N. Metal'nikov, L. V. Eremin, K. N. Shorin, and E. M. Gagin for help in carrying out the experiments. The authors are also grateful to Professor A. A. Kolomenskii, Professor D. D. Ivanenko, Professor A. A. Sokolov, I. M. Ternov, A. N. Lebedev, and I. S. Danilkin for help in comparing the experiment with theory and for a discussion of the results obtained.

[1]A. A. Kolomenskii and A. N. Lebedev, Dokl. Akad. Nauk SSSR **106**, 807 (1956), Soviet Phys.-Doklady **1**, 100 (1956).

[2]A. A. Sokolov and I. M. Ternov, JETP **25**, 698 (1953).

[3]M. Sands, Nuovo cimento **15**, 599 (1960).

[4]Атомная энергия (Atomic Energy) No 9, 154 (1960).

[5]Elder, Langmuir, and Pollock, Phys. Rev. **74**, 52 (1948).

[6]Korolev, Akimov, Markov, and Kulikov, Тр. X Всесоюзного совещания по спектроскопии (Transactions, Tenth All-Union Conference on Spectroscopy), v. 2, L'vov 1958, p. 24.

[7]A. A. Kolomenskii and A. N. Lebedev, Ускорители элементарных частиц (Accelerators for Elementary Particles), Fourth Appendix to Journal "Atomic Energy" for 1957, p. 31.

[8]A. A. Sokolov, Введение в квантовую электродинамику (Introduction to Quantum Electrodynamics), Fizmatizdat, 1958, Sec. 28.

[9]Sokolov, Ivanenko, and Ternov, Doklady Akad. Nauk SSSR **111**, 334 (1956), Soviet Phys.-Doklady **1**, 658 (1957).

Translated by J. G. Adashko
281

ELASTIC SCATTERING OF 8.7-Bev PROTONS BY EMULSION NUCLEI

B. P. BANNIK, V. G. GRISHIN, and L. V. SIL'VESTROV

Joint Institute for Nuclear Research

Submitted to JETP editor January 24, 1961

J. Exptl. Theoret. Phys. (U.S.S.R.) **40**, 1653-1657 (June, 1961)

The angular distribution of 8.7-Bev protons scattered elastically in nuclear emulsion is measured. Comparison is made with the optical model theory.

1. EXPERIMENTAL PROCEDURE

THE present work was undertaken to improve our earlier measurements of elastic proton scattering in nuclear emulsion.[1] A pellicle stack was irradiated with an internal 8.7-Bev proton beam in the proton synchrotron at the High-Energy Laboratory of the Joint Institute for Nuclear Research. The stack consisted of 10×20 cm type-R NIKFI pellicles 400μ thick; the beam intensity was $\sim 3 \times 10^4$ protons/cm^2. The proton beam, with an angular spread of $\sim 0.1°$, traversed the stack at an angle of $0.1 - 0.2°$ to the plane of the emulsion. An MBI-9 microscope with 60×15 magnification was used to search for and measure scatterings.

For scanning we selected tracks satisfying the conditions of (1) relativistic ionization and (2) no visually perceptible angle between a track and the proton beam axis, nor track dip with respect to the emulsion plane.

Scattering events were searched for by accelerated on-track scanning.[2] We recorded track deflections for which the projected scattering angle φ on the emulsion plane was about 0.1° or larger. φ was measured with the accuracy $\Delta\varphi = 0.05°$ in track sections of length $l = 3$ mm.* All events with projected angle $\varphi > 0.17°$ were remeasured with $l = 1$ mm. In this way a 1-mm track section was determined within which scattering had occurred; the scattering point was then located.

All events exhibiting $\varphi > 0.17$ after the second measurement were remeasured relative to two or three close-lying tracks, with $l = 3$ mm. In addition to φ, we measured the projected angle θ on a plane perpendicular to the emulsion plane. The relative measurements were performed in order to exclude events resulting from distortions in the emulsion. The accuracy of the relative measurements was $\Delta\varphi = 0.04°$. An event was associated with distortion if a deflection with $\varphi \geq 0.1°$ was observed in a corresponding section of even one neighboring track. The great density of proton tracks insured high efficiency in excluding cases of distortion by means of the relative measurements.

The relative measurements of 331 events showed that 4 events resulted from distortions; $\varphi < 0.17°$ for 25 events; 2 events were induced by secondary particles; in 12 events $\varphi > 2°$ or $\theta > 2°$. Careful scanning showed that 16 events were stars. All of these events were excluded in plotting the angular distribution of elastic scattering in the range $0.17° < \varphi < 2°$.

A certain fraction of the plates was scanned for the purpose of recording track deflections with projected angles of at least 0.25°. These events were used to plot the angular distribution for $\varphi \geq 0.3°$. Thirteen of these events were excluded from the total data.

The efficiency of our on-track scanning technique for detecting scattering could differ from 100% at the beginning and termination of each track. In order to avoid scanning errors at the beginnings of tracks all events (17 instances) in the first three millimeters were excluded. A study of the distribution of scattering events along the lengths of tracks showed that scanning efficiency decreases at track terminations. We therefore excluded all events (41 instances) found in the last nine millimeters.

In estimating the scanning efficiency in the middle of a track it was assumed that events with $\varphi \geq 0.3$ were detected with 100% efficiency (see reference 2). The efficiency was estimated for φ in the range $0.2 - 0.3°$ by comparing the number of events having φ in this range with the number of events having θ in the range $0.2 - 0.3°$. The two results were identical within error limits. Assuming azimuthal symmetry of scattering, it therefore followed that the detection efficiency for events

*Angles were measured as described in reference 1.

Angle range, deg	Distribution of N events in emulsion plane: From reference 1,* L = 151.6 m	Present work, L = 151.6 m	Total, L = 224.2 m	Calculated for L = 224.2 m: Re f = +14.4 Fermi units	Re f = −14.4 Fermi units	Re f = 0	Spatial distribution, (dN/dΩ) × 10⁻⁴: Measured, L = 123 m	Calculated for Re f = 0, L = 123 m
0.2—0.3		66.5**±9	98±13	96.6	131.7	83.8	141±27	126.1
0.3—0.4	50.2±10	46±7	70±8	69.8	85.5	51.3	76±14	65.2
0.4—0.5	33.5±8	20±5	36±6	46.0	53.1	31.7	49.2±9.0	38.2
0.5—0.6	18.8±6	17±4	26±5	26.7	31.4	17.9	21.8±5.2	21.4
0.6—0.7	8.4±4	8.5±3	12.5±4	16.6	21.4	9.8	11.0±3.3	11.1
0.7—0.8	2.1	6.5	7.5	9.9	14.5	5.2	6.3±2.3	4.5
0.8—0.9	—	4.5	4.5	6.5	9.5	3.3	3.6±1.6	2.0
0.9—1.0	4.2	4.5	6.5	6.2	8.8	2.6	2.6±1.3	1.5
1.0—1.1	—	6	6	5.4	7.9	2.0	3.4±1.4	1.3
1.1—1.2	6.3	5	8	4.1	5.7	1.5	3.1±1.3	1.2
1.2—1.3	4.2	2	4	3.3	4.6	1.1	0.9±0.7	0.8
1.3—1.4	—	1	1	2.0	2.8	0.5	0.4±0.4	0.4
1.4—1.5	—	2	2				1.2±0.7	
1.5—1.6	—	1.5	1.5				—	
1.6—1.7	2.1	1.5	2.5				0.3±0.3	
1.7—1.8		2	3				0.6±0.5	
1.8—1.9		—	—				0.6±0.4	
1.9—2.0		—	—				0.3±0.3	

*Data obtained for L = 72.54 m and converted for L = 151.6 m.

**When a scattering angle equalled the angle at the end of a 0.1° interval of the table, one-half event was assigned to each of the adjoining intervals.

with φ in the range 0.2 — 0.3° was close to 100%.

A total of 201 scattering events remained after the exclusion of events at track ends. For $\varphi > 0.3°$ we used events recorded in the scanning of a total combined track length L = 151.6 m; for φ from 0.17° to 0.3°, L = 123 m.

2. DISCUSSION OF RESULTS

The distributions obtained in the present and earlier work are given in the accompanying table. Since the results of the two experiments agreed within error limits a combined angular distribution was plotted (see the figure).* The table also gives the solid-angle distribution of scattering events from the total scanned track length L = 123 m, assuming azimuthal scattering symmetry.

The figure includes theoretical curves for the dependence of the differential cross section on the projected scattering angle. The calculations were based on the optical model taking into account the interference of nuclear and Coulomb scattering† and assuming that in the laboratory system the real part of the nucleon-nucleon forward-scattering amplitude is Re $f_{NN}(0) = 0$, +14.4, or −14.4 Fermi units.‡ In calculating the differential cross section corresponding to Re $f_{NN}(0) = 0$ we used the total nucleon-nucleon interaction cross section averaged over the nucleons within the nucleus ($\bar{\sigma} = 38$ mb), computed from measurements of p-p and p-n scattering cross sections.[4] The differential cross section for Re $f_{NN}(0) = \pm 14.4$ Fermi units and $\bar{\sigma} = 38$ mb was obtained by linear extrapolation, using the results for Re $f_{NN}(0) = 0$ and $\bar{\sigma} = 38$ mb and for Re $f_{NN}(0) = 0$ or $\pm$ 14.4 Fermi units and $\bar{\sigma} = 34$ mb.

We shall now estimate the sensitivity of the curves to the parameters used in the calculations. Measurements in the emulsion give $\bar{\sigma}$ with ±10% accuracy,* corresponding to ±7% shifts of the calculated curves for small angles.

According to Hofstadter,[7] the uncertainty of the radial parameter is ±2%, which for small angles results in ±2% inaccuracy of the calculated curves. For large angles ($\varphi > 1°$), up to 100% error results in the calculated curves.

Uncertainty regarding the form of the nucleon density distribution in the nucleus (trapezoidal, Fermi, or Gaussian distribution) results in ±2% inaccuracy of the calculated cross sections.

When calculating errors amounting to 3% are added, the total error of the calculated cross sections is of the order 10% for small angles φ.

*In the angle range $0.2° < \varphi < 0.3°$ some events were overlooked because of the selection criterion. This loss was estimated at ~ 5 events, for which the angular distribution was not corrected.

†Details of the calculation are given in reference 3.

‡This corresponds to an effective potential of 30 Mev for nucleon-nucleus interactions.

*From data kindly furnished by the authors of reference 5 we have estimated the mean free path for inelastic interactions of 8.7-Bev protons in the emulsion. From the result $\bar{R}_{inel} = 33.7^{+1.3}_{-1.6}$ cm it follows that $\bar{\sigma} = 38^{+4}_{-6}$ mb.[6] In our earlier paper we used $\bar{R}_{inel} = 34.7 \pm 1.5$ cm and, correspondingly, $\bar{\sigma} = 36 \pm 5$ mb. The measurements of $\bar{R}_{inel}$ in the emulsion thus are not inconsistent with each other or with the value $\bar{\sigma} = 38$ mb used in the calculations.

A χ^2 test of goodness of fit between the experimental histogram and the theoretical curves indicated agreement with probability 0.3 for Re $f_{NN}(0) = +14.4$ Fermi units, with probability 0.001 for Re $f_{NN}(0) = 0$, and with probability < 0.001 for Re $f_{NN}(0) = -14.4$ Fermi units.

Taking into account the uncertainty of the calculated curves, we can conclude that the results exclude Re $f_{NN}(0) = -14.4$, that they perhaps do not exclude Re $f_{NN}(0) = 0$, and that they are in good agreement with Re $f_{NN}(0) = +14.4$.

There also remains the possibility that some events taken to be elastic scatterings were actually inelastic interactions.* We estimated the contribution to the measured cross section from inelastic processes which could have been mistaken for elastic processes.

Quasi-elastic proton-neutron scattering was estimated from the measured cross section for quasi-elastic scattering of protons by bound protons.[8] Assuming identical cross sections for quasi-elastic scattering by bound protons and by neutrons, we estimated ~ 7 quasi-elastic neutron scatterings in 225 m of path within the emulsion. Two of these scatterings fall within the angle interval $0 - 1°$ and about five within the interval $1 - 2°$.†

In calculating nuclear excitation accompanying scattering it was assumed that the ratio $\sigma_{scat}/\sigma_{exc}$ of the elastic scattering cross section to the excitation cross section depends only on the transferred momentum. Using nuclear excitation measurements at E = 185 Mev,[9] for our experimental conditions we obtain $\sigma_{scat}/\sigma_{exc} \approx 100$ at scattering angles $0.2 - 0.6°$ and $\sigma_{scat}/\sigma_{exc} \approx 10$ at $1 - 2°$. The Coulomb excitation cross section was determined for $\varphi \lesssim 0.5°$, since Coulomb scattering falls off sharply above 0.5°. The contribution from Coulomb excitation was of the order 1% or less. The contribution from diffractive pion production[10] was calculated to be less than 1% of the total cross section and $\sim 10\%$ in the interval $1 - 2°$. From the angular distribution of secondary relativistic particles in nuclear reactions single-pronged stars were estimated to occur in 1% of the total number of events.

*The possible background of inelastic interactions at small φ lends support to the exclusion of Re $f_{NN}(0) = -14.4$, but makes it more difficult to choose between Re $f_{NN}(0) = 0$ and Re $f_{NN}(0) = +14.4$.

†Quasi-elastic proton-neutron scattering can produce an excited nucleus decaying by the emission of β rays with a few Mev. A corresponding track should then be observable at the scattering point. In the present work, in 201 scatterings within the range $0.2° < \varphi < 2.0°$ not a single event of this type was observed.

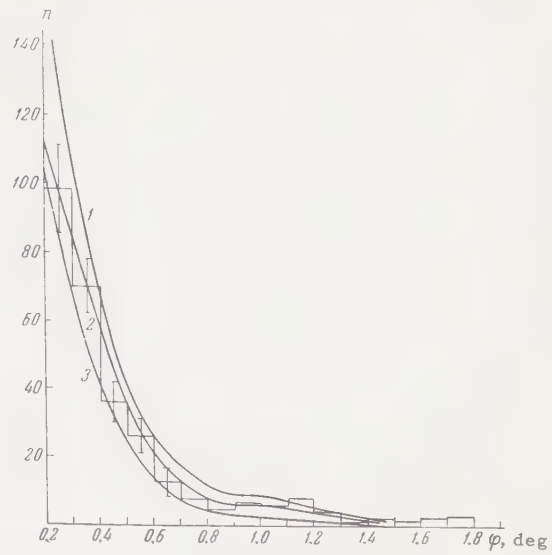

Angular distribution of 8.7-Bev protons scattered elastically in nuclear emulsion. Theoretical curves 1, 2, and 3 correspond to Re $f_{NN}(0) = -14.4$, +14.4, and 0, respectively. n is the number of events in a 0.1° interval.

Multiple scatterings on 37 tracks were measured as a control. The distribution of mean second differences for each scattered particle was compared with the analogous distribution for the primary protons. The parameters of the distributions were identical within error limits.

A strikingly large number of scatterings occurred at angles from 1 to 2°, totaling 27 events (including some events involving nuclear recoil), whereas the optical model indicates ~ 7 events for Re $f_{NN}(0) = 0$. The observed discrepancy cannot be accounted for solely by the inelastic reactions, which amount to 40% according to the estimates given above. It can reasonably be assumed that the discrepancy results from inaccuracy of the calculated cross sections at large angles.

The authors are deeply indebted to M. I. Podgoretskii for numerous valuable discussions and very considerable assistance, and to I. M. Gramenitskii and V. N. Strel'tsov for assistance and suggestions.

The authors also wish to thank the laboratory assistants G. A. Nurusheva, G. P. Tyupikova, T. A. Zhuravleva, É. V. Esina, and M. A. Varganova for performing measurements and scanning; also O. V. Kol'ga and M. I. Filippova for assistance with the calculations.

[1] Bannik, Grishin, Danysh, Lyubimov, and Podgoretskii, JETP **37**, 1575 (1959), Soviet Phys. JETP **10**, 1118 (1960).

[2] B. P. Bannik and M. I. Podgoretskii, Приборы и техника эксперимента (Instrum. and Exptl. Techniques) No. 3, 36 (1960).

[3] B. P. Bannik and V. G. Grishin, JETP **39**, 94 (1960).

[4] Von Dardel, Frisch, Mermod, Milburn, Piroué, Vivargent, Weber, and Winter, Phys. Rev. Letters **5**, 333 (1960); Perez-Mendez, Atkinson, Hess, and Wallace, Bull. Am. Phys. Soc. **4**, 253 (1959).

[5] Wang Shu-Fen, Vishki, Gramenitskii, Grishin, Dalkhazhav, Lebedev, Nomofilov, Podgoretskii, and Strel'tsov, JETP **39**, 957 (1960), Soviet Phys. JETP **12**, 663 (1961).

[6] V. S. Barashenkov, Usp. Fiz. Nauk **72**, 53 (1960), Soviet Phys.-Uspekhi **3**, 689 (1961).

[7] R. Hofstadter, Revs. Modern Phys. **28**, 214 (1956).

[8] V. A. Nikitin and É. N. Tsyganov, JETP **40**, 1027 (1961).

[9] T. A. J. Maris and H. Tyrén, Nuclear Phys. **3**, 35 (1957); H. Tyrén and T. A. J. Maris, Nuclear Phys. **6**, 82; 446 (1958).

[10] I. Ya. Pomeranchuk and E. I. Feĭnberg, Doklady Akad. Nauk SSSR **93**, 439 (1953).

Translated by I. Emin
282

INVESTIGATION OF ELECTRON BUNCHES IN A MICROTRON

V. P. BYKOV

Physics Laboratory, Academy of Sciences U.S.S.R.

Submitted to JETP editor January 25, 1961

J. Exptl. Theoret. Phys. (U.S.S.R.) 40, 1658-1666 (June, 1961)

A technique is developed for measuring charge density in electron bunches produced when electrons are accelerated in a microtron. Measurements performed on the microtron of the Institute for Physics Problems showed that the effective length of the bunches is $0.05 - 0.07\lambda$, where λ is the wavelength of the accelerating field. The electron distribution in a bunch corresponds on the whole to the theory of microtron operation.

THE principle of the microtron, which is a powerful source of bunched electrons, was published as long ago as 1944.[1] The earliest microtrons[2,3] had low efficiency, owing to the difficulty of capturing electrons into accelerating orbits. The electrons were obtained through unregulated cold emission and were captured in a region traversed by all orbits. These difficulties were overcome and the current considerably increased in the microtron of of the Institute for Physics Problems (IPP).[4]

A limit to the increase of current and energy in a microtron is imposed by the requirement of coherent emission of electron bunches. It is therefore of interest to investigate the size of bunches experimentally.

Electron bunching in microtrons depends mainly on the size of the region of phase stability, which was investigated theoretically by Henderson et al.[5] and by Kolomenskii.[6] The former gave numerical results, while the latter used an analytic method supplemented by numerical calculations. The results of the two investigations are in essential agreement.

From Kolomenskii's work it follows that stable phases range from 0 to 32.5°, in accordance with the inequality*

$$0 < \mathrm{tg}\varphi_s < \mathrm{tg}(\varphi_s)_{lim} = 2/\pi.$$

A particle traversing the resonator will undergo phase oscillations if it is not in a stable phase. The frequency ν of these oscillations at small amplitudes is given by

$$\cos\nu = 1 - \pi\mathrm{tg}\varphi_s.$$

The departure of ν from this equation increases with the amplitude of phase oscillations (see Fig. 4 in reference 6). Phase trajectories can be plotted in a plane, with ordinates representing the difference between the particle energy and the corresponding stable energy, and with abscissas representing the phase. The phase trajectories remain closed up to a certain limiting amplitude. The limiting trajectory bounds the phase stability region of the microtron. The longitudinal dimension of bunches in a microtron beam is obviously determined mainly by the extent of the phase stability region along the abscissal axis. Theoretical calculations show that the length of bunches must be about 0.1λ, where λ is the wavelength of the accelerating field.

An oscilloscopic study of electron bunching was made on the IPP microtron operated in its first mode[4] and producing a 5 milliamp pulsed current at 7.3 Mev in the 12th orbit. This method had been used previously by Tzopp[7] to investigate electron bunching in a linear accelerator. The sweep was produced by a sinusoidal voltage of the same frequency as the accelerating frequency. All electron bunches traversed the deflecting system in the same phase, but the beginning and end of each bunch were in slightly different phases and were deflected differently. The bunch size was determined from these deflections and the sweep speed.

The deflecting system was a toroidal resonant cavity, where the electric field was perpendicular to the electron velocity. This resonator was placed in the 12th (i.e., last) orbit of the microtron (Fig. 1). Electrons were deflected vertically, i.e., parallel to the magnetic field of the microtron. Power was fed to the resonator from the waveguide of the microtron by means of a coaxial line.

A fluorescent screen was positioned 360 mm after the resonator along the 12th orbit. An electron bunch traced a bright vertical band on this screen, which was observed visually by television.

*tg = tan.

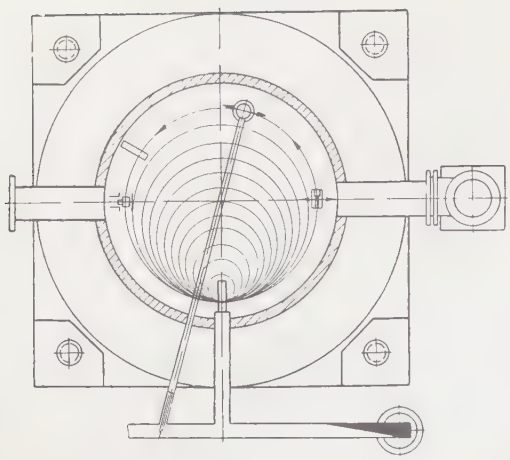

FIG. 1. General scheme of microtron.

The height h of this band was related to the bunch length l by

$$h/u = l/v, \tag{2}$$

where u is the sweep rate and v is the electron velocity ($v \approx c$). Thus

$$l \approx hc/u. \tag{3}$$

For the purpose of determining the sweep rate, the deflection amplitude A must be known, i.e., the maximum deflection for the given resonator power, since $u = \omega A$. However, zero deflection accompanied the maximum sweep rate. Therefore the phase difference between the rf oscillations in the sweep resonator and the electron bunches had to be changed by at least $\pi/2$.

Since it was difficult to construct a phase shifter that would not affect the power in the sweep resonator, we employed a different measuring technique free of this defect. The sweep resonator was now shifted along the electron trajectory by bending the coaxial line. This varied the phase between the rf field in the sweep resonator and the entering electrons. It is easily seen that the resonator had to be shifted by only the length of a bunch (16 mm). The screen on which electron bunches were displayed contained a narrow horizontal slit, behind which an electron collector was placed to permit quantitative measurements. Electron density in the bunches was thus measured electrically besides being observed visually.

If the voltage in the accelerating resonator is $U = U_0 \sin \omega t$, the current in the last orbit traversing this resonator is some periodic function of phase or time $J(\omega t)$, which must be determined. The voltage in the sweep resonator was generally different in phase from that in the accelerating resonator, and would thus be described by $\sin(\omega t + \varphi)$. φ remains constant during the measurements. The current through the sweep resonator is*

$$J(\omega t + \omega s/v) = J[\omega(t + s/v)], \tag{4}$$

where S is the length of the electron trajectory between the accelerating and the sweep resonator. The additional term $\omega s/v$ depends on the electron time of flight from the former to the latter.

The only electrons passing through the slit in the screen will obviously be those traversing the sweep resonator close to the voltage phases $2n\pi$, i.e.,

$$\Omega t = 2n\pi - \varphi_1. \tag{5}$$

This phase region is given by

$$\Delta\varphi = \omega\tau, \tag{6}$$

where τ is the time of beam passage through the slit; $\tau = d/u$, where d is the width of the slit, $u = \omega A$ is the sweep speed, and A is the sweep (or deflection) amplitude (30 — 40 mm). In our case

$$\Delta\varphi = \omega d/u = d/A \approx 0.8^\circ. \tag{7}$$

During each period, for a given position of the sweep resonator the charge passing through the slit in the screen is

$$\left\{ J\left(\omega t + \omega \frac{s}{v}\right)_{\omega t = 2n\pi - \varphi_1} \right\} \tau = J\left(\omega \frac{s}{v} - \varphi_1\right) \frac{d}{\omega A}. \tag{8}$$

The mean current during a pulse is therefore

$$J\left(\omega \frac{s}{v} - \varphi_1\right) \frac{d}{\omega T A} = \frac{d}{2\pi A} J\left(\omega \frac{s}{v} - \varphi_1\right). \tag{9}$$

Multiplying by the duty cycle, we obtain the mean current at the collector:

$$J_c = \frac{d\nu_0\tau_0}{2\pi A} J\left(\omega \frac{s}{v} - \varphi_1\right), \tag{10}$$

where ν_0 is the pulse repetition rate and τ_0 is the pulse duration.

By varying the path s we obviously obtain J, the electron distribution, as a function of the phase. It is very clear that the measurements are essentially independent of the voltage amplitude in the sweep resonator, which determines only the resolution or accuracy of the method.

The sweep resonator (Fig. 2) was a toroidal resonant cavity with tapered capacitive bulges.

*The current through the sweep resonator will generally be smaller than that through the accelerating resonator, because of the presence of a diaphragm. For the sake of simplicity we shall neglect this difference.

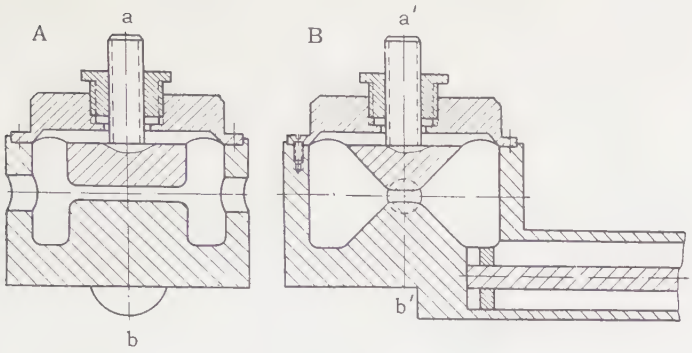

FIG. 2. Sweep resonator.

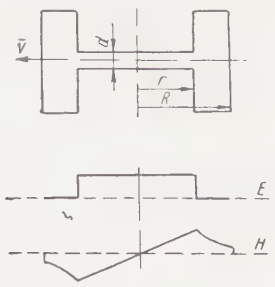

FIG. 3

This resonator had to be positioned in the 12th orbit without encroaching on the 11th orbit; the distance between orbits was $\sim\lambda/\pi = 32$ mm. This circumstance determined the shape of the resonator; a toroidal quasi-static resonator can be made considerably smaller than λ. The resonator was coupled inductively to the coaxial line by means of a bottom aperture (Fig. 2). A collar was moved along the center conductor of the line to regulate the coupling, which was adjusted to make the loaded Q of the resonator one-half of the unloaded value. There was thus no reflected wave in the coaxial line at resonance. The inner conductor had a 6-mm diameter, the inside diameter of the outer conductor was 14 mm, and the wave impedance of the line was $\sim 50\,\Omega$.

The inner conductor was centered by means of teflon disks arranged to coincide with standing-wave voltage nodes in the resonator when untuned. The vacuum in the coaxial line was maintained through a number of openings in the outer conductor for the purpose of connecting the line to the microtron vacuum chamber. The line was connected to the waveguide (Fig. 1) by a stub terminating the center conductor. The coupling was varied within rather wide limits by changing the length of stub in the waveguide. The center conductor was a tube through which cooling water was circulated.

The shifting of the sweep resonator through bending of the coaxial line was performed by a selsyn-driven screw mechanism. For the purpose of investigating different parts of the electron beam, a cooled diaphragm with an aperture of 0.4-mm diameter, which could be shifted radially, was positioned in the last orbit ahead of the sweep resonator.

The fluorescent screen contained a horizontal slit 0.4 mm wide. The electron collector, a thick-walled lead Faraday cylinder, was located 110 mm behind the slit, and was connected to a high-sensitivity (10^{-12} amp) current amplifier. (The amplifier of a standard "Cactus" dosimeter was used.) The high sensitivity of the amplifier required shielding of the Faraday cylinder from rf induction in the microtron chamber.

Signals from the amplifier were fed to an EPP-09 automatic potentiometer, whose tape motion was synchronized with the shifting of the sweep resonator. A curve representing the electron distribution in a bunch was thus traced automatically on the tape.

The production of a sufficiently large sweep amplitude on the screen required large rf power dissipation in the sweep resonator. For the purpose of calculating this power we considered the electron motion in the toroidal resonator (Fig. 3), where the field distribution was assumed to be quasi-stationary. The effect of the resonator magnetic field on the motion of a relativistic electron is of the same order of magnitude as that of the electric field and must be taken into account. Calculations showed that after traversing the sweep resonator an electron has the vertical momentum component

$$\Delta p_z = \frac{eE_0}{c}\frac{\lambda}{2\pi}\cos(\varphi+\psi_0)\{2\sin\psi_1 - \psi_1^2[\mathrm{Si}(\psi_0) - \mathrm{Si}(\psi_1)] - (\sin\psi_1 - \psi_1\cos\psi_1)\}, \quad (11)$$

where E_0 and λ are the amplitude and wavelength of the electric field in the resonator, φ is the phase of electron transit through the center of the resonator, $\psi_0 = 2\pi R/\lambda$, and $\psi_1 = 2\pi r/\lambda$. The first term within the braces results from the electric field, while the second and third terms result from the magnetic field. These terms have the values 1.65, -0.38, and -0.27, respectively.

We thus see that the effect of the magnetic field is opposed to that of the electric field and equals 40% of the latter. The sweep amplitude A is related to the acquired momentum $(\Delta p)_{max}$ by

$$A = (\Delta p)_{max}\, cL/E = (eE_0/E)L\lambda/2\pi, \quad (12)$$

where L is the distance from the resonator to the screen and E is the total electron energy. The electric field E_0 is determined from the power absorbed in the resonator:

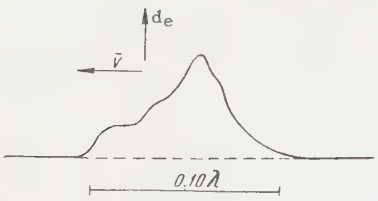

FIG. 4. Electron distribution along the length of a bunch. d_e is the electron density.

$$E_0 = \sqrt{8QW/fdr^2}\ , \qquad (13)$$

where Q is the quality factor of the sweep resonator, W is the absorbed power, f is the frequency, and d and r are the resonator dimensions. The sweep amplitude is thus

$$A = (e/E)\sqrt{8QW/fdr^2}\ . \qquad (14)$$

The parameters of our apparatus are Q = 3000, L = 36 cm, $f = 3 \times 10^9$ cps, d = 0.8 cm, r = 1.75 cm.

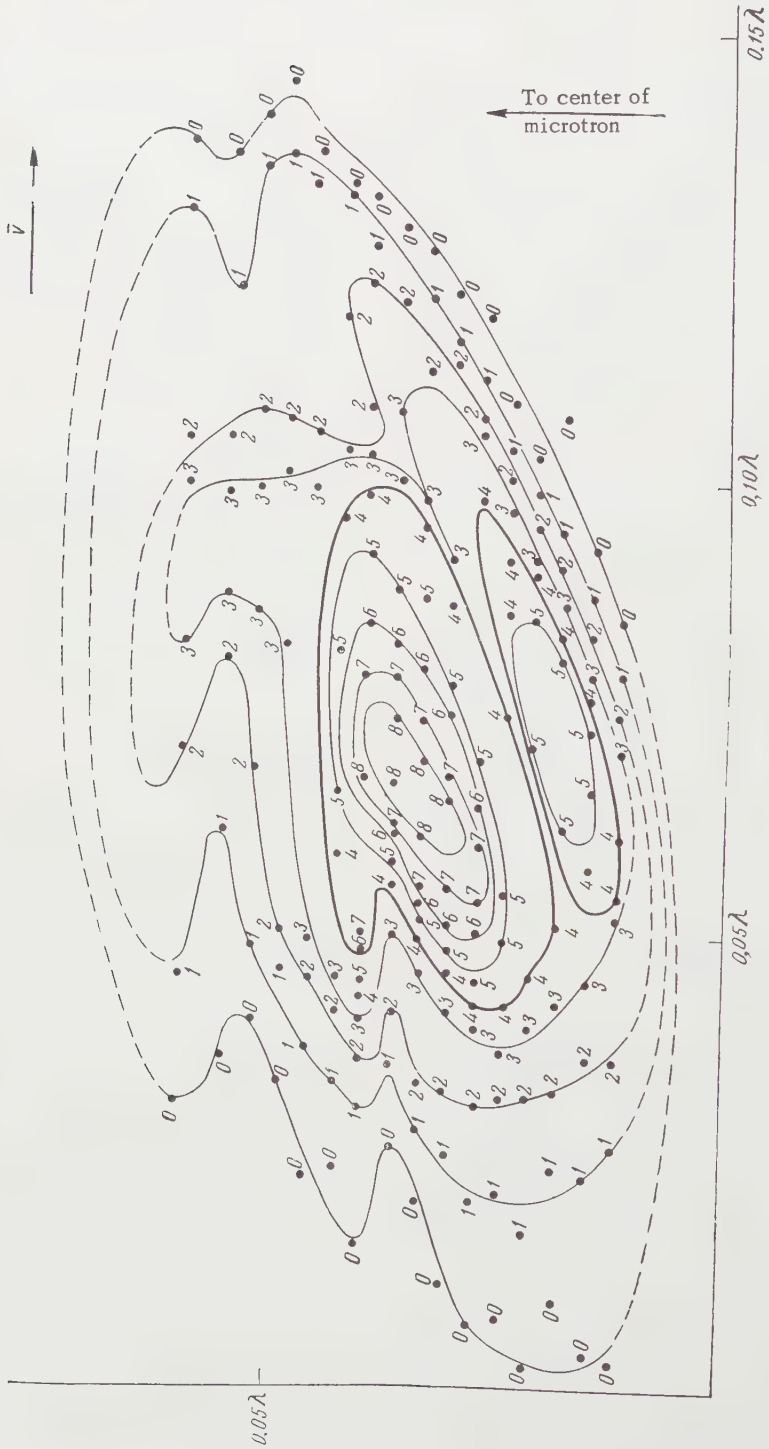

FIG. 5

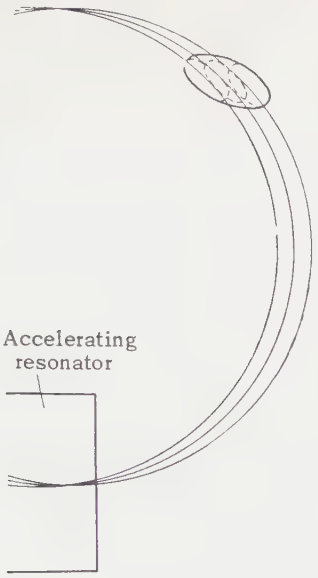

FIG. 6

and E = 7.3 Mev. At the power level W = 40 kw this gives the sweep amplitude A ≈ 2.8 cm. During the experiment the resonator absorbed 50 — 60 kw, and the sweep amplitude was 30 — 40 mm.

We shall now estimate the possible errors from several sources. First of all, when the coaxial line is bent the sweep resonator does not move along a circle but along a more complex curve, thus displacing the resonator with respect to the electron trajectory. Furthermore, since the beam is of finite width, it is shifted relative to the resonator axis. However, the field changes in the resonator close to the electron trajectory are proportional to the square of the displacement Δx:

$$\Delta E/E \sim \Delta H/H \sim (\Delta x/\lambda)^2. \qquad (15)$$

We thus see that even with a 3-mm displacement the field change does not exceed some tenths of one percent and can be neglected.

Furthermore, the bending of the coaxial line changes its electrical length to some extent; this can change the phase in the sweep resonator. It is suggested by Krasnushkin's[8] investigation that the change of electrical length of the line as a fraction of the wavelength is

$$\Delta = l_0 a^2/\lambda r^2, \qquad (16)$$

where l_0 is the length of the bent section, a is the radius of the line, and r is the radius of curvature of the bend. The actual radius of curvature was at least 200 cm. For a = 0.7 cm and l_0 = 39 cm we have $\Delta = 5 \times 10^{-5}$, corresponding to 0.02° phase difference, which is considerably below the resolving power of the apparatus. An experimental check showed that the phase change associated with the shifting of the resonator was under 0.5° in each instance.

FIG. 7. Phase diagram. Δε is the departure of energy from equilibrium.

Longitudinal displacement of the sweep resonator, changing the distance L to the screen, can also result in errors. The sweep speed will therefore differ for the measurements at the beginning and end of a bunch, respectively; the difference, δu/u = δL/L, is ~3%. The electron density at the beginning of a bunch will therefore be about 3% greater than at the end. This error can be excluded by a suitable correction.

Finally, the electron energy spread (±0.5%)[5,6] also induces some error. The measurements will contain an error of the same magnitude, since the sweep speed is inversely proportional to the energy.

The pulsed operation of the microtron is also very important for the accuracy of the measurements. Oscillations are set up in the sweep resonator, with its smaller Q, more rapidly than in the accelerating resonator, where oscillations build up in 1 μsec. However, the stable accelerating mode is established abruptly, since acceleration does not occur until the field amplitude in the accelerating resonator reaches a certain critical value.

An oscillogram of the accelerated current presents rectangular pulses 2 μsec long with steep edges. The rise time does not exceed 0.2 μsec. Thus the build-up processes cannot induce an error above 10%. The total systematic error of the measurements does not exceed 12 — 15%.

Figure 4 shows a typical record of the electron distribution in a bunch for a given diaphragm position. The electron density distribution over an entire bunch was determined by analyzing several plots corresponding to different diaphragm positions. The results are shown in Fig. 5, where the axes are parallel and perpendicular, respectively, to the direction of electron motion. The curves represent equal density levels bearing numbers proportional to the electron density.

The length of a bunch can be estimated from the diaphragm. If the length l is taken to mean the separation of two points where the electron density is half of the maximum, we have $l \approx 0.05 - 0.07\lambda$ or $5 - 7$ mm.

The error in l resulting from cathode instability is $20 - 25\%$, based on repeated measurements. The operation of the microtron is stable for a few hours on the average. However, the stability requirements of our measurements were very rigorous; as a result, some instability of cathode emission appeared.

The existence of two maxima in a bunch has not previously been explained satisfactorily. The total length of a bunch is 0.14λ, which considerably exceeds the theoretical length of the phase stability region (0.10λ). This is accounted for by the angle spread in the velocities of electrons leaving the accelerating resonator. These electrons will therefore move along noncoincident orbits (Fig. 6), resulting in a lengthening of the bunches at orbital points most distant from the accelerating resonator.

In order to understand the electron distribution in a bunch we must consider how a phase diagram is filled in. Electrons emerging from the resonator for the first time are distributed uniformly along some curve AB intersecting the phase diagram (Fig. 7). In subsequent passes through the resonator this curve is transformed in a complex manner, since the frequency of phase oscillations depends on their amplitude. The curve ultimately just about fills the entire phase region. Some inhomogeneity of the magnetic field as well as possible fluctuations of the rf amplitude produces additional interspersion of electrons in the phase diagram. Electrons corresponding to large amplitudes of the phase oscillations will be smeared over a larger area than those close to the equilibrium position. This can obviously account for the experimentally observed electron distribution.

Incomplete coverage of the phase diagram by the shifting of the original curve would produce fine structure in a bunch. The second maximum in a bunch could possibly be the remnant of this fine structure.

I wish to thank P. L. Kapitza for his interest, and S. P. Kapitza for directing this research. I also wish to thank L. A. Vaĭnshteĭn and V. N. Melekhin for many valuable discussions.

[1] V. I. Veksler, Doklady Akad. Nauk SSSR **43**, 346 (1944); J. Phys. U.S.S.R. **9**, 153 (1945).

[2] Redhead, Le Caine, and Henderson, Can. J. Phys. **A28**, 73 (1950).

[3] Henderson, Heymann, and Jennings, Proc. Phys. Soc. (London) **B66**, 654 (1953).

[4] S. P. Kapitza, Bykov, and Melekhin, JETP **39**, 997 (1960), Soviet Phys. JETP **12**, 693 (1961).

[5] Henderson, Heymann, and Jennings, Proc. Phys. Soc. (London) **B66**, 41 (1953).

[6] A. A. Kolomenskii, J. Tech. Phys. (U.S.S.R.) **30**, 1347 (1960), Soviet Phys.-Tech. Phys. **5**, 1278 (1961).

[7] L. É. Tzopp, Радиотехника и электроника (Radio Engineering and Electron Physics) **4**, 1936 (1959).

[8] P. E. Krasnushkin, Уч. зап. МГУ, (Science Notes, Moscow State University), Physics. v. 2, No. 75, p. 9.

Translated by I. Emin
283

ON THE NATURE OF SPIN-LATTICE INTERACTION IN CHROME CORUNDUM. I.

G. M. ZVEREV

Institute for Nuclear Physics, Moscow State University

Submitted to JETP editor January 30, 1961

J. Exptl. Theoret. Phys. (U.S.S.R.) 40, 1667-1671 (June, 1961)

The temperature dependence of the spin-lattice relaxation time of corundum containing various amounts of chromium has been studied by continuously changing the temperature from 4 to 90° K. At small concentrations, the relaxation is determined by the Kronig-Van Vleck mechanism. At high chromium concentrations a new spin-lattice mechanism arises, which apparently is due to an exchange interaction between pairs of chromium ions. The spin-lattice relaxation of chrome corundum samples irradiated in a reactor has been investigated. The measurements were made at 3.2 cm by the CW saturation technique.

1. INTRODUCTION

CHROME corundum (ruby) is now widely used as the working substance in paramagnetic amplifiers. Spin-lattice relaxation plays a very important role in the operation of these amplifiers. Hence a considerable number of experimental papers have been devoted to the study of spin-lattice relaxation in chrome corundum.[1-5]

It has been established,[2] that at liquid-helium temperatures the spin-lattice relaxation time τ_1, measured by the CW saturation method, depends strongly on the concentration of paramagnetic ions, e.g., for a sample with a chromium concentration $c = 5 \times 10^{-4}$ the magnitude of τ_1 is 4.4×10^{-2} sec, and for a concentration of 4×10^{-3}, $\tau_1 = 6 \times 10^{-4}$ sec. (Concentration is defined as the ratio of the number of Cr^{3+} ions to the number of Al^{3+} ions in the corundum lattice.) At liquid-nitrogen temperatures the dependence of the relaxation time on concentration is weaker[2,5]: for the same samples τ_1 is respectively 1.3×10^{-4} and 2.7×10^{-5} sec. The Kronig[6] and Van Vleck[7] classical theory of spin-lattice relaxation, which was developed for isolated paramagnetic ions in a crystal lattice, does not contain a dependence on the concentration of the paramagnetic ions.

Experiments by the pulse method have shown that the spin-lattice relaxation process at low temperatures is complicated by cross relaxation effects.[8,9] Cross relaxation has explained a number of anomalies in the relaxation phenomena at low temperatures (cross saturation, the presence of "fast" exponents in the process of recovery of the intensity of saturated lines, etc.) However, cross relaxation cannot explain the concentration dependence of τ_1; while it equalizes the spin temperature of different transitions, it cannot change the rate of energy interchange between the spin system and the lattice.

A single relaxation mechanism is insufficient to explain all of the experimental data at low temperatures. It is natural to suppose that several mechanisms take part simultaneously in the spin-lattice relaxation process, each one predominating at a different temperature.

The goal of our investigation of spin-lattice relaxation in chrome corundum was the elucidation of the nature of these mechanisms. All the measurements were made at a frequency of 9400 Mc by the CW saturation method.

2. INVESTIGATION OF SPIN-LATTICE RELAXATION IN IRRADIATED CHROME CORUNDUM.

Van Vleck pointed out as early as 1941, that at low temperatures a limit to the rate of spin-lattice relaxation could exist because of the lack of low-frequency oscillators for the transfer of the energy to the walls of the sample.[10] This idea has been extensively discussed more recently by Gorter, van der Marel, and Bölger,[11] by Townes and his co-workers,[12] and by others.

The limitation due to the lack of low-frequency phonons is withdrawn if there exist processes that widen the frequency band of oscillators interacting with the spins. The scattering of phonons by cracks and lattice defects can serve as such processes. We have made a comparison of the spin-lattice relaxation times of samples having the same concentration of chromium, but a different concentration of defects.

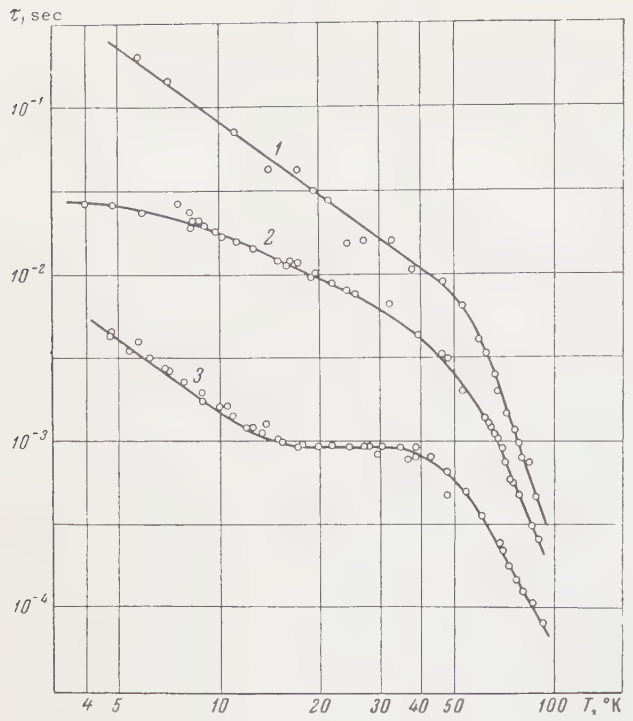

The lattice defects (principally in the form of atoms displaced from their equilibrium positions) were created by irradiation with fast neutrons and gamma rays in the active zone of a reactor. The number of defects in the irradiated samples was of the order of 10^{19} cm^{-3}.[13] After irradiation, the electron paramagnetic resonance spectrum in parallel orientation ($\theta = 0°$) was measured. The line positions had not changed, but transitions between the levels with quantum numbers $+3/2$ and $+1/2$ were significantly widened: the width had increased from 15 to 70 oe. The line corresponding to the transition $+1/2 \longleftrightarrow -1/2$ was unchanged.*

The spin-lattice relaxation time τ_1 of the transition $+1/2 \longleftrightarrow -1/2$ in the parallel orientation, for the irradiated sample with chromium concentration of 2×10^{-4}, turned out to be three times shorter than τ_1 for the non-irradiated control sample of the same concentration. For samples of concentration 8×10^{-4} the relaxation time τ_1 of the irradiated sample was only 1.3 times shorter than τ_1 for the corresponding control sample.

These experiments were conducted at T = 4.2°K. At 77° K the relaxation times of the irradiated samples were the same as those of the control samples. It is to be noted that the number of low-frequency phonons in the control sample should not increase significantly with an increase in chromium concentration, since the scattering from isomorphous paramagnetic centers in the crystal is not significant, and the number of defects in the lattice of the non-irradiated samples is not large (no line broadening due to lattice non-ideality was observed in the samples of both concentrations studied).

Thus, phonon effects play a role only in samples with a low chromium content.* At higher concentrations new relaxation mechanisms appear, not limited by a lack of low-frequency oscillators.

3. INVESTIGATION OF THE TEMPERATURE DEPENDENCE OF τ_1 IN THE RANGE 4 — 90° K.

The different mechanisms of spin-lattice relaxation should show up differently at different temperatures. The results of Manenkov and Prokhorov[2] show that the sharp dependence of τ_1 on concentration at helium temperatures is replaced at T = 77° K by a weaker dependence. At room temperature τ_1 is practically identical for all concentrations. It would be extremely interesting to follow the course of the temperature dependence of τ_1 for different concentrations by continuously changing the temperature. To this end a special apparatus was constructed, with the cavity enclosed by a liquid-helium cooled jacket.[15] By heating the cavity it was possible to obtain any temperature between 2 and 60° K for a prolonged length of time. The temperature was monitored with a carbon thermometer. Use of liquid nitrogen as a coolant makes the higher temperature region 60 — 100° K available for study.

The line width of chrome corundum does not depend on temperature. We used a cavity whose loaded Q likewise did not change with temperature. Hence it was possible to study the dependence of τ_1 on T by measuring the power necessary to saturate a given transition at different temperatures. The results of these measurements for three different chromium concentrations are shown in the

*The noticeable widening of the transitions $+3/2 \leftrightarrow +1/2$ is due to the following circumstance. The energy of these transitions ($h\nu = \pm 2D \mp g_{\parallel} \beta H$) depends on the values of the spin Hamiltonian parameters D and $g_{\parallel}$. The disturbance to the regularity of the crystallographic surroundings causes the electric field at the location of a chromium ion to change slightly from ion to ion. This change leads to a variation in the values of the spin Hamiltonian parameters such that the variation in D is very much greater than the variation in $g_{\parallel}$. The theory[14] gives the following relation between the parameters: $2D = \lambda(g_{\parallel} - g_{\perp})$. Since the g-factors are close to one another, the dispersion of the values of D exceeds by three orders the dispersion of the g-factors.

*Attempts to detect a dependence of spin-lattice relaxation time on size (for the concentration of 2×10^{-4}) were unsuccessful; τ_1 was the same within 10% for samples, the smallest linear dimensions of which differed by a factor of four.

figure. The relaxation time studied was that of the transition $+\frac{1}{2} \longleftrightarrow -\frac{1}{2}$. The angle θ was chosen equal to 5°, in order to avoid the possibility of cross relaxation with the transition $-\frac{1}{2} \longleftrightarrow +\frac{3}{2}$.

Curve 1 shows the temperature dependence of the spin-lattice relaxation time for a sample having a chromium concentration $c = 2 \times 10^{-4}$. At temperatures below 50° K, $\tau_1 \sim T^{-1.5}$, and in the interval 64 — 90° K, $\tau_1 \sim T^{-7}$. Curve 2 is for a sample with $c = 8 \times 10^{-4}$. In this case, $\tau_1 \sim T^{-5}$ in the 64 — 90° K interval; it is impossible to characterize the temperature region below 50° K by a single power law. Curve 3 corresponds to a concentration of 2.8×10^{-3}. In the interval 4.2 — 12° K, $\tau_1 \sim T^{-1.3}$; at temperatures from 15 — 32° K, the relaxation time is practically constant, and in the 64 — 90° K range, the magnitude of $\tau_1 \sim T^{-4}$. The precision of the relative measurements of τ_1 is ±10%.

4. DISCUSSION OF THE RESULTS

The curves of τ_1 as a function of temperature for the three chromium concentrations are essentially different in character.

Curve 1, which pertains to the most dilute sample, corresponds approximately to the Kronig-Van Vleck mechanism. Up to 50° K, the relaxation is basically due to the direct process of absorption and emission of single phonons. At higher temperatures processes of Raman scattering of phonons prevail; hence in this range τ_1 strongly depends on temperature ($\tau_1 \sim T^{-7}$).

With an increase in paramagnetic-ion concentration, a new mechanism enters into the relaxation process. It appears particularly pronounced in curve 3, corresponding to the sample with chromium concentration 2.8×10^{-3}. This mechanism shortens the spin-lattice relaxation time at helium temperatures. In the temperature interval 4 — 32° K the relaxation is completely determined by this mechanism; at higher temperatures the Kronig-Van Vleck mechanism also takes part. It is likely that the mechanism that determines the concentration dependence of τ_1 at helium temperatures is relaxation through the exchange interaction of pairs of chromium ions.

The optical investigations of Shawlow, Wood, and Clogston[16] have shown that the fluorescence spectrum of ruby has certain lines which cannot be attributed to transitions between levels of individual Cr^{3+} ions: at a chromium concentration of 3×10^{-4} these lines are absent, and at higher concentrations their intensity increases approximately as the square of the concentration.

The weak lines appearing in the vicinity of the electron paramagnetic resonance lines that belong to transitions between levels of individual Cr^{3+} ions are also associated with exchange interactions of ion pairs.[17]

It can be considered that exchange interaction is also responsible for the anomalies in the relaxation process at low temperatures. At very low paramagnetic-ion concentration, when the number of exchange pairs is small, spin-lattice relaxation is determined by the Kronig-Van Vleck mechanism. This is confirmed by the fact that at extremely low concentrations there is no dependence on concentration. With an increase in concentration the contribution of the exchange relaxation mechanism becomes important. At concentrations of 5×10^{-4} — 5×10^{-3} this mechanism will come in strongly at helium temperature. At still higher concentrations this mechanism will show up even at nitrogen temperatures.

Curve 3 of the figure shows how the probability of exchange relaxation changes with changing temperature. At temperatures of 4.2 — 12° K, τ_1 is approximately proportional to T^{-1}. With further increase in temperature, τ_1 is independent of temperature. The temperature dependence of τ_1 in the interval 32 — 90° K reflects the simultaneous participation of a mechanism giving a T^{-7} dependence and one independent of temperature.

In order to explain the existence of the "plateau" in curve 3 of the figure, we have to suppose that there is an exchange heat reservoir, as postulated by Bloembergen and Wang.[18] In this model the energy of the spin system is first transferred to the exchange reservoir, and from there falls directly into the lattice. At very low temperatures the rate of transfer of energy from the spin system is determined by the transfer process out of the exchange reservoir into the lattice, which depends on temperature. At higher temperatures the probability of a relaxation transition is determined by the process of energy transfer from the system into the exchange reservoir, which does not depend on temperature.

The process of spin-lattice relaxation by means of exchange of ion pairs includes the process of transfer of excitation from the spins of single Cr ions to spins of associated pairs. This transfer undoubtedly occurs through cross spin relaxation and can include spin diffusion processes.

Note that the "plateau" in the curve cannot be successfully explained by a single cross-relaxation process, if this curve is obtained by the CW method. Cross relaxation changes only the effective width of the saturated line.

The author thanks Prof. A. M. Prokhorov for many discussions and valuable suggestions, and also N. I. Naumkin, N. G. Petelina, and V. P. Kiryukhin for assistance in performing the experiment.

[1]Davis, Strandberg, and Kyhl, Phys. Rev. **111**, 1268 (1958).

[2]A. A. Manenkov and A. M. Prokhorov, JETP **38**, 729 (1960), Soviet Phys. JETP **11**, 527 (1960).

[3]Pace, Sampson, and Thorp, Phys. Rev. Letters **4**, 18 (1960).

[4]R. A. Armstrong and A. Szabo, Canad. J. Phys. **38**, 1304 (1960).

[5]J. C. Gill, Quantum Electronics, ed. by C. H. Townes (Columbia Univ. Press, New York, 1960), p. 333.

[6]R. Kronig, Physica **6**, 33 (1939).

[7]J. H. Van Vleck, Phys. Rev. **57**, 426 (1940).

[8]Bloembergen, Shapiro, Pershan, and Artman, Phys. Rev. **114**, 445 (1959).

[9]B. Bölger, Quantum Electronics, ed. by C. H. Townes (Columbia Univ. Press, New York, 1960), p. 337.

[10]J. H. Van Vleck, Phys. Rev. **59**, 724 (1941).

[11]Gorter, Van der Marel, and Bölger, Physica **21**, 103 (1955).

[12]Giordmaine, Alsop, Nash, and Townes, Phys. Rev. **109**, 302 (1958).

[13]G. J. Dienes and G. H. Vineyard, Radiation Effects in Solids (Interscience, New York, 1957).

[14]W. Low, Paramagnetic Resonance in Solids, Academic Press, New York, 1960.

[15]G. M. Zverev, Приборы и техника эксперимента (Instr. and Exptl. Tech.), in press.

[16]Shawlow, Wood, and Clogston, Phys. Rev. Letters **3**, 271 (1959).

[17]Rimai, Statz, Weber, de Mars, and Koster, Phys. Rev. Letters **4**, 125 (1960).

[18]N. Bloembergen and S. Wang, Phys. Rev. **93**, 72 (1954).

Translated by L. M. Matarrese
284

LEPTONIC DECAY OF THE Λ HYPERON AND THE PROBABILITY OF THE $K_{\mu 2}$ AND K_{e3} PROCESSES

G. M. GANDEL'MAN

Submitted to JETP editor June 27, 1960

J. Exptl. Theoret. Phys. (U.S.S.R) **40**, 1672-1675 (June, 1961)

A new postulate is introduced for the divergence of the vector part of the strangeness-violating baryon current. The Gell-Mann and Levy[1] postulate is taken for the divergence of the axial vector part, but with the π-meson operator replaced by the K-meson operator. As a result it is found to be possible to relate the probability for the leptonic decay of the Λ particle to the probability for the $K_{\mu 2}$ and K_{e3} processes. The theory leads to the conclusion that the vector variant plays a most important role in the leptonic decay of the Λ particle.

INTRODUCTION

RECENTLY Gell-Mann and Levy[1] introduced a certain postulate for the divergence of the axial vector part of the strong current and succeeded in finding a relation between the decay probability of the charged π meson and the β interaction coupling constant. The lifetime of the charged pion obtained by them coincides with that obtained by Goldberger and Treiman,[2] who made use of dispersion relation techniques with only certain intermediate states taken into account, and is in good agreement with experiment.

The Gell-Mann and Levy hypothesis refers essentially to the baryon current only, not including strange particle, responsible for β decay, μ capture and the decay of the charged pion. When these results are generalized to the case of strong interactions including strange particles, it is therefore necessary to satisfy both the condition of parity conservation and strangeness conservation.

To generalize the ideas of Gell-Mann and Levy[1] to the case of the baryon current including strange particles ($K_{\mu 2}$, K_{e2}, $K_{\mu 3}$ and K_{e3} decays and β decay of the Λ particle) one can introduce an additional postulate referring to the divergence of the vector part of the baryon current, which now no longer vanishes. The simplest form of the postulates follows from strangeness and parity conservation considerations, and we assume that the K meson is pseudoscalar. Thus we assume that

$$\partial_\alpha P_\alpha = ia\varphi_K, \tag{1}$$

$$\partial_\alpha V_\alpha = ib\varphi_\pi\varphi_K. \tag{2}$$

The first equation, giving the divergence of the axial vector current, is the same as assumed by Gell-Mann and Levy[1] but with the π-meson field operator replaced by the K-meson operator.[3] The divergence of the vector current is assumed to be equal to the product of the π- and K-field operators.

In Sec. 1 we discuss the consequences of such a hypothesis. It turns out that the $K_{\mu 2}$ and K_{e2} decay probabilities can be expressed in terms of the constant a, and the $K_{\mu 3}$ and K_{e3} decay probabilities in terms of the constant b. In Sec. 2 the probability for the leptonic decay $\Lambda \to p + e + \nu$ is obtained and found to depend on the constants a and b.

The new postulate, Eq. (2), here introduced means in fact that the vector part of the leptonic Λ decay is mainly connected with the intermediate state K meson + π meson.

1. PROBABILITY OF THE $K_{\mu 2}$ AND K_{e3} DECAYS

The matrix element for the $K_{\mu 2}$ decay is given by

$$\langle \mu\nu \,|\, K\rangle = 2^{-1/2} G \langle 0 \,|\, P_\lambda \,|\, K\rangle \bar{u}_\mu \gamma_\lambda (1+\gamma_5) u_\nu \delta (p_K - p_\mu - p_\nu). \tag{3}$$

On the basis of Eq. (1) we find, as in reference 1, that

$$\langle 0 \,|\, P_\lambda(x) \,|\, K\rangle = -a \sqrt{Z_{3K}}\, (p_{K\lambda}/m_K^2) \langle 0 \,|\, \varphi_{Kr}(x) \,|\, K\rangle; \tag{4}$$

the matrix element of the renormalized $\varphi_{Kr}(x)$ between a meson state and vacuum is the same as that of the free field between the states of a free particle and the free vacuum.

It is now easy to express the $K_{\mu 2}$ probability in terms of $a\sqrt{Z_{3K}}/m_K^2$. An elementary comparison with experimental data (see, for example, Okun's review,[4] p. 469) yields

$$a\sqrt{Z_{3K}}/m_K^2 = 0{,}0375\ m, \tag{5}$$

where m is the nucleon mass and m_K is the K-meson mass.

Let us consider now the K_{e3} process. Because of the pseudoscalarity of the K meson only the vector current contributes to the matrix element of this process

$$\langle e\nu\pi\,|\,K\rangle = G2^{-1/2}\langle\pi\,|\,V_\alpha\,|\,K\rangle\,\bar{u}_e\gamma_\alpha\,(1+\gamma_5) \times u_\nu\delta\,(p_K - p_e - p_\nu - p_\pi). \tag{6}$$

Because $V_\alpha \sim \varphi_\pi\varphi_K$ [according to Eq. (2)] it follows from invariance considerations that

$$\langle\pi\,|\,V_\alpha\,|\,K\rangle = [c_1\,(p_\pi + p_K)_\alpha + c_2\,(p_\pi - p_K)_\alpha]\,\langle\pi\,|\,\varphi_\pi\varphi_K\,|\,K\rangle, \tag{7}$$

but, in addition,

$$\partial_\alpha V_\alpha - ib\varphi_\pi\varphi_K, \tag{8}$$

i.e., $(p_\pi - p_K)_\alpha V_\alpha = b\varphi_\pi\varphi_K$, where b is a constant.

There are grounds for expecting that c_1 and c_2 depend on k^2 only weakly. We shall consider them to be constant. Then it follows immediately from Eqs. (7) and (8) that

$$c_2 = 0, \qquad c_1 = b/(m_K^2 - m_\pi^2). \tag{9}$$

The equality $c_2 = 0$ means that the probabilities for $K_{\mu3}$ and K_{e3} are in a definite ratio: $W_{\mu3}/W_{e3} = 0.6875$. This results from the data given by Okun'[4] (p. 473), since in our case $f_1 = f_2$, $g = 2f$ (in the notation of the above-mentioned review), which is not in bad agreement with the experimental value 0.765.[5]

Thus,

$$\langle\pi\,|\,V_\alpha\,|\,K\rangle = [b/(m_K^2 - m_\pi^2)]\,\sqrt{Z_{3K}}\,\sqrt{Z_{3\pi}}\,(p_K + p_\pi)_\alpha \times\langle\pi\,|\,\varphi_{\pi r}\varphi_{Kr}\,|\,K\rangle. \tag{10}$$

The last matrix element is of the same order of magnitude as the free-field matrix element. This is valid in the case when $K\pi$ scattering processes contribute insignificantly to this matrix element. Therefore Eq. (11) below is valid only approximately. By making use of Eq. (10) one can find the probability for K_{e3} decay. Comparing the resultant formula with the experimental value we obtain

$$b\sqrt{Z_{3K}Z_{3\pi}}/(m_K^2 - m_\pi^2) \approx 0.16. \tag{11}$$

2. LEPTONIC DECAY OF THE Λ PARTICLE

The amplitude for this decay is

$$2^{-1/2}G\bar{u}_e\gamma_\alpha\,(1+\gamma_5)\,u_\nu\,[\langle p\,|\,V_\alpha\,|\,\Lambda\rangle + \langle p\,|\,P_\alpha\,|\,\Lambda\rangle]. \tag{12}$$

On the basis of Eqs. (1) and (2) we have

$$\langle p\,|\,k_\alpha P_\alpha\,|\,\Lambda\rangle = a\sqrt{Z_{3K}}\,\langle p\,|\,\varphi_{Kr}\,|\,\Lambda\rangle, \tag{13a}$$

$$\langle p\,|\,k_\alpha V_\alpha\,|\,\Lambda\rangle = b\sqrt{Z_{3K}}\,\sqrt{Z_{3\pi}}\,\langle p\,|\,\varphi_{\pi r}\varphi_{Kr}\,|\,\Lambda\rangle; \tag{13b}$$

$$k = p_\Lambda - p, \quad \langle p\,|\,\varphi_{Kr}\,|\,\Lambda\rangle = i\,(k^2 + m_K^2)^{-1}\,g_\Lambda\bar{u}_p\gamma_5 u_\Lambda L\,(k^2) \tag{14}$$

Here g_Λ is the strong interaction coupling constant, k is the Λ-nucleon momentum transfer, and $L(k^2)$ is the form factor of the vertex part.

It follows from relativistic invariance considerations that

$$\langle p\,|\,V_\alpha\,|\,\Lambda\rangle = \bar{u}_p\,\{\gamma_\alpha f_1 + f_2\,(\gamma_\alpha\hat{k} - \hat{k}\gamma_\alpha) + f_3 k_\alpha\}\,u_\Lambda,$$
$$\langle p\,|\,P_\alpha\,|\,\Lambda\rangle = \bar{u}_p\,\{\gamma_\alpha h_1 + h_2\,(\gamma_\alpha\hat{k} - \hat{k}\gamma_\alpha) + h_3 k_\alpha\}\,\gamma_5 u_\Lambda. \tag{15}$$

From here it follows that

$$\langle p\,|\,k_\alpha V_\alpha\,|\,\Lambda\rangle = \bar{u}_p\,\{f_1\hat{k} + k^2 f_3\}\,u_\Lambda, \tag{16a}$$

$$\langle p\,|\,k_\alpha P_\alpha\,|\,\Lambda\rangle = \bar{u}_p\,\{h_1\hat{k} + k^2 h_3\}\,\gamma_5 u_\Lambda. \tag{16b}$$

Making use of Eqs. (13a) and (14) and comparing them with Eq. (16b) for* $k^2 \to 0$, we obtain

$$-h_1\,(m_\Lambda + m) = a\sqrt{Z_{3K}}\,g_\Lambda L\,(0)/m_K^2, \tag{17}$$

whereas using Eq. (5) we obtain

$$-h = 0.0375\,g_\Lambda\,L\,(0)m/(m_\Lambda + m). \tag{18}$$

The here obtained value of h_1 agrees with the results of Albright,[6] who made use of the dispersion technique of Goldberger and Treiman.[2]

If we assume $g_\Lambda^2/4\pi = 2.6$[6] and $L(0) \approx 1$, then $-h_1 = 0.1$.

Let us consider next the vector matrix element

$$\langle p\,|\,k_\alpha V_\alpha\,|\,\Lambda\rangle = b\sqrt{Z_{3K}}\,\sqrt{Z_{3\pi}}\,\langle p\,|\,\varphi_{\pi r}\,\varphi_{Kr}\,|\,\Lambda\rangle.$$

The matrix element $\langle p\,|\,\varphi_{\pi r}\varphi_{Kr}\,|\,\Lambda\rangle$ is connected with the process shown in the Figure. For small momentum transfers k it follows from invariance considerations that

$$\langle p\,|\,\varphi_{\pi r}\,\varphi_{Kr}\,|\,\Lambda\rangle = i\alpha\,(g_\Lambda g/m)\,\bar{u}_p u_\Lambda. \tag{19}$$

Making use of Eqs. (19) and (11) and comparing with Eq. (16a) we obtain

$$(m_\Lambda - m)\,f_1 = b\sqrt{Z_{3K}}\,\sqrt{Z_{3\pi}}\,g_\Lambda\,g\alpha/m \approx 0.16\,(m_K^2 - m_\pi^2)\,g_\Lambda g\alpha/m, \tag{20}$$

whence

$$\left|\frac{f_1}{h_1}\right| \approx \frac{0.16}{0.0375}\,\frac{\alpha g}{L\,(0)}\,\frac{m_K^2 - m_\pi^2}{m^2}\,\frac{m_\Lambda + m}{m_\Lambda - m}. \tag{21}$$

An exact evaluation of α presents a difficult problem. It is necessary to remember that there are in fact two identical diagrams, one with the intermediate state $K^-\pi^0$, the other with $K^0\pi^+$. In the second case the matrix element is twice as large. Therefore the Feynman integral of the diagram (see the figure) calculated in perturbation theory must be multiplied by 3. A perturbation

*Generally speaking the quantity k^2 is of the order of m_π^2 (the pion mass) in the decay $\Lambda \to p + e^- + \nu$. For the form factor of this decay, however, the characteristic mass is m_K^2, and the ratio m_π^2/m_K^2 may be ignored so that the limit $k^2 \to 0$ can be taken.

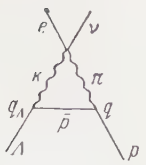

theory calculation, the details of which will be left out, leads to the value $\alpha = 0.016$.

If we assume $L(0) \approx 1$, $g^2/4\pi = 15$, then we get $f_1/h_1 \approx 2.76$. For the product of the leptonic decay probability by the lifetime τ of the Λ particle we then obtain (ignoring the form factor h_2)

$$W_\Lambda \tau = 0.4 \cdot 10^{-3}.$$

The experimental value[7] is approximately 1.3×10^{-3}.

At this time the experimental data on the decay $\Lambda \rightarrow p + e + \nu$ are most meager. The constant α also cannot be precisely calculated. However even in the roughest form of perturbation theory one obtains a not very large deviation from experiment.

The result obtained here indicates that in the Λ leptonic decay the main contribution is most likely to come from the vector part of the interaction. This can be checked experimentally most conveniently by utilizing the fact that the Λ particle is almost completely polarized; it then follows that for the axial vector covariant a strong asymmetry of the electron emission with respect to the Λ spin direction should be observed, whereas for the vector covariant no such asymmetry should be seen (this is correct to the extent that the proton recoil may be ignored).

In conclusion I express sincere gratitude to Ya. B. Zel'dovich for interest in the problem and to L. B. Okun' for interesting discussion.

[1] M. Gell-Mann and M. Levy, Nuovo cimento **16**, 705 (1960).

[2] M. L. Goldberger and S. B. Treiman, Phys. Rev. **110**, 1178 (1958).

[3] J. Nambu, preprint.

[4] L. B. Okun', Usp. Fiz. Nauk **68**, 449 (1959); Ann. Revs. Nuc. Sci. **9**, 61 (1959).

[5] Bruin, Holthuizen, and Jongejans, Nuovo cimento **9**, 422 (1958).

[6] C. H. Albright, Phys. Rev. **114**, 1648 (1959).

[7] Crawford, Cresti, Good, Kalbfleisch, Stevenson, and Ticho, Phys. Rev. Lett. **1**, 377 (1958); Nordin, Orear, Reed, Rosenfeld, Solmitz, Taft, and Tripp, Phys. Rev. Lett. **1**, 380 (1958).

Translated by A. M. Bincer
385

THE CONDUCTION-ELECTRON INTERACTION INDUCED BY SPIN WAVES IN A FERROMAGNETIC SUBSTANCE

S. V. VONSOVSKII and M. S. SVIRSKII

Institute for the Physics of Metals, Academy of Sciences, U.S.S.R.; Chelyabinsk State Pedagogical Institute

Submitted to JETP editor September 20, 1960

J. Exptl. Theoret. Phys. (U.S.S.R.) 40, 1676-1681 (June, 1961)

We use the s-d exchange model of a ferromagnetic metal and Bogolyubov's method in the theory of superconductivity to study the interaction between conduction electrons which is induced by their exchange coupling with the inner (3d and 4f) shells which determine the spontaneous magnetic moment of the ferromagnetic. We show that in contradistinction to the electron-electron interaction induced by phonons, this coupling is repulsive by nature and thus inhibits the establishment of a superconducting state in ferromagnetic metals.

1. It is well known that the exchange interaction between the conduction electrons and the electrons taking part in the atomic magnetic order in ferromagnetics leads to two factors which influence the establishment of superconductivity: 1) a shift of the Fermi sphere for conduction electrons with different spin directions, and 2) an extra interaction between the conduction electrons produced by the spin waves. The first of these factors* was shown earlier by us[1,2] to impede the establishment of superconductivity in a ferromagnetic. There are, however, two opposite opinions about the influence of the second factor.

On the one hand, Kasuya[3] has shown that in the rare earth metals the effective interaction between conduction electrons which is induced by the s-f exchange is repulsive in character and impedes thus the attraction caused by the phonons which leads to superconductivity. Kasuya did, however, not take into account the shift of the Fermi surface for conduction electrons with different spin directions and his conclusions refer therefore to antiferromagnetics, in which such a shift does not occur,[4] rather than to ferromagnetics. On the other hand, Akhiezer and Pomeranchuk[5] considered the interaction between a pair of conduction electrons $k\uparrow$, $-(k+\chi)\downarrow$ (see figure)† which was caused by the exchange of spin waves of a ferromagnetic and they came to the conclusion that this interaction

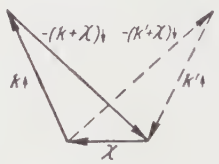

had the character of an additional attraction which thus assists the appearance of superconductivity. In view of such a difference in points of view about the nature of the interaction between conduction electrons induced by spin waves it is of interest to consider this problem using the method proposed by Bogolyubov,[6] and that will be the aim of the present paper.

2. The Hamiltonian of a system of conduction electrons which interact with the spin waves of a ferromagnetic can be written in the form[7]

$$H = U_0 + \sum_k \varepsilon_{k\uparrow} c_{k\uparrow}^+ c_{k\uparrow} + \sum_k \varepsilon_{-(k+\chi)\downarrow} c_{-(k+\chi)\downarrow}^+ c_{-(k+\chi)\downarrow} + \sum_g \omega_g b_g^+ b_g - \frac{1}{\sqrt{N}} \sum_{k,k'} J c_{-(k+\chi)\downarrow}^+ c_{k'\uparrow} b_{k'+k+\chi}^+ + \text{c.c.}, \quad (1)$$

where

$$\varepsilon_{k\uparrow} = E_k + \tfrac{1}{2}\mu J - E_F, \qquad \varepsilon_{k\downarrow} = E_k - \tfrac{1}{2}\mu J - E_F$$

are the energies of the conduction electrons with momentum k with spins directed to the left and to the right, respectively, counted from the energy E_F of the Fermi surface; μ is the excess per crystal lattice site of d-electrons with the predominant spin orientation; N is the number of lattice sites; J is the s-d exchange parameter which we assume approximately to be independent of k (see reference 5); ω_g is the energy of a spin wave of momentum g; $c_{k\uparrow}^+$, $c_{k\downarrow}^+$ and $c_{k\uparrow}$, $c_{k\downarrow}$ are the electron Fermi-operators, and b_g^+ and b_g the

*It is clear that the Meissner effect does not impede the influence of this factor as the exchange interaction is connected with an electrostatic and not with a magnetic interaction.

†In the figure we have indicated by dotted lines the pairs after the exchange of a spin wave.

spin wave Bose-operators; U_0 is a constant. The extra momenta χ of the conduction electrons with their spins to the left in (1) are chosen in agreement with Akhiezer and Pomeranchuk's data (see reference 5) in such a way that

$$|k+\chi| \gtrless k_{F\downarrow} \text{ when } |k| \gtrless k_{F\uparrow}, \tag{2}$$

where $k_{F\uparrow}$ and $k_{F\downarrow}$ are respectively the radii of the Fermi spheres for electrons with "left-handed" and "right-handed" spins in k space. The extra momenta χ are thus, generally speaking, different for different momenta.

It is clear that we can not use Bogolyubov's general canonical transformation,[6] as in the case under consideration we study the interaction of pairs whose total momentum χ is not equal to zero. All the same, it turns out to be possible to carry out a similar transformation applicable both when the Fermi sphere is shifted and when the total momentum of the electron pairs is non-vanishing. To do this we change over from the operators $c_{k\uparrow}$, $c_{(k+\chi)\downarrow}$ to new Fermi operators α_{k0} and α_{k1} through the transformation

$$c_{k\uparrow} = u_{k\uparrow}\alpha_{k0} + v_{k\uparrow}\alpha^+_{k1}, \qquad c_{(k+\chi)\downarrow} = u_{k\uparrow}\alpha_{-k1} - v_{k\uparrow}\alpha^+_{-k0}, \tag{3}$$

where $u_{k\uparrow}$ and $v_{k\uparrow}$ are real numbers satisfying the relations

$$u^2_{k\uparrow} + v^2_{k\uparrow} = 1, \qquad u_{k\uparrow} = u_{-k\uparrow}, \qquad v_{k\uparrow} = -v_{-k\uparrow}. \tag{4}$$

Using (3) and (4) one obtains easily the inverse transformation

$$\alpha_{k0} = u_{k\uparrow}c_{k\uparrow} - v_{k\uparrow}c^-_{-(k+\chi)\downarrow}, \qquad \alpha_{k1} = u_{k1}c_{-(k+\chi)\downarrow} + v_{k\uparrow}c^+_{k\uparrow} \tag{5}$$

and one can easily show that α_{k0} and α_{k1} satisfy all commutation relations of Fermi-operators.

In the ground state

$$\begin{aligned} u_{k\uparrow} &= 1, \quad v_{k\uparrow} = 0 \quad \text{when} \quad |k| > k_{F\uparrow}, \\ u_{k\uparrow} &= 0, \quad v_{k\uparrow} = 1 \quad \text{when} \quad |k| < k_{F\uparrow}. \end{aligned} \tag{6}$$

It follows from (5) that

$$\begin{aligned} &\alpha_{k0} = c_{k\uparrow}, \ \alpha_{k1} = c_{-(k+\chi)\downarrow} \text{ when } |k| > k_{F\uparrow} \text{ and } |k+\chi| > k_{F\downarrow}; \\ &\alpha_{k0} = -c^+_{-(k+\chi)\downarrow}, \\ &\alpha_{k1} = c^+_{k\uparrow} \qquad \text{when } |k| < k_{F\uparrow} \text{ and } |k+\chi| < k_{F\downarrow}, \end{aligned} \tag{7}$$

so that when $|k| > k_{F\uparrow}$ the operator α_{k0} describes the annihiliation of an electron with right-hand spin above the Fermi sphere of radius $k_{F\uparrow}$, and the operator α_{k1} the annihilation of an electron with left-hand spin above the Fermi sphere with radius $k_{F\downarrow}$. When $|k| < k_{F\uparrow}$ the operator α_{k0} describes the annihilation of a left-hand hole under the Fermi-sphere of radius $k_{F\downarrow}$ and α_{k1} the annihilation of a right-hand hole under the Fermi sphere of radius $k_{F\uparrow}$. In the general case when $u_{k\uparrow}v_{k\uparrow} \neq 0$ the operator α_{k0} (or α_{k1}) describes for $|k| > k_{F\uparrow}$ the superposition of a left-hand electron (or a left-hand hole) above the Fermi-sphere of radius $k_{F\downarrow}$ and a right-hand hole (or a right-hand electron) under the Fermi-sphere of radius $k_{F\uparrow}$. A similar superposition of electrons and holes also occurs when $|k| < k_{F\uparrow}$. The transformation (3), and (5) by itself thus does not yet solve the problem of whether bound pairs can be formed. To solve this problem one must find the equation for $u_{k\uparrow}v_{k\uparrow}$ and study the possibility that that product is different from zero.

It is clear from (6) that $u_{k\uparrow}$ and $v_{k\uparrow}$ characterize the occupation of k space by right-hand holes and electrons respectively. The fact that one then succeeds in obtaining also information about the distribution of left-hand holes and electrons is due to the fact that according to (2) knowledge of the position of k relative to the Fermi surface of radius $k_{F\uparrow}$ gives us information about the position of $k+\chi$ relative to the Fermi-sphere of radius $k_{F\downarrow}$. It thus turns out to be sufficient here to restrict ourselves to only the first two parameters (for which we shall drop in the following the index $\uparrow$) of the four parameters[1] $u_{k\uparrow}$, $v_{k\uparrow}$, $u_{k\downarrow}$, and $v_{k\downarrow}$.

Substituting (3) into (1) one can transform the Hamiltonian to the form

$$H = U_1 + H_0 + H_1 + H_2 + H_3, \tag{8}$$

where

$$U_1 = U_0 + \sum_k [\varepsilon_{k\uparrow} + \varepsilon_{k+\chi,\downarrow}]\, v^2_k, \tag{9}$$

$$H_0 = \sum_k [(\varepsilon_k u^2_k - \varepsilon_{k+\chi,\downarrow}v^2_k)\,\alpha^+_{k0}\alpha_{k0} + (\varepsilon_{k+\chi,\downarrow}u^2_k - \varepsilon_{k\uparrow}v^2_k)\,\alpha^+_{k1}\alpha_{k1}] + \sum_g \omega_g b^+_g b_g, \tag{10}$$

$$H_1 = -\frac{1}{\sqrt{N}} \sum_{k,\,k'} J\,(u_k v_{k'}\alpha^+_{k1}\alpha^+_{k'1} - u_{k'}v_k\alpha_{k0}\alpha_{k'0})\, b^+_{k'+k+\chi} + \text{c.c.}, \tag{11}$$

$$H_2 = -\frac{1}{\sqrt{N}} \sum_{k,\,k'} J\,(u_k u_{k'}\alpha^+_{k1}\alpha_{k'0} - v_k v_{k'}\alpha_{k0}\alpha^+_{k'1})\, b^+_{k'+k+\chi} + \text{c.c.}, \tag{12}$$

$$H_3 = \sum_k (\varepsilon_{k\uparrow} + \varepsilon_{k+\chi,\downarrow})\, u_k v_k\, (\alpha^+_{k0}\alpha^+_{k1} + \alpha_{k1}\alpha_{k0}). \tag{13}$$

It follows from (11) to (13) that the terms containing the operators $\alpha^+_{k0}\alpha^+_{k1}$ describing the creation of pairs occur in H_3 and can also be obtained if H_1 and H_2 operate simultaneously. If we put the coefficients of the terms which contain the operators $\alpha^+_{k0}\alpha^+_{k1}$ (since in the ground state the creation of excited pairs is forbidden[6]), we get in second approximation the compensation equation

$$\xi_k u_k v_k = -\frac{1}{2N}(u^2_k - v^2_k)\sum J^2 u_{k'}v_{k'}[\omega_{g=k'+k+\chi} + \varepsilon_{k+\chi,\downarrow}u^2_k - \varepsilon_{k\uparrow}v^2_k + \varepsilon_{k'+\chi,\downarrow}u^2_{k'} - \varepsilon_{k'\uparrow}v^2_{k'}]^{-1}, \tag{14}$$

where

$$2\xi_k = \varepsilon_{k\uparrow} + \varepsilon_{k+\chi,\downarrow} - \frac{1}{N}\sum_{k'}{}' J^2 (u_{k'}^2 - v_{k'}^2)$$
$$\times [\omega_{g=k'+k+\chi} + \varepsilon_{k+\chi,\downarrow} u_k^2 - \varepsilon_{k\uparrow} v_k^2$$
$$+ \varepsilon_{k'+\chi,\downarrow} u_{k'}^2 - \varepsilon_{k'\uparrow} v_{k'}^2]^{-1}. \quad (15)$$

If we take into account that $E_{kF\downarrow} - E_{kF\uparrow} = \mu J$ and that relative to the Fermi surface E_F the relations

$$\varepsilon_{k+\chi,\downarrow} - \varepsilon_{k\uparrow} = E_{k+\chi} - E_k - \mu J \approx E_{k_F\downarrow} - E_{k_F\uparrow} - \mu J = 0$$

hold, we can in the limits of the approximation which we have used put

$$\varepsilon_{k+\chi,\downarrow} u_k^2 - \varepsilon_{k\uparrow} v_k^2 = \xi_k (u_k^2 - v_k^2) = \tilde{\varepsilon}_k. \quad (16)$$

We then get for Eq. (14)

$$\xi_k u_k v_k = -\tfrac{1}{2}(u_k^2 - v_k^2)\, c_k, \quad (17)$$

where

$$c_k = \frac{1}{N}\sum_{k'} J^2 u_{k'} v_{k'} [\omega_{g=k'+k+\chi} + \tilde{\varepsilon}_k + \tilde{\varepsilon}_{k'}]^{-1}. \quad (18)$$

From (17) and (4) it follows that

$$u_k^2 = \tfrac{1}{2}[1 + \xi_k (\xi_k^2 + c_k^2)^{-1}], \quad v_k^2 = \tfrac{1}{2}[1 - \xi_k (\xi_k^2 + c_k^2)^{-1}], \quad (19)$$

$$u_k v_k = -\tfrac{1}{2} c_k (\xi_k^2 + c_k^2)^{-1}, \qquad \tilde{\varepsilon}_k = \xi_k^2 (\xi_k^2 + c_k^2)^{-1}; \quad (20)$$

these relations differ formally from the usual relations[6] by the sign of the product $u_k v_k$. Substituting this product from (20) into (18) we get an equation for c_k

$$c_k = -\frac{1}{2N}\sum_{k'} J^2 (\omega_{g=k'+k+\chi} + \tilde{\varepsilon}_k + \tilde{\varepsilon}_{k'})^{-1} c_{k'} (\xi_{k'}^2 + c_{k'}^2)^{-1}. \quad (21)$$

Equation (21) differs also by the sign of the right-hand side from the analogous equation for the case of an interaction produced by phonons which occurs in the work by Bogolyubov, Tolmachev, and Shirkov (see reference 6). The quantity

$$J^2(\omega_{g=k'+k+\chi} + \tilde{\varepsilon}_k + \tilde{\varepsilon}_{k'})^{-1}$$

is thus positive and Eq. (21) has only the trivial solution: $c_k = 0$. Equation (19) goes then over into (6) which is satisfied in the ground state.

We have thus shown that the interaction between the conduction electrons caused by the exchange of spin waves in a ferromagnetic is repulsive by nature and can not assist the formation of a superconducting state.

3. The contrasting character of the phonon and the ferromagnon (spin-wave) effective interaction between conduction electrons can also be seen directly from comparing the expression

$$\hbar\omega_g |M_g|^2 [(\varepsilon_k - \varepsilon_{k+g})^2 - (\hbar\omega_g)^2]^{-1} c_{k'-g,\downarrow}^{+} c_{k'\downarrow} c_{k+g,\uparrow}^{+} c_{k\uparrow}, \quad (22)$$

which occurs in second perturbation theory approximation for the interaction between two electrons with spins in opposite directions which is produced by the exchange of a virtual longitudinal phonon[8] with the analogous expression*

$$\Omega^{-1} a^3 \Delta^2 [\varepsilon_{k\uparrow} - \varepsilon_{k+g,\downarrow} - \theta (ag)^2]^{-1} c_{k'-g,\uparrow}^{+} c_{k'\downarrow} c_{k+g,\downarrow}^{+} c_{k\uparrow}, \quad (23)$$

which occurs in the same approximation for the interaction produced by the exchange of ferromagnons.[5] Indeed, introducing the creation and annihilation operators for a $(k\uparrow, k'\downarrow)$ pair:

$$b_{kk'}^{+} = c_{k\uparrow}^{+} c_{k'\downarrow}^{+}, \qquad b_{kk'} = c_{k'\downarrow} c_{k\uparrow} \quad (24)$$

(unlike reference 8 we do not assume here that $k' = -k$) and using the commutation relations for the Fermi-operators $c_{k\uparrow}$ and $c_{k\downarrow}$ we can transform (22) and (23) to

$$\hbar\omega_g |M_g|^2 [(\varepsilon_k - \varepsilon_{k+g})^2 - (\hbar\omega)^2]^{-1} b_{k+g,k'-g}^{+} b_{kk'}, \quad (22')$$

$$-\Omega^{-1} a^3 \Delta^2 [\varepsilon_{k\uparrow} - \varepsilon_{k+g,\downarrow} - \theta(ag)^2] b_{k'-g,k+g}^{+} b_{kk'}. \quad (23')$$

The difference in the signs of (22′) and (23′) shows† that in the first case the "phonon interaction" is attractive near the Fermi surface, while in the second case the "ferromagnon interaction" is repulsive.‡ The physical cause of this difference is** that in the first case transitions of electrons are not accompanied by a change in their spin orientation while such a change does take place in the second case.

Indeed, if, for instance, there are initially two electrons in the states $k\uparrow$ and $k\downarrow$ with opposite spins, absorption of a phonon may lead to a transi-

*The notation in (22) and (23) is the same as in references 5 and 8; we note merely that in reference 5 expression (23) was written down without taking into account in the numerator the operator which is essential for grouping the electrons in pairs and thus for the determination of the sign of the matrix element. See also the text of reference 8 after Eq. (2.7) for this problem.

†In order to avoid misunderstandings we note that it is clear from (24) that $b_{k+g,k'-g} \neq -b_{k'-g,k+g}$ so that (22′) and (23′) indeed have opposite signs. Interchanging the indices of $b_{k+g,k'-g}^{+}$ in (22′) and (23′) means only that in the first case the pair $(k\uparrow, k'\downarrow)$ goes over into the pair $(k+g\uparrow; k'-g\downarrow)$ and in the second case into the pair $(k'-g\uparrow; k+g\downarrow)$.

‡We note that Cooper[10] also considered pairs with $\chi \neq -0$, and that the binding energy of the pair turned out to be energetically preferred only in the case of a negative matrix element of the interaction energy. The difference in sign of the matrix elements of the interactions caused on the one hand by longitudinal phonons and on the other hand by spin waves which we obtained means thus that the latter interaction will not lead to the Cooper effect.

**See also the concluding remark in a note by the present authors.[9]

tion $k\uparrow \rightarrow k + g\uparrow$ while the absorption of a ferromagnon must lead to the transition $k\downarrow \rightarrow k + g\uparrow$. Two electrons which before the transition are in different states $k\uparrow$ and $k\downarrow$ must after the above mentioned transitions turn out to be in the same state $k + g\uparrow$ which is forbidden by the Pauli principle. It follows thus that the exchange of a spin wave inhibits the effect caused by the exchange of a longitudinal phonon.

What we have said so far allows us also to conclude that the opposition to the establishment of the superconducting state is not a basic property of the exchange of a spin wave, but will occur generally whenever a quasi-particle with unit spin is exchanged. In particular, there are some grounds for assuming that transverse phonons have unit spin. In metals (not necessarily ferromagnetics) the exchange of transverse phonons as well as the well-known Coulomb repulsion can thus inhibit the establishment of superconductivity. This problem we propose to consider in more detail at a later time.

[1] S. V. Vonsovskii and M. S. Svirskii, Doklady Akad. Nauk SSSR **122**, 204 (1958), Soviet Phys. Doklady **3**, 949 (1958).

[2] S. V. Vonsovskii and M. S. Svirskii, JETP **39**, 384 (1960), Soviet Phys. JETP **12**, 272 (1961).

[3] T. Kasuya, Progr. Theoret. Phys. (Kyoto) **20**, 980 (1958).

[4] B. V. Karpenko, Физика металлов и металловедение (Physics of Metals and Metallography) **9**, 794 (1960), Phys. Metals Metallogr. **9**, no. 5, 146 (1960).

[5] A. I. Akhiezer and I. Ya. Pomeranchuk, JETP **36**, 859 (1959), Soviet Phys. JETP **9**, 605 (1959).

[6] N. N. Bogolyubov, V. V. Tolmachev, and D. V. Shirkov, Новый метод в теории сверхпроводимости (New Method in the Theory of Superconductivity) AN SSSR, 1958 (English translation by Consultants Bureau).

[7] S. V. Vonsovskii and E. A. Turov, JETP **24**, 419 (1953).

[8] J. Bardeen, L. N. Cooper, and J. R. Schrieffer, Phys. Rev. 108, 1175 (1957).

[9] S. V. Vonsovskii and M. S. Svirskii, JETP **37**, 1494 (1959), Soviet Phys. JETP **10**, 1060 (1960).

[10] L. N. Cooper, Phys. Rev. **104**, 1189 (1956).

Translated by D. ter Haar
286

ANGULAR DISTRIBUTION FUNCTION FOR PARTICLES IN A SHOWER PRODUCED BY A PRIMARY PARTICLE OF A GIVEN ENERGY

V. V. GUZHAVIN and I. P. IVANENKO

Institute of Nuclear Physics, Moscow State University

Submitted to JETP editor October 14, 1960

J. Exptl. Theoret. Phys. (U.S.S.R.) 40, 1682-1694 (June, 1961)

The angular distribution functions for electrons and photons in a cascade shower produced by a primary electron or photon of finite energy E_0 are deduced in approximation A of the cascade theory.[1] The angular distribution functions of the shower particles are also derived in the case when the electrons and photons are continuously produced along the whole shower path by some non-electromagnetic penetrating component.

MANY papers have been devoted to the determination of the angular distribution function of particles in cascade showers. In the multiple-scattering small-angle approximation (Landau approximation), this function was obtained by several authors.[1-6] In some papers[7-9] the angular problem was solved without assuming the particle scattering angles to be small and without using the Landau approximation. In most of these investigations, only the so-called "equilibrium" angle function was studied, i.e., the function integrated over the entire depth of the layer of the substance in which the cascade developed. In all the indicated papers, the authors neglected the dependence of the cascade parameter s on the angle θ, i.e., they obtained essentially expressions valid only for $E_0 = \infty$ (E_0 is the energy of the shower-producing primary).

One of us[10] obtained for the shower particles an angular-distribution equilibrium function valid for any finite value of E_0. We have previously[11] calculated approximately the particle angular distribution functions in a shower produced by a primary of specified finite energy. The purpose of the present investigation was the derivation of exact expressions for the sought angle functions for many particular cases.

1. Let us write the principal equations of the cascade theory, assuming the particle deviation angles to be small and regarding the scattering as multiple, so that $\cos\theta$ can be replaced by unity and the Laplacian operator can be expressed in the form $\Delta_\theta = \theta^{-1}(\partial/\partial\theta)(\theta\partial/\partial\theta)$:

$$\begin{aligned}\partial P(E_0, E, t, \theta)/\partial t &= L_1[P(E_0, E, t, \theta),\\ &\Gamma(E_0, E, t, \theta)] + (E_k^2/4E^2)\,\Delta_\theta P(E_0, E, t, \theta),\\ \partial\Gamma(E_0, E, t, \theta)/\partial t &= L_2[P(E_0, E, t, \theta), \Gamma(E_0, E, t, \theta)].\end{aligned} \tag{1}$$

Here $P(E_0, E, t, \theta)$ and $\Gamma(E_0, E, t, \theta)$ are the sought electron and photon distribution functions over the energy E, the depth t (measured in shower units), and the angle of deflection from the shower axis θ (two-dimensional angle); L_1 and L_2 are integral operators that account for the radiative retardation and pair production;[1] $E_k = E_s(L_{res}/L_{rad})^{1/2}$; $E_s = 21$ Mev. Usually we assume $E_k = E_s$. The boundary conditions

$$P(E_0, E, 0, \theta) = \delta(E_0 - E)\,\delta(\theta), \qquad \Gamma(E_0, E, 0, \theta) = 0$$

or

$$P(E_0, E, 0, \theta) = 0, \qquad \Gamma(E_0, E, 0, \theta) = \delta(E_0 - E)\,\delta(\theta)$$

correspond either to one primary electron vertically incident on the boundary of the layer of matter at t = 0, or, analogously, to one photon.

Let us expand the functions P and Γ in Bessel functions of zero order, using the relations

$$P(E_0, E, t, \theta) = \int_0^\infty D_P(E_0, E, t, k)\,J_0(k\theta)\,k\,dk,$$

$$D_P(E_0, E, t, k) = \int_0^\infty P(E_0, E, t, \theta)\,J_0(k\theta)\,\theta\,d\theta,$$

and analogously for the functions Γ. Multiplying (1) by $J_0(k\theta)\,\theta$ and integrating with respect to θ from zero to infinity, we obtain

$$\begin{aligned}\partial D_P(E_0, E, t, k)/\partial t &= L_1[D_P(E_0, E, t, k), D_\Gamma(E_0, E, t, k)]\\ &- (E_k^2/4E^2)\,k^2 D_P(E_0, E, t, k),\\ \partial D_\Gamma(E_0, E, t, k)/\partial t &= L_2[D_P(E_0, E, t, k), D_\Gamma(E_0, E, t, k)].\end{aligned} \tag{2}$$

We seek the functions D_P and D_Γ in the form

$$D_{P,\Gamma}(E_0, E, t, k) = \frac{1}{4\pi^2 i}\int_{\delta-i\infty}^{\delta+i\infty}\frac{ds}{E}\left(\frac{E_0}{E}\right)^s\sum_{m=0}^{\infty}\left(-\frac{E_k^2k^2}{4E^2}\right)^m\psi_m^{P,\Gamma}(s, t). \tag{3}$$

Substituting (3) in (2) and equating coefficients of equal powers of $(-E_k^2k^2/4E^2)$, we obtain equations for the determination of $\psi_m^{P,\Gamma}(s, t)$:

$$\partial\psi_0^P(s,t)/\partial t + A(s)\psi_0^P(s,t) - B(s)\psi_0^\Gamma(s,t) = 0,$$
$$\partial\psi_0^\Gamma(s,t)/\partial t - C(s)\psi_0^P(s,t) + \sigma_0\psi_0^\Gamma(s,t) = 0,$$
$$\partial\psi_m^P(s,t)/\partial t + A(s+2m)\psi_m^P(s,t) - B(s+2m)\psi_m^\Gamma(s,t) - \psi_{m-1}^P(s,t) = 0,$$
$$\partial\psi_m^\Gamma(s,t)/\partial t - C(s+2m)\psi_m^P(s,t) + \sigma_0\psi_m^\Gamma(s,t) = 0,$$
$$m \geqslant 1.$$

The explicit expressions and the values of the functions $A(s)$, $B(s)$, $C(s)$, as well as the functions $\lambda_1(s)$, $\lambda_2(s)$, and $H_1(s)$, which will be introduced subsequently, can be found in reference 1. Multiplying the preceding equations by $e^{-\lambda t}$ and integrating with respect to t from zero to infinity, we obtain equations for the functions $\psi_m(s, \lambda)$. The form of the functions $\psi_m^{P,\Gamma}(s, t=0)$ is determined by the initial conditions. It is easily seen that in the case of a primary electron the only non-vanishing functions are

$$\{\psi_0^P(s,\lambda)\}^P = 1/\psi(\lambda, s),$$
$$\{\psi_0^\Gamma(s,\lambda)\}^P = C(s)/\psi(\lambda, s)(\lambda+\sigma_0),$$

and in the case of a primary photon

$$\{\psi_0^P(s,\lambda)\}^\Gamma = \frac{B(s)}{\psi(\lambda, s)(\lambda+\sigma_0)},$$
$$\{\psi_0^\Gamma(s,\lambda)\}^\Gamma = \frac{B(s)C(s) + \psi(\lambda, s)(\lambda+\sigma_0)}{\psi(\lambda, s)(\lambda+\sigma_0)^2}.$$

Here

$$\psi(\lambda, s) = [\lambda - \lambda_1(s)][\lambda - \lambda_2(s)]/(\lambda+\sigma_0),$$

where $\lambda_1(s)$ and $\lambda_2(s)$ are the roots of the equation $\psi(\lambda, s) = 0$. In the case of the primary electron we obtain for $\{\psi_m^P(s,\lambda)\}^P$ the following expressions:

$$\{\psi_1^P(s,\lambda)\}^P = 1/\psi(\lambda, s)\psi(\lambda, s+2),$$
$$\{\psi_2^P(s,\lambda)\}^P = 1/\psi(\lambda, s)\psi(\lambda, s+2)\psi(\lambda, s+4),$$
$$\ldots\{\psi_n^P(s,\lambda)\}^P = 1/\psi(\lambda, s)\psi(\lambda, s+2)\ldots\psi(\lambda, s+2n).$$

Hence, taking the inverse Laplace transform, neglecting terms proportional to $\exp\{\lambda_2(s)t\}$, $\exp\{\lambda_2(s+2)t\}$, $\exp\{\lambda_1(s+2)t\}$, $\exp\{\lambda_1(s+4)t\}$, etc., and substituting the resultant expression for $\{\psi_m^P(s,t)\}^P$ in (3), we obtain*

$$D_P^P(E_0, E, t, k) = \frac{1}{4\pi^2 i}\int_{\delta-i\infty}^{\delta+i\infty}\frac{ds}{E}\left(\frac{E_0}{E}\right)^s H_1(s)\,e^{\lambda_1(s)t} \times\left\{1 - \frac{E_k^2k^2}{4E^2}\frac{1}{\psi[\lambda_1(s), s+2]} + \left(\frac{E_k^2k^2}{4E^2}\right)^2 \times\frac{1}{\psi[\lambda_1(s), s+2]\psi[\lambda_1(s), s+4]} + \ldots + (-1)^n \times\left(\frac{E_k^2k^2}{4E^2}\right)^n\frac{1}{\psi[\lambda_1(s), s+2]\ldots\psi[\lambda_1(s), s+2n]} + \ldots\right\}.$$

*It should be noted that this method of analysis makes it possible to take the discarded terms into account.

Integrating $D_P^P(E_0, E', t, k)$ with respect to E' from E to infinity, we obtain the function $D_N^P(E_0, E, t, k)$, which determines the number of electrons with energy greater than E.

Let us approximate the function $\psi_0(\lambda, s)$ by the following expression:[1]

$$\psi(\lambda, s) = \psi_0(\lambda, s) = f(\lambda)[s - s_1(\lambda)]/s. \quad (4)$$

Substituting $\psi_0(\lambda, s)$ in $D_P^P(E_0, E, t, k)$ and $D_N^P(E_0, E, t, k)$, summing the series, and using the formula for the inversion of the Fourier-Bessel transform, we obtain

$$\{P(E_0, E, t, \theta)\}^P = \frac{1}{4\pi^2 i}\int_{\delta-i\infty}^{\delta+i\infty}\frac{ds}{E}\left(\frac{E_0}{E}\right)^s H_1(s)\,e^{\lambda_1(s)t} \times\int_0^\infty\left[1 + \frac{E_k^2k^2}{4E^2f(\lambda_1)}\right]^{-s/2-1} J_0(k\theta)\,k\,dk.$$

After evaluating the integral with respect to k, we get

$$\{P(E_0, E, t, \theta)\}^P = \frac{1}{4\pi^2 i}\int_{\delta-i\infty}^{\delta+i\infty}\frac{ds}{E}H_1(s)\,e^{ys+\lambda_1(s)t}\frac{z^{(4+s)/2}K_{s/2}(z)}{\theta^2 2^{s/2}\Gamma(1+s/2)},$$

$$\{N_P(E_0, E, t, \theta)\}^P = \frac{1}{4\pi^2 i}\int_{\delta-i\infty}^{\delta+i\infty}\frac{ds}{s}H_1(s)\,e^{ys+\lambda_1(s)t}\frac{z^{(2+s)/2}K_{(2-s)/2}(z)}{\theta^2 2^{(s-2)/2}\Gamma(s/2)},$$

where $\{N_P(E_0, E, t, \theta)\}^P$ is the electron angular distribution function, integrated over E. Here $y = \ln(E_0/E)$, $z = E\theta/P$, where $P = E_k/2\sqrt{f(\lambda_1)}$, $K_\nu(z)$ is the modified Bessel function of second kind of order ν, and $\Gamma(s)$ is the gamma function of argument s. If we calculate the integral with respect to s in $\{N_P(E_0, E, t, \theta)\}^P$ by the method of steepest descent, neglecting the dependence of s on θ, we obtain Belen'kii's results[1] for the case $E_0 = \infty$:

$$\{N_P(E_0, E, t, \theta)\}^P = \{N_P(E_0, E, t)\}^P\frac{z^{(2+s)/2}K_{(2-s)/2}(z)}{2\pi\theta^2 2^{(s-2)/2}\Gamma(s/2)}. \quad (5)$$

In this same approximation we obtain for $\{P(E_0, E, t, \theta)\}^P$ the expression

$$\{P(E_0, E, t, \theta)\}^P = \{P(E_0, E, t)\}^P\frac{z^{(4+s)/2}K_{s/2}(z)}{2\pi\theta^2 2^{s/2}\Gamma(1+s/2)}. \quad (6)$$

The quantities y, s, and t in (5) and (6) are related by the equation $y + \lambda_1'(s)t = 0$, which coincides with the corresponding relation in one-dimensional cascade theory. Let us calculate $\{N_P(E_0, E, t, \theta)\}^P$ and $\{P(E_0, E, t, \theta)\}^P$ by the method of steepest descent more accurately, taking the dependence of s on θ into account, i.e., assuming E_0 to be a finite quantity. Then*

*In all formulas of Sec. 1 we have $a = \lambda_1'(s)t$ and $L = \lambda_1''(s)t$; in all formulas of Sec 2, we have

$$a = \lambda_1'(s)t - \lambda_1'(s)/[\lambda_1(s) + \mu],$$
$$L = \lambda_1''(s)t - \{\lambda_1''(s)[\lambda_1(s) + \mu] - [\lambda_1'(s)]^2\}/[\lambda_1(s) + \mu]^2.$$

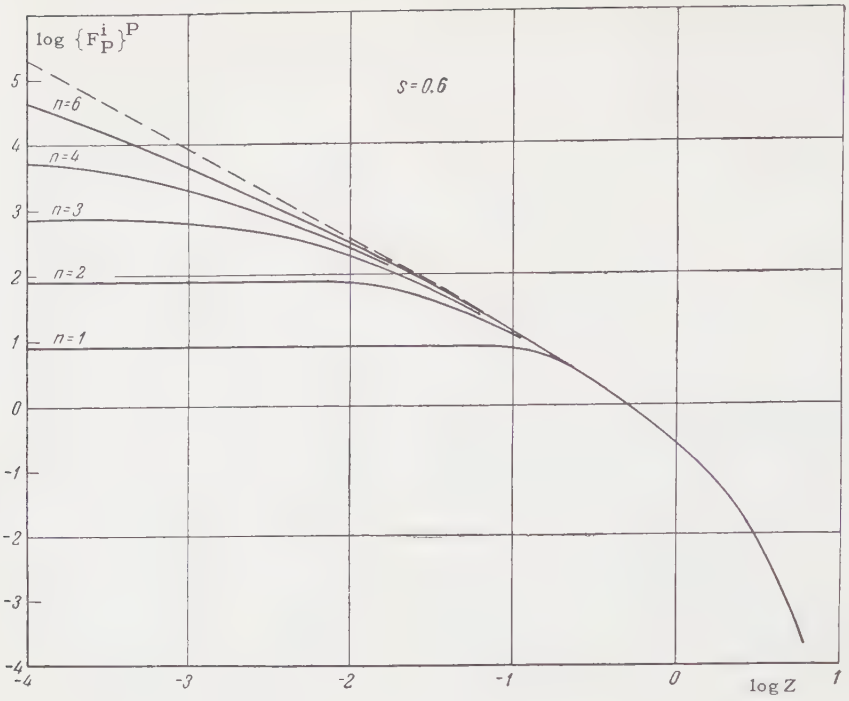

FIG. 1

$$\{N_P(E_0, E, t, \theta)\}^P = H_1(s)\, f_1[s, K_{(2-s)/2}(z), L], \quad (5')$$

and s is determined by the condition $\varphi_1\left(s, \frac{2-s}{2}, a\right) = 0$, where

$$\varphi_1(s, \nu, a) = y + a + 0.5 \ln z + (d/ds) \ln K_\nu(z);$$

$$f_1[s, K_\nu(z), L] = \frac{z^{(2+s)/2} \exp\{ys + \lambda_1(s)\, t\}\, K_\nu(z)}{2\pi\theta^2 2^{s/2}\Gamma(1+s/2)\{2\pi[L + (d^2/ds^2)\ln K_\nu(z)]\}^{1/2}}.$$

Analogously we find

$$\{P(E_0, E, t, \theta)\}^P = H_1(s)\, f_1[s, K_{s/2}(z), L]\, z/E; \quad (6')$$

s is determined by the condition $\varphi_1(s, s/2, a) = 0$. When $z \ll 1$, (5′) and (6′) can be rewritten in a more convenient form

$$\{N_P(E_0, E, t, \theta)\}^P|_{z\ll 1} = f_2\left[s, \frac{2-s}{2}, L\right] 2^{1-s} H_1(s)\, z^s \Gamma(1-s/2)/\Gamma(s/2); \quad (5'')$$

Here s is determined by the condition $\varphi_2\left(s, \frac{2-s}{2}, a\right) = 0$, where

$$\varphi_2(s, \nu, a) = y + a + \ln z - 0.5 \ln 2 - 0.5\,\psi(\nu) + 1/2\,\nu.$$

Analogously

$$\{P(E_0, E, t, \theta)\}^P_{z\ll 1} = H_1(s)\, f_2[s, s/2, L]\, z^2/E; \quad (6'')$$

s is determined by the condition $\varphi_2(s, s/2, a) = 0$. Here

$$f_2(s, \nu, L) = \frac{\exp\{ys + \lambda_1(s)\, t\}}{2\pi\theta^{2s}\{2\pi[L + (d/ds)(0.5\psi(\nu) - 1/2\nu)]\}^{1/2}}.$$

In these formulas $\psi(x) = d \ln\Gamma(x+1)/dx$. When $z \ll 1$, the value of s for the function $\{N_P\}^P$ cannot be greater than 2 (if $\bar{s}$ is one-dimensional it is less than 2). The value of s for $\{N_P\}^P$ depends on z, approaching $s = 2$ as $z \to 0$, where for $\{P\}^P$ the value of s is independent of z when $z \ll 1$.

When $z \gg 1$, (5′) and (6′) assume the form

$$\{N_P(E_0, E, t, \theta)\}^P|_{z\gg 1} = \{N_P(E_0, E, t)\}^P f_3(s, z)\, s, \quad (5''')$$

$$\{P(E_0, E, t, \theta)\}^P|_{z\gg 1} = \{P(E_0, E, t)\}^P f_3(s, z)\, z. \quad (6''')$$

Here s is determined by the condition $\varphi_3(s, a) = y + a + 0.5 \ln z = 0$, and

$$f_3(s, z) = \frac{z^{(1+s)/2} e^{-z}}{2^{(3+s)/2}\pi^{1/2}\theta^2\Gamma(1+s/2)}.$$

By way of an example illustrating the application of the formulas obtained for $E_0 \neq \infty$, Figs. 1, 2, and 3 show the function $\{N_P(E_0, E, t, \theta)\}^P$, calculated by formulas (5′), (5″), and (5‴) for three values of the parameter s. The abscissas represent log z, where $z = E\theta/2\sqrt{2.29}$. The ordinates represent the logarithm of the quantity

$$\{F_P^i(E_0, z, s)\}^P = 2\pi P^2 \{N_P(E_0, E, t, \theta)\}^P / E^2 \{N_P(E_0, E, t)\}^P.$$

The solid curves correspond to different values of $(E_0/E) = 10^n$. The dotted curves are calculated, in accordance with references 1 and 7, for the case $(E_0/E) = \infty$. The values of the cascade parameter s are indicated in the figures. It is evident from the figures that the less the ratio E_0/E and the less z, i.e., the less θ, the greater the influence of the finite E_0 on the form of the angular distribution functions, as expected from physical considerations.

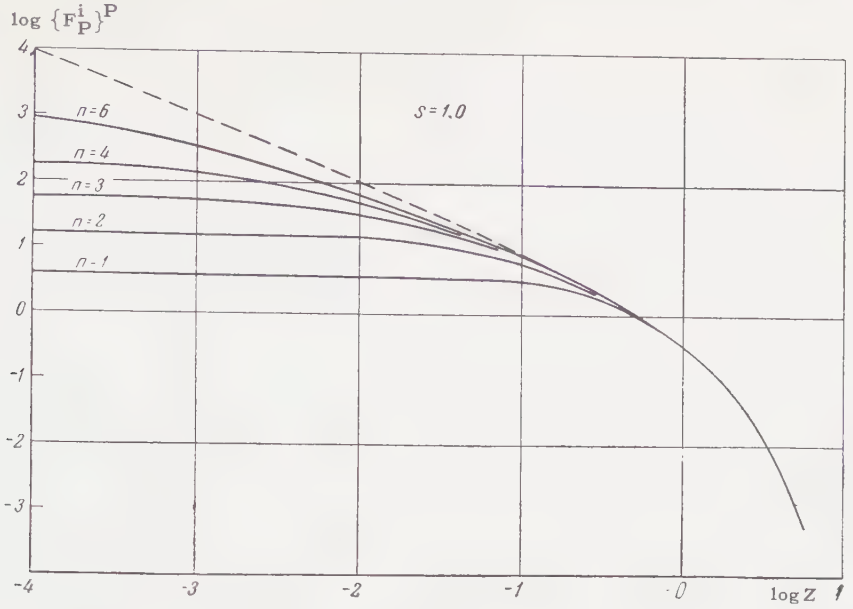

FIG. 2

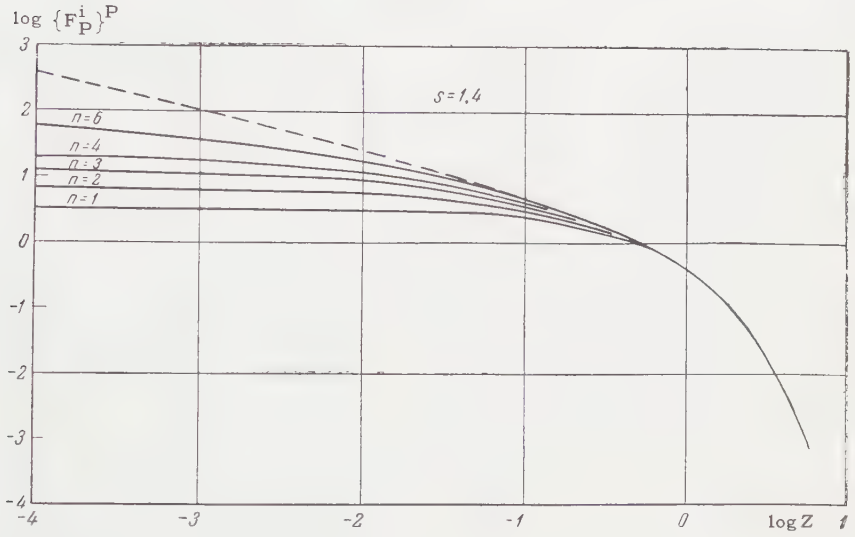

FIG. 3

Let us derive expressions for the photon angular distribution function. Replacing $\psi(\lambda, s)$ by $\psi_0(\lambda, s)$, assuming that approximately $C(s) = 1/s$, and using the Fourier-Bessel transform, we obtain

$$\{\Gamma(E_0, E, t, \theta)\}^P = \frac{1}{4\pi^2 i}\int_{\delta-i\infty}^{\delta+i\infty} \frac{ds}{E}\left(\frac{E_0}{E}\right)^s \frac{C(s)\, e^{\lambda_1(s)t}}{\lambda_1(s) - \lambda_2(s)} \times \int_0^\infty \left[1 + \frac{E_k^2 k^2}{4E^2 f(\lambda_1)}\right]^{-s/2} J_0(k\theta)\, k\,dk.$$

Integrating with respect to k and calculating the integral with respect to s in $\{\Gamma(E_0, E, t, \theta)\}^P$ by the method of steepest descents without allowance for the dependence of s on θ ($E_0 = \infty$), we obtain

$$\{\Gamma(E_0, E, t, \theta)\}^P = \{\Gamma(E_0, E, t)\}^P \frac{z^{(2+s)/2} K_{(2-s)/2}(z)}{2\pi\theta^2 2^{(s-2)/2}\Gamma(s/2)}, \quad (7)$$

where s is determined by the condition $y + \lambda_1'(s)t = 0$. Integrating $\{\Gamma(E_0, E', t, \theta)\}^P$ with respect to E′ from E to infinity, we obtain the angular distribution function integrated over the energy

$$\{N_\Gamma(E_0, E, t, \theta)\}^P = \{N_\Gamma(E_0, E, t)\}^P \frac{sF_1(s, z)}{2\pi\theta^2 2^{(s-2)/2}\Gamma(s/2)}, \quad (8)$$

where s is determined by the same condition as in (7), and

$$F_1(s, z) = z^s \int_z^\infty dz' z'^{-s/2} K_{(2-s)/2}(z').$$

For convenience in comparison with experiment, it is expedient to introduce angular distribution functions normalized to unity

$$\int_0^\infty F(s, z)\, z\,dz = 1.$$

We note that these functions F(s, z) can be

readily obtained from the corresponding functions of angular distribution for the total number of particles

$$\{F^{d}_{P,\Gamma}(s,z)\}^{P}=2\pi\frac{P^{2}}{E^{2}}\frac{\{P,\Gamma(E_0,E,t,\theta)\}^{P}}{\{P,\Gamma(E_0,E,t)\}^{P}},$$

$$\{F^{i}_{P,\Gamma}(s,z)\}^{P}=2\pi\frac{P^{2}}{E^{2}}\frac{\{N_{P,\Gamma}(E_0,E,t,\theta)\}^{P}}{\{N_{P,\Gamma}(E_0,E,t)\}^{P}}.$$

Let us write them in explicit form

$$\{F^{d}_{P}(s,z)\}^{P}=\frac{z^{s/2}K_{s/2}(z)}{2^{s/2}\Gamma(1+s/2)},\quad \{F^{i}_{\Gamma}(s,z)\}^{P}=\frac{sF_1(s,z)}{2^{(s-2)/2}\Gamma(s/2)\,z^{2}},$$

$$\{F^{i}_{P}(s,z)\}^{P}=\{F^{d}_{\Gamma}(s,z)\}^{P}=\frac{z^{(s-2)/2}K_{(2-s)/2}(z)}{2^{(s-2)/2}\Gamma(s/2)}.$$

From a comparison of these formulas we see that the electron angular distribution function, normalized to unity and integral in E, is the same as the photon angular distribution function, which is differential in E. At the maximum of the shower (when s = 1) the foregoing expressions assume a particularly simple form

$$\{F^{d}_{P}(1,z)\}^{P}=e^{-z},\qquad \{F^{i}_{\Gamma}(1,z)\}^{P}=-\mathrm{Ei}(-z)/z,$$
$$\{F^{i}_{P}(1,z)\}^{P}=\{F^{d}_{\Gamma}(1,z)\}^{P}=e^{-z}/z.$$

We now calculate for $\{\Gamma^{P}\}$ and $\{N_{\Gamma}\}^{P}$ the integral with respect to s by the method of steepest descent, taking into account the dependence of s on θ. Then

$$\{\Gamma(E_0,E,t,\theta)\}^{P}=f_1\left[s,\frac{2-s}{2};L\right]sH_3(s)/E; \qquad (7')$$

s is determined by the conditions $\varphi_1\left(s,\frac{2-s}{2},a\right)=0$, and $H_3(s)=C(s)/[\lambda_1(s)-\lambda_2(s)]$. Analogously,

$$\{N_{\Gamma}(E_0,E,t,\theta)\}^{P}=H_3(s)\,sf_1[s,F_1(s,z),L]. \qquad (8')$$

Here s is determined by the condition $\varphi_4(s,a)=y+a+(d/ds)\ln F_1(s,z)=0$.

As before, the expression (7′) can be simplified for $z\ll 1$ and $z\gg 1$. When $z\ll 1$ we have

$$\{\Gamma(E_0,E,t,\theta)\}^{P}|_{z\ll 1}=H_3(s)\,f_2\left[s,\frac{2-s}{2},L\right]s\cdot 2^{1-s}z^{s}\Gamma(1-s/2)/\Gamma(s/2)\,E;$$

s is determined by the relation $\varphi_2\left(s,\frac{2-s}{2},a\right)=0$. When $z\gg 1$ we have

$$\{\Gamma(E_0,E,t,\theta)\}^{P}|_{z\gg 1}=\{\Gamma(E_0,E,t)\}^{P}f_3(s,z)\,s, \qquad (7''')$$

where s is determined by the relation $\varphi_3(s,a)=0$.

Let us consider now the angular distribution of particles in a shower produced by a primary photon. As in the case of a primary electron, we seek the solution in the form (3). Calculating the corresponding integral with respect to s by the method of steepest descent, disregarding the dependence of s on θ, we obtain

$$\{P(E_0,E,t,\theta)\}^{\Gamma}=2\{P(E_0,E,t)\}^{\Gamma}f_4[s,K_{s/2}(z)]\,z/s, \qquad (9)$$

$$\{N_P(E_0,E,t,\theta)\}^{\Gamma}=2\{N_P(E_0,E,t)\}^{\Gamma}f_4[s,K_{(2-s)/2}(z)]. \qquad (10)$$

Here s is determined by the condition of the one-dimensional theory, and

$$f_4[s,K_\nu(z)]=z^{(s+2)/2}K_\nu(z)/2\pi\theta^{2}2^{s/2}\Gamma(s/2).$$

If we calculate in the expressions for $\{P\}^{\Gamma}$ and $\{N_P\}^{\Gamma}$ the integrals with respect to s with allowance for the dependence of s on θ, i.e., for $E_0\neq\infty$, we obtain

$$\{P(E_0,E,t,\theta)\}^{\Gamma}=H_4(s)\,f_1[s,K_{s/2}(z),L]\,z/E, \qquad (9')$$

$$\{N_P(E_0,E,t,\theta)\}^{\Gamma}=H_4(s)\,f_1[s,K_{(2-s)/2}(z),L]; \qquad (10')$$

s is determined by the condition $\varphi_1(s,\nu,a)=0$, and $H_4(s)=B(s)/[\lambda_1(s)-\lambda_2(s)]$.

If $z\ll 1$ or $z\gg 1$, the preceding formulas can be written in simpler form. When $z\ll 1$ we get

$$\{P(E_0,E,t,\theta)\}^{\Gamma}|_{z\ll 1}=H_4(s)\,f_2[s,s/2,L]\,z^{2}/E, \qquad (9'')$$

$$\{N_P(E_0,E,t,\theta)\}^{\Gamma}|_{z\ll 1}=H_4(s)\,f_2\left[s,\frac{2-s}{2},L\right]2^{1-s}z^{s}\Gamma(1-s/2)/\Gamma(s/2), \qquad (10'')$$

s is determined by the condition $\varphi_2(s,\nu,a)=0$ (with $\bar{s}<2$). When $z\gg 1$ we get

$$\{P(E_0,E,t,\theta)\}^{\Gamma}|_{z\gg 1}=\{P(E_0,E,t)\}^{\Gamma}f_3(s,z)\,z, \qquad (9''')$$

$$\{N_P(E_0,E,t,\theta)\}^{\Gamma}|_{z\gg 1}=\{N_P(E_0,E,t)\}^{\Gamma}f_3(s,z). \qquad (10''')$$

Here s is determined by the condition $\varphi_3(s,a)=0$.

We consider the angular distribution function of the photons in the shower due to the primary photon. After making all the necessary calculations, we obtain the following final expressions. Disregarding the dependence of s on θ,

$$\{\Gamma(E_0,E,t,\theta)\}^{\Gamma}=(2\pi)^{-1}e^{-\sigma_0 t}\delta(E_0-E)\,\delta(\theta)+2\{\Gamma(E_0,E,t)\}^{\Gamma}f_4[s,K_{(2-s)/2}(z)], \qquad (11)$$

$$\{N_\Gamma(E_0,E,t,\theta)\}^{\Gamma}=(2\pi)^{-1}\delta(\theta)\,e^{-\sigma_0 t}+2\{N_\Gamma(E_0,E,t)\}^{\Gamma}f_4[s,F_1(s,z)]\,z^{-(s+2)/2}; \qquad (12)$$

s is determined by the condition of the one-dimensional theory. If the dependence of s on θ is taken into account,

$$\{\Gamma(E_0,E,t,\theta)\}^{\Gamma}=(2\pi)^{-1}e^{-\sigma_0 t}\delta(E_0-E)\,\delta(\theta)+H_4(s)\,C(s)\,f_1[s,K_{(2-s)/2}(z),L]\,s/[\lambda_1(s)+\sigma_0]\,E, \qquad (11')$$

where s is determined by the condition $\varphi_1\left(s,\frac{2-s}{2},a\right)=0$. Further

$$\{N_\Gamma(E_0, E, t, \theta)\}^\Gamma = (2\pi)^{-1}e^{-\sigma_0 t}\delta(\theta) + H_4(s)C(s)f_1[s, F_1(s, z), L]\, s/[\lambda_1(s) + \sigma_0]\, z^{(s+2)/2}; \quad (12')$$

s is determined by the condition $\varphi_4(s, a) = 0$.

When $z \ll 1$, making allowance for the dependence of s on θ, we get

$$\{\Gamma(E_0, E, t, \theta)\}^\Gamma|_{z\ll 1} = e^{-\sigma_0 t}\delta(E_0 - E)\,\delta(\theta)/2\pi + H_4(s)\,C(s)\,f_2\left[s, \frac{2-s}{2}, L\right] s\, 2^{1-s}z^s\Gamma(1 - s/2)/[\lambda_1(s) + \sigma_0]\,\Gamma(s/2)\,E; \quad (11'')$$

s is determined by the condition $\varphi_2\left(s, \frac{2-s}{2}, a\right) = 0$. For $z \gg 1$ we get

$$\{\Gamma(E_0, E, t, \theta)\}^\Gamma|_{z\gg 1} = \frac{\delta(E_0 - E)\,\delta(\theta)}{2\pi}e^{-\sigma_0 t} + \{\Gamma(E_0, E, t)\}^\Gamma f_3(s, z)\, s; \quad (11''')$$

where s is determined by the condition $\varphi_3(s, a) = 0$.

For the corresponding functions, normalized to one particle, we obtain the following expressions:

$$\{F_P^d(s, z)\}^\Gamma = \frac{z^{s/2}K_{s/2}(z)}{2^{s/2}\Gamma(1 + s/2)},\quad \{F_P^i(s, z)\}^\Gamma = \frac{z^{(s-2)/2}K_{(2-s)/2}(z)}{2^{(s-2)/2}\Gamma(s/2)}.$$

The functions $\{\Gamma\}^\Gamma$ and $\{N_\Gamma\}^\Gamma$ are each a sum of two terms, the first of which contains $\delta(\theta)$ and consequently complicated expressions are obtained for $\{F_\Gamma^d(s, z)\}^\Gamma$ and $\{F_\Gamma^i(s, z)\}^\Gamma$. Simpler and more convenient expressions can be obtained by normalizing to unity only the second, non-singular term. Then the corresponding functions assume the form

$$\{\tilde{F}_\Gamma^d(s, z)\}^\Gamma = \frac{z^{(s-2)/2}K_{(2-s)/2}(z)}{2^{(s-2)/2}\Gamma(s/2)},\quad \{\tilde{F}_\Gamma^i(s, z)\}^\Gamma = \frac{sF_1(s, z)}{2^{(s-2)/2}\Gamma(s/2)\,z^2}.$$

From a comparison of the electron angular distribution functions normalized to unity we see that they are independent of the nature of the shower-producing particle at all depths t. For the corresponding photon functions, this conclusion is valid only for depths $t > 1$, where the effect of the term with the δ-function can be neglected. Consequently, the nature of the primary particle must be taken into account only in calculations of the photon angular distribution at depths $t \lesssim 1$. We note that in this case it is necessary to include some of the terms which we have previously discarded—those proportional to $\exp\{\lambda_2(s)t\}$ etc. The method of calculation used in the present paper enables us in principle to take these terms into account. The table lists the asymptotic behavior of the normalized angular distribution functions for $z \to 0$ at different values of s.

2. We now obtain the angular distribution functions of the particles in the case when some penetrating radiation of non-electromagnetic nature, which is absorbed as $e^{-\mu t}$, generates electrons or photons continuously along the entire path of development of the electron-photon shower. Let $S_P(E_0, E, t, \theta)$ electrons and $S_\Gamma(E_0, E, t, \theta)$ photons be generated in a single energy and angle interval of unit thickness.

The fundamental equations of this problem can then be written in the form

$$\partial P(E_0, E, t, \theta)/\partial t = L_1[P(E_0, E, t, \theta), \Gamma(E_0, E, t, \theta)] + (E_k^2/4E^2)\,\Delta_\theta P + S_P(E_0, E, t, \theta),$$

$$\partial\Gamma(E_0, E, t, \theta)/\partial t = L_2[P(E_0, E, t, \theta), \Gamma(E_0, E, t, \theta)] + S_\Gamma(E_0, E, t, \theta). \quad (1')$$

Asymptotic behavior of normalized angular distribution functions as $z \to 0$ in the case $E_0 = \infty$

Form of function	Region of variation of s	Asymptotic expression of the function
$\{F_P^d(s,z)\}^P$, $\{F_P^d(s,z)\}^\Gamma$	$s > 0$	$\sim 1/s$
	$0 < s < 2$	$\sim 2^{1-s}\Gamma(1 - s/2)/z^{2-s}\Gamma(s/2)$
$\{F_P^i(s, z)\}^P$, $\{F_P^i(s, z)\}^\Gamma$	$s = 2$	$\sim -\ln z$
	$s > 2$	$\sim 1/(s-2)$
	$0 < s < 2$	$\sim 2^{1-s}\Gamma(1 - s/2)/z^{2-s}\Gamma(s/2)$
$\{F_\Gamma^d(s, z)\}^P$, $\{F_\Gamma^d(s, z)\}^\Gamma$	$s = 2$	$\sim -\ln z$
	$s > 2$	$\sim 1/(s-2)$
	$0 < s < 2$	$\sim s2^{1-s}\Gamma(1 - s/2)(-\ln z)/z^{2-s}\Gamma(s/2)$
$\{F_\Gamma^i(s, z)\}^P$, $\{F_\Gamma^i(s, z)\}^\Gamma$	$s = 2$	$\sim (\ln z)^2$
	$s > 2$	$\sim s/(s-2)^2$

We take the source functions in two forms:*

1) $S_P(E_0, E, t, \theta) = 0$,
$S_\Gamma(E_0, E, t, \theta) = \delta(E_0 - E)\,\delta(\theta)\,e^{-\mu t}$,
2) $S_P(E_0, E, t, \theta) = \delta(E_0 - E)\,\delta(\theta)\,e^{-\mu t}$,
$S_\Gamma(E_0, E, t, \theta) = 0$.

1) In this case, making the necessary calculations, we obtain the function $P(E_0, E, t, \theta)$ in the form

$$\{P(E_0, E, t, \theta)\}^{s\Gamma} = \frac{1}{4\pi^2 i}\int_{\delta-i\infty}^{\delta+i\infty} \frac{ds}{E}\left(\frac{E_0}{E}\right)^s \frac{H_4(s)\exp[\lambda_1(s)\,t]\,z^{(4+s)/2}K_{s/2}(z)}{[\lambda_1(s)+\mu]\,\theta^2 2^{s/2}\Gamma(1+s/2)}. \quad (13)$$

Let us calculate the integral with respect to s in (13) without regard of the dependence of s on θ. We then sum the series in the second term, and, integrating with respect to k, obtain finally

$$\{P(E_0, E, t, \theta)\}^{s\Gamma} = 2\{P(E_0, E, t)\}^{s\Gamma} f_4[s, K_{s/2}(z)]\,z/s, \quad (14)$$

$$\{N_P(E_0, E, t, \theta)\}^{s\Gamma} = 2\{N_P(E_0, E, t)\}^{s\Gamma} f_4[s, K_{(2-s)/2}(z)]. \quad (15)$$

Here $\{P(E_0, E, t)\}^{s\Gamma}$ and $\{N_P(E_0, E, t)\}^{s\Gamma}$ are functions of the one-dimensional development of a cascade shower, generated by the penetrating radiation,[1] while the quantity s is determined by the condition y + a = 0.

Evaluating the integral, with allowance for the dependence of the saddle point on θ, we obtain

$$\{P(E_0, E, t, \theta)\}^{s\Gamma} = H_4(s)\,f_1[s, K_{s/2}(z), L]\,z/E\,[\lambda_1(s)+\mu], \quad (14')$$

$$\{N_P(E_0, E, t, \theta)\}^{s\Gamma} = H_4(s)\,f_1[s, K_{(2-s)/2}(z), L]/[\lambda_1(s)+\mu]. \quad (15')$$

The quantity s is defined here by the condition $\varphi_1(s, \nu, a) = 0$. The expressions (14) and (15) become simpler when $z \ll 1$ and $z \gg 1$:

$$\{P(E_0, E, t, \theta)\}^{s\Gamma}|_{z\ll 1} = H_4(s)\,f_2[s, s/2, L]\,z^2/E\,[\lambda_1(s)+\mu], \quad (14'')$$

$$\{N_P(E_0, E, t, \theta)\}^{s\Gamma}|_{z\ll 1} = H_4(s)\,f_2[s, (2-s)/2, L]\,2^{1-s}z^s\Gamma(1-s/2)/\Gamma(s/2), \quad (15'')$$

where s is determined by the condition $\varphi_2(s, \nu, a) = 0$. Further,

$$\{P(E_0, E, t, \theta)\}^{s\Gamma}|_{z\gg 1} = \{P(E_0, E, t)\}^{s\Gamma} f_3(s, z)\,z, \quad (14''')$$

$$\{N_P(E_0, E, t, \theta)\}^{s\Gamma}|_{z\gg 1} = \{N_P(E_0, E, t)\}^{s\Gamma} f_3(s, z)\,s, \quad (15''')$$

where s is determined by the condition $\varphi_3(s, a) = 0$.

For the photon angular distribution functions, analogous calculations for the case $E_0 = \infty$ lead to

$$\{\Gamma(E_0, E, t, \theta)\}^{s\Gamma} = \frac{\delta(E_0 - E)\,\delta(\theta)}{2\pi(\sigma_0 - \mu)}(e^{-\mu t} - e^{-\sigma_0 t}) + 2\{\Gamma(E_0, E, t)\}^{s\Gamma} f_4[s, K_{(2-s)/2}(z)], \quad (16)$$

$$\{N_\Gamma(E_0, E, t, \theta)\}^{s\Gamma} = \frac{\delta(\theta)}{2\pi(\sigma_0 - \mu)}(e^{-\mu t} - e^{-\sigma_0 t}) + 2\{N_\Gamma(E_0, E, t)\}^{s\Gamma} f_4[s, F_1(s, z)]\,z^{-(s+2)/2}, \quad (17)$$

where s is determined by the condition y + a = 0. If the dependence of s on θ is included, we get

$$\{\Gamma(E_0, E, t, \theta)\}^{s\Gamma} = \frac{\delta(E_0 - E)\,\delta(\theta)}{2\pi(\sigma_0 - \mu)}(e^{-\mu t} - e^{-\sigma_0 t}) + H_4(s)\,C(s)\,f_1[s, K_{(2-s)/2}(z), L]\,s/E\,[\lambda_1(s) + \sigma_0]\,[\lambda_1(s) + \mu], \quad (16')$$

where s is determined by the same condition as in (15');

$$\{N_\Gamma(E_0, E, t, \theta)\}^{s\Gamma} = \frac{\delta(\theta)}{2\pi(\sigma_0 - \mu)}(e^{-\mu t} - e^{-\sigma_0 t}) + H_4(s)\,C(s)\,f_1[s, F_1(s, z), L]\,s/[\lambda_1(s) + \sigma_0]\,[\lambda_1(s) + \mu]\,z^{(2+s)/2}, \quad (17')$$

and s is determined by the condition $\varphi_4(s, a) = 0$. When $z \ll 1$ and $z \gg 1$, the foregoing formulas can be more conveniently written as

$$\{\Gamma(E_0, E, t, \theta)\}^{s\Gamma}|_{z\ll 1} = \frac{\delta(E_0 - E)\,\delta(\theta)}{2\pi(\sigma_0 - \mu)}(e^{-\mu t} - e^{-\sigma_0 t}) + H_4(s)\,C(s)\,f_2[s, (2-s)/2, L] \times \frac{s2^{1-s}z^s\Gamma(1-s/2)}{E[\lambda_1(s)+\sigma_0][\lambda_1(s)+\mu]\Gamma(s/2)}; \quad (16'')$$

here s is determined by the condition $\varphi_2[s, (2-s)/2, a] = 0$. Further,

$$\{\Gamma(E_0, E, t, \theta)\}^{s\Gamma}|_{z\gg 1} = \{\Gamma(E_0, E, t)\}^{s\Gamma} f_3(s, z)\,s, \quad (16''')$$

where s is determined by the condition $\varphi_3(s, a) = 0$.

2) Our problem can also be solved when electrons of given energy are generated along the entire path of the shower. The general outline of the solution is the same as given in item 1). We therefore give only the final results.

If we assume $E_0 = \infty$, i.e., disregard the dependence of s on θ, we obtain the following expressions for the angular distribution functions of the electrons:

$$\{P(E_0, E, t, \theta)\}^{sP} = 2\{P(E_0, E, t)\}^{sP} f_4[s, K_{s/2}(z)]\,z/s, \quad (18)$$

$$\{N_P(E_0, E, t, \theta)\}^{sP} = 2\{N_P(E_0, E, t)\}^{sP} f_4[s, K_{(2-s)/2}(z)]. \quad (19)$$

In (18) and (19), s is determined by the condition y + a = 0.

If the dependence of s on θ is taken into account, we obtain

$$\{P(E_0, E, t, \theta\}^{sP} = H_1(s)\,f_1[s, K_{s/2}(z), L]/E\,[\lambda_1(s) + \mu], \quad (18')$$

*The solutions obtained with these sources can play the role of Green's functions for sources of more complicated form.

where s is determined from $\varphi_1(s, s/2, a) = 0$, and

$$\{N_P(E_0, E, t, \theta)\}^{sP} = H_1(s) f_1[s, K_{(2-s)/2}(z), L]/[\lambda_1(s) + \mu], \quad (19')$$

where s is determined from $\varphi_1[s, (2-s)/2, a] = 0$.

Formulas (18′) and (19′) can be rewritten for $z \ll 1$ and $z \gg 1$ as

$$\{P(E_0, E, t, \theta)\}^{sP}|_{z\ll 1} = H_1(s) f_2[s, s/2, L] z^2/E [\lambda_1(s) + \mu], \quad (18'')$$

$$\{N_P(E_0, E, t, \theta)\}^{sP}|_{z\ll 1} = H_1(s) f_2[s, (2-s)/2, L] 2^{1-s} z^s \Gamma(1-s/2)/\Gamma(s/2); \quad (19'')$$

Here s is given by the condition $\varphi_2(s, \nu, a) = 0$. Further,

$$\{P(E_0, E, t, \theta)\}^{sP}|_{z\gg 1} = \{P(E_0, E, t)^{sP} f_3(s, z) z, \quad (18''')$$

$$\{N_P(E_0, E, t, \theta)\}^{sP}|_{z\gg 1} = \{N_P(E_0, E, t)\}^{sP} f_3(s, z) s. \quad (19''')$$

The quantity s is determined in (18‴) and (19‴) by the condition $\varphi_3(s, a) = 0$.

For the photon angular distribution functions, disregarding the dependence of s on θ, we obtain

$$\{\Gamma(E_0, E, t, \theta)\}^{sP} = 2\{\Gamma(E_0, E, t)\}^{sP} f_4[s, K_{(2-s)/2}(z)], \quad (20)$$

$$\{N_\Gamma(E_0, E, t, \theta)\}^{sP} = 2\{N_\Gamma(E_0, E, t)\}^{sP} f_4[s, F_1(s, z)] z^{-(s+2)/2}. \quad (21)$$

In (20) and (21) s is determined by the condition $y + a = 0$. With allowance for the dependence of s on θ we get

$$\{\Gamma(E_0, E, t, \theta)\}^{sP} = H_3(s) f_1[s, K_{(2-s)/2}(z), L] s/E [\lambda_1(s) + \mu], \quad (20')$$

$$\{N_\Gamma(E_0, E, t, \theta)\}^{sP} = H_3(s) f_1[s, F_1(s, z), L] s/[\lambda_1(s) + \mu]. \quad (21')$$

In (20′) and (21′) s is defined by $\varphi_4(s, a) = 0$. When $z \ll 1$ or $z \gg 1$ we can rewrite (20′) as

$$\{\Gamma(E_0, E, t, \theta)\}^{sP}|_{z\ll 1} = H_3(s) f_2[s, (2-s)/2, L] s 2^{1-s} z^s \Gamma(1-s/2)/E [\lambda_1(s) + \mu] \Gamma(s/2), \quad (20'')$$

where s is given by $\varphi_2[s, (2-s)/2, a] = 0$ and

$$\{\Gamma(E_0, E, t, \theta)\}^{sP}|_{z\gg 1} = \{\Gamma(E_0, E, t)\}^{sP} = f_3(s, z) s, \quad (20''')$$

where s is given by the condition $\varphi_3(s, a) = 0$.

We note that in the formulas of Sec. 2 the cascade parameter s cannot be greater than s_μ, corresponding to equilibrium of the secondary electron-photon showers and the primary radiation, no matter what value t has. Therefore the form of the energy spectrum in the region of large energies differs greatly from the energy spectrum of the ordinary shower, generated by a primary particle of specified energy. Consequently, the angular distribution function under consideration, particularly in the region $\theta \ll 1$, will differ greatly from the corresponding function of the ordinary shower.

[1] S. Z. Belen'kii, Лавинные процессы в космических лучах (Cascade Processes in Cosmic Rays), Gostekhizdat, 1948. S. Z. Belen'kii and I. P. Ivanenko, Usp. Fiz. Nauk **69**, 591 (1959), Soviet Phys. Uspekhi **2**, 912 (1960).

[2] M. H. Kalos and J. M. Blatt, Australian J. Phys. **7**, 543 (1954).

[3] J. Nishimura and K. Kamata, Prog. Theor. Phys. **6**, 262 (1951).

[4] L. Eyges and S. Fernbach, Phys. Rev. **82**, 23 (1951).

[5] L. Eyges and S. Fernbach, Phys. Rev. **82**, 287 (1951).

[6] G. Moliere, Kosmische Strahlung, hrsg. von Heisenberg, Berlin, Springer-Verlag (1953).

[7] B. A. Chartress and H. Messel, Phys. Rev. **104**, 517 (1956).

[8] J. W. Garner, Proc. Phys. Soc. **A75**, 482 (1960).

[9] J. Nishimura and K. Kamata, Suppl. Progr. Theor. Phys. **6**, 93 (1958).

[10] I. P. Ivanenko, Doklady Akad. Nauk SSSR **122**, 367 (1958), Soviet Phys. Doklady **3**, 962 (1959).

[11] V. V. Guzhavin and I. P. Ivanenko, Proc. Intl. Conf. on Cosmic Rays, July 1959. Acad. Sci. Press **2**, 253 (1960).

Translated by J. G. Adashko
287

LIGHT ABSORPTION BY ELECTRONS OF NONMETALLIC CRYSTALS IN AN ELECTRIC FIELD

V. A. YAKOVLEV

Stalingrad Pedagogical Institute

Submitted to JETP editor October 2, 1960; resubmitted January 12, 1961

J. Exptl. Theoret. Phys. (U.S.S.R.) 40, 1695-1698 (June, 1961)

The effect is determined of a strong electric field on the optical absorption coefficient due to the conduction electrons of a nonmetallic crystal (semiconductor, insulator).

THERE are several mechanisms for the absorption of infrared radiation in semiconductors: 1) intrinsic absorption; 2) absorption due to local states; 3) lattice absorption; 4) free-carrier absorption.[1] Recently attention has been given to the effect of external fields on these mechanisms, e.g., on the intrinsic absorption.[2,3] This interest is due in particular to the fact that semiconductor devices (p-n junctions, transistors) operate under conditions which create strong electric fields in them. However, no theory has yet been given which takes into account the effect of a field on the remaining three mechanisms. In connection with the prospective use of semiconductors to amplify and generate infrared radiation,[4] the carrier absorption mechanism merits particular study, since it can be a competing process.

In the absence of a field, the mechanism under consideration consists of the absorption of a photon and the transition of an electron between levels of a single conduction band (in an n-type semiconductor). However, by virtue of the selection rules,[1] a direct transition in a single band is forbidden, so that it only occurs through intermediate states, with the participation of lattice vibrations or impurity centers. From the viewpoint of perturbation theory this process is of the second order. However, because the selection rules mentioned are determined by the wave functions of the electrons in the perfect lattice, it can be anticipated that they cease to apply when the wave functions are significantly changed owing to the strict periodicity of the lattice field being destroyed. The character of the optical absorption by the electron should also change. We shall consider changes of this type, assuming that the periodicity is destroyed by an external homogeneous electric field. As a result, we will show that under defined conditions a sufficiently strong field can so change the electron states that direct transitions (in the first order of perturbation theory), with simultaneous absorption (emission) of a photon, become possible between levels of the conduction band as altered by the field.

It is convenient to expand the wave functions in terms of Wannier functions:[5]

$$\psi(r) = \sum_{n,m} \Phi_n(\mathbf{r}_m)\, w_n(\mathbf{r} - \mathbf{r}_m), \tag{1}$$

where $w_n(\mathbf{r} - \mathbf{r}_m)$ is the Wannier function of the n-th band localized at the lattice site $\mathbf{m}(l_x, l_y, l_z)$. The coefficients Φ_n are determined from the system of equations[5]

$$(E_n^0(\mathbf{p}) + \mathbf{rF} - E)\,\Phi_n = -\sum_{n' \neq n} \mathbf{F}\mathbf{r}_{nn'}\Phi_{n'}. \tag{2}$$

Here $\mathbf{F}/e$ is the electric field strength, $\mathbf{r}_{nn'}$ are the coordinate matrix elements, and $E_n^0(\mathbf{p})$ is the operator obtained from the expression for the energy in the n-th band as a function of the quasi-momentum in the absence of the field, by replacing $\hbar\mathbf{k}$ by the momentum operator $\mathbf{p}$.

In the zero-order approximation, we neglect the effect of the energy bands on one another by discarding the right-hand side of (2). This means that we ignore the Zener effect,[6] which occurs in very large fields of the order of 10^6 v/cm. Of the equations obtained for the separate bands, we will consider below only the equation for the conduction band.

In order to determine Φ_n and E, an explicit form of $E_n^0(\hbar\mathbf{k})$ is needed, which forces us to use an approximate model. With a view to revealing the conditions under which the effect of the field on the states will be significant, we will use the "strong coupling" approximation,[7] which, for a simple cubic lattice, gives:

$$E_n^0 = E_n - 2\alpha_n \sum_{i=1}^{3} \sin^2\left(\frac{a_i k_i}{2}\right), \tag{3}$$

where $\mathbf{a_i}$ are the primitive translations, $2\alpha_n$ is the width of the band. Limiting the summation in (3) to nearest neighbors only corresponds to assuming that the band is narrow.[7] If we put

$$\Phi_n(r) = \int \varphi(p) \exp(-i\,\mathbf{rp}/\hbar)\, d\tau_p,$$

then we obtain from (2)

$$\varphi(p) = A \exp\left[\frac{i}{\hbar}\sum_{s=1}^{3}\left(\frac{C_s p_s}{F_s} - \alpha_n \frac{\sin ak_s}{aF_s}\right)\right]. \quad (4)$$

Using the series expansion of $\exp(-iz\sin\varphi)$ in terms of Bessel functions,[8] we reduce Φ_n to the form

$$\Phi_n(r) = AJ_{k'}(-\alpha_n/aF_x)\, J_{k''}(-\alpha_n/aF_y)\, J_{k'''}(-\alpha_n/aF_z),$$

$$k' = C_1/aF_x + x/a, \qquad k'' = C_2/aF_y + y/a,$$
$$k''' = C_3/aF_z + z/a. \quad (5)$$

The requirement that the wave function be finite can only be satisfied when J_k is a Bessel function of the first kind, and k′, k″, k‴ are whole numbers. The energy spectrum of the electrons in the band then becomes

$$E = E_n - 3\alpha_n + \sum_i aF_i s_i, \quad (6)$$

where s_1, s_2, s_3 are whole numbers replacing C_i/aF_i, and the normalized wave function is

$$\psi_{s_1 s_2 s_3}(r) = \sum_{l_i} J_{s_x - l_x}\left(\frac{-\alpha_n}{aF_x}\right) J_{s_y - l_y}\left(\frac{-\alpha_n}{aF_y}\right) J_{s_z - l_z}\left(\frac{-\alpha_n}{aF_z}\right)$$
$$\times w_n(\mathbf{r} - \mathbf{r}_m). \quad (7)$$

Since the external field does not change the number of states in the band, the limits of the variables s_i are given by the relationships

$$-N_i/2 \leqslant s_i \leqslant N_i/2, \quad (8)$$

where N_i is the number of elementary cells in the crystal in the i axis direction.

The wave function (7) and the discrete spectrum (6) which have been obtained correspond to finite motion of the electron. We emphasize that this result is essentially related to the assumption that transitions of electrons from one band to another can be neglected. The possibility that the energy of an electron in the crystal in a homogeneous field can be quantized has been discussed under similar assumptions by I. Lifshitz and Kaganov, using a different method,[9] for an arbitrary dispersion law $E_n(\hbar\mathbf{k})$ as applied to metals. This quantization cannot, however, give observable effects in metals. In fact, for the quantum character of the states to be displayed, it is necessary that the amplitude of the periodic (in the quasi-classical sense) motion, which is of the order $2\alpha_n/F$, shall be smaller than the mean free path. Even for large current densities $j = 10^2$ amp/cm^2, the attainable fields F/e in metals amount to $10^{-8} - 10^{-6}$ cgs esu, so that $2\alpha_n/F \approx 10^4$ cm, which greatly exceeds the mean free path.[9] In semiconductors and insulators fields of $F/e \approx 10^4$ cgs esu can be realized when the energy gap separating off the conduction band is sufficiently large. If, moreover, the width of the band is small, so that, for example, $2\alpha_n \sim 0.1$ ev, then $2\alpha_n/F$ is 10^{-6} cm. The mean free path in a number of semiconductors (Ge, Si) attains $10^{-5} - 10^{-4}$ cm, which greatly exceeds the amplitude of the periodic motion.[10]

Assuming that all the required conditions are satisfied in our model, we will calculate the optical absorption coefficient due to electrons of the band. The interaction of an electron with light is given in the coordinate representation (1) by the operator

$$\delta V = e\,\mathbf{A}\mathbf{p}/mc, \quad (9)$$

where $\mathbf{p}$ is the momentum operator, $\mathbf{A}$ is the vector potential:

$$\mathbf{A} = (\Omega\varepsilon)^{-1/2}\sum_{\sigma,t} q_\sigma \xi_{\sigma t} \exp(i\,\sigma\mathbf{r}), \quad (10)$$

where σ is the photon wave vector, $\xi_{\sigma t}$ are the unit polarization vectors, and Ω is the volume of the crystal. The matrix element of the transition from the state s_x, s_y, s_z to the state s'_x, s'_y, s'_z is

$$\langle \psi_{s'} | \delta V | \psi_s \rangle = \frac{e}{mc\sqrt{\Omega\varepsilon}} \sum_{\sigma, l, l'} q_\sigma \prod_{i=1}^{3} J_{s_i - l_i}\left(\frac{-\alpha_n}{eF_i}\right) J_{s'_i - l'_i}\left(\frac{-\alpha_n}{aF_i}\right)$$
$$\times \int w_n(\mathbf{r} - \mathbf{r}_l)\,(\xi_\sigma \mathbf{p})\, e^{i\sigma\mathbf{r}} w_n(\mathbf{r} - \mathbf{r}_{l'})\, d\tau. \quad (11)$$

The integral in (11) admits the following transformation:

$$\int w_n(\mathbf{r} - \mathbf{r}_l)\,(\xi_\sigma \mathbf{p})\, e^{i\sigma\mathbf{r}} w_n\ (\mathbf{r} - \mathbf{r}_{l'})\ d\tau$$
$$= e^{i\sigma\mathbf{r}_l} \int w_n(\boldsymbol{\rho})\,(\xi_\sigma \mathbf{p})\, e^{i\sigma\mathbf{p}} w_n(\boldsymbol{\rho} - (\mathbf{r}_{l'} - \mathbf{r}_l))\, d\tau.$$

Since the region in which the function $w_n(\rho)$ is localized has linear dimensions of the order of the lattice constant, a, but the wavelength of light $\lambda \gg a$, then we put $e^{i\sigma\cdot\rho} = 1$ in the integral. The matrix element (11) can only be non-zero if account is taken of the overlapping of the Wannier functions for neighboring cells.

Taking the cubic symmetry into account, we obtain the relations

$$A_0 = \int w_n(\boldsymbol{\rho})\, p_x w_n(\boldsymbol{\rho} \pm \mathbf{a}_1)\, d\tau = \int w_n(\boldsymbol{\rho})\, p_y w_n(\boldsymbol{\rho} \pm \mathbf{a}_2)\, d\tau$$
$$= \int w_n(\boldsymbol{\rho})\, p_z w_n(\boldsymbol{\rho} \pm \mathbf{a}_3)\, d\tau;$$
$$A_1 = \int w_n(\boldsymbol{\rho})\, p_x w_n(\boldsymbol{\rho} \pm \mathbf{a}_2)\, d\tau = \int w_n(\boldsymbol{\rho})\, p_x w_n(\boldsymbol{\rho} \pm \mathbf{a}_3)\, d\tau. \quad (12)$$

The fundamental formula determining the absorption coefficient μ is

$$\mu = \bar{P}\sqrt{\varepsilon}/c, \tag{13}$$

$$\bar{P} = \frac{2\pi}{\hbar}\sum_{s,\,s'} |\langle\psi_{s'}|\delta V|\psi_s\rangle|^2 \rho(E_{s'}) f(E_s) \tag{14}$$

where $\bar{P}$ is the total absorption probability, calculated for 1 sec, $f(E_S)$ is the electron distribution function (Maxwell-Boltzmann) normalized to the number of electrons N, ϵ is the optical dielectric constant, and $\rho(E)$ is the density of electronic states on an energy scale.

Because of the complexity of (11), calculation using formula (14) presents great difficulty for an arbitrary flux direction. We therefore evaluate μ for the particular case when the light flux is directed along the x axis of the crystal. We will also assume that the radiation is unpolarized, so that

$$\bar{\xi}_{\sigma z} = \bar{\xi}_{\sigma y} = 0, \qquad \overline{\xi^2_{\sigma y}} = \overline{\xi^2_{\sigma z}} = \tfrac{1}{2}.$$

In the optical frequency region considered, $\omega \approx 10^{14}$ and for all attainable fields $\hbar\omega \gg |\alpha_n \sin(\sigma a/2)|$. With these assumptions we obtain

$$\mu = \frac{2\pi n e^2 (A_0 + 2A_1)^2}{m^2 c\omega\sqrt{\varepsilon}\, aF} J^2_{\hbar\omega/\alpha F}\left(\frac{\alpha_n}{aF}\sin\frac{\sigma a}{2}\right) \tag{15}$$

($n = N/\Omega$). Because also $\sigma\alpha \ll 1$, then when $\alpha_n \sim 0.1 - 1$ ev we have, for all frequency ranges, $\hbar\omega \gg aF$. This inequality permits us to use an asymptotic form of the function $J_p(x)$,[8] and to bring (15) to the final form

$$\mu = \frac{n e^2 (A_0 + 2A_1)^2}{m^2 c\sqrt{\varepsilon}\,\hbar\omega^2}\,(1 - e^{-\hbar\omega/kT})\, e^{-F_0(\omega)/F},$$

$$F_0(\omega) \approx \frac{\hbar\omega}{2a}\ln\left(\frac{\hbar\omega}{\alpha_n \sin(\sigma a)}\right). \tag{16}$$

The multiplier $(1 - e^{-\hbar\omega/kT})$ takes the induced radiation into account. For small fields ($F < F_0$), the absorption μ is small, and disappears as $F \to 0$. For fields $F > F_0$, the quantity μ tends to saturation. It is of interest to note that the frequency dependence of the absorption μ is the inverse of that which was observed under the experimental conditions used by V. Vavilov and Britsyn[3] where the intrinsic absorption mechanism apparently dominated: with increasing frequency the absorption gets smaller. This fact can serve to separate the contribution of free carriers to the absorption in a field from other contributions in the total absorption coefficient.

We remark finally that the effect discussed should be expected in semiconductors with impurity bands the width of which is small, and that at sufficiently low temperatures the applicability conditions of the calculations given improve.

[1]N. I. Fan, Usp. Fiz. Nauk **64**, 315 (1958).

[2]L. V. Keldysh, JETP **34**, 1138 (1958), Soviet Phys. JETP **7**, 788 (1958).

[3]V. S. Vavilov and K. I. Britsyn, Физика твердого тела **2**, 1937 (1960), Soviet Physics-Solid State **2**, 1746 (1961).

[4]Basov, Krokhin, and Popov, Usp. Fiz. Nauk **72**, 161 (1960), Soviet Phys. Uspekhi **3**, 702 (1961).

[5]E. N. Adams, Phys. Rev. **85**, 41 (1952).

[6]C. Zener, Proc. Roy. Soc. **A145**, 523 (1934).

[7]F. Seitz, "The Modern Theory of Solids" (McGraw Hill, New York, 1940).

[8]I. M. Ryzhik and I. S. Gradshteĭn, Таблицы интегралов (Tables of Integrals), IIL, (1951).

[9]I. M. Lifshitz and M. I. Kaganov, Usp. Fiz. Nauk **69**, 419 (1959), Soviet Phys. Uspekhi **2**, 831 (1960).

[10]Coll. Полупроводники в науке и технике (Semiconductors in Science and Technology) **1**, AN SSSR 1957.

Translated by K. F. Hulme
288

ELECTRON POLARIZABILITY AND DIAMAGNETIC SUSCEPTIBILITY OF NEUTRAL ATOMS IN THE THOMAS-FERMI MODEL

T. TIETZ

Lodz University, Poland

Submitted to JETP editor November 6, 1960

J. Exptl. Theoret. Phys. (U.S.S.R.) 40, 1699-1704 (June, 1961)

The Latter potential is employed to calculate the following quantities for a free neutral atom: the field at the atomic nucleus due to the variation of density, the total induced quadrupole moment, and the change in the gradient of the electric field at the nucleus produced by an external charge. These quantities turn out to be finite, in contrast to the result obtained on the basis of the usual statistical theory of the atom. Also the diamagnetic susceptibility of atoms is calculated according to the Thomas-Fermi model corresponding to the effective charge distribution of Latter and Byatt.

IT is well known[1] that in the statistical theory of Thomas and Fermi[2] (T.F.) for a free neutral atom the field at the nucleus, the total induced quadrupole moment, and also the gradient of the electric field at the atomic nucleus due to the external charge cannot be evaluated since these quantities all diverge in this theory. In this paper we shall show that if we assume for the potential of a free neutral atom the Latter potential,[3] then all the quantities enumerated above become finite.

We assume that the electric field is due to a single charge +e situated at a large distance R from the nucleus along the positive X axis. If R is measured in units of the Bohr radius a_0, then the dipole part of the potential energy (in Rydberg units) is given by the expression

$$H_1 = -2R^{-2}r\cos\vartheta, \tag{1}$$

where ϑ is the angle between the X axis and the radius vector **r** directed from the nucleus to an electron of the filled shell. The momentum p of an electron in the presence of the external charge +e at the point X = R is given in the case of the Latter potential by the expression

$$\begin{aligned} &\frac{p^2}{2m} = \frac{Ze^2}{r}\varphi(x) + \frac{e^2 r\cos\vartheta}{R^2} \quad \text{for} \quad \frac{Ze^2}{r}\varphi(x) \geqslant \frac{e^2}{r}, \\ &\frac{p^2}{2m} = 0 + \frac{e^2 r\cos\vartheta}{R^2} \quad \text{for} \quad \frac{Ze^2}{r}\varphi(x) < \frac{e^2}{r}. \end{aligned} \tag{2}$$

Here $\varphi(x)$ is the T. F. function for a free neutral atom, while the dimensionless variable x is related to r in the following manner:[2]

$$x = 2Z^{1/3}r\,(3\pi/4)^{-2/3}a_H^{-1}. \tag{3}$$

If we denote by p_0 the momentum of the electron in the absence of the external charge, then we have for $\Delta p = p - p_0$

$$p_0\Delta p = me^2 rR^{-2}\cos\vartheta, \tag{4}$$

where

$$\begin{aligned} &p_0 = (2mZ\varphi e^2/r)^{1/2} \quad \text{for} \quad Z\varphi(x) \geqslant 1, \\ &p_0 = 0 \qquad\qquad\quad \text{for} \quad Z\varphi(x) < 1. \end{aligned} \tag{5}$$

The change in density $\Delta\rho$ corresponding to Δp has the form

$$\Delta\rho = 8\pi p_0^2\Delta p/h^3. \tag{6}$$

By utilizing formulas (4) — (6) we find in the case of the Latter potential for the field at the nucleus produced by the increment $\Delta\rho$ the expression

$$E_l(0) = \frac{e}{2R^2}\int_0^{x_0}[x\varphi(x)]^{1/2}dx. \tag{7}$$

To obtain a rough estimate of the momentum induced in the filled shells of the T.F. theory we shall express the momentum p corresponding to the maximum energy E = 0 in terms of the nuclear quadrupole moment Q:

$$\begin{aligned} &\frac{p^2}{2m} = \frac{Ze^2}{r}\varphi(x) + \frac{e^2Q(3\cos^2\vartheta - 1)}{4r^2} \quad \text{for} \quad \frac{Ze^2}{r}\varphi(x) > \frac{e^2}{r}, \\ &\frac{p^2}{2m} = 0 + \frac{e^2Q(3\cos^2\vartheta - 1)}{4r^2} \quad \text{for} \quad \frac{Ze^2}{r}\varphi(x) < \frac{e^2}{r}. \end{aligned} \tag{8}$$

Here $\varphi(x)$ is the T.F. function at the point x of the electron cloud, r is the length of the vector from the nucleus to this point, ϑ is the angle between r and the symmetry axis of Q. Since the electron density is $\rho = 8\pi p^3/3h^3$, then the density $\Delta\rho$ due to the second term in (8) is given by relation (6),

while the change in the momentum Δp associated with the term containing Q is equal to

$$(p_0 \Delta p)/m = e^2 Q (3 \cos^2 \vartheta - 1)/4r^3 \qquad (9)$$

(p_0 is the maximum momentum p for Q = 0).

On taking (6), (8), and (9) into account we obtain for $\Delta\rho$ the expression

$$\Delta\rho = \pi (2me^2/h^2r^2)^{3/2} (Z\varphi/r)^{1/2} Q (3 \cos^2 \vartheta - 1). \qquad (10)$$

The potential due to this $\Delta\rho$ corresponds to the quadrupole moment induced by the nuclear quadrupole moment Q. The total induced quadrupole moment Q will be obtained from (10) by integration over the angles and over r. In the case of the Latter potential we obtain

$$Q_i = \frac{3}{10} Q \int_0^{x_0} [\varphi(x)]^{1/2} dx, \qquad (11)$$

where the sign of Q_i is such that the nuclear moment q is screened. It can be concluded from (11) that the gradient of the electric field at the nucleus due to the external charge is altered by an amount

$$\Delta\left(\frac{\partial E_x}{\partial x}\right) = \frac{2e}{R^3} \cdot \frac{3}{10} \int_0^{x_0} [x\varphi(x)]^{1/2} dx. \qquad (12)$$

It can be seen from (7), (11), and (12) that in the case of the Latter potential the quantities E_i, Q_i and $\Delta(\partial E_x/\partial x)$ exist. The upper limit of integration x_0 in the aforementioned formulas is obtained from the relation $Z\varphi(x_0) = 1$.

Table I. The values of $R^2e^{-1}E_i(0)$ obtained in the present work and by Sternheimer[1] for the case of the T.F. D. model for different values of the slope at x = 0

Z	Sternheimer		Present work	
	x_0	$R^2e^{-1}E_i(0)$	x_0	$R^2e^{-1}E_i(0)$
18	7.25 6.66 5.46	2.98 2.73 2.22	6.2558	1.96
57	9.66 3.81	3.50 1.47	11.8352	3.36

In Table I we compare our results for $E_i(0)$ with those obtained by Sternheimer[1] for Z = 18 and Z = 57. We obtain the integral of $[\varphi(x)x]^{1/2}$ numerically by utilizing the tables of the T.F. functions due to Taima and Kobayashi [4]. The Thomas-Fermi-Dirac (T.F.D.) solutions with a smaller negative slope at x = 0 have a minimum at large x corresponding to a neutral atom; they were cut off at a distance x_0. The smallest value for $(R^2/e)E_i(0)$ is the best one. It can be seen from Table I that our results agree with Sternheimer's results.

Table II. Effect of the induced quadrupole moment*

Element	Z	$Q, 10^{-24}$ cm^2	Sternheimer $Q_c, 10^{-24}$ cm^2	Present work $Q_c, 10^{-24}$ cm^2
Lu	71	5.9[a] 7,0[b]	6,7[a] 8.0[b]	8.1[a] 9.2[b]
Eu	63	1.2[c] 2,5[d]	2,0[c] 4.2[d]	3.3[c] 4.1[d]

*The indices correspond to the different isotopes: a – Lu^{175}, b – Lu^{176}, c – Eu^{151}, d – Eu^{153}.

In Table II we compare our numerical results for the corrected nuclear quadrupole moment $Q_c = Q + Q_i$ with Sternheimer's quantum mechanical calculations.[5] It can be seen from Table II that the agreement is only rough.

We now go on to consider the diamagnetic susceptibility according to the T. F. model in the case of the Latter potential. It is well known that the original T. F. model cannot explain the molar diamagnetic susceptibility of free neutral atoms because of the excessive smearing out of the electron cloud in this model.

For the diamagnetic susceptibility of a gram-atom of the substance χ_d one obtains the dependence of χ_d on Z in the form $\chi_d = \text{const} \cdot Z^{1/3}$. The constant in this formula gives according to the T.F. model excessively large values of χ. For this reason this formula has been corrected in different ways with the best agreement being obtained in the case of a free neutral atom if one evaluates χ_d according to a modified T.F. model, viz., according to the Fermi-Amaldi model. The T.F.D. model usually does not lead to any better results than the Fermi-Amaldi model.

In this paper we evaluate χ_d by utilizing the Latter potential and also by assuming Byatt's expression[6] for the effective charge $Z_p(r)$. The susceptibility per gram atom is given by the formula

$$\chi_d = -(7.923 \cdot 10^{-7}) a_0^{-2} \left(0 \left| \sum_j r_j^2 \right| 0\right), \qquad (13)$$

where r_j is the distance of the j-th electron from the nucleus, a_0 is the Bohr radius, and 0 denotes the ground state of the atom. For a spherically symmetric atom we have

$$\left(0 \left| \sum_j r_j^2 \right| 0\right) = 6 \int_0^{\infty} Z_p(r)\, r\, dr, \qquad (14)$$

where $Z_p(r)$ is the effective charge. In the T.F. model the charge Z_p is related to the T.F. function for the free neutral atom $\varphi_0(x)$ by the expression $Z_p = Z\varphi_0(x)$. Here Z is the atomic

Table III. Numerical values of the constants c_i and b_i in (19)

Element	c_1	c_2	c_3	b_1	b_2	b_3	Element	c_1	c_2	c_3	b_1	b_2	b_3
He	1.25	—0.25	0.0	1.75	3.845	0.0	O	1.25	—0.35	0.1	0.991	1.63	18.3
Ne	1.0	0.0	0.0	0.978	0.0	0.0	Fe	0.25	0.56	0.19	0.335	0.828	3.76
Ar	0.659	0.341	0.0	0.574	2.77	0.0	As	0.295	0.705	0.0	0.387	1.295	0.0
Kr	0.415	0.51	0.075	0.378	1.48	7.0	Hg	0.19	0.56	0.25	0.257	0.779	3.16
C	1.25	—0.44	0.19	0.828	1.41	4.29							

Table IV. Values of the quantity $-10^6 \chi_d$ obtained according to the different models

Element	He	Ne	Ar	Kr	Xe
T. F. model (uncorrected)	—	67.0	81.0	10.20	11.70
Fermi-Amaldi model	—	12.62	21.67	37.34	49.53
T. F. D. model	—	14.33	22.15	35.51	45.96
Hartree-Fock model	—	8.06	—	31.10	—
According to formula (18)	—	14.21	24.60	42.15	64.0
According to formula (20)	1.73	8.39	19.97	38.61	—
Experimental	—	6.8	19.5	28.0	42.4

Table V. Gram-atom susceptibility $-10^6 \chi_d$

Element	C	O	Fe	As	Hg
According to formula (18)	6.71	12.50	33.34	61.60	75.11
According to formula (20)	8.38	6.55	31.90	28.57	61.40
Experimental	6.2[8]	4.6[8]	—	23.2[9]	38.1[9]

number, $x = r/\mu$, where $\mu = 0.88534\, a_0 Z^{-1/3}$. In the case of the Latter potential Z_p, as is well known, is given by the formula

$$Z_p = Z\varphi_0(x), \quad \text{if} \quad Z\varphi_0(x) \geqslant 1,$$
$$Z_p = 0, \quad \text{if} \quad Z\varphi_0(x) < 1. \tag{15}$$

On taking this into account we write (14) for the case of the Latter potential:

$$\left(0 \left| \sum_j r_j^2 \right| 0\right) = 6 \int_0^{r_0} Z\varphi_0(x)\, r\, dr. \tag{16}$$

The upper limit of integration r_0 is given by the equation $Z\varphi_0(x_0) = Z\varphi_0(r_0/\mu) = 1$. By utilizing the expression obtained earlier[7]

$$\varphi_0(x) = (1 + bx + cx^2)^{-3/2}, \tag{17}$$

where $b = 0.7105$, $c = 0.03919$, we obtain in accordance with (13), (16) and (17) the expression for χ_d:

$$-10^6 \chi_d = 21.411\, Z^{1/3} \left[\frac{2 + bx_0}{\sqrt{1 + bx_0 + cx_0^2}} - 2 \right], \tag{18}$$

with $Z\varphi_0(x_0) = 1$. The function $\varphi_0(x)$ of the form (17) gives a very good approximation to the exact values of $\varphi_0(x)$ in the interval from $x = 0$ to $x = 1000$. The maximum error in this case amounts to less than 3%.

Ruark was the first to propose (cf. reference 6) that the following expression should be utilized for the effective charge Z_p

$$Z_p = Z\,[c_1 e^{-b_1 r/\mu} + c_2 e^{-b_2 r/\mu} + c_3 e^{-b_3 r/\mu}]. \tag{19}$$

The constants c_i and b_i in the last formula depend on Z. Byatt has calculated these constants with great accuracy for several values of Z. In Table III are given numerical values of c_i and b_i as functions of Z.

By utilizing (19), (16), and (13), we obtain for χ_d the expression

$$-10^6 \chi_d = 3.7260 Z^{1/3} [c_1 b_1^{-2} + c_2 b_2^{-2} + c_3 b_3^{-2}]. \tag{20}$$

In Table IV the values of χ_d evaluated by us in accordance with expressions (18) and (20) are compared with numerical values obtained in the original T.F. model (cf. reference 2), in the modified Fermi-Amaldi model, in the T.F.D. and the Hartree-Fock models, and also with experimental data. It may be seen from Table IV that expression (18) gives better results than the original T.F. model, although they are still too large in comparison with experiment. Formula (20) gives better results than (18), and this means that the charge Z_p obtained from (19) is very close to the true Hartree-Fock effective charge distribution.

In Table V we give values of χ_d, obtained from (20) and (18) for a number of substances which are not listed in Table 4; experimental data[8,9] are also shown there. As is well known, these data are not very definite, since it is difficult to find experimentally the diamagnetic susceptibility for atoms other than those shown in Table IV.

It can be seen from Tables IV and V that formula (19) for Z_p can be utilized for the description of the problem of interest to us.

From the present work it follows that the quantities $E_i(0)$, Q_i and $\Delta(\partial E_x/\partial x)$ [formulas (7), (11) and (12)], obtained with the aid of the Latter potential have finite values. Numerically they agree with the experimental data only very roughly. In order to obtain better agreement it is necessary to carry out a quantum mechanical averaging. Table II shows that Q_i evaluated with the aid of the Latter potential gives a somewhat worse result than the more elaborate T.F.D. model. It can be seen from Table IV that the diamagnetic susceptibility obtained with the aid of the Latter potential gives better results than the uncorrected T.F. theory. The results of Table IV provide evidence that the Latter potential, in principle, leads to values comparable to those obtained in the T.F.D. and the Fermi-Amaldi models.[10]

[1] R. M. Sternheimer, Phys. Rev. **96**, 951 (1954).

[2] P. Gombas, Die statistische Theorie des Atoms und ihre Anwendungen, Springer Verlag, Vienna, 1949.

[3] R. Latter, Phys. Rev. **99**, 510 (1955).

[4] S. Kobayashi and T. Taima, Table of the Exact Values of the T.F. Function, Kagava University, Japan, 1956.

[5] R. M. Sternheimer, Phys. Rev. **102**, 80 (1950).

[6] W. J. Byatt, Phys. Rev. **104**, 1298 (1956).

[7] T. Tietz, Nuovo cimento **4**, 1192 (1956).

[8] E. C. Stoner, Magnetism, London, 1930.

[9] Handbook of Chemistry and Physics, 3rd ed. (Chemical Rubber Publishing Co., Cleveland, Ohio).

[10] S. Kobayashi, J. Phys. Soc. Japan **14**, 1039 (1959).

Translated by G. Volkoff
289

THEORY OF THE ABSORPTION OF SOUND IN DILUTE He^3 IN He II SOLUTIONS

A. F. ANDREEV

Institute for Physics Problems, Academy of Sciences, U.S.S.R.

Submitted to JETP editor November 10, 1960; resubmitted February 18, 1961

J. Exptl. Theoret. Phys. (U.S.S.R.) **40**, 1705-1709 (June, 1961)

We have evaluated the absorption coefficient of first sound due to second viscosity in dilute solutions of He^3 in He II. The processes that lead to the establishment of equilibrium in the phonon and roton numbers are regarded as the slow processes which cause second viscosity. We compare our results with experiments.

KHALATNIKOV[1] obtained phenomenologically the following expression for the coefficient of absorption of first sound of frequency ω in dilute solutions of He^3 in He II:

$$\alpha(x) = \frac{\omega^2}{2\rho c^3}\left\{\frac{4}{3}\eta + \zeta_2 + \frac{Dc^2}{\rho}\left(\frac{\partial\rho}{\partial x}\right)^2 \frac{m_3 x}{kT}\right\}, \qquad (1)$$

where ρ is the density of the solution, c the sound velocity in it, η, ζ_2, and D respectively the coefficients of first viscosity, second viscosity, and diffusion, x the He^3 concentration, and m_3 the mass of a He^3 atom.

The second term in (1), which is connected with the second viscosity, is the main contribution to the absorption coefficient. The processes that establish the number of excitations (see reference 2) are, as in the case of pure He II, the slow processes that cause second viscosity.

The measurements by Harding and Wilks[3] have shown that the absorption of sound decreases appreciably when the He^3 concentration is increased. This indicates that the coefficient of second viscosity ζ_2 must depend strongly on the concentration. In the present paper we evaluate the sound absorption connected with second viscosity.

Equilibrium in solution for a given number of excitations is much faster established than equilibrium in the number of excitations. We shall therefore assume that the first equilibrium is established, i.e., that the excitation distribution functions are the equilibrium ones, but that the chemical potential is different from zero. As far as impurity excitations are concerned, their number is given (it is equal to the number of impurity atoms) and we shall thus assume the "impurity gas" to be in complete equilibrium.

The basic processes which in pure He II accompany a change in the number of excitations are the five-phonon process and the processes where a phonon-roton scattering changes a phonon into a roton, and vice versa. We must elucidate the influence of impurities on the speed with which the number of phonons and rotons changes. In the following we consider the most probable of the processes which are of interest to us: scattering by impurities involving three phonons or involving roton-phonon interchanges.

IMPURITY SCATTERING INVOLVING THREE PHONONS

The Hamiltonian for the interaction between impurities and phonons is of the form (see reference 4)

$$V = -\frac{1}{2}(\mathbf{Pv} + \mathbf{vP}) + \frac{\partial\Delta}{\partial\rho}\rho' + \frac{1}{2}\frac{\partial^2\Delta}{\partial\rho^2}\rho'^2 + \frac{1}{6}\frac{\partial^3\Delta}{\partial\rho^3}\rho'^3, \qquad (2)$$

where Δ is the zero energy of the impurity, ρ' the change in density due to the presence of phonons, $\mathbf{v}$ the velocity of the medium, connected with the presence of phonons, and $\mathbf{P} = -i\hbar\nabla$ the momentum operator of the impurity.

Our problem consists in calculating the probability that an impurity makes a transition from a state i with momentum $\mathbf{P}$ into a state f with momentum $\mathbf{P}'$ during which a phonon with momentum $\mathbf{p}_1$ is absorbed and two phonons with momenta $\mathbf{p}_2$ and $\mathbf{p}_3$ are emitted.

We apply the method of approximate quantization of the nonlinear equations of hydrodynamics, developed by Landau and Khalatnikov,[5] and we perform our calculations in a manner similar to theirs, taking terms of fourth order in ρ' into account (this is necessary because three phonons are involved in the process considered by us); we then get for the matrix element for the above-mentioned transition the expression

$$M \equiv V_{fi} = \frac{A}{c}\left(\frac{\rho}{2c}\right)^{3/2}(p_1 p_2 p_3)^{1/2}\{M_{12} + M_{13} + M_{23}\},$$

where

$$M_{12} = -\frac{(p_1-p_3)^2}{p_1p_2[1-\mathbf{n}_1\mathbf{n}_2+3\gamma(p_1-p_2)^2]}\left\{\frac{P}{\rho^2}(\mathbf{n}_1+\mathbf{n}_3,\ \mathbf{m})\right.$$
$$\left.\times(1+\mathbf{n}_1\mathbf{n}_3) - \frac{\partial\Delta}{\partial\rho}\left(\frac{3n_1n_3}{\rho c^2}-\frac{B}{c^3}\right)+\frac{1}{c}\frac{\partial^2\Delta}{\partial\rho^2}\right\};$$

M_{13} is obtained from M_{12} by the substitution $\mathbf{n}_2 \to \mathbf{n}_3$, $\mathbf{n}_3 \to \mathbf{n}_2$, $\mathbf{p}_2 \to \mathbf{p}_3$; M_{23} is obtained from M_{12} by the substitution $\mathbf{n}_1 \to \mathbf{n}_3$, $\mathbf{n}_3 \to \mathbf{n}_1$, $\mathbf{p}_1 \to -\mathbf{p}_3$;

$$A = c^2/\rho + {}^1/_2\,\partial c^2/\partial\rho, \qquad B = c^2/\rho - \partial c^2/\partial\rho;$$

the constant γ is defined by the dependence of the phonon energy ϵ_{ph} on the momentum p: $\epsilon_{ph} = c(p-\gamma p^3)$: $\mathbf{n}_1$, $\mathbf{n}_2$, $\mathbf{n}_3$, and $\mathbf{m}$ are unit vectors in the directions of the momenta $\mathbf{p}_1$, $\mathbf{p}_2$, $\mathbf{p}_3$, and $\mathbf{P}$, respectively.

The absolute square of the matrix element M can easily be integrated over the directions of the vectors $\mathbf{m}$, $\mathbf{n}_1$, $\mathbf{n}_2$, and $\mathbf{n}_3$:

$$W \equiv \int |M|^2 do\,do_1\,do_2\,do_3 = \frac{A^2}{c^2}\left(\frac{\rho}{2c}\right)^3\frac{(4\pi)^4}{6\gamma}p_1p_2p_3\left(K+\frac{4P^2}{3\rho^4}\right)$$
$$\times\left\{\frac{(p_1-p_2)^2}{p_1^2p_2^2}+\frac{(p_1-p_3)^2}{p_1^2p_3^2}+\frac{(p_2+p_3)^2}{p_2^2p_3^2}\right\},$$
$$K = \left(\frac{\partial\Delta}{\partial\rho}\right)^2\left(\frac{3}{\rho^2c^2}+\frac{B^2}{c^6}\right)+\frac{1}{c^2}\left(\frac{\partial^2\Delta}{\partial\rho^2}\right)^2+\frac{2B}{c^4}\frac{\partial\Delta}{\partial\rho}\frac{\partial^2\Delta}{\partial\rho^2}. \qquad (3)$$

In integrating we have used the fact that $\gamma p^2 \ll 1$ (p is a momentum of the order of the average phonon momentum).

The probability dw for the transition in which we are interested is determined by the perturbation-theory formula

$$dw = 2\pi\hbar^{-1}|M|^2\,\delta(E_f - E_i)\,d\mathbf{p}_2\,d\mathbf{p}_3/(2\pi\hbar)^6,$$

where E_f and E_i are the energies of the final and initial states.

If one uses the momentum conservation law one sees easily that as $P, p_1, p_2, p_3 \ll mc$, where m is the effective impurity mass

$$E_f - E_i \approx c(p_1 - p_2 - p_3).$$

We are interested in the rate of change of the total number of phonons N_{ph} per unit time, due to the process considered:

$$\dot{N}_{ph} = \iiint\{N(P)\,n(p_1)\,[1+n(p_2)]\,[1+n(p_3)]$$
$$-N(P')\,n(p_2)\,n(p_3)\,[1+n(p_1)]\}\,dw\,d\mathbf{P}\,d\mathbf{p}_1\,(2\pi\hbar)^{-6}. \qquad (4)$$

Here

$$N(P) = (2\pi\hbar)^3\frac{x\rho}{m_3}(2\pi mkT)^{-3/2}\exp\left\{-\frac{P^2}{2mkT}\right\}$$

is the impurity distribution function and $n(p)$ the phonon distribution function.

If the number of phonons is not equal to its equilibrium value, this means that $n(p)$ contains a non-vanishing chemical potential μ_{ph}

$$n(p) = [\exp\{[\varepsilon_{ph}(p) - \mu_{ph}]/kT\} - 1]^{-1}.$$

If the deviation from equilibrium is a small one,

$$n(p) = n_0(p) + n_0(p)\,[1+n_0(p)]\,\mu_{ph}/kT, \qquad (5)$$

where $n_0(p)$ is the equilibrium distribution function.

Using (5) we transform (4) to

$$\dot{N}_{ph} = -\frac{\mu_{ph}}{kT}\iiint N(p)\,n_0(p_1)\,[1+n_0(p_2)]$$
$$\times[1+n_0(p_3)]\,dw\,\frac{d\mathbf{P}d\mathbf{p}_1}{(2\pi\hbar)^6}. \qquad (6)$$

Integrating in (6) over the angles, integrating over p_1 to get rid of the δ-function, and using (3) we get

$$\dot{N}_{ph} = -(2\pi\hbar)^{-12}\frac{\mu_{ph}}{kT}\int_0^\infty dP\int_0^\infty dp_2\int_0^\infty dp_3 N(P)\,P^2(p_2+p_3)^2p_2^2p_3^2$$
$$\times e^{c(p_2+p_3)/kT}\,[e^{c(p_2+p_3)/kT}-1]^{-1}$$
$$\times\,[e^{cp_2/kT}-1]^{-1}[e^{cp_3/kT}-1]^{-1}W. \qquad (7)$$

We can without great loss of accuracy neglect in the denominator of (7) unity as compared to $\exp\{c(p_2+p_3)/kT\}$, and we can then again perform the integration in (7) and we get

$$\dot{N}_{ph} = -\Gamma_{phi}\mu_{ph}, \quad \Gamma_{phi} = x\frac{64\pi^2\beta\rho Q}{(2\pi\hbar)^9m_3c^{10}\hbar}\left(\frac{K}{4}+\frac{mkT}{\rho^4}\right)(kT)^8. \qquad (8)$$

In (8) we have used the notation

$$\beta = 36.3, \qquad Q = \frac{A^2}{c^2}\left(\frac{\rho}{2c}\right)^3\frac{(4\pi)^4}{6\gamma}.$$

The quantity K contains the derivatives $\partial\Delta/\partial\rho$ and $\partial^2\Delta/\partial\rho^2$ which we do not know and which we shall therefore in the following determine from the experiments.

The three-phonon process can occur also in pure He II through scattering by a roton, but calculations show that its contribution is small compared with the contribution from the five-phonon process (at low temperatures) or as compared to that from the roton-scattering process involving a roton-phonon transition (at higher temperatures).

IMPURITY SCATTERING INVOLVING A ROTON-PHONON TRANSITION

We must now calculate the probability for a transition of the impurity from a state with momentum $\mathbf{P}$ to a state with momentum $\mathbf{P}'$ during which a phonon with momentum $\mathbf{p}$ is absorbed and a roton with momentum $\mathbf{P}_1$ is emitted.

It is clear that the phonon that takes part in this process must be very energetic. We shall assume that it interacts with the impurity in the same way as the roton, but that it has a different dispersion law. We get thus for the probability of the above mentioned process

$$dw = 2\pi\hbar^{-1}|v_{ir}|^2\,\delta(E_1 - E_2)\,d\mathbf{P}_1/(2\pi\hbar)^3, \qquad (9)$$

where $v_{ir} = 8 \times 10^{-38}$ erg-cm^3 is the impurity-roton interaction constant, and E_1 and E_2 are the energies of the initial and final states.

We are interested in the rate of change in the number of excitations due to this process; this rate of change is, moreover, determined by the formula

$$\dot{N}_r = -\dot{N}_{ph} = \frac{\mu_{ph} - \mu_r}{kT} \iiint n_0(p)\, N(P)\, dw \frac{dp dP}{(2\pi\hbar)^6}, \quad (10)$$

where μ_r is the roton chemical potential.

Khalatnikov[2] has shown that we can estimate in this way only an upper limit for the quantities which we evaluate, i.e., we get from (10)

$$\dot{N}_r = -\dot{N}_{ph} = \Gamma_{phri}(\mu_{ph} - \mu_r), \quad (11)$$

where

$$\Gamma_{phri} \lesssim x \frac{2\sqrt{2\pi}}{\hbar^4} |v_{ir}|^2 \frac{P_0^2 \Delta_r^2 \sqrt{m_r}}{(2\pi\hbar c)^3} \frac{\rho}{m_3} (kT)^{-1/2} e^{-\Delta_r/kT}$$

$$= 1.1 \cdot 10^{51} x T^{-1/2} e^{-\Delta_r/kT}. \quad (11')$$

Here, P_0, Δ_r and m_r are the roton spectrum parameters. The exact value of Γ_{phri} will be determined from experiments.

THE SOUND ABSORPTION COEFFICIENT

The following expressions hold for the rate of change of the number of phonons and rotons in pure He II:[2]

$$\dot{N}_{ph} = -(\Gamma_{ph} + \Gamma_{phr})\mu_{ph} + \Gamma_{phr}\mu_r,$$
$$\dot{N}_r = -\Gamma_{phr}\mu_r + \Gamma_{phr}\mu_{ph}, \quad (12)$$

where one must take for Γ_{ph} and Γ_{phr} the values

$$\Gamma_{ph} = 6.3 \cdot 10^{42} T^{11}, \qquad \Gamma_{phr} = 6.5 \cdot 10^{50} e^{-2\Delta_r/T}. \quad (13)$$

When there are impurities present we must according to (8) and (11) replace Γ_{ph} by $\Gamma_{ph} + \Gamma_{phi}$ and Γ_{phr} by $\Gamma_{phr} + \Gamma_{phri}$ in (12), i.e., we have now instead of (12)

$$\dot{N}_{ph} = -(\Gamma_{ph} + \Gamma_{phi} + \Gamma_{phr} + \Gamma_{phri})\mu_{ph} + (\Gamma_{phr} + \Gamma_{phri})\mu_r,$$
$$\dot{N}_r = -(\Gamma_{phr} + \Gamma_{phri})\mu_r + (\Gamma_{phri} + \Gamma_{phr})\mu_{ph}. \quad (14)$$

The coefficient for the absorption of sound of not too high a frequency in pure He II, due to second viscosity, is given by the equation (see reference 2)

$$\tilde{\alpha}(0) = \frac{\omega^2}{2\rho c^3}\left[\frac{1}{\Gamma_{ph}}\left(\frac{\partial\rho}{\partial\mu_r} + \frac{\partial\rho}{\partial\mu_{ph}}\right)^2 + \frac{1}{\Gamma_{phr}}\left(\frac{\partial\rho}{\partial\mu_r}\right)^2\right]_{\rho, S_0},$$

where S_0 is the entropy per unit mass of pure He II. As the sound velocity is independent of the impurity concentration[1] at low concentrations we can compare (12) and (14) and immediately write down for the solution

$$\tilde{\alpha}(x) = \frac{\omega^2}{2\rho c^3}\left[\frac{1}{\Gamma_{ph} + \Gamma_{phi}}\left(\frac{\partial\rho}{\partial\mu_r} + \frac{\partial\rho}{\partial\mu_{ph}}\right)^2 + \frac{1}{\Gamma_{phr} + \Gamma_{phri}}\left(\frac{\partial\rho}{\partial\mu_r}\right)^2\right]_{\rho, S, x}, \quad (15)$$

where S is the entropy per unit mass of the solution.

We transform this last expression in terms of p, T, x, μ_r, and μ_{ph} using the fact that the derivative $(\partial\rho/\partial T)_{p,x}$ is small:

$$\tilde{\alpha}(x) = \frac{\omega^2 c}{2\rho}\left[\frac{1}{\Gamma_{ph} + \Gamma_{phi}}\left(\frac{\partial\rho}{\partial\mu_r} + \frac{\partial\rho}{\partial\mu_{ph}}\right)^2 + \frac{1}{\Gamma_{phr} + \Gamma_{phri}}\left(\frac{\partial\rho}{\partial\mu_r}\right)^2\right]_{\rho, T, x}. \quad (16)$$

Using the thermodynamic identity (for constant concentration)

$$d\Phi = -SdT + \frac{1}{\rho}dp - \frac{N_{ph}}{\rho}d\mu_{ph} - \frac{N_r}{\rho}d\mu_r,$$

we get the following expressions for the derivatives occurring in (16)

$$\partial\rho/\partial\mu_{ph} = \rho(\partial N_{ph}/\partial p)_{T,x} - N_{ph}/c^2,$$
$$\partial\rho/\partial\mu_r = \rho(\partial N_r/\partial p)_{T,x} - N_r/c^2. \quad (17)$$

One can conclude from the work of Dash and Taylor[6] that

$$\frac{\partial}{\partial x}\frac{\partial\rho}{\partial\mu_{ph}} \sim \frac{\partial\rho}{\partial\mu_{ph}}, \qquad \frac{\partial}{\partial x}\frac{\partial\rho}{\partial\mu_r} \sim \frac{\partial\rho}{\partial\mu_r},$$

but it follows from (8) that

$$\Gamma_{phi}/x > 2{,}7 \cdot 10^{44} T^9 \gg \Gamma_{ph} \text{ when } T \sim 1^\circ K.$$

The main concentration dependence of $\tilde{\alpha}(x)$ comes thus from taking Γ_{phi} and Γ_{phri} into account and we can thus in (16) put

$$\partial\rho/\partial\mu_r = (\partial\rho/\partial\mu_r)_0, \qquad \partial\rho/\partial\mu_{ph} = (\partial\rho/\partial\mu_{ph})_0,$$

where $(\partial\rho/\partial\mu)_0$ is the value for pure He II. The values for $(\partial\rho/\partial\mu_r)_0$ and $(\partial\rho/\partial\mu_{ph})_0$ were calculated by Khalatnikov:[2]

$$\left(\frac{\partial\rho}{\partial\mu_r}\right)_0 = -N_r\left[\frac{\Delta_r}{T}\left(\frac{N_r}{N_{ph}} - 23.2\right) - 22.5\right] \Big/ c^2\left[\left(\frac{\Delta_r^2}{T^2} + \frac{\Delta_r}{T} + \frac{3}{4}\right)\frac{N_r}{N_{ph}} + \frac{\pi^4}{9}\right], \quad (18)$$

$$\left(\frac{\partial\rho}{\partial\mu_{ph}}\right)_0 = -N_r\left[6.4\frac{\Delta_r^2}{T^2} + 9.4\frac{\Delta_r}{T} + 9.3\right] \Big/ c^2\left[\left(\frac{\Delta_r^2}{T^2} + \frac{\Delta_r}{T} + \frac{3}{4}\right)\frac{N_r}{N_{ph}} + \frac{\pi^4}{9}\right].$$

Thus:

$$\tilde{\alpha}(x) = \frac{\omega^2 c}{2\rho}\left[\frac{1}{\Gamma_{ph} + \Gamma_{phi}}\left[\left(\frac{\partial\rho}{\partial\mu_r}\right)_0 + \left(\frac{\partial\rho}{\partial\mu_{ph}}\right)_0\right]^2 + \frac{1}{\Gamma_{phr} + \Gamma_{phri}}\left(\frac{\partial\rho}{\partial\mu_r}\right)_0^2\right]. \quad (19)$$

In the figure we have given a comparison of the values of the sound absorption coefficient deter-

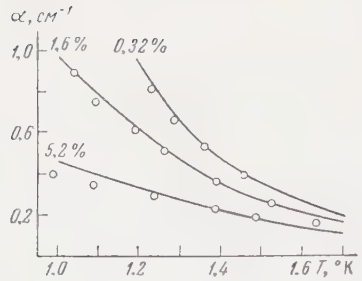

mined from Eq. (19) (adding to it the quantity $2\omega^2\eta/3\rho c^3$ which at high temperatures becomes appreciable) with the experimental data of Harding and Wilks,[3] where we have put

$$\Gamma_{\text{phi}} = 1.4 \cdot 10^{44} x T^8 \,(1.3 + 1.9T),$$

which corresponds to

$$K\rho^4 = 5.3 \cdot 10^{-39} \text{g}^2\,\text{cm}^2\,\text{sec}^{-2}$$

$$\Gamma_{\text{phri}} = x \cdot 0.7 \cdot 10^{50} T^{-1/2} e^{-\Delta_r/T};$$

the value of η was evaluated by Zharkov.[7]

In conclusion the author expresses his gratitude to I. M. Khalatnikov for his assistance with this paper and to V. N. Zharkov for valuable remarks.

[1] I. M. Khalatnikov, JETP **23**, 265 (1952).
[2] I. M. Khalatnikov, JETP **20**, 243 (1950).
[3] G. O. Harding and J. Wilks, Phil. Mag. **3**, 1469 (1958).
[4] I. M. Khalatnikov and V. N. Zharkov, JETP **32**, 1108 (1957), Soviet Phys. JETP **5**, 905 (1957).
[5] L. D. Landau and I. M. Khalatnikov, JETP **19**, 657 (1949).
[6] J. G. Dash and R. D. Taylor, Phys. Rev. **107**, 1228 (1957).
[7] V. N. Zharkov, JETP **33**, 929 (1957), Soviet Phys. JETP **6**, 714 (1958).

Translated by D. ter Haar
290

DOUBLE DISPERSION RELATIONS AND THE PHOTOPRODUCTION OF PIONS. II

N. F. NELIPA and V. A. TSAREV

P. N. Lebedev Physics Institute, Academy of Sciences, U.S.S.R.

Submitted to JETP editor November 17, 1960

J. Exptl. Theoret. Phys. (U.S.S.R.) 40, 1710-1712 (June, 1961)

An approximate estimate of the contribution of the annihilation of a nucleon pair into a π meson and a γ quantum to the π-meson photoproduction amplitude is made by using previously derived[1] integral equations.

THE aim of the present paper is the approximate evaluation of the contribution of the process of annihilation of a nucleon pair into a meson and photon to the π-meson photoproduction amplitude. A system of integral equations derived previously by one of the authors[1] will be utilized.

If one assumes that there exists a resonance in the π-π interaction with angular momentum J = 1 and isospin T = 1 and that this resonance is sufficiently narrow, one can write according to Eq. (5.6) of reference 1 (we assume that only the isoscalar part of the amplitude will contribute to the two-meson approximation)*

$$\Delta E_{0+} = (\Lambda/e)\left\{C_1[r_1^1 I_1 + r_1^2 I_5 - 4kqr_1^3] - C_2[r_2^1 I_2 + r_2^2 I_6] + \tfrac{1}{2} qC_2\left[r_4^1 I_3 - \tfrac{8}{3}\alpha kqr_4^1\right]\right\}, \quad (1.1)$$

$$\Delta E_{1-} = (\Lambda/e)\left\{C_1[r_1^1 I_2 + r_1^2 I_6] - C_2[r_2^1 I_1 + r_2^2 I_5 - 4kqr_2^3] - qC_1\left[r_3^1 I_3 - \tfrac{8}{3}\alpha kqr_3^1\right] + qC_2 r_4^1 I_3\right\}, \quad (1.2)$$

$$\Delta M_{1+} = (\Lambda/2e)\left\{C_1[r_1^1 I_2 + r_1^2 I_6] - C_2 r_2^1 I_4 - \tfrac{1}{2} qC_1\left[r_3^1 I_3 - \tfrac{8}{3}\alpha kqr_3^1\right]\right\}, \quad (1.3)$$

$$\Delta M_{1-} = (\Lambda/e)\left\{-C_1[r_1^1 I_2 + r_1^2 I_6] + C_2[r_2^1 I_1 + r_2^2 I_5 - 4kqr_2^3] + \tfrac{1}{2} qC_1\left[r_3^1 I_3 - \tfrac{8}{3}\alpha kqr_3^1\right]\right\}. \quad (1.4)$$

We have used the following abbreviations:

$$I_1 = \ln\frac{a+1}{a-1} \equiv \beta, \quad I_2 = -2 + a\beta, \quad I_3 = 2a + (1-a^2)\beta,$$

$$I_4 = -6a + (3a^2-1)\beta, \quad I_5 = 4kq(2E_\mu k - 1),$$

$$I_6 = -\tfrac{1}{3}8q^2k^2,$$

$$C_1 = -\frac{1}{4kq}\frac{W-M}{8\pi W}\sqrt{(E_k+M)(E_M+M)},$$

$$C_2 = -\frac{1}{4k}\frac{W-M}{8\pi W}\sqrt{\frac{E_k+M}{E_M+M}};$$

$a = (2E_\mu k - 1)/2qk$, Λ is the photon-meson coupling constant.

*We shall use the notation of reference 1 throughout.

The values of r_k^i are:

$$r_1^1 = Q_1 + \frac{2(W-M)^2-1}{2(W-M)}Q_3,$$

$$r_2^1 = -Q_1 + \frac{2(W+M)^2-1}{2(W+M)}Q_3,$$

$$r_3^1 = (W-M)Q_2 - Q_3, \qquad r_4^1 = -(W+M)Q_2 - Q_3,$$

$$r_1^2 = Q_3\alpha, \qquad r_2^2 = Q_3\alpha/2(W+M),$$

$$r_1^3 = r_1^1\alpha + Q_3/2(W-M), \qquad r_2^3 = r_2^1\alpha + Q_3/2(W+M).$$

Here

$$Q_1 \approx -0.55\xi, \qquad Q_2 = -Q_1/t_r, \qquad Q_3 = \xi/2\sqrt{t_r};$$

$$\xi = \gamma t_r^2/(t_r+\gamma)\sqrt{t_r-1}.$$

In deriving the above formulae, we used the following expressions for the amplitudes of photoproduction of π mesons on mesons and of the annihilation of nucleon pairs into two mesons, which have to be inserted into Eqs. (5.6) and (A.5) of reference 1. The form of the π-π resonance was chosen[2] as

$$f_{\pi\pi} = \gamma/(t_r - t - i\gamma q^3),$$

where $q = (t/4-1)^{1/2}$ is the meson momentum in the intermediate state, t_r is the energy of the meson-meson scattering resonance, and γ is a parameter characterizing the widths of the resonance.

The expression for the amplitudes $T_\pm$ of the process of annihilation of a nucleon pair into two mesons* is written as[2,3]

$$T_\pm = f_{\pi\pi}\int_{-\infty}^{a}\frac{\mathrm{Im}f_\pm(t')dt'}{f_{\pi\pi}(t')(t'-t-i\varepsilon)} = f_{\pi\pi}N_\pm(t).$$

In obtaining $N_\pm(t)$ we have utilized the connection between $T_\pm(t)$ and the isovector parts of the nucleon formfactors.[4]

*We use here the following connection between the partial amplitudes $G_{l\pm1,1}$ [see Eq. (A.15) of reference 1] and the coefficients in the expansion of $T_\pm^1$ in helicity states:[3] $G_{l+1,1} = \frac{1}{3}3^{-1/2}(T_+^1 + \sqrt{2}\,T_-^1)$; $G_{l-1,1} = 6^{-1/2}(-T_+^1 + 2^{-1/2}T_-^1)$.

In the determination of the π-meson photoproduction amplitude on π mesons we have made use* of the solution of Gourdin and Martin:[5]

$$F_{\gamma\pi} = \frac{1}{8}\Lambda f_\pi \left[\frac{(t-4)(t-1)}{t}\right]^{1/2} \frac{2t_r - t - 1}{2t_r + t - 3},$$

$$f_\pi = \frac{t_r + \gamma}{t_r - t - i\gamma q^3}$$

(f_π is the meson formfactor).

It should be noted that the expression (1) has been obtained without an expansion in powers of 1/M.

With the presently available experimental data it is not possible to determine uniquely the parameters which enter the formulae (1). However, the limits within which these parameters are determined are not too large: the parameter t_r lies between ~ 15 and ~ 25, and $1.7 \leq q_r^3 \leq 3$.[2] Therefore we have carried through an evaluation[6] in the region close to threshold ($E_\gamma \leq 250$ Mev in the laboratory system) for a few choices of the parameters, remaining within the indicated limits.

From these evaluations it can be seen that the additions to the multipoles do not exceed a few percent of the results obtained by simple dispersion relations.[7] The additions to the coefficients A and B, which characterize the angular distribution of the photoproduction are, a few percent, and those to the coefficient C are on the order 10 — 20%. In both cases it was assumed that $\Lambda/e = 1$. These results are close to analogous results obtained by somewhat other methods.[8]

In conclusion we thank P. N. Komolov and A. T. Matachun for numerical computations.

*We note that our choice of the form of the solution of $F_{\gamma\pi}$, which differs from the solution of Gourdin and Martin,[5] influences in the present calculation only the choice of the constant A.

[1] N. F. Nelipa, JETP **40**, 1085 (1961), Soviet Phys. JETP **13**, 766 (1961).

[2] Bowcock, Cottingham, and Lurie, Nuovo cimento **16**, 918 (1960).

[3] W. R. Frazer and J. R. Fulco, Phys. Rev. **117**, 1609 (1960).

[4] W. R. Frazer and J. R. Fulco, Phys. Rev. Letters **2**, 365 (1959).

[5] M. Gourdin and A. Martin, Nuovo cimento **16**, 78 (1960).

[6] N. F. Nelipa and V. A. Tsarev, Report, Phys. Inst. Acad. Sci., (1960).

[7] Chew, Goldberger, Low, and Nambu, Phys. Rev. **106**, 1345 (1957).

[8] J. Ball, Univ. of Calif. Report W 7405 (1960) (unpublished).

Translated by M. Danos
291

ON THE PROBLEM OF ABOVE-BARRIER REFLECTION OF HIGH-ENERGY PARTICLES

V. L. POKROVSKII and I. M. KHALATNIKOV

Institute for Physics Problems, Academy of Sciences of the U.S.S.R.

Submitted to JETP editor December 16, 1960

J. Exptl. Theoret. Phys. (U.S.S.R.) 40, 1713-1719 (June, 1961)

A regular method is given for calculating in the quasi-classical approximation the amplitude for above-barrier reflection of a particle from a one-dimensional potential barrier, by the use of the properties of the potential in the complex plane.

In a previous paper[1] an expression has been found for the amplitude for reflection of a particle from a one-dimensional potential barrier in the quasi-classical approximation, and it was shown that in cases in which the potential U is an analytic function which has no singularities on the real axis the reflection amplitude is exponentially small and can be put in the form of an iteration series in which all the terms are of the same order. This problem has been treated earlier in a number of papers.[2-4] In these papers, however, the authors confined themselves to only the first terms of the iteration series and consequently obtained an incorrect coefficient for the exponential. For this same reason the results found in references 3 and 4 for the three-dimensional problem of the scattering of high-energy particles by centers of force in the region of classically inaccessible angles are also incorrect.

The method of reference 1 is, however, extremely cumbersome. Although it provides an elucidation of the structure of the series, it requires a knowledge of the answer for some particular case. The purpose of the present note is to present a much simpler and more regular method for getting the amplitude for above-barrier reflection (without requiring previous knowledge of the answer for any particular case).

The present method, like the so-called Zwaan method,[5,6] is based on an investigation of the behavior of the wave function in the complex plane. Let $U(x)$ be an analytic function of x which has no singularities on the real axis, and such that the particle energy $E > U(x)$ for all real x. We shall assume that the particle is quasi-classical:

$$kd \gg 1, \qquad k = \sqrt{2mE}, \tag{1}$$

where d is a characteristic dimension of the potential $U(x)$.

The Schrödinger equation

$$d^2\psi/dx^2 + p^2\psi = 0, \qquad p^2 = 2m(E - U) \tag{2}$$

has a solution ψ_0 that behaves asymptotically like e^{ip_+x} for $x \to +\infty$. Then for $x \to -\infty$ the function ψ_0 behaves like $ae^{ip_-x} + be^{-ip_-x}$, where $p_\pm^2 = \lim p^2(x)$ for $x \to \pm\infty$, and a and b are constants. The reflection amplitude A is the ratio b/a.

It is well known that in the quasi-classical approximation considered here the equation (2) has approximate solutions of the form[7]

$$\psi_\pm = \frac{1}{\sqrt{p}} \exp\left(\pm i \int_{\bar{x}}^{x} p\,dx\right), \tag{3}$$

where x is an arbitrary lower limit. The solutions $\psi_\pm$ can be interpreted as waves traveling in opposite directions. The general solution can be represented in the form

$$\psi = a\psi_+ + b\psi_-, \tag{4}$$

where a and b are constants. This way of writing the function has meaning, however, only in cases in which the two terms in the right member of Eq. (4) are of the same order of magnitude, since the solutions themselves are inexact and the separation into waves traveling in different directions is defined only to the fractional accuracy $\sim 1/kd$.

The coefficients a and b take on exact meanings only for $x \to \pm\infty$, where $p(x) \to p_\pm = \text{const}$. In the case considered we have for $x \to +\infty$

$$a = \exp\left[i \int_{\bar{x}}^{\infty} (p - p_+)\,dx - ip_+\bar{x}\right], \qquad b = 0.$$

According to what has been said, as we go along the real axis the coefficient a remains unchanged to accuracy $1/kd$, and b is everywhere not larger than order of magnitude $1/kd$. For real x ($|x| \lesssim d$), however, the exact value of b is not defined. Therefore we cannot determine the value of b for $x \to -\infty$ by moving along the real axis.

The idea of the method is to leave the real axis and move in the complex plane along a line L on which the two waves are of the same order of magnitude. First of all it is clear that the condition

$$\operatorname{Im} \int^{x} p dx = \text{const} \tag{5}$$

must hold on the line L, since otherwise one of the exponentials will increase and the other will decrease. Furthermore, this line must pass through zeroes or singularities of the function p^2. In fact, otherwise the solutions ψ_+ will be correct to accuracy 1/kd along the entire line L and all of the difficulties still remain.

Thus we can try to find the coefficient b in the following way. We continue the solution that behaves like e^{ip_+x} for $\operatorname{Re} x \to +\infty$ away from the real axis into the upper half-plane of x until we get to the first line L that satisfies the stated condition. This can always be done, because the potential vanishes for $|x| \to \infty$. We then move along L to a zero or singularity x_0 of the function p^2. Near x_0 the solution ψ_+ with which we came to the point will be irregular, and we must "join it on" to the solution of the approximate equation obtained from Eq. (2) by expanding p^2 in powers of $x - x_0$. We then make the passage around the point x_0 that is necessary to get to the branch of L that goes toward $\operatorname{Re} x \to -\infty$. By moving along this branch and then going down to the real axis we get the coefficient b.

Let us begin with the case $U/E \lesssim 1$. In this case the simplest and most likely situation is that x_0 is a simple root of the function p^2. In analogy with the case of below-barrier reflection we shall speak of a complex "turning point," since x_0 satisfies the equation

$$U(x_0) = E. \tag{6}$$

Near x_0 we can write approximately

$$p = C\sqrt{x - x_0}; \qquad \int_{x_0}^{x} p dx = \tfrac{2}{3} C (x - x_0)^{3/2}. \tag{7}$$

It is obvious that the lines $\operatorname{Im} \int_{x_0}^{x} p\,dx$ go out from the point x_0 at angles of $2\pi/3$ with each other. Two of them are the branches of the curve L, as is shown in Fig. 1, which represents schematically the level lines of $\operatorname{Im} \int_{x_0}^{x} p\,dx$. Near x_0 Eq. (2) is of the form

$$\psi'' + C^2 (x - x_0)\psi = 0. \tag{8}$$

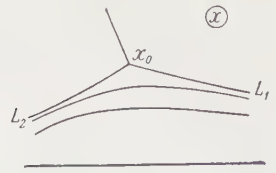

FIG. 1

The solution of this equation that goes over into the wave traveling "to the right" on the "right" branch L_1 takes the form

$$\psi = C\sqrt{x - x_0} H_{1/3}^{(1)}\left(\tfrac{2}{3} C (x - x_0)^{3/2}\right). \tag{9}$$

Using the well known asymptotic formulas for the Hankel functions, one can show that for $C(x - x_0)^{3/2} \gg 1$ the function (9) has the form

$$C\sqrt{x - x_0} H_{1/3}^{(1)}\left(\tfrac{2}{3} C (x - x_0)^{3/2}\right) \to \frac{1}{\sqrt{p}} \exp\left(i \int_{x_0}^{x} p dx - i \frac{5\pi}{12}\right). \tag{10}$$

This solution differs from ψ_0 by a constant factor. Since we are concerned only with the ratio $A = b/a$, the value of this factor is of no importance for what follows.

Let us now go over to the branch L_2; to do so we make a rotation by the angle $-2\pi/3$ and express the function $H_{1/3}^{(1)}$ on the branch L_2 in terms of its value and that of $H_{1/3}^{(2)}$ on L_1. To do so we use the relation (cf., e.g., reference 8)

$$H_{1/3}^{(1)}(e^{-i\pi} z) = H_{1/3}^{(1)}(z) + e^{-i\pi/3} H_{1/3}^{(2)}(z). \tag{11}$$

Using the asymptotic formulas for $H_{1/3}^{(1)}(z)$ and $H_{1/3}^{(2)}(z)$ for large positive z, we get on L_2

$$\begin{aligned}\psi &= C\sqrt{x - x_0} H_{1/3}^{(1)}\left(\tfrac{2}{3} C (x - x_0)^{3/2}\right) \\ &\to \frac{1}{\sqrt{p}}\left[\exp\left(-i \int_{x_0}^{x} p dx - i \frac{5\pi}{12}\right)\right. \\ &\left. + e^{-i\pi/3} \exp\left(i \int_{x_0}^{x} p dx + i \frac{5\pi}{12}\right)\right].\end{aligned} \tag{12}$$

We see that on L_2 the two waves in fact are of the same order of magnitude and therefore can be distinguished. Their coefficients remain the same also for $\operatorname{Re} x \to -\infty$.

We still have to go over from functions of the type $\exp\left(\pm i \int_{x_0}^{x} p\,dx\right)$ to functions that behave like $\exp(\pm i p_- x)$ for $x \to -\infty$. To do this we use the obvious relations

$$\int_{x_0}^{x} p dx = p_- x - \varphi_0, \qquad \varphi_0 = \int_{-\infty}^{x_0} (p - p_-)\, dx + p_- x_0, \tag{13}$$

and thus get from Eq. (12)

$$\psi \to \frac{1}{\sqrt{p}}\left[e^{ip_- x} e^{-i(\varphi_0 + 5\pi/12)} + e^{-i\pi/3} e^{-ip_- x} e^{i(\varphi_0 + 5\pi/12)}\right]. \tag{14}$$

We emphasize that the coefficient of $\exp\left(i\int_{x_0}^{x} p\,dx\right)$ is not changed, since in the passage below the point x_0

$$\exp\left(i\int_{x_0}^{x} p dx\right) \gg \exp\left(-i\int_{x_0}^{x} p dx\right).$$

From Eq. (14) we find

$$A = b/a = -ie^{2i\varphi_0}. \tag{15}$$

It is not hard to extend this result to the case in which p^2 has at x_0 a singularity or zero of the form $p^2 = C^2(x-x_0)^{2\beta-2}$ (with $\beta > 0$). In this case the solution of the equation

$$\psi'' + C^2 (x - x_0)^{2\beta-2}\psi = 0,$$

that goes over into a wave running to the right on L_1 has the form[8]

$$\psi = H^{(1)}_{1/2\beta}\left(\frac{C}{\beta}(x - x_0)^{\beta}\right) \to \frac{1}{\sqrt{p}} \exp\left\{i\int_{x_0}^{x} p dx - \frac{i\pi}{4}\left(\frac{1}{\beta} + 1\right)\right\}.$$

The level lines of $\operatorname{Im}\int_{x_0}^{x} p\,dx = 0$ go out from x_0 at angles π/β with each other. Therefore in this case the passage from L_1 to L_2 is equivalent to a change of the argument of $(x-x_0)^{\beta}$ by $-\pi$. Using the general formula for rotation by $-\pi$

$$H^{(1)}_{\nu}(e^{-i\pi}z) = \frac{\sin 2\nu\pi}{\sin \nu\pi} H^{(1)}_{\nu}(z) + e^{-\nu\pi i} H^{(2)}_{\nu}(z)$$

and the asymptotic formulas for $H^{(1),(2)}(z)$, we get

$$A = -i\left(\sin\frac{\pi}{\beta} \Big/ \sin\frac{\pi}{2\beta}\right) e^{2i\varphi_0},$$

where φ_0 is defined by Eq. (13). For $\beta = 3/2$ we get the result already known.

If on the single line L there are not one but several singularities (on zeroes) $x_1, x_2, \ldots$ of the function p^2, their contributions to A are additive if the condition

$$\left|\int_{x_i}^{x_{i+1}} p dx\right| \gg 1 \tag{16}$$

is satified. If, on the other hand, the condition (16) is not satisfied, it is necessary to treat the equation with close-space singularities.

If we abstract from accidental coincidences, the situation with two close-spaced zeroes arises in the case of small values of the ratio $(E-U)/E$. In this case the energy of the particle is not much above the barrier, and near the point on the real axis of x at which U takes its maximum value there are two closely spaced complex conjugate roots of p^2. Here, however, there is no need to go off into the complex plane, since the line L coincides with the real axis. Physically this is associated with the fact that in this case the reflection coefficient is not small. This situation has been treated in detail earlier (cf. e.g., reference 6).

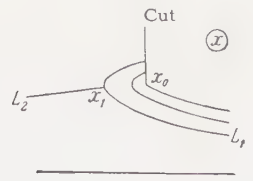

FIG. 2

A zero and a pole are close together for small values of the ratio U/E. In fact, the potential U takes large values equal to E only in the complex plane near a singularity. Let us consider the case of a simple pole x_0, near which $U(x)$ has the form

$$U(x) = U_0 x_0/(x - x_0). \tag{17}$$

Then the root x_1 of the function $p^2 = 2m(E-U)$ is determined from the equation

$$x_1 = x_0(1 + U_0/E). \tag{18}$$

The condition for the zero and pole to be close together is

$$\left|\int_{x_1}^{x} p dx\right| \sim \left|\frac{U_0}{E} k x_0\right| \lesssim 1. \tag{19}$$

Near x_0 and x_1 we have

$$p^2 = k^2 (x - x_1)/(x - x_0), \tag{20}$$

$$\int_{x_0}^{x} p dx = k\left[\sqrt{(x-x_0)(x-x_1)} - \frac{U_0 x_0}{2E} \ln\left(\frac{x - x_0 - (U_0 x_0/2E) + \sqrt{(x-x_0)(x-x_1)}}{-U_0 x_0/2E}\right)\right]. \tag{21}$$

The position of the level lines of $\operatorname{Im}\int_{x_1}^{x} p\,dx$ near x_0 and x_1 is shown schematically in Fig. 2. A cut is taken through the point x_0, which is a singular point of the Eq. (2). As L one can take, for example, the line $\operatorname{Im}\int_{x_1}^{x} p\,dx = 0$.* Its two branches L_1, L_2 are shown in Fig. 2. Obviously for $|x - x_0| \gg |x_1 - x_0|$ the passage from L_1 to L_2 corresponds to a rotation through the angle $-\pi$.†

*At first glance it seems natural to take for L the line $\operatorname{Im}\int_{x_0}^{x} p\,dx = 0$. Unfortunately, however, this line has only one branch and does not go to infinity in one of the directions (cf. Fig. 2).

†We emphasize that in the case of the pole the results of going around above and below are not the same, since in going around above we cross the cut. In the case in which the point x_0 was a simple zero of p^2 the results of going around above and below coincided, since a simple zero of p^2 is not a singular point of the equation (2).

The solutions of the approximate equation*

$$\psi'' + k^2[(x - x_1)/(x - x_0)]\psi = 0 \qquad (22)$$

are of the form

$$\psi = W_{\pm\lambda,1/2}(\pm z), \qquad \lambda = -\tfrac{1}{2} ikx_0U_0/E, \qquad z = -2ik(x - x_0), \qquad (23)$$

where $W_{\lambda,\mu}$ are the Whittaker functions (cf. reference 8). The asymptotic formulas for the Whittaker functions for large $|z|$ are of the form

$$W_{\mu,\lambda} \sim e^{-z/2}z^{\lambda} \qquad (|\arg z| < \pi). \qquad (24)$$

We see that for large values of $k(x - x_0)$ on the branch L_1

$$W_{\lambda,1/2}(z) \to E^{1/4}\exp\left(\lambda \ln\frac{\lambda}{e} + i\int_{x_1}^{x} pdx\right) \qquad \left(\arg z = -\frac{\pi}{2}\right). \qquad (25)$$

On L_2 the second solution $W_{-\lambda,\frac{1}{2}}$ has the asymptotic formula

$$W_{-\lambda,1/2}(-z) \to E^{1/4}\exp\left(-\lambda \ln\frac{-\lambda}{e} - i\int_{x_1}^{x} pdx\right), \qquad (26)$$

and we shall set $-\lambda = e^{-i\pi\lambda}$, $-z = e^{-i\pi}z$.

Equation (22) is noninvariant under change of sign of $(x - x_0)$, and therefore there is no linear connection between $W_{\lambda,\mu}(-z)$ and $W_{\pm\lambda,\mu}(\pm z)$. Equation (22) is, however, invariant under rotation through 2π around the point x_0. Therefore there does exist a linear connection between $W_{\lambda,\mu}(e^{-2\pi i}z)$ and $W_{\pm\lambda,\mu}(\pm z)$ (cf. reference 10):

$$W_{\lambda,\mu}(e^{-2\pi i}z) = e^{-2\pi i\lambda}W_{\lambda,\mu}(z) - \frac{2\pi i e^{-i\pi\lambda}}{\Gamma(1/2 + \mu - \lambda)\,\Gamma(1/2 - \mu - \lambda)}W_{-\lambda,\mu}(-z). \qquad (27)$$

On L_2 the argument of z is $-3\pi i/2$. Therefore in the right member of Eq. (27) we have $\arg(\pm z) = \pm i\pi/2$. Using the asymptotic formulas (24) and going over, as in the case of the simple zero, to solutions that behave like $\exp(\pm ip_-x)$ for $x \to -\infty$, we get

$$A = F(\lambda)\exp\left\{2i\left[\int_{-\infty}^{x_1}(p - p_-)\,dx + p_-x_1\right]\right\}, \qquad (28)$$

$$F(\lambda) = 2\pi i e^{-2\lambda\ln(-\lambda/e)}/\Gamma(-\lambda)\,\Gamma(1 - \lambda). \qquad (29)$$

If $|\lambda| \sim U/\hbar v \gg 1$, then $F(\lambda) \approx -i$, and Eq. (28) goes over into Eq. (15). In the opposite case with $U/\hbar v \ll 1$ we have $F(\lambda) \approx -2\pi i\lambda$, and Eq. (28) gives the Born approximation:

$$A = -2\pi i\lambda e^{2ip-x_0}. \qquad (30)$$

Taking the square of the absolute value of the scattering amplitude (28), we get the reflection coefficient

$$R = |A|^2 = |F(\lambda)|^2\exp\left\{4i\,\mathrm{Im}\int_{-\infty}^{x_1} pdx\right\}. \qquad (31)$$

In the one-dimensional case the formulas of Gol'dman and Migdal[3] and of Saxon and Schiff[4] give the same result

$$A = -2\pi i\lambda\exp\left\{2i\left[\int_{-\infty}^{x_1}(p - p_-)\,dx + p_-x_1\right]\right\}.$$

This differs from Eq. (28) by the replacement of the function $F(\lambda)$ by the quantity $-2\pi i\lambda$. As we have shown, this is correct only in the Born case $U/\hbar v \ll 1$. In the case $U/\hbar v \sim 1$ the results of references 3 and 4 are correct only in order of magnitude.

In conclusion the writers express their deep gratitude to L. D. Landau for helpful discussions.

*An analogous equation has been considered by Denisov[9] in connection with a different problem; in Denisov's case, however, unlike the present problem, the zero and pole were on the real axis, which decidedly alters the situation.

[1] Pokrovskii, Savvinykh, and Ulinich, JETP **34**, 1272, 1629 (1958), Soviet Phys. JETP **7**, 879, 1119 (1958).

[2] L. I. Schiff, Phys. Rev. **103**, 443 (1956).

[3] I. I. Gol'dman and A. B. Migdal, JETP **28**, 394 (1954), Soviet Phys. JETP **1**, 304 (1955).

[4] D. S. Saxon and L. I. Schiff, Nuovo cimento **6**, 614 (1957).

[5] E. C. G. Stueckelberg, Helv. Phys. Acta **5**, 369 (1932).

[6] E. C. Kemble, Phys. Rev. **48**, 549 (1935).

[7] L. D. Landau and E. M. Lifshitz, Квантовая механика (Quantum Mechanics), Vol. 1, Gostekhizdat 1948, pp. 192-193. [Transl., Pergamon, 1958].

[8] I. M. Ryzhik and I. S. Gradshteĭn, Таблицы интегралов (Tables of Integrals), Gostekhizdat, 1951.

[9] N. G. Denisov, Радиотехника и электроника (Radio Engineering and Electron Physics) **4**, 388 (1959).

[10] Higher Transcendental Functions, Bateman Manuscript Project, McGraw-Hill, 1953. H. Buchholz, Die confluente hypergeometrische Function, Springer-Verlag, 1953.

Translated by W. H. Furry
292

CONCERNING THE THEORY OF SPIN-LATTICE RELAXATION IN RADICALS IN LIQUIDS

I. V. ALEKSANDROV and G. M. ZHIDOMIROV

Institute of Chemical Physics, Academy of Sciences, U.S.S.R.

Submitted to JETP editor December 19, 1960

J. Exptl. Theoret. Phys. (U.S.S.R.) 40, 1720-1724 (June, 1961)

Spin-lattice relaxation times due to the interaction between the spin and the vibrations of individual atoms of a radical are calculated for radicals in a liquid. It is demonstrated that the direct, as well as the combinational ("two-phonon") relaxation transitions yield, as a rule, larger relaxation times than the Brownian rotational motion of the radical.

McCONNELL[1] has considered the mechanism of spin-lattice relaxation associated with the Brownian rotational motion of a radical as a whole in a liquid. In this case the relaxation transitions are due to the anisotropy of the spin-orbit and the hyperfine interactions and to the rotation of the radical. Al'tshuler and Valiev[2] have proposed a different mechanism for the spin-lattice relaxation associated with the interaction of the spin with the orbital motion of the electron and with the normal vibrations of the complex ion in solution; however, as will be shown here, the method of calculation proposed by Al'tshuler and Valiev[2] is incorrect. In this paper we shall examine in greater detail this mechanism for spin-lattice relaxation as applied to radicals in liquids.

We shall discuss relaxation processes associated with the intramolecular vibrations due to the Fermi interaction of the electron spin **S** with the nuclear spin **I** (the contribution of the spin-orbit $(\mathbf{S}\cdot\mathbf{L})$ and of the dipole-dipole $(\mathbf{S}\cdot\mathbf{I})$ interactions usually turns out to be smaller in the case of radicals; we also note that, if necessary, these interactions can be easily taken into account within the framework of the calculation proposed below). The spin-Hamiltonian of the unpaired electron interacting with one of the nuclei of the radical has the form

$$\mathcal{H} = g\beta\,\mathbf{SH} + A\,\mathbf{SI}, \tag{1}$$

where the constant describing the Fermi interaction is $A = A(Q)$, Q is the diplacements of the nucleus of spin I from its equilibrium position R, and the remaining notation is the usual one. Following Al'tshuler and Valiev,[2] we shall assume that the vibrations take place classically, i.e., $Q = Q(t)$. By expanding the quantity A in a power series in terms of the small displacements from the equilibrium position, and by restricting ourselves to the linear and the quadratic terms, we obtain

$$\mathcal{H} = \mathcal{H}_0 + V_1(t) + V_2(t), \qquad \mathcal{H}_0 = g\beta\,\mathbf{SH} + A_0\,\mathbf{SI}, \tag{2}$$

where

$$V_1(t) = A_1\frac{Q(t)}{R}\mathbf{SI}, \qquad V_2(t) = A_2\frac{Q^2(t)}{2R^2}\mathbf{SI},$$
$$A = A_0 + A_1 Q(t)/R + A_2 Q^2(t)/R^2. \tag{3}$$

In formulas (2) and (3), $Q(t)$ is a random function describing the vibration of the nucleus under consideration, modulated by the random interactions with the surrounding medium.

We first evaluate the probability of relaxation transition per unit time due to the term $V_1(t)$. By regarding the quantity V_1 as a perturbation we obtain for the transition probability between the magnetic levels k and k'[3]

$$w_{kk'} = \frac{A_1^2}{\hbar^2}\,\frac{\overline{Q^2(t)}}{R^2}\,|(k|\,\mathbf{SI}\,|k')|^2\int_{-\infty}^{\infty}\varphi(\tau)\,e^{i\omega_{kk'}\tau}\,d\tau, \tag{4}$$

where $\hbar\omega_{kk'}$ is the spacing between the levels k and k', and $\varphi(\tau) = \overline{Q(t)Q(t+\tau)}/\overline{Q^2}$ is the correlation function for the random variable Q.

In the case when the interaction of the vibrations with the medium is large (much larger than the energy of the natural vibrations of the nucleus) it is reasonable to assume for the correlation function

$$\varphi(\tau) = \exp\{-|\tau|/\tau_c\}, \tag{5}$$

where τ_c is some characteristic correlation time. Then we immediately obtain from (4)

$$w_{kk'} = \frac{A_1^2}{\hbar^2}\,\frac{\overline{Q^2}}{R^2}\,|(k|\,\mathbf{SI}\,|k')|^2\,\frac{2\tau_c}{1+\omega_{kk'}^2\tau_c^2}, \tag{6}$$

i.e., an expression analogous to formula (9) of the paper of Al'tshuler and Valiev.[2] However, in the case under consideration of strong interaction it is not possible to relate the quantity τ_c to the op-

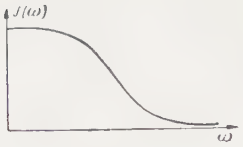

FIG. 1.

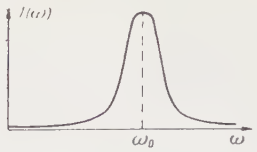

FIG. 2.

tical characteristics of an individual intramolecular vibration (as is done in reference 2). Indeed, the correlation function (5) yields for the spectral density of the nuclear vibrations $J(\omega)$ the curve shown in Fig. 1, and this corresponds to a continuous optical spectrum and to the absence of any spectral lines due to the natural vibrations of the nucleus.

However, if the interaction of the natural vibrations with the medium is small and may be treated as a perturbation of the characteristic vibrations, then a different expression is obtained for the correlation function. Representing the quantity $Q(t)$ in the form

$$Q(t) = q(t)\cos(\omega_0 t + \eta(t)), \tag{7}$$

where ω_0 is the natural frequency of the vibrations, while q and η are respectively the random amplitude and phase of the oscillator, and assuming that $q(t)$ and $\eta(t)$ are not correlated with one another, we obtain the correlation function for the quantity $Q(t)$ in the form

$$\varphi(\tau) = \exp\{-|\tau|/\tau_c\}\cos\omega_0\tau. \tag{8}$$

In this case we obtain from (4)

$$w_{kk'} = \frac{A_1^2}{\hbar^2}\frac{\overline{q^2}}{R^2}|(k|\mathrm{SI}|k')|^2\frac{2\tau_c}{1+(\omega_0-\omega_{kk'})^2\tau_c^2}. \tag{9}$$

For $\omega_0\tau_c \gg 1$ the spectral density $J(\omega)$ has the form shown in Fig. 2; the maximum at $\omega = \omega_0$ corresponds in the optical spectrum to a line due to the natural vibration of the nucleus, the breadth of this maximum being of the order of $1/\tau_c$.

We note that formulas (6) and (9) lead to essentially different results, for in all the cases of interest to us we have $\omega_0 \gg \omega_{kk'}$.

As an example we evaluate the probability of the relaxation transition for an unpaired electron in the C atom of the CH fragment caused by the vibrations of the C-H bond (modulated by the motion of the medium). The constant A for the CH fragment has been evaluated by McConnell:[4]

$$A = \frac{8\pi}{3}g\beta g_H\beta_H\frac{I(C\pi)-I(\pi H)}{2I(CH)}|\Psi(0)|^2, \tag{10}$$

where g_H is the g-factor for the proton, β_H is the nuclear magneton, $\Psi(0)$ is the value of the 1s-wave function for the H atom at the origin; $I(C\pi)$ is the exchange integral between the 2p-orbit for the unpaired electron of the C atom and the hybridized orbit of the C atom responsible for the C-H bond; $I(\pi H)$ is the exchange integral between the 2p-orbit of the C atom and the 1s-orbit of the H atom; $I(CH)$ is the exchange integral between the hydridized orbit of the C atom and the 1s-orbit of the H atom. Keeping in mind that $I(\pi H) \ll I(C\pi)$, we note that the dependence of A on Q is essentially determined by the dependence on Q of the exchange integral $I(CH)$. The latter can be approximated by the formula[5]

$$I(CH) = I_0\exp\{-Q/R\}. \tag{11}$$

Thus, in formula (3) $A_1 = A_0$, and for the transition probability we have

$$w_{kk'} = \frac{A_0^2}{\hbar^2}\frac{\overline{q^2}}{R^2}|(k|\mathrm{SI}|k')|^2\frac{2\tau_c}{1+(\omega_0-\omega_{kk'})^2\tau_c^2}. \tag{12}$$

The quantity A_0 can be estimated from the hyperfine structure of the electron paramagnetic resonance (e.p.r.) spectra of the aromatic radicals, while $\overline{q^2}$ and τ_c can be estimated as in the paper by Al'tshuler and Valiev;[2] finally, on assuming for the natural frequency of the vibrations of the C-H bond a magnitude of the order of $10^{14}-10^{15}$ sec^{-1}, we obtain

$$w_{kk'} \sim 1-10^{-3}\ \mathrm{sec}^{-1}$$

and this corresponds to a spin-lattice relaxation time of the order of 10^3-1 sec. Taking the relaxation mechanism associated with deformational vibrations into account does not lead to any essential increase in the quantity $\omega_{kk'}$ which would be sufficient to explain the experimental data.

The direct process considered above, that of transfer of energy from the spin system to thermal motion, is a process involving the transfer to the oscillator of a quantum of energy $\hbar\omega_{kk'}$, which is considerably smaller than the mean self energy of the oscillator. As can be seen from formula (9), the probability of this process is proportional to the spectral density of the coordinate of the oscillator far from the maximum ($w_{kk'} \sim J(\omega_{kk'})$, $\omega_{kk'} \ll \omega_0$; cf. Fig. 2), and this is responsible for the low probability of relaxation transitions. From this point of view one might expect that those second order processes will turn out to be more ef-

fective which are associated with changes (actual or virtual) in the vibrational energy of the oscillator by a quantity of the order of $\hbar\omega_0$, which evidently occur with a probability proportional to the value of $J(\omega)$ at the maximum.

If, as before, we treat the nuclear vibrations classically, then the effect just mentioned can be evaluated by taking into account the term $V_2(t)$ in the spin Hamiltonian (2). Let the two-dimensional distribution function for the random variable q be given by the normal distribution function

$$F(q_1, q_2, \tau) = \frac{1}{2\pi\sigma^2(1-\rho^2)^{1/2}} \exp\left\{-\frac{q_1^2+q_2^2-2\rho q_1 q_2}{2\sigma^2(1-\rho)^2}\right\}, \quad (13)$$

where $\sigma^2 = \overline{q^2}$ is the mean square amplitude of the oscillator, while $\rho = \rho(\tau)$ is the correlation function for the random changes of the amplitude. For the random phase η we can choose a distribution function of the form

$$P(\eta_1, \eta_2, \tau) = (2\pi)^{-1}\delta(\eta_1 - \eta_2)\exp\{-|\tau|/\tau_c\} + (2\pi)^{-2}(1 - \exp\{-|\tau|/\tau_c'\}), \quad (14)$$

where τ_c' is a time of the order of magnitude of the time between collisions. The distribution function (14) describes a process in which the phase of the oscillator does not change in the intervals between collisions, while the phase after a collision is not correlated with the value of the phase before the collision. We note that the function $P(\eta_1, \eta_2, \tau)$ could also have been chosen of a different form; for what follows it is essential only that all the values of the phase should be equally probable, and that the correlation of $\eta(t)$ and $\eta(t+\tau)$ should decrease with increasing time τ.

Further, we represent $V_2(t)$ in the form

$$V_2(t) = V_2'(t) + \overline{V_2(t)} = V_2'(t) + B\,\mathbf{SI} \quad (15)$$

and include the constant quantity $B = A_2\overline{Q^2(t)}/2R^2$ in A_0. Then for the evaluation of the probability of a transition under the influence of $V_2(t)$ we can apply a formula analogous to (4), where $\varphi(\tau)$ now denotes

$$\varphi(\tau) = \overline{Q^2(t)\,Q^2(t+\tau)}/\overline{Q^4(t)} \quad (16)$$

[formula (4) is inapplicable to $V_2(t)$, since the quantity $\overline{V_2(t)\,V_2(t+\tau)}$ does not tend to zero as $\tau \to \infty$].

By using (13) and (14) we easily obtain

$$\varphi(\tau) = \tfrac{1}{2}\rho^2\sigma^4 + \tfrac{1}{8}\sigma^4\exp\{-|\tau|/\tau_c'\}\cos 2\omega_0\tau\,(1+2\rho^2). \quad (17)$$

Finally, by choosing $\rho(\tau)$ in the form $\rho(\tau) = \exp(-|\tau|/\tau_c)$, we obtain for the transition probability

$$w_{kk'} = \frac{A_2^2}{8\hbar^2R^4}|(k|\,\mathbf{SI}\,|k')|^2(\bar{q}^2)^2\frac{4\tau_c}{1+4\omega_{kk'}^2\tau_c^2}. \quad (18)$$

In expression (18) we have omitted the terms corresponding to the last term in (17), which leads in the expression for the spectral density of the quantity $Q^2(t)$ to a maximum at the frequency $\omega = 2\omega_0$.

Estimating the quantity $w_{kk'}$ by means of formula (18) in exactly the same manner in which we made an estimate of formula (12) we find that for $\omega_0 \sim 10^{14} - 10^{15}$ sec^{-1} we have $w_{kk'} \sim 10^3 - 1$ sec^{-1}. Thus, the combined transition indeed turns out to be more effective than the direct transition discussed by Al'tshuler and Valiev.[2]

Formulas (9) and (18) show that the mechanism of spin-lattice relaxation in radicals in liquids associated with the vibrational motion turns out to be, as a rule, less important ($T_1 \gtrsim 10^{-3}$ sec) then the mechanism proposed by McConnell[1] ($T_1 \sim 10^{-5}$ sec). The predominance of the "vibrational" mechanism can apparently be expected in cases when: 1) the anisotropy Δg of the g-factor and the anisotropy ΔA of the hyperfine interaction are both very small ($A\overline{q^2}/R^2 > \Delta A$ and $A\overline{q^2}/R^2 > \Delta g\beta H_0$; H_0 is the constant external magnetic field), or 2) the hyperfine splitting is large, and the constant A is determined by exchange integrals which depend on the coordinates corresponding to low frequency vibrations.

The authors wish to thank Professor N. D. Sokolov for discussions.

[1] H. M. McConnell, J. Chem. Phys. **25**, 709 (1956).

[2] S. A. Al'tshuler and K. A. Valiev, JETP **35**, 946 (1958), Soviet Phys. JETP **8**, 661 (1959).

[3] Bloembergen, Purcell, and Pound, Phys. Rev. **73**, 679 (1948).

[4] H. M. McConnell, J. Chem. Phys. **24**, 764 (1956).

[5] S. A. Al'tshuler, Thesis, Physics Institute, Academy of Sciences, U.S.S.R., 1954.

Translated by G. Volkoff
293

BRANCHING OF ELECTRON AND PHOTON GREEN'S FUNCTIONS

V. G. VAKS

Submitted to JETP editor November 22, 1960

J. Exptl. Theoret. Phys. (U.S.S.R.) **40**, 1725-1727 (June, 1961)

The branchings of the electron Green's function G(p) and the photon Green's function D(k) at the respective points $p^2 = m^2$ and $k^2 = 0$ are discussed. In electrodynamics the branching of G(p) indicates a nonstationary behavior of the amplitude of the one-electron state, and with the usual gauge for the potentials this amplitude increases with the time; this is connected with the indefinite metric. A branching of D(k) at $k^2 = 0$ arises as a consequence of the weak three-photon and photon-neutrino interactions, but the singularity of the function at this point is a weak one, so that the one-photon state remains stationary.

In the nonrelativistic case the Fourier component of the Green's function

$$G(\mathbf{p}, \tau) = \frac{1}{2\pi}\int G(\mathbf{p})\, e^{-ip_0\tau}\, dp_0$$

is equal to the probability amplitude for finding the initial state $\Phi_{0\mathbf{p}} = a^+_{\mathbf{p}}|\,\mathrm{vac}\,\rangle$ in the state

$$\Phi_{\mathbf{p}}(\tau) = \exp(-iH\tau)\,\Phi_{0\mathbf{p}},$$

obtained from $\Phi_{0\mathbf{p}}$ after the time τ.[1] We shall derive analogous relations in the relativistic case. If the Schrödinger operator ψ of the spinor field has the form

$$\psi(\mathbf{x}) = \sum_{\mathbf{p}\lambda}(u_{\mathbf{p}\lambda}e^{i\mathbf{px}}a_{\mathbf{p}\lambda} + v^*_{-\mathbf{p}\lambda}e^{-i\mathbf{px}}b^+_{\mathbf{p}\lambda}),$$

then

$$G_1(\mathbf{p}, \tau) = \langle a_{\mathbf{p}\lambda}e^{-iH\tau}a^+_{\mathbf{p}\lambda}\rangle = \frac{1}{4\varepsilon_p}\,\mathrm{Sp}\; G(-\mathbf{p}, \tau)(\hat{p}+m),$$

$$G_2(\mathbf{p}, \tau) = \langle b^+_{\mathbf{p}\lambda}e^{-iH\tau}b_{\mathbf{p}\lambda}\rangle = \frac{1}{4\varepsilon_p}\,\mathrm{Sp}\; G(\mathbf{p}, \tau)(\hat{p}-m). \quad (1)$$

Here $\tau > 0$, the averaging is over the physical vacuum, and $p_0 = \epsilon_{\mathbf{p}} = (\mathbf{p}^2 + m^2)^{1/2}$; the notations are those of Feynman. In electrodynamics the function G(p) has a well known branching at the point $p^2 = m^2$,[2,3]

$$G(p) \underset{p^2\to m^2}{=} i\,\frac{\hat{p}+m}{(p^2+m^2)^{1+\beta}}, \qquad \beta = \frac{\alpha}{2\pi}(3 - d_{l0}). \quad (2)$$

For $d_{l0} < 3$ (for example, for the commonly used $d_{l0} = 1$ or $d_{l0} = 0$) we have $\beta > 0$, and according to Eqs. (1) and (2) this means an increase of the amplitude of the one-electron state with time:

$$G_1(\mathbf{p}, \tau) = \mathrm{const}\cdot\exp(-i\varepsilon_p\tau + \beta\ln\varepsilon_p\tau). \quad (3)$$

The increase of the amplitude, Eq. (3), is connected with the indefinite metric in electrodynamics. In addition to the "no-quantum" state $\Phi_{0\mathbf{p}\lambda} = a^+_{\mathbf{p}\lambda}|\,\mathrm{vac}\,\rangle$ the state vector contains states of negative norm with longitudinal and scalar quanta, which are physically indistinguishable from $\Phi_{0\mathbf{p}\lambda}$ by gauge invariance. The complete norm of the state $\exp(-iH\tau)\times\Phi_{0\mathbf{p}\lambda}$ is conserved, according to general theorems.[4]

In the usual case of states with positive norms the replacement of the pole of the Green's function by a branch point describes a damping of the one-particle state. Such a branching is due to the presence of a spectrum of two-particle excitations joining on continuously to the one-particle ones. Since through the weak interaction a photon can go over into two photons and two neutrinos, a replacement of the pole by a branch point must occur in its Green's function $D_{rn}(k)$. If the quantity $k^2D_{rn}(k)$ went to zero for $k^2 \to 0$, the photon would be in principle unstable, dissociating in time into a pair of massless particles with the same direction of motion. Let us find the form of the branching of D(k).

In lowest order in k, when we take into account CP invariance and symmetry in the particles, the three-photon vertex part must have the form

$$e_{1i}e_{2k}e_{3l}\Gamma_{ikl} = a\varepsilon_{iklm}\,[e_{1i}e_{2k}e_{3l}(k_{1m}(k_3^2 - k_2^2) + k_{2m}(k_1^2 - k_3^2) + k_{3m}(k_2^2 - k_1^2)) - 2(e_{1i}e_{2k}k_{1l}k_{2m}(e_3k_3) + e_{2i}e_{3k}k_{2l}k_{3m}(e_1k_1) + e_{3i}e_{1k}k_{3l}k_{1m}(e_2k_2))]. \quad (4)$$

Here ϵ_{iklm} is the unit antisymmetric tensor, e_i, k_i are the polarization and momentum vectors of the quanta, and $k_1 + k_2 + k_3 = 0$. The expression (4) is gauge invariant: in a longitudinal external field, for example, $e_3 = k_3 f(k_3^2)$, the scattering amplitude of a real photon with $k_1^2 = k_2^2 = 0$ is zero; the general case can be reduced to this by means of dispersion relations. If we derive the interaction (4) from the known weak and electromagnetic interactions, we get for the constant a the estimate $a \sim e^3G^2\Lambda^2\mu^{-4}$, where $G^2 \sim 10^{-13}$, μ is the

mass of the π meson, and Λ is the momentum at which the four-fermion interaction is effectively cut off.[5]

Similarly, the amplitude for transition of a quantum into two neutrinos must have the form[6]

$$e_r \Gamma_r = b_1 e_r \sigma_r + b_2 \sigma_r e_n (\delta_{rn} k^2 - k_r k_n). \quad (5)$$

Here $\sigma_r = (\boldsymbol{\sigma}, 1)$ is the two-rowed matrix spin vector; we are using the two-component representation. The case $b_1 \neq 0$ corresponds to a charged massless particle, and we have treated it earlier;[7] we here take $b_1 = 0$. On the assumption of a direct $(e\nu, e\nu)$ interaction the quantity b_2 has the order of magnitude $b_2 \sim G e \mu^{-2} \ln(\Lambda/m)$.

Setting, as usual,

$$D_{rn}(k) = k^{-4} [d_t (\delta_{rn} k^2 - k_r k_n) + d_l k_r k_n],$$

$$d_t = [1 - 4\pi\Pi(k^2)]^{-1},$$

we find that the contribution of the processes in which we are interested to the imaginary part of Π is

$$2 \operatorname{Im} \Pi(k^2) = \begin{cases} [4a^2 + b_2^2/12\pi] k^4, & k^2 > 0, \\ 0, & k^2 < 0. \end{cases}$$

From this we have

$$d_t^{-1}(k^2) = 1 - k^4 (8a^2 + b_2^2/6\pi) (\ln(-k^2) + \text{const}). \quad (6)$$

Because transitions to two-particle states are strongly forbidden, the singularity in d_t is rather weak, and there is no "infrared" damping. Thus the hypothetical case $b_1 \neq 0$,[7] for which $d_t^{-1} = 1 - (b_1^2/6\pi) \ln(-k^2)$, is the only one in which the photon is not rigorously stable.

We note, finally, that the expression (4) can be interesting in itself as the phenomenological amplitude of a "purely electromagnetic" process that does not conserve parity.[8,6] For example, it describes a rotation of the plane of polarization of a photon in scattering by a Coulomb field. These effects are small, however, if we use the estimate for a given here.

[1] V. M. Galitskii and A. B. Migdal, JETP **34**, 139 (1958), Soviet Phys. JETP **7**, 96 (1958).

[2] A. A. Abrikosov, JETP **30**, 96 (1956), Soviet Phys. JETP **3**, 71 (1956).

[3] N. N. Bogolyubov and D. V. Shirkov, Introduction to the Theory of Quantized Fields, Interscience, 1959, Secs. 43, 44.

[4] A. I. Akhiezer and V. B. Berestetskii, Квантовая электродинамика (Quantum Electrodynamics), Second edition, Fizmatgiz, 1959, Sec. 16.

[5] B. L. Ioffe, JETP **38**, 1608 (1960), Soviet Phys. JETP **11**, 1158 (1960).

[6] Ya. B. Zel'dovich and A. M. Perelomov, JETP **39**, 1115 (1960), Soviet Phys. JETP **12**, 777 (1961).

[7] V. G. Vaks, JETP **40**, 792 (1961), Soviet Phys. JETP **13**, 556 (1961).

[8] Ya. B. Zel'dovich, JETP **33**, 1531 (1957), Soviet Phys. JETP **6**, 1184 (1958).

Translated by W. H. Furry
294

SUPPRESSION OF TWO-MESON ANNIHILATION IN ANTIPROTON-PROTON INTERACTION

É. O. OKONOV

Joint Institute for Nuclear Research

Submitted to JETP editor December 26, 1960

J. Exptl. Theoret. Phys. (U.S.S.R.) 40, 1728-1731 (June, 1961)

It is demonstrated that the suggestions made by various authors to explain the suppression of the $p + \bar{p} \to \pi^- + \pi^+$ reaction can be distinguished experimentally. Annihilation involving the emission of K mesons is examined from the viewpoint of the various proposals and corresponding experiments are suggested.

ONE of the most interesting experimental facts is the suppression of the two-meson annihilation in the antiproton-proton interaction. Among 3000 annihilation stars in a propane bubble chamber (antiproton momentum ~ 1 Bev/c) Goldhaber et al. (cited in Sakurai[1]) did not observe a single two-meson annihilation event (see Sakurai,[1] p. 29).

In the studies of annihilation of antiprotons with momentum up to 1.15 Bev/c in a hydrogen bubble chamber[2] altogether only two events were found, that the authors could interpret as the reaction

$$\bar{p} + p \to \pi^- + \pi^+. \qquad (1)$$

At that an estimate of 1/400 was given for the upper limit of the relative probability of this process. This number is significantly smaller than estimates made on the basis of various versions of the statistical theory which gives good agreement with experiment for the average multiplicity of pions in annihilation. According to these estimates the two-meson annihilation should amount to 2 — 10%.[3-7] Nevertheless the possibility that the suppression of the two-meson annihilation could be explained within the framework of some version of the statistical theory cannot be excluded (see, for example, Desai[8]).

Various assumptions regarding the character of the annihilation process have been made in order to explain the above mentioned experimental fact. Thus, for example, Okonov[9] suggested that the annihilation proceeds mainly through the singlet state of the $\bar{p}p$ system, for which the two-meson transition is forbidden by existing selection rules. He proposed experiments in which three-meson annihilations would be studied with the aim of establishing the presence or absence of a dependence on the spin (and isospin) state of the $\bar{p}p$ system of the annihilation transition matrix.* Sakurai[1] suggested that the annihilation proceeds through intermediate bosons, each of which rapidly decays into two or three pions. Since in the annihilation act on a free nucleon at least two such bosons should be emitted two-mesonic (and also three-mesonic) annihilations would be suppressed.† Finally, Shirokov and the author[11] have shown that annihilation into two pions is forbidden if the charge parity of the $\bar{p}p$ system is opposite to the one that follows from Dirac's equation. The observation of two events of annihilation into $\pi^-\pi^+$ seemingly excludes this last possibility. However, if one takes into account the difficulties noted by Chamberlain,[2] in the identification of two-mesonic annihilation events then, apparently, the question of the forbiddenness of reaction (1) cannot be considered as definitely settled.‡

It should be noted that the study of the reactions

$$\bar{n} + p \to \pi^0 + \pi^+, \qquad (2)$$

$$\bar{p} + n \to \pi^- + \pi^0 \qquad (3)$$

permits one to distinguish between the proposals here discussed. Indeed, if the suppression of reaction (1) is due to statistical factors, then reactions (2) and (3) will also be suppressed. An analogous situation would result if the annihilation proceeds through intermediate bosons, however in

*A study of this question within the framework of the Ball and Chew model shows that such a dependence should take place.[10]

†Annihilation into two (three) pions could arise in this case, in principle, only through virtual interactions of the intermediate bosons.

‡For example, it cannot be excluded that the events represented annihilation into π^- and π^+ with the emission of a soft photon.

that case three-meson annihilations should be suppressed to the same extent. The simultaneous suppression of reactions (1) — (3) could be caused by dominant annihilation in the singlet state of any $\bar{N}N$ system independently of isospin (and not only of the $\bar{p}p$ system). The same experimental situation arises in the case when the annihilation proceeds not only mainly through the singlet state, but basically in the state of isospin 1.* In that case, as already indicated by the author,[9] the question about the dominance of annihilation in the $^1S_0$ state can be settled by studying three-meson annihilations.

If it should turn out that reaction (1) is forbidden while reactions (2) and (3) are allowed, then two of the above discussed possibilities will remain:

a) the charge parity of the $\bar{p}p$ system is opposite to the one that follows from Dirac's equation, i.e., $C_{\bar{p}p} = -1$;

b) the Dirac parity holds, but the dominance of annihilation in the singlet state is true only for the $\bar{p}p$ system (and not for $\bar{N}N$ in general). This is possible, for example, if the amplitudes for the annihilation transitions in the triplet state with isospin 0 and 1 are equal in magnitude and opposite in phase.

The versions a) and b) can be distinguished by the energy dependence of reactions (2) and (3). This is easily shown in the framework of the selection rules based on the so-called G-parity,† first introduced by Lee and Yang.[12] For the Dirac version of charge parity one has for the $\bar{n}p$ ($\bar{p}n$) system $G = (-1)^{l+s+1}$, and if $C_{\bar{p}p} = -1$ then $G = (-1)^{l+s}$ (l and s are the values of the orbital angular momentum and spin respectively of the $\bar{N}N$ system). When it is noted that the 2π transition of the $\bar{N}N$ system is possible only in the triplet state ($s = 1$), and that the G-parity of the $\pi\pi$ system is $+1$, then it is seen that reactions (2) and (3) are possible in version a) for odd values of orbital angular momentum (1, 3, ...), and in version b) for even values of l (0, 2, ...).

This means that in the region of not too large energies (up to $E_{\bar{p}} \sim 50$ Mev) in the version a) the cross section for reactions (2) and (3) will rise like $E^{1/2}$, and in the version b) will fall like $E^{-1/2}$. Further if the estimates of Desai[10] are correct, who showed that the capture of a stopped antiprotons proceeds mainly from the S state, then the relative yield of reaction (3) will sharply increase (decrease) in going over to annihilation in flight [respectively for versions a) and b)]. Study of reaction (2) is in principle preferable, since it permits the observation of the elementary process, however from the experimental point of view it is connected with definite difficulties. Apparently it is best to observe such a process in an antiproton beam with the help of a hydrogen bubble chamber, making use of the antineutrons produced by charge exchange: $\bar{p} + p \rightarrow \bar{n} + n$. The kinematic analysis of such an event makes it possible, in principle, to determine the energy of the antineutron annihilated as a result of a subsequent interaction. In any case the probability of such a process should be no smaller, than the probability of antiproton double scattering, which was observed in a large hydrogen bubble chamber.*

As regards reaction (3) information can be deduced from already existing experimental data on the annihilation of antiprotons on deuterons. Here, however, it is necessary to select events in which the proton remaining after annihilation carries away little momentum.

All the indications are that the system K^-K^+ ($K^0\bar{K}^0$) has the same symmetry properties as the $\pi^-\pi^+$ system.[13] Therefore, if the reaction (1) is suppressed because the annihilation proceeds predominantly through the singlet state or because of a non-Dirac charge parity of the $\bar{p}p$ state, the reaction

$$\bar{p} + p \rightarrow K + \bar{K} \tag{4}$$

will also be suppressed.†

At the same time the reactions

$$\bar{n} + p \rightarrow \bar{K}^0 + K^+, \tag{5}$$

$$\bar{p} \quad n \rightarrow K^- + K^0 \tag{6}$$

will, generally speaking, not be suppressed [provided, of course, that the suppression of (4) is not due to statistical factors]. Nothing more definite can be said about the behavior of reactions (5) and (6), as long as no definite information is available on the parity of the $\bar{K}^0K^+$ (K^-K^0) system.

An analysis of annihilation stars in a hydrogen bubble chamber failed to produce a single event that could be reliably interpreted as $\bar{p} + p \rightarrow K^-$

*In this connection it should be noted that in the Fermi-Yang model the existence of the pion indicates a strong attractive interaction between the nucleon and antinucleon in the singlet state with isospin 1.

†G-conjugation stands for the consecutive operations of charge conjugation and rotation by 180° in isospace: $G = C \exp(i\pi I_2)$.

*Up till now ~200 events of double antiproton scattering were registered in a large hydrogen bubble chamber.[2]

†Obviously the same conclusions would follow for a Dirac parity if $C_{K\bar{K}} = -1$.

$+ K^+$; this results in an upper limit for the relative probability of this process of 0.1%.[2]

Among 3000 annihilation stars in propane, annihilations with production of K^- and K^+ are, apparently, also absent. Indeed, the kinematic pictures of annihilation into $\pi^-\pi^+$ and K^-K^+ are very similar. The only difference consists of slightly different values of the momenta of the π and K mesons (for annihilation at rest the momenta are 0.93 and 0.8 Bev/c respectively). Consequently, annihilations into K^-K^+ could not have been missed. It is known that in the annihilation of antiprotons on nuclei a significant number of K mesons is produced. Thus, in a propane bubble chamber the fraction of annihilation stars containing K mesons amounts to 4% at $E_p = 70$ Mev, and to more than 5% at $E_p = 500$ Mev.[14]

It follows from these results that the contribution of reaction (4) must be at least a 100 times smaller, as compared to other processes that lead to production of K mesons in annihilation. These processes could consist of reaction (6) or of annihilation with emission of several pions in addition to the K-meson pair; the latter process has already been observed in emulsions.[15]

The relative probability of the latter process, according to various versions of the statistical theory, is several times larger than the contribution of reactions (4) — (6).[3-5] However, comparison with predictions of the statistical theory cannot serve as a reliable criterion for establishing the existence and degree of suppression of reaction (4). As a first step one must compare the yields of reactions (4) — (6), which should be of the same order in the absence of some factors, other than statistical, that might act to suppress reaction (4).

In those cases where the antiproton annihilates by interacting with two nucleons reactions of the following type could occur:[16]

$$\bar{p} + (2N) \to \bar{\Lambda}(\Sigma) + K, \qquad \bar{p} + (2N) \to \Xi + 2K.$$

A similar reaction (with emission of a Λ^0 and K^0) was recently observed in the annihilation of an antiproton on a carbon nucleus in a propane bubble chamber.[17] The relative probability of such processes can be estimated from the number of hyperons emitted in annihilation. This probability (as well as the probability for the $\bar{K}$ meson produced in the annihilation to give rise to a hyperon in the same nucleus) increases with increasing atomic weight of the nucleus. However the relative yield of K mesons from annihilations in emulsions ($A_{av} \approx 40$) and in propane bubble chambers ($A_{av} = 12$) is approximately the same ($\sim 4\%$). This makes one think that annihilation processes with the emission of hyperons do not play a decisive role.

The author expresses gratitude to M. I. Shirokov for discussion and valuable remarks.

[1] S. Sakurai, Ann. Phys. **11**, 1 (1960).

[2] O. Chamberlain, Proc. of the 1960 Ann. Intern. Conf. on High Energy Physics at Rochester (1961).

[3] Belen'kii, Maksimenko, Nikishov, and Rosental', Usp. Fiz. Nauk **62**, 1 (1957).

[4] Barkas, Birge, et al., and Amaldi, Baroni, et al., Phys. Rev. **105**, 1037 (1957).

[5] Z. Koba and G. Takeda, Progr. Theor. Phys. **19**, 269 (1958).

[6] E. Eberle, Nuovo cimento **8**, 610 (1958).

[7] J. V. Lepore and M. Neuman, Phys. Rev. **98**, 1484 (1955).

[8] B. Desai, Phys. Rev. **119**, 1390 (1960).

[9] É. Okonov, JETP **39**, 1059 (1960), Soviet Phys. JETP **12**, 738 (1960).

[10] B. Desai, Phys. Rev. **119**, 1385 (1960).

[11] M. I. Shirokov and É. O. Okonov, JETP **39**, 285 (1960), Soviet Phys. JETP **12**, 204 (1960).

[12] T. D. Lee and C. N. Yang, Nuovo cimento **3**, 749 (1956).

[13] D. Amati and B. Vitale, Fortschr. Physik **7**, 375 (1959).

[14] G. and S. Goldhaber, Fowler, and Powell, Bull. Am. Phys. Soc. **4**, 357, 368 (1959).

[15] Amaldi, Baroni, Belletini, Castagnoli, Ferro-Luzzi, and Manfredini, Nuovo cimento **14**, 977 (1959).

[16] É. Okonov, JETP **36**, 1597 (1959), Soviet Phys. JETP **9**, 1134 (1959).

[17] E. Segré, Science **132**, 9 (1960).

Translated by A. M. Bincer
295

MAGNETIC DIPOLE TRANSITIONS IN EVEN-EVEN NUCLEI WITH QUADRUPOLE COLLECTIVE EXCITATIONS

D. P. GRECHUKHIN

Submitted to JETP editor December 28, 1960

J. Exptl. Theoret. Phys. (U.S.S.R.) 40, 1732-1737 (June, 1961)

It is shown that for collective models with quadrupole excitations the branching ratio and interference phase shift of M1 and E2 radiation in a mixed M1 + E2 nuclear transition do not depend on the specific structure of the collective nuclear models. The ratio of the quantities $\delta^2(M1/E2) = W(M1; I_1 \to I_2)/W(E2; I_1 \to I_2)$ for two different M1 + E2 transitions of a given nucleus is a function only of the transition energies and nuclear spin states involved in the radiation process. By comparing this quantity with the experimental data one can estimate to what extent the collective degrees of freedom are smeared out with increasing excitation energy of the nucleus.

1. It has been variously proposed to describe the spectra of even-even nuclei in the intervals $60 \leq A \leq 196$ and $A > 210$ by means of the vibration model,[1,2] the axial-rotator model,[1,2] and the non-axial rotator model,[5] in which quadrupole collective excitations of the nucleus are considered. Common to all these models is the assumption that the excitation spectrum and the radiation properties of the nucleus can be described in terms of the parameters $\alpha_{2\mu}$ of the deformation of the nuclear surface, and their derivatives $\dot{\alpha}_{2\mu}$, regarded as dynamic variables ($\alpha_{2\mu}$ and $\dot{\alpha}_{2\mu}$ are defined in the laboratory system throughout). It is assumed here that the coordinates $\alpha_{2\mu}$ and the generalized momenta $\pi_{2\mu} = B_{2\mu}\dot{\alpha}^*_{2\mu}$, where B_2 is the inertia parameter of the collective motion of the nucleus, obey the commutation rule

$$[\pi_{2\mu}\alpha_{2\mu'}]_- = -i\hbar\delta_{\mu\mu'}$$

and the corresponding excitations of the nucleus are of the boson type.

This naturally raises the question of how accurately a boson-type collective excitation can be built up from the nucleons of the nucleus. It is of interest to estimate experimentally the accuracy of separation of such excitations. As will be shown below, a study of the angular correlations in a cascade of gamma quanta, one of which is a mixed M1 + E2 radiation of the nucleus, enables us to make this estimate.

2. The angular correlation functions (with and without detection of the quantum polarization) in a cascade that includes the nuclear transition $I_1 \to I_2$ with mixed M1 + E2 radiation depend essentially on the branching ratios of the M1 and E2 transitions

$$\delta^2(M1/E2,\ I_1 \to I_2) = W(M1;\ I_1 \to I_2)/W(E2;\ I_1 \to I_2) \tag{1}$$

and the relative phase ξ of the reduced matrix elements of the E2 and M1 transitions, which we define through

$$\delta e^{i\xi} = i\sqrt{\frac{\overline{50}}{3}}\frac{1}{\omega}\frac{\langle I_2 \| M1 \| I_1\rangle}{\langle I_2 \| E2 \| I_1\rangle}, \tag{2}$$

it being assumed here that δ is always positive; ω is the energy of the nuclear radiation transition $I_1 \to I_2$, expressed in $m_e c^2$ units (multiples of 0.511 Mev).

The reduced matrix elements of the M1 and E2 transitions are defined by the equations

$$\langle I_2 \| M1 \| I_1\rangle C^{I_1 M_1}_{I_2 M_2 1M} = \left\langle I_2 M_2 \left| \sum_{i=1}^{A} r_i\, Y^{0^*}_{1M}\, \mathbf{j}_i \right| I_1 M_1 \right\rangle, \tag{3}$$

$$\langle I_2 \| E2 \| I_1\rangle C^{I_1 M_1}_{I_2 M_2 2M} = \left\langle I_2 M_2 \left| \sum_{p=1}^{Z} e r_p^2\, Y^*_{2M} \right| I_1 M_1 \right\rangle. \tag{4}$$

All the quantities are best defined in units for which $\hbar = m_e = c = 1$ and $e^2 = 1/137$; the nuclear radius is $R_0 = 0.43A^{1/3}e^2$, corresponding to $R_0 = 1.2 \times 10^{-13}A^{1/3}$ cm. $C^{a\alpha}_{b\beta c\gamma}$ is the Clebsch-Gordan coefficient and Y_{LM} are spherical vector harmonics (see reference 4).

In order to define δ and ξ uniquely, we give the angular correlation function for two gamma-quanta in the cascade $I_1(M1 + E2)I_2(L)I_3$, where L is the multipolarity of the second quantum

$$W(\theta_{12}) = \sum_{\kappa=0,2,4} C_\kappa P_\kappa(\cos\theta_{12}); \tag{5}$$

$$C_\varkappa = C^{L1}_{L1\varkappa 0}(2\varkappa+1)\, u(\varkappa L I_2 I_3;\ L I_2)$$
$$\times\{C^{21}_{21\varkappa 0}\, u\,(2I_1\varkappa I_2; I_2 2) + \delta^2 C^{11}_{11\varkappa 0}\, u\,(1I_1\varkappa I_2;\ I_2 1)$$
$$+ 2\delta\cos\xi\, C^{10}_{10\varkappa 0}\, u(21\varkappa 1;\ 11)\, u\,(1I_1\varkappa I_2;\ I_2 2)\}. \qquad (6)$$

Here u(abcd, ef) is the normalized Racah function, tables for which are found in the paper by Yang.[5]

For the inverse cascade $I_3(L)I_2(M1+E2)I_1$, the gamma-quantum correlation function is also given by (5) and (6), but it is necessary to reverse in (6) the sign of the interference term proportional to $\delta\cos\xi$. The angular correlation functions with and without detection of quantum polarizations are described in greater detail in the review of Biederharn and Rose.[6]

3. A sufficiently accurate correlation experiment will thus enable us to find two physical parameters of the radiative transition of the nucleus $I_1 \to I_2$, namely $\delta^2(M1/E2, I_1 \to I_2)$ and $\cos\xi$. Let us consider these quantities in the collective models of the nucleus.

In all the previously mentioned collective models of the nucleus[1-3] the operators of the E2 and M1 transitions in terms of the variables $\alpha_{2\mu}$ and $\dot\alpha_{2\mu}$ have the following form:

the E2 transition operator

$$e\sum_{p-1}^{Z} r_p^2 Y^*_{2M} \to \int \rho_p(\mathbf{r})\, r^2 Y^*_{2M}(\mathbf{r})\, dv \approx \frac{3}{4\pi} ZR_0^2 e\alpha_{2M} + \ldots, \qquad (7)$$

the M1 transition operator

$$\sum_{i=1}^{A} r_i\, Y^{0*}_{1M}\, \mathbf{j}_i \to \int \mathbf{j}_N\, r\, Y^{0*}_{1M}\, dv = \hat J^{(0)}_M + \hat J^{(1)}_M + \ldots \qquad (8)$$

Here

$$\hat J^{(0)}_M = -\sqrt{\frac{15}{4\pi}}\, g_R \frac{e}{M}\sum_{m\nu} C^{1M}_{2m2\nu}\,\alpha_{2\nu} B_2\,\dot\alpha_{2m}, \qquad (9)$$

$$\hat J^{(1)}_M = -\frac{5\sqrt{3}}{2\pi}\, g_R \frac{e}{M} C^{20}_{2020}\sum_{m\nu\mu_1\mu_2} C^{1M}_{2m2\nu} C^{2\nu}_{2\mu_1 2\mu_2}\,\alpha_{2\mu_1}\alpha_{2\mu_2} B_2\,\dot\alpha_{2m}, \qquad (10)$$

M is the mass of the nucleon in m_e units ($M = 1840$) and g_R is the gyromagnetic ratio for the collective motion of the nucleus in the hydrodynamic model, $g_R = Z/A$.

In the derivation of (7) — (9) it is usually assumed that the charge density of the nuclear transition, $\rho_p(\mathbf{r})$, is uniformly spread over the volume of the nucleus, and the collective current of the nuclear transition, $\mathbf{j}_N$ is determined in terms of the rate of flow of the nuclear liquid

$$\mathbf{V} = \tfrac{1}{2}\sum_m \dot\alpha_{2m}\nabla r^2 Y_{2m}. \qquad (11)$$

We note, however, that these model assumptions are essential only for the values of the coefficients of the operators of the E2 and M1 transitions of the nucleus, whereas the functional dependence of E2 and M1 operators on the variables α_{2m} and $\pi^*_{2m} = B_2\dot\alpha_{2m}$ does not involve the models. In order for relations (7) and (8) to hold, it is sufficient to assume that the expansion terms containing the higher powers of α_{2m} and π_{2m} are small and can be neglected. We note also that the operators $B_2\dot\alpha_{2m}$ and $\alpha_{2\mu}$ freely commute in (10).

The specific forms of the operators $\alpha_{2\mu}$ and $\pi_{2\mu}$ may differ in the vibration and rotation models; for the vibrator, $\alpha_{2\mu}$ and $\pi_{2\mu}$ can be represented in terms of operators of creation and annihilation of quadrupole phonons $\hat c^+_\mu$ and $\hat c_\mu$, while in the rotation models $\alpha_{2\mu}$ and $\pi_{2\mu}$ act on the angles of orientation of the deformed nucleus. In both models, however, the operator $\hat J^{(0)}_M$ (see reference 1) is proportional to the angular momentum operator of the nucleus I, for which we have according to Bohr[1]

$$(-1)^\nu \hat I_{-\nu} = i\sqrt{10}\sum_{mq} C^{1\nu}_{2m2q}\,\alpha_{2q} B_2\,\alpha_{2m}, \qquad (12)$$

and in the particular case of the vibration model

$$(-1)^\nu \hat I_{-\nu} = \frac{i\sqrt{10}}{2}\sum_{mq} C^{1\nu}_{2m2q}\,[(-1)^m \hat c^+_{-m}\hat c_q - (-1)^q \hat c^+_{-q}\hat c_m]. \qquad (13)$$

Formula (13) for the operator $\hat I_{-\nu}$ holds also for the anharmonic vibrator, inasmuch as the state function $\Psi_{IM;i}$ of the vibrator can be expanded in terms of the states χ^n_{IM} of the harmonic vibrator (n is the number of phonons):

$$\Psi_{IM;\,i} = \sum_n a_{in}\chi^n_{IM}. \qquad (14)$$

Applying the operator $(-1)^\nu \hat I_{-\nu}$ (13) to $\Psi_{IM;i}$, we get

$$(-1)^\nu \hat I_{-\nu}\Psi_{IM;\,i} = \sum_n a_{in}\,(-1)^\nu \hat I_{-\nu}\chi^n_{IM}$$
$$= (-1)^\nu\sqrt{I(I+1)}\, C^{IM-\nu}_{IM1-\nu}\Psi_{IM-\nu;\,i}. \qquad (15)$$

Thus, regardless of the specific structure, the operator $\hat J^{(0)}_M$ makes no contribution to the radiative M1 transition of the nucleus, and the probability of the M1 transition is determined by the operator $\hat J^{(1)}_M$.

The operator $\hat J^{(1)}_M$ can be expressed in terms of the operator of the E2 transition, proportional to $\alpha_{2\mu}$, and the operator of angular momentum of the nucleus $\hat I_{-\nu}$:

$$\hat J^{(1)}_M = i g_R \frac{e}{M}\frac{5\sqrt{3}}{7\pi}\sum_{\nu\mu} C^{1M}_{1\nu 2\mu}\,\alpha_{2\mu}\hat I_{-\nu}(-1)^\nu. \qquad (16)$$

Relation (16) for $\hat J^{(1)}_M$ is not self-evident. It was obtained by Davydov and Filippov and given without

proof in reference 7, where relation (16) was used to calculate the probability of the M1 transition between the states $2' \to 2$ of a non-axial nucleus.

Relation (16) can be obtained from (10) by using the following equation for the Clebsch-Gordan coefficients

$$\sum_{\mu_1\mu_2} C^{1M}_{2m2\nu} C^{2\nu}_{2\mu_1 2\mu_2} \xi_{\mu_1\mu_2} = -2\sqrt{\frac{5}{7}} \sum_{\mu_1\mu_2} C^{1M}_{1n2\mu_1} C^{1n}_{2m2\mu_2} \xi_{\mu_1\mu_2}, \quad (17)$$

where $\xi_{\mu_1\mu_2} = \xi_{\mu_2\mu_1}$ is an arbitrary symmetrical function of $\mu_1\mu_2$ [a derivation of (17) is given in the Appendix]. It is not necessary to consider here the specific action of the operators $\alpha_{2\mu}$ and $\pi_{2\mu}$ on the wave function of the nucleus. Relation (16) holds for any model with collective quadrupole excitations of the nucleus.

4. Using (16) and taking into account the result of the action of the operator $(-1)^\nu I_{-\nu}$ on the wave function of the nucleus Ψ_{IM} [see (15)], we obtain after summation over the magnetic quantum numbers the following expression for the matrix element of the M1 transition of the nucleus

$$\langle \Psi^*_{I_2M_2} | \hat{J}^{(1)}_M | \Psi_{I_1M_1} \rangle = \langle I_2 \| M1 \| I_1 \rangle C^{I_1M_1}_{I_2M_2 1M}$$
$$= -ig_R \frac{e}{M} \frac{3}{7\pi}\sqrt{5}\sqrt{I_1(I_1+1)}\, u(I_2 I_1 11; 2I_1)$$
$$\times \langle I_2 \| \alpha_2 \| I_1 \rangle C^{I_1M_1}_{I_2M_2 1M}, \quad (18)$$

and for the operator of the E2 transition we get

$$\langle \Psi^*_{I_2M_2} | \frac{3}{4\pi} ZeR_0^2 \alpha_{2M} | \Psi_{I_1M_1} \rangle = \langle I_2 \| E2 \| I_1 \rangle C^{I_1M_1}_{I_2M_2 2M} \quad (19)$$
$$= \frac{3}{4\pi} ZeR_0^2 \langle I_2 \| \alpha_2 \| I_1 \rangle C^{I_1M_1}_{I_2M_2 2M},$$

where we have from the definition of the reduced matrix element

$$\langle I_2 M_2 | \alpha_{2M} | I_1 M_1 \rangle = C^{I_1M_1}_{I_2M_2 2M} \langle I_2 \| \alpha_2 \| I_1 \rangle. \quad (20)$$

The quantity $\langle I_2 \| \alpha_2 \| I_1 \rangle$ depends essentially on the structure of the model, but the branching ratio of the M1 and E2 transitions does not contain this matrix element.

Using (18) and (19) for the experimentally measured quantities $\delta^2(\mathrm{M1/E2}, I_1 \to I_2)$ and $\cos\xi$, we obtain, according to (1) and (2)

$$\cos\xi = 1, \quad (21)$$

$$\delta^2(M1/E2,\ I_1 \to I_2)$$
$$= \frac{500}{441}(I_1+I_2+3)(I_1-I_2+2)(I_2-I_1+2)$$
$$\times (I_1+I_2-1)(g_R/Z\omega MR_0^2)^2; \quad (22)$$

here ω is the transition energy in units of mc^2 (0.511 Mev). Formulas (21) and (22) are valid for all the collective models with quadrupole excitations, independently of the specific structure of the model; only these formulas are inapplicable for certain transitions of the strictly harmonic vibrator, which proceed via annihilation of two phonons.

In general, the quantities $(g_R/Z)^2$ can not be considered known, since the coefficients in the operators of the M1 and E2 transitions depend on the models assumped. It is therefore more convenient to compare the ratio of two values of $\delta^2(\mathrm{M1/E2})$ for different mixed M1 + E2 nuclear transitions $I_1 \to I_2$, and $I_3 \to I_4$. In this case the unknown factor $(g_R/Z)^2$ drops out of the final result

$$\frac{\delta^2(M1/E2,\ I_1 \to I_2)}{\delta^2(M1/E2,\ I_3 \to I_4)}$$
$$= \left(\frac{\omega_{34}}{\omega_{12}}\right)^2 \frac{(I_1+I_2+3)(I_1-I_2+2)(I_2-I_1+2)(I_1+I_2-1)}{(I_3+I_4+3)(I_3-I_4+2)(I_4-I_3+2)(I_3+I_4-1)}. \quad (23)$$

5. The deviation of the experimental values from the quantities (22) and (23), predicted by the collective models of the nucleus, may be due to the inaccuracy in the separation of the collective degrees of freedom. In this case the contribution of the single-particle admixture can change the result appreciably. Actually, the estimated probability of the most intense single-particle M1 transition between the levels of one spin-orbit doublet is

$$W_{\mathrm{s.p.}}(M1) \approx \frac{e^2\omega^3}{M^2} \frac{\mu_n^2}{3} \frac{m_e c^2}{\hbar}, \quad (24)$$

where μ_n is the magnetic moment of the nucleon in magnetons, whereas the collective M1 transitions have a probability

$$W_{\mathrm{col}}(M1) \approx \frac{e^2\omega^3}{M^2} \frac{g_R^2}{\pi} \beta^2 \frac{m_e c^2}{\hbar}, \quad (25)$$

where $\beta^2 = \langle \sum_\mu |\alpha_{2\mu}|^2 \rangle$ is the nuclear deformation. Thus

$$W_{\mathrm{s.p.}}(M1)/W_{\mathrm{col}}(M1) \approx (\mu_n/g_R\beta)^2. \quad (26)$$

Neglecting the contribution of the single-particle transitions to the probability of the nuclear E2 transition, and taking them into account only in the M1 transition, we obtain a rough estimate for $\delta^2(\mathrm{M1/E2},\ I_1 \to I_2)$:

$$\delta^2(M1/E2,\ I_1 \to I_2)$$
$$\approx [1 + a^2(\mu_n/\beta g_R)^2]\, \delta^2_{\mathrm{col}}(M1/E2,\ I_1 \to I_2), \quad (27)$$

where δ^2_{col} is given by (22).

The parameter a^2 is a measure of the admixture of the single-particle states. Its structure can be made more precise only with a specific microscopic model of the excitations of the nucleus. Since $(\mu_n/\beta g_R)^2 \approx 10^2 - 10^3$, even a small admixture of single-particle transitions changes the value of $\delta^2(\mathrm{M1/E2})$ appreciably. The sign of

cos ξ can also change when the admixture of single-particle transitions becomes considerable.

We are thus able to estimate experimentally the purity of separation of the collective degrees of freedom for even-even nuclei, where the reduced probability of the E2 transitions is appreciably greater than the single-particle estimate. Unfortunately, there are not enough exact and complete data at present to make this analysis possible. The available experimental values of δ^2(M1/E2) apparently do not contradict the estimates of the collective models,[8] but the accuracy of these data is low. It is of exceeding interest to measure the values of δ^2(M1/E2) for several transitions of one and the same nucleus, so as to be able to trace the "smearing" of the collective degrees of freedom of the nucleus with increasing nuclear excitation energy.

APPENDIX

Relation (17) can be obtained by successive application of the expansion formula

$$C^{1M}_{Nn2\mu_2}C^{Nn}_{2m2\mu_1}=\sum_A(-1)^{1+N+A}\,u\,(2221;\;AN)\,C^{1M}_{Aa2\mu_1}C^{Aa}_{2m2\mu_2}. \tag{A.1}$$

We have

$$\sum_{\mu_1\mu_2}\xi_{\mu_1\mu_2}C^{1M}_{2m2\nu}C^{2\nu}_{2\mu_12\mu_2}=u\,(2221;\;12)\sum_{\mu_1\mu_2}\xi_{\mu_1\mu_2}C^{1M}_{2\mu_21n}C^{1n}_{2m2\mu_2}$$
$$+\sum_{\mu_1\mu_2}\xi_{\mu_1\mu_2}\{u\,(2221;\;22)\,C^{1M}_{2n2\mu_2}C^{2n}_{2m2\mu_1}$$
$$+u\,(2221;\;32)\,C^{1M}_{3n2\mu_2}C^{3n}_{2m2\mu_1}\}. \tag{A.2}$$

Using the symmetry $\xi_{\mu_1\mu_2}=\xi_{\mu_2\mu_1}$ ($\xi_{\mu_1\mu_2}$ is an arbitrary function symmetrical in $\mu_1\mu_2$) and transforming, in accordance with (A.1), the terms in the curly brackets, we obtain with allowance for the numerical values of the u-functions

$$\sum_{\mu_1\mu_2}\xi_{\mu_1\mu_2}C^{1M}_{2m2\nu}C^{2\nu}_{2\mu_12\mu_2}$$
$$=\left[-\frac{1}{2}\sqrt{\frac{7}{5}}-\frac{13}{20}\sqrt{\frac{7}{5}}\right]\sum_{\mu_1\mu_2}C^{1M}_{1n2\mu_1}C^{1n}_{2m2\mu_2}\xi_{\mu_1\mu_2}$$
$$+\sum_{\mu_1\mu_2}\xi_{\mu_1\mu_2}\left\{\frac{3}{20}C^{1M}_{2n2\mu_1}C^{2n}_{2m2\mu_2}+\frac{3}{10}\sqrt{\frac{2}{5}}C^{1M}_{3n2\mu_1}C^{3n}_{2m2\mu_2}\right\}. \tag{A.3}$$

Applying formula (A.1) successively at each stage to the terms with $N\neq 1$ in the curly brackets, and separating each time the new terms with $N=1$, we obtain a geometric progression

$$\sum_{\mu_1\mu_2}\xi_{\mu_1\mu_2}C^{1M}_{2m2\nu}C^{2\nu}_{2\mu_12\mu_2}=-\sqrt{\frac{7}{5}}\left(\frac{1}{2}+\frac{13}{20}\left[1+\frac{3}{10}+\left(\frac{3}{10}\right)^2+\ldots\right]\right)$$
$$\times\sum_{\mu_1\mu_2}\xi_{\mu_1\mu_2}C^{1M}_{1n2\mu_2}C^{1n}_{2m2\mu_1}, \tag{A.4}$$

and after summing this series we arrive at formula (17).

[1] A. Bohr, Kgl. Danske Vid. Selsk. Mat. Fys. Medd. **26**, 14 (1952).

[2] Alder, Bohr, Huus, Mottelson, and Winter, Revs. Modern Phys. **28**, 432 (1956).

[3] A. S. Davydov and G. F. Filippov, JETP **35**, 440 (1958), Soviet Phys. JETP **8**, 303 (1959).

[4] Berestetskii, Dolginov, and Ter-Martirosyan, JETP **20**, 527 (1950).

[5] H. A. Jahn, Proc. Roy. Soc. **A205**, 192 (1951).

[6] L. C. Biedenharn and M. E. Rose, Revs. Modern Phys. **25**, 729 (1953).

[7] A. S. Davydov and G. F. Filippov, JETP **35**, 703 (1958), Soviet Phys. JETP **8**, 488 (1959).

[8] E. P. Grigor'ev and M. P. Avotina, Izv. Akad. Nauk SSSR, Ser. Fiz. **24**, 324 (1960), Columbia Tech. Transl. p. 311.

Translated by J. G. Adashko
296

ELECTROMAGNETIC CORRECTIONS TO WEAK INTERACTIONS

I. F. GINZBURG and V. V. SEREBRYAKOV

Institute of Mathematics with Computational Center, Siberian Division, Academy of Sciences, U.S.S.R.

Submitted to JETP editor December 31, 1960

J. Exptl. Theoret. Phys. (U.S.S.R.) 40, 1738-1745 (June, 1961)

The procedure for calculating electromagnetic corrections to weak interactions is studied. It is shown that at present there is no basis for asserting that the coupling constants of various weak interaction processes are equal or unequal with an accuracy better than electromagnetic.

A number of papers appeared in recent years containing calculations of electromagnetic corrections to the simpler weak interaction processes (μ and β decays[1-5]). The total weak interaction Lagrangian is usually taken in the form[6]

$$L_G = G : j^+ j :, \tag{0.1}$$

where j is a parity-nonconserving charged current:

$$j = (\bar{e}O\nu) + (\bar{\mu}O\nu) + (\bar{n}Op) + \ldots,$$
$$O^\mu = \gamma^\mu a_+, \qquad a_\pm = \tfrac{1}{2}(1 \pm i\gamma^5). \tag{0.2}$$

Afterwards one proceeds in the standard manner used in field theory to calculate corrections to the probabilities and cross sections obtained from Eq. (0.1) due to electromagnetic

$$L_e = e \sum_\alpha : \bar{c}_\alpha \hat{A} c_\alpha : + \ldots \tag{0.3}$$

and strong (n stands for nucleon)

$$L_g = g : \bar{n}\gamma^5 n\pi : + \ldots \tag{0.4}$$

interactions.

When this is done one studies, in effect, two different problems. The first problem consists of finding more accurate expressions for angular and energetic distributions in μ and β decays with electromagnetic corrections taken into account. To the study of this problem are devoted the papers of Behrends, Finkelstein, Kinoshita, and Sirlin,[1] Durand, Landovitz, and Marr,[2] Berman,[4] and Kuznetsov,[3] in which, however, bremsstrahlung terms connected with recoil are not fully taken into account. (The corresponding correction terms for μ decay were obtained, in effect, in Kuznetsov's second paper.[7])

The second problem consists of the determination of the renormalization of the coupling constants of the various weak interaction processes as a consequence of the interactions (0.3) and (0.4). Gell-Mann and Feynman have proposed the conserved vector current hypothesis,[6] according to which the vector part of the weak interaction does not undergo renormalization due to strong interactions. In the papers of Goldberger and Treiman and Chou Kuang Chao[8] the magnitude of the renormalization due to strong interactions is discussed for the axial vector current in β decay and other processes (its value is taken from experiments on the asymmetry in β decay; see, e.g., Alikhanov[9]). (The observed deviations from the V-A scheme (V-A $\rightarrow$ V-λA) in β decay may also be explained within this framework by taking into account only electromagnetic corrections with appropriate form factors. This means that experiment could be consistent with the absence of renormalization of the axial vector current due to strong interactions. In this connection one should also note Nambu's work.[10])

It is also known that the β decay of mirror nuclei ($0^+ \rightarrow 0^+$ transitions) is due to only the vector part of the weak interaction, which, as indicated, is not renormalized by the strong interactions. In these decays, as in μ decay, the basic weak interaction is deformed only by electromagnetic corrections. The coupling constants in these cases turn out to be very close in magnitude. This raises the question of comparing the electromagnetically renormalized coupling constants in these processes. The near equality of these constants has been discussed in a number of papers.[1,2,5]

The present work is devoted to an analysis of the starting assumptions that form the basis of such a comparison. It turns out that in the framework of contemporary field theory it is not possible to determine uniquely the renormalized coupling constants. In different processes these constants

may be determined only simultaneously with a certain (generally speaking arbitrary) normalization constant. At the moment it does not seem possible to establish a relation between the normalization constants in different processes. The gauge invariance property, contrary to the expectations of a number of authors,[1,2,5] does not save the situation. It follows therefore that a comparison of coupling constants for the above mentioned processes to an accuracy better than electromagnetic makes no sense.

Below we formulate and prove the concept of renormalization for the class of problems under consideration. We then prove the gauge invariance of the method of calculation used. In the end we consider the implications of the indicated facts for μ and β decay.

1. RENORMALIZABILITY

It is known that the four-fermion interaction (0.1) is not renormalizable, although for observable processes the inclusion of terms of higher order in G does not, apparently, change the V-A form.[11] Therefore a consistent discussion of terms of higher order in G is at this time simply impossible.* As a result we are forced to consider a semi-phenomenological theory in which only first order terms in G are kept, but all terms of the perturbation theory expansion in e and g corresponding to Eqs. (0.3) and (0.4) are taken into account. The justification of this approach is usually found in the extraordinary smallness of G.

We shall show that such a theory is renormalizable in the conventional sense. This means that the divergent expressions that appear in the course of calculations using perturbation theory can be eliminated by introducing into the Lagrangian counter terms of the type (0.3), (0.4), (0.1) and of the type of the free field Lagrangian or, which is the same, by renormalizing the masses and wave functions of the particles and the coupling constants of the interactions.

As is known, by an appropriate redefinition of the T products at the equal argument points, it is possible to reduce these infinite renormalizations to finite arbitrary multiplicative factors in the indicated quantities and in the simpler Green's functions related to them. Below, when referring to operations with divergent quantities, we shall understand operations with finite (defined up to a constant) quantities that result after the T products are redefined. One may also consider these divergent quantities to be regularized by the introduction of an appropriate cut-off. Then the above-noted finite arbitrariness in the determination of the coupling constants and particle masses corresponds, in part, to the circumstance that there is no need to choose the cut-off momenta to be the same in different, unrelated to each other, Feynman diagrams.

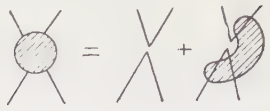

FIG. 1

We shall carry out our considerations on the simplest examples of μ and β decay, following the presentation in the book by Bogolyubov and Shirkov (Chap. 4).[12] We shall restrict ourselves in the matrix elements to only first order terms in G arising from the Lagrangians

$$L_\mu = G{:}(\bar{\mu}O\nu)\,(\bar{\nu}Oe){:} = G{:}(\bar{\mu}Oe)\,(\bar{\nu}O\nu){:}, \tag{1.1}$$

$$L_\beta = G{:}(\bar{n}Op)\,(\bar{\nu}Oe){:} = \tfrac{1}{2}{:}[\bar{n}(G_V\gamma^\mu + G_A\gamma^\mu i\gamma^5)p]\,(\bar{\nu}\gamma^\mu a_+ e){:} \qquad (G_V = G_A = G). \tag{1.1'}$$

As indicated above we will, however, take into account all terms of the perturbation-theory series corresponding to Eqs. (0.3) and (0.4). After the usual renormalizations of the coupling constants e and g, and the masses and wave functions of the particles, there remains in such a theory only one (logarithmic) divergence, corresponding to the diagram of Fig. 1. This is easily established by the conventional counting of the powers involved in the diagram.

For such G-vertices we can write an equation which, in terms of Feynman diagrams, corresponds to Fig. 1:

$$-iS_\mu = G{:}\,(\bar{\mu}Fe)\,(\bar{\nu}O\nu){:} = G{:}\,(\bar{\mu}Oe)\,(\bar{\nu}O\nu){:} + G{:}\,(\bar{\mu}Te)\,(\bar{\nu}O\nu){:}, \tag{1.2}$$

$$-iS_\beta = \tfrac{1}{2}{:}\,\bar{n}_\alpha p_\beta \bar{\nu}_\delta e_\gamma\,{:}\,F_{\alpha\beta;\,\gamma\delta} = \tfrac{1}{2}{:}\,[\bar{n}\,(G_V\gamma^\mu + G_A\gamma^\mu i\gamma^5)\,p]\,(\bar{\nu}\gamma^\mu a_+ e){:} + \tfrac{1}{2}{:}\,\bar{n}_\alpha p_\beta \bar{\nu}_\delta e_\gamma\,{:}\,R_{\alpha\beta;\,\gamma\delta}. \tag{1.2'}$$

In other words

$$F_{\alpha\beta} = O_{\alpha\beta} + T_{\alpha\beta}, \tag{1.3}$$

$$F_{\alpha\beta;\,\gamma\delta} = GO_{\alpha\beta}O_{\gamma\delta} + R_{\alpha\beta;\,\gamma\delta}. \tag{1.3'}$$

Here T and R are contributions due to the strong and electromagnetic interactions. They are logarithmically divergent.

After some transformations, in which use is made of the operator structure of the strong and

*It should be noted in addition that so far no processes of higher order in G have been observed.

electromagnetic interactions,* of the properties of direct products of operators† (see, e.g., Slavnov and Sukhanov[13]), and of the two-component nature of the neutrino, the divergent parts of R and T are isolated. In this way one obtains, as usual,

$$T_{\alpha\beta} = (Z - 1)\, O_{\alpha\beta} + T^{\mathrm{reg}}_{\alpha\beta}, \tag{1.4}$$

$$R_{\alpha\beta;\,\gamma\delta} = [G_V (Z_1 - 1)\,\gamma^\mu + G_A\gamma^\mu i\gamma^5 (Z_2 - 1)]_{\alpha\beta} O_{\gamma\delta} + R^{\mathrm{reg}}_{\alpha\beta;\,\gamma\delta}. \tag{1.4'}$$

Here T^{reg} and R^{reg} are finite functions of the momenta and the renormalized constants e, g, m, M, μ, etc.

After introducing into the Lagrangian appropriate counter terms we find that the divergence under consideration leads to a multiplicative renormalization of the coupling constant G (the constants G_V and G_A in β decay):‡

$$G \to ZG; \tag{1.5}$$

$$G_V \to Z_1 G_V, \quad G_A \to Z_2 G_A, \quad Z_1 \neq Z_2. \tag{1.5'}$$

It should be noted once more, that after the separation (1.4) of T(R) into a regularized and divergent part there remains in the definition of $T^{reg}(R^{reg})$ a finite arbitrariness, corresponding to different possible choices of the subtraction constants. This arbitrariness corresponds to the finite multiplicative renormalization of the type (1.5). At that the constants Z and $Z_1(Z_2)$ are in no way related to each other or to the analogous constants of other renormalizations (electromagnetic and strong). At first sight it seems that the situation is opposite in electrodynamics where the subtraction constant for the vertex diagram is related to the subtraction constant for the fermion self energy diagram as a consequence of gauge invariance. This contradiction with electrodynamics is apparent only, the G-vertex diagram being only superficially similar to the vertex diagram in electrodynamics. This distinction will be discussed in more detail in the next Section.

*For the here relevant most strongly divergent parts these interactions give direct products of the type $(\gamma^5\gamma^\mu) \times (\gamma^\mu\gamma^5)$ and $(\gamma^\mu\gamma^\nu) \times (\gamma^\nu\gamma^\mu)$ respectively.

†The following of them are of importance to us: $C_\pm^{-1}(\gamma^\alpha\gamma^\beta\gamma^\mu a_\pm) \times (\gamma^\mu a_+\gamma^\alpha\gamma^\beta) = D_\pm^{-1}(\gamma^\mu a_\pm\gamma^\alpha\gamma^\beta)(\gamma^\mu a_+\gamma^\alpha\gamma^\beta) = (\gamma^\mu a_\pm)(\gamma^\mu a_+)$ ($C_\pm$ and $D_\pm$ are certain numbers irrelevant for the calculations).

‡This result may also be derived by writing the S matrix as

$$S = T\left\{\left[1 + i\int L_G(x)\,dx\right]\exp\left[i\int dx\,(L_e(x) + L_g(x))\right]\right\}$$

and then computing its matrix elements as variational derivatives with respect to appropriate fields. The electromagnetic and strong divergences are in that case separated from the divergence in the G-vertex.

Thus, after the renormalization of the coupling constants e, g, and G, the particle masses and their wave functions, the theory under consideration contains no divergences.

2. GAUGE INVARIANCE

We have indicated at the end of the preceding section that the renormalization constants Z and $Z_1(Z_2)$ are unrelated to each other or to the analogous constants for other electromagnetic or strong Green's functions (diagrams). In contrast to this in a number of papers[1,3-5] it has been in essence assumed that the constant Z is related to the renormalization constant for the fermion mass operator by a relation of the type of Ward's identity in electrodynamics. We shall now show that the requirement of gauge invariance in the processes under consideration does not impose any restrictions on the constant Z and that therefore the above indicated arbitrariness in the determination of the constant Z persists.

To prove this it is necessary to show that the procedure for calculating electromagnetic corrections to weak interactions is gauge invariant. We shall show that the matrix element of the weak interaction, including electromagnetic and strong-interaction corrections, is after renormalization independent of the field intensity of longitudinal and scalar photons d_l. A full proof of this assertion is somewhat clumsy in perturbation theory; we shall therefore not present it but will limit ourselves to the consideration of only the terms of lowest order in e. The proof can also be carried out with the help of contour integration. In that case one need only to repeat almost verbatim the corresponding discussion in the book by Bogolyubov and Shirkov[12] (Sec. 41).

It is more convenient to give the proof for the μ-decay process. The generalization to processes in which the contribution of the strong interactions is relevant presents no difficulty; we leave it out here only to avoid a greater, as compared to μ decay, complexity. We shall write the weak interaction matrix element in the form

$$-iS_\mu = G{:}(\bar{\mu}Fe)\,(\bar{\nu}O\nu){:}.$$

FIG. 2

At that $$GF = G(O + \sum_{n\geqslant 1} e^{2n} F_n). \quad (2.1)$$

Since we are concerned with a theory in which the electromagnetic renormalizations of the charge e, and the particle masses and wave functions, have already been carried out, it is sufficient in second order to consider only the diagram of Fig. 2, in fourth order the six diagrams of Fig. 3,* etc.

In the series (2.1) the term of the 2n-th order in e is a polynomial of n-th order in d_l:

$$F_n = \sum_{k=0}^{n} d_l^k F_n^{(k)}. \quad (2.2)$$

To second order in e we have

$$F_1^{(1)} = \frac{1}{(2\pi)^4} \int \frac{\hat{k}}{k^2} \frac{\hat{p} - \hat{k} + \mu}{k^2 - 2pk} O \frac{\hat{q} - \hat{k} + m}{k^2 - 2qk} \frac{\hat{k}}{k^2} dk.$$

Here p and q are the momenta of the electron and muon respectively. Since in Eq. (2.1) F stands between the operators $\bar{\psi}_\mu$ and ψ_e, which satisfy their respective Dirac equations, it follows that

$$F_1^{(1)} = C_1 O. \quad (2.3)$$

Here C_1 is a "divergent constant":

$$C_1 = \frac{1}{(2\pi)^4} \int \frac{dk}{k^4}.$$

An analogous discussion of the fourth order terms in e, when the Dirac equations for the electron and muon and Lorentz invariance are taken into account, leads to the result

$$F_2^{(2)} = F_{2a}^{(2)} + F_{2b}^{(2)} = C_2^{(2)} O, \quad (2.4)$$

$$F_2^{(1)} = C_2^{(1)} O + C_1 F_1^{(0)}. \quad (2.5)$$

Here $C_2^{(2)}$ and $C_2^{(1)}$ are "divergent constants."

Substituting Eqs. (2.3) — (2.5) into Eq. (2.1) we find

$$GF = G(O + e^2 C_1 d_l O + e^2 F_1^{(0)} + e^4 d_l^2 C_2^{(2)} O + e^4 d_l C_1 F_1^{(0)} + e^4 d_l C_2^{(1)} O + e^4 F_2^{(0)} + \ldots).$$

Accurate to within terms of higher order this means that

$$GF = G''(O + e^2 F_1^{(0)} + e^4 F_2^{(0)} + \ldots) = G'' F^{(0)}. \quad (2.6)$$

Here G'' is the weak-interaction coupling constant, renormalized by longitudinal and scalar photons:

$$G'' = G(1 + e^2 C_1 d_l + e^4 C_2^{(2)} d_l^2 + e^4 C_2^{(1)} d_l + \ldots). \quad (2.7)$$

The function F^0 requires further renormalization, as stated in Sec. 1, however it no longer depends on d_l. Consequently the dependence on d_l is contained entirely in the renormalization of the coupling constant G. An analogous situation occurs in mesodynamics, where the renormalization constant of the vertex operator including electrodynamic corrections depends, as is easily seen, on d_l.

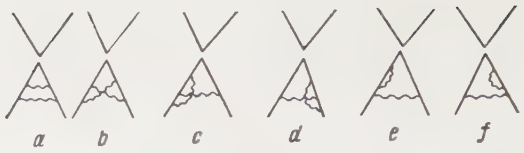

FIG. 3

Consequently, in order that the observable quantities be independent of d_l it is not necessary to impose any restrictions whatsoever on Z (Z_1 or Z_2). This is independent of what gauge invariant method is used to calculate other processes.

In contrast to this, in electrodynamics the condition of gauge invariance leads through the Ward identity to a relation between the normalization constants (or, which is the same, the cut-off momenta) for different processes. A relation is also established between the vertex diagram and the self-energy diagram. In this Section we have shown that the weak interaction matrix element is gauge invariant by itself, without imposing any conditions on the normalization constant. Therefore the normalization constant for the matrix element of each of the weak interaction processes is determined independently and represents an independent constant in the theory.

3. DISCUSSION

An elementary (but tedious) calculation of the matrix elements for μ and β decay, including bremsstrahlung, results in formulas for the probabilities of these processes of the type given in references 1 — 4 (including corrections due to recoil). These formulas, however, should contain additive terms corresponding to the finite arbitrariness noted above. At that it turns out, as was to be expected, that the parameters that characterize the spectrum (such as the Michel parameter and the asymmetry parameter) are independent of the normalization constant and are determined uniquely. At the same time the quantity G is determined from the lifetimes of the corresponding particles only in combination with the normalization constant C. Thus for μ decay it is only possible to determine the quantity $G[1 - (\alpha/2\pi)C] = G(1 - 0.001162\,C)$. No convincing arguments whatever are known at this

*Throughout we make use of the renormalized photon distribution function

$$D^{mn}(k) = k^{-2} d(k^2) [g^{mn} - k^{-2} k^m k^n] + d_l k^{-4} k^m k^n.$$

FIG. 4

time in favor of one or another choice of the normalization point.

In references 1, 3, and 4 a certain normalization for μ decay results essentially from the fact that the sum of the three divergent expressions, corresponding to the diagrams of Fig. 4, are assumed to be a definite number, in view of the generally accidental fact that the divergences cancel out. The authors of these papers forget, however, the arbitrariness that arises when divergent expressions are summed, and tacitly assume that the normalization constants (or, which is the same, the cut-off momenta) for the G-vertex and for the self energies of the electron and μ meson should necessarily coincide. The falsity of this point of view was discussed in Secs. 1 and 2. We can also note that the procedure used by these authors in substance prevents them from calculating corrections to the β decay even with a very rough account of the role of the strong interactions[8] through the constant form factor $\lambda = |G_A/G_V| = 1.2$.

With the help of dispersion-relations techniques Durand et al.[2] deduce unique expressions for the probabilities of μ and β decay, apparently from the condition that in the final expression the nonphysical photon mass λ_0 must vanish (i.e., in essence from the gauge invariance condition). It should, however, be noted that in applying the dispersion techniques to electromagnetic processes they automatically introduce into this field the determination of the renormalized coupling constant taken from the strong interactions. In reality the renormalized coupling constant can be determined in electrodynamics only when the emission of soft photons is taken into account. Therefore only the coupling constant determined in this way should be finite and independent of λ_0.* When this circumstance is taken into account the choice of a definite normalization point in the work of Durand et al.[2] is no longer unique.

In this way we are faced with a general situation in field theory of deducing experimental results from a theory in which the Lagrangians (0.1) — (0.4) are not fully known, and in which the constants (G, e, g, M, m, μ) entering these Lagrangians are not fully known. It is necessary, in addition, to specify a certain number C — the normalization constant. Only afterwards will the results be fully determined.

An analogous situation also arises in other versions of renormalizable theories. In electrodynamics, however, one usually introduces the additional boundary condition, which requires that the Coulomb law be satisfied at large distances. This means that the vertex operator is normalized at the point $k = 0$. In mesodynamics the determination of the g-charge as a subtraction at the point M corresponds to the normalization of the vertex operator as $\Lambda(M^2, M^2; m_\pi^2) = 1$. In the theory of μ and β decay there are no conditions of this type. For this reason we cannot have in this case a unique determination of the coupling constants G, G_A and G_V, related to each other. These constants can be determined only simultaneously with the normalization constant C, as discussed above.* Therefore, from our point of view, one should not talk about the existence of a discrepancy between theory and experiment, as is done by Feynman.[5]

If an intermediate boson, responsible for weak interactions, exists, one might expect that in that case it would be possible to relate the normalization constants for various weak interaction processes. However, until convincing arguments for the existence of such a boson are produced, the normalization constants of various processes (and, consequently, coupling constants) will remain unrelated to each other. It makes no sense therefore (even under the conserved vector current hypothesis) to talk at this time of the equality of coupling constants for various weak interaction processes to an accuracy better than the electromagnetic corrections.

In conclusion the authors express their gratitude to D. V. Shirkov and Ya. A. Smorodinskii for fruitful discussions, and also to A. I. Larkin, V. G. Vaks, and B. N. Valuev for valuable remarks.

[1] Behrends, Finkelstein, and Sirlin, Phys. Rev. **101**, 866 (1956). T. Kinoshita and A. Sirlin, Phys. Rev. **107**, 593, 638 (1957); **113**, 1652 (1959).

[2] Durand III, Landovitz, and Marr, Phys. Rev. Lett. **4**, 620 (1960).

[3] V. P. Kuznetsov, JETP **37**, 1102 (1960), Soviet Phys. JETP **10**, 787 (1960).

[4] S. Berman, Phys. Rev. **112**, 267 (1958).

*In the language of Durand et al.[2] the finite quantity should be the sum $G^2 + G^2C \ln(\lambda_0^2/m^2)$, and not G^2 itself.

*One can require the equality of renormalized coupling constants for various weak interaction processes. In that case the experimental lifetimes and cross sections will allow one to relate the normalization constants.

[5] R. P. Feynman, Rochester Conference on High Energy Physics, 1960 (preprint).

[6] M. Gell-Mann and R. P. Feynman, Phys. Rev. **109**, 193 (1958).

[7] V. P. Kuznetsov, JETP **39**, 1722 (1960), Soviet Phys. JETP **12**, 1202 (1961).

[8] M. L. Goldberger and S. B. Treiman, Phys. Rev. **110**, 1178 (1958). Chou Kuang-Chao, JETP **39**, 703 (1960), Soviet Phys. JETP **12**, 492 (1960).

[9] A. I. Alikhanov, Слабые взаимодействия и новейшие исследования β-распада (Weak Interactions and Recent Investigations of β Decay), Fizmatgiz. M., 1960.

[10] Y. Nambu, Axial Vector Current Conservation in Weak Interactions (preprint).

[11] R. A. Asanov and B. N. Valuev, On the Role of Higher Approximations for Weak Four-Fermion Interactions (preprint, Joint Institute for Nuclear Research).

[12] N. N. Bogolyubov and D. V. Shirkov, Introduction to Quantum Field Theory, Interscience, 1959.

[13] D. A. Slavnov and A. D. Sukhanov, The Vertex Function of the Four-Fermion Interaction in Perturbation Theory (preprint, Steklov Math. Inst. Acad. Sci.).

Translated by A. M. Bincer
297

MAGNETOHYDRODYNAMIC COMBUSTION

R. V. POLOVIN and V. P. DEMUTSKII

Physico-Technical Institute, Academy of Sciences, Ukr. S. S. R.

Submitted to JETP editor December 31, 1960

J. Exptl. Theoret. Phys. (U.S.S.R.) 40, 1746-1754 (June, 1961)

Possible combustion modes in a magnetohydrodynamic medium are determined. The types of magnetohydrodynamic shock and self-similar waves which can accompany magnetohydrodynamic combustion waves in the presence of a moving perfectly conducting piston are investigated. The piston velocity, the Alfvén velocity and the reaction energy are assumed to be sufficiently small. The conductivity of the medium is assumed to be infinite.

1. In recent years there has been an increased interest in new combustion modes. A number of papers is devoted to the problem of the combustion of fuel in a supersonic stream. In other papers, for example references 1 — 4, the effect of a magnetic field on detonation is investigated. In the present paper we investigate the effect of a magnetic field on the combustion process.

In ordinary hydrodynamics (in the absence of a magnetic field) two combustion modes are possible:

a) subsonic combustion

$$v_1 < c_1, \qquad v_2 < c_2; \tag{1}$$

b) supersonic combustion

$$v_1 > c_1, \qquad v_2 > c_2. \tag{2}$$

Here v is the velocity of the medium with respect to the discontinuity, c is the velocity of sound; subscript 1 refers to the region in front of the discontinuity and subscript 2 refers to the region behind the discontinuity.

If heating of the medium in front of the combustion wave occurs as a result of ordinary thermal conductivity then $v_1 \ll c_1$, and, therefore, supersonic combustion is usually impossible. Supersonic combustion can occur in the case of thermonuclear reactions when heating of the medium takes place by means of heat transfer by radiation; the supersonic combustion regime is also realized in the case of combustion in a supersonic stream.[5]

The difference between subsonic and supersonic combustion consists of the fact that in subsonic combustion the density is diminishing, while in supersonic combustion it is increasing.

In magnetohydrodynamics there exist three velocities of propagation of small disturbances: the Alfvén velocity $\mathbf{U} = \mathbf{H}/(4\pi\rho)^{1/2}$ and the velocities of propagation of the fast and the slow magnetoacoustic waves

$$U_\pm = \{U^2 + c^2 \pm [(U^2 + c^2)^2 - 4c^2 U_x^2]^{1/2}\}^{1/2}/\sqrt{2}$$

(the plus sign refers to the fast wave, and the minus sign refers to the slow wave, U_X is the component of the Alfvén velocity parallel to the direction of propagation of the wave). The existence of three characteristic velocities leads, as we shall see later, to the appearance of four magnetohydrodynamic combustion modes:

a) "slow" combustion

$$v_{1x} < U_{1-}, \qquad v_{2x} < U_{2-}; \tag{3}$$

b) "sub-Alfvén" combustion

$$U_{1-} < v_{1x} < U_{1x}, \qquad U_{2-} < v_{2x} < U_{2x}; \tag{4}$$

c) "super-Alfvén" combustion

$$U_{1x} < v_{1x} < U_{1+} \qquad U_{2x} < v_{2x} < U_{2+}; \tag{5}$$

d) "fast" combustion

$$U_{1+} < v_{1x}, \qquad U_x < v_{2x}. \tag{6}$$

(The subscript 1 refers to the region in front of the discontinuity, and the subscript 2 to the region behind the discontinuity; we recall that $U_- \leq U_X \leq U_+$.)

The difference between the four magnetohydrodynamic combustion modes lies not only in the different manner of density variation, but also in the different nature of variation of the magnetic field. As we shall show later, in the case of the slow and the super-Alfvén combustion the density is decreasing, while in the case of the sub-Alfvén and the fast combustion it is increasing. The magnetic field increases in the case of fast and slow combustion, and decreases in the case of the sub-Alfvén and the super-Alfvén combustion.

In magnetohydrodynamics, if the condition $U_1 \ll c_1$ is satisfied, slow, sub-Alfvén and super-Alfvén combustion can occur at temperatures common in the case of chemical reactions, and fast combustion can occur at thermonuclear temperatures.

Condensation discontinuities and photoionization discontinuities belong to the same type of discontinuities as combustion waves. Photoionization discontinuities occur in neutral interstellar gas in the case of intense radiation from a star (cf. references 6 — 8). The excess of photon energy over the ionization energy is released in the form of heat energy q. The velocity of propagation of a photoionization discontinuity can be both smaller than and greater than the velocity of sound.

2. At the surface of discontinuity the laws of conservation of mass, momentum and energy hold, and also the values of the tangential electric and of the normal magnetic field remain continuous:

$$\{(v_x - \zeta)/V\} = 0, \tag{7}$$

$$\{p + (v_x - \zeta)^2/V + H_y^2/8\pi\} = 0, \tag{8}$$

$$\{\gamma pV/(\gamma - 1) + (v_x - \zeta)^2/2 + v_y^2/2 + VH_y^2/4\pi - VH_xH_yv_y/4\pi\,(v_x - \zeta)\} = q, \tag{9}$$

$$\{(v_x - \zeta)\,v_y/V - H_xH_y/4\pi\} = 0, \tag{10}$$

$$\{H_xv_y - (v_x - \zeta)\,H_y\} = 0, \tag{11}$$

$$\{H_x\} = 0, \tag{12}$$

where $V \equiv 1/\rho$ is the specific volume, v is the velocity of the medium, ζ is the velocity of propagation of the combustion wave in the laboratory system of coordinates, p is the pressure, γ is the index of the Poisson adiabat which we assume for the sake of simplicity to be the same on both sides of the discontinuity, q is the energy released at the surface of discontinuity ($q > 0$); the x axis is directed normal to the discontinuity, and the system of coordinates is chosen in such a way as to make $H_Z \equiv 0$ and $v_Z \equiv 0$.

The conservation laws (7) — (12) are insufficient to determine the combustion mode uniquely. In order for combustion actually to take place it is necessary that in addition the evolutionary conditions should also be satisfied.[9-11] They consist of the requirement that the number of divergent waves on both sides of the surface of discontinuity should be equal to the number of independent boundary conditions.

Unlike shock waves and overcompressed detonation waves, the speed of propagation of a combustion wave in a medium at rest does not depend on the amplitude of the wave, but is determined by the physico-chemical characteristics of the medium in front of the wave.[12] Therefore, when a combustion wave is perturbed the velocity of propagation of the wave remains constant. This leads to the result that in order for the evolutionary conditions to be satisfied in ordinary hydrodynamics (in the absence of a magnetic field) the number of diverging waves must be equal to three, while in magnetohydrodynamics the number of diverging waves must be equal to seven. From this it follows that only such combustion waves are possible for which the inequalities (1), (2), and (3) — (6) are satisfied. The evolutionary conditions (3) — (6) restrict the number of waves which can be simultaneously propagated in one direction.

In the case of fast combustion the combustion wave can be followed by a fast magnetoacoustic (shock or self-similar) wave, and this can be followed by an Alfvén discontinuity, and, finally, by a slow (shock or self-similar) wave. Not a single one of the magnetohydrodynamic waves can be propagated ahead of the fast combustion wave.

In the case of super-Alfvén combustion the fast (shock or self-similar) wave leads, followed by a super-Alfvén combustion wave, then by an Alfvén discontinuity and, finally, by a slow wave.

In the case of sub-Alfvén combustion the fast wave leads, followed by the Alfvén discontinuity, then by a sub-Alfvén combustion wave and, finally, by a slow wave.

In the case of slow combustion the fast wave leads, followed by the Alfvén discontinuity, then by a slow wave and, finally, by a slow combustion wave.

Some of these waves may be absent.

3. In order to distinguish the actually occurring evolutionary waves from the unrealizable nonevolutionary ones, we utilize the (v_{1X}, v_{2X}) plane in which the characteristic velocities U_-, U_X, U_+ are marked (cf. Fig. 1).

We first consider shock waves unaccompanied by a release of energy ($q = 0$). By utilizing the boundary conditions (7) — (12) ($\zeta = 0$) we can determine the Hugoniot line in the (v_{1X}, v_{2X}) plane. From the calculations of Bazer and Ericson[13,14] it follows that the values v_{1X} and v_{2X} lie on the line 1—2—3—4—5—6 in the case of slow waves, and on the line 7—8—9 for fast waves (cf. Fig. 1). The line 0—1—4—8—32 corresponds to the absence of a discontinuity $v_{1X} = v_{2X}$.

The segments 1—2—3—4 and 8—9 correspond to compressional shock waves $v_{1X} > v_{2X}$. In such waves the entropy is increasing.[14-15]

For $v_{1X} \to \infty$ the line 8—9 has the asymptote $v_{2x}^2 = (\gamma - 1)\,U_{2+}^2/2\gamma + (\gamma + 1)\,U_{2x}^2/2\gamma$ $(U \ll c)$.

The segments 4—5—6—1 and 7—8 correspond to rarefaction shock waves $v_{1X} < v_{2X}$. In such waves the entropy is decreasing and, therefore, such waves cannot be realized.

The conditions for the shock waves to be evolutionary are of the following form[9,18-19]:

a) for the slow wave

$$U_{1-} < v_{1x} < U_{1x}, \qquad v_{2x} < U_{2-}; \tag{13}$$

b) for the fast wave

$$U_{1+} < v_{1x}, \qquad U_{2x} < v_{2x} < U_{2+} \tag{14}$$

The regions (13) and (14) are marked in Fig. 1 by vertical shading.

As can be seen from Fig. 1, the fast compression wave is an evolutionary wave along the whole segment 8—9, i.e., for arbitrary amplitudes. The slow compressional shock wave is evolutionary only along the segment 1—2. Along the segment 2—3—4 the slow compressional shock wave is a nonevolutionary one, and cannot be realized in spite of the fact that the entropy in such a wave is increasing.

We now consider discontinuities at which energy is released ($q > 0$). Such discontinuities are shown for $U \ll c$ and $q \ll c^2$ by the lines 0—10—11—12—4—13—14—15—4—16—17 and 18—19—20 in Fig. 1. Near the point $v_{1X} = U_{1-}$, $v_{2X} = U_{2-}$ these lines are described by the equation

$$(v_{1x} - U_{1-})^2 - (v_{2x} - U_{2-})^2 = \tfrac{3}{2}(\gamma - 1)\, q c_1^{-4} U_{1x}^2 U_{1y}^2, \tag{15}$$

near the point $v_{1X} = U_{1X}$, $v_{2X} = U_{2X}$ they are described by the equation

$$(v_{1x} - U_{1x})^2 - [1 - 2(\gamma - 1)\, q\, U_{1y}^{-2}]\,(v_{2x} - U_{2x})^2 = 0 \tag{16}$$

and, finally, near the point $v_{1X} = U_{1+}$, $v_{2X} = U_{2+}$ they are described by the equation

$$(v_{1x} - U_{1+})^2 - (v_{2x} - U_{2+})^2 = \tfrac{1}{2}(\gamma^2 - 1)\, q. \tag{17}$$

For $v_{1X} \ll U_{1-}$ this line is described by the equation

$$v_{2x} = [1 + (\gamma - 1)\, c_1^{-2} q]\, v_{1x}. \tag{18}$$

The segment 0—10 corresponds to slow combustion (rarefaction wave), the segment 15—4 corresponds to sub-Alfvén combustion (compression wave), the segment 4—16 corresponds to super-Alfvén combustion (rarefaction wave) and, finally, the segment 18—19 corresponds to fast combustion (compression wave). The segments 14—15 and 19—20 correspond to detonation in the case of slow and fast waves (compressional waves). Points 15 and 19 correspond to Chapman-Jouguet detonation in the case of slow and fast waves. The

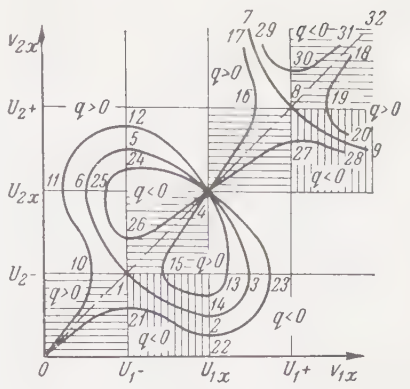

FIG. 1

segments 10—11—12—4—13—14 and 16—17 correspond to nonevolutionary discontinuities and, therefore, cannot be realized.

Figure 1 also shows discontinuities corresponding to absorption of energy ($q < 0$). Such discontinuities correspond to the lines 0—21—22—23—4—24—25—26—4—27—28 and 29—30—31. The segment 21—22 corresponds to ionization in the case of a slow shock wave, the segment 27—28 corresponds to ionization in the case of a fast shock wave.[4]

The boundary conditions (10)—(12) enable us to determine the change in the magnetic field in combustion waves.

From (10) and (11) it follows that

$$H_{2y} = \frac{1/\rho_1 - H_x^2/4\pi j^2}{1/\rho_2 - H_x^2/4\pi j^2} H_{1y} \tag{19}$$

($j = \rho_1 v_{1X} = \rho_2 v_{2X}$). From Eqs. (3)—(6) and (19) it follows that in all four magnetohydrodynamic combustion waves the transverse magnetic field H_y does not change sign. Taking into account the fact that both in slow and in super-Alfvén combustion the density is decreasing ($\rho_2 < \rho_1$), while in the case of sub-Alfvén and of fast combustion the density is increasing ($\rho_2 > \rho_1$), we obtain from (19) that in cases of slow and of fast combustion the transverse magnetic field H_y is increasing, while in cases of sub-Alfvén and super-Alfvén combustion the transverse magnetic field is decreasing.

4. We now go on to the question of the types of magnetohydrodynamic waves that can accompany a combustion wave. In order to simplify the problem we assume that the medium is bounded by a perfectly conducting piston moving with constant velocity **u**. Moreover, we assume that the piston velocity and the Alfvén velocity U are both much smaller than the velocity of sound c, and that the reaction energy q is much smaller than the square of the velocity of sound. We restrict ourselves to

the case in which the magnetic field, the piston velocity and the normal to the piston surface all lie in the same plane (the xy plane).

We first consider fast combustion. The conservation laws (7) — (12) enable us to express the discontinuities in the velocity, and the discontinuity in the specific volume, in terms of the velocity of propagation of the combustion front v_{1X} with respect to a stationary medium ($\zeta = 0$). The corresponding formulas can be greatly simplified in the limiting case $v_{1X} \gg c$:

$$\Delta_c v_x = (\gamma - 1)\, q/v_{1x}, \qquad \Delta_c v_y = -(\gamma - 1)\, U_x U_y q/v_{1x}^3,$$
$$\Delta_c V = -(\gamma - 1)\, qV/v_{1x}^2. \tag{20}$$

As a result of electrodynamic viscosity[20] the relative velocity of the medium is equal to zero at the surface of the piston. Therefore, the sum of the discontinuities of the velocity for all the waves is equal to the velocity of the piston:

$$\Delta_c \mathbf{v} + \Delta_+ \mathbf{v} + \Delta_A \mathbf{v} + \Delta_- \mathbf{v} = \mathbf{u}, \tag{21}$$

where $\Delta_c \mathbf{v}$ denotes the discontinuity in the velocity of the combustion wave. $\Delta_\pm$ is the discontinuity for the fast and the slow magnetohydrodynamic waves (without release or absorption of energy) and Δ_A is the amount of the Alfvén discontinuity. These discontinuities in the velocity are related to the discontinuity in the specific volume by means of the following relations:[4]

$$\Delta_+ v_x = -c\left(1 - \frac{\gamma+1}{4}\frac{\Delta_+ V}{V}\right)\frac{\Delta_+ V}{V},$$

$$\Delta_+ v_y = \frac{U_x U_y}{c}\left(1 - \frac{3-\gamma}{4}\frac{\Delta_+ V}{V}\right)\frac{\Delta_+ V}{V}; \tag{22}$$

$$\Delta_- v_x = -U_x \frac{\Delta_- V}{V}, \qquad \Delta_- v_y = -\frac{c^2}{U_y}\frac{\Delta_- V}{V}; \tag{23}$$

$$\Delta_A v_x = 0, \qquad \Delta_A v_y = 2U_y. \tag{24}$$

Formulas (23) are valid only if the additional restriction $|\Delta_- V/V| \ll U_y^2/c^2$ is imposed.

By taking the components of expression (21) along the x and y axes, and by expressing $\Delta_\pm \mathbf{v}$ in terms of $\Delta_+ V$ and $\Delta_- V$, we obtain a system of two equations in two unknowns: $\Delta_+ V$ and $\Delta_- V$. This system enables us to find the amplitudes of the fast and the slow magnetohydrodynamic waves, $\Delta_+ V$ and $\Delta_- V$. If $\Delta_\pm V < 0$ then the corresponding wave will be a shock wave, if $\Delta_\pm V > 0$, then the wave will be a self-similar one.

The possible types of magnetohydrodynamic waves accompanying a fast combustion wave are shown in Fig. 2a. In this diagram the longitudinal component of the velocity of the piston u_X has been plotted along the abscissa, and the transverse component u_Y has been plotted along the ordinate. (For the sake of definiteness we assume that the components H_X, H_Y of the magnetic field in the unperturbed medium are positive.) The letters C, S, R, A denote respectively the presence of the following waves: combustion, shock, rarefaction, and Alfvén discontinuity. The plus sign refers to the fast wave, the minus sign refers to the slow wave. The sequence in which the letters appear coincides with the sequence in which the waves follow each other.

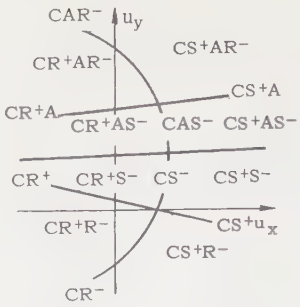

FIG. 2a

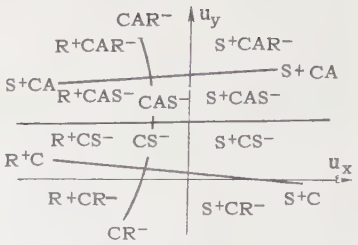

FIG. 2b

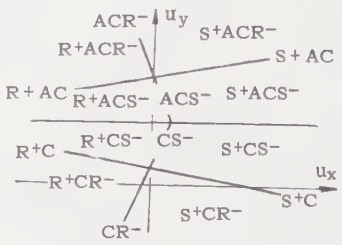

FIG. 2c

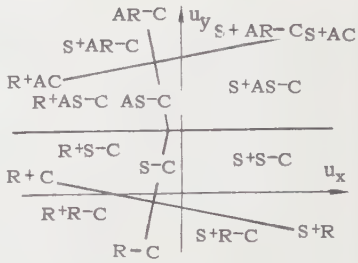

FIG. 2d

The origin in Fig. 2a lies in the region CR^+R^-. This means that in the case when the piston is at rest the fast combustion wave leads the others, it is followed first by the fast rarefaction wave and, finally, by the slow rarefaction wave. The same sequence of waves will also occur in the case when the piston is moving outward ($u_X < 0$, $u_Y = 0$). If the piston is moving inward ($u_X > 0$, $u_Y = 0$), then for sufficiently low velocity u_X we shall have the same combination of waves: CR^+R^-. As the piston velocity is increased the amplitudes of the fast and of the slow rarefaction waves diminish and, finally, vanish at the point where the horizontal axis intersects the lines CR^-, CS^-, CR^+, CS^+. (In the first approximation these lines intersect in one point.) As the piston velocity is increased further, we enter the region CS^+S^-.

In the case of transverse motion of the piston ($u_X = 0$) in the direction opposite to the direction of the transverse magnetic field in the unperturbed medium ($u_Y < 0$, $H_Y > 0$), with sufficiently low velocity $|u_Y|$ the same sequence of waves CS^+S^- occurs as in the case of the piston at rest. As the velocity $|u_Y|$ is increased the amplitude of the fast rarefaction waves diminishes and, finally,

vanishes on the line CR^-. This line separates the region CR^+R^- from the region CS^+R^- which is entered as the piston velocity $|u_y|$ is increased further.

In the case of the transverse motion of the piston ($u_x = 0$) in the direction of the magnetic field ($u_y > 0$, $H_y > 0$) with a sufficiently low velocity the same sequence of waves CR^+R^- occurs as in the case of the piston at rest. As the piston velocity is increased, the amplitude of the slow rarefaction wave diminishes and vanishes on the line CR^+. As the piston velocity u_y increases further a slow shock wave appears (regions CR^+S^-) whose amplitude increases with increasing piston velocity. Since in the case of the slow shock wave the transverse magnetic field H_y diminishes[17] (without changing sign), an increase in the transverse piston velocity u_y in the region CR^+S^- corresponds to a decrease in the transverse magnetic field H_y at the surface of the piston. When the piston velocity u_y becomes equal to

$$U_y - \frac{\gamma - 1}{2} \frac{U_y q}{c v_{1x}}$$

[cf. formula (28)], the transverse magnetic field H_y behind the slow shock wave (i.e., at the surface of the piston) vanishes.

As the piston velocity u_y increases further a sharp qualitative change in the flow pattern takes place. Behind the fast rarefaction wave R^+ an Alfvén wave A appears which changes the direction of the magnetic field by 180°, and the Alfvén wave is followed by a slow shock wave S^-. On the line separating the regions CR^+S^- and CR^+AS^- the amplitude of the slow shock wave reaches a maximum. As the piston velocity u_y increases the amplitude of the slow shock wave decreases, and this leads to an increase in the absolute value of the transverse magnetic field $|H_y|$ at the surface of the piston. In this case the transverse magnetic field at the surface of the piston is directed opposite to the transverse magnetic field in the unperturbed medium. Along the line CR^+A the amplitude of the slow shock wave vanishes, and as u_y increases further a slow rarefaction wave appears (region CR^+AR^-).

If we continue to increase the transverse piston velocity u_y, then the amplitude of the fast rarefaction wave diminishes, and vanishes along the line CAR^-. A further increase in the velocity of the piston u_y leads to the appearance of a fast shock wave (region CS^+AR^-). As can be seen from Fig. 2a, fast combustion is possible for any arbitrary piston velocity u.

The equations of the lines bounding the various regions in Fig. 2a are of the following form:

the lines CR^-, CS^-, CAS^-, CAR^-

$$u_x + \frac{U_x}{2c^2}(u_y - 2U_y)\, u_y - (\gamma - 1)\frac{q}{v_{1x}} = 0, \qquad (25)$$

the lines CR^+, CS^+

$$u_y + \frac{U_x U_y}{c^2} u_x - (\gamma - 1)\frac{U_x U_y q}{v_{1x} c^2} = 0, \qquad (26)$$

the lines CR^+A, CS^+A

$$u_y - 2U_y - \frac{U_y}{c} u_x + (\gamma - 1)\frac{U_y q}{v_{1x} c} = 0. \qquad (27)$$

The line separating the regions CR^+S^- and CR^+AS^-, and also the line between the regions CS^+S^- and CS^+AS^-, is determined by the equation

$$u_y - U_y - \frac{1}{2}\frac{U_y}{c} u_x + \frac{\gamma - 1}{2}\frac{U_y q}{v_{1x} c} = 0. \qquad (28)$$

5. We now proceed to consider super-Alfvén combustion. The discontinuities in the velocity and in the specific volume in a super-Alfvén combustion wave are determined in the limiting case $U_{1X} \ll v_{1X} \ll U_{1+}$ by the relations

$$\Delta_c v_x = -(\gamma - 1)\, q v_{1x}/c^2, \qquad \Delta_c v_y = (\gamma - 1)\, U_x U_y q / v_{1x} c^2;$$
$$\Delta_c V = (\gamma - 1)\, qV/c^2. \qquad (29)$$

The possible types of magnetohydrodynamic waves accompanying a super-Alfvén combustion wave are shown in Fig. 2b.

The equations of the lines bounding the various regions of Fig. 2b are of the following form:

the lines CR^-, CS^-, CAS^-, CAR^-

$$u_x + \frac{U_x}{2c^2}(u_y - 2U_y)\, u_y + (\gamma - 1)\frac{q v_{1x}}{c^2} = 0, \qquad (30)$$

the lines R^+C, S^+C

$$u_y + \frac{U_x U_y}{c^2} u_x - (\gamma - 1)\frac{U_x U_y q}{v_{1x} c^2} = 0, \qquad (31)$$

the lines R^+CA, S^+CA

$$u_y - 2U_y - \frac{U_y}{c} u_x + (\gamma - 1)\frac{U_y}{c^2} q = 0. \qquad (32)$$

The line separating the regions R^+CS^- and R^+CAS^-, and also the line separating the regions S^+CS^- and S^+CAS^- are determined by the equation

$$u_y - U_y - \frac{1}{2}\frac{U_y}{c} u_x + \frac{\gamma - 1}{2}\frac{U_y q}{c^2} = 0. \qquad (33)$$

As can be seen from Fig. 2b, super-Alfvén combustion is possible for any arbitrary piston velocity u.

6. We now consider sub-Alfvén combustion in the limiting case $U_X - v_{1X} \ll U_X$. The discontinuities in the velocity and in the specific volume in the sub-Alfvén combustion wave are determined by the relation

$$\Delta_c v_x = 2(\gamma - 1)\frac{U_x - v_{1x}}{U_y^2} q, \qquad \Delta_c v_y = (\gamma - 1)\frac{q}{U_y},$$

$$\Delta_c V = -2(\gamma - 1)\frac{U_x - v_{1x}}{U_x U_y^2} qV. \tag{34}$$

The possible types of magnetohydrodynamic waves accompanying a sub-Alfvén combustion wave are shown in Fig. 2c. The equations of the lines bounding the various regions in Fig. 2c have the following form:

the lines CR^-, CS^-

$$u_x - \frac{U_x U_y}{c^2} u_y + (\gamma - 1)\frac{U_x}{c^2} q = 0, \tag{35}$$

the lines ACS^-, ACR^-

$$u_x + \frac{U_x U_y}{c^2}(u_y - 2U_y) + (\gamma - 1)\frac{U_x}{c^2} q = 0, \tag{36}$$

the lines R^+C, S^+C

$$u_y + \frac{U_x U_y}{c^2} u_x - (\gamma - 1)\frac{q}{U_y} = 0, \tag{37}$$

the lines R^+AC, S^+AC

$$u_y - 2U_y - \frac{U_y}{c} u_x + (\gamma - 1)\frac{q}{U_y} = 0. \tag{38}$$

As can be seen from Fig. 2c, sub-Alfvén combustion is possible for any arbitrary piston velocity u.

7. Finally, we consider slow combustion in the limiting case $v_{1X} \ll U_X$. The discontinuities in the velocity and in the specific volume in the slow combustion wave are determined by the relations

$$\Delta_c v_x = -(\gamma - 1)\, q v_{1x}/c^2,$$

$$\Delta_c v_y = -(\gamma - 1)\, U_y q v_{1x}/c^2 U_x,$$

$$\Delta_c V = (\gamma - 1)\, qV/c^2. \tag{39}$$

The possible types of magnetohydrodynamic waves accompanying the slow combustion wave are shown in Fig. 2d.

The equations of the lines bounding the various regions in Fig. 2d have the following form:

the lines R^-C, S^-C

$$u_x - \frac{U_x U_y}{c^2} u_y + (\gamma - 1)\frac{q v_{1x}}{c^2} = 0, \tag{40}$$

the lines AS^-C, AR^-C,

$$u_x + \frac{U_x U_y}{c^2}(u_y - 2U_y) + (\gamma - 1)\frac{q v_{1x}}{c^2} = 0, \tag{41}$$

the lines R^+C, S^+C

$$u_y + \frac{U_x U_y}{c^2} u_x + (\gamma - 1)\frac{U_y q v_{1x}}{c^2 U_x} = 0, \tag{42}$$

the lines R^+AC, S^+AC

$$u_y - 2U_y - \frac{U_y}{c} u_x - (\gamma - 1)\frac{U_y q v_{1x}}{c^2 U_x} = 0. \tag{43}$$

As can be seen from Fig. 2d, slow combustion is possible for any arbitrary piston velocity u.

The authors express their gratitude to A. I. Akhiezer for valuable discussions.

[1] É. Larish and I. Shekhtman, JETP **35**, 203 (1958), Soviet Phys. JETP 8, 139 (1959).

[2] Gross, Chinitz, and Rivlin, J. Aero Space Sci. **27**, 283 (1960).

[3] G. A. Lyubimov, Dokl. Akad. Nauk SSSR **126**, 532 (1959), Soviet Phys. Doklady **4**, 526 (1960).

[4] V. P. Demutskii and R. V. Polovin, J. Tech. Phys. (U.S.S.R.) **31**, 419 (1961), Soviet Phys. Tech. Phys. **6**, 302 (1961).

[5] Ya. B. Zel'dovich and A. S. Kompaneets, Теория детонации (The Theory of Detonation), Gostekhizdat, 1955, p. 112.

[6] S. R. Pottasch, Revs. Modern Phys. **30**, 1053 (1958).

[7] F. D. Kahn, ibid. **30**, 1058 (1958).

[8] A. Goldsworthy, ibid. **30**, 1062 (1958).

[9] Akhiezer, Lyubarskii, and Polovin, JETP **35**, 731 (1958), Soviet Phys. JETP 8, 507 (1959).

[10] I. M. Gel'fand, Usp. Mat. Nauk **14**, 87 (1959).

[11] R. V. Polovin, Usp. Fiz. Nauk **72**, 33 (1960), Soviet Phys. Uspekhi **3**, 677 (1961).

[12] L. D. Landau and E. M. Lifshitz, Механика сплошных сред (Mechanics of Continuous Media), Gostekhizdat, 1953.

[13] J. Bazer and W. B. Ericson, Astrophys. J. **129**, 758 (1959).

[14] W. B. Ericson and J. Bazer, Phys. Fluids **3**, 631 (1960).

[15] S. V. Iordanskii, Dokl. Akad. Nauk SSSR **121**, 610 (1958), Soviet Phys. Doklady **3**, 736 (1959).

[16] R. V. Polovin and G. Ya. Lyubarskii, JETP **35**, 510 (1958), Soviet Phys. JETP 8, 351 (1959).

[17] R. V. Polovin and G. Ya. Lyubarskii, Ukr. Phys. J. **3**, 571 (1958).

[18] V. M. Kontorovich, JETP **35**, 1216 (1958), Soviet Phys. JETP 8, 851 (1959).

[19] S. I. Syrovat-skii, JETP **35**, 1466 (1958), Soviet Phys. JETP 8, 1024 (1959).

[20] G. Ya. Lyubarskii and R. V. Polovin, Dokl. Akad. Nauk SSSR **128**, 684 (1959), Soviet Phys. Doklady **4**, 977 (1960).

Translated by G. Volkoff
298

SINGULARITY IN THE SCHWARZSCHILD SOLUTION OF THE GRAVITATION EQUATIONS

Yu. A. RYLOV

Moscow State University

Submitted to JETP editor January 3, 1961

J. Exptl. Theoret. Phys. (U.S.S.R.) 40, 1755-1757 (June, 1961)

Schwarzschild's solution of the gravitational field equations has a singularity at the gravitational radius. It is shown that this singularity can be removed by a suitable choice of coordinate system. Examples of such coordinate systems are given.

THE centrally symmetric solution of Einstein's field equations in empty space is (see reference 1, Sec. 97)

$$ds^2 = \left(1 - \frac{1}{r}\right) dt^2 - \left(1 - \frac{1}{r}\right)^{-1} dr^2 - r^2 d\sigma^2,$$
$$d\sigma^2 = d\vartheta^2 + \sin^2\vartheta \cdot d\varphi^2. \qquad (1)$$

The units have been chosen so that $c = 1$ and $\alpha = 2kM/c^2 = 1$. The solution (1) has a singularity at $r = 0$ and also at $r = 1$, which is the so-called gravitational radius. Finkelstein has attempted to remove the singularity at the gravitational radius by a suitable choice of coordinate system.[2] In his coordinates the line element is

$$ds^2 = \left(1 - \frac{1}{r}\right) dt^2 + \frac{2}{r} dt dr + \left(1 + \frac{1}{r}\right) dr^2 - r^2 d\sigma^2. \qquad (2)$$

This line element suffers from the disadvantage that g_{tt} changes sign at $r = 1$, which means that for $r > 1$ t is a time-like coordinate, while for $r < 1$, t is a space-like coordinate. It should also be pointed out that Finkelstein's coordinates are not orthogonal. Fronsdal[3] embedded the Scharzschild space in a flat six dimensional manifold and showed that for a stationary metric (i.e. independent of coordinate time), the singularity at $r = 1$ could not be removed by a coordinate transformation. If nonstationary metrics were allowed, then the singularity at $r = 1$ could be removed. Although Fronsdal showed how this could be done, he did not actually do it.

The purpose of the present note is to present some coordinate systems which do not have the singularity.

Consider the coordinate transformation

$$\tau = t - \int \frac{r dr}{(r-1) f(r)}, \qquad \xi = \int \frac{r f(r)}{r-1} dr - t, \qquad (3)$$

where $f(r)$ satisfies the conditions $f'(1) \neq 0$, $f^2(1) = 1$, $f^2(r) > 1$ for $r > 1$, $f^2(r) < 1$ for $r < 1$.

In the new coordinate system the line element is

$$ds^2 = \frac{r-1}{r(1 - f^{-2}(r))} \left(d\tau^2 - \frac{d\xi^2}{f^2(r)}\right) - r^2 d\sigma^2. \qquad (4)$$

$f(r)$ has been chosen so that $1 - f^{-2}$ has a first order zero at $r = 1$, so that the line element (4) does not have a singularity at $r = 1$.

For the particular case $f(r) = r^2 - r + 1$, we have

$$\tau = t - \frac{1}{2} \ln \frac{(r-1)^2}{r^2 - r + 1} + \frac{1}{\sqrt{3}} \tan^{-1} \left[\frac{2}{\sqrt{3}}\left(r - \frac{1}{2}\right)\right],$$
$$\xi = r^3/3 + r + \ln|r - 1| - t. \qquad (5)$$

The transformation (5) is single valued (in both directions) for all values of (r, t). Upon carrying out the further transformation $\rho = (3\xi)^{1/3}$, the expression (4) takes the form

$$ds^2 = \frac{(\psi^2 - \psi + 1)^2}{(\psi^2 - \psi + 2)\psi^2} d\tau^2 - \frac{\rho^4 d\rho^2}{(\psi^2 - \psi + 2)\psi^2} - \psi^2 d\sigma^2, \qquad (6)$$

in the coordinates (ρ, τ), where $\psi = \psi(\rho^2/3 + \tau)$ and $\psi(y)$ is defined by the equation

$$y = \frac{\psi^3}{3} + \psi + \frac{1}{2} \ln(\psi^2 - \psi + 1) + \frac{1}{\sqrt{3}} \tan^{-1}\left[\frac{2}{\sqrt{3}}\left(\psi - \frac{1}{2}\right)\right]. \qquad (7)$$

Since the right hand side of (7) is a monotonic function of ψ, $\psi(y)$ is a single valued function of its argument. For finite τ and $\rho \to \infty$ (6) may be written in the approximate form

$$ds^2 = (1 - 1/\rho)\, d\tau^2 + (1 + 1/\rho)\, d\rho^2 - \rho^2 d\sigma^2. \qquad (8)$$

Formula (8) agrees with (1) for large values of $\rho = r$. Thus for $\rho \to \infty$ the coordinate system (ρ, τ) is the same as Schwarzschild's coordinate system, but differs from the latter in that it has no singularity at the gravitational radius.

Upon substituting $f(r) = \sqrt{r}$ in (3) we obtain

$$x^1 = \frac{2\sqrt{r}}{3}(r + 3) + \ln\left|\frac{\sqrt{r} - 1}{\sqrt{r} + 1}\right| - t,$$
$$x^0 = t - 2\sqrt{r} - \ln\left|\frac{\sqrt{r} - 1}{\sqrt{r} + 1}\right|; \qquad (9)$$

$$ds^2 = (dx^0)^2 - \left[\tfrac{3}{2}(x^1 + x^0)\right]^{-2/3} (dx^1)^2 - \left[\tfrac{3}{2}(x^1 + x^0)\right]^{4/3} d\sigma^2; \qquad (10)$$

$$r = [\tfrac{3}{2}(x^1 + x^0)]^{2/3},$$
$$t = x^0 + 2[\tfrac{3}{2}(x^1 + x^0)]^{1/3} + \ln\left|\frac{[3(x^1 + x^0)/2]^{1/3} - 1}{[3(x^1 + x^0)/2]^{1/3} + 1}\right|. \quad (11)$$

The coordinate system (x^0, x^1) has the following properties: 1) the time coordinate is the time read by a clock moving on the coordinate lines x^1, ϑ, φ = const, 2) the lines x^1, ϑ, φ = const are geodesics, so that the coordinate system (x^0, x^1) can be realized by freely falling bodies carrying clocks. It is a "freely falling" coordinate system. It follows from (11) that the transformation from (x^0, x^1) to (r, t) is single valued. The transformation from (r, t) to (x^0, x^1) is double valued, which corresponds to the two possible square roots of r. This can be explained as follows: in the coordinate system (r, t) a freely falling body (x^1, ϑ, φ = const) will reach $r = 0$ in a finite proper time, and upon "reflection" will retrace its path. This explains the double-valuedness of the transformation (9), with a branch point at $r = 0$. In other words, the point (r, t) can correspond to an incoming particle or an outgoing particle.

In conclusion, we should like to point out (see also reference 4) that the singularity at $r = 1$ in Schwarzschild's coordinate system is associated with the fact that the coordinates change character upon passing through $r = 1$: the space-like coordinates become time-like, while the time-like ones become space-like. This is clear from (1), for if $r > 1$, then r is space-like ($g_{rr} < 0$) and t is time-like ($g_{tt} > 0$), while for $r < 1$, the situation is reversed ($g_{rr} > 1$, $g_{tt} < 0$). The transformation (3) avoids this state of affairs; for suitable choice of $f(r)$ the coordinate ξ is space-like everywhere ($g_{\xi\xi} < 0$ everywhere), while τ is time-like everywhere ($g_{\tau\tau} > 0$ everywhere).

I should like to thank Prof. Ya. P. Terletskii for his interest in this work.

[1] L. D. Landau and E. M. Lifshitz, Теория поля (Theory of Fields), 2d ed., Gostekhizdat (1960);
[2] D. Finkelstein, Phys. Rev. **110**, 965 (1958).
[3] C. Fronsdal, Phys. Rev. **116**, 778 (1959).
[4] I. D. Novikov, Астрономический журнал **38**, No. 3 (1961), Soviet Astronomy **5**, in press.

Translated by R. Krotkov
299

CAUSALITY CONDITIONS IN QUANTUM FIELD THEORY

V. Ya. FAĬNBERG

P. N. Lebedev Physics Institute, Academy of Sciences, U.S.S.R.

Submitted to JETP editor January 4, 1961

J. Exptl. Theoret. Phys. (U.S.S.R.) 40, 1758-1767 (June, 1961)

It is shown that the Bogolyubov causality condition and the condition of local commutativity of the operators $\varphi(x)$ of an interacting field lead to identical expressions for the matrix elements of the S matrix on the mass shell. In the study of this problem the necessary and sufficient conditions are found for the local solubility of the equation for the Heisenberg operators $\varphi(x)$ on the assumption that the commutator of the currents, $[j(x), j(y)]$, vanishes outside the light cone; that is, the so-called Wightman problem is solved.

1. INTRODUCTION

THE fundamental problem of relativistic quantum field theory is that of finding the properties of the matrix elements of the S matrix on the mass shell of real particles, i.e., for free-particle values of the four-momenta of all incident and scattered particles, $p_i^2 = m_i^2$ (here $p_i^2 = (p_i^0)^2 - (\mathbf{p}_i)^2$, and i indicates the type of particle). In the case of the Lagrangian formulation these properties are a consequence of the Heisenberg equations for the operators of the interacting field and the commutation relations. For a formulation of the local properties of the theory without the assumption of the existence of a Lagrangian (i.e., a dynamical principle), however, it is necessary to go outside the limits of the mass shell in the S matrix. In the axiomatic approach there are two main methods for accomplishing such an extrapolation.

The first method was proposed by Bogolyubov[1,2] and is as follows.* The S matrix is represented in the form of a functional of the free-field operators $[\varphi_{in}(x)$ and $\varphi_{out}(x)]$

$$S = \sum_{n=0}^{\infty} \frac{1}{n!} \int d^4x_1 \ldots d^4x_n S_n(x_1, \ldots x_n) : \varphi_{in}(x_1) \ldots \varphi_{in}(x_n) : . \quad (1)$$

Here the colon indicates the normal product. For simplicity we shall consider the case of a neutral scalar field of mass m and assume that it does not form any bound states. The operators $\varphi_{in,out}(x)$ satisfy the homogeneous Klein-Gordon equation

$$(\Box - m^2)\, \varphi_{in,\, out}(x) = 0 \quad (2)$$

and obey the commutation relations

$$[\varphi_{in,\, out}(x),\ \varphi_{in,\, out}(y)] = -i\Delta(x-y,\ m)\,. \quad (3)$$

The S matrix is assumed unitary,

$$S^+S = 1, \quad (4)$$

and we have

$$\varphi_{out}(x) = S^+\varphi_{in}(x)\, S. \quad (5)$$

For the passage beyond the mass shell one defines the variational derivatives

$$\delta S/\delta\varphi_{in}(x) \equiv (\delta S(\eta)/\delta\eta(x))_{\eta=0}.$$

Here $S(\eta)$ is obtained from S by the replacement $\varphi_{in}(x) \to \varphi_{in}(x) + \eta(x)$, where $\eta(x)$ is an arbitrary external field.

Even though this departure from the mass shell is accomplished with preservation of Lorentz invariance, unitarity, and other necessary symmetry properties, it does not determine $S_n(x_1, \ldots x_n)$ unambiguously. To secure uniqueness and bring out the local properties of $S_n(x_1, \ldots x_n)$ one formulates the causality condition in the Bogolyubov method in the form

$$\delta j(x)/\delta\varphi_{in}(y) = 0, \qquad x \lesssim y \quad (6)$$

$x \lesssim y$ means that $x_0 < y_0$ or $(x-y)^2 < 0$, and $x \sim y$ means that $(x-y)^2 < 0$.) The current $j(x)$ is defined in the following way:

$$j(x) = iS^+ \frac{\delta S}{\delta\varphi_{in}(x)} = i\frac{\delta S}{\delta\varphi_{out}(x)} S^+. \quad (7)$$

In the other method, that of LSZ,[3,4] the current operator is also defined by means of Eq. (7).* The

*A detailed formulation of the initial axioms in the two methods can be found in papers by Bogolyubov and his coworkers[2] and by Lehmann, Symanzik, and Zimmermann (hereafter for brevity called LSZ).[3,4] Here we are interested mainly in the difference between the two methods in the formulation of the local properties of the theory.

*We disregard differences between the two approaches that are not important in this problem.[4]

interacting-field operator $\varphi(x)$ is introduced in terms of $j(x)$ as the retarded solution of the inhomogeneous Klein-Gordon equation

$$\varphi(x) = \varphi_{in}(x) - \int_{-\infty}^{+\infty} \Delta^K(x - x', m)\, j(x')\, d^4x' \qquad (8)$$

(the advanced solution is written in an analogous way). The requirement of causality, instead of being written as in Eq. (6), is formulated in this method as the vanishing of all the commutators of $\varphi(x)$ and $j(x)$ outside the light cone; that is, for $x \sim y$ we must have

$$[j(x), j(y)] = 0, \qquad (9a)$$

$$[\varphi(x), j(y)] = 0, \qquad (9b)$$

$$[\varphi(x), \varphi(y)] = 0. \qquad (9c)$$

In addition, in both methods one assumes the stability of the vacuum state and of the one-particle states.

It is not obvious that these two methods of going beyond the mass shell for the determination of the local properties of the S matrix are identical. Moreover, it has been asserted (cf. e.g., references 5, 6) that there are differences in principle between the two approaches (cf. end of Sec. 3).

The main purpose of the present paper is to show, without bringing in supplementary hypotheses (of the type of the adiabatic hypothesis) that the two methods are equivalent from the point of view of the properties of the matrix elements of the S matrix on the mass shell, but lead in general to different $S_n(x_1, \ldots x_n)$. It is important to emphasize that in the solution of this problem the need does not arise to make special use of the asymptotic conditions of LSZ.[3] The paper also contains the necessary and sufficient conditions for the existence of a causal [in the sense of Eqs. (9a) – (9c)] solution of Eq. (8) on the assumption that $j(x)$ obeys the condition (9a), without resort to the S matrix and to the connection (7) of the current $j(x)$ with S. This is the solution of a problem posed by Wightman.[7]

2. THE CONDITIONS FOR THE EXISTENCE OF LOCAL SOLUTIONS OF THE EQUATION (8)

In this section we shall study the local properties of Eq. (8), assuming that all of the operators that appear are the renormalized ones. Before proceeding to an exact statement of the problem, let us make two important remarks. Equation (8) has a number of remarkable properties.

First, owing to the relation

$$(\Box - m^2)\varphi(x) = j(x), \qquad (10)$$

it follows from (8) that if $[\varphi(x), \varphi(y)] = 0$ for $x \sim y$, then $[j(x), j(y)]$ also vanishes outside the cone, $(x-y)^2 < 0$; that is, the local property of $j(x)$ follows from that of $\varphi(x)$. The converse is in general untrue: the vanishing outside the light cone of the bracket $[j(x), j(y)]$ is not a sufficient condition for the local character of $\varphi(x)$. This fact will be of important use in what follows.

Second, the adiabatic hypothesis, which has been brought in particularly by Kaschluhn,[6] is in contradiction with Eq. (8) (on this point see papers by Haag, Hall and Wightman, and also Greenberg[8]). Moreover, even if this were not so, the adiabatic condition [in the sense of strong convergence: $\lim [\varphi(x) - \varphi_{in}(x)] = 0$ for $x_0 \to -\infty$] would be an additional assumption on the existence of a unitary connection between $\varphi(x)$ and $\varphi_{in}(x)$, which does not contain the assumption of the local character of $\varphi(x)$ [in the sense of Eq. (9)] and contains an implicit assumption of the finiteness of the renormalization in the theory.* Therefore we shall not resort to the adiabatic hypothesis.

Let us now state in its most general form the problem of the local properties of (8). In this connection we shall not use the connection (7) of the current $j(x)$ with the S matrix, and shall determine the necessary and sufficient conditions to be satisfied by the operator $j(x)$ in order for the solution of (8) for $\varphi(x)$ to be local, on the assumption that $j(x)$ commutes outside the light cone. This statement of the problem is equivalent to the Wightman problem.[7]

First we shall show (for later use) that the Bogolyubov causality condition (6), together with Eq. (7), is sufficient for the local properties (9a) – (9c) of the operators $\varphi(x)$ and $j(x)$ to hold. In fact, it follows from Eqs. (6) and (7) that

$$\delta j(x)/\delta\varphi_{in}(y) - \delta j(y)/\delta\varphi_{in}(x) = -i[j(x), j(y)] = 0, \quad x \sim y, \qquad (11)$$

$$\delta j(x)/\delta\varphi_{in}(y) = -i\theta(x_0 - y_0)[j(x), j(y)], \qquad (12)$$

apart from quasi-local terms, which will always be omitted in what follows.

*Finally, there is an argument against the introduction of the adiabatic hypothesis in the original idea of formulating the theory in the language of matrix elements of the S matrix, which from the very beginning avoids as far as possible all "unobservable" quantities such as unrenormalized operators, masses, charges, and so on.

Let us now take the simplest commutator $[\varphi(x), j(y)]$. Using Eqs. (8), (11), and (12) and the formula*

$$[\varphi_{in}(x),\ j(y)] = -i\int \Delta(x-x', m)\frac{\delta j(y)}{\delta\varphi_{in}(x')}\,d^4x', \quad (13)$$

we transform $[\varphi(x), j(x)]$ to the form†

$$\begin{aligned}[\varphi(x), j(y)] &= -i\int \Delta(x-x',m)\frac{\delta j(y)}{\delta\varphi_{in}(x')}\,d^4x'\\ &-\int \Delta^R(x-x', m)\,[j(x'), j(y)]\,d^4x'\\ &= -\int \Delta^R(x-x', m)\,\theta(x_0'-y_0)\,[j(x'), j(y)]\,d^4x'\\ &-\int \Delta^A(x-x', m)\,\theta(y_0-x_0')[j(x'), j(y)]\,d^4x. \end{aligned} \quad (14)$$

From this expression it can be seen that $[\varphi(x), j(x)] = 0$ when $x \sim y$, since the first and second terms on the right in Eq. (14) contribute only inside the upper and lower light cones, respectively. In an entirely analogous way it can be shown that $[\varphi(x), \varphi(y)] = 0$ when $x \sim y$.

Let us now return to the problem stated earlier. The causality condition (6) suggests that in the general case it is convenient to try to find $\delta j(x)/\delta\varphi_{in}(y)$ in the form

$$\delta j(x)/\delta\varphi_{in}(y) = -i\theta(x_0-y_0)[j(x),\ j(y)] + \Lambda(x,\ y), \quad (15)$$

where $\Lambda(x,y)$ is an as yet arbitrary operator, whose properties must be established on the basis of the requirement (9b) of commutativity of the operators $\varphi(x)$ and $j(x)$ outside the light cone. Using (13) and (15), we get

$$\begin{aligned}[\varphi(x),\ j(y)] &= -i\int \Delta(x-x',\ m)\,\Lambda(y,\ x')\,d^4x'\\ &-\int \Delta^R(x-x', m)\,\theta(x_0'-y_0)\,[j(x'),\ j(y)]\,d^4x'\\ &-\int \Delta^A(x-x',\ m)\,\theta(y_0-x_0')\,[j(x'), j(y)]\,d^4x'. \end{aligned} \quad (16)$$

Unlike (14), Eq. (16) has on the right an additional operator term

$$F(x,\ y) \equiv -i\int \Delta(x-x',\ m)\,\Lambda(y,\ x')\,d^4x'. \quad (17)$$

In the spacelike region $x \sim y$ the second and third terms in (16) drop out for the same reasons as in the case of (14). From this it immediately follows that the vanishing of $F(x,y)$ outside the cone $(x-y)^2 = 0$ is the necessary and sufficient condition for the existence of a causal solution of (8) [causal in the sense of (9a) and (9b)].‡

It is convenient to consider instead of $\Lambda(x,y)$ an arbitrary matrix element $\langle p|\Lambda(x,y)|p'\rangle$ between states with total four-momenta p and p'. These states are also characterized by the momenta of the particles that occur in them. Invariance under translations gives

$$\begin{aligned}\langle p|\Lambda(x,\ y)|p'\rangle &= \exp(iQy)\,\langle p|\Lambda(x-y,\ 0)|p'\rangle\\ &\equiv \exp(iQ\ y)\,\lambda(x-y), \end{aligned} \quad (18)$$

where $Q = p - p'$. (We do not write out the other variables on which $\lambda(x)$ depends.) Introducing the notation

$$\langle p|F(x,\ y)|p'\rangle \equiv \exp(iQy)\,f(x-y),$$

we get instead of (7)

$$f(x) = \int \Delta(x-x', m)\,\lambda(x')\,d^4x'. \quad (19)$$

We shall now show that $f(x)$ vanishes outside the light cone $(x^2 < 0)$ if and only if the Fourier transform $\tilde{\lambda}(k)$ of the function $\lambda(x)$ is a polynomial of finite degree in k on both sheets of the hyperboloid

$$k^2 - m^2 = 0. \quad (20)$$

The sufficiency of the condition is easily proved. By hypothesis, on the hyperboloid (20)

$$\tilde{\lambda}(k) = \sum_{l=0}^{n} \tilde{\lambda}_l P_l(k), \quad (21)$$

where $P_l(k)$ are polynomials in k,* and the coefficients $\tilde{\lambda}_l$ do not depend on k.

Substituting (21) in (19), we at once find that

$$f(x) = \sum_{l=0}^{n} \tilde{\lambda}_l P_l\left(-i\frac{\partial}{\partial x}\right)\Delta(x, m). \quad (22)$$

The proof of the necessity of the condition can be given on the basis of the following theorem of Bogolyubov and Vladimirov[9] on the analytic continuation of generalized functions,† which we shall formulate suitably for the application to our case.

Let there be given two generalized functions $f_R(x)$ and $f_A(x)$, which vanish in the respective regions

$$x_0 < 0 \text{ or } x^2 < 0, \qquad x_0 > 0 \text{ or } x^2 < 0. \quad (23)$$

Let their Fourier transforms $f_{R,A}(k)$ coincide in the region

$$k^2 < m^2. \quad (24)$$

Then one can find a positive integer n such that in

*This formula is a consequence of Eq. (3) and the assumption that all operators are functionals of $\varphi_{in}(x)$ [or of $\varphi_{out}(x)$].

†We have used the relation $\Delta(x,m) = \Delta^R(x,m) - \Delta^A(x,m)$.

‡Naturally we assume that the solution in the form (8) exists, i.e., that the integral in (8) converges for an arbitrary matrix element of $j(x)$.

*From considerations of invariance, $P_l(k)$ can be represented as a polynomial in the various invariants that can be constructed from k and the other four-vectors that occur in $\tilde{\lambda}(k)$.

†I take occasion to express my sincere gratitude to V. S. Vladimirov, who called my attention to the proof given here.

the region (24) these functions can be represented in the form

$$f_R(k) = f_A(k) = \sum_{l=0}^{n} P_l(k)\ \Phi_l(k^2) \ldots, \qquad (25)$$

where $P_l(k)$ are polynomials, and the functions $\Phi_l(k^2)$ admit of analytic continuation to the entire plane of the complex variable z except the cut*

$$\operatorname{Im} z = 0, \qquad \operatorname{Re} z \geqslant m^2. \qquad (26)$$

The important points for us in this theorem are, first, that the $\Phi_l(k^2)$ depend on k only through the invariant k^2, and second, that from the analytic character of $\Phi_l(z)$ there follows the representation

$$\Phi_l(z) = \int_{m^2}^{\infty} \frac{\rho_l(\zeta)\, d\zeta}{\zeta - z}. \qquad (27)$$

Furthermore,

$$f_{R,A}(k) = \lim \sum_{l=0}^{n} P_l(k)\ \Phi_l(z)$$

$$\text{for } z \to k^2 \pm ik_0\varepsilon; \qquad \varepsilon > 0 \qquad (28)$$

and, consequently,

$$f_R(k) - f_A(k) = 2\pi i \sum_{l=0}^{n} P_l(k)\ \varepsilon(k_0)\ \rho_l(k^2) \qquad (29)$$

in the region $k^2 \geq m^2$.

If we now set

$$f_{R,A}(x) = \pm\, \theta(\pm x_0)\, f(x), \qquad (30)$$

where f(x) is defined by (19), then these functions satisfy all of the conditions of the theorem. The conditions (23) are satisfied owing to the fact that $f(x) = 0$ for $x^2 < 0$. The Fourier transform $\tilde{f}(k)$ of the function $f(x) = f_R(x) - f_A(x)$ is of the form

$$\tilde{f}(k) = 2\pi i \varepsilon(k_0)\delta(k^2 - m^2)\, \tilde{\lambda}(k), \qquad (31)$$

i.e., it clearly satisfies the condition (24). Now, comparing (29) and (31), we find

$$(2\pi i)^{-1} \tilde{f}(k) = \varepsilon(k_0)\, \delta(k^2 - m^2)\, \tilde{\lambda}(k) = \sum_{l=0}^{n} P_l(k)\ \rho_l(k^2)\ \varepsilon(k_0).$$

From this it follows that $\rho_l(k^2) = \delta(k^2 - m^2)\,\tilde{\lambda}_l$. This proves the necessity of the representation (21) for $\tilde{\lambda}(k)$ on the hyperboloid (20).†

It is easily verified that the necessary and sufficient restrictions on $\Lambda(x, y)$ in (15) which we have found, and which follow from the requirement that the commutator $[\varphi_{in}(x), j(y)]$ vanish outside the light cone, automatically assure also that the commutator (9c) is zero outside the light cone.

Let us point out two consequences of the conditions (15) and (21) for the local solubility of (8).

1. On the mass shell $\Lambda(x, y)$ behaves like a quasi-local operator. Let us consider

$$I \equiv \int \exp(-ikx)\, \langle p | \Lambda(x, y) | p' \rangle\, d^4x, \qquad (32)$$

for $k^2 = m^2$. Transforming I by means of (18) and (21), we find

$$I = \exp[i(Q - k)y] \sum_{l=0}^{n} \tilde{\lambda}_l P_l(k). \qquad (33)$$

On the other hand, we can get (33) from (32) if we set

$$\langle p | \Lambda(x, y) | p' \rangle = \exp(iQy) \sum_{l=0}^{n} \tilde{\lambda}_l P_l\left(-i\frac{\partial}{\partial x}\right)\delta(x - y). \qquad (34)$$

2. Owing to the different natures of the terms $i\theta(x_0 - y_0)[j(x), j(y)]$ and $\Lambda(x, y)$ in the right member of (15) it is obvious that they cannot compensate each other. In particular this means that if $\delta j(x)/\delta\varphi_{in}(y) = 0$, or in other words if the operator j(x) does not depend on $\varphi_{in}(y)$, Eq. (8) has no local solutions for $\varphi(x)$. The examples considered by Wightman and Epstein[7] refer to just this class of operators j(x), and consequently do not satisfy the conditions for local solubility of (8).

3. THE EQUIVALENCE OF THE TWO APPROACHES ON THE MASS SHELL

Let us find the additional restrictions on the operator $\Lambda(x, y)$ in (15) that are required by the unitarity of the S matrix and the relation (7) between j(x) and S. Substitution of (15) in (11) gives

$$\Lambda(x, y) = \Lambda(y, x). \qquad (35)$$

Taking the second variational derivative of $S^+S = 1$ with respect to $\varphi_{in}(x)$ and using (7) and (15), we get

$$\Lambda(x, y)^* = \Lambda(x, y). \qquad (36)$$

Thus the necessary conditions for the local solubility of the equation (8) along with a unitary S matrix and the connection (7) between j(x) and S are (15), (21), (35), and (36).

Let us now compare the reduction formulas in the two methods. If we start from the causality conditions (6), then according to (11)

$$[a_{in}(\mathbf{q}), j(x)] = -i(2\pi)^{-3/2} \int \frac{e^{iqy} d^4y}{(2q_0)^{1/2}}\, \theta(x_0 - y_0)\, [j(x), j(y)], \qquad (37)$$

where

*In what follows we shall assume for simplicity that the $\Phi_l(z)$ fall off for $|z| \to \infty$.

†We note that the representation (21) also follows from the integral representation of Jost, Lehmann, and Dyson.[10]

$$q_0 = +(\mathbf{q} + m^2)^{1/2}.$$

From the local solubility of (8) it follows that

$$[a_{in}(\mathbf{q}),\ j(x)] = (2\pi)^{-3/2}\int \frac{e^{iqy}\,d^4y}{(2q_0)^{1/2}}\{-i\theta(x_0-y_0)\,[j(x), j(y)] + \Lambda(x, y)\}. \quad (38)$$

But when $q^2 = m^2$ [cf. Eqs. (32) — (34)] $\Lambda(x, y)$ in Eq. (38) behaves like a quasi-local operator, which we have not taken into account in (37). Therefore the reduction formulas (37) and (38) in the two methods give identical results. Similarly it can be shown that in both methods

$$\left[a_{in}(q),\ \frac{\delta S}{\delta\varphi_{in}(x)}\right] = -(2\pi)^{-3/2}\int \frac{e^{iqy}\,d^4y}{(2q_0)^{1/2}}\,ST(j(x), j(y)). \quad (39)$$

From this we quickly find that an arbitrary matrix element $\langle p_1, \ldots, p_n | S | q_1, \ldots, q_m\rangle$ can be put in the form ($p_i \neq q_j$)

$$(-i)^{m+n}(2\pi)^{-\frac{3(n+m)}{2}}\prod_{i=1}^{n}(2p_i^0)^{-1/2}\prod_{j=1}^{m}(2q_j^0)^{-1/2} \times\int\exp\left(\sum_{i=1}^{n}p_ix_i - \sum_{j=1}^{m}q_jy_j\right) \times\langle 0|Tj(x_1)\ldots j(x_n)\,j(y_1)\ldots j(y_m)|0\rangle\prod_i d^4x_i\prod_j d^4y_j, \quad (40)$$

where we have dropped quasi-local terms.

We summarize briefly the results that have been obtained. First, the Bogolyubov causality condition (6) and the causality conditions in the form (9a) — (9c) together with Eq. (8) lead to identical expressions (40) for the matrix elements of the S matrix on the mass shell. Second, in solving this problem there is no need to use the asymptotic conditions in the form proposed by LSZ.[4] This is a sharpening of the initial postulates in the second method of extrapolation as compared with the original formulation of LSZ.[3,4] Third and last, it is important to note that the addition to $S_n(x_1, \ldots x_n) = (-i)^n\langle 0|Tj(x_1)\ldots j(x_n)|0\rangle$ of terms $\Lambda_n(x_1, \ldots x_n)$ which behave like quasi-local terms on the mass shell (and owing to the unitarity of S have the property $\Lambda_n^* = \Lambda_n$ and are symmetric under interchange of any pair, $x_i \leftrightarrow x_j$) does not destroy the local [in the sense of Eq. (9)] properties of the operators $\varphi(x)$ and $j(x)$ constructed from this S matrix by means of (7) and (8), but does contradict the causality condition in the form (6).

It is interesting to compare these results with those of other papers. In the papers of LSZ[3,4] the basic initial postulates include along with the causality conditions (9a) — (9c) the asymptotic conditions

$$\langle\Psi|a(\mathbf{q}, x_0)|\Phi\rangle \to \langle\Psi|a_{in,\,out}(\mathbf{q})\,\Phi\rangle, \qquad x_0 \to \mp\infty, \quad (41)$$

where $|\Psi\rangle$ and $|\Phi\rangle$ are arbitrary states and

$$a(\mathbf{q}, x_0) = (2\pi)^{-3/2}\int dx\left\{f_q^*(x)\frac{\partial\varphi(x)}{\partial x_0} - \varphi(x)\frac{\partial f_q^*(x)}{\partial x_0}\right\},$$

$$f_q(x) = (2q_0)^{-1/2}\exp(iqx), \qquad q_0 = +(\mathbf{q}^2 + m^2)^{1/2}.$$

The causality conditions (9a) — (9c) are never used explicity in references 3, 4, 11, and 12 to obtain covariant expressions for the matrix elements of S, nor to derive the various relations between the Green's functions, the multiple retarded commutators, and the expansions of $\varphi(x)$ and $j(x)$ in functional series in $\varphi_{in}(x)$ or $\varphi_{out}(x)$. This has created the illusion that the asymptotic conditions (41), without causality, are sufficient for the obtaining of these relations, and that in general such relations can also be correct in a nonlocal theory. Kaschluhn[5] was the first to show that the application of the asymptotic conditions in the papers of LSZ is not sufficiently well defined, and the expression for the matrix elements $\langle p|S|p'\rangle$ in the form (40) does not follow from the asymptotic conditions alone. If, however, one uses the asymptotic conditions as they are used in the papers of LSZ[3, 4,11] then the operators $\varphi(x)$ of the interacting field must necessarily commute outside the light cone, in order that there be no contradictions with relativistic invariance.

These conclusions of Kaschluhn are fully confirmed by the results of the present paper. Furthermore, if we start from Eqs. (8) and (9a) — (9c), then, as has already been remarked, there is no need to use the asymptotic conditions (41). As for the possibility that there exist nonlocal solutions of (8), without resorting to Eqs. (9a) — (9c) or to Eq. (6), and to additional assumptions of the type of the adiabatic hypothesis, in our opinion the question remains an open one.* Whereas the role of the asymptotic conditions (41) in the derivation of Eq. (40) from Eqs. (8) — (9c) is not an essential one, the requirements of causality, Eqs. (9a) and (9b) are of decisive importance.

Here it is necessary to emphasize once more that the condition (9a) on one hand, and the conditions (9b) and (9c) on the other, are not equivalent. This result of the present paper contradicts Kaschluhn's conclusion[6] that "the commutation condition for the operators of the interacting field

*We note that if we start from Eq. (8), without assuming the connection (7) between $j(x)$ and the S matrix, the possibility of the existence of nonlocal solutions can be settled in a trivial way (see the analysis given for the Wightman example). This possibility, it is true, is of no interest from the physical point of view.

cannot be interpreted as a condition on the reduced elements of the D matrix, from which follow some analytical consequences for the theory of dispersion relations" (cf. pages 4, 5, and 33 in reference 6). The mistake in this conclusion comes from the fact that in studying the various expressions involving operators $\varphi(x)$ of the interacting field Kaschluhn has actually nowhere taken into account the additional restrictions on the operators $\varphi(x)$ and $j(x)$ that arise from the conditions (9a) and (9b) for local behavior.

In connection with the equivalence of the two methods from the point of view of the properties of $S_n(x_1, \ldots x_n)$ in the S matrix (1) on the mass shell the question can arise: Where is the retardation condition imposed in the formation of causality in the form (9a) and (9b)? Essentially, it is contained in the expression of $\varphi(x)$ in terms of $j(x)$ in Eq. (8) by means of retarded (or advanced) Green's functions $\Delta^R(x, m)$ [or $\Delta^A(x, m)$ of the homogeneous Klein-Gordon equation. In this connection, however, it must hold apart from terms that vanish on the mass shell, i.e., it does not have to hold rigorously.

Comparing the two methods that have been considered, we note an important advantage of the Bogolyubov method, which is that the condition (6) is formulated and can be used without any resort to the operators $\varphi(x)$ of the interacting field and Eq. (8) for these operators. Moreover, for obtaining the expressions for $S_2(x_1, x_2)$ and $S_3(x_1, x_2, x_3)$ in Eq. (1), which correspond to the single-particle and vertex Green's functions, in the forms

$$S_2 = -\langle 0 | Tj(x_1), j(x_2) | 0 \rangle,$$
$$S_3 = -i\langle 0 | Tj(x_1), j(x_2), j(x_3) | 0 \rangle$$

and for studying their analytical properties, the causality conditions (6) are not only sufficient, but also necessary conditions. This is so because the contributions from $S_2(x_1, x_2)$ and $S_3(x_1, x_2, x_3)$ in Eq. (1) drop out on the mass shell. Therefore one cannot get unambiguous expressions for these functions by means of the conditions (9a) and (9b).

On the other hand, all of the difficulties of present quantum field theory in its Lagrangian formulation have their roots, as a rule, in the properties of just these simplest Green's functions. Therefore the existence of an additional arbitrariness in their definition, which does not contradict the local character in the sense of Eq. (9), may be due to deep causes. In any case the requirement (9) is weaker than Eq. (6), and in general widens the range of possibilities.

In conclusion we point out an interesting consequence of the theorem proved in Sec. 2: the commutators $[\varphi_{in,out}(x), j(y)]$, $[\varphi_{in,out}(x), \varphi(y)]$, and $[\varphi_{in}(x), \varphi_{out}(y)]$ do not vanish outside the light cone,* $(x-y)^2 < 0$, if we exclude the trivial case in which $\varphi_{in}(x) = \varphi_{out}(x)$ or $\varphi(x)$ and $j(x)$ do not depend on $\varphi_{in}(x)$ [or $\varphi_{out}(x)$]. For example,

$$[\varphi_{in}(x), j(y)] = \int \Delta(x - x', m)\, \theta(y_0 - x'_0)\, [j(x'), j(y)]\, d^4x' \neq 0 \text{ for } x \sim y$$

since otherwise it would be necessary for an arbitrary matrix element $\langle p | [j(x), j(y)] | p' \rangle$ to behave on the mass shell like a quasi-local operator [$\sim \delta(x-y)$ and its covariant derivative].

The method used in the present paper can be extended without particular difficulty to the case of several interacting fields and the presence of bound states.

[1] N. N. Bogolyubov, Izv. Akad. Nauk SSSR, Ser. Fiz. **19**, 237 (1955), Columbia Tech. Transl. p. 215.

[2] N. N. Bogolyubov and D. V. Shirkov, Introduction to Quantized Field Theory, Interscience, 1959. Bogolyubov, Medvedev, and Polivanov, Вопросы теории дисперсионных соотношений (Problems in the Theory of Dispersion Relations), Fizmatgiz, 1958.

[3] Lehmann, Symanzik, and Zimmermann, Nuovo cimento **1**, 205 (1955).

[4] Lehmann, Symanzik, and Zimmermann, Nuovo cimento **6**, 319 (1957).

[5] F. Kaschluhn, Nuovo cimento **12**, 541 (1959).

[6] F. Kaschluhn, On the Asymptotic and Causality Conditions in Quantum Field Theory, II, Preprint r-517, Dubna, 1960.

[7] A. Wightman, Report at the International Conference on High-Energy Physics, Kiev, 1959. A. Wightman and H. Epstein, Ann. of Phys. **11**, 201 (1960).

[8] R. Haag, Nuovo cimento suppl. **14**, 131 (1959); Kgl. Dansk. Vidensk. Selskab, mat.-fys. medd. **29**, No. 12 (1955). D. Hall and A. S. Wightman, Kgl. Dansk. Vidensk. Selskab, mat.-fys. medd. **31**, No. 5 (1957). O. W. Greenberg, Phys. Rev. **115**, 706 (1959).

*In this case Miyatake's assertion[13] that vanishing of the commutator $[\varphi_{in}(x), \varphi_{out}(y)]$ outside the light cone is a condition for causality in a local theory seems strange, to say the least.

[9] N. N. Bogolyubov and V. S. Vladimirov, Научн. докл. высш. шк. (Sci. Rep. of the Universities, Phys. Math. Sci.) **3**, 26 (1958).

[10] R. Jost and H. Lehmann, Nuovo cimento **5**, 1598 (1957). F. J. Dyson, Phys. Rev. **110**, 1460 (1958).

[11] Glaser, Lehmann, and Zimmermann, Nuovo cimento **6**, 1122 (1957).

[12] K. Nishijima, Progr. Theor. Phys. **17**, 765 (1957); Phys. Rev. **119**, 485 (1960).

[13] Y. Miyatake, Progr. Theor. Phys. **21**, 562 (1959).

Translated by W. H. Furry
300

COLLISION INTEGRAL FOR CHARGED PARTICLES

V. P. SILIN

P. N. Lebedev Physics Institute, Academy of Sciences, U.S.S.R.

Submitted to JETP editor January 4, 1961

J. Exptl. Theoret. Phys. (U.S.S.R.) 40, 1768-1774 (June, 1961)

The equation for the correlative distribution function with screening of the interaction of charged particles taken into account, which was obtained earlier by Klimontovich and Temko, is here solved. The correlative function is found. The collision integral is obtained for a system consisting of several types of nonrelativistic charged particles; this integral is suitable in particular for the description of states very different from the thermodynamic equilibrium state. It is shown that the screening of the Coulomb interaction is described by a complex permittivity tensor. This has made possible an extension to the case of relativistic distributions and the obtaining of the relativistic collision integral with the screening of the fields of the charged particles taken into account.

1. Klimontovich and Temko[1] have extended results obtained by Bogolyubov[2] to the quantum case and have shown that the collision integral $J_\alpha(\mathbf{p}_\alpha)$ for charged particles is determined by the formula

$$\frac{N_\alpha}{V} J_\alpha = \frac{i}{2\hbar}\int \frac{d\mathbf{k}}{(2\pi)^3}\left\{h_\alpha\left(\mathbf{k}, \mathbf{p}_\alpha + \frac{\hbar\mathbf{k}}{2}\right) - h_\alpha\left(\mathbf{k}, \mathbf{p}_\alpha - \frac{\hbar\mathbf{k}}{2}\right) - h_\alpha\left(-\mathbf{k}, \mathbf{p}_\alpha + \frac{\hbar\mathbf{k}}{2}\right) + h_\alpha\left(-\mathbf{k}, \mathbf{p}_\alpha - \frac{\hbar\mathbf{k}}{2}\right)\right\}, \quad (1.1)$$

where N_α/V is the number of particles of type α per unit volume, and the function $h_\alpha(\mathbf{k}, \mathbf{p}_\alpha)$ is connected with the correlative function $g_{\alpha\beta}(\mathbf{r}_\alpha - \mathbf{r}_\beta, \mathbf{p}_\alpha, \mathbf{p}_\beta)$ by the relation

$$h_\alpha(\mathbf{k}, \mathbf{p}_\alpha) = \sum_\beta \frac{N_\alpha}{V}\frac{N_\beta}{V} \nu_{\alpha\beta}(k) \int d\mathbf{p}_\beta G_{\alpha\beta}(\mathbf{k}, \mathbf{p}_\alpha, \mathbf{p}_\nu). \quad (1.2)$$

Here

$$G_{\alpha\beta}(\mathbf{k}, \mathbf{p}_\alpha, \mathbf{p}_\beta) = \int e^{-i\mathbf{k}\mathbf{r}}\, d\mathbf{r}\, g_{\alpha\beta}(\mathbf{r}, \mathbf{p}_\alpha, \mathbf{p}_\beta),$$

$$\nu_{\alpha\beta}(k) = \int e^{i\mathbf{k}\mathbf{r}}\, d\mathbf{r}\, \frac{e_\alpha e_\beta}{r}.$$

Furthermore, according to the work of Klimontovich and Temko[1] one has the following equation which determines the correlative function:

$$\begin{aligned}\frac{N_\alpha}{V}\frac{N_\beta}{V}\nu_{\alpha\beta}(k)\, G_{\alpha\beta}(\mathbf{k}, \mathbf{p}_\alpha, \mathbf{p}_\beta) &= \frac{1}{\hbar}\left\{i\pi\delta\left(\frac{\mathbf{k}\mathbf{p}_\alpha}{m_\alpha} - \frac{\mathbf{k}\mathbf{p}_\beta}{m_\beta}\right)\right.\\ &+ P\frac{1}{\mathbf{k}\mathbf{p}_\alpha/m_\alpha - \mathbf{k}\mathbf{p}_\beta/m_\beta}\Big\}\Big\{\nu_{\alpha\alpha}(k)\,\nu_{\beta\beta}(k)\frac{N_\alpha}{V}\frac{N_\beta}{V}\\ &\times [f_\alpha(\mathbf{p}_\alpha + \hbar\mathbf{k}/2)\, f_\beta(\mathbf{p}_\beta - \hbar\mathbf{k}/2)\\ &- f_\alpha(\mathbf{p}_\alpha - \hbar\mathbf{k}/2)\, f_\beta(\mathbf{p}_\beta + \hbar\mathbf{k}/2)]\\ &+ (N_\alpha/V)\,\nu_{\alpha\alpha}(k)\,[f_\alpha(\mathbf{p}_\alpha + \hbar\mathbf{k}/2)\\ &- f_\alpha(\mathbf{p}_\alpha - \hbar\mathbf{k}/2)]\, h_\beta(-\mathbf{k}, \mathbf{p}_\beta)\\ &- (N_\beta/V)\,\nu_{\beta\beta}(k)\,[f_\beta(\mathbf{p}_\beta + \hbar\mathbf{k}/2)\\ &- f_\beta(\mathbf{p}_\beta - \hbar\mathbf{k}/2)]h_\alpha(\mathbf{k}, \mathbf{p}_\alpha)\Big\}. \end{aligned} \quad (1.3)$$

The symbol P means that here and in what follows the singular integrals are to be taken by using the principal value.

In the paper of Klimontovich and Temko[1] this equation was not solved, although it was shown that such an equation must lead to screening of the interaction of the particles at large distances. Screening of the Coulomb interaction in the quantum collision integral was obtained by Konstantinov and Perel'[3] in the case of states differing slightly from the state of thermodynamic equilibrium. Here, by solving Eq. (1.3), we shall obtain a collision integral that is valid for the description of states decidedly different from the equilibrium state. In the classical theory the analogous treatment for collisions of electrons with electrons has been carried out in papers by Balescu[4] and Lenard.[5]

2. We introduce functions of the complex variable ω,

$$H(\omega, \mathbf{k}, \pm) = \frac{1}{2\pi i}\sum_\alpha \int \frac{d\mathbf{p}_\alpha}{\omega - \mathbf{k}\mathbf{p}_\alpha/m_\alpha} h_\alpha(\pm\mathbf{k}, \mathbf{p}_\alpha), \quad (2.1)$$

which have no singularities in either the upper or lower half-plane, but which have a discontinuity on passage across the real axis. On the real axis the limit H^+ of the function analytic in the upper half-plane and the limit H^- of the function analytic in the lower half-plane obey the Sokhotskii-Plemel' relations

$$H^\pm(\omega) = \frac{1}{2\pi i}\sum_\alpha \int d\mathbf{p}_\alpha\, h_\alpha(\mathbf{p}_\alpha)\left\{P\frac{1}{\omega - \mathbf{k}\mathbf{p}_\alpha/m_\alpha} \mp i\pi\delta\left(\omega - \frac{\mathbf{k}\mathbf{p}_\alpha}{m_\alpha}\right)\right\}. \quad (2.2)$$

From Eq. (1.3) we have

$$h_\alpha(\mathbf{k}, \mathbf{p}_\alpha) = \frac{2\pi i \nu_{\alpha\alpha}(k) N_\alpha / V}{\hbar \varepsilon^-(\mathbf{k}\mathbf{p}_\alpha / m_\alpha, \mathbf{k})}\left[f_\alpha\left(\mathbf{p}_\alpha + \frac{\hbar\mathbf{k}}{2}\right) F^-\left(\frac{\mathbf{k}\mathbf{p}_\alpha}{m_\alpha}, \mathbf{k}, -\right) - f_\alpha\left(\mathbf{p}_\alpha - \frac{\hbar\mathbf{k}}{2}\right) F^-\left(\frac{\mathbf{k}\mathbf{p}_\alpha}{m_\alpha}, \mathbf{k}, +\right)\right] + \frac{\nu_{\alpha\alpha}(k)}{\hbar}\frac{N_\alpha}{V}\left[f_\alpha\left(\mathbf{p}_\alpha + \frac{\hbar\mathbf{k}}{2}\right) - f_\alpha\left(\mathbf{p}_\alpha - \frac{\hbar\mathbf{k}}{2}\right)\right] 2\pi i \frac{H^-(\mathbf{k}\mathbf{p}_\alpha / m_\alpha, \mathbf{k}, -)}{\varepsilon^-(\mathbf{k}\mathbf{p}_\alpha / m_\alpha, \mathbf{k})}, \quad (2.3)$$

where ϵ^- and F^- are the limits on approaching the real axis from below of the functions

$$\varepsilon(\omega, \mathbf{k}) = 1 + \frac{2\pi i}{\hbar}[F(\omega, \mathbf{k}, +) - F(\omega, \mathbf{k}, -)], \quad (2.4)$$

$$F(\omega, \mathbf{k}, \pm) = \frac{1}{2\pi i}\sum_\alpha \int \frac{d\mathbf{p}_\alpha}{\omega - \mathbf{k}\mathbf{p}_\alpha / m_\alpha} \nu_{\alpha\alpha}(k) \frac{N_\alpha}{V} f_\alpha\left(\mathbf{p}_\alpha \pm \frac{\hbar\mathbf{k}}{2}\right). \quad (2.5)$$

It follows from Eqs. (1.3) and (2.3) that for the solution of the system of singular integral equations (1.3) it is sufficient to determine the functions $H(\omega, \mathbf{k}, \pm)$. The corresponding equations for the determination of these functions can be obtained in the following way. Let us multiply Eq. (2.3) by $\delta(\omega - \mathbf{k}\mathbf{p}_\alpha / m_\alpha)$ and integrate over $\mathbf{p}_\alpha$. On summing the result of the integration over α, we get

$$[H^-(\omega, \mathbf{k}, +) - H^+(\omega, \mathbf{k}, +)]\,\varepsilon^-(\omega, \mathbf{k}) - H^-(\omega, \mathbf{k}, -)\,[\varepsilon^-(\omega, \mathbf{k}) - \varepsilon^+(\omega, \mathbf{k})] = (2\pi i / \hbar)\,[F^+(\omega, \mathbf{k}, -) F^-(\omega, \mathbf{k}, +) - F^+(\omega, \mathbf{k}, +) F^-(\omega, \mathbf{k}, -)]. \quad (2.6)$$

We get a second equation by changing the signs of ω and $\mathbf{k}$ in Eq. (2.6):

$$[H^-(\omega, \mathbf{k}, -) - H^+(\omega, \mathbf{k}, -)]\,\varepsilon^+(\omega, \mathbf{k}) - H^+(\omega, \mathbf{k}, +)\,[\varepsilon^-(\omega, \mathbf{k}) - \varepsilon^+(\omega, \mathbf{k})] = (2\pi i / \hbar)[F^+(\omega, \mathbf{k}, -) F^-(\omega, \mathbf{k}, +) - F^+(\omega, \mathbf{k}, +) F^-(\omega, \mathbf{k}, -)]. \quad (2.7)$$

The system (2.6) and (2.7) enables us to determine the functions H.

To solve (2.6) and (2.7) we subtract one equation from the other. The result is the following relation:

$$[H^-(\omega, \mathbf{k}, +) - H^-(\omega, \mathbf{k}, -)]\,\varepsilon^-(\omega, \mathbf{k}) = [H^+(\omega, \mathbf{k}, +) - H^+(\omega, \mathbf{k}, -)]\varepsilon^+(\omega, \mathbf{k}). \quad (2.8)$$

The left member of this relation is analytic in the lower half-plane of the complex variable ω, and the right member is analytic in the upper half-plane. The analytic function with zero discontinuity on the line that separates the regions of analyticity is obviously analytic in the entire plane of the complex variable. The condition that the distribution functions go to zero at infinitely large momenta means that both the right and left members of Eq. (2.8) go to zero at infinity, and from this and the condition that

$$\varepsilon^\pm(\omega, \mathbf{k}) \neq 0 \quad (2.9)$$

we get

$$H(\omega, \mathbf{k}, +) = H(\omega, \mathbf{k}, -) \equiv H(\omega, \mathbf{k}). \quad (2.10)$$

The absence of zeroes of the functions $\epsilon^\pm(\omega, \mathbf{k})$ in the regions in which they are analytic has a simple physical meaning. The fact is that the function $\epsilon(\omega, \mathbf{k})$ is connected with the complex permittivity tensor $\epsilon_{ij}(\omega, \mathbf{k})$ of the plasma by the relation*

$$k^2 \varepsilon(\omega, \mathbf{k}) = k_i k_j \varepsilon_{ij}(\omega, \mathbf{k}).$$

In this connection, the condition (2.9) corresponds to the absence of undamped and increasing self-consistent oscillations of the density (so called longitudinal plasma waves†) in the state in which the distribution of the particles is described by the functions $f_\alpha(\mathbf{p}_\alpha)$. In other words, the condition (2.9) is the condition for the stability of the system of charged particles against perturbations associated with changes of the charge density. In what follows it is assumed that this condition is satisfied.‡

Equation (2.10) enables us to write Eq. (2.6) in the following form

$$\frac{H^-(\omega, \mathbf{k})}{\varepsilon(\omega, \mathbf{k})} - \frac{H^+(\omega, \mathbf{k})}{\varepsilon^+(\omega, \mathbf{k})} = \frac{F^+(\omega, \mathbf{k}, -) + F^+(\omega, \mathbf{k}, +)}{2\varepsilon^+(\omega, \mathbf{k})} - \frac{F^-(\omega, \mathbf{k}, -) + F^-(\omega, \mathbf{k}, +)}{2\varepsilon^-(\omega, \mathbf{k})} - \frac{F^+(\omega, \mathbf{k}, -) + F^+(\omega, \mathbf{k}, +) - F^-(\omega, \mathbf{k}, -) - F^-(\omega, \mathbf{k}, +)}{2\varepsilon^+(\omega, \mathbf{k})\,\varepsilon^-(\omega, \mathbf{k})}. \quad (2.11)$$

This equation determines the discontinuity of the function H/ϵ on the real axis of the plane of the complex variable ω. As is well known,[6,7] the problem of the determination of an analytic function $\mathfrak{A}$ which goes to zero at infinity from its discontinuity a on a path L is solved [as can be seen without difficulty from the Sokhotskii-Plemel' relations of the type of Eq. (2.3)] by the formulas**

*Regarding the complex permittivity tensor of a plasma see reference 9.

†The damped plasma oscillations which are often considered correspond to zeroes of the analytic continuation of the function $\varepsilon(\omega, \mathbf{k})$ to adjacent sheets of the complex variable ω.

‡We note that for the obtaining of the collision integral it is sufficient for the condition (2.9) to be satisfied on the path of integration of the formulas (2.1) and (2.5). The condition then corresponds to the absence of self-consistent oscillations capable of being absorbed and emitted by particles with the distributions f_α.

**Furthermore,

$$\mathfrak{A}^+(z) = \frac{1}{2} a(z) + \frac{1}{2\pi i}\int_L \frac{dz'}{z' - z} a(z'),$$

$$\mathfrak{A}^-(z) = \frac{1}{2} a(z) + \frac{1}{2\pi i}\int_L \frac{dz'}{z' - z} a(z')$$

$$\mathfrak{A}^+(z) - \mathfrak{A}^-(z) = a(z) \text{ on } L, \quad \mathfrak{A}(z) = \frac{1}{2\pi i}\int_L \frac{dz' a(z')}{z'-z}.$$

Therefore the solution of Eq. (2.11) can be written in the following form:

$$\frac{H(\omega, \mathbf{k})}{\varepsilon(\omega, \mathbf{k})} = -\frac{F(\omega, \mathbf{k}, +) + F(\omega, \mathbf{k}, -)}{2\varepsilon(\omega, \mathbf{k})} + \frac{1}{2\pi i}\int \frac{d\omega'}{\omega' - \omega} \times \frac{F^+(\omega', \mathbf{k}, -) + F^+(\omega', \mathbf{k}, +) - F^-(\omega', \mathbf{k}, -) - F^-(\omega', \mathbf{k}, +)}{2\varepsilon^+(\omega', \mathbf{k})\varepsilon^-(\omega', \mathbf{k})}. \tag{2.12}$$

3. Equations (2.12), (2.3), and (1.3) enable us to write an explicit expression for the correlative function in a system of charged particles. We note that a knowledge of this function can be necessary, for example, for the determination of the energy of the system of particles in a nonequilibrium state. It is obvious that now we can also write an expression for the collision integral. We note that Eq. (2.11) suffices for this purpose, because Eq. (1.1) contains the difference $h_\alpha(\mathbf{k}, \mathbf{p}_\alpha) - h_\alpha(-\mathbf{k}, \mathbf{p}_\alpha)$. Substituting the expressions obtained in Eq. (1.1), we find

$$\frac{N_\alpha}{V} J_\alpha(\mathbf{p}_\alpha) = \sum_\beta \frac{N_\alpha}{V}\frac{N_\beta}{V}\int \frac{d\mathbf{p}'_\alpha}{(2\pi\hbar)^3} d\mathbf{p}'_\beta w_{\alpha\beta}(\mathbf{p}_\alpha, \mathbf{p}'_\alpha) \times \delta(\mathbf{p}'_\alpha + \mathbf{p}'_\beta - \mathbf{p}_\alpha - \mathbf{p}_\beta)\,\delta(p'^2_\alpha/2m_\alpha + p'^2_\beta/2m_\beta - p^2_\alpha/2m_\alpha - p^2_\beta/2m_\beta)\,[f_\alpha(\mathbf{p}_\alpha) f_\beta(\mathbf{p}_\beta) - f_\alpha(\mathbf{p}'_\alpha) f_\beta(\mathbf{p}'_\beta)], \tag{3.1}$$

$$w_{\alpha\beta}(\mathbf{p}_\alpha, \mathbf{p}'_\alpha) = \frac{2\pi v^2_{\alpha\beta}\left(\left|\frac{\mathbf{p}_\alpha - \mathbf{p}'_\alpha}{\hbar}\right|\right)}{\hbar\,\varepsilon^+\left(\frac{p'^2_\alpha - p^2_\alpha}{2\hbar m_\alpha}, \frac{\mathbf{p}'_\alpha - \mathbf{p}_\alpha}{\hbar}\right)\varepsilon^-\left(\frac{p'^2_\alpha - p^2_\alpha}{2\hbar m_\alpha}, \frac{\mathbf{p}'_\alpha - \mathbf{p}_\alpha}{\hbar}\right)}. \tag{3.2}$$

We note that (3.2), like the original (1.3), has been obtained on the assumption that the interaction is weak. This means that for very small impact parameters Eq. (3.2) must not be used. In the case of states only slightly different from the state of thermodynamic equilibrium, for which we can use the linear approximation, Eq. (3.2) goes over into the formula of the paper of Konstantinov and Perel'.[3]

In the classical limit, which corresponds to sufficiently distant collisions, Eq. (3.1) takes the form

$$\frac{N_\alpha}{V} J_\alpha = \frac{\partial}{\partial p^i_\alpha}\sum_\beta \int d\mathbf{p}_\beta I^{ij}_{\alpha\beta}\left(\frac{\mathbf{p}_\alpha}{m_\alpha}, \frac{\mathbf{p}_\beta}{m_\beta}\right)\left[\frac{\partial f_\alpha}{\partial p^j_\alpha} f_\beta - f_\alpha \frac{\partial f_\beta}{\partial p^j_\beta}\right]\frac{N_\alpha}{V}\frac{N_\beta}{V}, \tag{3.3}$$

$$I^{ij}_{\alpha\beta}(\mathbf{v}_\alpha, \mathbf{v}_\beta) = \int \frac{d\mathbf{k}}{(2\pi)^3}\frac{k^i k^j \pi v^2_{\alpha\beta}(k)\delta(\mathbf{kv}_\alpha - \mathbf{kv}_\beta)}{\varepsilon^+_{\mathrm{cl}}(\mathbf{kv}_\alpha, \mathbf{k})\,\varepsilon^-_{\mathrm{cl}}(\mathbf{kv}_\alpha, \mathbf{k})}, \tag{3.4}$$

where ϵ_{cl} is given as a function of the complex variable ω by the formula

$$\varepsilon_{\mathrm{cl}}(\omega, \mathbf{k}) = 1 + \sum_\alpha \frac{4\pi e^2_\alpha}{k^2}\frac{N_\alpha}{V}\int \frac{d\mathbf{p}_\alpha}{\omega - \mathbf{kp}_\alpha/m_\alpha}\left(\mathbf{k}\frac{\partial f_\alpha}{\partial \mathbf{p}_\alpha}\right). \tag{3.5}$$

In the special case of electron-electron collisions the formula (3.4) corresponds to the formula obtained by Balescu and by Lenard.[4,5] We note that in Eq. (3.4) the integral diverges at large values of k, which correspond to small impact parameters; this is due to the fact that here the classical approximation cannot be applied, as it is in the passage from Eq. (3.1) to Eq. (3.3). The necessity of cutting off the integral in Eq. (3.4) can be connected with the lack of validity of perturbation theory, which with the Boltzmann distribution begins to fail at the impact parameter $\rho_{\min} \sim e^2/\kappa T$.

Finally, if we neglect the difference between ϵ_{cl} and unity, the expression (3.3) goes over into the collision integral for charged particles in the form that was given by Landau.[8] Here also at large impact parameters one must resort to cutting off the integral, which converges automatically in our treatment. The convergence is due to the consistent inclusion of effects of polarization of the medium as described by the permittivity.

4. The results of the preceding section regarding the collision integral mean that in calculating collision probabilities we must use instead of the Coulomb field the expression for the field of a particle in a plasma, with the complex permittivity taken into account. This is particularly clear from Eq. (3.2). Here the value of the complex permittivity corresponds to the first approximation of perturbation theory, and in the nonquantum case, to which we confine ourselves from now on, is given by[9]

$$\varepsilon_{ij}(\omega, \mathbf{k}) = \delta_{ij} + \sum_\alpha \frac{4\pi e^2_\alpha}{\omega}\frac{N_\alpha}{V}\int \frac{d\mathbf{p}_\alpha}{\omega - \mathbf{kv}_\alpha} v^i_\alpha \frac{\partial f_\alpha}{\partial p^l_\alpha} \times\left(\delta_{jl}\left[1 - \frac{\mathbf{kv}_\alpha}{\omega}\right] + \frac{k_l v^j_\alpha}{\omega}\right). \tag{4.1}$$

Here, as before, we are dealing with analytic functions that have cuts along the real axis.

Only the longitudinal interaction plays any part in the nonrelativistic approximation, and therefore in the formulas written above it is the quantity $k_i k_j \epsilon_{ij}$ that appears. In the nonrelativistic case this is no longer true. We shall now proceed to the consideration of this case. Here we shall not deal with the equation for the correlative functions, but shall at once take into account the polarization of the medium, and use the permittivity for the determination of the field in the plasma.

It is clear that for what follows we must define the probability of collision between two particles. For this we need to know in the nonquantum limit the quantity

$$\lim_{\hbar\to 0} w_{\alpha\beta}(\mathbf{p}_\alpha, \mathbf{p}_\alpha + \hbar\mathbf{k})\,\hbar/2,$$

where $w_{\alpha\beta}$ is the probability of a collision of particles α and β with change of the momentum of particle α from $\mathbf{p}_\alpha$ to $\mathbf{p}_\alpha + \hbar\mathbf{k}$. This quantity serves in the following way to determine the kernel of the collision integral, which obviously is still of the form (3.3):

$$I^{ij}_{\alpha\beta}(\mathbf{v}_\alpha, \mathbf{v}_\beta) = \int \frac{d\mathbf{k}}{(2\pi)^3} k_i k_j \delta(\mathbf{k}\mathbf{v}_\alpha - \mathbf{k}\mathbf{v}_\beta) \lim_{\hbar\to 0} w_{\alpha\beta}(\mathbf{p}_\alpha, \mathbf{p}_\alpha + \hbar\mathbf{k})\,\hbar/2. \quad (4.2)$$

Equation (4.2) can easily be obtained by going to the limit $\hbar = 0$ in the quantum collision integral.

For the calculation of the scattering probability we must determine the fields. Using the gauge in which the scalar potential is zero, we can write the following equations for the Fourier components of the vector potential of the field produced by the uniform motion of a charge e_β with the velocity v_β in a medium with the complex permittivity tensor $\epsilon_{ij}(\omega, \mathbf{k})$:

$$a_{ij}(\mathbf{k}\mathbf{v}_\beta, \mathbf{k})\, A_j \equiv \{(\mathbf{k}\mathbf{v}_\beta)^2 c^{-2}\varepsilon_{ij}(\mathbf{k}\mathbf{v}_\beta, \mathbf{k}) - k^2\delta_{ij} + k_i k_j\}\, A_j = -4\pi c^{-1} e_\beta v^i_\beta, \quad (4.3)$$

from which we have

$$A_i = -(4\pi/c)\, e_\beta a^{-1}_{ij}(\mathbf{k}\mathbf{v}_\beta, k)\, v^j_\beta. \quad (4.4)$$

According to Møller's paper,[10] with our gauge

$$\lim_{\hbar=0} w_{\alpha\beta}(\mathbf{p}_\alpha, \mathbf{p}_\alpha + \hbar\mathbf{k})\,\hbar/2 = \pi |e_\alpha c^{-1}\mathbf{v}_\alpha \mathbf{A}|^2. \quad (4.5)$$

Therefore for the collision integral we get

$$I^{ij}_{\alpha\beta}(\mathbf{v}_\alpha, \mathbf{v}_\beta) = \frac{(4\pi e_\alpha e_\beta)^2}{c^4} \int \frac{d\mathbf{k}}{(2\pi)^3} \pi k_i k_j \delta(\mathbf{k}\mathbf{v}_\alpha - \mathbf{k}\mathbf{v}_\beta) \times |v^i_\alpha a^{-1}_{ij}(\mathbf{k}\mathbf{v}_\alpha, \mathbf{k})\, v^j_\beta|^2. \quad (4.6)$$

In the special case of an isotropic distribution the complex permittivity tensor has the form

$$\varepsilon_{ij}(\omega, \mathbf{k}) = \varepsilon^{tr}(\omega, k)(\delta_{ij} - k^{-2}k_i k_j) + k^{-2}k_i k_j \varepsilon^{l}(\omega, k). \quad (4.7)$$

Here we have, according to Eq. (4.1)*

$$\varepsilon^{tr}(\omega, k) = 1 + \sum_\alpha \frac{2\pi e^2_\alpha}{\omega k^2} \int \frac{d\mathbf{p}_\alpha}{\omega - \mathbf{k}\mathbf{v}_\alpha} [\mathbf{k}[\mathbf{v}_\alpha \mathbf{k}]] \frac{\partial f_\alpha}{\partial \mathbf{p}_\alpha} \frac{N_\alpha}{V},$$

$$\varepsilon^{l}(\omega, k) = 1 + \sum_\alpha \frac{4\pi e^2_\alpha}{k^2} \int \frac{d\mathbf{p}_\alpha}{\omega - \mathbf{k}\mathbf{v}_\alpha} \left(\mathbf{k}\frac{\partial f_\alpha}{\partial \mathbf{p}_\alpha}\right) \frac{N_\alpha}{V}.$$

Then the formula (4.6) can be simplified and takes the following form:

$$I^{ij}_{\alpha\beta}(\mathbf{v}_\alpha \mathbf{v}_\beta) = (4\pi e_\alpha e_\beta)^2 \int \frac{d\mathbf{k}}{(2\pi)^3} \frac{\pi k_i k_j}{k^4} \delta(\mathbf{k}\mathbf{v}_\alpha - \mathbf{k}\mathbf{v}_\beta) \times \left| \frac{1}{\varepsilon^l(\mathbf{k}\mathbf{v}_\alpha, \mathbf{k})} + \frac{k^2 \mathbf{v}_\alpha \mathbf{v}_\beta - (\mathbf{k}\mathbf{v}_\alpha)^2}{(\mathbf{k}\mathbf{v}_\alpha)^2 \varepsilon^{tr}(\mathbf{k}\mathbf{v}_\alpha, \mathbf{k}) - k^2 c^2} \right|^2. \quad (4.8)$$

In the limit $\epsilon^l = \epsilon^{tr} = 1$ Eq. (4.8) goes over into Eq. (22) of the paper of Klimontovich,[11] and therefore it corresponds to the relativistic collision integral of Belyaev and Budker.[12]

The integral in Eq. (4.8) must be cut off at large k for the same reasons as in the nonrelativistic treatment. At small k, corresponding to large impact parameters, the integral converges. We shall show in particular that in the case of relativistic temperatures the longitudinal and transverse permittivities lead to cutting off at distances of the order of the Debye radius. For this purpose we note that in the region of small values of $\mathbf{k}\mathbf{v}_\alpha$ we can use for the permittivities the approximate formulas[9,13]

$$\varepsilon^l \sim (kr_D)^{-2}, \qquad \varepsilon^{tr} \sim iv_T/(\mathbf{k}\mathbf{v}_\alpha)\, kr^2_D,$$

where v_T is the thermal velocity. The formula for ϵ^l corresponds to the Debye screening, and the formula for ϵ^{tr} corresponds to the region of the anomalous skin effect, for which $\epsilon^{tr}(\omega, k) \sim i/\omega k$.

It is clear that under conditions in which v_T is close to the speed of light, these approximate expressions for the permittivities lead to a cutting off at impact parameters of the order of the Debye radius. If, on the other hand, $v_T \ll c$, then unlike the longitudinal permittivity, which leads to a cutting off of the logarithmic divergence at the Debye radius, the transverse permittivity cuts off the divergence at parameters $\sim (c/v_T) r_D$. Under these conditions, however, the contribution of the transverse interaction to the collision integral is only a small correction. Therefore for the Boltzmann distribution there is no large error in cutting off both the transverse and the longitudinal interactions at the Debye radius.

We note that the kernel (4.8) can be used not only in the case of an isotropic distribution, but also in the case of a small departure from isotropy. For this purpose it is assumed to be possible to linearize the collision integral. In the case of a decidedly anisotropic distribution, such as occurs, for example, in the collision of beams of charged particles that are neutral taken on the whole, it is necessary to use the collision integral with the kernel (4.6).

Note added in proof (May 12, 1961). It was stated above that in Eq. (4.6), as indeed always when a collision integral of the Landau type[8] is being used, it is necessary to cut off the integration for large k. This shortcoming is absent for the ordinary Boltzmann collision integral, which holds also in our case and is written in the form (3.1) with the energy of the particle replaced by its relativistic value. One then has for the transition probability for distributions independent of the spin the following expression

*$[\mathbf{k}[\mathbf{v}_\alpha \mathbf{k}]] = \mathbf{k} \times [\mathbf{v}_\alpha \times \mathbf{k}]$.

$$W(\mathbf{p}_\alpha, \mathbf{p}_\beta; \mathbf{p}'_\alpha, \mathbf{p}'_\beta) = \frac{2\pi}{\hbar} \frac{(4\pi e_\alpha e_\beta)^2}{4E_\alpha(\mathbf{p}_\alpha) E_\alpha(\mathbf{p}'_\alpha) E_\beta(\mathbf{p}_\beta) E_\beta(\mathbf{p}'_\beta)}$$
$$\times \left\{ c^2 [p'^r_\alpha p^i_\alpha + p'^i_\alpha p^r_\alpha] - \frac{1}{2} \delta_{ir} ([E_\alpha(p'_\alpha) - E_\alpha(\mathbf{p}_\alpha)]^2 - c^2 [\mathbf{p}'_\alpha - \mathbf{p}_\alpha]^2) \right\}$$
$$\times \left\{ c^2 [p'^l_\beta p^j_\beta + p'^j_\beta p^l_\beta] - \frac{1}{2} \delta_{lj} ([E_\beta(\mathbf{p}'_\beta) - E_\beta(\mathbf{p}_\beta)]^2 - c^2 [\mathbf{p}'_\beta - \mathbf{p}_\beta]^2) \right\}$$
$$\times a^{-1}_{ij} \left(\frac{E_\beta(\mathbf{p}_\beta) - E_\beta(\mathbf{p}'_\beta)}{\hbar}, \frac{\mathbf{p}_\beta - \mathbf{p}'_\beta}{\hbar} \right)$$
$$\times a^{-1}_{rl} \left(\frac{E_\alpha(\mathbf{p}_\alpha) - E_\alpha(\mathbf{p}'_\alpha)}{\hbar}, \frac{\mathbf{p}_\alpha - \mathbf{p}'_\alpha}{\hbar} \right). \qquad (4.9)$$

In these formulas one must use the quantum expression for the permittivity tensor.

[1] Yu. L. Klimontovich and S. V. Temko, JETP **33**, 132 (1957), Soviet Phys. **6**, 102 (1958). S. V. Temko, Научн. докл. высш. шк., физ.-мат. науки (Scient. Notes of the Universities, Phys.-Math Sci.) **2**, 189 (1958).

[2] N. N. Bogolyubov, Проблемы динамической теории в статистической физике (Problems of Dynamical Theory in Statistical Physics), Gostekhizdat, 1946.

[3] O. V. Konstantinov and V. I. Perel', JETP **39**, 861 (1960), Soviet Phys. JETP **12**, 597 (1961).

[4] R. Balescu, Physics of Fluids **3**, 52 (1960).

[5] A. Lenard, Ann. of Phys. **10**, 390 (1960).

[6] N. I. Muskhelishvili, Сингулярные интегральные уравнения (Singular Integral Equations), Gostekhizdat, 1946.

[7] F. D. Gakhov, Краевые задачи (Boundary-value Problems), Fizmatgiz, 1958.

[8] L. D. Landau, JETP **7**, 203 (1936); Physik. Z. Sowjetunion **10**, 154 (1936).

[9] A. A. Rukhadze and V. P. Silin, Электромагнитные свойства плазмы и плазмоподобных сред (Electromagnetic Properties of Plasmas and Plasma-Like Media), Atomizdat, 1961.

[10] C. Møller, Z. Physik **70**, 786 (1931).

[11] Yu. L. Klimontovich, JETP **38**, 1212 (1960), Soviet Phys. JETP **11**, 876 (1960).

[12] S. T. Belyaev and G. I. Budker, Doklady Akad. Nauk SSSR **107**, 807 (1956), Soviet Phys.-Doklady **1**, 218 (1957).

[13] V. P. Silin, JETP **38**, 1577 (1960), Soviet Phys. JETP **11**, 1136 (1960).

Translated by W. H. Furry
301

SPATIAL DISPERSION IN A RELATIVISTIC PLASMA

V. N. TSYTOVICH

P. N. Lebedev Physics Institute, Academy of Sciences, U.S.S.R.

Submitted to JETP editor January 4, 1961

J. Exptl. Theoret. Phys. (U.S.S.R.) 40, 1775-1787 (June, 1961)

The dielectric constant of a relativistic plasma $\epsilon_{ij}(\omega, \mathbf{k})$ is considered with pair production taken into account. The effect of recoil on the Cerenkov absorption is also considered. The spectra for longitudinal and transverse plasma oscillations are analyzed at high densities and temperatures, in which case absorption due to pair production is possible in addition to Cerenkov absorption.

1. Spatial dispersion in an ultrarelativistic plasma has been considered by Silin[1] in the classical (nonquantum) limit. The classical analysis cannot be used at high plasma temperatures and densities. For example, at densities $N \sim 10^{32}$ cm^{-3} the natural frequency of the longitudinal oscillations is of the order of twice the mass of the electron (for $\hbar = c = 1$) and the processes of virtual and real pair production have an important effect on the dielectric constant.

However, even at low densities the relativistic quantum-mechanical calculation makes it possible to take account of recoil in the Landau damping of the longitudinal waves.[2] This damping is an inverse Cerenkov effect for the longitudinal waves, in which the wave is absorbed by free plasma electrons by virtue of the transfer of momentum to the medium (Fig. 1a). The quantum-mechanical effect of recoil on Cerenkov radiation of particles in a medium was first considered by Ginzburg.[3]

In addition to Cerenkov absorption (cf. Fig. 1a), at high densities it is possible to have absorption due to pair production (Fig. 1b); the latter process is allowed by the conservation laws because part of the momentum is taken up by the medium itself. This damping mode is possible for both the longitudinal and transverse electromagnetic waves (in appropriate regions of ω and $\mathbf{k}$). The process shown in Fig. 1a is also possible for the transverse waves.

The production of pairs in a medium has been treated by Saakyan,[4] who used a phenomenological quantum-electrodynamical description, but the spatial dispersion of the dielectric constant was not taken into account.*

*Furthermore, the expression used for $\varepsilon(\omega)$ in reference 4 is not applicable at high densities and temperatures.

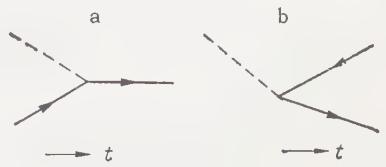

FIG. 1

2. When spatial dispersion is taken into account in an isotropic plasma, the dielectric constant becomes a three-dimensional tensor:*[6]

$$\varepsilon_{ij} = \delta_{ij} + 4\pi\omega^{-1}\sigma_{ij} = \varepsilon^t(\delta_{ij}\mathbf{k} - \mathbf{k}^{-2}k_ik_j) + \varepsilon^l\mathbf{k}^{-2}k_ik_j, \quad (1)$$

$$j_i = \sigma_{ij}(\omega,\mathbf{k})E_j, \quad \sigma_{ij}(\omega,\mathbf{k}) = \sigma^t(\delta_{ij} - \mathbf{k}^{-2}k_ik_l) + \sigma^l\mathbf{k}^{-2}k_ik_j, \quad (2)$$

where j_i is the four-dimensional Fourier component of the current, E_j is the Fourier component of the electric field, σ^l, σ^t, ϵ^l, and ϵ^t are respectively the longitudinal and transverse (in the three-dimensional sense) electrical conductivity and dielectric constant.

The four-dimensional representation can also be used:

$$j_\mu = \Pi_{\mu\nu}(\omega, k)A_\nu, \quad \Pi_{ik} = i\omega\sigma_{ik}, \quad \Pi_{i4} = \Pi_{4i} = -ik_i\sigma^l,$$
$$\Pi_{44} = -i(\mathbf{k}^2/\omega)\sigma^l, \quad (3)$$

where A_ν is the Fourier component of the potential. The relation between $\Pi_{\mu\nu}$ and σ_{ik} can be obtained easily from Eq. (1) if E_j is expressed in terms of the potentials and j_4 is found from the equation of continuity: $j_4 = -(1/i\omega)k_ij_i$. The relation in (3) can be substituted in Maxwell's equations:

$$(k_\lambda^2\delta_{\mu\nu} - k_\mu k_\nu - 4\pi\Pi_{\mu\nu})A_\nu = 4\pi j_\mu^0, \quad (4)$$

where j_μ^0 is the Fourier component of the external current.

*Hereinafter we use $\hbar = c = 1$; $i, j = 1, 2, 3$; $\mu, \nu = 1, 2, 3, 4$.

If the external source is given by a δ-function we obtain the following equation for the Green's function D:

$$(k_\lambda^2\delta_{\mu\nu} - k_\mu k_\nu - 4\pi\Pi_{\mu\nu})\, D_{\nu\sigma} = 4\pi\delta_{\mu\sigma}. \tag{5}$$

The equations for the Green's function in quantum statistics has been investigated in detail by Fradkin.[7] The equations for the time Green's functions in quantum statistics have been considered by Kogan[8] and Bonch-Bruevich.[9]

3. To terms of order e^2, the causal polarization operator $\Pi^c_{\mu\nu}$ is made up additively of the corresponding operators for the electrons and the ions. As an example let us consider the electrons:

$$\Pi^c_{\mu\nu}(\omega, \mathbf{k}) = \frac{ie^2}{(2\pi)^4}\int \mathrm{Sp}\,\gamma_\mu G(\mathbf{p}+\mathbf{k},\ \omega+\lambda)\,\gamma_\nu G(\mathbf{p}, \lambda)\, d\mathbf{p}d\lambda, \tag{6}$$

where the γ_μ are the Dirac matrices while $G(\mathbf{p}, \lambda)$ is the electron Green's function in the momentum representation:

$$G(\mathbf{p}, \lambda) = \int \mathrm{Tr}\,[\rho T(\hat{\psi}_1\hat{\bar{\psi}}_2)]\, e^{-i\mathbf{p}\mathbf{r}+i\lambda t}\, d\mathbf{r}dt, \tag{7}$$

where $\mathbf{r} = \mathbf{r}_1 - \mathbf{r}_2$, $t = t_1 - t_2$, T is the sign of the time ordering, ρ is the density matrix ($\mathrm{Tr}\,\rho = 1$), $\hat{\psi}_1 \equiv \hat{\psi}(\mathbf{r}_1, t_1)$ and $\hat{\bar{\psi}}_2 = \hat{\bar{\psi}}(\mathbf{r}_2, t_2)$ are operators in the interaction representation:

$$\hat{\psi}(\mathbf{r}, t) = \exp\,[it(\hat{H}_0 - \mu\hat{N}_0)]\,\hat{\psi}(\mathbf{r})\,\exp\,[-it(\hat{H}_0 - \mu\hat{N}_0)],$$

μ is the chemical potential of the system, $\hat{H}_0$ is the Hamiltonian for the free Dirac particles, $\hat{N}_0$ is the operator for the conservation of the difference in the number of particles and antiparticles, Sp denotes summation over the spin indices, and Tr is the statistical average.

Expanding $\hat{\psi}$ in plane waves and substituting in Eq. (7) we have*

$$G(\mathbf{p}, \omega) = G^-(\mathbf{p}, \omega)\,(m - i\hat{p}^-)/2\varepsilon_\mathbf{p} + G^+(\mathbf{p}, \omega)\,(m - i\hat{p}^+)/2\varepsilon_\mathbf{p}, \tag{8}$$

$$\hat{p} = \gamma_\mu p_\mu, \qquad p^-_\mu = \{\mathbf{p}, i\varepsilon_\mathbf{p}\}, \qquad p^+_\mu = \{\mathbf{p}, -i\varepsilon_\mathbf{p}\};$$

$$G^\pm(\mathbf{p}, \omega) = \frac{1}{i}\left\{\frac{n^\pm_\mathbf{p}}{\varepsilon_\mathbf{p} \mp \mu \pm \omega + i\delta} + \frac{1 - n^\pm_\mathbf{p}}{\varepsilon_\mathbf{p} \mp \mu \pm \omega - i\delta}\right\}, \tag{9}$$

where $\varepsilon_\mathbf{p} = \sqrt{\mathbf{p}^2 + m^2}$ is the modulus of the energy while $n^\pm_\mathbf{p}$ is respectively the mean number of positrons and electrons with energy $\varepsilon_\mathbf{p}$ for the density matrix ρ. The expression for $G(\mathbf{p}, \omega)$ in the nonrelativistic limit (without the positron part) has been given, for example, by Kogan.[8]

*The chemical potential appears with opposite sign in the expression for the mean number of positrons, since the number of positrons $n^+_\mathbf{p}$ is

$$1 - n^-_{\varepsilon<0} = 1 - \{\exp(-\varepsilon - \mu)\beta + 1\}^{-1} = \{1 + \exp(\varepsilon + \mu)\beta\}^{-1}.$$

The further calculations are very simple. It is necessary to substitute (8) in (6), compute the traces of the γ-matrices by the conventional rule,[10] and integrate the resultant expression with respect to λ, taking account of the fact that the products of the terms $G^\pm$, which contain poles in different half-planes of the complex variable λ, make a contribution to the integral. We give the result for the longitudinal and transverse parts of the dielectric constant ϵ^l and ϵ^t:*

$$\varepsilon^{l,t} = 1 - \frac{4\pi e^2}{\omega^2}\int f(\varepsilon_\mathbf{p})\, d\mathbf{p}\left\{\frac{\varepsilon_\mathbf{p} - \varepsilon_{\mathbf{p}-\mathbf{k}}}{(\varepsilon_\mathbf{p} - \varepsilon_{\mathbf{p}-\mathbf{k}})^2 - \omega^2}\,\Lambda^{l,t}_- + \frac{\varepsilon_\mathbf{p} - \varepsilon_{\mathbf{p}-\mathbf{k}}}{(\varepsilon_\mathbf{p} + \varepsilon_{\mathbf{p}-\mathbf{k}})^2 - \omega^2}\,\Lambda^{l,t}_+\right\} + \delta\varepsilon^{l,t}_B,$$

$$\Lambda^l_\pm = 1 \mp \frac{\varepsilon^2_\mathbf{p} + (\mathbf{pk}) - 2(\mathbf{pk})^2/\mathbf{k}^2}{\varepsilon_\mathbf{p}\varepsilon_{\mathbf{p}-\mathbf{k}}},$$

$$\Lambda^t_\pm = 1 \mp \frac{m^2 - (\mathbf{pk}) + (\mathbf{pk})^2/\mathbf{k}^2}{\varepsilon_\mathbf{p}\varepsilon_{\mathbf{p}-\mathbf{k}}}, \quad f(\varepsilon_\mathbf{p}) = 2(2\pi)^{-3}(n^-_\mathbf{p} + n^+_\mathbf{p}),$$

$$\delta\varepsilon^t_B\omega^2 = (\omega^2 - k^2)\,\delta\varepsilon^l_B = \Pi_B = \frac{e^2}{\pi^2}\int \Lambda^t_+ \frac{\varepsilon_\mathbf{p} + \varepsilon_{\mathbf{p}-\mathbf{k}}}{(\varepsilon_\mathbf{p} + \varepsilon_{\mathbf{p}-\mathbf{k}})^2 - \omega^2}\, d\mathbf{p}; \tag{10}$$

the quantity $\delta\epsilon^{l,t}$ is obtained from that part of the polarization operator which does not vanish when $n^+_\mathbf{p} = n^-_\mathbf{p} = 0$; after the standard renormalization, this quantity gives the usual expression for the vacuum polarization† (cf. reference 10).

*The causal operator $\Pi^c_{\mu\nu}$ can only be used to find the real parts of ε^l and ε^t and the momentum integrals are to be understood in the sense of the principal value. The imaginary part of the causal operator will not correspond to the imaginary parts of ε^l and ε^t, which are determined by the retarded Green's function for the photon. The imaginary parts can be found by means of the Kramers-Kronig relations for σ^l and σ^t and the easily derived formula

$$\frac{1}{\pi}\int\!\!\!\!\!\!-\frac{dx}{x-\omega}\int\!\!\!\!\!\!-\frac{\varphi(y)}{f(y)-x}\,dy = -\pi\int dy\,\varphi(y)\,\delta(f(y)-\omega),$$

where the slash denotes an integral in the sense of the principal value. Thus, to obtain the imaginary parts the energy denominators must be replaced by $-i\pi\delta$-functions or, what is the same, for the complex ε^l and ε^t in Eq. (10) we are to understand ω in the sense of $\omega = \omega + i\delta$ with $\delta \to +0$.

†The relation between $\delta\varepsilon^t$ and $\delta\varepsilon^l$ follows from the four-dimensional tranversality of the vacuum polarization operator. The real parts of $\delta\varepsilon$ are small also away from the light cone ($\omega \approx k$), and will be neglected hereafter. However, the imaginary part of $\delta\varepsilon$ is very important for the description of pair production in the medium by a photon. In particular, if the imaginary part of $\delta\varepsilon$ is not taken into account a meaningless result is obtained; the amplitude of the wave increases because of pair production, i.e., the oscillations are excited rather than damped. The imaginary part of $\delta\varepsilon$ is usually not considered because it vanishes everywhere except far from the light cone $\omega^2 > 4m^2 + k^2$ (cf. below). The dispersion curves for the longitudinal and transverse waves can only fall in this region if the particle density of the medium is greater than 10^{32} cm^{-3} (cf. below).

In the nonrelativistic limit Eq. (10) coincides with the familiar expressions (cf. reference 6) obtained from the kinetic equation. If the positron contribution is neglected ($n_{\mathbf{p}}^{+} = 0$) in the nonquantum-mechanical ($\mathbf{k} \ll \mathbf{p}$) ultrarelativistic limit $p \gg m$, the equations in (10) lead to the results obtained by Silin[1] by means of the kinetic equation. Below we shall only discuss results not contained in reference 1.

It should be emphasized that the positron contribution cannot be neglected in the ultrarelativistic limit if the system has attained total equilibrium. In this case the chemical potential of the system μ must be found from the relation

$$\frac{2}{(2\pi)^3}\int (n_{\mathbf{p}}^{-} - n_{\mathbf{p}}^{+})\, dp = N, \tag{11}$$

where N is the difference between the number of particles and antiparticles in the system.

4. Spatial dispersion can be neglected in the limit of small wave vectors $\mathbf{k}$, and the real part becomes*

$$\operatorname{Re}\varepsilon(\omega) = 1 - \frac{4\pi e^2}{\omega^2}\int f(\varepsilon_{\mathbf{p}})\,\frac{4\varepsilon_{\mathbf{p}}(1 - p^2/3\varepsilon_{\mathbf{p}}^2)\,d\mathbf{p}}{4\varepsilon_{\mathbf{p}}^2 - \omega^2}. \tag{12}$$

At relatively low frequencies $\omega \ll 2\epsilon_{\mathbf{p}}$ Eq. (12) yields the well-known expression

$$\operatorname{Re}\varepsilon(\omega) = 1 - \frac{\omega_0^2}{\omega^2}, \qquad \omega_0^2 = 4\pi e^2\int \frac{f(\varepsilon_{\mathbf{p}})}{\varepsilon_{\mathbf{p}}}\left(1 - \frac{1}{3}\frac{p^2}{\varepsilon_{\mathbf{p}}^2}\right)d\mathbf{p}. \tag{13}$$

When $n_{\mathbf{p}}^{+} = 0$ the expression for the natural plasma frequency ω_0 in ultrarelativistic ($\mathbf{p} \gg m$) degenerate and nondegenerate gases coincides with the expression given by Silin.[1] If, however, a system at relativistic temperatures reaches total equilibrium, then at sufficiently high temperatures $\mu = 0$, $n_{\mathbf{p}}^{+} \approx n_{\mathbf{p}}^{-} = [\exp(p\beta) + 1]^{-1}$ and

$$\omega_0^2 = 2\zeta(2)\, e^2/3\pi\beta^2, \tag{14}$$

where ζ is the Riemann zeta function.

At high frequencies $\omega \gg 2\epsilon_{\mathbf{p}}$

$$\operatorname{Re}\varepsilon(\omega) = 1 + Z/\omega^4,$$

$$Z = 16\pi e^2\int f(\varepsilon_{\mathbf{p}})\,\varepsilon_{\mathbf{p}}\left(1 - \frac{1}{3}\frac{\mathbf{p}^2}{\varepsilon_{\mathbf{p}}^2}\right)d\mathbf{p}. \tag{15}$$

For nonrelativistic temperatures $Z = 16\pi e^2 mN$ whereas for ultrarelativistic temperatures, if the positron contribution is neglected ($n_{\mathbf{p}}^{+} = 0$), in a nondegenerate gas $Z = 32\pi e^2 N/\beta$ while in a degenerate gas $Z = 4\pi e^2 N p_0$ ($p_0 = 2\pi[3N/8\pi]^{1/3}$ is the limiting momentum at the Fermi surface). For total equilibrium and ultrarelativistic temperatures

$$Z = 120 e^2\zeta(4)/\pi\beta^4. \tag{16}$$

5. To obtain the imaginary part of $\epsilon^{l,t}$ we must replace the energy denominators by δ functions which express the conservation of momentum and energy for the diagrams in Fig. 1. In momentum space $\mathbf{p}$ we introduce a cylindrical coordinate system with Z axis in the direction of the wave vector $\mathbf{k}$. With no loss of generality (formally, we replace $\mathbf{p}$, the variable of integration in Eq. (10), by $\mathbf{p} \pm \mathbf{k}/2$) we can set the initial momentum of the electron equal to $\mathbf{p} - \mathbf{k}$ so that $\mathbf{p}$ is finite and the energy conservation relation for Cerenkov dissipation* (Fig. 1a)

$$\omega = \varepsilon_{\mathbf{p}} - \varepsilon_{\mathbf{p}-\mathbf{k}} \tag{17}$$

allows us to find the electron momentum component p_z as a function of k, ω and $\epsilon_\perp = \sqrt{p_\perp^2 + m^2}$ ($\mathbf{p}_\perp$ is the momentum perpendicular to $\mathbf{k}$).

Equation (17) has two roots

$$p_z^{\pm} = k/2 \pm (\omega/k)\,\varkappa,$$
$$\varkappa = [\varepsilon_\perp^2/(1 - \omega^2/k^2) + k^2/4]^{1/2}. \tag{18}$$

Substituting Eq. (17) in $\epsilon_{\mathbf{p}}$ and $\epsilon_{\mathbf{p}-\mathbf{k}}$ we obtain different signs for the two possible values $\epsilon_{\mathbf{p}}^{\pm}$ and $\epsilon_{\mathbf{p}-\mathbf{k}}^{\pm}$ (ϵ^{+} denotes ϵ for $p_z = p_z^{+}$ while ϵ^{-} denotes ϵ for $p_z = p_z^{-}$). Equation (17) is satisfied only by p_z^{+} and

$$\varepsilon_{\mathbf{p}}^{+} = \omega/2 + \varkappa, \qquad \varepsilon_{\mathbf{p}-\mathbf{k}}^{+} = \varkappa - \omega/2. \tag{19}$$

On the other hand, the values p_z^{-}, $\epsilon_{\mathbf{p}}^{-} = \kappa - \omega/2$, $\epsilon_{\mathbf{p}-\mathbf{k}}^{-} = \omega/2 + \kappa$ satisfy the conservation law $\omega = \epsilon_{\mathbf{p}-\mathbf{k}} - \epsilon_{\mathbf{p}}$ which corresponds to another possible absorption process in which the initial momentum is $\mathbf{p}$ and the final momentum is $\mathbf{p} + \mathbf{k}$. It thus follows that Cerenkov dissipation is possible only when $\kappa^2 > \omega^2/4$ or, what is the same thing, when $\omega/k \ll 1$. This result means that Cerenkov damping occurs only for phase velocities smaller than the velocity of light when recoil is taken into account.

The energy conservation relation for dissipation due to pair production $\omega = \epsilon_{\mathbf{p}} + \epsilon_{\mathbf{p}-\mathbf{k}}$ has the same solutions (18) for p_z as (17). Both values $p_z^{\pm}$ satisfy the conservation relation; the signs must be chosen in the following manner: $\epsilon_{\mathbf{p}}^{\pm} = \omega/2 \pm \kappa$. For $\epsilon_{\mathbf{p}}^{\pm}$ to be positive we require $\omega^2/4 > \kappa^2$; this is possible only when $\omega^2/k^2 > 1$. Thus dissipation due to pair production arises only when the phase velocity of the wave is greater than the velocity of light.

*Equation (12) coincides with the expression obtained by Fradkin.[7]

*To be specific we take $\omega > 0$.

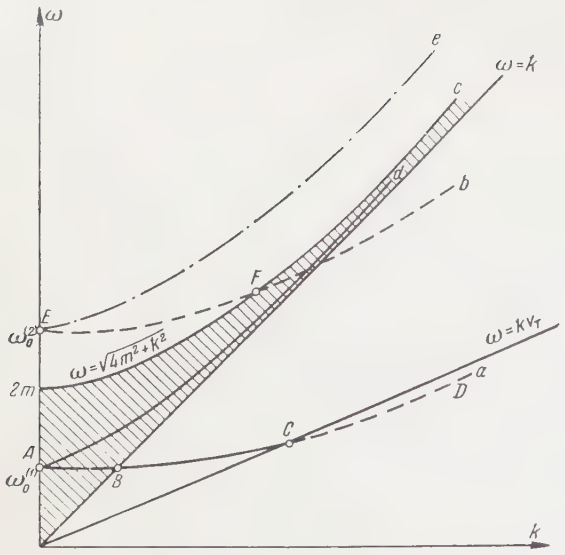

FIG. 2. a – dispersion curve for longitudinal waves for low densities, d – dispersion curve for transverse waves for low densities, b – dispersion curve for longitudinal waves for high densities, e – dispersion curve for transverse waves for high densities, BC – region of weak damping, CD – region of strong damping, EF – region of damping due to pair production.

However, there is an energy threshold for the latter process; this threshold follows from the requirement that the quantity under the radical in the expression for κ must be positive. Since the distribution contains particles with arbitrary momenta, in particular, momenta parallel to $\mathbf{k}$ ($p_\perp = 0$), it is sufficient to satisfy this condition for $\epsilon_\perp^2 = m^2$:

$$\omega^2 > 4m^2 + k^2. \tag{20}$$

In the $\omega - k$ plane the line $\omega = k$ and the curve $\omega^2 = 4m^2 + k^2$ define the region in which neither of the dissipation mechanisms considered above is possible (the cross-hatched region in Fig. 2). This region is bordered on both sides by regions in which the absorption is relatively small.

6. The calculation of the imaginary parts of $\epsilon^{l,t}$ is simplified by the fact that the integration over p_z can be carried out in elementary fashion by means of δ-functions. Thus, for the imaginary part of ϵ^l, which describes the Cerenkov absorption of the longitudinal waves, we have from Eq. (10)

$$\operatorname{Im}\varepsilon^l_{\text{cer}} = \frac{8\pi^3 e^2}{k^3}\int_{\varkappa_0}^{\infty}\left(\varepsilon^2 - \frac{k^2}{4}\right)\left[f\left(\varepsilon - \frac{\omega}{2}\right) - f\left(\varepsilon + \frac{\omega}{2}\right)\right]d\varepsilon, \tag{21}$$

where $\varkappa_0 = \varkappa\big|_{e_\perp = m}$. If the positrons are neglected, in a Boltzmann gas $f(\epsilon) = 2(2\pi)^{-3}e^{(\mu-\epsilon)\beta}$ and after an elementary integration we have

$$\operatorname{Im}\varepsilon^l_{\text{cer}} = \frac{4e^2}{k^3\beta}e^{\mu\beta}\operatorname{sh}\frac{\omega\beta}{2}\left\{\frac{m^2}{1-\omega^2/k^2} + \frac{2}{\beta}\varkappa_0 + \frac{2}{\beta^2}\right\}e^{-\beta\varkappa_0}. \tag{22}$$

*sh = sinh.

The integration is also elementary for a degenerate gas.

The imaginary part of ϵ^t, which describes Cerenkov absorption (Fig. 1a), is computed in similar fashion

$$\operatorname{Im}\varepsilon^t_{\text{cer}} = \frac{4\pi^3 e^2}{\omega^2 k}\left(1 - \frac{\omega^2}{k^2}\right)\int_{\varkappa_0}^{\infty}\left(\varepsilon^2 + \frac{k^2}{2} - \varkappa_0^2\right)\left[f\left(\varepsilon - \frac{\omega}{2}\right) - f\left(\varepsilon + \frac{\omega}{2}\right)\right]d\varepsilon. \tag{23}$$

In particular, for a Boltzmann electron gas

$$\operatorname{Im}\varepsilon^t_{\text{cer}} = \frac{4e^2(1-\omega^2/k^2)}{\omega^2 k\ \beta^3}\left(1 + \beta\varkappa_0 + \frac{k^2\beta^2}{4}\right)e^{(\mu-\varkappa_0)\beta}\operatorname{sh}\frac{\omega\beta}{2}. \tag{24}$$

The damping due to pair production (Fig. 1b) is computed in similar fashion from Eq. (10):

$$\operatorname{Im}\varepsilon^l_{\text{pair}} = -\frac{8\pi^3 e^2}{k^3}\frac{\omega}{|\omega|}\int_0^{\varkappa_0}\left(\frac{k^2}{4} - \varepsilon^2\right)\left[f\left(\varepsilon + \frac{\omega}{2}\right) + f\left(\frac{\omega}{2} - \varepsilon\right)\right]d\varepsilon + \operatorname{Im}\delta\varepsilon^l_{\text{pair}}, \tag{25}$$

$$\operatorname{Im}\varepsilon^t_{\text{pair}} = -\frac{4\pi^3 e^2}{\omega^2 k}\left(\frac{\omega^2}{k^2} - 1\right)\frac{\omega}{|\omega|}\int_0^{\varkappa_0}\left(\frac{k^2}{2} - \varkappa^2 + \varepsilon^2\right)\left[f\left(\frac{\omega}{2} + \varepsilon\right) + f\left(\frac{\omega}{2} - \varepsilon\right)\right]d\varepsilon + \operatorname{Im}\delta\varepsilon^t_{\text{pair}}, \tag{26}$$

$$\operatorname{Im}\delta\varepsilon^l_{\text{pair}} = \frac{\omega^2}{\omega^2 - k^2}\operatorname{Im}\delta\varepsilon^t_{\text{pair}} = \frac{e^2\varkappa_0}{3k^3}\left(k^2 + \frac{2m^2}{\omega^2/k^2 - 1}\right). \tag{27}$$

In particular, for a Boltzmann gas ($\operatorname{Im}\epsilon_{\text{pair}} = \operatorname{Im}\tilde{\epsilon}_{\text{pair}} + \operatorname{Im}\delta\epsilon_{\text{pair}}$)

$$\operatorname{Im}\tilde{\varepsilon}^t_{\text{pair}} = -\frac{4e^2}{k^3\beta^3}e^{-\beta(\omega/2-\mu)}\frac{\omega}{|\omega|}\left[\left(\frac{k^2\beta^2}{4} - 2 - \varkappa_0^2\beta^2\right)\operatorname{sh}\varkappa_0\beta + 2\varkappa_0\beta\operatorname{ch}\varkappa_0\beta\right], \tag{28}$$

$$\operatorname{Im}\tilde{\varepsilon}^t_{\text{pair}} = -\frac{4e^2}{\omega^2 k\beta^2}\frac{\omega}{|\omega|}\left(\frac{\omega^2}{k^2} - 1\right)e^{-\beta(\omega/2-\mu)}\left[\left(1 + \frac{k^2\beta^2}{4}\right)\operatorname{sh}\varkappa_0\beta - \varkappa_0\beta\operatorname{ch}\varkappa_0\beta\right], \tag{29}$$

*ch = cosh.

7. We now consider the spectrum of electromagnetic oscillations and the damping. We start with the longitudinal waves, for which

$$\varepsilon^l(\omega, \mathbf{k}) = 0.$$

For weak damping $\bar{\omega} = \omega - i\gamma$ ($\gamma \ll \omega$) (cf. reference 6)

$$\operatorname{Re}\varepsilon^l(\omega, \mathbf{k}) = 0, \qquad \gamma = \operatorname{Im}\varepsilon^l \Big/ \frac{\partial}{\partial\omega}\operatorname{Re}\varepsilon^l. \tag{30}$$

At relatively low densities $\omega_0 \ll 2m$ there is a region of ω and $\mathbf{k}$ in which the spatial dispersion of the longitudinal waves can be considered weak ($k \ll \omega$) for any temperature $1/\beta$:

$$\operatorname{Re}\varepsilon^l(\omega, k) = \varepsilon(0) - \omega_0^2/\omega^2 - (k^2/\omega^2)\,u^l(\omega^2), \tag{31}$$

$$\varepsilon(0) = 1 - \pi e^2\int d\mathbf{p} f(\varepsilon_p)\frac{1}{\varepsilon_p^2}\left(1 - \frac{1}{3}\frac{\mathbf{p}^2}{\varepsilon_p^2}\right), \tag{32}$$

$$u^l(\omega^2) = \varepsilon(0) - 1 + \frac{4\pi e^2}{\omega^2}\int d\mathbf{p} f(\varepsilon_p)\frac{\mathbf{p}^2}{\varepsilon_p^3}\left(1 - \frac{3}{5}\frac{\mathbf{p}^2}{\varepsilon_p^2}\right), \tag{33}$$

while ω_0 is given by Eq. (13).

Together with Eqs. (22) and (31), the dispersion equations (30) lead to a spectrum of weakly damped longitudinal oscillations:

$$\omega^2 = \frac{1}{\varepsilon(0)}(\omega_0^2 + k^2 u^l (\omega_0^2/\varepsilon(0))), \tag{34}$$

$$\gamma = \sqrt{\frac{\pi}{8}} \frac{1}{k^3 d^3} \omega_0 \left(\frac{2}{\omega_0 \beta} \operatorname{sh} \frac{\omega_0 \beta}{2}\right) \frac{1}{1-\omega^2/k^2} e^{-\beta \varkappa_0};$$

$$d^2 = (4\pi N e^2 \beta)^{-1}. \tag{35}$$

It should be noted that while Eq. (34) is valid for undamped oscillations ($k < \omega$) and ultrarelativistic temperatures,* the damping expression (35) applies only for nonrelativistic temperatures because the expansion in (31) does not apply in the region $k > \omega$ for $u^l \sim 1$ (u^l is of the order of the mean square thermal velocity of the particles). For this reason we have neglected terms of order $1/\beta m \ll 1$ in Eq. (22). When $\omega_0 \beta \ll 1$, $k \gg \omega$ and $k \ll m$, Eq. (35) gives the familiar Landau damping.[2] As is well known, in this case the oscillations are weakly damped at wavelengths large compared with the Debye radius $dk \ll 1$ (dashed line in Fig. 2).

We now consider the extent to which damping is reduced at nonrelativistic temperatures when recoil is taken into account in absorption (the $k^2/4$ term in the expression for κ_0^2). When $k^2/4 \ll m^2$ there is an additional factor $\exp[-\beta(k^2/8m)\times\sqrt{1-\omega^2/k^2}$ which can reduce the damping at $k \gg \omega$ if $k^2 \gg 8m/\beta$. For wavelengths of the order of the Debye radius this gives $\beta^2 \gg 8/\omega_0^2$; if the gas is nondegenerate $N \ll 2m^{3/2}(2\pi\beta)^{-3/2}$ we find

$$\beta m \gg 8\pi/e^4 = 0.5 \cdot 10^6, \tag{36}$$

where (36) must be satisfied with a margin of at least two orders of magnitude. In other words, the damping can decrease only at sufficiently low temperatures. It also follows from Fig. 2 that a region of undamped and weakly damped oscillations exists for $\omega \gg 2m$ when $k \sim m$. It is easy to verify that Eq. (30) always has real solutions in this region. We find $\epsilon^l|_{\omega=k}$ for this region. Integrating over the angles, we have from Eq. (10):

$$\operatorname{Re} \varepsilon^l(\omega, k)|_{\omega=k} = 1 - \omega_l^2/\omega^2,$$

$$\omega_l^2 = 4\pi e^2 \int f(\varepsilon_p) \left[\frac{2}{p} \ln \frac{\varepsilon_p + p}{m} - \frac{1}{\varepsilon_p}\right] dp. \tag{37}$$

At nonrelativistic temperatures $\omega_l^2 \approx \omega_0^2$ whereas for ultrarelativistic temperatures there is an additional factor of order $\ln(\alpha/m\beta)$, where $\alpha \sim 1$. Thus, it is convenient to seek a solution of Eq. (30) in the region $k \approx \omega \approx \omega_l$ taking $k = \omega_l + \Delta k$, $\omega = \omega_l + \Delta\omega$, and expanding in Δk and $\Delta\omega$:

*In this case $\omega^2 = \omega_0^2/\varepsilon(0) + k^2[8/5 - 1/\varepsilon(0)]$.

$$\operatorname{Re}\left\{\Delta\omega \left.\frac{\partial \varepsilon^l}{\partial \omega}\right|_{\omega=k=\omega_l} + \Delta k \left.\frac{\partial \varepsilon^l}{\partial k}\right|_{\omega=k=\omega_l}\right\} = 0;$$

$$\operatorname{Re} \left.\frac{\partial \varepsilon^l}{\partial \omega}\right|_{\omega=k=\omega_l} = \frac{8\pi e^2}{\omega_l^3} \int \frac{f(\varepsilon_p)}{\varepsilon_p} \left[\frac{2\varepsilon_p^2}{m^2} - \frac{\varepsilon_p}{p} \ln \frac{\varepsilon_p + p}{m}\right] dp, \tag{38}$$

$$\operatorname{Re} \left.\frac{\partial \varepsilon^l}{\partial k}\right|_{\omega=k=\omega_l} = -\frac{8\pi e^2}{\omega_l^3} \int \frac{f(\varepsilon_p)}{\varepsilon_p} \left[1 + 2\frac{\varepsilon_p^2}{m^2} - \frac{3\varepsilon_p}{p} \ln \frac{\varepsilon_p + p}{m}\right] dp. \tag{39}$$

It follows that the slope of the dispersion curve with respect to the line $\omega = k$ (Fig. 2) decreases rapidly as the temperature increases

$$\Delta\omega/\Delta k = 1 - \tfrac{1}{3} m^2 \beta^2 \ln(2C\sqrt{e}/m\beta), \tag{40}$$

where C is the Euler constant.

Equation (38) is used to determine the damping. Thus, for ultrarelativistic temperatures close to threshold ($\Delta k \ll \omega_l$)

$$\gamma = \omega_l \pi m^2 \beta^2 \frac{\operatorname{sh}(\omega_l \beta/2)}{\omega_l \beta/2} \left[\frac{3\omega_l}{2\Delta k \ln \Lambda} + 2 + 2\left[\frac{3\omega_l}{2\Delta k \ln \Lambda} + \frac{\omega_l^2 \beta^2}{4}\right]^{1/2}\right]$$
$$\times \exp\left[-\left(\frac{3\omega_l}{2\Delta k \ln \Lambda} + \frac{\omega_l^2 \beta^2}{4}\right)^{1/2}\right], \quad \Lambda = \frac{2C\sqrt{e}}{m\beta}. \tag{41}$$

At threshold ($\omega \approx k$) the damping is exponentially small at any temperature.

The damping is described by Eq. (41) for any density, in particular for $\omega_l \gg 2e_p$. At high densities ($\omega_l \gg 2m$) the gas is always ultrarelativistic.* To analyze the damping far from threshold we use the fact that the dispersion curve approaches $\omega = k$ in the ultrarelativistic limit. For arbitrary ω we write $k = \omega + \Delta k$. Using Eq. (39) with Eq. (30) we can express Δk as a function of ω

$$\frac{\Delta k}{\omega} = \frac{\omega^2 - \omega_l^2}{\omega_s^2}, \quad \omega_s^2 = 8\pi e^2 \int \frac{f(\varepsilon_p)}{\varepsilon_p} \left(1 + 2\frac{\varepsilon_p^2}{m^2} - \frac{3\varepsilon_p}{p} \ln \frac{\varepsilon_p + p}{m}\right) dp. \tag{42}$$

Since ω_s^2 is of order $\omega_l^2/m^2\beta^2 \gg \omega_l^2$, Eq. (42) gives the dispersion curve up to frequencies of approximately $\omega_l/m\beta \gg \omega_l$. In the region $\omega_l \ll \omega \ll \omega_l/m\beta$ the damping is given by

$$\gamma = \frac{\pi}{48} \omega m^2 \beta^2 \frac{\operatorname{sh}(\omega\beta/2)}{\omega\beta/2} \left[\frac{m^2\beta^2\omega_s^2}{2\omega^2} + 2\left(\frac{m^2\beta^2\omega_s^2}{2\omega^2} + \frac{\omega^2\beta^2}{4}\right)^{1/2} + 2\right]$$
$$\times \exp\left[-\left(\frac{m^2\beta^2\omega_s^2}{2\omega^2} + \frac{\omega^2\beta^2}{4}\right)^{1/2}\right] \tag{43}$$

and ceases to be exponentially small only when $\omega \sim \omega_l/m\beta$; however, it is still rather small: $\gamma/\omega \sim m^2\beta^2 \ll 1$.

When $k \gg \omega$ and $m\beta \ll 1$, in the classical limit the quantity $\operatorname{Im} \epsilon^l$ coincides with the results of reference 1. The oscillations are strongly damped in this case.

*The limiting momentum for a degenerate gas p_0 is high when $\omega_l = 2m$: this momentum is given by $p_0^2/m^2 = 9\pi/2e^2 \gg 1$.

8. At high densities and temperatures the longitudinal oscillations can be damped as a result of pair production (Fig. 1b). The dispersion curve for the longitudinal oscillations must intersect the line $\omega^2 = 4m^2 + k^2$ (cf. Fig. 2) for this to occur. To analyze the pair-production damping we calculate Re ϵ^l for an ultrarelativistic Boltzmann electron gas by means of Eq. (10)*

$$\operatorname{Re}\varepsilon^l = 1 + \frac{4\pi N e^2\beta}{k^2} + \frac{4\pi N e^2\beta}{k^2(1-k^2/\omega^2)(\varepsilon_1-\varepsilon_2)} \times \left[\frac{m^2+\varepsilon_1(k^2-\omega^2)/2\omega}{\sqrt{\varepsilon_1^2-m^2}}\ln\frac{\varepsilon_1+\sqrt{\varepsilon_1^2-m^2}}{m} + \frac{m^2+\varepsilon_2(k^2-\omega^2)/2\omega}{\sqrt{\varepsilon_2^2-m^2}}\ln\frac{\varepsilon_2+\sqrt{\varepsilon_2^2-m^2}}{m}\right],$$

where

$$\varepsilon_{1,2} = \omega/2 \pm \varkappa^2, \qquad \omega\beta \ll 1, \qquad k\beta \ll 1, \qquad m\beta \ll 1. \quad (44)$$

It follows from Eq. (44) that on the curve $\omega^2 = 4m^2 + k^2$

$$\operatorname{Re}\varepsilon^l = 1 - \frac{4\pi N e^2\beta}{k^2}\left[\frac{\sqrt{4m^2+k^2}}{k}\ln\frac{k+\sqrt{k^2+4m^2}}{2m} - 1\right]. \quad (45)$$

In particular, as $k \to 0$, Re $\epsilon^l \to 1 - \pi N e^2\beta/3m$.

At high densities $N > 10^{33}$ cm^{-3}, Re ϵ^l can vanish. When k increases, the function $1 - \operatorname{Re}\epsilon^l$ decreases monotonically at threshold, corresponding to the intersection of the curve $\omega^2 = 4m^2 + k^2$ with the dispersion curves for all high densities N.

The behavior of the dispersion curve close to threshold can be described approximately by expanding the relation $\epsilon^l(\omega, k) = 0$ in powers of $\Delta\omega = \omega - \omega_0$ and $\Delta k = k - k_0$, where k_0 and ω_0 define the point at which the dispersion curve intersects the threshold $\omega_0^2 = 4m^2 + k_0^2$. By definition $\epsilon^l(\omega_0, k_0) = 0$ so that

$$\frac{\Delta\omega}{\Delta k} = -\left(\frac{\partial\varepsilon^l}{\partial k}\Big/\frac{\partial\varepsilon^l}{\partial\omega}\right)_{\omega_0, k_0}. \quad (46)$$

The derivatives which appear here can be computed from Eq. (44):

$$\left.\frac{\partial\varepsilon^l}{\partial k}\right|_{\omega_0, k_0} = 4\pi N e^2\beta\left[\frac{3\sqrt{k_0^2+4m^2}}{k_0^4}\ln\frac{k_0+\sqrt{k_0^2+4m^2}}{2m} - \frac{1}{4k_0m^2} - \frac{3}{k_0^3}\right], \quad (47)$$

$$\left.\frac{\partial\varepsilon^l}{\partial\omega}\right|_{\omega_0, k_0} = -\frac{4\pi N e^2\beta}{k_0^2}\left[\frac{1}{k_0}\ln\frac{k_0+\sqrt{k_0^2+4m^2}}{2m} - \frac{1}{4m^2}\sqrt{k_0^2+4m^2}\right]. \quad (48)$$

*The real parts of ε^l and ε^t were computed exactly for a Boltzmann gas. Equation (44) is obtained as a limiting case of the resulting complicated expressions, which are not given here.

When $k_0 \ll m$ we have $\Delta\omega = (3k_0/40m)\Delta k$. When $k_0 \gg 2m$, we have $\Delta k = \Delta\omega$. The approximate behavior of the longitudinal dispersion curve at high densities and temperatures is shown in Fig. 2 (dashed line).

The damping factor close to the pair-production threshold can be found easily from Eqs. (27) and (30):*

$$\frac{\gamma^l_{\text{pair}}}{2m} = \frac{1}{32}e^2\sqrt{\frac{\Delta\omega}{m}}, \qquad k_0 \ll m,$$

$$\frac{\gamma^l_{\text{pair}}}{k_0} = \frac{2e^2}{3}\sqrt{\frac{\Delta\omega}{m}}\left(\frac{m}{k_0}\right)^{3/2}\frac{1}{\ln 0.37\, k_0/m}, \qquad k_0 \gg m. \quad (49)$$

We note that, in contrast with Cerenkov damping, the pair-production damping vanishes close to threshold not exponentially but as $\sqrt{\Delta\omega}$.

9. We now consider the transverse plasma oscillations. Separating the real and imaginary parts in the transverse dispersion equation

$$\omega^2\varepsilon^t = k^2, \quad (50)$$

we obtain for weak damping

$$\omega^2 \operatorname{Re}\varepsilon^t = k^2, \qquad \gamma = \omega^2 \operatorname{Im}\varepsilon^t / \frac{\partial}{\partial\omega}\omega^2 \operatorname{Re}\varepsilon^t. \quad (51)$$

It follows from (51) that $k^2 \ll \omega^2$ corresponds to Re $\epsilon^t \ll 1$. In other words, the frequency ω must be close to the plasma frequency ω_0 [Eq. (13)] if the spatial dispersion is to be weak.

At frequencies far from the plasma frequency spatial dispersion is important only at relativistic temperatures. If we assume that Re ϵ^t is approximately unity so that $\omega \sim k$, we can write in accordance with Eq. (51) $\omega = k$ in Eq. (10), the expression for ϵ^t. Thus we find

$$\varepsilon^t(\omega, \omega) = 1 - \frac{\omega_t^2}{\omega^2}, \qquad \omega_t^2 = 4\pi e^2\int\frac{f(\varepsilon_p)}{\varepsilon_p}dp. \quad (52)$$

In the ultrarelativistic limit ω_t^2 is $3/2$ times larger than ω_0^2. At low densities ($\omega_0^2 \ll 4m^2$) the dispersion curve for the transverse oscillations lies inside the region in which there is neither Cerenkov nor pair-production damping (cf. Fig. 2).

Pair-production damping appears at high densities. To analyze the spectrum of transverse os-

*The temperature effects contained in Eqs. (28) and (29) reduce the damping to some extent; however, this reduction is small for a Boltzmann gas because the corresponding terms contain the small factor $\exp(\mu\beta) \ll 1$. These terms, which are proportional to β^2, are omitted in Eq. (49). It is also easy to write general formulas for an ultrarelativistic Boltzmann gas by dividing Eq. (27) by $\partial\varepsilon/\partial\omega$ from Eq. (44). For a degenerate gas the contributions of Im $\varepsilon^l_{\text{pair}}$ and Im $\delta\varepsilon^l_{\text{pair}}$ are of the same order of magnitude and decrease together for $\mu > \omega/2 + \varkappa$, whereas for $\omega/2 > \mu + \varkappa$ we have Im $\varepsilon^l_{\text{pair}}$ = Im $\delta\varepsilon^l_{\text{pair}}$.

cillations we calculate Re ϵ^t by means of Eq. (10) for $m\beta \ll 1$, $\omega\beta \ll 1$, $k\beta \ll 1$:

$$\text{Re}\,\varepsilon^t = 1 - \omega_t^2/\omega^2 - \tfrac{1}{2}(\varepsilon^l - 1)(1 - k^2/\omega^2), \qquad (53)$$

where Re ϵ^l is given by Eq. (44).

The dispersion curve for the transverse oscillations is obtained from Eq. (53):

$$\varepsilon^t = 3 - 2\omega_t^2/(\omega^2 - k^2). \qquad (54)$$

It is apparent that Eq. (53) and the curve $\omega^2 = 4m^2 + k^2$ can intersect only for a limited range of densities

$$1 < \omega_t^2/4m^2 < {}^3/_2. \qquad (55)$$

If the second inequality in (55) is not satisfied the dispersion curve lies above $\omega^2 = 4m^2 + k^2$ everywhere, that is to say, it lies in the region in which the oscillations are damped by pair production. Then, for weak spatial dispersion ($k \ll \omega$), using Eqs. (28) and (51) we find

$$\gamma^t_{\text{pair}}/\omega = \tfrac{1}{12}e^2\sqrt{1 - 4m^2/\omega_0^2}\,(1 + 2m^2/\omega_0^2). \qquad (56)$$

This result corresponds to weak damping.

An approximate analytical solution of Eq. (54) can be found at high frequencies. We seek a solution of Eq. (54) in the form $\omega^2 = \omega_S^2 + k^2$ where $\omega_S^2 > 4m^2$ and $k^2 \gg \omega_S^2$. Then

$$\varepsilon^l \approx 1 - (\omega_t^2/k^2)\ln(k^2/\omega_s^2)$$

and for values of k/ω_S which are not excessively large, the third term in Eq. (53) is approximately $(\omega_t^2/2k^4)\,\omega_S^2 \ln(k^2/\omega_S^2)$ i.e., one order higher than the second term. Writing $\epsilon^l \approx 1$ in Eq. (54) we obtain $\omega_S^2 = \omega_t^2$, i.e., for the accuracy required here we can use Eq. (52). In this case the damping due to pair production is

$$\frac{\gamma^t_{\text{pair}}}{\omega} = \frac{e^2}{12}\frac{\omega_t^2}{\omega^2}\sqrt{1 - \frac{4m^2}{\omega_t^2}}\left(1 + \frac{2m^2}{\omega_t^2}\right). \qquad (57)$$

The temperature corrections $\delta\gamma^t_{\text{pair}}$ given by (29) are small for an ultrarelativistic Boltzmann gas. For $\mu\beta \ll 1$ these corrections are proportional to β^2; when $\omega\beta \gg 1$ they are exponentially small.

$$\frac{\delta\gamma^t_{\text{pair}}}{\omega} = -\frac{e^2}{12}\frac{\pi\omega_t^2}{\omega^2}\left(1 + \frac{2m^2}{\omega^2}\right)\sqrt{1 - \frac{4m^2}{\omega_t^2}}\,\omega_t^2\beta^2 \quad \text{for } \omega\beta \ll 1. \qquad (58)$$

Equation (57) is valid for a degenerate gas when $\mu + \kappa < \omega/2$; when $\omega/2 + \kappa < \mu$ the damping vanishes.

10. We discuss further the possibility of realizing the inequality Re $\epsilon^t > 1$ for the transverse oscillations. We consider the limiting case Re $\epsilon^t \gg 1$ or, what is the same thing, $k^2 \gg \omega^2$. It follows from Eq. (10)* that for $k^2 \gg 4\epsilon^2$

$$\varepsilon^t = 1 + \frac{\Lambda}{\omega^2 k^2}\left(1 + 3\frac{\omega^2}{k^2}\right), \qquad (59)$$

$$\Lambda = \frac{16\pi e^2}{3}\int\frac{p^2}{\varepsilon_p} f(\varepsilon_p)\,dp. \qquad (60)$$

The condition Re $\epsilon^t \gg 1$ is then actually possible when $\Lambda \gg \omega^2, k^2$, i.e., at very high densities. Thus, for a nondegenerate ultrarelativistic electron gas $\Lambda = 32\pi e^2 N/\beta$ and for a degenerate gas, $\Lambda = 8\pi e^2 N p_0$ where p_0 is the limiting momentum at the Fermi surface.

In this case the transverse oscillations are damped because of the inverse Cerenkov effect. This damping is exponentially small ($k\beta \gg 1$) for a nondegenerate electron gas [cf. Eq. (24)]

$$\gamma_{\text{cer}}/\omega = \tfrac{1}{128}\pi\,(\text{Re}\,\varepsilon^t)\,k^3\beta^3 e^{-\beta k/2}. \qquad (61)$$

A particle moving in a medium with $\epsilon^t > 1$ will experience Cerenkov losses; in the region in which the medium is transparent these losses are given by the well-known expression (cf. reference 6):

$$W^t = 2e^2\int_0^\infty \omega d\omega \int_0^\infty \frac{q^3 dq}{q^2 + \omega^2/v^2}\,\delta\left[q^2 + \omega^2\left(\frac{1}{v^2} - \varepsilon^t\left(\omega, \sqrt{q^2 + \frac{\omega^2}{v^2}}\right)\right)\right], \qquad (62)$$

where v is the particle velocity and W^t is the energy loss per unit path of the particle. Making the substitution $\epsilon^t = 1 + \Lambda/\omega^2 k^2$ throughout, we have

$$W^t = \frac{e^2}{2v^2\sqrt{\Lambda}}\int_0^{\omega_{max}} \omega d\omega\,(\omega_{max}^2 - \omega^2), \qquad (63)$$

where $\omega_{\text{max}}^2 = v^2\sqrt{\Lambda}$. Thus, a wide spectrum is radiated (up to $\omega = \omega_{\text{max}}$). Finally, after integrating over frequency we have

$$W^t = \tfrac{1}{8}e^2\omega_{max}^2. \qquad (64)$$

11. The static magnetic susceptibility of a relativistic electron gas has been investigated by Silin and Rukhadze.[11] The dielectric constant found in the present work can be utilized to find a more general expression that takes account of the positron contribution. We shall use for $\chi \ll 1$ the definition

$$\chi(0) \approx \frac{\omega^2}{k^2}(\varepsilon^t - \varepsilon^l) = \frac{\omega^2}{k^2}(\varepsilon^t - 1) \quad \text{for } \omega, k \to 0. \qquad (65)$$

Using Eq. (10) we have

$$\chi = \frac{4}{3}\frac{e^2\pi}{(2\pi)^3}\int_0^\infty \frac{n_p^- + n_p^-}{\varepsilon_p}\,dp, \qquad (66)$$

*When $\omega^2 \ll \Lambda/k^2 \ll k^2$ the second term in the round bracket can be neglected.

which differs from the result obtained in reference 11 only in that there is an additional term $n_{\mathbf{p}}^{+}$. In particular, at equilibrium with respect to pair production ($\mu \approx 0$)

$$\chi = (e^2/6\pi^2) \ln (2.9/m\beta). \qquad (67)$$

A similar modification, specifically, a term with $n_{\mathbf{p}}^{+}$, must be introduced into the expression for the shielding radius for a static field (Debye radius) found in reference 1:

$$r_D^{-2} = -4\pi e^2 \int \frac{2}{(2\pi)^3} d\mathbf{p} \left(\frac{dn_{\mathbf{p}}^{-}}{d\varepsilon_{\mathbf{p}}} + \frac{dn_{\mathbf{p}}^{+}}{d\varepsilon_{\mathbf{p}}} \right). \qquad (68)$$

In particular, when $\mu = 0$

$$r_D^{-2} = (8e^2/\pi\beta^2)\, \zeta(2). \qquad (69)$$

This dependence of the Debye radius on temperature has been indicated by Fradkin.[7]

I am very much indebted to V. P. Silin and A. A. Rukhadze for acquainting me with the contents of their book on the effect of spatial dispersion in plasmas and for many valuable discussions.

I also wish to take this opportunity to thank V. L. Ginzburg, E. L. Feĭnberg, and E. S. Fradkin for their interest in this work and for useful comments.

[1] V. P. Silin, JETP **38**, 1577 (1960), Soviet Phys. JETP **11**, 1136 (1960).

[2] L. D. Landau, JETP **16**, 574 (1946).

[3] V. L. Ginzburg, JETP **11**, 620 (1941).

[4] G. S. Saakyan, JETP **38**, 1593 (1960), Soviet Phys. JETP **11**, 1147 (1960).

[5] G. S. Saakyan, JETP **38**, 843 (1960), Soviet Phys. JETP **11**, 610 (1960).

[6] V. P. Silin and A. A. Rukhadze, Электромагнитные свойства плазмы и плазмоподобных сред (Electromagnetic Properties of Plasmas and Plasma Media) Atomizdat (in preparation).

[7] E. S. Fradkin, JETP **36**, 1286 (1959), Soviet Phys. JETP **9**, 912 (1959); Dissertation, Phys. Inst. Acad. Sci. 1960.

[8] Sh. M. Kogan, Doklady Akad. Nauk SSSR **126**, 546 (1959), Soviet Phys.-Doklady **4**, 604 (1959).

[9] V. L. Bonch-Bruevich, ibid., **126**, 539 (1959), transl. p. 596.

[10] A. I. Akhiezer and V. B. Berestetskii, Квантовая электродинамика (Quantum Electrodynamics), 2d Ed., Fizmatgiz, 1959.

[11] V. P. Silin and A. A. Rukhadze, JETP **38**, 645 (1960), Soviet Phys. JETP **11**, 463 (1960).

Translated by H. Lashinsky
302

SPECTRUM OF GALACTIC AND SOLAR COSMIC RAYS

S. I. SYROVAT-SKII

P. N. Lebedev Physics Institute, Academy of Sciences, U.S.S.R.

Submitted to JETP editor January 4, 1961

J. Exptl. Theoret. Phys. (U.S.S.R.) 40, 1788-1793 (June, 1961)

A differential energy spectrum of galactic cosmic rays has been obtained in the form of a power law with an exponent $\gamma = 2.5$ by assuming that the source energy is equally divided between the magnetic field, turbulence, and cosmic rays. If a constant pressure is assumed to be maintained when the solar cosmic rays leave the region in which they were produced, a value $\gamma = 3.5$ is obtained for nonrelativistic cosmic rays and $\gamma = 5$ for ultrarelativistic rays.

To interpret the observed exponent of the cosmic-ray spectrum

$$N(E)\,dE = KE^{-\gamma}dE, \tag{1}$$

where E is the total energy of the particle, K is a constant, and γ is the spectrum exponent ($\gamma = 2.5$ for galactic cosmic rays), the scheme first suggested by Fermi[1] is usually employed. In this scheme γ is obtained under the assumptions that the energy of the particles increases exponentially with a time constant $1/\alpha$ during the acceleration process and that the absorption of the particles follows an experimental law with a lifetime T. Then

$$\gamma = 1 + 1/\alpha T. \tag{2}$$

Subsequently, the lifetime with respect to nuclear collisions, which led to a strong unobserved dependence of γ on the atomic number of the cosmic-ray nucleus, was replaced by the mean time T in which the particles leave the region of acceleration.[2] In order to obtain the spectrum (1) and (2) in this scheme, it has to be assumed, moreover, that the conditions of acceleration, i.e., the parameters, α and T, and, what is particularly important, the injection of the particles do not change over the time interval necessary for the particles to acquire the maximum observed energy. Under these assumptions and with a suitable choice of parameters α and T, one can obtain the value of γ required by experiment.

It should be noted that the rather severe assumptions on the character of the acceleration and injection processes and chiefly the strong dependence of γ on specific values of α and T make the foregoing scheme for the production of the cosmic-ray spectrum highly unconvincing.

As a matter of fact, the conditions of the acceleration of cosmic rays in powerful explosive processes such as the flare-up of supernovae, which are apparently the basic sources of cosmic radiation in our Galaxy,[3] are not stationary both during the early stages of the flare-up and during the subsequent expansion of the shells. The chromospheric flare process on the Sun is also known not to be a stationary one.[4] Therefore the assumption that the rate of acceleration is constant and that the particles are injected uniformly is doubtful and should somehow be generalized.[5] Furthermore, the similarity of the radio spectra of different discrete sources (radiogalaxies) is evidence, according to the present views, of the similarity of the cosmic-ray spectra in these sources. At the same time, the energies of the internal motion, the magnetic fields, and the size of various galaxies, which determine the parameters α and T, can differ basically. It is very unlikely that the parameters α and T for each of these objects take on purely by chance values leading precisely to $\gamma \approx 2.5$.

The foregoing remarks apply in no lesser degree to the spectrum of cosmic rays produced in solar flares. Despite considerable oscillations in the duration and strength of the flares, the spectrum of the produced cosmic rays always appears to be more or less stable.

It is therefore natural to assume that the constancy of the cosmic-ray spectrum from various objects is some general property of the dynamics of magnetized cosmic gaseous masses and the thermodynamics of the relativistic cosmic-ray gas. We present below some simple arguments indicating that the spectrum of galactic cosmic rays and cosmic rays of solar origin can be ob-

tained, under certain assumptions, from the general thermodynamical requirements without regard to the specific mechanism of the acceleration of the cosmic rays.

1. GALACTIC COSMIC RAYS

An important result of observations and their interpretation is the conclusion that both in individual galactic nebulae producing strong radio waves and in our Galaxy as a whole, and also, apparently, in other galaxies, the energy is distributed equally between the kinetic energy of the gaseous masses, magnetic energy, and energy of relativistic particles.[5] The equality of the magnetic and kinetic energies of turbulent motion of a magnetized conducting medium is apparently a general consequence of the behavior of magnetohydrodynamic systems.* As regards the establishment of the energy equilibrium between cosmic rays and the magnetic field, thus far there have been only qualitative discussions.[8,9]

One can make the following arguments in favor of the establishment of such an equilibrium. The production of cosmic rays and their acceleration is apparently a fundamental property of a turbulent magnetized plasma on a cosmic scale. If such a plasma occupies a limited volume, then, as the cosmic-ray energy increases, a limit will be reached at which it will no longer be possible to retain the cosmic rays in this volume. In this case, the equilibrium in the volume will be preserved at the expense of the escape of part of the cosmic rays as soon as the energy begins to exceed some critical value depending on the magnetic field intensity. It is natural to assume (if only from dimensional considerations) that this state of equilibrium is reached when there is a uniform distribution of energy between the above-mentioned three components. Thus we henceforth assume that the magnetized gaseous cloud with intense internal motion attains relatively rapidly a state of equilibrium in which

$$W_{\text{c.r.}} = W_{\text{turb}} = W_{\text{magn}} = W/3, \tag{3}$$

where W is the total energy of the cloud and consists of the turbulent energy W_{turb}, the magnetic field energy W_{magn}, and the cosmic-ray energy $W_{\text{c.r.}}$.

According to present ideas (see, e.g., reference 3), the clouds producing cosmic rays are, first of all, nebulae and supernova shells. It is also not impossible that a similar role can be played by the rapidly rotating region close to the galactic nucleus.

We shall assume, further, that the injection of new fast particles has ceased and the decrease in energy of the cloud occurs mainly through the escape of relativistic particles. The latter may be due to the diffusion of relativistic particles towards the boundaries of the cloud or to the ejection of "bunches" of cosmic rays as a result of local disturbances of the magnetic field and the boundaries of the cloud. Then the equation of the energy balance based on (3) has the form

$$dW \equiv d(3n\bar{E}_k) = \bar{E}_k dn, \tag{4}$$

where n is the number of relativistic particles in the nebula and $\bar{E}_k$ is the average kinetic energy. Here $-\bar{E}_k\, dn$ is the drop in energy due to the escape of cosmic-ray particles. Hereafter, only the ultrarelativistic energy region in which $E_k \approx E$ will be considered for galactic cosmic rays.

Equation (4) gives the following relation between the number of cosmic-ray particles remaining in the cloud and their average energy:*

$$n = \text{const} \cdot \bar{E}^{-1,5}. \tag{5}$$

The differential spectrum of the particles emitted from the nebula then has the form

$$N(E)\,dE = -dn = \text{const} \cdot E^{-2,5}\,dE. \tag{6}$$

Here we have replaced the average energy of the particles by their true energy E. Such a substitution, of course, is valid if the particle spectrum inside the cloud is close to being monoenergetic, which would correspond to the quite natural assumption that all the accelerated particles are injected during a small interval of time,[11] and, consequently, the acceleration of all the relativistic particles is approximately the same. This assumption, however, is not a necessary one. For any particle spectrum in the cloud, the spectrum outside it (6) is preserved if the mechanism of acceleration of the cosmic rays is such that the increase in energy is proportional to the energy

*The present state of the problem of magnetohydrodynamic turbulence and the existing ideas are discussed in a review article by the author.[6] Although the question of the character of stationary turbulence has not yet been clarified theoretically, all the available data indicate that, at least in cosmic conditions, the magnetic energy tends to be equal to the total kinetic energy of the turbulence, and not to the energy of the smallest eddies, as is sometimes assumed (see e.g. reference 7).

*In the general case, if in the state of equilibrium the cosmic-ray energy amounts to a fraction δ of the remaining forms of energy, then, as shown by the author,[10] $n = \text{const} \cdot \bar{E}^{-(1+\delta)}$.

of the particle (see Appendix). Such a law for the increase of energy is very common. In particular, it is valid for all regular mechanisms of acceleration (mechanisms of the first order) and also for the Fermi statistical acceleration in the relativistic region and the statistical betatron mechanism (see, e.g., reference 3).

Hence, regardless of the character of the acceleration and the energy spectrum of the particles inside the nebula, the cosmic-ray spectrum in the surrounding space will have the form (6), in good agreement with what is observed for galactic cosmic rays.

We note that within the framework of the scheme, the cosmic-ray spectrum inside the sources is in no way connected with the observed galactic cosmic-ray spectrum, and is, in principle, quite arbitrary. At the same time, in the interpretation of radio waves of galactic nebula as synchrotron radiation of relativistic electrons, the relativistic electron spectrum in the nebula-shells of supernovae usually proves to be close to the spectrum of galactic cosmic rays. Thus if we assume the same mechanism for the production of cosmic rays and relativistic electrons or the secondary nature of the latter (production of relativistic electrons in collisions between cosmic rays and atoms of the nebula gas), we can conclude that the cosmic-ray spectrum in the sources is similar to the cosmic ray spectrum observed at the earth.

It should be mentioned, however, that the spectra of radio-wave electrons in galactic nebulae sometimes differ essentially from the galactic cosmic-ray spectrum. Thus, for example, Crab nebula, which according to present notions is one of the most typical sources of cosmic rays, has a relativistic-electron spectrum characterized by an exponent $\gamma = 1.7$, while it follows from general considerations that the relativistic-electron spectrum, either from cosmic-ray origin or in the case of their secondary nature, can be only a soft cosmic-ray spectrum. Moreover, the very question of the nature of the relativistic electrons of galactic nebulae is still far from clear. Hence there is not yet any serious basis to require that the mechanism by which the spectrum is produced must lead to the same spectrum for relativistic particles both inside and outside the source.

2. COSMIC RADIATION FROM SOLAR FLARES

As distinct from galactic gaseous nebulae, parts of the solar chromosphere responsible for cosmic rays should be regarded as energetically isolated. In fact, the chromospheric flares usually leading to the appearance of solar cosmic rays represent a local phenomenon on the sun's surface; as a rule, they occur close to sunspots and are apparently mainly caused by the magnetic fields of the spots.[12] It is reasonable to assume that, as a result of some accelerating process in the solar chromosphere, a cavity filled with fast particles and maintained by the pressure of the external magnetic field is formed. Under sufficiently large pressure from these particles and a slow dissipation of their energy, the retaining magnetic field is ruptured and the contents of the cavity are ejected into the space around the sun. Then, if we consider the external pressure resulting from the strong magnetic field of the spots to be practically constant during the process of ejection of the particles from the cavity, we can use the thermodynamical relation

$$dH = \overline{E}_k dn, \tag{7}$$

where H is the heat function of the system, n is the number of particles, and $\overline{E}_k$ is the average energy of the particles in the cavity. The presence of the heat function in (7) at once reflects the fact that the system is not an isolated one; as more particles leave, the average energy of the particles in the cavity increases at the expense of the work done by the external pressure.

The cosmic-ray gas can be regarded as an ideal gas with a constant specific-heat ratio κ. Then

$$H = \varkappa \mathscr{E} = \varkappa n \overline{E}_k, \tag{8}$$

where $\mathscr{E}$ is the total kinetic energy of the particles in the cavity. From Eqs. (7) and (8) it follows that the relation between the number of particles in the cavity and the average energy per particle is

$$n = \text{const} \cdot \overline{E}_k^{-\varkappa/(\varkappa-1)} . \tag{9}$$

The spectrum of the particles leaving the cavity therefore has the form

$$N(E_k)\, dE_k = -dn = \text{const} \cdot E_k^{-\gamma}, \tag{10}$$

where

$$\gamma = (2\varkappa - 1)/(\varkappa - 1). \tag{11}$$

As in the derivation of the expression (6), the substitution of the true energy in (10) for the average energy is valid under very general assumptions (see Appendix).

Let us consider briefly the choice of the specific-heat ratio κ for the cosmic-ray gas. As shown by Ginzburg and the author,[3] for a strictly regular acceleration between approaching parallel

walls, $\kappa = 3$ in the nonrelativistic case and $\kappa = 2$ in the relativistic case. For regular betatron acceleration, the corresponding values are $\kappa = 2$ and $\kappa = 3/2$. These values were obtained under the assumption that the energy is channeled into one (in the case of walls) or two (for betatron acceleration) degrees of freedom of the particle. Actually, if the walls are not strictly parallel, and also owing to scattering on inhomogeneities of the magnetic field, the end result is that all degrees of freedom of the particle are equally privileged. Then, as should be the case for an ideal gas, $\kappa = 5/3$ in the nonrelativistic case and $\kappa = 4/3$ in the relativistic case. For these values of κ, the spectrum of solar cosmic rays, owing to (10) and (11), will be exponential with $\gamma = 3.5$ in the region of nonrelativistic energies and $\gamma = 5$ in the region of ultrarelativistic energies.

The experimental data indicate[13] that γ is already close to five for solar cosmic rays in the region of comparatively low energies ($E_k \gtrsim 100$ Mev for protons). This means that the spectrum turns out to be softer than would follow from the arguments developed above. One should keep in mind, however, that the solar cosmic-ray spectrum can become softer as the cosmic rays travel from the sun to the earth, owing to the large velocity of diffusion of the faster particles. Moreover, any losses in the cavity considered above (radiation, viscous, and Joule dissipation) and the fact that the external pressure does not remain constant as the cavity contracts should also lead to a softening of the spectrum.

APPENDIX

Let the differential energy spectrum of relativistic particles in the source have the form

$$\nu(E, t)\, dE = n(t)\, f(E, t)\, dE, \qquad \int_0^\infty f(E, t)\, dE = 1. \quad \text{(A.1)}$$

Then, after all the relativistic particles have left the source, their spectrum outside the nebula will be

$$N(E)\, dE = -dE \int_0^\infty f(E, t)\, \frac{dn}{dt}\, dt. \quad \text{(A.2)}$$

Using the relation between the average energy of a particle in a nebula $\bar{E}(t) = \int_0^\infty f(E, t)\, E\, dE$ and their number $n(t)$ [see (5) and (9)], which we write in the general form

$$n(t) = \text{const} \cdot [\bar{E}(t)]^{-(\gamma-1)}, \quad \text{(A.3)}$$

we obtain, by (A.2),

$$N(E)\, dE = \text{const} \cdot dE \int_{\bar{E}(0)}^\infty f(E, t)\, [\bar{E}(t)]^{-\gamma}\, d\bar{E}(t). \quad \text{(A.4)}$$

For particles with a monochromatic spectrum in the nebula $f(E, t) = \delta[E - \bar{E}(t)]$, we at once obtain

$$N(E)\, dE = \text{const} \cdot E^{-\gamma} dE, \qquad E > E(0). \quad \text{(A.5)}$$

If $f(E, t)$ is an arbitrary function which, as a result of the acceleration of the particle, varies with time according to the law

$$E(t) = E(0)\, \varphi(t), \quad \text{(A.6)}$$

then

$$f(E, t) = \frac{1}{\varphi(t)}\, f\left(\frac{E}{\varphi(t)}\right), \qquad \bar{E}(t) = \bar{E}(0)\, \varphi(t)$$

and we obtain from (A.4)

$$N(E)\, dE = \text{const} \cdot dE \int_1^\infty f\left(\frac{E}{\varphi}\right) \frac{d\varphi}{\varphi^{\gamma+1}}$$

$$= \text{const} \cdot E^{-\gamma} dE \int_0^E f(E_0)\, E_0^{\gamma-1}\, dE_0. \quad \text{(A.7)}$$

If in the high-energy region the initial spectrum of the particles in the source drops sufficiently rapidly with an increase in energy (faster than $E^{-\gamma}$) then, for $E \gg \bar{E}(0)$, we once again obtain the spectrum (A.5).

[1] E. Fermi, Phys. Rev. **75**, 1169 (1949).

[2] Morrison, Olbert, and Rossi, Phys. Rev. **94**, 440 (1954).

[3] V. L. Ginzburg and S. I. Syrovat-skii, Usp. Fiz. Nauk **71**, 411 (1960), Soviet Phys.-Uspekhi **3**, 504 (1961).

[4] A. B. Severnyĭ, Изв. Крымск. астрофиз. обс. (News of the Crimean Astrophysical Observatory) **20**, 22 (1958).

[5] V. L. Ginzburg, Usp. Fiz. Nauk **51**, 343 (1953); **62**, 27 (1957).

[6] S. I. Syrovat-skii, Usp. Fiz. Nauk **62**, 247 (1957).

[7] L. D. Landau and E. M. Lifshitz, Электродинамика сплошных сред (Electrodynamics of Continuous Media), Gostekhizdat, Moscow, 1957, Sec. 55.

[8] E. N. Parker, Phys. Rev. **109**, 1328 (1958).

[9] S. B. Pikel'ner, Астроном. ж. **38**, 21 (1961), Soviet Astronomy **5**, 14 (1961).

[10] S. I. Syrovat-skii, Вопросы магнитной гидродинамики и динамики плазмы (Collection: Problems of Magnetic Hydrodynamics and Plasma Dynamics), Acad. Sci. Latv. S.S.R., Riga, 1959, p. 45.

[11] A. A. Korchak and S. I. Syrovat-skii, Dokl. Akad. Nauk SSSR **122**, 792 (1958), Soviet Phys.-Doklady **3**, 983 (1958).

[12] A. B. Severnyĭ and V. P. Shabanskii, Астроном. ж. **37**, 609 (1960), Soviet Astronomy **4**, 583 (1961).

[13] Charakhch'yan, Tulinov, and Charakhch'yan, JETP **38**, 1031 (1960), Soviet Phys. JETP **11**, 742 (1960).

Translated by E. Marquit
303

ANGULAR CORRELATIONS IN STATISTICAL NUCLEAR REACTIONS

V. M. STRUTINSKII

Submitted to JETP editor January 5, 1961

J. Exptl. Theoret. Phys. (U.S.S.R.) 40, 1794-1802 (June, 1961)

The correlation between the directions of emission of particles emitted in succession by a nucleus with a large angular momentum is considered. Simple analytical expressions have been obtained for the angular correlation of two particles under the condition that the final nucleus remains in a state with a small angular momentum. The correlations between the directions of emission of a particle and of the fission fragments accompanying the particle emission are also considered.

THE dependence of the nuclear level density on the angular momentum of the nucleus leads to an anisotropy in the angular distribution of particles emitted by a compound nucleus.[1-3] A similar effect leads to an anisotropy in the fission of the nucleus. When two particles are emitted in succession or when fission takes place after the emission of a particle, an angular correlation occurs between the direction of emission of the particles or between the direction of emission of the particles and the direction of the fragments. As distinct from the particle angular correlations, usually considered in nuclear physics when one has in mind transitions between strictly defined quantum states, individual levels of the nucleus are not allowed in statistical nuclear reactions, and the angular correlation of the particles, as well as the angular distribution, arises as a result of averaging over a large number of nuclear states. The effects arising in this way can usually be given a classical interpretation (see references 1 — 3). In this connection, it is entirely natural to apply quasi-classical methods of calculation.

ANGULAR CORRELATION OF PARTICLES

We shall first consider the simple case of a cascade consisting of only two particles. The probability that a nucleus with an angular momentum $\mathbf{j}_1$ emits the first particle in the direction $\mathbf{n}_1$ and the second particle in the direction $\mathbf{n}_2$ is

$$W_{\mathbf{j}_1}(1, 2)\, d\Omega_1 d\Omega_2 = \iint \frac{d\Gamma^{(1)}_{p_1}(\mathbf{j}_1, \mathbf{j}_2; \mathbf{l}_1, \mathbf{n}_1)}{\Gamma^{(1)}_{tot}(j_1)} \frac{d\Gamma^{(2)}_{p_2}(\mathbf{j}_2, \mathbf{j}_3; \mathbf{l}_2, \mathbf{n}_2)}{\Gamma^{(2)}_{tot}(j_2)}, \quad (1)$$

where $d\Gamma^{(1)}_{p_1}(\mathbf{j}_1, \mathbf{j}_2, \mathbf{l}_1, \mathbf{n}_1)$ is the partial width for the emission of a particle p_1 with orbital angular momentum $\mathbf{l}_1$ in the direction $\mathbf{n}_1$ by a nucleus with an angular momentum $\mathbf{j}_1$; $d\Gamma^{(2)}_{p_2}$ is the analogous quantity for the emission of the second particle; $\mathbf{j}_1$, $\mathbf{j}_2$, and $\mathbf{j}_3$ are the angular momenta of the initial, intermediate, and final nuclei, respectively, and $\Gamma^{(1)}_{tot}$ and $\Gamma^{(2)}_{tot}$ are the total decay widths of the initial and intermediate nuclei:

$$\Gamma^{(1)}_{tot} = \Gamma^{(1)}_{p_1}(j_1) + \Gamma^{(1)}_{n}(j_1) + \ldots$$

and similarly for $\Gamma^{(2)}_{tot}$; $\Gamma^{(1)}_{p_1}(\mathbf{j}_1)$ is the total width for the emission of particle p_1 by the initial nucleus and $\Gamma^{(2)}_{p_2}(\mathbf{j}_2)$ is the analogous quantity for the emission of particle p_2 by the intermediate nucleus:

$$\Gamma^{(1)}_{p_1}(j_1) = \int d\Gamma^{(1)}_{p_1}(\mathbf{j}_1, \mathbf{j}_2,; \mathbf{l}_1, \mathbf{n}_1). \quad (2)$$

For $d\Gamma^{(1)}_{p_1}$ we can use the quasi-classical expression[1-3]

$$d\Gamma^{(1)}_{p_1}(\mathbf{j}_1, \mathbf{j}_2; \mathbf{l}_1, \mathbf{n}_1) = C_1 (\rho^{(2)}(j_2)/\rho^{(1)}(j_1))\, T_1(\mathbf{l}_1) \times \delta^3(\mathbf{j}_1 - \mathbf{j}_2 - \mathbf{l}_1)\, \delta(\mathbf{l}_1\mathbf{n})\, d^3j_2 d^3\, l_1 d\Omega_1. \quad (3)$$

In formula (3), $\delta^3(\mathbf{x})$ and $\delta(x)$ are the three-dimensional and one-dimensional δ-functions, respectively; $T_1(l_1)$ and $T_2(l_2)$ are the barrier factors for particles p_1 and p_2; $\rho^{(1)}$, $\rho^{(2)}$, and $\rho^{(3)}$ are the level densities of the initial, intermediate, and final nuclei. The explicit form of the dependence of these factors and the coefficients C_1 and C_2 on the energy will not be necessary for the discussion below.

Using (3), we obtain for the total partial width $\Gamma^{(2)}_{p_2}(\mathbf{j}_2)$

$$\Gamma^{(2)}_{p_2}(j_2) = 4\pi C_2 \int l_2^{-1} T_2(l_2)\, \frac{\rho^{(3)}(\mathbf{j}_2 - \mathbf{l}_2)}{\rho^{(2)}(j_1)}\, d^3 l_2. \quad (4)$$

The quantity $\Gamma^{(1)}_{p_1}(\mathbf{j}_1)$ is expressed in a similar way. Substituting (3) and (4) into (1), we can represent $W_{\mathbf{j}_1}(1, 2)$ in the form

$$W_j(1, 2) = \frac{1}{(2\pi)^2} \int\int d^3 l_1\, d^3 l_2 \gamma^{(1)}_{p_1}(j_1)\, \gamma^{(2)}_{p_2}(j_2)\, \rho^{(2)}(\mathbf{j}_1 - \mathbf{l}_1) \times \rho^{(3)}(\mathbf{j}_1 - \mathbf{l}_1 - \mathbf{l}_2)\, \frac{T_1(l_1)\, T_2(l_2)}{N_1(j_1)\, N_2(|\mathbf{j}_1 - \mathbf{l}_1|)}\, \delta(\mathbf{l}_1\mathbf{n}_1)\, \delta(\mathbf{l}_2\mathbf{n}_2), \quad (5)$$

where $\gamma^{(1)}_{p_1}(j_1)$ is the relative probability for the emission of particle p_1 by a nucleus with an angular momentum j_1:

$$\gamma^{(1)}_{p_1}(j_1) = \Gamma^{(1)}_{p_1}(j_1)/\Gamma^{(1)}_{tot}(j_1). \tag{6}$$

$N_1(j_1)$ and $N_2(j_2)$ in (5) are the normalizing factors:

$$N_1(j_1) = \frac{1}{2\pi}\int\int d^3\Omega_1 d^3 l_1 T_1(l_1)\,\rho^{(2)}(\mathbf{j}_1 - \mathbf{l}_1)\,\delta(\mathbf{l}_1\mathbf{n}_1) \cdot \int \frac{d^3 l_1}{l_1} T_1(l_1)\,\rho^{(2)}(\mathbf{j}_1 - \mathbf{l}_1). \tag{7}$$

$N_2(j_2)$ is expressed in a similar way.

As can be seen from (5),

$$\int\int W_{j_1}(1,2)\,d\Omega_1 d\Omega_2 = \gamma^{(1)}_{p_1}(j_1)\int \frac{d^3 l_1}{l_1}\frac{T_1(l_1)\,\rho^{(2)}(\mathbf{j}_1 - \mathbf{l}_1)}{N_1(j_1)}\,\gamma^{(2)}_{p_2}(|\mathbf{j} - \mathbf{l}|) \tag{8}$$

represents the relative probability of emission of a pair of particles p_1 and p_2 by a nucleus with an angular momentum j_1.

Generally speaking, the dependence of the integrand of (5) on the orientation of the momenta is determined if the dependence of the level density of the nucleus on the angular momentum is known. In the statistical theory of the nucleus

$$\rho(j) = \rho_0(u)\exp(-\alpha j^2), \tag{9}$$

where $\alpha = \hbar^2/2\mathcal{J}T$, $\mathcal{J} = 2AmR^2/5$ is the moment of inertia, and T is the temperature of the nucleus. For such a form of $\rho(j)$, we cannot integrate over $\mathbf{l}_1$ and $\mathbf{l}_2$ in (5) in general form.

We shall consider the important special case in which the nucleus remains in a state with small angular momentum after the emission of the second particle. Setting in (5)

$$\rho^{(3)}(\mathbf{j}_1 - \mathbf{l}_1 - \mathbf{l}_2) = \rho_0\delta^3(\mathbf{j}_1 - \mathbf{l}_1 - \mathbf{l}_2), \tag{10}$$

we obtain

$$W_j(1,2) = \frac{1}{2\pi^2}\gamma^{(1)}_{p_1}(j_1)\,N_1^{-1}(j_1)\int d^3 l_1 f(|\mathbf{j}_1 - \mathbf{l}_1|)\,T_1(l_1) \times \delta(\mathbf{l}_1\mathbf{n}_1)\,\delta(\mathbf{j}_1\mathbf{n}_2 - \mathbf{l}_1\mathbf{n}_2), \tag{11}$$

where

$$f(|j_2|) = \gamma^{(2)}_{p_2}(j_2)\,j_2\,\rho^{(2)}(j_2), \qquad \mathbf{j}_2 = \mathbf{j}_1 - \mathbf{l}_1.$$

Assuming that $j \gg l_1$, we expand the function $f(j_2)$ into a series in the small quantity $x = (\mathbf{l}_1\mathbf{j}_1)/j_1^2$:

$$f(j_2) \approx f(j_1)(1 + a_1 x + a_2 x^2 + \ldots). \tag{12}$$

The coefficients a_1 and a_2 are

$$a_1 = 2\alpha_2 j_1^2 - 1 + q_1,$$

$$a_2 = 2\alpha_2^2 j_1^4 - \tfrac{1}{2} - 2\alpha_2 j_1^2 + q_2 - q_1 + 2\alpha_2 j_1^2 q_1, \tag{13}$$

where q_1 and q_2 are determined from the equality

$$\gamma^{(2)}_{p_2}(j_2) = \gamma^{(2)}_{p_2}(j_2)(1 + q_1 x + q_2 x^2 + \ldots). \tag{14}$$

We shall consider the important special case in which one counter is located at a right angle to the beam and another is moved either in the plane of the beam or in a plane perpendicular to it. We denote by θ_1, θ_2, Φ_1, Φ_2 the angular coordinates of the directions $\mathbf{n}_1$ and $\mathbf{n}_2$, and by ϑ_l, φ_l, ϑ_f, φ_f the angular coordinates of the vectors l_1 and j_1. Of course, $\vartheta_j = \frac{1}{2}\pi$. We shall consider these special cases separately.

1. Both counters are in the perpendicular plane ($\theta_1 = \theta_2 = \frac{1}{2}\pi$). After integrating in (5) over the directions of the vector $\mathbf{l}_1$, we obtain

$$W_j(1,2) = \frac{2}{(2\pi)^2}\gamma^{(1)}(j_1)\frac{f(j_1)}{N_1(j_1)}\int_0^\infty \frac{l_1\,dl_1\,T_1(l_1)(1 + a_1\bar{x} + a_2\bar{x^2} + \ldots)}{[l_1^2\sin^2\omega - (j_1 n_2)^2]^{1/2}},$$

$$\bar{x} = \cos(\varphi_j - \omega)\sin\varphi_j/\sin\omega, \tag{15}$$

where ω is the angle between the counters ($\omega = \Phi_1 - \Phi_2$). Expression (15) should be integrated over all values of the angle φ_j for which the expression in the denominator of the integrand is positive. The result is expressed in terms of elliptic integrals. In the limiting case of practical interest $j \gg l$, we obtain

$$W_j = \frac{1}{16\pi^2}\gamma^{(1)}_{p_1}(j)\,\gamma^{(2)}_{p_2}(j)\left(1 + \frac{a_1 - a_2}{2}\frac{\bar{l^2}}{j^2}\sin^2\omega\right),$$

$$\bar{l^2} = \int_0^\infty l^3 T_1(l)\,dl \Big/ \int_0^\infty l T_1(l)\,dl. \tag{16}$$

In the derivation of (16) we took for $N_1(j)$ the approximate expression

$$N_1(j) \approx 4\pi\rho^{(2)}(j)\int_0^\infty l T_1(l)\,dl. \tag{17}$$

We have discarded terms at least as small as l^4/j^4.

Expression (16) should still be integrated over $|\mathbf{j}|$, where we must take into account the probability of capture of an incident particle with an angular momentum j:

$$\overline{W}_j(1,2) = \int_0^\infty j^3 T_j(j)\,dj \Big/ \int_0^\infty j T_j(j)\,dj, \tag{18}$$

where $T_j(j)$ is the coefficient of absorption of an incident particle with angular momentum j. If the emission of the second recorded particle is a single or basic process, then $\gamma^{(2)}_{p_2} \equiv 1$, and $q_1 = q_2 = 0$. In this case we obtain for $\overline{W}$

$$\overline{W}(1,2) \approx 1 + \tfrac{1}{2}\alpha_2\bar{l^2}\left[4 - \tfrac{1}{2}(\alpha_2 j_0^2)^{-1}\ln(\bar{j_0^2}/\bar{l^2}) - \alpha_2 j_0^2\right]\sin^2\omega. \tag{19}$$

In the derivation of (19), $T_j(j)$ was taken in the form

$$T_j(j) \approx T_j^{(cl)}(j) = \begin{cases} 1, & j \leqslant j_0 \\ 0, & j > j_0 \end{cases}. \tag{20}$$

For an idea as to the size of the correlation effect, we shall consider the specific reaction Cu(α, 2p) studied by Lassen and Sidorov.[4] For an α particle energy of ~ 20 Mev and an energy of 6 — 9 Mev for the first proton, the intermediate nucleus can decay only by two modes: the emission of a sub-barrier proton with an energy of $\sim 1-2$ Mev or the radiation of a γ quantum. For $\alpha_2 = 0.05$, which corresponds to the rigid-body moment of inertia of the intermediate nucleus, and for $\overline{l^2} = 3-4$ and $j_0^2 = 50$, we obtain the value +0.1 for the coefficient of $\sin^2\omega$ in (19). The magnitude and sign of the coefficient strongly depend on the relation between the parameters $\alpha_2\overline{l^2}$ and $\alpha_2\overline{j^2}$. For a larger value of j_0^2, for example, in the case of high-energy α particles, the coefficient drops to zero and then becomes negative.

The measurement of the angular correlation between two protons in the perpendicular plane in the reaction Ni^{58}(α, 2p) (E_α = 32 Mev) was carried out by Bodansky et al.[5] Their result corresponds to a value of approximately −0.15 for the coefficient of $\sin^2\omega$. This value is in agreement with (19). It is assumed here that the reaction can be regarded as a transition of an excited nucleus produced by the capture of an α particle to the ground state or close to the ground state through the emission of two protons, which is not an obvious assumption.

2. Counters and beam in the same plane. Two cases should be distinguished here: a) $\theta_2 = \frac{1}{2}\pi$, $\Phi_1 = \Phi_2 = 0$ or π and b) $\theta_1 = \frac{1}{2}\pi$. We shall first consider case a. Inserting (12) into the integral (11) and integrating over l and over the directions of the vector $\mathbf{j}$, we obtain, in the same approximation as in (19),

$$W_j(1,2) = (1/16\pi^3)\,\gamma^{(1)}_{p_1}(j)\,\gamma^{(2)}_{p_2}(j)\,(1 + (\overline{l^2}/2j^2) \times (\tfrac{1}{2} + a_1)\cos^2\theta_1). \quad (21)$$

Apart from terms of order higher than l^4/j^4, the angular distribution of the first particle for a fixed direction of emission of the second is determined in this case by the single coefficient a_1.

Inserting in (21) the expression (13) for a_1 and setting $q_1 = q_2 = 0$ in the latter, we obtain, after integration over j,

$$\overline{W}(1,2) \sim 1 + [\alpha_2\overline{l^2} - (\overline{l^2}/2j_0^2)\ln(j_0/l_0)]\cos^2\theta_1. \quad (22)$$

As in the case of (19), the coefficient of $\cos^2\theta_1$ can change sign if the angular momentum of the compound nucleus changes. If the angular momentum is large, so that $\alpha_2 j^2 \gg 1$, then the angular distribution of the first particle does not depend on j if the direction of emission of the second is fixed at the angle $\theta_2 = \frac{1}{2}\pi$. This is in contrast to the usual angular distribution of particles in which the anisotropy equals $\frac{1}{2}\alpha_2^2\overline{l^2}\overline{j^2}$.[1,2]

We shall consider case b, in which $\theta_1 = \pi/2$. Here, after integration over the directions of the vectors $\mathbf{l}$ and $\mathbf{j}$, we obtain from (11)

$$W_j(1,2) = \frac{1}{4\pi^2}\frac{\gamma^{(1)}_{p_1}(j)\,f(j)}{jN(j)}\int_0^\infty W_{l,j}\,lT_1(l)\,dl,$$

$$W_{l,j}(1,2) = \sin^{-1}\theta_2\,[A(k) + (a_2 l^2/3j^2)\,B(k)];$$

$$A(k) = \frac{2}{\pi}\times\begin{cases}K(k), & k = l\,\mathrm{tg}\,\theta_2/j \leqslant 1,\\ k^{-1}K(k^{-1}), & k \geqslant 1,\end{cases}$$

$$B(k) = \frac{2}{\pi}\times\begin{cases}K(k) + E(k) - k^{-2}[K(k) - E(k)], & k \leqslant 1,\\ k^{-1}[K(k^{-1}) + E(k^{-1}) - k^2(K(k^{-1}) - E(k^{-1}))], & k \geqslant 1,\end{cases} \quad (23)^*$$

where K(k) and E(k) are the complete elliptic integrals of the first and second kinds, respectively:

$$K(k) = \int_0^{\pi/2}(1 - k^2\sin^2\varphi)^{-1/2}d\varphi,$$

$$E(k) = \int_0^{\pi/2}(1 - k^2\sin^2\varphi)^{1/2}d\varphi.$$

The function $W_{j,l}(1,2)$ describes the angular correlation of the particles for fixed j and l. The dependence of $W_{j,l}$ on the angle θ_2 is determined mainly by the factor $1/\sin\theta_2$, which results from the fact that for $l_1 \ll j$, the orbital angular momentum of the second particle has a direction close to $\mathbf{j}$ and, consequently, lies in the plane perpendicular to the beam. The deviations of $\mathbf{l}_2$ from this plane, which are connected with the fact that the first particle carries away a certain angular momentum, lead to a deviation of the angular distribution from $1/\sin\theta_2$. These deviations are described by the factor in the brackets in the expression for $W_{j,l}$. The function $W_{j,l}$ strongly depends on the angle in the small-angle region $\theta_2 \lesssim l_1/j$. At large angles, the deviations from $1/\sin\theta_2$ are small ($\sim l_1^2/j^2$):

$$\overline{W} \sim \sin^{-1}\theta_2\,\{1 + (\overline{l_1/4j^2})\,\mathrm{ctg}^2\theta_2 + \ldots\}. \quad (24)^\dagger$$

In (24), we have discarded terms of the order $l_1^4 \times \cot^4\theta_2/j^4$.

It is natural to compare the angular distribution (23) of the second particle for a fixed direction of emission of the first particle with the angular distribution of the second particle for the free emission of the first. Normalized to unity for $\theta_2 = \theta/2$, this angular distribution is given by the expression

*tg = tan.

†ctg = cot.

$$[\sin^{-1}(l/j\sin\theta_2)]/\sin^{-1}(l/j), \qquad (25)$$

which is readily obtained from (11). Comparing (25) and (24), we find that, for $\theta_2 \gtrsim l/j$, the angular distribution of the second particle, when the counter registering the first particle is connected, changes by the quantity

$$\Delta W_{l,j} = \tfrac{1}{12}\sin^{-1}\theta_2\,\overline{(l^2/j^2)}\,\mathrm{ctg}^2\,\theta_2. \qquad (26)$$

It should be borne in mind that the distribution $\sim 1/\sin\theta_2$ is valid only with quasi-classical accuracy in the region $\theta_2 \gtrsim l_1/j$ and is not at all valid for $\theta_2 \lesssim l_1/j$. In this case, the effect of the angular correlation can therefore be established only when the angular distribution of the second particle, for a fixed direction of emission of the first particle (close to $\theta_1 = \frac{1}{2}\pi$), is compared with the angular distribution for free emission. This is the essential difference between this case and the two preceding cases, for which the result of the zero approximation—isotropy—is known exactly and the inexactness of the quasi-classical approximation leads to an unimportant error in the value of the coefficients.

For $a_1 = a_2 = 0$, one can obtain the following general expression for the angular correlation function $W_{j,l}(1, 2)$, valid for any orientation of the counters relative to the beam and relative to each other $[\rho^{(3)}(j_3) = \rho_0\delta^3(j_3)]$:

$$W_{j,l} = \frac{2}{\pi}\sin^{-1}\theta_2 \times \begin{cases} K(\varkappa), & \varkappa = l\sin\gamma/j\sin\theta_2 \leqslant 1, \\ \varkappa^{-1}K(\varkappa^{-1}), & \varkappa \geqslant 1, \end{cases} \qquad (27)$$

where γ is the angle between the counters.

If for the barrier factor $T_1(l)$ we use the classical expression similar to (2), then expression (27) for $W_{j,l}$ can be integrated over l. As a result, we obtain

$$W_j(1, 2)|_{\mathrm{av}\ l} = \sin^{-1}\theta_2 \begin{cases} \varkappa_0^{-1}E(\varkappa_0^{-1}), & \varkappa_0 = l_0\sin\gamma/j\sin\theta_2 \leqslant 1, \\ \varkappa_0^{-2}[E(\varkappa_0) - (1-\varkappa_0^2)K(\varkappa_0)], & \varkappa_0 \geqslant 1. \end{cases} \qquad (28)$$

Besides the correlation of two particles when the final nucleus remains in a state with a small angular momentum, as was considered above, other cases may also be of interest. In particular, with the aid of (11), it is not difficult to calculate the angular correlation between two particles when, for example, the level density of the final nucleus as well as the initial and intermediate nuclei weakly depend on the angular momentum. This can happen if the excitation energy of the final nucleus is comparatively high and the angular momentum of the initial nucleus is not very large. It is also easy to obtain the generalization of formula (5) to the case of a large number of particles in cascade. The probability of registering m particles in the directions $n_1, n_2, \ldots, n_m$ is

$$W_{j_1}(1,\ldots,m) = \frac{1}{(2\pi)^2}\int d^3l_1\ldots d^2l_m \prod_{i=1}^{m}\gamma_{p_i}^{(i)}(j_i)\,\rho^{(i+1)}(j_{i+1}) \times T_i(l_i)N_i^{-1}(j_i)\delta(\mathbf{l}_i\mathbf{n}_i),$$
$$j_1 = j_1 - \sum_{k=1}^{i-1} l_k. \qquad (29)$$

If the direction of emission of one of the particles in the experiment is not registered, expression (29) should be integrated over the angular variables of the corresponding particle. The angular correlation in this case depends also on the parameters characterizing the emission of the unregistered particle. This circumstance causes the results of the angular correlation experiment to be less definite. If, however, the unobserved particle is light and the registered particles are heavy, for example, α particles, the correlation will be approximately the same as if only two particles were emitted.

If identical particles are registered, the expression for the angular correlation should be symmetrized in a suitable way. This may not be necessary, however, if the energy of the particles is also registered in the experiment. Since the probability of emission of a particle strongly depends on the particle energy and the excitation energy of the nucleus, it is often possible to establish which particle is first and which is second. This applies, in particular, to the above-mentioned reaction[4] Cu $(\alpha, 2p)$, where the second proton is a sub-barrier particle and consequently the probability that a particle of such energy is emitted from the nucleus first is negligibly small.

ANGULAR CORRELATION BETWEEN A PARTICLE AND FISSION FRAGMENTS

Formally, this case of angular correlation can be regarded as a special case of the angular correlation of two particles. In formula (5), instead of the level density of the final nucleus $\rho^{(3)}$, we should insert the product of the level densities of the fragments and introduce the corresponding summation over the fragment spins. It will be more convenient, however, to consider first the distribution of the number of total spin states of the fragments $\mathbf{S} = \mathbf{j}' + \mathbf{j}''$. This distribution coincides formally with (9), where for the constant α we have

$$\alpha \equiv 1/2K_0^2 = (1/\mathcal{J}' + 1/\mathcal{J}'')T^*,$$

here $\mathcal{J}'$, $\mathcal{J}''$, and T^* are the moments of inertia

and temperature of the fragments.[6] Hence, to calculate the angular correlation between the particle and the fragments, one can use directly formula (5), where $\rho^{(3)}(j_3)$, $\mathbf{j}_3$, and $\mathbf{l}_2$ are replaced by the distribution function $\rho(\mathbf{S})$, the vector $\mathbf{S}$, and the orbital angular momentum of the fragments $\mathbf{l}'$, respectively. The barrier factor $T_f(l')$ can be set equal to unity, since the mass of the fragments is large and the classical limitation on the size of the angular momentum is not important, even when the energy of the nucleus is only slightly above the fission threshold. The integration over l' can then be carried out in general form. After integrating over l', we obtain

$$W_j(p, f) = \frac{1}{(2\pi)^2} \frac{\gamma_p^{(1)}(j_1)}{N_1(j_1)} \int d^3 l_1 \gamma_f^{(2)}(j_2)\ \rho^{(2)}(j_2)\ \delta(\mathbf{l}_1\mathbf{n}_1)\ \Re(\mathbf{j}_2\mathbf{n}_f), \tag{30}$$

where $\mathbf{j}_2 = \mathbf{j}_1 - \mathbf{l}_1$, and $\mathbf{n}_1$ and $\mathbf{n}_f$ are the directions of emission of the particle and the fragments; $\gamma_f^{(2)}$ is the relative probability of fission of the intermediate nucleus; the function

$$\Re(\mathbf{j}_2\mathbf{n}_f) = R(j^2/2K_0^2) \exp(-K^2/2K_0^2),\ K = \mathbf{j}_2\mathbf{n}_f \tag{31}$$

is the projection of the angular momentum of the intermediate nucleus on the direction of fission. In (31)

$$R(z) = \int_{-1}^{1} e^{-zx^2} dx.$$

Function (31) gives the distribution of the number of cases of fission with a value K. The expression given above for K_0^2 corresponds to the assumption made in the derivation of (30) that the fission probability is determined by the statistical weight of the fragments. One may also assume that the probability of fission with a given value of $|K|$ is determined by the statistical distribution of K in the transition nucleus for a deformation approximately corresponding to a saddle point. The distribution of K in this case coincides with (31), but the constant K_0^2 is equal to $T^{*-1}(\mathcal{J}_{\parallel}^{-1} - \mathcal{J}_{\perp}^{-1})^{-1}$, where $\mathcal{J}_{\parallel}$ and $\mathcal{J}_{\perp}$ are the moments of inertia of the transition nucleus relative to the axis of symmetry and perpendicular to it, T^* is the transition nucleus temperature (see also reference 6).

It should be kept in mind that, strictly speaking, the angular distribution of the fragments is determined by the distribution of K at infinity.[7] Since the projection of the orbital angular momentum of the fragments on the direction of fission is equal to zero, the distribution of the projection K of the total angular momentum of the system $\mathbf{j} = \mathbf{l}' + \mathbf{S}$ on the fission direction coincides with the distribution of the resultant spin of the fragments on this direction. Thus, the problem is only whether the distribution of the projection of vector $\mathbf{S}$ is determined by the level density of the fragments or whether it coincides with the distribution of K in the "transition" nucleus. On the basis of the data available at the present time, one can conclude that the second assumption corresponds more closely to reality, at least for fission close to the threshold and for low excitation of the initial nucleus. From the formal point of view, the existence of these two different approaches is not important, since in both cases the distribution of K is given by the same expression, namely (31).

If the angular momentum of the compound nucleus is sufficiently large, so that the inequality

$$j^2/2K_0^2 \gg 1, \tag{32}$$

is satisfied, expression (31) for N(K) goes over into $j_2\delta(\mathbf{j}_2\mathbf{n}_f)$, and (30) then formally coincides with (11). Hence all the expressions obtained above for the angular correlation of particles also describe the correlation between the particle and the fragments for a nucleus with a sufficiently large angular momentum. An outward sign that condition (32) is fulfilled is the closeness of the fragment angular distribution to $1/\sin\theta_f$.[8] This usually occurs in the case of fission induced by the capture of heavy ions. The large angular momentum of the compound nucleus formed upon capture of heavy particles also enhances the fissionability of the nucleus and, consequently, increases the probability that the nucleus undergoes fission immediately after the emission of the registered particle.

With the aid of formula (30), one can find an angular correlation between the particle and the fission fragments also when condition (32) is not fulfilled. We shall consider, in particular, the case in which

$$lj/2K_0^2 \ll 1. \tag{33}$$

The parameter $j^2/2K_0^2$ can then have any value, but cannot be so large that inequality (33) is not fulfilled. Making the same approximation as in the derivation of (16), we write $W_j(p, f)$ in the form

$$W_j(p, f) \approx \frac{1}{(2\pi)^3} \gamma_p^{(1)}(j)\ \gamma_f^{(2)}(j)\ \Re(\mathbf{j}\mathbf{n}_f) \left(4\pi \int_0^{\infty} l dl T(l)\right)^{-1} \times \int d^3 l\, T(l)\ \delta(\mathbf{l}\mathbf{n}_1)\ (1 + r(\mathbf{l}\mathbf{j}) + \ldots) \exp\{(\mathbf{l}\mathbf{n}_f)\ [2(\mathbf{j}\mathbf{n}_f) - \mathbf{l}\mathbf{n}_f]/2K_0^2\}, \tag{34}$$

where

$$\mathbf{j} \equiv \mathbf{j}_1, \quad \mathbf{l} = \mathbf{l}_1;$$

$$1 + r(\mathbf{l}\mathbf{j}) + \ldots = G(\mathbf{j} - \mathbf{l})/G(j), \tag{35}$$

$$G(j) = \gamma_f^{(2)}(j)\ \rho^{(2)}(j)\ R^{-1}(j^2/2K_0^2). \tag{36}$$

We shall consider the case in which the direction of emission of the particle and the direction of the fission fragments lie in a plane perpendicular to the beam. We expand the exponential factor in the integrand of formula (34) into a series and integrate over 1. After averaging over the directions of the vector j, we obtain

$$W_j(p, f) = (1/16\pi^3)\,\gamma_p^{(1)}(j)\,\gamma_f^{(2)}(j)\exp(-z/2)\,I_0(z/2)$$
$$\times\{1 - (\overline{l^2}/4K_0^2)\sin^2\omega_f + (l^2j^2/8K_0^4)(1 + 2K_0^2 r)$$
$$\times[1 - I_1(z/2)/I_0(z/2)]\sin^2\omega_f + \ldots\}, \qquad (37)$$

where $z = j^2/2K_0^2$, I_0 and I_1 are Bessel functions of imaginary argument. Expression (37) should still be averaged over the quantity $|j|$ with a weight $jT_j(j)$.

The coefficient r in (37) depends, generally speaking, on j. To determine r, we must use the explicit expressions for $\rho^{(2)}(j_2)$ (9), R(z), and $\gamma_f^{(2)}(j_2)$. For $\gamma_f^{(2)}$, we can take the statistical expression

$$\gamma_f^{(2)}(j_2) = \{1 + \gamma_n^{(2)}(j_2)/\gamma_f^{(2)}(j_2)\}^{-1},$$

$$\gamma_n^{(2)}(j_2)/\gamma_f^{(2)}(j_2) = (\Gamma_n(0)/\Gamma_f(0))\exp[(\alpha_3 - \alpha_1)\,j_2^2]\,R^{-1}(j_2^2/2K_0^2). \qquad (38)$$

Setting

$$\rho^{(2)}(j_2) \approx \rho^{(2)}(j)\,(1 + 2\alpha_2(lj) + \ldots),$$

$$R(j_2^2/2K_0^2) \approx R(j^2/2K_0^2)\,(1 - s(lj) + \ldots),$$

$$\gamma_f^{(2)}(j_2) \approx \gamma_f^{(2)}(j)\,(1 - t(lj) + \ldots),$$

we obtain

$$r = 2\alpha_2 + s - t.$$

The coefficient r is a quantity of the same order of smallness as $1/2K_0^2$. The parameter $\overline{j^2}/2K_0^2$ can be determined independently with the help of the anisotropy of the fragment angular distribution.[8] Measurement of the angular correlation between the particle and the fragments permits one to obtain additional information concerning the orbital angular momentum of the particle and the dependence of the fission probability on the angular momentum.

We note that in formula (37) the dependence on the angle does not disappear for j = 0. This is connected with the fact that there is a known correlation between the directions of the two particles in a state with total angular momentum j = 0. The probability of the angle ω is proportional to the square of the Legendre polynomial

$$P_l^2(\cos\omega) \sim 1/\sin\omega \qquad (39)$$

for $l \gg 1$. This expression agrees with (16) if in the latter we set j = 0. The term in formula (37) not depending on j "trails along" with the correlation (39) and goes over into it for $l^2/2K_0^2 \gg 1$.

[1] V. M. Strutinskii, Сб. материалов Всесоюзн. конф. по ядерной реакции (Collection: All-Union Conference on Nuclear Reactions), Moscow, 1957.

[2] T. Erikson and V. Strutinski, Nuclear Phys. **8**, 284 (1958).

[3] T. Erikson, Nuclear Phys. **17**, 250 (1960).

[4] N. O. Lassen and V. A. Sidorov, Nuclear Phys. **19**, 579 (1960).

[5] D. Bodansky et al., Cyclotron Research, Univ. Washington Ann. Reports, 1960.

[6] V. M. Strutinskii, Атомная энергия (Atomic Energy) **2**, 508 (1957).

[7] V. M. Strutinskii, JETP **30**, 606 (1956), Soviet Phys. JETP **3**, 638 (1956).

[8] I. Halpern and V. Strutinski, Proc. of the Second Intern. Conf. on the Peaceful Uses of Atomic Energy, Geneva, 1958, Vol. 15, paper P/1513.

Translated by E. Marquit
304

ELECTROMAGNETIC WAVES IN A MEDIUM POSSESSING A CONTINUOUS ENERGY SPECTRUM. II.

V. S. MASHKEVICH

Kiev Polytechnic Institute

Submitted to JETP editor January 11, 1961

J. Exptl. Theoret. Phys. (U.S.S.R.) 40, 1803-1811 (June, 1961)

An electromagnetic-wave theory in which spatial dispersion is taken into account is applied to the case of exciton states. Propagation of waves in an infinite crystal and their transmission through a plane-parallel plate are considered. The absorption of electromagnetic waves in the presence of spatial dispersion is investigated.

IN a previous work[1] the equations of the electromagnetic field in a non-conducting medium in the presence of spatial dispersion were obtained:

$$\Delta \mathscr{E}^{\perp}_{x'}(\mathbf{r}) + \gamma \mathscr{E}^{\perp}_{x'}(\mathbf{r}) + 4\pi\gamma \int K^{\perp}_{x'y'}(\mathbf{r}, \mathbf{r}')\, \mathscr{E}^{\perp}_{y'}(\mathbf{r}')\, d\mathbf{r}' = 0, \quad (1)$$

$$\mathscr{E}^{\parallel}_{x'}(\mathbf{r}) = -4\pi \int K^{\parallel}_{x'y'}(\mathbf{r}, \mathbf{r}')\, \mathscr{E}^{\perp}_{y'}(\mathbf{r}')\, d\mathbf{r}', \quad (2)$$

where $\mathscr{E}^{\perp}(\mathbf{r})$, $\mathscr{E}^{\parallel}(\mathbf{r})$ are the solenoidal and irrotational parts of the electric field intensity, $\gamma = \mu\omega^2/c^2$, and summation over repeated indices is understood. The polarizability kernel is

$$K_{x'y'}(\mathbf{r}, \mathbf{r}') = K^{\perp}_{x'y'}(\mathbf{r}, \mathbf{r}') + K^{\parallel}_{x'y'}(\mathbf{r}, \mathbf{r}')$$

$$= \frac{1}{\hbar\omega} \sum_n{}' (E_n - E_0) \left[\frac{(0 \mid G_{x'}(\mathbf{r}) \mid n)(n \mid G_{y'}(\mathbf{r}') \mid 0)}{E_n - E_0 - \hbar\omega - i\varepsilon_n(\omega)} \right.$$

$$\left. - \frac{(n \mid G_{x'}(\mathbf{r}) \mid 0)(0 \mid G_{y'}(\mathbf{r}') \mid n)}{E_n - E_0 + \hbar\omega + i\varepsilon_n(-\omega)} \right], \quad (3)$$

$$\operatorname{div}_{\mathbf{r}} K^{\perp}_{y'}(\mathbf{r}, \mathbf{r}') = 0, \quad \operatorname{curl}_{\mathbf{r}} K^{\parallel}_{y'}(\mathbf{r}, \mathbf{r}') = 0. \quad (4)$$

Here E_0 is the energy of the ground state, E_n is the energy of the excited state; ϵ_n is connected with the lifetime of the state in the usual fashion, and $G(\mathbf{r})$ is the operator of the electric moment per unit volume.

In the present work, we shall apply these results to the case of exciton states of the crystal. This case was considered by Pekar,[2,3] who started from the differential equation derived by him for the polarization and with additional boundary conditions which require the vanishing of the exciton part of the polarization on the surface of the crystal. However, these conditions, even if one uses the wave functions of the exciton states chosen by Pekar, are approximate in the first place, and in the second place, are applicable only in the case of an isolated exciton band, transition to which is permitted in the dipole approximation.

The analysis in this paper is based on the integral-differential equation (1), which automatically takes into account the additional conditions and requires only the choice of the exciton wave functions (Pekar's functions were used for this purpose). This makes it possible to obtain general results which include Pekar's results as a special case and which show where the approximation in the latter lies.

1. WAVES IN AN INFINITE CRYSTAL

The Hamiltonian of the infinite crystal commutes with the translation operators $\hat{T}_n$ ($\mathbf{n}$ is the lattice vector). Therefore, one can use the eigenfunctions of $\hat{T}_n$ in the calculation of matrix elements entering into (3); the corresponding eigenvalues are $e^{i\mathbf{k}\cdot\mathbf{n}}$, where $\mathbf{k}$ is the quasi-momentum of the exciton ($-\pi \le \mathbf{k}\cdot\mathbf{a}_i < \pi$), and $\mathbf{a}_i$ ($i = 1, 2, 3$) is the basic lattice vector. It follows from translational symmetry that the quantity

$$f(\mathbf{r}, \mathbf{k}, \alpha) = \exp(-i\mathbf{k}\mathbf{r})(0 \mid G(\mathbf{r}) \mid \mathbf{k}\alpha),$$

(α are the other variables that enumerate the states along with $\mathbf{k}$) has the same period as the lattice, and can be expanded in the vectors of the reciprocal lattice $\mathbf{b}$:

$$f(\mathbf{r}, \mathbf{k}, \alpha) = \sum_{\mathbf{b}} g(\mathbf{b}, \mathbf{k}, \alpha)\, e^{i2\pi\mathbf{b}\mathbf{r}}.$$

Transforming to the variables $\mathbf{k}$, α in (3), we obtain

$$K_{x'y'}(\mathbf{r}, \mathbf{r}') = K^{+}_{x'y'}(\mathbf{r}, \mathbf{r}') + K^{-}_{x'y'}(\mathbf{r}, \mathbf{r}'), \quad (5)$$

$$K^{\pm}_{x'y'}(\mathbf{r}, \mathbf{r}') = \frac{L^3}{(2\pi)^3 \hbar\omega} \sum_{\alpha}{}' \int \Gamma^{\pm}(\mathbf{k}, \alpha) \times \sum_{\mathbf{bb}'} g^{\pm}_{x'y'}(\mathbf{b}, \mathbf{b}', \mathbf{k}, \mathbf{k}, \alpha) \exp\{\mp i\mathbf{k}(\mathbf{r} - \mathbf{r}') \mp i2\pi(\mathbf{br} - \mathbf{b}'\mathbf{r}')\}\, d\mathbf{k};$$

$$\Gamma^{\pm}(\mathbf{k}, \alpha) \quad \mp \frac{E(\mathbf{k}, \alpha) - E_0}{E(\mathbf{k}, \alpha) \mp i\varepsilon(\mathbf{k}, \alpha, \mp\omega) - E_0 \pm \hbar\omega},$$

$$g^{+}_{x'y'}(\mathbf{b}, \mathbf{b}', \mathbf{k}, \mathbf{k}', \alpha) = g^{*}_{x'}(\mathbf{b}, \mathbf{k}, \alpha)\, g_{y'}(\mathbf{b}', \mathbf{k}', \alpha), \quad g^{-} = g^{+*}, \tag{6}$$

$L \to \infty$ are the dimensions of the fundamental region.

We shall assume that the macroscopic field $\mathcal{E}^{\perp}(\mathbf{r})$ entering in (1) is a smooth function of its coordinates. Then, in the integration over $\mathbf{r}'$, the main contribution is made to the part due to K^+ by the terms with $\mathbf{b}' = 0$ and with small $\mathbf{k}$, since K^+ does not contain any singularities. When $\mathbf{k}$ is small, the matrix element $(0|\mathbf{G}(\mathbf{r})|\mathbf{k}\cdot\alpha)$ is a smooth function of the coordinates: when $\mathbf{k} = 0$, it has the same period as the lattice, as a consequence of which, being a macroscopic quantity, it is constant. Therefore, $\mathbf{g}(\mathbf{b}, \mathbf{k}, \alpha)$ is small for $\mathbf{b} \neq 0$ and small $\mathbf{k}$. The circumstances mentioned lead to the result that the part of the polarization which is due to K^+ is locally associated with the field.

Following Pekar,[2] we limit ourselves to consideration of states for which $\mathbf{k}$ and only $\mathbf{k}$ is a continuous quantum number. In this case α is discrete and one can separate components in K^- for which $E(0, \alpha)$ differs appreciably from $E(\omega) = E_0 + \hbar\omega$. Like K^+, they yield the local part of the polarization. Taking it into account that $f^*(z^*)$ is the analytic continuation in the complex plane of the function $f^*(z)$, and that the functions $\mathbf{k}$ entering into (6) may not be analytic at the point $\mathbf{k} = 0$, we can write (1) in the form

$$\Delta\mathcal{E}^{\perp}_{x'}(\mathbf{r}) + \gamma\beta^{\perp}_{x'y'}\mathcal{E}^{\perp}_{y'}(\mathbf{r}) + 4\pi\gamma\int \chi^{\perp}_{x'y'}(\mathbf{r}, \mathbf{r}')\,\mathcal{E}^{\perp}_{y'}(\mathbf{r}')\, d\mathbf{r}' = 0, \tag{7}$$

$$\beta^{\perp}_{x'y'} = \delta_{x'y'} + \frac{4\pi L^3}{\hbar\omega}\Big[\sum_{\alpha}\Gamma^{+}\Big(-ai\frac{\partial}{\partial\mathbf{r}}, \alpha\Big) \times g^{+\perp}_{x'y'}\Big(0, 0, \Big(-ai\frac{\partial}{\partial\mathbf{r}}\Big)^{*} - ai\frac{\partial}{\partial\mathbf{r}}, \alpha\Big) + \sum_{\alpha}{}'\Gamma^{-}\Big(-ai\frac{\partial}{\partial\mathbf{r}}, \alpha\Big) \times g^{-\perp}_{x'y'}\Big(0, 0, -ai\frac{\partial}{\partial\mathbf{r}}, \Big(-ai\frac{\partial}{\partial\mathbf{r}}\Big)^{*}, a\Big)\Big]_{a=+0}. \tag{8}$$

The prime on the summation sign in (8) means that the components containing the singularity are omitted; $\chi^{\perp}$ is obtained from K^-, which appears in (6), by replacement of g^- by $g^{-\perp}$ and $\sum_{\alpha}$ by $\sum_{\alpha}'' = \sum_{\alpha} - \sum_{\alpha}'$; $g^{\pm\perp}_{x'y'}$ is obtained from $g^{\pm}_{x'y'}$ by replacing $g_{x'}$ by the projection $g^{\perp}_{x'}$ of this quantity, on the plane perpendicular to $\mathbf{k} + 2\pi\mathbf{b}$.

We seek a solution of (7) in the form

$$\mathcal{E}_{\mathbf{n}}(\mathbf{r}) = \sum_{s}\mathbf{c}_s \exp(i\mathbf{n}\varkappa_s\mathbf{r}), \qquad n^2 = 1, \tag{9}$$

$$\mathbf{nc}_s = 0 \tag{10}$$

subject to a condition that guarantees the smoothness of the field

$$|\varkappa_s| \ll \pi/d \tag{11}$$

(d is the lattice constant), which should be satisfied for those s for which c_s is large. Computing the integral over $\mathbf{k}$ in (7) by a method similar to that used in the Appendix, we find that $\varkappa_s$ and c_s are determined from

$$-\varkappa^2 c_{x'} + \gamma\beta^{\perp}_{\mathbf{n}x'y'}c_{y'} + \frac{4\pi\gamma L^3}{\hbar\omega}\sum_{\varkappa}{}''\Gamma^{-}_{\mathbf{n}}(\varkappa, \alpha)\, g^{-\perp}_{\mathbf{n}x'y'}(0, 0, \varkappa, \varkappa^*, \alpha)\, c_{y'} = 0 \tag{12}$$

and (10), where the subscripts of g and Γ indicate the direction of $\mathbf{k}$, and $\beta^{\perp}_{\mathbf{n}x'y'}$ is obtained from (8) by setting $a = 0$ and writing Γ and g with the index $\mathbf{n}$. From (12) one can obtain (in the corresponding case and approximation) the results of Pekar,[2] which refer to a transverse field in an infinite crystal. $\mathcal{E}^{\parallel}(\mathbf{r})$ can be found with the help of (2) and (9).

2. WAVES IN A THICK PLATE

We consider the normal incidence of a wave on a plane-parallel plate of a cubic crystal. As wave functions of the exciton state, we choose the functions[2]

$$\Phi_{\alpha\mathbf{k}} = 2^{-1/2}(\Psi_{\alpha\mathbf{k}} - \Psi_{\alpha\widetilde{\mathbf{k}}}),$$

where $\Psi_{\alpha\mathbf{k}}$ is the wave function of the infinite crystal,

$$\widetilde{\mathbf{k}}\mathbf{a}_{1,2} = \mathbf{k}\mathbf{a}_{1,2} \equiv k_{1,2}, \qquad -\widetilde{\mathbf{k}}\mathbf{a}_3 = \mathbf{k}\mathbf{a}_3 \equiv k_3 = \pi\nu/(N+1),$$
$$\nu = 1, \ldots, N,$$

$\mathbf{a}_{1,2}$ are parallel to the surfaces of the plate, N is the number of elementary cells that make up the thickness of the plate l.

We direct the z axis normal to the plate so that $z = 0$ and l on the surfaces. Now the polarizability kernel is obtained in the form (5), where

$$K^{\pm}_{x'y'}(\mathbf{r}, \mathbf{r}')$$

$$= \frac{L^2}{(2\pi)^2 2\hbar\omega} \sum_{\alpha} \sum_{k_3=-k_N}^{k_N} \int \Gamma^{\pm}(\mathbf{k}, \alpha) \sum_{bb'} \exp\{\mp i [k_3 b_{3z} z + k_x (x - x') + k_y (y - y') + (k_1 b_{1z} + k_2 b_{2z})(z - z') + 2\pi (\mathbf{br} - \mathbf{b}'\mathbf{r}')]\} \times [g^{\pm}_{x'y'}(\mathbf{b}, \mathbf{b}', \mathbf{k}, \mathbf{k}, \alpha) \exp(\pm i k_3 b_{3z} z') - g^{\pm}_{x'y'}(\mathbf{b}, \mathbf{b}', \mathbf{k}, \tilde{\mathbf{k}}, \alpha) \exp(\mp i k_3 b_{3z} z')]\, dk_x\, dk_y, \quad (13)$$

where $k_N = \pi N/(N+1)$, $\mathbf{b}_i$ $(i = 1, 2, 3)$ is the fundamental vector of the reciprocal lattice.

As above, we can separate in (13) the components that give the local contribution to the polarization. We then arrive at Eq. (7), in which one must now integrate over the volume $L^2 l$, $\beta^{\perp}$ is obtained from (8) by the replacement of L^3 by $L^2 l$, and $\chi^{\perp}$ from the K^- appearing in (13) by replacement of g^- by $g^{-\perp}$ and $\sum_{\alpha}$ by $\sum_{\alpha}''$.

It is not difficult to prove that a solution of (7) which does not depend on x and y, exists with the given kernel. We further assume that one can separate excitons with transverse and longitudinal polarizations in a cubic crystal at small k. Finally, the tensors entering into (7) in the case of a cubic crystal reduce to scalars; therefore, one can consider a field with fixed polarization. Let $\mathcal{E}(z)$ be directed along the y axis. Omitting the corresponding signs, we obtain

$$\frac{d^2\mathcal{E}(z)}{dz^2} + \eta\, \mathcal{E}(z) + \frac{\rho}{2l} \sum_{\alpha}'' \sum_{bb'} \int_0^l \chi(z, z', b, b', \alpha)\, \mathcal{E}(z')\, dz' = 0. \quad (14)$$

Here the sum over α takes into account only the transverse excitons, $b = nb_{3z}$ (n an integer), $\eta = \gamma\beta$, $\rho = 4\pi\gamma L^2 l/\hbar\omega$,

$$\chi(z, z', b, b', \alpha) = \exp[i2\pi(bz - b'z')] \sum_{k=-k_N}^{k_N} \Gamma_0^-(k, \alpha)\, g_0(b, k, \alpha) \times \exp(ikz)\, [g_0^*(b', k, \alpha) \exp(-ikz') - g_0^*(b', -k, \alpha) \times \exp(ikz')], \quad (15)$$

where

$$f_0(b, k) = f(nb_3, \mathbf{k})|_{k_x, y=0}, \qquad f = \Gamma, g.$$

As is shown in the Appendix, the solution of (14) has the form

$$\mathcal{E}(z) = \sum_s c_s \exp(i\varkappa_s z), \quad (16)$$

where $\varkappa_s$ are the roots of the equation

$$-\varkappa^2 + \eta + \rho \sum_{\alpha}'' g_0^-(0, 0, \varkappa, \varkappa^*, \alpha)\, \Gamma_0^-(\varkappa, \alpha) = 0, \quad (17)$$

and it is assumed that (11) is satisfied for all s for which c_s is large; the quantities c_s satisfy the equations

$$\sum_s c_s \sum_b [k^+_{\alpha q} r_s^+(b, k^+_{\alpha q}, \alpha) + (\varkappa_s - 2\pi b)\, r_s^-(b, k^+_{\alpha q}, \alpha)] = 0,$$

$$\sum_s c_s \exp(i\varkappa_s l) \sum_b \exp(-2\pi b l)\, [k^-_{\alpha q} r_s^+(b, k^-_{\alpha q}, \alpha) + (\varkappa_s - 2\pi b)\, r_s^-(b, k^-_{\alpha q}, \alpha)] = 0,$$

$$r_s^{\pm}(b, k, \alpha) = [g_0^*(b, k^*, \alpha) \pm g_0^*(b, -k^*, \alpha)]\, [(\varkappa_s - 2\pi b)^2 - k^2]^{-1}, \quad (18)$$

where $k^{\pm}_{\alpha q}$ are the roots of the equation

$$E_0(k, \alpha) - i\varepsilon_0(k, \alpha, \omega) - E(\omega) = 0, \qquad q = 1, \ldots, m_{\alpha}, \quad (19)$$

and the sign on $k_{\alpha q}$ denotes the sign of the imaginary part.

The number of components in (16) exceeds the number of equations in (18) by two, so that there are exactly two independent quantities among the c_s. The results that have been given are valid in the case of a sufficiently thick plate. From (16), the Maxwell boundary conditions, and the additional conditions (18), one can find the waves reflected from and emerging from the plate. The corresponding formulas are very cumbersome in the general case and we shall not write them out.

3. EXCITONS OF ZERO AND FIRST ORDER

We consider the simplest case in which the sum (17) contains only one component, and $E(\omega) \approx E_0(0, \alpha)$. Under these conditions, (11) is satisfied for all s and we can therefore set $\kappa = 0$ in the numerator of Γ in (17), and expand $E_0(\kappa, \alpha)$ in the denominator and in (19) in powers of κ, restricting ourselves to the quadratic term. Moreover, we can neglect the dependence of ϵ_0 on κ and ω. In this case (19) yields two roots $k^- = -k^+$, which are small, and which makes it possible to neglect components in (18) with $b \neq 0$. Omitting α, we get from (17) — (19)

$$-\varkappa^2 + \eta + \rho g_0^-(0, 0, \varkappa, \varkappa^*)\, [E_0(0) - E_0] \times (\xi\varkappa^2 - i\varepsilon - \zeta)^{-1} = 0; \quad (20)$$

$$\sum_s c_s [k^+ r^+(0, k^+) + \varkappa_s r^-(0, k^+)] = 0,$$

$$\sum_s c_s \exp(i\varkappa_s l)\, [k^- r^+(0, k^-) + \varkappa_s r^-(0, k^-)] = 0; \quad (21)$$

$$\xi (k^{+})^2 - i\varepsilon - \zeta = 0, \qquad (22)$$

where $\zeta = E(\omega) - E_0(0)$, $\xi = \hbar^2/2m^*$, m^* is the effective mass of the exciton.

We consider two cases, in which

$$g_0 \equiv g_0(0, 0) \neq 0$$

and

$$g_0 = 0, \qquad g_0' \equiv (dg_0(0, k)/dk)_0 \neq 0.$$

In these cases, we can speak of excitons of zero and first order, respectively (or of dipole and quadrupole excitons). Excitons of zero order are found in anthracene, and of first order in copper oxide (references to the corresponding experiments are given in the paper of Pekar et al.[4]). For excitons of zero order, we can regard $g_0(0, k) = g_0$ in (20) and (21); here, (20) — (22) are identical with the corresponding results of Pekar.[2,3] Thus the results derived are approximately valid for frequencies arbitrarily close to the resonant frequency point $\mathbf{k} = 0$.

We now consider excitons of first order, assuming $g_0(0, k) = g_0' k$ for them. Here the solutions of (20) are $\pm\kappa_j$, $j = 1, 2$,

$$\varkappa_j^2 = \{\xi\eta + \zeta + i\varepsilon + \alpha + (-1)^j [(\xi\eta + \zeta + i\varepsilon + \alpha)^2 - 4\xi\eta(\zeta + i\varepsilon)]^{1/2}\}/2\xi,$$

where $\alpha = \rho |g_0'| [E_0(0) - E_0]$, which are identical with the corresponding results of Pekar et al.[4] It is now convenient to write (16) in the form

$$\mathscr{E}(z) = \sum_{j=1,2} [c_j^+ \exp(i\varkappa_j z) + c_j^- \exp(-i\varkappa_j z)].$$

In corresponding fashion, (21) yields

$$\sum_{j=1,2} \gamma_j (c_j^+ - c_j^-) = 0,$$

$$\sum_{j=1,2} \gamma_j [c_j^+ \exp(i\varkappa_j l) - c_j^- \exp(-i\varkappa_j l)] = 0,$$

$$\gamma_j = \varkappa_j [\varkappa_j^2 - (k^+)^2]^{-1}. \qquad (23)$$

Let the incident, reflected, and transmitted waves have respectively the forms

$$\mathscr{E}_0 \exp(ik_0 z), \qquad R \exp(-ik_0 z), \qquad B \exp(ik_0 z).$$

From the Maxwell boundary conditions and the additional conditions (23), we find*

$$R = A(u^2 - v^2 - w^2), \qquad B = A i 2uw \exp(-ik_0 l);$$

$$A = \mathscr{E}_0 (u^2 - v^2 + w^2 + i2vw)^{-1},$$

$$u = \gamma_1 / \sin \varkappa_2 l - \gamma_2 / \sin \varkappa_1 l,$$

$$v = \gamma_1 \operatorname{ctg} \varkappa_2 l - \gamma_2 \operatorname{ctg} \varkappa_1 l, \qquad w = (\gamma_1 \varkappa_2 - \gamma_2 \varkappa_1)/k_0.$$

*ctg = cot.

In the case of a semi-infinite crystal, we then obtain

$$B_\infty = 0, \qquad R_\infty = \mathscr{E}_0 (\gamma_1 - \gamma_2 - w)(\gamma_1 - \gamma_2 + w)^{-1},$$

which gives the generalization of the corresponding Fresnel formula with account of spatial dispersion.

We note that in the case of excitons of first order one should have, for greater consistency, considered higher approximations in the material equations.[5]

4. WAVES IN A PLATE OF ARBITRARY THICKNESS

As is seen from the Appendix, the solution of Eq. (14) used above is inappropriate for sufficiently small l. Here we obtain a solution appropriate for arbitrary l, limiting ourselves to the case in which the sum over α in (14) contains only one component (an isolated exciton band) and $E(\omega) \approx E_0(0)$. In this case the terms of the sum over k in (15) vanish, for smooth functions $\mathscr{E}(z)$, with increase in $|k|$ so that for all z the principal role in the last component of (14) is played by terms with small $|k|$, as a consequence of which one can discard terms with b and $b' \neq 0$ and keep the first non-vanishing term in the expansion of $g_0(0, k)$ in powers of k. We note that for excitons of zero order this agrees in accuracy with the approximate theory of Pekar.[2]

In the case of excitons of zero order, we obtain in this fashion

$$\frac{d^2\mathscr{E}'(t)}{dt^2} + \eta'\mathscr{E}'(t) + \int_0^\pi \sum_{n=1}^\infty f_0'(n) \sin nt \sin nt' \mathscr{E}'(t')\, dt' = 0,$$

$$t = (\pi/l) z, \qquad \mathscr{E}'(t) = \mathscr{E}(z),$$

$$\eta' = (l/\pi)^2 \eta, \qquad f'(n) = (l/\pi)^3 f(k_n),$$

$$f_0(k_n) = \begin{cases} (2\rho/l) |g_0|^2 \Gamma_0^-(k_n), & n \leqslant N \\ 0, & n > N. \end{cases} \qquad (24)$$

We now seek the solution of (24) in the form

$$\mathscr{E}'(t) = \sum_{n=1}^\infty a_n \sin nt, \qquad 0 < t < \pi.$$

Taking it into account that

$$\frac{d\mathscr{E}'}{dt} = \frac{c_0}{2} + \sum_{n=1}^\infty [na_n - d_0 + (-1)^n (c_0 + d_0)] \cos nt,$$

$$c_0 = (2/\pi)[\mathscr{E}'(\pi) - \mathscr{E}'(0)], \qquad d_0 = (2/\pi)\mathscr{E}'(0), \qquad (25)$$

we can differentiate termwise the cosine series[6] and obtain

$$a_n = n[d_0 - (-1)^n (c_0 + d_0)][n^2 - \eta' - (\pi/2) f_0'(n)]^{-1}.$$

Further, denoting

$$\sigma_p = \sum_{n=1}^{\infty} (-1)^{pn} \left[\eta' + \frac{\pi}{2} f_0'(n)\right]\left[n^2 - \eta' - \frac{\pi}{2} f_0'(n)\right]^{-1},$$

we obtain

$$d\mathscr{E}'/dt|_0 = c_0/2 + d_0\sigma_2 - (c_0 + d_0)\sigma_1,$$
$$d\mathscr{E}'/dt|_\pi = c_0/2 + d_0\sigma_1 - (c_0 + d_0)\sigma_2. \qquad (26)$$

(25), (26) express $\mathscr{E}'$ and $d\mathscr{E}'/dt$ on the surface of the plate in terms of the constants c_0 and d_0, which play the role of arbitrary constants.

With the help of the Maxwell boundary conditions, we find the amplitudes of the reflected and transmitted waves:

$$R_0 = A_0 [k_0^2 l^2 - 4(\sigma_2 - \sigma_1)(1 - \sigma_1 - \sigma_2)],$$

$$B_0 = A_0 i 2k_0 l (1 - 2\sigma_1) \exp(-ik_0 l);$$

$$A_0 = \mathscr{E}_0 [k_0^2 l^2 + 4(\sigma_2 - \sigma_1)(1 - \sigma_1 - \sigma_2) + 2ik_0 l (1 - 2\sigma_2)]^{-1}.$$

In the case of excitons of first order, (14) and (15) yield the following expression in the approximation under consideration:

$$\frac{d^2\mathscr{E}'(t)}{dt^2} + \eta'\mathscr{E}'(t) + \int_0^\pi \sum_{n=1}^{\infty} f_1'(n) \cos nt \cos nt' \mathscr{E}'(t')\, dt' = 0,$$

where $f_1(k_n)$ is obtained from $f_0(k_n)$ by replacing $|g_0|^2$ by $|g_0'|^2 k_n^2$. Working in a fashion similar to the above, we obtain the amplitudes of the reflected and transmitted waves

$$R_1 = A_1 [4k_0^2 l^2 (\sigma_1' - \sigma_2')(1/\eta' - \sigma_1' - \sigma_2') + \pi^4],$$

$$B_1 = A_1 i \cdot 2k_0 l \pi^2 (1/\eta' - 2\sigma_1') \exp(-ik_0 l);$$

$$A_1 = \mathscr{E}_0 [4k_0^2 l^2 (\sigma_1' - \sigma_2')(1/\eta' - \sigma_1' - \sigma_2') - \pi^4 - i2k_0 l\pi^2 (1/\eta' - 2\sigma_2')]^{-1},$$

$$\sigma_p' = \sum_{n=1}^{\infty} (-1)^{pn} \left[n^2 - \eta' - \frac{\pi}{2} f_1'(n)\right]^{-1}.$$

5. ABSORPTION

In the presence of spatial dispersion, there is meaning to considering only absorption throughout the entire volume:

$$\overline{W} = i\omega \int \mathscr{E}_y(\mathbf{r})\, P_y^*(\mathbf{r})\, d\mathbf{r} + \text{compl. conj.}$$

where the bar denotes averaging over the period, while $\mathscr{E}_y(\mathbf{r})$ and $P_y(\mathbf{r})$ are the amplitudes of the electric field intensity and polarization. We resolve $\mathscr{E}_y(\mathbf{r})$ into a solenoidal part and an irrotational part, in accord with which we obtain

$$\overline{W} = W^\perp + W^\parallel,$$

$$W^{\perp,\parallel} = i\omega \int \mathscr{E}_y^{\perp,\parallel}(\mathbf{r})\, P_y^*(\mathbf{r})\, d\mathbf{r} + \text{compl. conj.} \qquad (27)$$

Further, substituting (2), in the expression

$$P_{x'}(\mathbf{r}) = \int K_{x'y'}(\mathbf{r}, \mathbf{r}')\, \mathscr{E}_{y'}^{\perp}(\mathbf{r}')\, d\mathbf{r}' \qquad (28)$$

obtained in reference 1, and (3) in (24), and taking (4) into account, we find that $W^{\parallel} = 0$. Finally, by introducing (28) and the relation $K_{x'y'} = Q_{x'y'} + R_{x'y'}$ which figures in reference 1, ($Q_{x'y'}$, $R_{x'y'}$ are the Hermitian and anti-Hermitian parts of the kernel) into (27) we obtain

$$\overline{W} = -2i\omega \int R_{x'y'}(\mathbf{r}, \mathbf{r}')\, \mathscr{E}_{x'}^{\perp *}(\mathbf{r})\, \mathscr{E}_{y'}^{\perp}(\mathbf{r}')\, d\mathbf{r}\, d\mathbf{r}'.$$

Thus the absorption for a given field is determined by the anti-Hermitian part of the polarizability kernel, just as the absorption is determined by the anti-Hermitian part of the polarizability tensor in the absence of spatial dispersion.

It is seen from (3) that $R_{x'y'} \sim \epsilon$ when $\hbar\omega \neq E_n - E_0$. Therefore, upon satisfaction of the inequality mentioned, the absorption must tend to zero if $\epsilon \to 0$. It is not difficult to prove that the expressions obtained above for R, B, R_0, B_0 and R_1, B_1 satisfy this condition.

In conclusion we note that in this research, just as in reference 1, we did not make any distinction between the average and effective values of the field. Therefore, the results obtained apply only to the case in which these values are identical. The general case needs special consideration.

APPENDIX

We consider the integral which appears in (14):

$$I(z, b, b', \alpha) = \int_0^l \chi(z, z', b, b', \alpha)\, \mathscr{E}(z')\, dz',$$

where $\mathscr{E}(z)$ is given by Eq. (16). In view of the fact that (14) is a differential equation, it suffices in the case of large l to know I for z not too close to the boundary values. For such z the principal contribution to I is made in the summation over k in (15) by the immediate vicinity of the points $\pm \mathrm{Re}\,\kappa_S$ and $\mathrm{Re}\,k_{\alpha q}$. Let us consider the contribution made by the points $\pm \mathrm{Re}\,\kappa_S$. In view of (11), only the terms with b and b' = 0 are important:

$$I_s(z, 0, 0, \alpha) = c_s \Gamma_0^- (-i\partial/\partial z, \alpha)\, g_0(0, -i\partial/\partial z, \alpha) \times [g_0^*(0, (-i\partial/\partial z)^*, \alpha)\, I_s^-(z) - g_0^*(0, (i\partial/\partial z)^*, \alpha)\, I_s^+(z)],$$

$$I_s^{\pm}(z) = \int_0^l \sum_k^{(s)} \exp[ik(z \pm z') + i\varkappa_s z']\, dz',$$

where the summation is carried out over the values $k = (\pi/l)\nu$ which lie close to the points $\pm \mathrm{Re}\,\kappa_S$. Inasmuch as the vicinities of the points mentioned

make the principal contribution, we can extend the summation over all k. Then

$$I_s(z, 0, 0, \alpha) = 2lc_s g_0^- (0, 0, \varkappa_s, \varkappa_s^*, \alpha)\, \Gamma_0^- (\varkappa_s, \alpha) \exp(i\varkappa_s z). \tag{A.1}$$

We now consider the contribution of the points $k_{\alpha q}$:

$$I_\alpha = \sum_q \sum_s c_s \sum_k^{(q)} \exp[i(2\pi b + k) z]\, \Gamma_0^- (k, \alpha)\, g_0 (b, k, \alpha) \times \left\{ g_0^* (b', k, \alpha) \frac{\exp[i(\varkappa_s - k - 2\pi b')l] - 1}{i(\varkappa_s - k - 2\pi b')} - g_0^* (b', -k, \alpha) \frac{\exp[i(\varkappa_s + k - 2\pi b')l] - 1}{i(\varkappa_s + k - 2\pi b')} \right\},$$

where the summation over k includes the vicinity of the points $k_{\alpha q}$. We transform from summation over k to integration; this is possible in the case of sufficiently large l. Here, we must replace e^{ikl} in the second term in curly brackets by the equivalent expression e^{-ikl} to obtain a smoother function of k. Furthermore, we can close the contour of integration in the lower half-plane in the interval containing $e^{ik(z-l)}$, and in the upper half-plane in the interval containing e^{ikz}. Then, with the aid of residues, we find

$$I_\alpha = -2l \sum_q \sum_s c_s e^{i2\pi bz} \{\exp[ik_{\alpha q}^- (z - l) + i(\varkappa_s - 2\pi b')l] \times p_s (b, b', k_{\alpha q}^-, \alpha) + \exp(ik_{\alpha q}^+ z)\, p_s (b, b', k_{\alpha q}^+, \alpha)\},$$

$$p_s (b, b', k, \alpha) = \left[\frac{g_0^- (b, b', k, k^*, \alpha)}{\varkappa_s - k - 2\pi b'} - \frac{g_0^- (b, b', k, -k^*, \alpha)}{\varkappa_s + k - 2\pi b'} \right] \frac{E_0 (k, \alpha) - E_0}{dE_0 (k, \alpha)/dk}. \tag{A.2}$$

Taking into account (A.1), (A.2), (16) and (14), it is easy to obtain (17), (18). We write (17) in the form

$$\varphi(\varkappa) + \psi(\varkappa) = 0;$$

$$\varphi(\varkappa) = (-\varkappa^2 + \eta) \prod_\alpha'' [E_0 (\varkappa, \alpha) - i\varepsilon_0 (\varkappa, \alpha, \omega) - E(\omega)],$$

$$\psi(\varkappa) = \rho \sum_\alpha'' g_0^- (0, 0, \varkappa, \varkappa^*, \alpha) \times \prod_{\alpha' \neq \alpha} [E_0 (\varkappa, \alpha') - i\varepsilon_0 (\varkappa, \varkappa', \omega) - E(\omega)].$$

$\varphi(\kappa)$ and $\psi(\kappa)$ are analytic functions of κ. The number of components in (16), N_1, is equal to the number of zeros of $\varphi(\kappa) + \psi(\kappa)$ lying close to the origin of the coordinates, in accord with (11). The number of equations in (18) is $N_2 = \sum_\alpha'' m_\alpha$. We shall show that $N_1 = N_2 + 2$. We draw the closed contour C in the plane passing through the points $-\pi/d$, $+\pi/d$ so that for them $|\kappa| \geq \pi/d$ and $\varphi(\kappa)$, $\psi(\kappa)$ do not vanish on them. Inasmuch as $|\kappa|$ is large on C, then $|\varphi(\kappa)| > |\psi(\kappa)| > 0$ on C. Then, by Rouche's theorem,[7] the number of zeros of $\varphi(\kappa) + \psi(\kappa)$ inside C is identical with the number of zeros of $\varphi(\kappa)$, which is obviously equal to $N_2 + 2$.

[1] V. S. Mashkevich, JETP **38**, 906 (1960), Soviet Phys. JETP **11**, 653 (1960).

[2] S. Pekar, JETP **33**, 1022 (1957), Soviet Phys. JETP **6**, 785 (1958).

[3] S. I. Pekar, JETP **34**, 1176 (1958), Soviet Phys. JETP **7**, 813 (1958).

[4] Pekar, Brodin, and Tsekvava, Paper at the IV Conference on the Theory of Superconductivity, Reports of the Conference, Tiflis, 1960.

[5] V. S. Mashkevich, Изв. Высш. уч. зав., Физика (News of the Colleges, Physics) **4**, 217 (1960).

[6] G. P. Tolstov, Ряды Фурье (Fourier Series), Gostekhizdat, 1951.

[7] M. A. Lavrent'ev and B. V. Shabat, Методы теории функций комплексного переменного (Methods of the Theory of Functions of a Complex Variable), Gostekhizdat, 1951.

Translated by R. T. Beyer
305

THE EFFECT OF DIFFUSION ON THE SCATTERING OF NEUTRONS AND PHOTONS BY CRYSTAL IMPERFECTIONS AND ON THE MÖSSBAUER EFFECT

M. A. KRIVOGLAZ

Institute of Metal Physics, Academy of Sciences, Ukrainian S.S.R.

Submitted to JETP editor January 11, 1961

J. Exptl. Theoret. Phys. (U.S.S.R.) 40, 1812-1824 (June, 1961)

The broadening of the energy distribution of neutrons or photons which are quasi-elastically scattered by crystal defects resulting from diffusion is investigated. The macroscopic approximation is not used and the diffusion mechanism is taken into account explicitly. The broadening may be appreciable in the scattering of neutrons and photons which are emitted without recoil by nuclei in a crystal, and also in certain cases of Rayleigh scattering of light at high temperatures. The analogous broadening should occur for the spectral distribution in the absorption and emission spectra in the Mössbauer effect for the case of high temperatures. The characteristic dependence is found of the broadening on the magnitude and orientation of the wave vector, and this makes it possible in principle to investigate the mechanism of diffusion and the type of defect.

1. INTRODUCTION

THE diffuse scattering of neutrons by defects in a crystal at sufficiently low temperatures can be divided into inelastic scattering associated with thermal vibrations and having a continuous energy distribution, and elastic scattering whose energy distribution is described by a δ function $\delta(E)$ (where E is the change in energy on scattering). At high temperatures, however, defects (atoms injected in interstices, vacancies at lattice sites, etc.) give an appreciable diffusion mobility. A defect moving at random even in the absence of vibration can transfer energy to a neutron, as a result of which the δ function in the energy distribution of the scattered neutrons is smeared out, and the scattering becomes completely inelastic.

The influence of the diffuse motion of the atoms of a liquid on the scattering of neutrons has been treated by means of the macroscopic approximation in references 1 — 3. This approximation is applicable for the case of very slow neutrons or small scattering angles. For large differences q_1 of the wave vectors of the scattered and incident waves, the results depend essentially on the geometry of the diffusion jumps of the atoms, and the macroscopic approximation ceases to be applicable. In the case of scattering by defects, for each of several possible mechanisms of diffusion the geometry of the diffusion jumps is known, which makes it possible to construct a theory of the energy distribution of scattered neutrons which is also applicable for large q_1. As we shall see from the results obtained below, it is just this case which is especially interesting, since the comparison of theory with the experimental data regarding the case of large q_1 makes it possible in principle to obtain valuable information concerning the type of defects in the crystal and concerning the mechanism of diffusion. In certain cases, even for small q_1, the macroscopic treatment does not allow one to carry out the investigation. In this connection, we shall treat in Sec. 2 the influence of diffusion on the energy distribution of scattered neutrons without using the macroscopic approximation.

It is obvious that the diffusion of defects must give rise to the same sort of broadening of the energy distribution of scattered x rays. But, since the energy of x-ray photons is approximately 10^5 times greater than the energy of thermal neutrons, while the natural width of x-ray levels is much greater than this broadening, its experimental detection by ordinary methods is impossible. The possibility of such an observation has arisen in connection with the discovery of extremely narrow energy distributions of photons (x rays or γ quanta) which are emitted by long-lived excited states of nuclei of certain isotopes in a crystal, and can be studied with high precision by using the resonant nuclear absorption of the photons (the Mössbauer effect).[4] (For reference to other

work, we refer to the summary of Belozerskii and Nemilov.[5]) With respect to this we discuss in Sec. 3 the influence of diffuse motion on the energy distribution of such photons.

If the defects can occur only at sites of one type, then for small values of q_1 the magnitude of the broadening produced by diffusion falls off like q_1^2. For the scattering of light waves in this case, the broadening is approximately 10^7 times smaller than for the scattering of x rays and is completely insignificant. If, however, the defects may be present at positions of several different types, then, as we shall show later, as $q_1 \to 0$ the broadening tends to a non-zero limit, and may be appreciable for the scattering of light at high temperatures. Therefore in Sec. 3 we also discuss the influence of diffusion on the scattering of light.

Diffusion may also appreciably affect the energy distribution of the emitted radiation if, during the lifetime of the excited state of the radiating atom (nucleus), it succeeds in shifting such a distance that the phase difference between the waves radiated in the initial and final points is comparable with π. The corresponding broadening of the emission line may become appreciable at high temperatures in the case of the Mössbauer effect and also in the case of no-phonon emission of light, if the radiating defects can be at several different sites. These effects will be treated in Sec. 4.

2. THE INFLUENCE OF DIFFUSION OF DEFECTS ON THE SCATTERING OF THERMAL NEUTRONS

The atoms of a crystal carry out motions of two types: oscillations around their equilibrium positions, and diffusion jumps to new equilibrium positions. If the diffusion can be neglected, then there remain only the oscillations of the atoms which lead to a reduction in the amplitude of elastic scattering of the s-th atom by the Debye factor e^{-M_s}, where $M_S = \frac{1}{2}\overline{(\mathbf{q}_1 \cdot \mathbf{u}_S)^2}$ and the $\mathbf{u}$'s are the thermal displacements of the atoms.

We take account of the diffuse motion for the case where the probability W of diffusion jumps to neighboring positions is considerably less than the effective frequency of oscillation of the atom ω_0. In practice the criterion $W \ll \omega_0$ is always satisfied. We denote by $E = \hbar\omega$ the change in energy of the neutrons during scattering. As will be shown later, diffusion leads to a smearing of the energy distribution of the elastic scattering in the region $\omega \lesssim W$. In the following we shall treat just this region of low values of ω (corresponding to long times in the time-correlation function). In this case we may treat the oscillations simply by introducing the factor e^{-M_s} into the scattering amplitude.

Suppose that point defects (or defects of finite dimensions) can occupy positions of several types, $1, 2 \ldots, \nu, \ldots, n$. We shall assume that the concentration of defects c_ν is small ($c_\nu \ll 1$), that they are distributed randomly, and that in the absence of these defects the non-ideality of the crystal can arise only from the presence of isotopes of different types. The detailed distribution of the defects can be characterized by assigning the numbers $c_{r\nu}(t)$, equal to one or zero, if at the time t at the position r of the ν-th type there is or is not a defect. The amplitude of scattering of monochromatic neutrons by a single crystal containing defects, at the time t, is proportional to the sum

$$a(t) = \sum_{r\nu} c_{r\nu}(t) \exp(i\mathbf{q}_1\mathbf{R}_{r\nu}) \Big\{\varphi_\nu + \sum_s{}' [A_s - \bar{A}_s + b_s(sS_s)] \times \exp(i\mathbf{q}_1\delta\mathbf{R}_{sr\nu}) \exp(i\mathbf{q}_1, \mathbf{R}_s - \mathbf{R}_{r\nu})\Big\}$$
$$+ \sum_s{}'' [A_s - \bar{A}_s + b_s(sS_s)] \exp(i\mathbf{q}_1, \mathbf{R}_s + \delta\mathbf{R}_s),$$
$$\varphi_\nu = \sum_s \bar{A}_s \exp(i\mathbf{q}_1\,\delta\mathbf{R}_{sr\nu}) \exp(i\mathbf{q}_1,\ \mathbf{R}_s - \mathbf{R}_{r\nu}). \qquad (1)$$

Here $\mathbf{q}_1 = \mathbf{k}_2 - \mathbf{k}_1$ is the difference of the wave vectors of the scattered and incident waves; s numbers the atoms (both those which are at the sites of any sublattice of the ideal crystal, and those belonging to the defects); the summation Σ' goes over atoms which move together with the center of the defect $r\nu$ (if the defect is an added atom, then the sum reduces to a term corresponding to this atom); the summation Σ'' goes over all the other atoms; A_S and b_S are the constants A'_S and b'_S in the expression for the energy of interaction of a neutron with the nucleus s:

$$V_s(\mathbf{r}) = [A'_s + b'_s(sS_s)]\,\delta(\mathbf{r} - \mathbf{R}_s)$$

($\mathbf{s}$ and $\mathbf{S}_S$ are the spins of the neutron and the s-th nucleus), multiplied by the Debye factor e^{-M_s}; $\bar{A}_S$ is the average value (over the isotopes) of the quantity A_S; $\delta\mathbf{R}_{sr\nu}$ is the static displacement of the s-th atom with radius vector $\mathbf{R}_S$, resulting from the influence of the defect at the $\mathbf{r}\nu$ location with radius vector $\mathbf{R}_{r\nu}$; $\delta\mathbf{R}_S = \sum_{r\nu} c_{r\nu}(t)\,\delta\mathbf{R}_{sr\nu}$ is the total displacement of the s-th atom. For small concentrations of defects we may keep in the sum for $\delta\mathbf{R}_S$ just the terms corresponding to the nearest defect. (This point

is explicitly taken into account in the formula for φ_ν.)

The differential cross section (per unit solid angle and per unit energy range) for the scattering of neutrons is (cf., for example, reference 1) expressible in the form

$$\sigma'(\mathbf{q}_1, \omega) = \frac{m^2}{8\pi^3\hbar^5} \int_{-\infty}^{\infty} dt\, e^{-i\omega t} \langle a(t)\, a^*(0)\rangle.$$

Here m is the neutron mass, $\langle \ldots \rangle$ denotes an average over the initial configuration of defects and over the possible types of their diffusion jumps, the bar denotes an averaging over isotopes and over nuclear spins. In the average over isotopes and spins of the product of expressions (1), $a(t)a^*(0)$ is different from zero only for terms of the type

$$[A_s - \bar{A}_s + b_s(\mathrm{sS}_s)]\,[A_{s'} - \bar{A}_{s'} + b_{s'}(\mathrm{sS}_{s'})]$$

with $s = s'$, corresponding to the same atom. As a result of the motion of defects, this atom at various times may be located at different positions (with different $\mathbf{R}_S$). Then for the atoms moving together with the defect [corresponding to Σ' in (1)] the change of $\mathbf{R}_S$ is the same as the change of $\mathbf{R}_{r\nu}$, so that $\mathbf{R}_S - \mathbf{R}_{r\nu}$ does not depend on t. The other atoms [corresponding to Σ'' in (1)] during the motion of the defect (for example, a vacancy) from $r\nu$ to $r'\nu'$ may (in a not completely determined way) move to other sites, which are displaced from the old ones by $\mathbf{R}_S(r\nu r'\nu')$. In the corresponding term in $a(t)a^*(0)$ as a result there appears a factor $\exp[i\mathbf{q}_1 \cdot \mathbf{R}_S(r\nu r'\nu')]$, and in these terms we must take an average $\langle\langle \ldots \rangle\rangle$ over the possible types of such displacements of the atoms s.

In calculating $\langle a(t)a^*(0)\rangle$ we shall also take into account that in this case of small concentration, where we neglect configurations of low probability, we may set

$$\exp\left\{i\mathbf{q}_1 \sum_{r\nu} [c_{r\nu}(t) - c_{r\nu}(0)]\, \delta\mathbf{R}_{sr\nu}\right\} - 1$$
$$= \sum_{r\nu r'\nu'} c_{r\nu}(t)\, c_{r'\nu'}(0)\, [\exp(i\mathbf{q}_1, \delta\mathbf{R}_{sr\nu} - \delta\mathbf{R}_{sr'\nu'}) - 1].$$

Then, substituting (1) in the expression for $\sigma'(\mathbf{q}_1, \omega)$ and subtracting the cross section for scattering by a crystal not containing defects, we find the expression for the change in the scattering cross section $\sigma(\mathbf{q}_1, \omega)$ due to defects:

$$\sigma(\mathbf{q}_1, \omega) = \frac{m^2}{8\pi^3\hbar^5} \frac{k_2}{k_1} \sum_{r\nu r'\nu'} \int_{-\infty}^{\infty} dt e^{-i\omega t} \langle c_{r\nu}(t)\, c_{r'\nu'}(0)\rangle$$
$$\times [F_{\nu\nu'} \exp(i\mathbf{q}_1, \mathbf{R}_{r\nu} - \mathbf{R}_{r'\nu'}) + \Phi_{\nu\nu'}(\mathbf{R}_{r\nu} - \mathbf{R}_{r'\nu'})]. \quad (2)$$

Here

$$F_{\nu\nu'} = \varphi_\nu \varphi^*_{\nu'} + \sum_s{}' \overline{[(A_s - \bar{A}_s)^2} + \overline{B_s^2}] \exp(i\mathbf{q}_1, \delta\mathbf{R}_{sr\nu} - \delta\mathbf{R}_{sr'\nu'}), \quad (3)$$

$$\Phi_{\nu\nu'}(\mathbf{R}_{r\nu} - \mathbf{R}_{r'\nu'}) = \sum_s{}'' \overline{[(A_s - \bar{A}_s)^2}$$
$$+ \overline{B_s^2}]\, [\ll \exp\{i\mathbf{q}_1 \mathbf{R}_s(r\nu r'\nu')\}$$
$$\times \exp(i\mathbf{q}_1, \delta\mathbf{R}_{sr\nu} - \delta\mathbf{R}_{sr'\nu'}) \gg - 1],$$
$$B_s^2 = b_s^2 S_s(S_s + 1)/4. \quad (4)$$

Going over in (2) from the quantities $c_{r\nu}$ to their Fourier components

$$c_{\mathbf{k}\nu}(t) = \frac{1}{N} \sum_r c_{r\nu}(t) \exp(i\mathbf{k}\mathbf{R}_{r\nu}) \quad (5)$$

(where N is the number of unit cells), we obtain the following expression for the differential cross section for inelastic scattering ($\omega \neq 0$):

$$\sigma(\mathbf{q}_1, \omega) = N_g \frac{m^2}{4\pi^2\hbar^5} \frac{k_2}{k_1} \left\{\sum_{\nu\nu'} [F_{\nu\nu'} \exp(2\pi i \mathbf{K}_n \mathbf{R}_{\nu\nu'})\, f_{\nu\nu'}(\mathbf{q}, \omega)\right.$$
$$\left. + \sum_{\mathbf{k}} \Phi_{\nu\nu'\mathbf{k}} f_{\nu\nu'}(\mathbf{k}, \omega)]\right\}. \quad (6)$$

Here

$$f_{\nu\nu'}(\mathbf{q}, \omega) = \frac{N^2}{N_g} \frac{1}{2\pi} \int_{-\infty}^{\infty} \langle c_{\mathbf{q}\nu}(t)\, c^*_{\mathbf{q}\nu'}(0)\rangle\, e^{-i\omega t} dt,$$
$$\Phi_{\nu\nu'}(\mathbf{R}_{r\nu} - \mathbf{R}_{r'\nu'}) = \sum_{\mathbf{k}} \Phi_{\nu\nu'\mathbf{k}} \exp(i\mathbf{k}, \mathbf{R}_{r\nu} - \mathbf{R}_{r'\nu'}), \quad (7)$$

where $\mathbf{q} = \mathbf{q}_1 - 2\pi\mathbf{K}_n$, $\mathbf{K}_n$ is the reciprocal lattice vector which is closest to the vector $\mathbf{q}_1/2\pi$, N_g is the number of defects in the crystal, $\mathbf{R}_{\nu\nu'} = \mathbf{R}_{r\nu} - \mathbf{R}_{r\nu'}$. The summation over $\mathbf{k}$ is taken over the values $\mathbf{k}/2\pi$ lying in a cell of the reciprocal lattice.

Thus the problem of determining the energy distribution of neutrons scattered by defects reduces to finding the time correlation function for the Fourier components $c_{\mathbf{q}\nu}$ and $c_{\mathbf{q}\nu'}$. This transition from the quantities $c_{r\nu}$ to their Fourier components greatly simplifies the computation.

First we consider the simplest case, where the defects are located at positions of just one type and move from one position to another, overcoming potential barriers of the same height. We denote by ρ the vector joining the initial and final position in a diffusion jump, and by w the probability of transition of the defect from a given position to a definite neighboring position. If at the time t one of the quantities $c(\mathbf{R}_r) = c_r$ is equal to unity, then at the time $t + dt$ its average value will be

$$1 - dt \sum_\rho w = 1 - zw\, dt$$

(where z is the number of positions to which the diffusion jump can go), while the quantities

$c(\mathbf{R}_r + \rho)$ take the values wdt. As a result, in this case, the quantity $c_{\mathbf{k}}(t)$ satisfies the differential equation

$$dc_{\mathbf{k}}(t)/dt = -w\sum_{\rho}(1 - e^{i\mathbf{k}\rho})\, c_{\mathbf{k}}(t), \qquad (8)$$

i.e., $\langle c_{\mathbf{k}}(t)\, c^{*}_{\mathbf{k}}(0)\rangle$ depends exponentially on time:

$$\langle c_{\mathbf{k}}(t)\, c^{*}_{\mathbf{k}}(0)\rangle = \langle |c_{\mathbf{k}}(0)|^2\rangle \exp(-\alpha_{\mathbf{k}}|t|),$$
$$\alpha_{\mathbf{k}} = w\sum_{\rho}(1 - \cos \mathbf{k}\rho). \qquad (9)$$

Here we make use of the fact that $\langle c_{\mathbf{k}}(t)\, c^{*}_{\mathbf{k}}(0)\rangle$ is an even function of the time (cf., for example, reference 6, Sec. 117). Formula (9) is applicable for long times, where $t \gg 1/\omega_0$.

Taking into account the fact that for low concentration of randomly distributed defects $\langle |c_{\mathbf{k}}(0)|^2\rangle = N_g/N^2$, we obtain from (7) and (9) the following expression for the function $f(\mathbf{q}, \omega)$ (we omit the subscripts ν and ν' in this case):

$$f(\mathbf{q}, \omega) = \frac{1}{\pi}\frac{\alpha_{\mathbf{q}}}{\alpha^2_{\mathbf{q}} + \omega^2}. \qquad (10)$$

As we see from (10) and (9) for small q the width of the Lorentz curve $f(\mathbf{q}, \omega)$ falls off like q^2. The constant w which determines this width is related in this case to the diffusion coefficient D of defects in cubic crystals by the relation

$$D = \tfrac{1}{2} w\sum_{\rho}\rho_x^2, \qquad (11)$$

i.e., for small q we have $\alpha_{\mathbf{q}} = Dq^2$. In the more general case where the defects, just as in the preceding case, are located only at positions of one type, but can go over from this position to neighboring positions by overcoming potential barriers of various heights, the function $f(\mathbf{q}, \omega)$ can again be calculated from formula (10), but $\alpha_{\mathbf{k}}$ in this formula is now determined not by (9), but by the more general expression $\alpha_{\mathbf{k}} = \sum_{\rho} w_{\rho}(1 - \cos \mathbf{k}\cdot\rho)$, where w_{ρ} is the probability of transition of the defect from the position $\mathbf{R}_r$ to the position $\mathbf{R}_r + \rho$.

We give several examples of the application of the formulas obtained above to defects in cubic crystals of various structures. In all cases we shall assume that during diffusion jumps the defects go to nearest neighbor positions. If the defects are vacancies at the sites of a face-centered cubic lattice, then

$$\alpha_{\mathbf{k}} = 4\frac{D}{a^2}\Big(3 - \cos\frac{k_x a}{2}\cos\frac{k_y a}{2} - \cos\frac{k_x a}{2}\cos\frac{k_z a}{2} - \cos\frac{k_y a}{2}\cos\frac{k_z a}{2}\Big), \qquad (12)$$

where a is the length of a side of the cubic unit cell. This expression is also applicable to injected atoms which are located at the octahedral interstices of this lattice (the centers of the cubes and the midpoints of the edges).

In the case of vacancies at the sites of a body-centered cubic lattice

$$\alpha_{\mathbf{k}} = 8\frac{D}{a^2}\Big(1 - \cos\frac{k_x a}{2}\cos\frac{k_y a}{2}\cos\frac{k_z a}{2}\Big). \qquad (13)$$

For vacancies diffusing through one of the sublattices of a crystal with a lattice of the CsCl type

$$\alpha_{\mathbf{k}} = 2Da^{-2}(3 - \cos k_x a - \cos k_y a - \cos k_z a). \qquad (14)$$

The expression for $\alpha_{\mathbf{k}}$ in the case of vacancies on one of the sublattices of a crystal of the NaCl type is given by formula (12), in which we must replace a by 2a. For atoms which are injected at the centers of the cubic cells of this lattice, formula (14) can be used.

Formulas (12) — (14) and formula (10) for $f(\mathbf{q}, \omega)$ determine the Lorentz-shaped energy distribution of the scattered neutrons corresponding to the first term in (6). As we see from these formulas, for large q the width of this distribution may differ markedly from the width determined by the phenomenological formula $\alpha_{\mathbf{q}} = Dq^2$. For example, for $q_x = q_y = q_z = \pi/a$, formula (13) gives $\alpha_{\mathbf{q}} = 8D/a^2$, instead of the value $\alpha_{\mathbf{q}} = 3\pi^2 D/a^2$ from the phenomenological theory. From (9), and (12) — (14) we also see that the width $\alpha_{\mathbf{q}}$ of the distribution for large q must depend markedly on the orientation of the vector $\mathbf{q}$ relative to the axes of the single crystal. For example, for the vector $q_x a = \sqrt{3}\,\pi$, $q_y = q_z = 0$, which has the same length as the one given in the preceding example, (13) gives $\alpha_{\mathbf{q}} = 15.3\, D/a^2$, i.e., almost twice the value.

The second terms in (2) or (6) are important only for the case of relatively large incoherent scattering cross sections. The triple integral over $\mathbf{k}$ in the second term of formula (6) can be calculated for specific types of defects by using numerical integration. Here in the case of atoms injected into a lattice of Bravais type, the $\Phi_{\nu\nu'\mathbf{k}}$ are proportional to $|\varphi(\mathbf{k})|^2$ where

$$\varphi(\mathbf{k}) = \sum_{s}\exp(i\mathbf{q}_1\delta\mathbf{R}_{sr})\exp(-i\mathbf{k}\mathbf{R}_s).$$

The same factor determines the intensity of diffuse scattering of x rays or neutrons by static defects. Therefore it can be obtained from independent experimental data, or from computations

of such scattering. In the general case, one can find the frequency dependence of the second term in (6) for small ω. To do this we note that for small k, the functions $\Phi_{\mathbf{k}}$ for arbitrary defects in Bravais lattices with n = 1 can be written in the form $\Phi_{\mathbf{k}} = CN^{-1}|\varphi(\mathbf{k})|^2$, where C is the average value (over s) of $(A_S - \bar{A}_S)^2 + B_S^2$. Since, in addition, for small k we have $\varphi(\mathbf{k}) = \mathbf{q}_1 \cdot \mathbf{R}_{\mathbf{k}} = \mathbf{q}_1 \cdot \mathbf{e}_{\mathbf{k}} a_{\mathbf{k}}/k$, where $\mathbf{R}_{\mathbf{k}}$ is the Fourier component of $i\delta\mathbf{R}_S$, $\mathbf{e}_{\mathbf{k}}$ is a unit vector, and $a_{\mathbf{k}}$ for small k depends only on the direction (and not on the magnitude) of the vector $\mathbf{k}$ (cf. reference 7), so for small ω, in the sum in the second term in (6) the region of small k predominates, where $\alpha_{\mathbf{k}} \approx Dk^2$. Thus the integration can be carried out in general form and gives for cubic crystals

$$C \frac{v}{48\pi^3 \sqrt{2}} q_1^2 \int d\Omega a_k^2 \frac{1}{\sqrt{D\omega}}$$

(where v is the volume of a cell, $d\Omega$ is the element of solid angle). Thus if the second term in (6) is important, then for small ω the scattering cross section must increase like $\omega^{-1/2}$ (independent of q).

Now we consider the more general case where the defects may be present at different sites. Then the Fourier components are determined not by (8), but by a system of equations

$$dc_{\mathbf{k}\nu}(t)/dt = -\sum_{\nu'=1}^{n} a_{\nu\nu'}(\mathbf{k}) c_{\mathbf{k}\nu'}(t), \qquad \nu = 1, 2 \ldots n, \quad (15)$$

where the $a_{\nu\nu'}(\mathbf{k})$ are constants. Remembering that at t = 0

$$\langle c^*_{\mathbf{k}\nu}(0) c_{\mathbf{k}\nu'}(0)\rangle = N_{g\nu} N^{-2} \delta_{\nu\nu'} = x_\nu N_g N^{-2} \delta_{\nu\nu'},$$

where $N_{g\nu}$ is the number of defects at the ν positions and x_ν are their relative fractions, we obtain by the usual method (cf. reference 6, Sec. 120) expressions for the functions $f_{\nu\nu'}(\mathbf{q}, \omega)$ defined by formula (7),

$$f_{\nu\nu'}(\mathbf{q}, \omega) = \frac{1}{\pi} \mathrm{Re}\left(\frac{a(\mathbf{q})}{x} + \frac{i\omega}{x}\right)^{-1}_{\nu\nu'} = \sum_{i=1}^{n} \frac{A_i(\mathbf{q})}{\alpha_{\mathbf{q}i}^2 + \omega^2}, \quad (16)$$

where $a(\mathbf{q})/x$ is a matrix with matrix elements $a_{\nu\nu'}(\mathbf{q})/x_\nu$, and the matrix $1/x$ has matrix elements $\delta_{\nu\nu'}/x_\nu$. This last expression is obtained from the preceding by an expansion in elementary fractions. Here the "reciprocal relaxation times" $\alpha_{\mathbf{q}i}$ are determined by the roots y_i of the equation

$$|a_{\nu\nu'} - \delta_{\nu\nu'} y| = 0. \quad (17)$$

In each specific case it is not difficult to carry out the inversion of the matrix $a(\mathbf{q})/x + i\omega/x$ and to find $f_{\nu\nu'}(\mathbf{q}, \omega)$.

As an example we consider the case of atoms injected at the octahedral interstices of a body-centered cubic lattice (the centers of the faces and edges of cubic cells). In this case there are three types of interstices, which have two nearest-neighbor atoms located respectively along the x, y, and z axes. If the injected atoms carry out diffusion jumps to their nearest-neighbor interstices with probability w, then the system of differential equations (15) takes the form

$$dc_{\mathbf{k}\nu}(t)/dt = -4wc_{\mathbf{k}\nu}(t) + \sum_{\nu''=1(\nu''\neq\nu)}^{3} C_{\nu''} c_{\mathbf{k}\nu'}(t). \quad (18)$$

Here $\nu'' \neq \nu$ and $\nu'' \neq \nu'$, $C_{\nu''} = 2w \cos \mathbf{k} \cdot \boldsymbol{\rho}_{\nu''}$, where, for example, the vector $\boldsymbol{\rho}_1 = \frac{1}{2}a\mathbf{e}_x$ joins interstices of the second and third types.

Since all the positions are energetically equivalent, $x_\nu = 1/3$. Equation (17), which determines the quantities $\alpha_{\mathbf{q}i}$ in (16), is a cubic equation in this case:

$$D(y) = (y - 4w)^3 - (y - 4w)(C_1^2 + C_2^2 + C_3^2) + 2C_1C_2C_3 = 0. \quad (19)$$

The quantities $f_{\nu\nu'}(\mathbf{q}, \omega)$ are equal in this case [as one finds from (15), (16), and (18)] to

$$f_{11}(\mathbf{q}, \omega) = \frac{1}{3\pi} \mathrm{Re} \frac{(4w + i\omega)^2 - C_1^2}{-D(-i\omega)} = \frac{2}{9\pi} \frac{6w}{36w^2 + \omega^2} + \frac{2}{3\pi} \frac{wa^2q^2}{w^2a^4q^4 + 36\omega^2},$$

$$f_{12}(\mathbf{q}, \omega) = \frac{1}{3\pi} \mathrm{Re} \frac{(4w + i\omega)C_3 + C_1C_2}{-D(-i\omega)} = -\frac{1}{9\pi} \frac{6w}{36w^2 + \omega^2} + \frac{2}{3\pi} \frac{wa^2q^2}{w^2a^4q^4 + 36\omega^2}. \quad (20)$$

The second equalities in (20) are written for small q. The quantity w is related to the coefficient of diffusion of the injected atoms by the relation $w = 6D/a^2$.

As another example, we consider vacancies at the sites of an ordered solid solution of the type of β brass (with a lattice of the CsCl type). Suppose that a diffusion jump takes a vacancy from a site of one sublattice to one of the neighboring sites of the other sublattice [the case of the diffusion of vacancies over sites of a single sublattice is described by formulas (10) — (14)]. We shall denote by $w_1/8$ the probability of transition of a vacancy from a site of the first type to sites of the second type, and by $w_2/8$ the probability of the reverse transition. Then the time behavior of $c_{\mathbf{k}1}(t)$ and $c_{\mathbf{k}2}(t)$ is described by (15), in which

$$a_{11} = w_1, \qquad a_{12} = -w_2 C, \qquad a_{21} = -w_1 C, \qquad a_{22} = w_2,$$
$$C = \frac{1}{8} \sum_{\rho} \cos \mathbf{k}\rho, \qquad \rho = \frac{a}{2}(\pm \mathbf{e}_x \pm \mathbf{e}_y \pm \mathbf{e}_z).$$

Noting that

$$x_1 = w_2/(w_1 + w_2), \quad x_2 = w_1/(w_1 + w_2),$$

we obtain from (16)

$$f_{11}(\mathbf{q}, \omega) = \frac{1}{\pi} \frac{w_2}{w_1 + w_2} \operatorname{Re} \frac{w_2 + i\omega}{(w_1 + i\omega)(w_2 + i\omega) - w_1 w_2 C^2}$$

$$\underset{q \to 0}{=} \frac{4}{\pi} \frac{w}{w_1 + w_2} \operatorname{Re} \left[\frac{1}{w_1 + w_2 + i\omega} + \frac{w_2 / w_1}{w a^2 q^2 + i\omega} \right],$$

$$f_{12}(\mathbf{q}, \omega) = \frac{4wC}{\pi} \operatorname{Re} \frac{1}{(w_1 + i\omega)(w_2 + i\omega) - w_1 w^2 C^2}$$

$$\underset{q \to 0}{=} \frac{4}{\pi} \frac{w}{w_1 + w_2} \operatorname{Re} \left[-\frac{1}{w_1 + w_2 + i\omega} + \frac{1}{w a^2 q^2 + i\omega} \right],$$

$$w = \frac{1}{4} \frac{w_1 w_2}{w_1 + w_2}. \tag{21}$$

The energy distribution of the scattered neutrons which we have found takes a simpler form for the case where the coefficients $\Phi_{\nu\nu'\mathbf{k}}$ in formula (6) are equal to zero (for example, if the lattice contains only nuclei of one isotope with zero spin, or if we can neglect imperfections). As follows from (16), the energy distribution is then described by a superposition of Lorentz curves. In the two cases considered above, where there are two nonequivalent positions for defects, for small q the function $f(\mathbf{q}, \omega)$ is a sum of two Lorentz functions. One of them is described by a curve with a width proportional to q^2 and the coefficient of diffusion of the defects and coincides with the curve obtained from a macroscopic treatment. The width of the curve corresponding to the second function tends to a nonzero limit for $q \to 0$.

If all the quantities

$$F'_{\nu\nu'} = F_{\nu\nu'} \exp(2\pi i \mathbf{K}_n \mathbf{R}_{\nu\nu'})$$

are the same, then these second terms in the sum (6) cancel, and the energy distribution, just as for the case of defects of only one type, is described by a narrow Lorentz curve. In the general case, however, in this sum, in addition to the term corresponding to the narrow curve for small q, there must also be a term corresponding to the broad Lorentz curve and proportional to the differences of the quantities $F'_{\nu\nu'}$. Obviously the appearance of the broad component in the energy distribution cannot be obtained by means of the macroscopic theory which does not take into account the diffusion mechanism.

It is not difficult to show that the broad curve in the energy distribution, in addition to the narrow curve for small q, should be observed in all cases where the defects can go from positions of one type to positions of another type, where the different quantities $F'_{\nu\nu'}$ are not the same. In addition to the examples given above, the defects may also make such transitions between positions of different types in the case of injected atoms at tetrahedral or dodecahedral interstices of body-centered cubic lattices, in the case of atoms of vacancies injected into ordered alloys of different structures, in the case of a pair of vacancies, a pair of injected atoms, or an impurity atom-vacancy pair (where differently oriented pairs may be regarded as defects of different types) etc.

From the results obtained it follows that for each mechanism of diffusion of defects of a given type there should be a characteristic dependence of the width and shape of the energy distribution of scattered neutrons on the magnitude and orientation of the vector $\mathbf{q}$. If the type of defects giving rise to the scattering is known, this makes it possible in principle to make a choice between the various possible mechanisms of diffusion of defects, by comparing the dependence on $\mathbf{q}$ of the width, as calculated for these mechanisms, with the result of experiment. Thus one can, for example, study whether the diffuse jumps of the injected atoms and vacancies to nearest positions occurs as assumed in deriving the formulas given above, or to more remote locations; whether the diffusion in a given crystal occurs by means of vacancies or interstitial atoms. A comparison of calculated and measured energy distributions also makes it possible in principle to choose between various assumptions concerning the type of defects giving rise to the scattering. Thus, for example, the energy distribution, as shown above, is found to be qualitatively different (for small q) for vacancies and for injected atoms in body-centered cubic lattices, for atoms injected at octahedral and tetrahedral holes in face-centered cubic lattices, for isolated vacancies, for pairs of vacancies, etc.

If the coefficients $\Phi_{\nu\nu'\mathbf{k}}$ in formula (6) are different from zero, the analysis of the energy distribution is made more complicated (where for small q the width of the energy distribution of the second sum in (6) always tends to a nonzero value), but can also be carried out in each specific case.

To estimate the order of magnitude of the broadening of the energy distributions, let us consider the case where $D \sim 3 \times 10^{-5}$ cm^2/sec (diffusion of vacancies and injected atoms at temperatures close to the melting point; in the case of diffusion of H atoms, D may be 10 — 100 times greater). Setting $a^2 \sim 10^{-15}$ cm^2, we find

that formulas (12), (13), and (20) in this case give a maximum value of the width of the distribution of the order of $(3-6)\times 10^{-4}$ ev. Such a broadening can be detected experimentally. Obviously the difficulty in experimental investigation, aside from the need for obtaining a high resolution in the energy distribution, is related to the presence of an intense elastic scattering resulting from isotopes and spins of nuclei in the crystal, and also the presence of inelastic scattering by thermal vibrations which is especially intense in the case we are considering of high temperature.

The separating out of the scattering by defects from the total cross section for scattering is made easier by the fact that the energy distribution of the isotopic scattering for monochromatic incident neutrons is extremely narrow (its width is proportional to the self-diffusion coefficient which is much smaller than the coefficient of diffusion of the defects), while the energy distribution of the scattering by vibrations, on the other hand, is much broader than the distribution of scattering by defects. Obviously the defect concentration must be sufficiently high. It appears that with present-day technique of experiment the smearing of the energy distribution of neutrons scattered by injected atoms can be studied, for example, in Pd-H solutions. To study the scattering by vacancies, it may be convenient to use substitutional solutions (for example, Co-Al, Ni-Al), where the concentration of "structural" vacancies is high, or to introduce into the crystal impurities to increase the concentration of vacancies.

3. INFLUENCE OF DIFFUSION ON SCATTERING OF PHOTONS BY CRYSTAL DEFECTS

The diffusion of defects may lead to a similar broadening of the energy distribution of the elastic scattering of monochromatic photons (x rays or γ quanta) as for the case of neutron scattering. Just as before, let us consider the case where $W \ll \omega_0$ and $\omega \lesssim W$ and disregard the scattering by thermal vibrations. Then, in electron units, the intensity of the diffuse scattering of monochromatic photons by defects $I(\mathbf{q}_1, \omega)$, per unit solid angle and per unit frequency range, is given by a formula analogous to formula (6):

$$I(\mathbf{q}_1, \omega) = N_g \sum_{\nu\nu'} \varphi_\nu^* \varphi_{\nu'} \exp(2\pi i \mathbf{K}_n \mathbf{R}_{\nu\nu'}) f_{\nu\nu'}(\mathbf{q}, \omega). \qquad (22)$$

Here φ_ν is given by formula (1), if we make the substitution $\bar{A}_s \to f_s$, where f_s is the atomic scattering factor of the s-th atom multiplied by the Debye attenuation factor e^{-M_s}. The functions $f_{\nu\nu'}(\mathbf{q}, \omega)$ in (22) are again determined by formulas (7), (10), and (16) (where it is obvious that in the case of scattering of photons $\Phi_{\nu\nu'\mathbf{k}} = 0$).

Thus the investigation of the function $f(\mathbf{q}, \omega)$ which we carried out above for various specific cases is also applicable for the treatment of scattering of photons. In this case the energy distribution is obtained more simply because of the fact that $\Phi_{\nu\nu'\mathbf{k}} = 0$. As shown above, the magnitude of the broadening associated with diffusion of defects is less than or of the order of 10^{-3} ev. Therefore, as already pointed out in Sec. 1, this broadening cannot be observed if one uses ordinary x rays. However, by using the Mössbauer effect one can obtain photons with a very narrow energy distribution, and investigate their scattering by defects of another crystal which is used as a resonance absorption detector. Here the width of the energy distribution may be very small. For example, for Fe^{57} it amounts to approximately 6×10^{-9} ev. As a result, one can detect and study much smaller broadenings than by using neutrons. Even at low temperatures, where the diffusion coefficient of the defects considered above is $D \sim 10^{-9}$ cm^2/sec, the diffusion will give rise to a broadening $\sim 10^{-8}$ ev, which is comparable with the natural width.

If the broadening as a result of diffusion is of the same order as the natural width, then one must take into account the non-monochromatic nature of the incident radiation. Since in the case of monochromatic radiation the energy distribution of the scattered photons is described by a sum of Lorentz functions (16), for the case where the shape of the spectral line of the incident radiation is Lorentzian, the distribution of the scattered radiation will also be described by a sum of Lorentz functions with widths of the corresponding curves, each of which is equal to the sum of $\alpha_{\mathbf{q}i}$ and the width of the line of the incident radiation.

In the same way as for neutron scattering, the study of the dependence of the width of the energy distribution of scattered photons as a function of $\mathbf{q}$ enables one to investigate the mechanism of diffusion and to establish the nature of the defects (cf. Sec. 2). In the case of scattering of photons the analysis of the distribution is somewhat simpler, since $\Phi_{\nu\nu'\mathbf{k}} = 0$. Because of the higher resolution, the separation of the scattering into that by defects and that by vibrations also can be carried out more precisely than for the case of neutrons.

Formula (22) is also applicable to the case of scattering of light waves, but the expressions for the constants φ_ν are then changed (φ_ν will be

$\sim\lambda^2$, where λ is the wavelength). If the defects are located at positions of just one type, the width of the energy distribution is $Dq^2 = 16\pi^2 D\lambda^{-2}\sin^2\theta$, and even for the very highest values of D is several orders of magnitude smaller than the width of the spectral distribution of the incident radiation. If, however, the defect can undergo diffusion jumps between positions of different types, and the values of φ_ν for different ν are different, then there will be a term in the expression for $I(\mathbf{q}, \omega)$ whose graph is a Lorentz curve with a large width independent of λ. For example, in the case of scattering of light by injected atoms in a body-centered cubic lattice, according to (22) and (20), for $D > 10^{-7}$ cm^2/sec, this width is greater than 2×10^{-6} ev, i.e., it may be of the order of (or greater than) the width of the spectral distribution of the incident radiation. The intensity of the broad spectral curve in the scattered spectrum should depend in a characteristically strong way on the polarization of the light, but we shall not consider this question here.

4. INFLUENCE OF DIFFUSION ON THE MÖSSBAUER EFFECT

The diffuse motion of the atoms may not only lead to a broadening of the spectrum of elastic scattering, but also to a broadening of the absorption and emission spectra. This effect should be observed in the spectra of resonant absorption and emission of photons by nuclei in a crystal which is at high temperature. The intensity of such a recoilless emission of photons is proportional to the Debye attenuation factor e^{-M_S} for $\mathbf{q}_1$ equal to the wave vector of the emitted wave. In various cases where relatively soft photons are emitted, this factor is not very small even at high temperatures, which enables one to investigate the Mössbauer effect at such temperatures. For example, for Fe^{57} (with a photon energy of 14.4 kev) at $T = 2000°$ K, $M_S = 1.4$ if the Debye temperature is equal to 430° K.

Let us first consider the spectral distribution of the emitted (or absorbed) photons for the case where the natural width $\Gamma = 0$ and the emitting nuclei are located at sites of one sublattice. We shall denote by ω the difference between this frequency and the frequency of the radiation emitted in the absence of diffusion. Since we are considering recoilless radiation, we shall limit ourselves to the range of values $\omega \lesssim W$, where W is the probability of a diffusion jump of an atom. The expression for the spectral distribution of the photons emitted without recoil when we include diffusion of the atoms over sites of their own sublattice is not hard to obtain by using the adiabatic approximation and noting that the inter-nuclear motion is incomparably faster than the motion of the center of gravity of the nucleus. Denoting by $\sigma_p(\mathbf{q}_1)$ the integral cross section (over energy) of the resonance absorption of photons with wave vector $\mathbf{q}_1$ (and a given polarization) by a single nucleus, by N_p the total number of absorbing nuclei at the sites of the given sublattice, and by N the number of sites of the sublattice ($N_p \ll N$), we write the expression for the differential cross section of absorption $\sigma_p(\mathbf{q}_1, \omega)$ (per unit solid angle and per unit frequency range) in the form

$$\sigma_p(\mathbf{q}_1, \omega) = \frac{N^2}{2\pi}\sigma_p(\mathbf{q}_1)\int_{-\infty}^{\infty} dt\, e^{-i\omega t}\langle c_{\mathbf{q}}(t)\, c_{\mathbf{q}}^*(0)\rangle$$

$$= N_p\sigma_p(\mathbf{q}_1) f(\mathbf{q}, \omega). \qquad (23)$$

Here $c_{\mathbf{q}}$ is determined by formula (5), in which $c_{r\nu}$ now refers not to defects, but to nuclei of the absorbing isotope on the ν-th sublattice.

In order to obtain the differential equation describing the time behavior of $c_{\mathbf{q}}(t)$ for the vacancy mechanism of diffusion, we shall choose a "physically infinitesimal" time interval dt, which is much smaller than the interval between two diffusion jumps of an atom and much greater than the interval between two diffusion jumps of a vacancy. Because of the fact that for the vacancy mechanism there is a correlation between successive diffusion jumps of the atoms,[8] there exists a finite probability of transition of an atom during this infinitesimal time interval not only to the neighboring atoms, but also to more remote sites. Therefore our equation has the form

$$\frac{dc_{\mathbf{k}}(t)}{dt} = -\alpha_{\mathbf{k}} c_{\mathbf{k}}(t),$$

$$\alpha_{\mathbf{k}} = w_1\sum_{\rho_1}^{(1)}(1-\cos\mathbf{k}\rho_1) + w_2\sum_{\rho_2}^{(2)}(1-\cos\mathbf{k}\rho_2)$$

$$+ \ldots \approx \frac{D_S}{a^2}\sum_{\rho_1}^{(1)}(1-\cos\mathbf{k}\rho_1). \qquad (24)$$

Here the summations are extended over sites of the first, second, etc. coordination spheres, w_i is the probability of transition to a particular site of the i-th sphere. The approximate equation is written for cases of simple, body-centered, and face-centered cubic lattices. In deriving it, we use the fact that the self-diffusion coefficient D_S is equal to

$$D_S = \frac{1}{2}\sum_i w_i\sum_{\rho_i}\rho_{ix}^2$$

and that $w_2 \sim w_1/z^2 \sim 10^{-2}w_1$, so that with a slight

error we need keep only the first term in the sum over i.

From (23) and (24) it follows that for $\Gamma = 0$ the spectral distribution is described by the Lorentz function

$$\sigma_p(\mathbf{q}_1, \omega) = N_p \sigma_p(q_1)\, \pi^{-1} \alpha_q / (\alpha_q^2 + \omega^2). \qquad (25)$$

For $\Gamma \neq 0$ there is also a Lorentz distribution, but its width is equal to $\alpha_q + \Gamma$.*

From (24), (25), and (12) — (14) it follows that the broadening of the spectral distribution resulting from diffusion at high temperatures may be appreciable. For example, assuming that near the melting point $D_S = 10^{-8}$ cm^2/sec and that $a^2 = 10^{-15}$ cm^2, we find that for a body-centered cubic lattice for $q_x = q_y = q_z = \pi/a$, the broadening is equal to 10^{-7} ev, i.e., much larger than the width Γ for Fe^{57}. This broadening should depend exponentially on temperature and be strongly dependent on the direction of the vector $\mathbf{q}_1$. It is obvious that the investigation of such a dependence would enable one to establish whether the self-diffusion occurs via a vacancy mechanism or by diffusion jumps to neighboring lattice sites, as was assumed in deriving the formulas given above, or by some other mechanism, (for example, by means of diffusion over interstices).†

In various cases the resonance radiation may be emitted by nuclei which, because of the energy transfer in the preceding radioactive decay, have been ejected from lattice sites and are located in interstices. Then the broadening will be determined by the diffusion coefficient of interstitials, which is several orders of magnitude greater than the self-diffusion coefficient. A significantly larger broadening should therefore occur when the radiating atoms are close to grain boundaries (in a sample consisting of very tiny crystals prepared by diffusion methods at low temperatures) because of the large value of the coefficient of grain boundary diffusion. Apparently a larger broadening than for ordinary crystals should be observed in substitutional alloys. Finally, a large broadening (although much smaller than for gases) should be observed in the case of liquids.

In the absorption and emission of light by crystal defects which can undergo diffusion jumps between non-equivalent positions, there can also occur a diffusion broadening of the spectral curves (cf. Sec. 3). This effect may be appreciable, however, only if the electron-phonon interaction is sufficiently small (so that one can separate a line of a purely electronic transition) and the probability of thermal radiationless transitions from the excited state is small at these high temperatures.

Note added in proof (May 16, 1961): After this paper was sent to press, papers appeared which also consider the influence of diffusion on the Mössbauer effect in solids[9] and in liquids,[10] which obtain results overlapping the results of Sec. 4 of this paper. By using a quasi-classical model, the influence of diffusion on the scattering of neutrons by a liquid has also been treated[11] recently.

*It is not difficult to see that in a more detailed calculation, which does not use the concept of a "physically infinitesimal" time interval, in the expression for $\sigma_p(\mathbf{q}_1, \omega)$ there is an additional small term corresponding to a broad spectral distribution with a width greater than α_q by the factor D_S/D_V (where D_V is the coefficient of diffusion of the vacancies). The ratio of this term to the term considered in (25) is of the order of N_V/N, where N_V is the number of vacancies.

†The height of the potential barrier for the transition of an atom from a site to an interstitial position is usually much greater than the barrier height for transition from one interstitial position to another. Therefore if the diffusion occurs via a mechanism in which atoms move through interstices, then α_{qi} does not depend on $\mathbf{q}$ and is equal to the probability of transition of an atom from a site to an interstitial position. The temperature dependence of α_{qi} is then different from the temperature dependence of D_S.

[1] L. Van Hove, Phys. Rev. **95**, 249 (1954).
[2] G. H. Vineyard, Phys. Rev. **110**, 999 (1958).
[3] P. Schofield, Phys. Rev. Letters **4**, 239 (1960).
[4] R. L. Mössbauer, Z. Physik **151**, 124 (1958); Naturwissenschaften **45**, 538 (1958); Z. Naturforsch. **14a**, 211 (1959).
[5] G. N. Belozerskii and Yu. A. Nemilov, Usp. Fiz. Nauk **72**, 433 (1960), Soviet Phys.-Uspekhi **3**, 813 (1961).
[6] L. Landau and E. Lifshitz, Statistical Physics, Pergamon Press, 1958.
[7] M. A. Krivoglaz, JETP **34**, 204 (1958), Soviet Phys. JETP **7**, 139 (1958).
[8] J. Bardeen and C. Herring, Imperfections in Nearly Perfect Crystals, J. Wiley and Sons, New York, 1952. K. Compaan and Y. Haven, Trans. Faraday Soc. **52**, 786 (1956).
[9] K. S. Singwi and A. Sjölander, Phys. Rev. **120**, 1093 (1960).
[10] M. I. Podgoretskii and A. V. Stepanov, JETP **40**, 561 (1961), Soviet Phys. JETP **13**, 393 (1961).
[11] C. T. Chudley and R. J. Elliot, Proc. Phys. Soc. (London) **77**, 353 (1961).

Translated by M. Hamermesh
306

BEHAVIOR OF MULTIPLY CHARGED IONS IN A PLASMA

A. V. GUREVICH

P. N. Lebedev Physics Institute, Academy of Sciences, U.S.S.R.

Submitted to JETP editor January 11, 1961

J. Exptl. Theoret. Phys. (U.S.S.R.) **40**, 1825-1831 (June, 1961)

It is shown that under certain conditions the direction of motion of multiply charged ions in a singly ionized plasma in a fixed electric field must be opposite to that of the singly charged ions. Under these conditions the velocity of the multiply charged ions can be of approximately the same magnitude as the directed electron velocity while their energy can be one to three orders of magnitude greater than the thermal energy of the singly charged ions and the electrons.

1. We consider an ion of charge Ze in a fully ionized plasma, consisting of electrons and singly charged ions, in a fixed electric field. The motion of the ions is obviously described by the equation

$$M d\mathbf{v}/dt = eZ\mathbf{E} - \mathbf{F}_e - \mathbf{F}_i. \quad (1)$$

Here, M is the ion mass, $\mathbf{v}$ is the ion velocity, $\mathbf{F}_e + \mathbf{F}_i$ is the friction force which arises by virtue of the interaction with the plasma electrons ($\mathbf{F}_e$) and ions ($\mathbf{F}_i$).

Because of the reciprocal nature of the interaction between the electrons and the ions, $\mathbf{F}_e$ can be written in the form

$$\mathbf{F}_e = m\nu_{ei}(N_e/N_Z)(\mathbf{v} - \mathbf{v}_{e0})$$

(cf. reference 1, Sec. 63). Here, m is the mass, N_e is the number density, $\mathbf{v}_{e0}$ is the mean directed velocity of the electrons, N_Z is the number density of ions with charge Ze, and ν_{ei} is the frequency of collisions between the electrons and these ions. Hereinafter it is convenient to consider Eq. (1) in a coordinate system that moves with the singly charged ions. The expression for $\mathbf{F}_e$ can then be written in the form

$$\mathbf{F}_e = m\nu_{e0}Z^2(\mathbf{v} - \mathbf{v}_0), \quad (2)$$

where $\mathbf{v}_0 = \mathbf{v}_{e0} - \mathbf{v}_{i0}$ is the difference between the mean directed velocities of the electrons and the singly charged ions, while ν_{e0} is the effective collision frequency for collisions between electrons and singly charged ions in the fixed electric field:

$$\nu_{e0} = \tfrac{4}{3}\sqrt{2\pi}e^4 N m^{-1/2}(kT_e)^{-3/2}\ln\Lambda, \quad (3)$$

Here, $N = N_e = N_i$ is the number density for the electrons or single charged ions in the plasma, T_e is the electron temperature, k is the Boltzmann constant and $\ln\Lambda$ is the Coulomb logarithm.

Since $\mathbf{v}_0 = e\mathbf{E}/m\nu_{e0}$, the expression for $\mathbf{F}_e$, Eq. (2), can be written

$$\mathbf{F}_e = eZ^2\mathbf{E} + m\nu_{e0}Z^2\mathbf{v}. \quad (2a)$$

We note that this expression applies only when

$$|\mathbf{v} - \mathbf{v}_0| \ll v_{Te}, \quad (2b)$$

where v_{Te} is the thermal velocity of the electrons. In other words, the essential requirement is that the mean directed velocity of the electrons must be smaller than their thermal velocity. Dreicer[2] (cf. also reference 3) has shown that this requirement is satisfied only when $E \ll E_c = 4\pi e^3 N \ln\Lambda/kT_e$. For the effects considered in the present paper, we shall be interested in relatively weak fields in which this condition is obviously satisfied [cf. Eqs. (5) and (10)].* Furthermore, it follows from Eq. (2b) that the velocity of the multiply charged ion must be smaller than the thermal velocity of the electrons, a condition which we naturally assume to be satisfied.

However, the analagous condition for the interaction with the plasma ions, $v < v_{Ti}$, cannot be satisfied. When $v > v_{Ti}$ the collision frequency goes as v^{-3} while the frictional force goes as v^{-2}. When this circumstance is taken into account the force $\mathbf{F}_i$ is given by the approximate expression:

$$\mathbf{F}_i = m\nu_{e0}Z^2\gamma\mathbf{v}/[1 + (v/v_{Ti})^3],$$

$$\gamma = (M_0 T_e^3/mT_{i0}^3)^{1/2}. \quad (4)$$

*We note that because of this condition, Eq. (2a), which gives the friction force, does not apply if the plasma density approaches zero (for a fixed value of E). Consequently, the features of the behavior of multiply charged ions noted below do not appear in this case; these ions then move in the direction of the field, as expected.

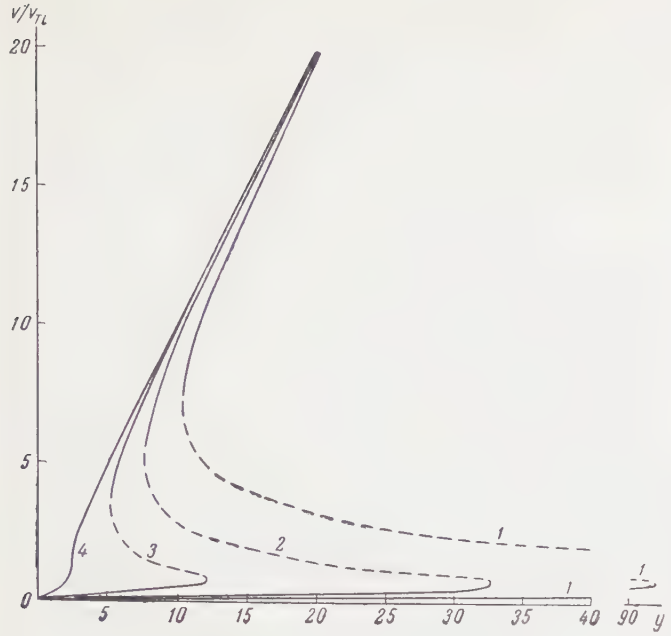

FIG. 1. The dependence of v/v_{Ti} on $y = e(Z-1) \times E/Zm\nu_{e0}v_{Ti} = (Z-1)v_0/Zv_{Ti}$ for different values of $\gamma = (M_0T_e^3/mT_{i0}^3)^{1/2}$; $\gamma = 172$, 60.8, 21.5, and 3 for curves 1, 2, 3, and 4, respectively.

Here, M_0, T_{i0} and v_{Ti} are respectively the mass, temperature, and thermal velocity of the plasma ions. The parameter γ is determined by the properties of the plasma in which the multiply charged ion is located. The value of γ is usually very large; for example, if $T_{i0} = T_e$, then in deuterium $\gamma \approx 60.8$ and in hydrogen $\gamma \approx 43$.

Equation (1) is now written in the form

$$M\mathrm{d}v/dt = -eZ(Z-1)\mathbf{E} - mv_{e0}Z^2\mathbf{v}[1 + \gamma/(1 + v/v_{Ti})^3)]. \quad (1a)$$

What is most obvious from the above is that a multiply charged ion moving with the singly charged ions in the plasma ($\mathbf{v} = 0$) is always acted on by a force in the direction of motion of the electrons. The origin of this force is easily understood if we consider that the force $e\mathbf{E}$ which the field exerts on the plasma ions (i.e., the singly charged ions) is exactly balanced by the friction caused by the interaction of these ions with the traveling electron stream. If a multiply charged ion is placed in this plasma, the force exerted on it by the field is larger by a factor of Z, while the friction force is larger by a factor of Z^2, so that the multiply charged ions are carried along by the electron stream.

Solving Eq. (1a) we can find the velocity of the multiply charged ion. The dependence of this velocity v on electric field, as determined from this equation for stationary conditions ($dv/dt = 0$), is shown in Fig. 1. It is obvious from the figure that in general the relation between v and E is not unique; in the region

$$3\gamma^{1/3}mv_{e0}v_{Ti}Z/2^{2/3}e(Z-1) \leqslant E \leqslant 2^{2/3}\gamma mv_{e0}v_{Ti}Z/3e(Z-1) \quad (5)$$

a given value of field corresponds to two stable stationary values of the velocity rather than one, as is usually the case (the third stationary value of the velocity, shown in Fig. 1 by the dashed line, is unstable).

In the first stationary state, which corresponds to the lower curve, the velocity of the multiply charged ions is small: $v_1 \approx v_0(Z-1)/\gamma Z$. In this case the interaction with the plasma ions (the force $\mathbf{F}_i$) is decisive. On the other hand, in the second stationary state, corresponding to the upper curve, the velocity of the multiply charged ion is very large: $v_2 \approx v_0(Z-1)/Z$. Under these conditions the interaction with the plasma electrons assumes the dominant role because the ion interaction becomes unimportant at high velocities ($v \gg v_{Ti}$). The energy of the multiply charged ion is always large in the second stationary state:

$$\varepsilon_2 = \frac{Mv_2^2}{2} = \frac{M}{M_0}\left(\frac{v_0}{v_{Ti}}\right)^2\left(\frac{Z-1}{Z}\right)^2 kT_{i0}.$$

This energy is many times (one to three orders of magnitude) greater than the thermal energy of the electrons or ions in the plasma. The characteristic time τ required for the ion to acquire an energy ϵ_2 is of order $M/m\nu_{e0}Z^2$.

As γ decreases the difference between the curves corresponding to the first and second states become smaller (cf. Fig. 1). These curves finally coalesce when $\gamma \leq 3$ [i.e., $T_e/T_{i0} \leq 2.1 \times (m/M_0)^{1/3}$] and in this case a given energy E corresponds to one stationary value of the velocity v.

With respect to a fixed observer (not with respect to a singly charged ion, as considered above) the velocity of the multiply charged ion is obviously $\mathbf{v} + \mathbf{v}_{i0}$, where $\mathbf{v}_{i0}$ is the mean velocity of the singly charged ions. Since the velocity $\mathbf{v}$ is always in the direction of motion of the electrons while the velocity $\mathbf{v}_{i0}$ is in the opposite direction, the multiply charged ion can move in either direction, depending on the ratio of the velocities v and v_{i0}. In particular, in a fully ionized equilibrium plasma (laminar) the velocity $\mathbf{v}_{i0}$ is very small (its magnitude is limited by the conservation of total momentum for the electrons and singly charged ions $v_{i0} = mv_{e0}/M_0$) so that v is almost always larger than v_{i0} (for $\gamma < M_0/m$). Thus, in an equilibrium plasma the multiply charged ion almost always moves in the same direction as the electrons. Under actual conditions, however,

the directed velocity of the singly charged ions can be appreciably greater;[4] in any case, it can be greater than the first stationary velocity of the multiply charged ions.* On the other hand, the second stationary velocity is always greater than v_{i0}.

Thus, the elementary analysis given above indicates that two substantially different stationary states of multiply charged ions in a plasma can occur at a single value of the field. However, this analysis does not tell us which of these states is actually realized. Since any velocity is possible, by virtue of the existing particle velocity distribution, any of the ions will, in general, always be in one state (i.e., the velocities of these ions will be grouped about one of the stationary values) while the other ions will be in the other. Transfer of ions between states is also possible. How many ions will be in each of the states at total equilibrium? These questions can be answered only when the velocity distribution of the multiply charged ions is analyzed.

2. In a fully ionized plasma the kinetic equation for the velocity distribution $f(\mathbf{v}, t)$ of ions with charge Ze is of the form

$$\frac{\partial f}{\partial t} - \frac{eZ(Z-1)E}{M}\left(\cos\theta\frac{\partial f}{\partial v} - \frac{\sin\theta}{v}\frac{\partial f}{\partial\theta}\right) - \frac{1}{v^2}\frac{\partial}{\partial v}\left\{v^2\left[\frac{M}{M_0}\nu_i(v)\, G\left(\frac{v}{(2kT_{i0}/M_0)^{1/2}}\right)\left(\frac{kT_{i0}}{M}\frac{\partial f}{\partial v} + vf\right)\right.\right.$$
$$\left.\left. + \frac{m}{M}\nu_{e0}Z^2\left(\frac{kT_e}{M}\frac{\partial f}{\partial v} + vf\right)\right]\right\} - \frac{\nu_i(v)}{2\sin\theta}H\left(\frac{v}{(2kT_{i0}/M_0)^{1/2}}\right)\frac{\partial}{\partial\theta}\left(\sin\theta\frac{\partial f}{\partial\theta}\right) = 0. \quad (6)$$

Here, θ is the angle between $\mathbf{E}$ and $\mathbf{v}$, $\nu_i(v) = 4\pi e^4 NZ^2 \ln\Lambda/M^2v^3$ is the collision frequency for collisions between multiply charged ions and singly charged ions, and $G(x)$ and $H(x)$ are the functions introduced by Chandrasekhar:[5]

$$G(x) = \Phi(x) - 2xe^{-x^2}/\sqrt{\pi},$$
$$H(x) = (1 - \tfrac{1}{2}x^{-2})\,\Phi(x) + e^{-x^2}/\sqrt{\pi}x,$$

where $\Phi(x)$ is the probability integral. When $x \gg 1$ the functions $G(x)$ and $H(x)$ are close to unity; when $x \ll 1$ we have

$$G(x) = 4x^3/3\sqrt{\pi},\quad H(x) = 4x/3\sqrt{\pi}.$$

It is obvious from Eq. (6) that the multiply charged ions, which move with singly charged plasma ions, are subject to a force $\mathbf{F} = -eZ\times(Z-1)\mathbf{E}$ in the direction of motion of the electrons.*

For low velocities $v \lesssim (kT_{i0}/M)^{1/2}$ it is natural to seek a solution of (6), as usual, (cf. reference 7) in the form

$$f = f_0(v) + f_1(v)\cos\theta + \chi(v,\theta), \qquad \chi \ll f_0. \quad (7)$$

The function f_1 is then easily found to be

$$\nu_i(v)H(x)f_1 - \frac{M}{M_0v^2}\frac{\partial}{\partial v}\left\{v^2\nu_i(v)\,G(x)\left(\frac{kT_{i0}}{M}\frac{\partial f_1}{\partial v} + vf_1\right)\right\} = \frac{eEZ(Z-1)}{M}\frac{\partial f_0}{\partial v}. \quad (7a)$$

In this case the function f_0 is Maxwellian with a characteristic temperature T_{i0}. It is obvious from Eqs. (7) and (7a) that at small velocities the distribution function is weakly dependent on the direction of the velocity.

On the other hand, at high velocities $v > (kT_{i0}/M)^{1/2}$ the distribution function is sensitive to the direction of the velocity. A method of solving an equation similar to Eq. (6) in the high-velocity region has been developed in reference 3; it is shown that at high velocities the distribution function decreases slowest in the direction of the acting force $\theta = 0$, i.e., in our case, in the direction opposite to the electric field. For velocities close to this direction ($\theta = 0$) the distribution function is of the form

$$f = (M/2\pi kT_{i0})^{3/2}N_1 \times\exp\left\{-\int_{v_1}^{v}\frac{Mv_i(v)\,Gv/M_0 + mv_{e0}Z^2v/M - eZ(Z-1)E/M}{\nu_i(v)\,GkT_{i0}/M_0 + \nu_{e0}Z^2kT_em/M^2}\,dv\right\}, \quad (8)$$

where N_1 is the number density of the multiply charged ions in the first equilibrium state and v_1 is the first root of the equation

$$\frac{M}{M_0}\nu_i(v)\,G\left(\frac{v}{(2kT_{i0}/M_0)^{1/2}}\right)v + \frac{m}{M}\nu_{e0}Z^2v - \frac{eZ(Z-1)E}{M} = 0. \quad (9)$$

Equation (8) is obtained as a first approximation in an expansion in powers of the parameter $(kT_{i0}/Mv_c^2)^{1/2}$ in the exponential term; it is valid only when $v < v_c$ where the critical velocity v_c

*The relation $mv_{e0} + M_0v_{i0} = 0$ breaks down even if the plasma contains a large number of neutral particles or multiply charged ions, but all the more so in the presence of essentially nonequilibrium processes such as may cause a marked increase in the transfer of electron momentum to the walls of the chamber or to the inhomogeneities of the magnetic field.

*Equation (6) is written in a coordinate system that moves with the singly charged plasma ions. The collision integral for collisions between the multiply charged ions and the electrons and ions in the plasma is used in the differential form given by Landau[6] (terms that describe collisions with electrons are written under the assumption that the ion velocity v is smaller than the mean thermal velocity of the electrons). For simplicity it is assumed that the singly charged ions have a Maxwellian distribution. The directed velocity of the electrons is taken to be $v_0 = eE/m\nu_{e0}$. Interactions between the multiply charged ions themselves are neglected.

is the mean root of Eq. (9). It is apparent that a critical velocity v_c does not exist for every value of the field: E must be larger than E_{c1} and smaller than E_{c2} where

$$E_{c1} = \frac{Z}{Z-1}\left(\frac{3m}{2\pi M_0}\right)^{1/3}\frac{4\pi e^3 N \ln\Lambda}{kT_e} \approx 1.7\,\frac{Z}{Z-1}\left(\frac{M_p}{M_0}\right)^{1/3}\frac{N}{10^{14}}\frac{\ln\Lambda}{kT_e},$$

$$E_{c2} = 0.21\,\frac{Z}{Z-1}\,\frac{4\pi e^3 N \ln\Lambda}{kT_{i0}} \approx 5.5\,\frac{Z}{Z-1}\,\frac{N}{10^{14}}\frac{\ln\Lambda}{kT_{i0}} \qquad (10)$$

(in the numerical expression kT_e and kT_i are given in ev and E is in v/cm; M_p is the mass of the proton).

If $E < E_{c1}$ or $E > E_{c2}$, the distribution function decreases monotonically with increasing v; when $E_{c1} < E < E_{c2}$ the function exhibits a second maximum. Thus if the field E lies between E_{c1} and E_{c2} the second stationary state indicated in the preceding section is possible. As expected, the field values E_{c1} and E_{c2} coincide with the limiting values of the field indicated by Eq. (5) to within a numerical factor of order unity.

Further, it has been noted above that if $E_{c2} > E > E_{c1}$, then Eq. (6) gives the distribution function only when $v \le v_c$. The form of the distribution function for $v > v_c$ can be found easily by means of the preceding method but now the origin in Eq. (6) must be displaced to the point v_2, corresponding to the second equilibrium value of the velocity, i.e., the second maximum in the distribution function in Eq. (8). In this case the velocity v_2 is naturally determined by the same relation, Eq. (9). As before, when $v > v_c$ the distribution function exhibits a maximum in the direction $\theta = 0$. In the first approximation it is

$$f(v') = \left(\frac{M}{2\pi kT_e}\right)^{3/2} N_2 \times \exp\left\{-\int_{v_2}^{v_2-v'} \frac{eZ(Z-1)E/M - m\nu_{e0}Z^2 v/M - M\nu_i(v)Gv/M_0}{\nu_{e0}Z^2 kT_e m/M^2 + \nu_i(v)\,GkT_{i0}/M_0}\,dv\right\}, \qquad (11)$$

where v′ is the velocity in the new coordinate system, while N_2 is the density of the multiply charged ions under consideration in the second equilibrium state (it is obvious that $N_Z = N_1 + N_2$ where N_Z is the total density of the indicated ions).

When $v = v_c$ the values of the functions in Eqs. (8) and (11) must obviously be the same at equilibrium; this condition then determines the ratio between the number of multiply charged ions in the first and second states at equilibrium:

$$\frac{N_2}{N_1} \approx \exp\left\{-\int_{v_1}^{v_2} \frac{M\nu_i(v)\,Gv/M_0 - m\nu_{e0}Z^2 v/M - eZ(Z-1)E/M}{\nu_i(v)\,GkT_{i0}/M_0 + \nu_{e0}Z^2 kT_e m/M^2}\,dv\right\}. \qquad (12)$$

It is important that the ratio N_2/N_1 is usually very sensitive to changes in the field E; when E is changed by the order of ten percent the ratio N_2/N_1 can change by a factor of ten. Consequently, it is natural to introduce a critical field E_c, defined by the condition $N_2(E_c) = N_1(E_c)$. When $E < E_c$ almost all the particles are in the first stationary state and when $E > E_c$ almost all the particles are in the second state. In this case the field E_c can be written in the form

$$E_c = \lambda\,(T_e/T_{i0})\,E_{c1},$$

where E_{c1} is determined by (10) and $\lambda(T_e/T_{i0})$ is the numerical factor given in Fig. 2. It is clear from the figure that λ is a rather weak function of the ratio T_e/T_{i0}.

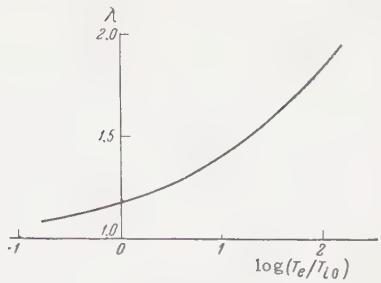

FIG. 2

Using the distribution function obtained for the multiply charged ions we can naturally compute the mean directed velocity v in the equilibrium state. The velocity v is given as a function of electric field in Fig. 3. It is obvious from the figure that near the value $E = E_c$ there is something like a transition from the first stationary state for the directed velocity, indicated in Sec. 1 (cf. Fig. 1), to the second, as expected.

We now estimate the characteristic time required for the establishment of the equilibrium

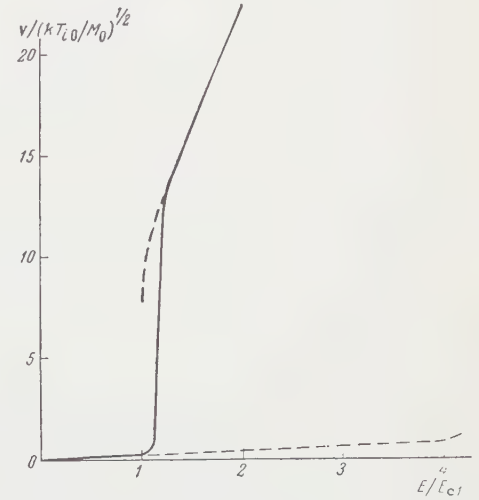

FIG. 3. The dependence of $v/(kT_{i0}/M_0)^{1/2}$ on E/E_{c1} for $T_e = T_{i0}$, $M_0/m = 3.7 \times 10^3$ (deuterium).

state under consideration. We assume, for example, that at the instant the field is switched on all the particles have low velocities so that the first stationary state is established in a time $\tau \approx M/m\nu_{e0}Z^2$. This state is naturally unstable when $E > E_c$: some of the multiply charged ions are continuously transferred to the second state. The flow of ions from the first state can be determined without difficulty if we make use of the results of references 3 and 8:

$$S = -\frac{dN_1}{dt} = \frac{N_1}{\sqrt{2\pi}} Z^2 \nu_{e0} \left(\frac{m}{M_0}\right)^{1/2} \left(\frac{T_e}{T_{i0}}\right)^{3/2} \left(\frac{E}{E_{c2}}\right)^{3/4} \times \exp\left\{-1.2\frac{M}{M_0}\frac{E_{c2}}{E}\right\}.$$

Thus the characteristic time for the establishment of the equilibrium state is

$$\Delta t \sim \left((M_0/m)^{1/2}/\nu_{e0}Z^2\right)\exp\left\{1.2ME_{c2}/M_0E\right\}.$$

This time is quite large when $M \gg M_0$. In this case $\tau \ll \Delta t$ and the first state indicated above becomes "quasi-stationary" when $E > E_c$. The same situation obtains for the second state when $E < E_c$. In Fig. 3 both of these conditions are shown by dashed lines. However, if $M \approx M_0$, then Δt and τ are of the same order of magnitude. In this case only the equilibrium state shown by the solid line in Fig. 3 is meaningful.

The author is indebted to V. L. Ginzburg and M. A. Leontovich for valuable discussion.

[1] Al'pert, Ginzburg, and Feĭnberg, Распространение радиоволн (Propagation of Radio Waves) Gostekhizdat, 1953.

[2] H. Dreicer, Phys. Rev. **115**, 238 (1959).

[3] A. V. Gurevich, JETP **39**, 1296 (1960), Soviet Phys. JETP **12**, 904 (1961).

[4] A. A. Ware, Nature **183**, 6 (1959).

[5] S. Chandrasekhar, Revs. Modern Phys. **15**, 1 (1943).

[6] L. D. Landau, JETP **7**, 203 (1937).

[7] V. L. Ginzburg and A. V. Gurevich, Usp. Fiz. Nauk **70**, 201 (1960), Soviet Phys.-Uspekhi **3**, 115 (1960).

[8] A. V. Gurevich, JETP **38**, 1597 (1960), Soviet Phys. JETP **11**, 1150 (1960).

Translated by H. Lashinsky
307

ON THE THEORY OF ENERGY DISSIPATION PROCESSES OF MOLECULAR OSCILLATIONS IN LIQUIDS

K. A. VALIEV

Kazan' Pedagogical Institute

Submitted to JETP editor January 14, 1961

J. Exptl. Theoret. Phys. (U.S.S.R.) 40, 1832-1837 (June, 1961)

The probabilities for energy dissipation of molecular oscillations in liquids are calculated. Exchange (short range) and electrostatic interaction forces between the molecules are taken into account. It is found that dissipation of vibrational energy due to exchange forces may explain the temperature course and the order of magnitude of the line widths of the molecular vibrational spectra in liquids. The role of electrostatic forces in energy dissipation is comparable with the role of exchange forces only in the case of complexes consisting of charged particles.

INTRODUCTION

THIS paper is devoted to a calculation of the lifetime of a liquid molecule in a definite vibrational state. The calculation has been carried out in order to elucidate the nature of the line widths of the vibrational (infrared and Raman) spectra of liquid molecules. The prevalent notion is that the width of the depolarization vibrational lines ($\rho \approx 6/7$) is due to a considerable extent to Brownian rotation of the anisotropic liquid molecules.[1,2] Estimates of the broadening due to dissipation of the vibrational energy have not yet been made. We consider first dissipation processes due to exchange short-range molecular interaction forces. Such forces act between all molecules, and the broadening that they induce will be present in the spectra of all liquids. We shall then consider dissipation processes due to electrostatic interaction between molecules in dipole liquids. In conclusion we shall discuss briefly the experimental data.

2. DISSIPATION OF VIBRATIONAL ENERGY OF MOLECULES. EXCHANGE INTERACTION OF PARTICLES

We single out one molecule in the liquid and describe its internal vibration by a set of normal coordinates Q_j; the atoms making up this molecule will be assigned numbers i; the atoms of the neighboring molecules will be designated A. In accordance with the problem posed, we must separate that part of the energy of exchange interaction of atoms i and A of two molecules, which depends on the coordinates Q_j. According to quantum-mechanical calculations, we choose for the exchange-interaction energy the expression (see Seitz[3])

$$H(R) = V_0 \exp(-\alpha R), \tag{1}$$

where R is the distance between the nuclei of the interacting atoms. We obviously have

$$R_{iA} = |\mathbf{r}_i^0 + \mathbf{s}_i - \mathbf{r}_A| = R_{iA}^0 - (\mathbf{R}_{iA}^0 \mathbf{s}_i)/R_{iA}^0, \tag{2}$$

where $\mathbf{r}_i^0 + \mathbf{s}_i$ and $\mathbf{r}_A$ are respectively the radius-vectors of atoms i and A; $\mathbf{s}_i$ is a small displacement of the atom i, due to the internal vibrations of the molecule.

Expanding (1) we obtain for the sought energy

$$H' = -\alpha V_0 \sum_{i,A} \exp(-\alpha R_{iA}^0)(\mathbf{R}_{iA}^0 \mathbf{s}_i)/R_{iA}^0. \tag{3}$$

We introduce the unit vector $\mathbf{n}_{iA}$, directed along $\mathbf{R}_{iA}^0$, and make in (3) the substitution

$$\mathbf{s}_i = \sum_j \frac{\partial \mathbf{s}_i}{\partial Q_j} Q_j; \tag{4}$$

Then the matrix element of the transition $n_j \to n_j - 1$ (n_j is the quantum number of oscillator Q_j) is

$$H'_{n_j \to n_j - 1} = -\alpha V_0 \sum_{i,A} \exp(-\alpha R_{iA}^0)(\mathbf{n}_{iA} \partial \mathbf{s}_i / \partial Q_j)(\hbar n_j / 2\mu_j \omega_j)^{1/2}. \tag{5}$$

Here μ_j and ω_j are the mass and frequency of the oscillator Q_j.

The time dependence of (5) is contained in $\mathbf{R}_{iA}$ and $\mathbf{n}_{iA}$, which vary at random as the molecules are displaced relative to one another. $\mathbf{R}_{iA}$, $\mathbf{n}_{iA}$ are coordinates that describe the translational

and rotational degrees of freedom of the molecules; in the transition $n_j \to n_j - 1$, the energy is transferred from the oscillator Q_j to the indicated degrees of freedom.

To calculate the transition probability we use the perturbation-theory formula

$$w_{n_j \to n_j - 1} = \hbar^{-2} \overline{|H_{n_j \to n_j - 1}|^2}\, \rho(\omega_j), \tag{6}$$

where $\rho(\omega_j)$ is the spectral density, calculated in terms of the normalized correlation function $g(\tau)$ of the random quantity H':[4]

$$\rho(\omega) = \int_{-\infty}^{+\infty} e^{-i\omega\tau} g(\tau)\, d\tau, \qquad g(\tau) = \overline{H'(0)\, H'(\tau)} / \overline{|H'(0)|^2}. \tag{7}$$

The interaction energy H' is greatly changed as the distance between the particles is changed by an amount on the order of the atomic diameter. We shall therefore use, as the time during which the values of H' are correlated, the time of the "sedentary" life of the molecule between the two jumps[5]

$$\tau_c = \tau_0 e^{E/RT}, \tag{8}$$

and the correlation function will be taken in the form $g(\tau) = \exp(-\tau/\tau_c)$. Then

$$\rho(\omega_j) = 2\tau_c/(1 + \omega_j^2 \tau_c^2). \tag{9}$$

The probability of the transition $n_j \to n_j - 1$ will be found with the aid of (5), (6), and (9):

$$w_{n_j \to n_j - 1} = \hbar^{-2} \frac{4\pi N V_0^2}{3} \sum_i \left| \frac{\partial s_i}{\partial Q_j} \right|^2 \frac{\hbar n_j}{2\mu_j \omega_j} e^{-2\alpha\Delta} \left(\frac{1}{4\alpha} + \frac{\Delta}{2} + \frac{\alpha\Delta^2}{2} \right) \rho(\omega_j). \tag{10}$$

Here N is the number of particles per cm^3 and Δ the shortest approach distance between the atoms i and A. In averaging the square of $|H'|$, the summation over A is replaced by integration over the volume.

A numerical estimate of (10), assuming the values $V_0 = 500$ ev, $1/\alpha = 0.4$ A, $\Delta = 3$ A, $N = 3 \times 10^{22}$, $\tau_c = 5 \times 10^{-12}$ sec, $\mu_j = 2 \times 10^{-24}$ g, $\omega_j = 2 \times 10^{14}$ sec^{-1}, and $\Sigma_i |\partial S_i / \partial Q_j|^2 = 1$, we get $w_{n_j \to n-1} \approx 25$ cm^{-1}.

3. DISSIPATION OF VIBRATIONAL ENERGY OF MOLECULES. ELECTROSTATIC INTERACTIONS

Let us consider the probability of dissipation of the vibrational energy of the molecules, due to electrostatic interactions between dipoles and a dipole liquid. The part of the dipole-dipole interaction dependent on the coordinates $Q_j^{(i)}$ of the vibrations of the molecule i is equal to

$$H' = \sum_j Q_j^{(i)} \sum_A R_{iA}^{-5} \left[R_{iA}^2 (\mathbf{d}_A \mathbf{D}_i^{(j)}) - 3 (\mathbf{d}_A \mathbf{R}_A)(\mathbf{D}_i^{(j)} \mathbf{R}_A) \right]. \tag{11}$$

Here $\mathbf{D}_i^{(j)} = \partial \mathbf{d}_i / \partial Q_j$; $\mathbf{d}_i$ and $\mathbf{d}_A$ are the dipole moments of the molecules i and A.

The time dependence of the energy H' is due to the rotational and translational diffusion of the particles. These motions will be regarded as independent, and their corresponding contributions to dissipation will be assumed additive. To calculate the correlation function $g(\tau)$ and the spectral density $\rho(\omega)$, we use the solutions (Green's functions) $u(q_0, 0; q, \tau)$ of the corresponding equations of free diffusion. For the rotational motion we find

$$g_{rot}(\tau) = \exp(-|\tau|/\tau_{rot}), \tag{12}$$

$$\rho_{rot}(\omega) = 2\tau_{rot}/(1 + \omega^2 \tau_{rot}^2), \qquad \tau_{rot} = 4(\pi\eta a^3/kT) = 4\tau_0. \tag{13}$$

Analogously we obtain for the translational motion[6]

$$\rho_t(\omega) = 36\tau_0 \left[(z^{-3} - 2z^{-5}) + e^{-z} \cos z\, (z^{-3} + 4z^{-4} + 2z^{-5}) + e^{-z} \sin z\, (z^{-3} - 2z^{-5}) \right], \qquad z = \sqrt{24\omega\tau_0}. \tag{14}$$

It is easy to find the limiting expressions for (14):

$$\rho_t(\omega) = 3/(4\sqrt{6}\omega^{3/2}\tau_0^{1/2}) \quad \text{for} \quad \omega\tau_0 \gg 1,$$
$$\rho_t(\omega) = (24/5)\tau_0 \quad \text{for} \quad \omega\tau_0 \ll 1. \tag{15}$$

After averaging $|H'|^2$ over the angles and the distances, using (13) and (15), we obtain the probability of the transition $n_j \to n_j - 1$ for $\omega_j \tau_0 \gg 1$:

$$w_{n_j \to n_j - 1} = \frac{8\pi N}{9} \frac{n_j \hbar^{-1}}{2\mu_j \omega_j} \frac{d^2 (D^{(j)})^2}{(2a)^3} \left[\frac{1}{2\omega_j^2 \tau_0} + \frac{\sqrt{3}}{4\omega_j^{3/2} \tau_0^{1/2}} \right]. \tag{16}$$

Here a is the radius of the molecule. A numerical estimate of the probability $w_{n_j \to n_j - 1}$, assuming the following values,

$N = 3 \cdot 10^{22}$, $d = 1.5\, D$, $D^{(j)} = 5 \cdot 10^{-10}$ cgs esu,[7]

$\tau_0 = 5 \cdot 10^{-12}$ sec,

$\omega_j = 10^{14}$ sec^{-1}, $2a = 4$Å, $\mu_j = 2 \cdot 10^{-24}$;

yields $w_{1 \to 0} = 4 \times 10^{11}$ sec^{-1}.

We have also calculated the probability of dissipation of the vibrational energy of ionic complexes formed in the solutions of metal-ion salts. To be specific, we consider octahedral complexes. The electric moments of the complex vanish under equilibrium. The internal vibrations disturb the symmetry of the complex, which acquires a quadrupole moment. The five independent components of the quadrupole moment, introduced in accordance with the formulas

$$D_0 = \frac{\sqrt{6}}{2} D_{zz},$$
$$D_{\pm 1} = \pm D_{xz} - i D_{yz}, \qquad 2D_{\pm 2} = D_{xx} - D_{yy} \mp 2D_{xy}, \tag{17}$$

are expressed in terms of the normal coordinates Q_j of the vibrations of the complex in the following manner:

$$D_0 = 6\sqrt{2}\, d Q_3,\ D_{\pm 1} = \pm 6d\,[Q_5 \mp i Q_6],$$
$$D_{\pm 2} = 2d\,[6 Q_2 \mp 3i Q_4 - 2\sqrt{3} Q_3]. \quad (18)$$

Here d is the dipole moment of the particles forming the complex. Then the particles carry equal charges q, and we must put qb in (18) in lieu of d (b is the distance between the particles in the complex). The components D_r in (18) are defined in a system of coordinates rotating together with the complex. In the laboratory system we write

$$D_p = \sum_{r=-2}^{2} T^{(2)}_{rp}(\theta, \psi, \varphi)\, D_r, \quad (19)$$

where $T^{(2)}_{rp}(\theta, \psi, \varphi)$ are generalized spherical functions.[8]

It is also easy to find the components of the tensor of the electric field intensity gradient of the dipole $\mathbf{d}_A(d_A, \alpha_A, \beta_A)$ at a distance $\mathbf{R}_A$ $(R_A, \theta_A, \varphi_A)$ from it (near the complex):

$$\sqrt{2/3}\,(\nabla\mathbf{E})^0_A = (\nabla\mathbf{E})^{zz}_A = d_A R_A^{-4}\Phi^0_A,\ (\nabla\mathbf{E})^{\pm 1}_A = \pm(\nabla\mathbf{E})^{xz}_A + i(\nabla\mathbf{E})^{yz}_A = d_A R_A^{-4}\Phi^{\pm 1}_A,$$
$$2(\nabla\mathbf{E})^{\pm 2}_A = (\nabla\mathbf{E})^{xz}_A - (\nabla\mathbf{E})^{yy}_A \pm 2i(\nabla\mathbf{E})^{xy}_A = d_A R_A^{-4}\Phi^{\pm 2}_A; \quad (20)$$

$$\Phi^0_A = (4\pi/\sqrt{7})[\sqrt{8}\, Y_3^{-1}(\theta)\, Y_1^1(\alpha) + \sqrt{8}\, Y_3^1(\theta)\, Y_1^{-1}(\alpha) - \sqrt{12}\, Y_3^0(\theta)\, Y_1^0(\alpha)],$$
$$\Phi^{-1}_A = (4\pi/\sqrt{7})[\sqrt{20}\, Y_3^{-2}(\theta)\, Y_1^1(\alpha) + \sqrt{6}\, Y_3^0(\theta)\, Y_1^{-1}(\alpha) - 4 Y_3^{-1}(\theta)\, Y_1^0(\alpha)],$$
$$\Phi^{-2}_A = (4\pi/\sqrt{7})[\sqrt{2}\, Y_3^{-1}(\theta)\, Y_1^{-1}(\alpha) - \sqrt{10}\, Y_3^{-2}(\theta)\, Y_1^0(\alpha) - \sqrt{30}\, Y_3^{-3}(\theta) Y_1^{-1}(\alpha)]. \quad (21)$$

The energy of interaction between the quadrupole moment of the complex and the electric field of the dipoles surrounding the complex will be written with the aid of (19) and (20):

$$H' = \frac{1}{6}\sum_{r=-2}^{2} D_r \sum_{p=-2}^{2} T^{(2)}_{rp}(\theta, \psi, \varphi) \sum_A (\nabla\mathbf{E})^p_A. \quad (22)$$

We give the calculated spectral density of H′:

$$\rho_{rot}(\omega) = 2\tau_r/(1 + \omega^2\tau_r^2),\ 1/\tau_r = 1/\tau_1 + 1/\tau_2,$$
$$\tau_1 = 4\pi\eta a_1^3/kT,\ \tau_2 = {}^4/_3\,\pi\eta a_2^3/kT; \quad (23)$$

a_1 and a_2 are the radii of the complex and of the solvent molecule. If H′ is disturbed by translational diffusion,

$$\rho_t(\omega) = 480\,\tau_0[({}^1/_4 z^{-3} - {}^3/_2 z^{-5} - 9z^{-7}) + e^{-z}\cos z\,(-{}^1/_4 z^{-3} - 3z^{-4} - {}^{15}/_2 z^{-5} + 9z^{-7}) + e^{-z}\sin z\,(-{}^1/_4 z^{-3} + {}^{15}/_2 z^{-5} + 18z^{-6} - 9z^{-7})]. \quad (24)$$

Determining the average of $|H'|^2$, we obtain for the probability that the energy of one of the oscillators of the complex (Q_2) will change by an amount $\hbar\omega_2$

$$w_{n_2 \to n_2 - 1} = \frac{1024\pi}{25}\frac{d^2 d_A^2 N}{\hbar^2 (2a)^3}\frac{\hbar n_2}{2\mu_2\omega_2}\left(\frac{16}{7}\tau_0 + 2\tau_r\right), \quad \omega\tau_0 \ll 1, \quad (25)$$

$$w_{n_2 \to n_2 - 1} = \frac{1024\pi}{25}\frac{d^2 d_A^2 N}{\hbar^2 (2a)^3}\frac{\hbar n_2}{2\mu_2\omega_2}\left(\frac{2}{\omega_2^2\tau_r} + \frac{5}{4\sqrt{6}\,\omega_2^{3/2}\tau_r^{1/2}}\right), \quad \omega\tau_0 \gg 1. \quad (26)$$

A numerical estimate of the probability by means of (26), using values typical of aqueous solutions, namely $d = d_A = 1.85$ D, $N = 3 \times 10^{22}$ cm^{-3}, $\mu_2 = 3.6 \times 10^{-22}$ g, $\omega_2 = 5 \times 10^{13}$ sec^{-1}, $2a = 4$ A, and $\tau_0 = \tau_r = 5 \times 10^{-12}$ sec yields $w_{1 \to 0} = 1.1 \times 10^{10}$ sec^{-1}. If the complex is made up of charged particles, we must replace d by the quantity qb $\approx 10^{-17}$ cgs esu; in this case $w_{1 \to 0} = 10^{12}$ sec^{-1} $= 5$ cm^{-1}.

We must note that the calculation given here is approximate, owing to the use of an expansion of the energy of electrostatic interaction between molecules in powers of the multipoles, an expansion which is correct only for large distances between molecules.

CONCLUSION

The experimental material on the line widths of the Raman and infrared spectra of molecules in liquids is scanty. The most systematic investigations of the line widths of Raman scattering in dipole organic liquids was carried out by Rakov.[2] He observed an exponential increase in the line width with increasing temperature: $\delta(T) = \Delta_0 + A\exp(-E/RT)$, and the values he obtained for the parameter E agreed closely with the viscosity barrier for the investigated liquid. In addition, a correlation was observed between the degree of depolarization ρ and the width of the line: the greater ρ, the broader the lines. These facts can be explained by assuming that one of the principal causes of Raman line broadening is Brownian rotation of the molecules with an anisotropic tensor of the derivative of the polarizability with respect to the normal coordinates of the vibrations. This source of broadening, however, is lacking in oscillations which have an isotropic tensor of the derivative of the polarizability.

It appears to us that the experimental data can be explained better by taking into account the dissipative broadening of the lines considered in the present paper. The temperature dependence predicted by (10), as well as the calculated order of

magnitude of the line width, coincide with those observed. The width of the polarized lines in dipole-free liquids is determined obviously essentially by the dissipation of the vibrational energy through exchange interactions. For depolarized lines, the dissipative broadening and the broadening due to Brownian rotation of the molecules will be additive; as a result, the greater ρ the greater the width.

We note that the contribution made by dissipation of the vibrational energy through exchange interactions to the line width depends greatly on the distance between molecules; in this connection, it would be interesting to observe the dependence of the line width on the pressure in the liquid. In addition, steric effects can be important; in complex molecules protected against external influences, vibrations may produce narrower lines.

In dipole liquids there is an additional dissipative broadening due to the presence of electrostatic interactions between molecules; judging from our estimate, this broadening is approximately one order of magnitude smaller than the broadening due to exchange interactions. Only in ionic complexes consisting of charged particles will the electrostatic and exchange interactions yield comparable contributions to the line widths.

[1] I. I. Sobel'man, Izv. Akad. Nauk. SSSR. ser fiz. 17, 554 (1953).

[2] A. V. Rakov, Оптика и спектроскопия (Optics and Spectroscopy) 7, 202 (1959).

[3] F. Seitz, The Modern Theory of Solids; McGraw-Hill, N. Y., 1940.

[4] M. S. Bartlett, Stochastic Processes, Cambridge Univ. Press, 1955.

[5] Ya. I. Frenkel', Кинетическая теория жидкостей (Kinetic Theory of Liquids), Akad. Nauk. SSSR, 1959, p. 197.

[6] K. A. Valiev, JETP **38**, 1222 (1960), Soviet Phys. JETP **11**, 883 (1960).

[7] M. V. Vol'kenshtein, Usp. Fiz. Nauk **18**, 153 (1937).

[8] Gel'fand, Minlos, and Shapiro, Представления группы вращений и группы Лоренца (Representations of Rotation and Lorentz Groups), Fizmatgiz 1958, p. 94.

Translated by J. G. Adashko
308

RESONANCE DIFFRACTION OF WAVES IN LAMELLAR INHOMOGENEOUS MEDIA

L. V. IOGANSEN

Submitted to JETP editor January 19, 1961

J. Exptl. Theoret. Phys. (U.S.S.R.) **40**, 1838-1843 (June, 1961)

A peculiar type of diffraction effect due to resonance accumulation of waves inside a lamellar system is observed when the waves are incident at an oblique angle on a finite laminar system. The main properties of this effect are elucidated and a characteristic length is derived which defines the distance along the layers from the boundary for which the effect can be observed.

RESONANCE phenomena can arise in wave propagation in inhomogeneous lamellar media. This takes place if the waves encounter two or more low-transmission, non-absorbing layers en route; these play the role of barriers, in the region between which standing waves can form. At resonance, the standing-wave amplitude between the barriers increases many times in comparison with the incident wave amplitude. Simultaneously, the transmission of the barriers for the incident wave can increase sharply. The quantum-mechanical phenomenon of the analogous process in nonplanar systems is the resonance transmission of de Broglie waves through a system of two potential barriers (Ramsauer effect) and also the resonance penetration of waves through a barrier according to Breit-Wigner.

These resonance phenomena in lamellar media are frequently encountered in practice: in acoustics, in wave propagation in a plasma, particularly in the ionosphere, in optical systems of the type of interference filters, Fabry-Perot etalons, etc. Many researches have been devoted to the analysis of resonance effects of this type (see, for example, reference 1). As a rule, the calculations here are carried out for infinite systems. The basis for this is the fact that in practice the dimensions of the systems are many orders of magnitude greater than the wavelength. Therefore, it is assumed that the diffraction effects from the boundaries of real systems are always small corrections which can safely be neglected.

The latter is not true, generally speaking; that is, the fact that the system is very large in comparison with the wavelength is not sufficient that the asymptotic theory of an infinite system can be used as a valid first approximation. In particular, a peculiar resonance diffraction effect takes place for oblique incidence of waves on a lamellar system. This process can propagate along the stratified system for many orders of wavelengths from its boundary. In this connection, a characteristic length of resonance diffraction l_0 appears and can be many orders larger than the wavelength. Only when the dimensions of the system are large in comparison with the characteristic resonance diffraction length l_0, and not with the wavelength, can one use the asymptotic theory of an infinite system as a first approximation.

The lack of understanding of this process, and the invalid application of the asymptotic theory in a number of cases, have already led to a radical disparity between theory and experiment as, for example, in total reflection filters.[2]

Until recently, mistaken attempts have been made to attribute these disparities to all sorts of imperfections of the system, inasmuch as the phenomenon of resonance diffraction has never been described or calculated up to now. Recently, a calculation of electromagnetic wave transmission through finite lamellar dielectric systems was carried out by the author.[3] It was established that the diffraction effects begin to play an important role at resonance. It was shown in the same place, in particular, that just these effects produce a sharp decrease in the transmission of total reflection filters. A complete calculation of the transmission coefficient of the finite total internal reflection filter is in excellent agreement with experimental data. Thus, the special case of the resonance diffraction effect was considered for the first time.[3]

The purpose of the present research was to formulate the basic general laws of resonance diffraction. It seems to us that this is of interest, since resonance diffraction is a rather general phenomenon which can arise for waves any nature obliquely propagating through lamellar media. To reduce the amount of calculation, we considered the case of scalar wave propagation

in the simplest semi-infinite resonant system. The results obtained can be written down in very simple form, which contains nothing that is specific to the nature of the waves and to the character of the actual resonant system. These results admit immediate generalization and make it possible to formulate the general laws of resonance diffraction.

We write down the scalar wave equation

$$\Delta\varphi - (n/c)^2 \ddot{\varphi} = 0. \tag{1}$$

Here $\varphi(\mathbf{r}, t)$ is the scalar wave function of the coordinates and time, n is a material constant of the medium (index of refraction), and c is the characteristic velocity. We consider the case of a harmonic time dependence $\varphi(\mathbf{r}, t) = \varphi(\mathbf{r})e^{i\omega t}$. In this case, we have from (1)

$$\Delta\varphi(\mathbf{r}) + k^2\varphi(\mathbf{r}) = 0, \tag{2}$$

where $k^2 = (n\omega/c)^2$.

We assume that the plane $z = 0$ separates media with different material constants. We require that the following boundary conditions be satisfied at the separation boundary:

$$\partial\varphi_1/\partial t = \partial\varphi_2/\partial t, \qquad \partial\varphi_1/\partial z = \partial\varphi_2/\partial z. \tag{3}$$

The equations (1) — (3) just considered can be used for the description of various wave processes. In particular, they describe the propagation of longitudinal sound waves in an elastic medium of constant density. In this case, φ is the velocity potential of the medium and c/n is the velocity of the sound waves. The same equations describe electromagnetic wave propagation in a nonmagnetic dielectric in the case in which the electric vector lies in the plane of separation of the two dielectrics. Here φ is the only nonvanishing component of the vector potential of the wave, c is the velocity of light in vacuum, and n is the index of refraction of the medium.

We take the plane of incidence of the waves on the boundary separating the media as the xz plane. We assume that the layered system is semi-infinite and fills the half-space $x > 0$. Consequently, the desired solution of the wave equation in the region $x < 0$ must be identically equal to zero. It is obvious that individual plane monochromatic waves are insufficient for the solution of the given diffraction problem. Below, we shall give the approximate solutions of the wave equation (1) obtained previously,[3] with the help of which one can solve our boundary problem.

We assume that total internal reflection takes place in the incidence of waves from medium I, which is located in the region $z < 0$, on medium II, located in the region $z > 0$. In medium I we shall have a wave consisting of a combination of deformed incident and reflected plane homogeneous waves:

$$\varphi(\mathbf{r}, t) = \left\{A\left(x - \frac{k_x}{k_z}z\right)\exp\left[-i(k_x x + k_z z)\right] + B\left(x + \frac{k_x}{k_z}z\right)\exp\left[-i(k_x x - k_z z)\right]\right\}e^{i\omega t}. \tag{4}$$

In medium II, we shall have a wave consisting of a combination of deformed inhomogeneous waves which grow and decay along the z axis:

$$\varphi(\mathbf{r}, t) = \left\{F\left(x + i\frac{k_x}{q_z}z\right)\exp\left[-i(k_x x + iq_z z)\right] + G\left(x - i\frac{k_x}{q_z}z\right)\exp\left[-i(k_x x - iq_z z)\right]\right\}e^{i\omega t}. \tag{5}$$

Here A, B, F, G are certain complex functions of their arguments:

$$k_x = (n\omega/c)\sin\alpha, \qquad k_x^2 + k_z^2 = (n\omega/c)^2, \qquad k_x^2 - q_z^2 = (n_1\omega/c)^2, \tag{6}$$

where ω is the circular frequency of the waves, c the characteristic velocity, α the angle of incidence of the waves from medium I on the plane of separation $z = 0$, n and n_1 the index of refraction of medium I and medium II, respectively. It is assumed that the angle of incidence is sufficiently large that the condition for total reflection is satisfied; i.e., $\sin\alpha \geq n_1/n$.

Generally speaking, Eqs. (4) and (5) are not exact solutions of the wave equation (1) for arbitrary form of the amplitude functions A, B, F, and G. They are exact solutions of (1) in the special case when these amplitudes are constant or are linear functions of their arguments. However, (4) and (5) are approximate solutions of (1), with accuracy up to first derivatives for arbitrary amplitudes A, B, F, and G, if these amplitudes are sufficiently slowly changing functions of their arguments. The condition "sufficiently slowly" in the given case means the smallness of the change of amplitudes over a distance of the order of a wavelength: $|\partial A/\partial x| \ll |k_x A|$, $|\partial A/\partial z| \ll |k_z A|$, etc. In practice, for the resonance diffraction phenomenon of interest to us, this condition of slowness of change of the amplitudes is always satisfied by a wide margin, and the Eqs. (4) and (5) can be taken practically as exact solutions. We shall call the waves (4) and (5) "orthogonal," which reflects the fact that the planes where the phases and amplitudes are constant, are mutually orthogonal.

Substituting (4) and (5) in (3), we get a differential relation connecting the amplitudes of the waves

(4) and (5) in the plane of separation z = 0. These equations can be solved with accuracy up to the first derivatives; one obtains the following direct and inverse systems of differential equations for the determination of A and B in terms of F and G, and vice versa:

$$A(x) = \frac{1}{2}\left(1 + i\frac{q_z}{k_z}\right)F(x) + \frac{1}{2}\left(1 - i\frac{q_z}{k_z}\right)G(x) - \frac{1}{2}\frac{k_x}{q_z k_z}\left(1 + \frac{q_z^2}{k_z^2}\right)[F'(x) - G'(x)],$$

$$B(x) = \frac{1}{2}\left(1 - i\frac{q_z}{k_z}\right)F(x) + \frac{1}{2}\left(1 + i\frac{q_z}{k_z}\right)G(x) + \frac{1}{2}\frac{k_x}{q_z k_z}\left(1 + \frac{q_z^2}{k_z^2}\right)[F'(x) - G'(x)]; \quad (7)$$

$$F(x) = \frac{1}{2}\left(1 - i\frac{k_z}{q_z}\right)A(x) + \frac{1}{2}\left(1 + i\frac{k_z}{q_z}\right)B(x) - \frac{1}{2}\frac{k_x}{q_z k_z}\left(1 + \frac{k_z^2}{q_z^2}\right)[A'(x) - B'(x)],$$

$$G(x) = \frac{1}{2}\left(1 + i\frac{k_z}{q_z}\right)A(x) + \frac{1}{2}\left(1 - i\frac{k_z}{q_z}\right)B(x) + \frac{1}{2}\frac{k_x}{q_z k_z}\left(1 + \frac{k_z^2}{q_z^2}\right)[A'(x) - B'(x)]. \quad (8)$$

We now proceed to consideration of resonant systems. The simplest resonant system consists of a single barrier located in front of an impenetrable wall. We shall call such a system a resonant condenser. Such a semi-infinite resonant condenser is shown in cross section in the drawing, with a totally reflecting sheet bounded by the region x > 0. Here the boundary medium I and the layer-resonator III possess large indices of refraction n and n_2, respectively. The totally reflecting layer II and the boundary medium IV possess small indices of refraction n_1 and n_1', respectively. It is assumed that the waves are incident from medium I on the separation boundary at such large angles of incidence α that complete internal reflection takes place in the planes P_{12} and P_{34}; i.e., the following conditions hold:

$$\sin\alpha \geqslant n_1/n \text{ and } \sin\alpha \geqslant n_1'/n.$$

The appearance of waves along the totally reflecting layer II is due to the smallness of its thickness d_1. In this case, the appearance of energy inside the resonator III has a resonance character and for certain fixed conditions depends on the thickness d_2 of the resonator. To be precise, upon satisfaction of definite resonance conditions, which are determined from the Eqs. (9) set forth below, the amplitude of the wave inside resonator III increases sharply in the case of an unbounded system. In the presence of a boundary,

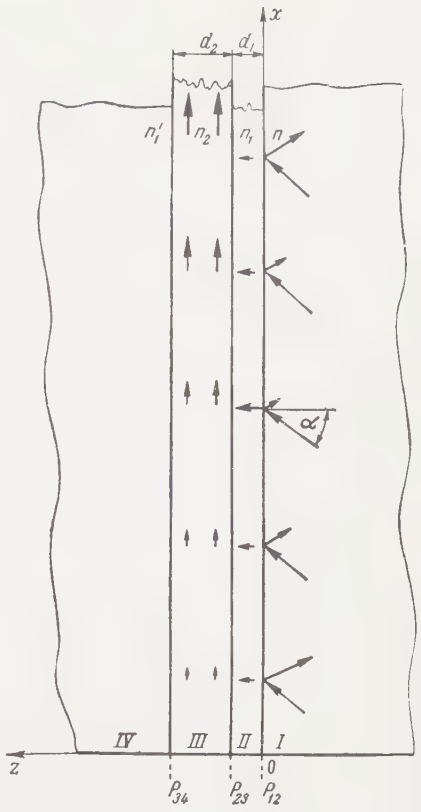

this resonance accumulation of waves will take place gradually in a certain portion adjacent to the boundary; that is, a special resonant diffraction layer appears with its own characteristic length. It is just this layer that we wish to discuss.

We note the curious fact* that in the case of oblique propagation of electromagnetic waves polarized in the plane of incidence in an unbounded lamellar plasma with continuously changing dielectric properties, the effect of leakage and resonant accumulation of energy takes place in the region behind the totally reflecting boundary, similar to what happens in the resonant condenser considered by us, in which the medium has properties which undergo discrete changes.[4] If we take into account the presence of the boundary in this case, then a characteristic length will obviously exist which is analogous to that obtained in the present research, over the extent of which flow of energy takes place into the region behind the barrier.

In the calculation of the semi-infinite resonant condenser shown in the drawing, one should determine eight complex amplitude functions, two for each of the media from I to IV. These amplitudes are connected by six matching conditions of the form (7) or (8) on the three boundary surfaces

*I am most grateful to V. L. Ginzburg who turned my attention to this point.

P_{12}, P_{23}, and P_{34}. Moreover, it is clear from physical considerations that the amplitude of the wave in medium IV which arises on the side $z > 0$ must be equal to zero, i.e., $F_{P_{34}}(x) \equiv 0$., since it would otherwise increase without limit as $z \to \infty$. In order that the problem be completely determined, one must assume one of the remaining amplitudes as given. We shall assume that the amplitude of the wave incident from I on P_{12} is given, and shall assume that an ordinary plane wave with constant amplitude A_1 is incident from medium I. Thus there remain six unknown complex amplitude functions, connected by the set of six linear differential equations of first order.

By making use of the approximate method developed earlier,[3] these equations can be integrated with accuracy up to first derivatives of slowly changing amplitudes. As a result, we obtain all six desired amplitude functions, expressed in terms of the amplitude A_1 of the wave incident on the system. These amplitudes depend in resonant fashion on the conditions in the resonator. The conditions of resonance are periodically repeated with change of thickness of the resonator d_2, and have the approximate form

$$\operatorname{tg}(k'_z d_2)_{\text{рез}} = -k'_z(q_z + q'_z)/(q_z q'_z - k'^2_z), \qquad (9)^*$$

where, by analogy with (6),

$$(k_x^2 + k'^2_z) = (n_2\omega/c)^2, \qquad (k_x^2 - q_z^2) = (n'_1\omega/c)^2. \qquad (10)$$

For exact resonance, the amplitudes of the waves inside resonator III in the region $x > 0$ are equal to

$$|A_{P_{23}}(x)| = |B_{P_{23}}(x)| = \left[\sqrt{(q_z^2 + k_z^2)(q_z^2 + k'^2_z)}/2q_z k'_z\right] \times \exp(q_z d_1)(1 - e^{-x/l_0})|A_I|, \qquad (11)$$

while the amplitude of the wave reflected from the leading plane of separation is equal to

$$|B_{P_{12}}(x)| = |1 - 2e^{-x/l_0}| \cdot |A_I|, \qquad (12)$$

where the characteristic length of resonant diffraction enters:

$$l_0 = (k_x/k_z)\,[(q_z^2 + k_z^2)(q_z^2 + k'^2_z)/(2q_z k'_z)^2] \exp(2q_z d_1) \times (d_2 + 1/q_z + 1/q'_z). \qquad (13)$$

For an infinite system in the region $x \gg l_0$ we have $e^{-x/l_0} \approx 0$; therefore, we find from (11) and (12):

$$|A_{P_{23}}(\infty)|^2/|A_I|^2 = [(q_z^2 + k_z^2)(q_z^2 + k'^2_z)/(2q_z k'_z)^2] \exp(2q_z d_1). \qquad (14)$$

From (12) we have $|B_{P_{12}}(\infty)| = |A_I|$; that is, the square of the modulus of the amplitude of the wave inside the resonator increases by a factor of $\exp(2q_z d_1)$ in comparison with the incident wave, while the amplitude of the reflected wave is equal to the amplitude of the incident wave.

The situation is different in the region $0 \leq x \lesssim l_0$. It is just in this region that the diffraction phenomena play a role. As is seen from (11), the amplitudes of the waves inside the resonator in this region increase monotonically from zero, gradually approaching the resonance value for an infinite system. On the other hand, the amplitude of the reflected wave, which at $x = 0$ is equal to the amplitude of the incident wave, gradually decreases, vanishing at $x = l_0 \ln 2$, and then increases again, approaching the amplitude of the incident wave.

The characteristic resonant diffraction length l_0, which is determined for exact resonance by the expression (13), can be written in the following simple form with the help of (6) and (14):

$$l_0 = [|A_{P_{23}}(\infty)|^2/|A_I|^2](d_2 + 1/q_z + 1/q'_z)\operatorname{tg}\alpha, \qquad (15)$$

that is, this length is equal to the effective thickness of the resonator, multiplied by the coefficient of amplification of the square of the amplitude of the wave inside the resonator and by the tangent of the angle of incidence. The effective thickness of the resonator is equal to its geometric thickness plus the effective depth of penetration of the waves in the totally reflecting medium adjoining it, which plays the role of the barrier.

In conclusion, we emphasize that the results obtained determined the general phenomenon of resonance diffraction, which is characteristic for any wave processes in lamellar media. The essence of this phenomenon consists of the fact that, in the oblique incidence of waves, there is always a certain region abutting the boundary of the system, in which a gradual leakage of the waves inside the resonator takes place. In this region, the amplitude of the waves inside the resonator gradually increases, as the distance from the boundary increases as $1 - e^{-x/l_0}$, from zero up to the resonant value of the amplitude of the wave inside an unbounded resonant system. The dimensions of the region in which these phenomena take place are determined by the characteristic length of resonance diffraction, which is in turn determined by Eq. (15).

*tg = tan.

[1] L. M. Brekhovskikh, Волны в слоистых средах (Waves in Layered Media), Academy of Sciences Press, 1957.

[2] A. F. Turner, J. phys. rad. **11**, 444 (1950). G. V. Rozenberg, Оптика тонко слойных покрытий (Optics of Thin-Film Coatings), Fizmatgiz, 1958.

[3] L. V. Iogansen, J. Tech. Phys. (U.S.S.R.), in press.

[4] N. G. Denisov, JETP **31**, 609 (1956), Soviet Phys. JETP **4**, 544 (1956); Gershman, Ginzburg, and Denisov, Usp. Fiz. Nauk **61**, 561 (1957).

Translated by R. T. Beyer
309

COULOMB EXCITATION OF Λ PARTICLES

B. N. VALUEV

Joint Institute for Nuclear Research

Submitted to JETP editor January 24, 1961

J. Exptl. Theoret. Phys. (U.S.S.R.) 40, 1844-1846 (June, 1961)

The electromagnetic transition $\Lambda \to \Sigma^0$ is examined. This transition is of interest in investigating the possibilities of experimental determination of the Σ^0 lifetime and in testing the validity of charge independence for strange particles (the $\Lambda + He_2^4 \to \Sigma^0 + He_2^4$ and $\Lambda + d \to \Sigma^0 + d$ reactions).

THE knowledge of the properties of strange particles is of great importance for any attempt to construct a theory of elementary particles and their interactions. The present paper is devoted to a discussion of the possibilities of an experimental determination of the Σ^0 lifetime, which has not as yet been measured.

As is known,[1] the matrix element corresponding to the electromagnetic transition $\Sigma^0 \to \Lambda + \gamma$ can be written as follows:

$$\bar{u}(p_\Lambda)\,[f(k^2)\,\sigma_{\mu\nu}k_\nu + g(k^2)\,k_\mu + h(k^2)\,\gamma_\mu]\,a_\pm u(p_\Sigma),$$

where $k = p_\Lambda - p_\Sigma$, $a_\pm = 1$ or γ_5 depending on the relative parity of Σ^0 and Λ. As a result of gauge invariance the term $g(k^2)k_\mu$ drops out and $h(0) = 0$. Consequently the decay probability is determined by the single quantity f, whose dimensions are those of a magnetic moment.

Direct measurement of the Σ^0 lifetime (in flight) may turn out to be inapplicable as a consequence of the very short lifetime of the Σ^0:

$$1/\tau = f^2\omega^3/\pi, \qquad \omega = (M_\Sigma^2 - M_\Lambda^2)/2M_\Sigma;$$

we set $\hbar = c = 1$, $\alpha = e^2/4\pi = 1/137$, i.e. $1/\tau = 4 \times 10^{18}(f/\mu_0)^2\ \mathrm{sec}^{-1}$, where $\mu_0 = e/2M$ with M the nucleon mass ($\hbar/\tau \sim 3(f/\mu_0)^2$ kev).

An estimate of f, analogous to Holladay's[2] estimates of the hyperon magnetic moments, yields $f \sim 2\mu_0$ if the hyperon-pion coupling constants and cut-off momentum are chosen to be the same as for the pion-nucleon interaction. It follows from detailed balance arguments that for small k^2 ($k^2 \lesssim m_\pi^2$) the transition $\Lambda \to \Sigma^0$ is determined by the same quantity since $f(k^2) \approx f(0)$ and $h(k^2) \approx 0$. It is therefore natural to use for the determination of the Σ^0 lifetime the inverse process, which can be realized through the interaction of a Λ particle with an electron in the Coulomb field of a nucleus. This is analogous to Primakoff's idea for the determination of the π^0 lifetime.[3] This possibility of determination of the Σ^0 lifetime has also been indicated by Pomeranchuk and Shmushkevich.[4*]

Since in nucleon - Λ particle collisions the transition $\Lambda \to \Sigma^0$ could take place as a result of strong interactions, and the nucleon cross section is of the order of 10^{-26} cm^2,[5] it would be preferable to use collisions with electrons to excite the particle. The relevant differential cross section is given by

$$d\sigma \approx 2\alpha f^2\, dk/k = \alpha f^2\, dT/T,$$

where $T = k^2/2m_e$ is the energy transferred to the electron if the latter is initially at rest. However the threshold for the reaction $\Lambda + e \to \Sigma^0 + e$ is ≈ 170 Bev.

The differential cross section for the excitation of the Λ particle by a Coulomb center is given by

$$d\sigma^{(\pm)} = Z^2\alpha f^2 S^{(\pm)} k^{-1}\, dk = Z^2\alpha f^2 S^{(\pm)} k^{-2} p_\Lambda p_\Sigma\, d\cos\theta,$$

$$S^{(\pm)} = 1 + \beta_\Lambda\beta_\Sigma\cos\theta - 2\,(\mathbf{k}\mathbf{p}_\Lambda)\,(\mathbf{k}\mathbf{p}_\Sigma)/k^2\varepsilon_\Lambda\varepsilon_\Sigma + m_\Lambda m_\Sigma/\varepsilon_\Lambda\varepsilon_\Sigma,$$

$$\beta_\Lambda = p_\Lambda/\varepsilon_\Lambda, \qquad \beta_\Sigma = p_\Sigma/\varepsilon_\Sigma, \qquad \cos\theta = (\mathbf{p}_\Lambda\mathbf{p}_\Sigma)/p_\Lambda p_\Sigma.$$

All quantities are in the laboratory frame of reference and (±) refers to even or odd relative Λ-Σ^0 parities. In the case of a nucleus it is necessary to include in the expression for $d\sigma$ the factor $F^2(k^2)$, where $F(k^2)$ is the nucleon form factor which may be determined experimentally by scattering electrons off the given nucleus.

If we introduce the quantity $\delta = p_\Lambda - p_\Sigma/p_\Lambda = (m_\Sigma - m_\Lambda)m_\Lambda/p_\Lambda^2$ and assume that $\delta \ll 1$, and $\beta_\Lambda = \beta_\Sigma = \beta$, then we easily obtain at small angles (which are precisely the ones that give the main

*The author is grateful to M. I. Podgoretskii and L. B. Okun' for informing him of this work and to I. Ya. Pomeranchuk for useful discussions.

contribution to the cross section) the following formulas:

$$d\sigma^{(+)} = Z^2\alpha f^2\beta^2 (\delta^2 + \theta^2)^{-2}\theta^2\, d\theta^2,$$
$$d\sigma^{(-)} = Z^2\alpha f^2 [\theta^2 + \delta^2 (1 - \beta^2)] (\delta^2 + \theta^2)^{-2}\, d\theta^2.$$

It is clear from the derived formulas that $d\sigma/d\theta^2$ ($d\sigma/d\theta^2 = \pi d\sigma/d\Omega$) has a sharp peak at $\theta = \delta$ with a width of the order of δ, and that the total cross section slowly (logarithmically) grows. $(d\sigma/d\theta^2)_{max} = Z^2\alpha f^2/4\delta^2$ grows rapidly with the Λ particle energy and may, in principle, exceed (at $\theta \sim \delta$) the cross section for the transition $\Lambda \to \Sigma^0$ due to strong interactions.

It is not hard to estimate the corresponding Λ particle energy. Let us suppose that the strong transition $\Lambda \to \Sigma^0$ is due to the exchange of a quantum of rest mass m. It is then easy to show that the cross section due to strong interactions is given by

$$d\sigma_s = \sigma_0 \frac{p_\Lambda}{m^2} \frac{d\theta^2}{(1 + p_\Lambda^2\theta^2/m^2)^2},$$

where σ_0 is the total cross section. It is natural to assume that σ_0 does not change rapidly with the energy and remains of the order of the geometrical cross section ($\sigma_0 = 2\pi A^{2/3} \times 10^{-26}$ cm^2). Under these assumptions we find that the cross section $d\sigma_e$ (electromagnetic) becomes of the order of $d\sigma_s$ at $p_\Lambda \sim 20$ Bev, $\theta \sim 10^{-4}$ for Z = 90, A = 200; in such a case the nucleus recoil energy is ~ 50 ev (we have set $f = 2\mu_0$, and $m = 2m_\pi$).

It is possible, however, to reduce the contribution due to strong interactions significantly by choosing for the target nucleus one with equal number of neutrons and protons ($I_3 = 0$), since for a system Z with given isotopic spin I and $I_3 = 0$ the transition $\Lambda + Z \to \Sigma^0 + Z$ is forbidden if charge independence is valid. The presence of Coulomb forces results in the nucleus not being in an eigenstate of $\hat{I}^2$, i.e., states with other values of I are admixed. From this point of view the most convenient nuclei are He_2^4 and deuterium. For He_2^4 we may set $|He_2^4> = |I = 0> + \gamma |I = 1>$. A rough estimate gives $|\gamma|^2 \lesssim 10^{-3}$.

If we limit ourselves to realistically measurable angles $\theta \sim 0.5°$, corresponding to $p_\Lambda \sim 3$ Bev and a recoil energy ~ 0.2 Mev, then we obtain for He_2^4 with $|\gamma|^2 \lesssim 10^{-3}$ in an analogous manner to what was done above

$$(d\sigma/d\theta^2)_e/(d\sigma/d\theta^2)_s \gtrsim 1.$$

(In these estimates we ignore contributions due to interference. It is an easy matter, however, to write down the general expression for $d\sigma$.) Consequently, under the above outlined experimental conditions the separation of the electromagnetic transition $\Lambda \to \Sigma^0$ is possible in principle, but it does require measuring cross sections of the order of 10^{-30} cm^2.

In addition to the coherent strong transition $\Lambda \to \Sigma^0$ considered by us, certain incoherent processes will also occur, for example $\Lambda + He_2^4 \to He_2^3 + n + \Sigma^0$. The contribution due to such processes may be reduced by selecting events with low energy recoil nuclei. Further, the angular dependence for such processes will be comparatively smooth, which will also be the case for bremsstrahlung of the Λ particle. The latter, apparently, may be ignored.

The author is grateful to the participants of the seminar of M. A. Markov's group for interest and to L. G. Zastavenko for discussions.

[1] G. Feldman and T. Fulton, Nucl. Phys. **8**, 106 (1958).

[2] W. G. Holladay, Phys. Rev. **115**, 1331 (1959).

[3] H. Primakoff, Phys. Rev. **81**, 899 (1951). A. V. Tollestrup et al, Proceedings of the 1960 Rochester Conference.

[4] I. Ya. Pomeranchuk and I. M. Shmushkevich, Nucl. Phys. **23**, 452 (1961).

[5] Crawford, Cresti, Good, Solmitz, Stevenson, and Ticho, Phys. Rev. Lett. **2**, 174 (1959).

Translation by A. M. Bincer
310

SINGULARITIES OF COSMOLOGICAL SOLUTIONS OF GRAVITATIONAL EQUATIONS. III

E. M. LIFSHITZ, V. V. SUDAKOV, and I. M. KHALATNIKOV

Institute of Physics Problems, Academy of Sciences, U.S.S.R.

Submitted to JETP editor January 25, 1961

J. Exptl. Theoret. Phys. (U.S.S.R.) **40**, 1847-1855 (June, 1961)

A general geometric analysis is given of the situation that leads to the appearance of a time singularity in solutions of gravitational equations in a synchronous system of reference [a system satisfying the conditions (1)]. This analysis, together with the previous results,[1,2] leads to the conclusion that such a singularity is absent in the general case of an arbitrary distribution of matter and gravitation field in space.

IN our previous papers[1,2] (cited below as I and II) the problem was posed of the investigation of the form of the cosmological solutions of the gravitational equations close to a time singularity; different types of such solutions were found. These results, together with the considerations set forth below, allow us to draw definite conclusions on the fundamental question—whether the existence of a time singularity is inevitable in cosmological models of the general theory of relativity.

1. GENERAL SOLUTION WITH FICTITIOUS SINGULARITY

As before, we shall use a reference frame that obeys the conditions

$$g_{00} = -1, \quad g_{0\alpha} = 0. \tag{1}$$

The vanishing of the components $g_{0\alpha}$ of the metric tensor is, as is well known, the necessary condition that guarantees the possibility of synchronization of clocks throughout all space (see, for example, reference 3, Sec. 84); therefore, the reference frame under consideration can be called synchronous. By virtue of the condition $g_{00} = -1$, the coordinate t is the world time in this case.

We have already mentioned in II the fact that the metric determinant g must necessarily vanish over a finite time duration in this reference frame because of one of the gravitational equations. To be precise, from the equation*

$$R_0^0 = \frac{1}{2}\frac{\partial}{\partial t}\varkappa_\alpha^\alpha + \frac{1}{4}\varkappa_\alpha^\beta \varkappa_\beta^\alpha = T_0^0 - \frac{1}{2}T_i^i \leqslant 0 \tag{2}$$

(all the notation is the same as in I and II), and with the aid of the algebraic inequality

$$\varkappa_\alpha^\beta \varkappa_\beta^\alpha \geqslant \frac{1}{3}(\varkappa_\alpha^\alpha)^2$$

we have

$$\frac{\partial}{\partial t}\varkappa_\alpha^\alpha + \frac{1}{6}(\varkappa_\alpha^\alpha)^2 \leqslant 0 \quad \text{or} \quad \frac{\partial}{\partial t}\frac{1}{\varkappa_\alpha^\alpha} \geqslant \frac{1}{6}. \tag{3}$$

For example, let $\kappa_\alpha^\alpha > 0$ at some instant of time. Then, upon decrease in t, the quantity $1/\kappa_\alpha^\alpha$ falls off, having always a finite (non-vanishing) derivative; it therefore must vanish (from the positive side) over a finite time interval. In other words, κ_α^α goes to $+\infty$ and, inasmuch as $\kappa_\alpha^\alpha = \partial \ln(-g)/\partial t$ [see I, (1.8)], then this means that the determinant $-g$ vanishes [but not more rapidly than t^6, from the inequality (3)]. If now $\kappa_\alpha^\alpha < 0$ at the initial moment, then this same result is obtained for increasing time.

We note that the presence of matter is not essential in this derivation: a zero on the right hand side of Eq. (2) (in the case of empty space) is sufficient to obtain the inequality (3).

However, this result still in no way proves the necessity of the existence in the metric of a real (physical) singularity that is not eliminated by a transformation of the reference frame. The singularity can be shown to be nonphysical, fictitious, associated simply with the character of the reference frame selected. The geometrical considerations given below show that this singularity, which is inescapable in the synchronous system, is actually fictitious in the general case.

In the synchronous reference frame, the time lines are goedesics in four-space. Actually, the four-vector $u^i = dx^i/ds$ tangent to the world line $x^1, x^2, x^3 = \text{const}$ has the components $u^\alpha = 0$ and

*For the energy-momentum tensor of the matter $T_i^k = (p + \varepsilon) \times u_i u^k + p\delta_i^k$ we have (in a synchronous reference frame)

$$T_0^0 - \frac{1}{2}T_i^i = -\frac{1}{2}(\varepsilon + 3p) - (p + \varepsilon)u_\alpha u^\alpha,$$

whence the negative character of this quantity is obvious. The same is valid also for the energy-momentum tensor of the electromagnetic field [$T_i^i = 0$, $T_0^0 = -(E^2 + H^2)/8\pi$].

$u^0 = 1$, and automatically satisfies the geodesic equations

$$du^i/ds + \Gamma^i_{kl} u^k u^l = \Gamma^i_{00} = 0, \quad (4)$$

inasmuch as the Christoffel symbols Γ^0_{00}, Γ^α_{00} in the conditions (1) are identically equal to zero. It is also easy to see that these lines are normal to the hypersurfaces $t = \text{const}$. Actually, the four-vector normal to such a hypersurface $n_i = -\partial t/\partial x^i$ has the covariant components $n_\alpha = 0$ and $n_0 = -1$. The corresponding contravariant components for the conditions (1) are $n^\alpha = 0$ and $n^0 = 1$, i.e., they are identical to the components of the four-vector u^i tangent to the time lines.

Conversely, these properties can be used for the geometrical construction of a synchronous reference frame in an arbitrary space-time. For this purpose, we choose as a reference any spatial hypersurface, i.e., a hypersurface the normal to which at each point has a time-like direction (lying within the light cone with vertex at this same point); all the interval elements on such a hypersurface are space-like. We then construct a family of geodesic lines normal to this hypersurface. If we now choose these lines as the coordinate time lines, and define the time coordinate t as the length of the geodesic line measured from the original hypersurface, we obtain a synchronous reference frame.

It is clear that such a construction, and thereby the choice of the synchronous reference frame, is always possible in principle.

But the geodesic lines of an arbitrary family generally intersect one another on certain enveloping hypersurfaces—the four-dimensional analogs of the caustic surfaces of geometrical optics. In other words, there is a geometrical reason for the appearance of the singularity, connected simply with the specific properties of the synchronous reference frame; obviously, therefore, it has no physical character.

An arbitrary metric of four-space also generally allows the existence of non-intersecting families of geodesics. On the other hand, the property of the curvature of the real space-time, which is expressed by the inequality $R^0_0 \leq 0$, shows that the metric allowed by the gravitational equations generally excludes the existence of such families, so that the time lines in any synchronous system of reference must necessarily intersect.*

From the analytic point of view, this means that in the synchronous reference frame the equations of gravitation have a general solution with a fictitious time singularity. Such a solution (for empty space) must contain eight arbitrary functions of the three space coordinates: 1) four "physically different" functions that are necessary to specify the gravitational field at some initial moment (see II, Sec. 1), 2) a single function which determines the initial hypersurface in the geometric construction described above, 3) three functions associated with the fact that the conditions (1) still permit arbitrary transformations of the space coordinates not involving the time.

The character of the singularity in the metric is already clear from geometric considerations. Above all, the caustic hypersurface must be time-like, inasmuch as it in any event includes time-like intervals in itself—elements of length of the geodesics at points of their tangency with the caustic.*

Furthermore, one of the principal values of the metric tensor vanishes on the caustic, corresponding to the fact that the distance between two neighboring geodesics (which intersect each other at their point of tangency to the caustic) vanishes (the corresponding principal direction obviously lies along the normal to the caustic). This distance vanishes as the first power of the distance to the point of intersection. Therefore, the principal value of the metric tensor, and with it the entire determinant $-g$, vanishes as the square of the distance just mentioned.

The method of analytic determination of the form of the general solution under study, close to a singularity, is described in the Appendix. One can make use of the arbitrariness in the selection of the spatial coordinates to write the first terms of the expansion of the metric in the neighborhood of the singularity in a form for which the spatial element of length d is given by the formula

$$dl^2 = g_{\alpha\beta} dx^\alpha dx^\beta = a_{ab} dx^a dx^b + (t - \varphi)^2 a_{33} dx_3^2 + 2(t - \varphi)^2 a_{a3} dx^a dx^3 . \quad (5)$$

Here the indices a, b run over the values 1, 2; the quantities a_{ab}, a_{3a}, a_{33}, are functions of all three coordinates. This form still permits an arbitrary transformation $x^{3'} = x^{3'}(x^1, x^2, x^3)$, which reduces to the transformation of the quantities a_{a3}, a_{33}, and the first terms of the expansion

*We naturally avoid the trivial exception – that of pencils of parallel lines in flat four-space. We note, however, that in the arbitrary selection of an initial hypersurface, the family of geodesic lines normal to it intersects also in the flat four-space. This circumstance reveals with particular clarity the fictitious character of the resultant singularity.

*A hypersurface is called time-like when the normal to it lies outside the light cones. The elements of the interval in such a hypersurface can lie both inside and outside the light cones, i.e., they can be both time- and space-like.

of the components g_{ab}. For example, one can use them to cause the function φ, which gives the shape of the caustic hypersurface, to be $\varphi = x^3$. After all this, only the transformations of the two coordinates x^1 and x^2 into one another remain. Therefore, only five arbitrary functions should remain in the metric (three coordinates), so that the six functions a_{ab}, a_{a3}, a_{33} must be related, as the consequence of the equations of gravitation, by a single equation.

The singularity in the metric (5) is not simultaneous—different space points achieve it at different moments of time. However, it is easy to see that one can always construct such a synchronous reference frame in which the singularity (fictitious) will be reached simultaneously throughout the entire space. It is clear that such a singularity cannot be located on the hypersurface tangent to the time lines at the points of their intersection, since the existence of time-like intervals at these points excludes beforehand the simultaneity of the singularity. Therefore, the time lines must intersect at a "manifold of points," which has a smaller number of dimensions than the hypersurface, i.e., which is a certain two-dimensional surface in four-space; it can be called the focal surface of the corresponding family of geodesics. By selecting an arbitrary focal surface, constructing all possible directions of normals to it from each of its points (all directions in the two-dimensional plane normal to the focal surface), and drawing geodesics in these directions, we at the same time construct a synchronous reference frame possessing the required property.

Thus the general solution of the gravitational equations can also be represented (by corresponding choice of a synchronous reference frame) in a form in which the singularity is simultaneous for the entire space. Of course, in such a form it contains the same four physically different arbitrary functions (three space coordinates) which suffice to specify the arbitrary initial distribution of the gravitational field. In comparison with the solution in the form (5), it contains one less arbitrary function: if we construct a synchronous reference frame, beginning with some initial hypersurface, then nowhere can an arbitrary hypersurface lead to the focusing of the geodesic lines constructed along the normals to it.*

As has already been mentioned, the fictitious nature of the singularity in the solutions considered is already obvious from its mode of construction; the singularity can be removed by transformation of the coordinates, but only at the price of foregoing synchronism of the reference frame. One can also establish directly the fact that, for example, the scalar component of the curvature tensor $R_{iklm}R^{iklm}$ has no singularity.

The introduction of matter does not change the qualitative character of the considered solutions, and the density of matter remains finite. This becomes evident, in particular, if we note that matter moves (in the synchronous reference frame) along world lines that do not coincide with the time lines, and are, generally speaking, not even geodesics.

Only the case of "dust-like" matter is an exception (the equation of state is $p = 0$). Such matter moves along geodesic lines. Therefore, the condition of synchronism of the reference frame in this case does not contradict the condition of its "accompaniment" of matter (which means that the matter moves along time lines), so that the reference frame can be chosen to be not only synchronous but at the same time accompanying (in the general case of an arbitrary equation of state, this is of course impossible). The density of matter then becomes infinite on the caustic simply as the result of the intersection of the trajectories of the particles. However, it is clear that this singularity of the density has no physical character, and is removed by the introduction of a conveniently small, but non-zero, value of the pressure of the matter.

2. GENERAL CONCLUSIONS

The geometric considerations set forth in the previous section essentially solve the problem of obtaining for the gravitational equations a general solution that has a singularity in the time—a solution the existence of which in the synchronous reference frame follows, as we have seen, from the inequality (3). However, the singularity in this solution is shown to be not physical but connected only with the specific properties of the reference frame employed.

*In a certain sense, this solution corresponds to a zero value of the function φ in the solution of (5); in this case the square of the interval $ds^2 = dt^2 - dl^2$ reduces at the singularity ($t = 0$) to the quadratic form $ds^2 = -a_{ab}dx^a dx^b$ of only two differentials. We emphasize, however, that it is not at all impossible to obtain the expansion of the metric in the neighborhood of such a singularity simply by setting $\varphi = 0$ in the formulas which refer to the solution of the form (5). We also point out that such a reference frame does not include all of space-time. This is clear from the fact that all the points of each hypersurface $t = \text{const}$ lie in it at the same time-distance from the spatial focal surface, i.e., these hypersurfaces as a whole are located in regions of absolute future or absolute past relative to the focal surface.

By the same token, any basis vanishes for the existence of a solution in addition to this one which would possess a real singularity and would also be general. In fact, an investigation, carried out by two of us, of the possible forms of such singularities has shown that the broadest solution with a real singularity is the solution found in II, with the metric

$$g_{\alpha\beta} \cong t^{2p_1} l_\alpha l_\beta + t^{2p_2} m_\alpha m_\beta + t^{2p_3} n_\alpha n_\beta ,$$
$$p_1 + p_2 + p_3 = p_1^2 + p_2^2 + p_3^2 = 1 . \qquad (6)$$

However, it contains one less arbitrary function of the coordinates then would be required for the general solution. Therefore, this solution also is only a special case, in spite of its broadness.*

Such a solution is unstable; there exists a type of small perturbations whose action destroys the state described by this solution. Inasmuch as the singularity in the synchronous system cannot vanish in general, this means that it goes over into a fictitious singularity under the action of the perturbation. If in the transformation process one sees to it that the singularity is simultaneous (which is always possible), then the process must terminate in a transition to the solution described in Sec. 1, with a simultaneous singularity for all space.

It is interesting to note that a solution of the form (6) exists even in the absence of matter, i.e., for empty space (and it then contains three physically different arbitrary functions—see II). The geometric constructions given in Sec. 1 also do not depend on the presence or absence of matter. All this supports the idea that the most general properties of cosmological solutions relative to the singularities in time appear already in the case of empty space, and matter does not change these properties in any qualitative fashion. This result is natural if we note that the gravitational properties of a set of short-wave gravitational waves chosen in appropriate fashion can imitate the gravitational properties of matter (with an equation of state $p = \epsilon/3$). The isotropic (Friedmann) solution occupies an exceptional position in this sense, as does its generalization, considered in I; these solutions exist only for a space filled with matter. However, this exception is connected with the high symmetry (homogeneity) of the distribution of matter peculiar to this solution, a distribution which cannot be realized in the imitation shown.

All the foregoing leads to the fundamental conclusion that the presence of a time singularity is not an essential property of the cosmological model of the general theory of relativity, and the general case of an arbitrary distribution of matter and gravitational field does not lead to the appearance of such a singularity.

We have referred constantly (here and in I, II) to the direction of approach to the singularity as being one wherein the time is decreased. In actuality, in view of the symmetry of the gravitational equations relative to time reversal, one could speak with equal success of the approach to the singularity in the direction of increasing time. Physically, however, in view of the physical nonequivalence of future and past, there is an essential difference between the two cases relative to the very statement of the problem. A singularity in the future can have physical meaning only if it is attainable under completely arbitrary conditions given at some previous instant of time; it is clear that there is no basis for maintaining that the distribution of matter and field, attained at some given moment in the process of evolution of the universe, corresponds to the specific conditions required for the realization of some particular solution of the equations of gravitation which possess a real singularity. Furthermore, if such a distribution is attained for any reason at some instant of time it will be inevitably destroyed subsequently, at least by the inevitable thermodynamic (or quantum) fluctuations. Therefore, the results that have been set forth exclude the possibility of the existence of a singularity in the future, and mean that the contraction of the world (if it should occur in general) should in final analysis alternate with its expansion. As to the past, a consideration based only on gravitational equations can only superimpose definite limitations on the attainable forms of the initial conditions, the full explanation of the character of which is impossible on the basis of the existing theory.

Finally, let us make one remark. All the previous study has been based on Einstein's general equations of gravitation in the form in which they follow logically from the general theory of reltivity. At the present time there exist no astronomical or theoretical grounds for introducing an additional "cosmological term" in these equations. This applies even more strongly to the completely arbitrary and groundless changes introduced into the gravitational equation by F. Hoyle.

*The systematic construction of all possible types of solutions with real singularities will be given in a subsequent paper. We take this opportunity to correct two errors which appear in II, in the formulas referring to the solution of (6). In Eq. (2.16) for $P^l_{l'}$, $P^m_{m'}$, and P^n_n the factor t^{-2p_3} is omitted. On the right hand side of Eq. (3.6) of II, $u_0^{(0)}$ should appear instead of $u_n^{(0)}$.

In conclusion, we express our sincere gratitude to L. D. Landau for numerous stimulating discussions. We also thank L. P. Pitaevskii for discussion of a number of questions.

APPENDIX

ANALYTIC CONSTRUCTION OF A GENERAL SOLUTION WITH FICTITIOUS SINGULARITY

By choosing the space coordinates in the fashion shown in the text (we designate them as $x^1 = x$, $x^2 = y$, $x^3 = z$), we seek the first terms of the expansion of the components of the metric tensor in the form

$$g_{ab} = a_{ab} + \tau b_{ab}, \quad g_{a3} = \tau^2 a_{a3}, \quad g_{33} = \tau^2 (a_{33} + \tau b_{33}),$$

where $\tau = t - z$, and the indices, which are denoted by the Latin letters (a, b, c, ...), take on the values 1 and 2 everywhere. All the coefficients of the expansion are functions of x, y, and t (for reasons which are made clear below, such an expansion is more convenient than one in τ for given x, y, and z). The components of the corresponding contravariant tensor are:

$$g^{ab} = a^{ab} - \tau b^{ab}, \quad g^{a3} = -a^{a3}, \quad g^{33} = \tau^{-2}(a^{33} - \tau b^{33}).$$

Here a^{ab} is a two-dimensional tensor inverse to the tensor a_{ab} and $a^{33} = 1/a_{33}$. All the operations of raising and lowering of indices for the other quantities are carried out with the help of a_{ab} and a_{33}; thus,

$$b^{ab} = a^{ac} a^{bd} b_{cd}, \quad a^{a3} = a^{ab} a^{33} a_{b3} \quad \text{etc.}$$

The components of the tensor $\kappa_{\alpha\beta}$ are computed, by definition, as

$$\varkappa_{\alpha\beta} = \dot{g}_{\alpha\beta}, \quad \varkappa_{\alpha}^{\beta} = g^{\beta\gamma}\varkappa_{\alpha\gamma}, \quad \varkappa^{\alpha\beta} = -\dot{g}^{\alpha\beta}$$

(the dot denotes everywhere differentiation with respect to t).

We carry out all the calculations below for the case of an empty space, and accordingly we use Eqs. (2.1) — (2.3) of II. First we find

$$R_0^0 \cong \frac{1}{2}\dot{\varkappa}_3^3 + \frac{1}{4}(\varkappa_3^3)^2 \cong \frac{1}{\tau a_{33}}(b_{33} + \dot{a}_{33}) = 0,$$

whence $b_{33} = -\dot{a}_{33}$. Further, simple calculation yields

$$R_{ab} \cong P_{ab} \cong -b_{ab}/2\tau^3 a_{33} = 0,$$

whence $b_{ab} = 0$, i.e., there are no terms linear in τ in the expansion of g_{ab} (this circumstance naturally simplifies the subsequent calculations, including the advantage of an expansion for given x, y, and t). The remaining equations do not give anything new in the approximations used.

Taking these results into account, we now write

$$\begin{aligned} g_{ab} &= a_{ab} + \tau^2 c_{ab} + \tau^3 d_{ab}, \\ g_{a3} &= \tau^2 (a_{a3} + \tau b_{a3}), \\ g_{33} &= \tau^2 (a_{33} - \tau \dot{a}_{33} + \tau^2 c_{33}). \end{aligned} \tag{A.1}$$

Here we have written out those of the subsequent terms of the expansion which are jointly determined in the transition to the next approximation in the gravitational equations.

We should now compute the first nonvanishing terms in Eqs. (2.1) — (2.3) of II, which appear upon substitution in them of Eqs. (A.1). These rather cumbersome computations are materially simplified if g_{33} is represented temporarily in the form of an expansion in powers of τ for given x, y, and z (and not x, y, and t). Carrying out the corresponding expansion of the function $a_{33}(x, y, z+\tau)$ [in the function $c_{33}(x, y, t)$ it suffices simply to replace t by z] we get

$$g_{33} = \tau^2 [a_{33}(x, y, z) + \tau^2 C_{33}(x, y, z)],$$

$$C_{33} = c_{33}(x, y, z) - \tfrac{1}{2} a''_{33}(x, y, z)$$

(′ denotes differentiation with respect to z), i.e., the term $\sim \tau^3$ drops out of the expansion. Of course, application of different expansions for different components $g_{\alpha\beta}$ requires a subsequent rereduction to like variables in the final result of the calculation; upon calculation of the first nonvanishing terms in the equations, however, this reduction is seen to amount simply to a replacemeny of z by t.

The contravariant components of the metric tensor will now be*

$$\begin{aligned} g^{ab} &= a^{ab} + \tau^2 (-c^{ab} + a_3^a a^{3b}) + \tau^3 (-d^{ab} + a_3^a b^{3b} + a_3^b b^{3a}), \\ g^{3a} &= -a^{a3} - \tau b^{a3}, \\ g^{33} &= \tau^{-2} a^{33} - C^{33} + a_a^3 a^{3a}. \end{aligned} \tag{A.2}$$

The determinant is

$$-g = \tau^2 a_{33} |a_{ab}| [1 + \tau^2 (C_3^3 + c_a^a - a^{a3} a_{a3})].$$

The components of the tensors $\kappa_{\alpha\beta}$ and $P_{\alpha\beta}$ are computed according to the given metric. The left sides of Eqs. (2.1) — (2.3) of II are then computed. We write down only the final result here of the rather involved calculations [after which we again return to the expansion of g_{33} in the form (A.1)]:

*If $g_{\alpha\beta} = g_{\alpha\beta}^{(0)} + h_{\alpha\beta}$ (where $h_{\alpha\beta}$ are small), then $g^{\alpha\beta} \cong g^{\alpha\beta(0)} - h^{\alpha\beta} + h_{\gamma}^{\alpha} h^{\beta\gamma}$. In the given case, we mean by $g_{\alpha\beta}^{(0)}$ the tensor with components $g_{ab}^{(0)} = a_{ab}$, $g_{a3}^{(0)} = 0$, $g_{33}^{(0)} = \tau^2 a_{33}$.

$$R_0^0 = c_a^a + 3c_3^3 - \tfrac{3}{2}\ddot{a}_{33}a^{33} - a^{3a}a_{3a} + \tfrac{1}{2}(\dot{a}_{ab}a^{ab})^{\cdot} + \tfrac{1}{4}\dot{a}_{ac}\dot{a}_{bd}a^{ab}a^{cd} = 0, \quad (A.3)$$

$$R_a^0 = \frac{1}{\tau a_{33}}[k_0 a_{a3} + \dot{a}_{a3} + 3b_{a3} - \dot{a}_{ab}a_3^b + a_{33}k_a] = 0, \quad (A.4)$$

$$R_3^0 = \frac{\tau}{2}[3a_{a3}b^{a3} + \dot{a}_{ab}c^{ab} - 3d_a^a - \dot{a}_{ab}a_3^a a^{3b} - 2\dot{c}_{ab}a^{ab} + \dot{a}_{a3}a^{a3} + k_0 a_{a3}a^{a3}] = 0, \quad (A.5)$$

$$R_a^b = -\frac{1}{2\tau a_{33}}[c_a^b k_0 + 3d_a^b + a_{3a}{}^{;b} + a_{3;a}^b - a_{33}a^{bc}\dot{a}_{ac}] = 0, \quad (A.6)$$

$$R_a^3 = \frac{1}{2\tau a_{33}}[-2c_{a;b}^b + 2c_{b;a}^b + c_a^b k_b - c_b^b k_a + 3\dot{a}_{3a} + 3b_{a3} - \dot{a}_{ab}a_3^b + \dot{a}_{bc}a^{bc}a_{3a}] = 0. \quad (A.7)$$

Here we use the notation

$$k_0 = (\ln a_{33})^{\cdot}, \quad k_a = \partial \ln a_{33}/\partial x^a,$$

and the operations of covariant differentiation are carried out over the two-dimensional tensor c_{ab} and the vector a_{3a} in the two-dimensional space with metric $g_{ab} = a_{ab}$.

So far as the component R_3^3 is concerned, it is identical in its principal terms with the sum R_a^a. Therefore, to obtain one additional relation it is necessary to compute the first nonvanishing terms in the difference $R_a^a - R_3^3$; in this case, it is convenient to subtract R_0^0 from it; this term is of the same order of magnitude. As a result of the calculation, we obtain

$$R_a^a - R_3^3 - R_0^0 = K + \tfrac{1}{4}(\dot{a}_{ab}a^{ab})^2 - \tfrac{1}{4}\dot{a}_{ac}\dot{a}_{bd}a^{ab}a^{cd} - 6c_3^3 + 3\ddot{a}_{33}a^{33} + a^{33}[c_{ab}c^{ab} - (c_a^a)^2] = 0, \quad (A.8)$$

where K is the two-dimensional scalar curvature derived from the metric $g_{ab} = a_{ab}$ (the two dimensional analog K_{ab} of the tensor T_{ik} reduces, as is well known, to a scalar: $K_{ab} = \frac{1}{2}Kg_{ab}$).

Equations (A.4) determine the coefficients b_{a3} (for the given functions a_{ab}, a_{a3}, and a_{33}). Then, eliminating d_a^b from Eqs. (A.5) and (A.6), we obtain the single equation

$$\dot{a}_{ab}c^{ab} + c_a^a k_0 - 2\dot{c}_{ab}a^{ab} = -2a_{3;a}^a + a_{33}a^{ab}\dot{a}_{ab} + k_a a_3^a,$$

which, together with the two equations of (A.7),

$$2c_{b;a}^b - 2c_{a;b}^b + c_a^b k_b - c_b^b k_a = -2\dot{a}_{3a} - \dot{a}_{bc}a^{bc}a_{3a} + k_0 a_{a3} + k_a a_{33},$$

determines the three quantities c_{ab}. The quantity c_{33} is determined from Eq. (A.3) and d_{ab} from Eq. (A.6). Equation (A.8) can then be considered as the relation connecting the quantities $a_{\alpha\beta}$ with one another.

Thus, all the coefficients of the expansion (A.1) are determined from the six coefficients a_{ab}, a_{a3}, and a_{33}, which are connected with one another by a single relation. In other words, the metric (A.1) contains five arbitrary functions.

[1] E. M. Lifshitz and I. M. Khalatnikov, JETP **39**, 149 (1960), Soviet Phys. JETP **12**, 108 (1961).

[2] E. M. Lifshitz and I. M. Khalatnikov, JETP **39**, 800 (1960), Soviet Phys. JETP **12**, 558 (1961).

[3] L. D. Landau and E. M. Lifshitz, Теория поля (Field Theory), 3rd edition, Fizmatgiz, 1960.

Translated by R. T. Beyer
311

SCATTERING OF K MESONS ON NUCLEONS AT LARGE ORBITAL MOMENTA

Yu. P. NIKITIN

Submitted to JETP editor January 25, 1961

J. Exptl. Theoret. Phys. (U.S.S.R.) 40, 1856-1858 (June, 1961)

Peripheral KN scattering is investigated by taking into account only two-pion exchange. The KN-scattering phase shifts are expressed in terms of the $K\pi$ coupling constant. A phase-shift analysis of experimental data on KN scattering, in which high phase shifts ($l \gtrsim 2$) are taken into account, can yield in principle information on the magnitude of the $K\pi$ interaction. The contribution of the single-hyperon diagram to the KN-scattering phase shift is discussed.

OKUN' and Pomeranchuk[1] have shown that in KN scattering with large orbital momenta the principal role is played by the two-pion diagram shown in Fig. 1. The scattering phase shifts at large orbital momenta are determined by the absorptive part of the amplitude in the vicinity of the nearest singularity of the transferred momentum q^2 (cf. reference 2). In this case the nearest singularity is located at $q^2 = 4\mu^2$, and the next singularity is only at $q^2 = 16\mu^2$. The large distance between these nearest singularities gives grounds for hoping that the two-pion diagram will make the main contribution to the phase shift of the KN scattering even when the orbital momenta are not very large.

According to the unitarity relation, the absorptive part of the diagram of Fig. 1 is determined by the amplitudes of the πN and $K\pi$ scattering. The general expression for the amplitude of the $K\pi$ scattering is

$$F_{\alpha\beta}(k_1, k_2, k_3, k_4) = F^{(1)}\delta_{\alpha\beta} - i\varepsilon_{\alpha\beta\gamma}\tau^K_\gamma F^{(2)}, \qquad (1)$$

where $F^{(1)}$ and $F^{(2)}$ are invariant functions of the scalar products of the momenta k_1, k_2, k_3, and k_4; α and β are the isotopic variables of the pion; τ^K is the isotopic spin of the kaon. The following symmetry conditions apply: as $k_3 \to k_4$ we have $F^{(1)} \to F^{(1)}$ and $F^{(2)} \to -F^{(2)}$; k_3 and k_4 are the pion momenta before and after scattering.

The amplitude of the πN scattering near the point $Q^2 = 4\mu^2$ has been calculated by Galanin et al.[2] and has the form

$$f_{\alpha\beta}\left(p, p';\ k+\frac{q}{2};\ k-\frac{q}{2}\right) = g^2\,\bar{u}(p')\left\{\tau^N_\beta\tau^N_\alpha\frac{\hat{k}}{\mu^2 - q^2/2 - 2kp} - \tau^N_\alpha\tau^N_\beta\frac{\hat{k}}{\mu^2 - q^2/2 + 2kp} + \frac{\alpha}{m}\delta_{\alpha\beta}\right\}u(p). \qquad (2)$$

The notation in (2) is as follows: $k_3 = k + q/2$; $k_4 = k_{q/2} - k$; p and p' are the nucleon momenta before and after scattering; τ^N is the isotopic spin of the nucleus; $\bar{u}(p')$ and $u(p)$ are four-component spinors describing the initial and final spin states of the nucleus, respectively; $g^2 = 14.5$ and $\alpha \approx 1.2$.

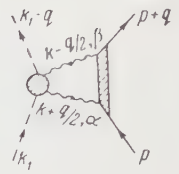

FIG. 1. Principal diagram of KN scattering at large orbital momenta.

The absorptive part of the amplitude of the KN scattering in the two-pion approximation, with allowance for Eqs. (1) and (2), can be readily calculated:

$$A(E, x) \approx \frac{3\lambda g^2\,\bar{u}(p')\,u(p)}{4(E+\omega)}\left[(\alpha - 1)\,x + \frac{\varepsilon}{2}\tan^{-1}\frac{2x}{\varepsilon}\right], \qquad (3)$$

where $x^2 = q^2/4\mu^2 - 1$, $\epsilon = \mu/m$ (μ is the pion mass and m the nucleon mass), ω is the kaon energy in the c.m.s., and E is the nucleon energy.

In the derivation of (3) it was assumed that the amplitudes of the $K\pi$ scattering are smooth functions of k in the region $|k^2_{\text{eff}}| \lesssim \mu^2/L$ (cf. references 2 and 3), and terms which are small near $q^2 = 4\mu^2$ were disregarded. The amplitude $F^{(2)} = \lambda$ was taken out at the point $q^2 = 4\mu^2$ and $k^2 = 0$ (see also reference 3), and the amplitude $F^{(2)}$ was discarded in view of the oddness in k. If we use for the $K\pi$ interaction the Lagrangian $\mathcal{L} = -4\pi\lambda\varphi^+_K\varphi_K\varphi^2_\alpha$, then λ is the constant of the πK interaction. If the functions $F^{(1)}$ and $F^{(2)}$ are not sufficiently smooth near this point, the expression (3) changes appreciably.

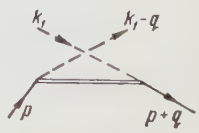

FIG. 2. Single-hyperon diagram of KN scattering.

The phase shifts of the KN scattering are expressed in terms of the absorptive part (3) as follows:[3]

$$\frac{(l+1)\,\delta_{l+}-l\delta_{l-}}{2l+1}\approx\frac{2\mu\xi}{\pi}\,Q_l(1+2\xi^2)\int_0^\infty dx^2\,e^{-Lx^2}\,A_0(x^2),$$

$$\frac{l\,(\delta_{l+}-\delta_{l-})}{2l+1}\approx\frac{4\mu^3\sqrt{1+\xi^2}}{\pi}\,Q_l(1+2\xi^2)\int_0^\infty dx^2\,e^{-Lx^2}\,A_1(x^2), \tag{4}$$

where $\xi=\mu/p$, $L=(l+1)\,\xi/\sqrt{1+\xi^2}$, $Q_l(1+2\xi^2)$ is the Legendre function of the second kind, A_0 and A_1 are the absorptive parts of the KN scattering amplitude without and with spin flip, respectively, δ_{l^+} and δ_{l^-} are the KN-scattering phase shifts, corresponding to a total momentum $j=l\pm\frac{1}{2}$. Formulas (4) are valid for $L\gg 1$. We note that by virtue of the assumed smooth behavior of the amplitude of the $K\pi$ scattering, the phase shifts are independent of the isotopic variables: $\delta_{l\pm}^{T=1}\approx\delta_{l\pm}^{T=0}$.

If we are interested in orbital momenta that are not very large, $L\ll 4m^2/\mu^2=180$, we readily obtain from (3) and (4)

$$\frac{(l+1)\,\delta_{l+}+l\delta_{l-}}{2l+1}\approx\frac{3g^2\lambda\mu\xi Q_l(1+2\xi^2)}{4\sqrt{\pi}L^{3/2}(E+\omega)}\left[\alpha-1+\sqrt{\pi}\,\zeta\left(1-\frac{2\zeta}{\sqrt{\pi}}\right)\right],$$

$$\frac{l\,(\delta_{l+}-\delta_{l-})}{2l+1}\approx\frac{3g^2\lambda\mu^2\varepsilon Q_l(1+2\xi^2)}{4\sqrt{\pi}L^{3/2}(E+m)(E+\omega)}\sqrt{1+\xi^2}\left[\alpha-1+\sqrt{\pi}\,\zeta\left(1-\frac{2\zeta}{\sqrt{\pi}}\right)\right], \tag{5}$$

where $\zeta=\varepsilon L^{1/2}/2\ll 1$ and $1\ll L\ll 180$.

It follows from (5) that in the approximation which is nonrelativistic with respect to the nucleon, $p\ll m$, but $p\sim\mu$ and $l\gg 1$, the ratio is

$$\frac{\delta_{l+}-\delta_{l-}}{\delta_{l+}+\delta_{l-}}\approx\frac{1}{\sqrt{2}}\left(\frac{\mu}{m}\right)^2,\ \text{i.e.}\ \delta_{l+}\approx\delta_{l-}. \tag{6}$$

This conclusion is also the consequence of the assumed smooth behavior of the amplitude of the $K\pi$ scattering. We note that by virtue of this assumption the peripheral phases of the elastic $\widetilde{K}N$ scattering are also calculated by formula (5) ($\widetilde{K}$ is the symbol for the anti-kaon).

In the analysis of the πN scattering[3] it was found that at small orbital momenta, $l\sim 2$, an important role may be played by the single-nucleon pole diagram, and therefore the two-pion approximation is not suitable for such small orbital momenta.

In the case of KN scattering, even a rough estimate* of the contribution of the single-hyperon states (Fig. 2) shows that regardless of the type of the KNY coupling (Y stands for the hyperon), the two-pion D phases predominate (accurate to $10-15\%$) over the single-hyperon phases in the kaon energy region $\omega_{kin}^{lab}\lesssim 180$ Mev, while the F phases predominate in the region $\omega_{kin}^{lab}\lesssim 400$ Mev. The calculated values of the phase shifts (for $\lambda<5$) do not exceed the experimental errors.[5]

Thus, the phase-shift analysis of the KN scattering, with allowance for the large phases ($l\gtrsim 2$), can in principle yield information on the magnitude of the $K\pi$ interaction, and also throw light on the limits of applicability of the two-pion approximation and its practical significance.

The author is grateful to I. Ya. Pomeranchuk for suggesting the topic and for guidance, and also to A. D. Galanin and A. F. Grashin for many useful advices and a discussion of the results.

[1] L. V. Okun' and I. Ya. Pomeranchuk, JETP **36**, 300 (1959), Soviet Phys. JETP **9**, 207 (1959).

[2] Galanin, Grashin, Ioffe, and Pomeranchuk, JETP **37**, 1663 (1959), Soviet Phys. JETP **10**, 1179 (1960).

[3] A. D. Galanin, JETP **38**, 243 (1960), Soviet Phys. JETP **11**, 177 (1960).

[4] R. T. Matthews and A. Salam, Phys. Rev. **110**, 569 (1958).

[5] L. W. Alvarez, Paper delivered at the Ninth International Conference on High-Energy Physics, Kiev, 1959.

Translated by J. G. Adashko
312

*For a rough estimate we used the KNY coupling constants given by Matthews and Salam,[4] and the $K\pi$ interaction constant was estimated at $\lambda\sim(m_k+\mu)\sqrt{\sigma_{K\pi}/4\pi}$, where $\sigma_{K\pi}$ is the $K\pi$-scattering cross section at low energies (it was assumed that $\sigma_{K\pi}\sim 1/\mu^2$).

EFFECT OF ANISOTROPY ON THRESHOLD PHENOMENA IN SUPERCONDUCTORS

V. L. POKROVSKII and M. S. RYVKIN

Institute for Radiophysics and Electronics, Siberian Division, Academy of Sciences, U.S.S.R.; Novosibirsk Pedagogical Institute

Submitted to JETP editor January 26, 1961

J. Exptl. Theoret. Phys. (U.S.S.R.) 40, 1859-1865 (June, 1961)

We consider the absorption of ultrasound and of electromagnetic waves in anisotropic superconductors at absolute zero at frequencies close to the threshold frequency ($\omega \sim 10^{11}$ to 10^{12} sec^{-1}). We show that the threshold frequency depends on the direction of propagation of the waves. The absorption near threshold is in the acoustic case proportional to $(\omega - \Omega_0)^{1/2}$ (Ω_0 is the threshold frequency). There is an essential difference in the electromagnetic case for the absorption in Pippard, London, or intermediate superconductors. If one averages over the direction, one obtains the linear increase of the absorption near threshold, as predicted for the isotropic model by the BCS theory,[1,2] only for intermediate superconductors.

INTRODUCTION

USING the conservation laws for energy and momentum we get for the absorption of a phonon (or photon) combined with the dissociation of a Cooper pair

$$\Phi(\mathbf{p}, \mathbf{q}) \equiv \varepsilon_{\mathbf{p}} + \varepsilon_{\mathbf{p}-\mathbf{q}} = \sqrt{\xi_{\mathbf{p}}^2 + \Delta_{\mathbf{p}}^2} + \sqrt{(\xi_{\mathbf{p}} - \mathbf{vq})^2 + \Delta_{\mathbf{p}-\mathbf{q}}^2} = \omega \qquad (1)$$

(we use throughout the notation introduced earlier[3]). The threshold frequency is determined by the minimum value of $\Phi(\mathbf{p}, \mathbf{q})$ for fixed $\mathbf{q}$. In the isotropic case, Δ = const and the minimum which is equal to 2Δ is attained on the line $\theta = \pi/2$ (θ is the angle between $\mathbf{v}$ and $\mathbf{q}$). The absorption of ultrasound and electromagnetic waves near threshold in the isotropic model was considered in a number of papers[1,2,4,5] and their results lead to the following conclusions.

The absorption of ultrasound[5] near threshold increases from zero to a magnitude of the order of c/v, where c is the sound velocity (strictly speaking this increase occurs over an exponentially small region of frequencies).

The absorption of electromagnetic waves[1,2,4] near threshold increases linearly as $\sim \omega - 2\Delta$.

We shall show in the following that the anisotropy of a superconductor changes the frequency dependence of the absorption fundamentally. This is caused by two circumstances:

1) The minimum of the left-hand side of (1) occurs for anisotropic superconductors not on the line $\theta = \pi/2$ as in the isotropic case, but in separate points on the Fermi surface. Because of this there is near threshold a contribution to the absorption from an appreciably smaller part of the Fermi surface than in the isotropic case.

2) In the electromagnetic case the decrease in the region of allowed dissociation of a pair is accompanied by an appreciable increase in the probability for dissociation and this leads to an increase in the absorption in the region immediately adjoining the threshold as compared to the absorption in isotropic superconductors.

ABSORPTION OF ULTRASOUND

We use a diagram technique for our calculations. To find the absorption it is necessary to evaluate the imaginary part of the polarization operator $\Pi(\mathbf{q}, \omega)$. We have shown earlier[5] that one can perform the calculation in the weak coupling approximation and that the results remain qualitatively correct also in the strong coupling approximation, which in actual fact occurs in superconductors. It is therefore sufficient to take into account the diagrams of Fig. 1 to calculate Im Π. Apart from numerical factors we then get (see reference 3)

$$\operatorname{Im}\Pi(\mathbf{q}, \omega) \sim \int d^3 p \left[u^2 v'^2 \mp \frac{\Delta\Delta'}{4\varepsilon\varepsilon'}\right] g^2 g'^2 \delta(\varepsilon \mp \varepsilon' - \omega), \qquad (2)$$

where $g = g(\mathbf{p})$ is a dimensionless function which characterizes the anisotropy of the electron-phonon interaction while the rest of the notation is the

FIG. 1

same as the one used before.[3] The primed quantities are here functions of the argument $\mathbf{p}-\mathbf{q}$. Assuming $q \ll p_0$ we can in the following put $\Delta' \approx \Delta$, $g' \approx g$. It is, however, impossible to put ξ and ξ', and ϵ and ϵ' equal to one another as near threshold the quantities ξ, vq, and Δ may be of the same order of magnitude. We have

$$\xi' = \xi - vq\cos\theta, \qquad \varepsilon' = \sqrt{\xi'^2 + \Delta^2}. \tag{3}$$

Owing to the δ-function, the integration in (2) is performed over a thin layer of thickness $\sim\Delta$ near the Fermi surface. This enables us to reduce the integration over momentum space to an integration over ξ and over the unit sphere which is the stereographic projection of the Fermi surface (see reference 3).

We get thus

$$\operatorname{Im}\Pi(\mathbf{q},\omega) \sim \iint g^4 \frac{\sin\theta\, d\theta\, d\varphi}{Kv} \times \int_{-\infty}^{\infty} d\xi \left[\left(1+\frac{\xi}{\varepsilon}\right)\left(1-\frac{\xi'}{\varepsilon'}\right) \frac{\Delta^2}{\varepsilon\varepsilon'}\right] \delta(\varepsilon+\varepsilon'-\omega) \tag{4}$$

(the direction of $\mathbf{q}$ is chosen as the polar axis); $K(\theta,\varphi)$ is the Gaussian curvature of the Fermi surface.

The roots of the equation $\epsilon + \epsilon' - \Delta = 0$ are determined by the equation

$$\xi_{1,2} = \tfrac{1}{2}\left\{vq\cos\theta \pm \omega\left[\frac{\omega^2 - v^2q^2\cos^2\theta - 4\Delta^2(\theta,\varphi)}{\omega^2 - v^2q^2\cos^2\theta}\right]^{1/2}\right\}. \tag{5}$$

For real phonons ($q = \omega/c$) this equation can be transformed to

$$\xi_{1,2} = \tfrac{1}{2}\left[\omega v c^{-1}\cos\theta \pm \sqrt{\omega^2 - \Omega^2(\theta,\varphi)}\right], \tag{6}$$

where

$$\Omega^2(\theta,\varphi) = 4\Delta^2(\theta,\varphi)/(1 - v^2c^{-2}\cos^2\theta). \tag{7}$$

The quantities ξ_1 and ξ_2 obviously satisfy the relations

$$\xi_1' = -\xi_2, \qquad \xi_2' = -\xi_1, \qquad \varepsilon_1' = \varepsilon_2, \qquad \varepsilon_2' = \varepsilon_1, \tag{8}$$

the geometric meaning of which is clear from Fig. 2.

If we perform the integration over ξ and use (8) we get

$$\operatorname{Im}\Pi(\mathbf{q},\omega) \sim \iint \frac{\sin\theta\, d\theta\, d\varphi}{Kv} g^4 \frac{(\xi_1+\varepsilon_1)(\xi_2+\varepsilon_2)+\Delta^2}{\xi_1\varepsilon_2 - \xi_2\varepsilon_1}. \tag{9}$$

The domain of integration in (9) is limited by the

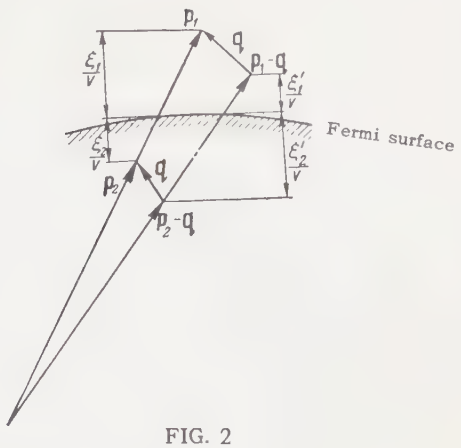

FIG. 2

conditions that the roots ξ_1 and ξ_2 be real

$$\omega^2 - \Omega^2(\theta,\varphi) \geqslant 0, \tag{10}$$

from which we get the inequality

$$|\cos\theta| \leqslant c\sqrt{\omega^2 - 4\Delta^2}/v\omega. \tag{11}$$

The threshold frequency Ω_0 is determined by the minimum value of $\Omega(\theta,\varphi)$. Since the ratio c/v ($c/v \sim 10^{-2}$ to 10^{-3}) is small, it follows from (11) that the minimum of $\Omega^2(\theta,\varphi)$ occurs near the line $\theta = \pi/2$. We expand Δ^2 in a power series in $x = \cos\theta$ and $\varphi - \varphi_0$, where φ_0 is the point where $\Delta^2(\pi/2,\varphi)$ is a minimum:

$$\Delta^2(x,\varphi) = \Delta_0^2[1 + ax + b(\varphi-\varphi_0)^2], \tag{12}$$

where $\Delta_0^2 = \min(\Delta^2(0,\varphi))$, and a and $b \sim 1$. Near this point we have

$$\Omega^2(x,\varphi) = 4\Delta_0^2[1 + ax + b(\varphi-\varphi_0)^2]/(1 - v_0^2c^{-2}x^2). \tag{13}$$

If we minimize this expression with respect to x we get at the minimum

$$x_0 = -\frac{a}{2}\left(\frac{c}{v_0}\right)^2, \qquad \Omega_0^2 = 4\Delta_0^2\left[1 - \frac{a^2}{4}\left(\frac{c}{v_0}\right)^2\right] \approx 4\Delta_0^2. \tag{14}$$

Near threshold we have

$$\omega^2 = \Omega_0^2(1+\alpha), \qquad \alpha \ll 1. \tag{15}$$

Using (10) and (13) we find that the domain of integration in the x,φ-plane is the interior of the ellipse

$$v_0^2c^{-2}(x-x_0)^2 + b(\varphi-\varphi_0)^2 \leqslant \alpha. \tag{16}$$

Evaluating the integral in (9) up to terms of order $\sim\alpha^{1/2}$ we get

$$\operatorname{Im}\Pi = Ac(\omega-\Omega_0)^{1/2}/v_0, \qquad A \sim g_0^4/K_0v_0\Omega_0^{1/2}. \tag{17}$$

It was shown earlier[3] that the damping of ultrasound is determined by the equation

$$\alpha_s(\mathbf{n}) = \gamma(\mathbf{n})\,\omega\,\operatorname{Im}\Pi, \tag{18}$$

where $\gamma(\mathbf{n})$ is some experimentally immeasurable function of the direction. We have thus near threshold

$$\alpha_s(\mathbf{n}) = B(\mathbf{n})\, c\, (\omega - \Omega_0)^{1/2}/v_0, \qquad B(\mathbf{n}) = \gamma(\mathbf{n})\, A\Omega_0. \quad (19)$$

The minimum of the quantity $\Omega^2(\theta, \varphi)$ occurs in the isotropic case everywhere along the line $\theta = \pi/2$. The integration is in that case performed over a "ribbon" of width $\sim c\sqrt{\alpha}/v_0$ girdling the equator of the unit sphere, and it leads to the result obtained before.[5]

ABSORPTION OF ELECTROMAGNETIC WAVES

The absorption is in this case also determined by the imaginary part of the polarization tensor $\Pi_{\alpha\beta}$. If we restrict our considerations to the diagrams of Fig. 1 we have (apart from numerical factors)

$$\operatorname{Im}\Pi_{\alpha\beta} \sim \int d^3p\, v_\alpha v_\beta \left[u^2u'^2 + v^2u'^2 - \frac{\Delta\Delta'}{2\varepsilon\varepsilon'}\right]\delta(\varepsilon + \varepsilon' - \omega). \quad (20)$$

Changing to an integration over ξ and over the unit sphere, we find

$$\operatorname{Im}\Pi_{\alpha\beta} \sim \iint \frac{\sin\theta\, d\theta\, d\varphi}{Kv} v_\alpha v_\beta \int_{-\infty}^{\infty} d\xi\, \frac{\varepsilon\varepsilon' - \xi\xi' - \Delta^2}{\varepsilon\varepsilon'}\delta(\varepsilon + \varepsilon' - \omega). \quad (21)$$

In our problem the characteristic dimension is the penetration depth δ, which is appreciably less than the wavelength in vacuo $2\pi c/\omega \sim c/\Delta$; there is thus no dispersion relation of the form $\omega = cq$. The roots of the equation $\epsilon + \epsilon' - \omega = 0$ are thus determined by (5), and the condition that they be real assumes the form

$$\omega^2 - v^2q^2\cos^2\theta - 4\Delta^2(\theta, \varphi) \geqslant 0. \quad (22)$$

If we evaluate the integral over ξ we get

$$\operatorname{Im}\Pi_{\alpha\beta} \sim \iint \frac{\sin\theta\, d\theta\, d\varphi}{Kv} v_\alpha v_\beta \frac{\varepsilon_1\varepsilon_2 + \xi_1\xi_2 - \Delta^2}{\xi_1\varepsilon_2 - \xi_2\varepsilon_1}. \quad (23)$$

The magnitude of the integral in (23) depends essentially on whether we are considering a Pippard, London, or intermediate metal.

a) Pippard metal, $vq \gg \Delta$. The threshold frequency Ω_0 is determined by the minimum value of the quantity $\Omega^2(\theta, \varphi) = v^2q^2\cos^2\theta + 4\Delta^2(\theta, \varphi)$. Because of the condition $vq \gg \Delta$ the minimum of $\Omega^2(\theta, \varphi)$ occurs near the line $\theta = \pi/2$. Calculations similar to the ones for the acoustic case give

$$\Omega^2(x, \varphi) = 4\Delta_0^2[1 + a_1x + b_1(\varphi - \varphi_0)^2 + (vq/2\Delta_0)^2x^2],$$
$$x_0 = -\frac{a_1}{2}\left(\frac{2\Delta_0}{v_0q}\right)^2, \qquad \Omega_0^2 = 4\Delta_0^2\left[1 - \frac{a_1^2}{4}\left(\frac{2\Delta_0}{v_0q}\right)^2\right] \cong 4\Delta_0^2. \quad (24)$$

We find from condition (22) that the domain of integration is the interior of the ellipse

$$\left(\frac{v_0q}{2\Delta_0}\right)^2(x - x_0)^2 + b_1(\varphi - \varphi_0)^2 \leqslant \alpha. \quad (25)$$

The absorption is essentially determined by the transverse components of the tensor $\Pi_{\alpha\beta}$ which do not contain Fermi-velocity components v_α and v_β proportional to the small quantity $\cos\theta$.

If we evaluate the integral in (23) up to the lowest powers of α and Δ_0/v_0q we get

$$\operatorname{Im}\Pi_{\alpha\beta} \sim \frac{v_{\alpha0}v_{\beta0}}{K_0v_0}\frac{\Delta_0}{v_0q}\left[\alpha^{3/2} + 3a_1^2\left(\frac{\Delta_0}{v_0q}\right)^2\alpha^{1/2}\right], \quad (26)$$

where $v_{\alpha0}$ and $v_{\beta0} \sim v_0$. There are in the Pippard case thus two regions of frequencies near threshold:

1) $\alpha \gg (\Delta_0/v_0q)^2$. In that case we have

$$\operatorname{Im}\Pi_{\alpha\beta} = A_1(\Delta_0/v_0q)(\omega - \Omega_0)^{3/2}, \qquad A_1 \sim v_{\alpha0}v_{\beta0}/K_0v_0\Omega_0^{3/2}. \quad (27)$$

2) $\alpha \ll (\Delta_0/v_0q)^2$. Then

$$\operatorname{Im}\Pi_{\alpha\beta} = A_2(\Delta_0/v_0q)^3(\omega - \Omega_0)^{1/2}, \qquad A_2 = 3A_1a_1^2\Omega_0. \quad (28)$$

The minimum of the quantity Ω^2 occurs in the isotropic model everywhere along the line $\theta = \pi/2$. If the frequency is close to the threshold frequency integration leads in that case to the result of references 2 and 4:

$$\operatorname{Im}\Pi_{\alpha\beta} \sim \Delta(\omega - \Omega_0)/vq. \quad (29)$$

A comparison of Eqs. (27) and (28) with (29) shows that the anisotropy reduces the absorption in region 1), but enhances it in region 2) which is in the immediate vicinity of the threshold.

Experiments to measure the absorption of electromagnetic waves (see, for instance, reference 6) are usually performed on polycrystalline superconductors and at various angles of incidence. In that case one must average the result (26) over the various directions. The role of the threshold frequency for such experiments is played by twice the absolute minimum of the quantity Δ. An effective contribution to the averaged absorption is given near threshold only by those great circles on the stereographic projection of the Fermi surface which pass through a small ellipse (with semi-axes $\sim\sqrt{\alpha}$) which lies near the points where $\Delta(\theta, \varphi)$ is an absolute minimum. These circles occupy a band of width $\sim\sqrt{\alpha}$ on the sphere.

The averaging thus results in an additional small factor $\sqrt{\alpha}$ in Eq. (26). Moreover, in this case we must put in that equation $a_1 = 0$. The experimentally observed absorption must thus

for such experiments be proportional to $\sim \alpha^2$.

b) London metal, $vq \ll \Delta$. The point where $\Omega^2(x, \varphi)$ is a minimum is in that case practically the same as the point where the energy gap $\Delta(x, \varphi)$ has its absolute minimum. Near threshold we have

$$\omega^2 - \Omega^2(x, \varphi) = 4\Delta_m^2 [\alpha - a_2 (x - x_0)^2 - b_2 (\varphi - \varphi_0)^2] \geqslant 0.$$

Evaluating the integral in (23) we get

$$\operatorname{Im} \Pi_{\alpha\beta} \sim \frac{v_\alpha v_\beta}{K_0 v_0} \left(\frac{v_0 q}{2\Delta_m}\right)^2 x_0^2 \alpha^{1/2}. \qquad (30)$$

The averaging over directions introduces in this case no added small factors.

c) Intermediate metal, $vq \sim \Delta$. In this case, which is the most interesting from an experimental point of view, the quantity $\Omega^2(x, \varphi)$ has its minimum in some point x_1, φ_1 which neither lies on the line $x = 0$ nor is the same as the point where $\Delta(x, \varphi)$ is a minimum. The threshold frequency $\Omega_0 = \min\ \Omega(x, \varphi)$ has therefore no simple relation with the values of the energy gap.

The integration is in this case performed over the interior of the ellipse

$$a_3 (x - x_1)^2 + b_3 (\varphi - \varphi_1)^2 \leqslant \alpha. \qquad (31)$$

The numerator of the integrand in (23) is not small (as far as the parameter α is concerned) while the denominator is of the order of $\sqrt{\alpha}$. The absorption changes thus in this case, as in the case of the London metal, near threshold proportional to $x_0^2 \alpha^{1/2}$ but the factor $(v_0 q/\Omega_0)^2$ which occurs in the expression for $\operatorname{Im} \Pi_{\alpha\beta}$ instead of the factor $(v_0 q/2\Delta_m)^2$ in (30) is not small.

Averaging over the directions gives for intermediate metals an additional small factor $\sqrt{\alpha}$. In fact, the absolute threshold frequency is in that case equal to $2\Delta_m$ and occurs for any directions of $\mathbf{q}$ which are perpendicular to the Fermi velocity in the point where the gap has its absolute minimum. The integration over directions is therefore performed over a narrow band of width $\sim\sqrt{\alpha}$ near the line $\theta_q = \pi/2$ and this leads to the factor $\sqrt{\alpha}$.

The absorption in polycrystalline samples of intermediate metals is thus proportional to $\omega - 2\Delta_m$. We note that the isotropic BCS model also leads to the same result (both for intermediate and for London metals). We emphasize once again that the agreement of qualitative results for the isotropic and for the averaged anisotropic model occurs only for the intermediate superconductors.

CONCLUSION

There are as yet no experiments on the absorption of ultrasound in the threshold region, since the corresponding frequencies cannot yet be attained. The only experiment we know of, in which the frequency dependence of the absorption of electromagnetic waves near threshold was measured at low temperatures, is described by Richards and Tinkham.[6] The total number of experimental points and the experimental accuracy are insufficient to compare theory and experiment. Moreover, the majority of the data obtained in that paper refer to intermediate metals for which the results of the isotropic model are the same as those for the averaged anisotropic model. The linear increase of the absorption with frequency is apparently verified experimentally.

The fact that the threshold frequencies for In, Hg, and Pb measured by the above mentioned authors[6] turned out to be larger than the ones predicted by the isotropic theory ($\Omega_0 = 3.5\, kT_c$) is very surprising. Indeed, in a real polycrystalline superconductor the threshold frequency is determined by the minimum value of the gap, and in the relation $\Delta(0) = 1.75\, kT_c$ of the isotropic model $\Delta(0)$ stands for some average over directions of the magnitude of the gap. Similar experiments in a region near the threshold with Pippard metals and also with single crystals are thus very desirable.

Experiments with single crystals are moreover important for the following reason. A measurement of the threshold frequency Ω_0 in Pippard metals allows us to find the minimum value of the energy gap on the great circle of the stereographic projection of the Fermi surface perpendicular to a given direction $\mathbf{n}$ ($\mathbf{n} = \mathbf{q}/q$). We have shown earlier[3] that one can obtain the same result by studying the absorption of ultrasound at frequencies below the threshold frequency at low temperatures ($T \ll \Delta$).

There are already experiments about the anisotropic absorption of ultrasound in that region.[7] It would be very useful to compare the experimental data obtained by Bezuglyĭ and co-workers[7] with electromagnetic measurements near threshold.

Pokrovskii and Toponogov[8] developed a method which allows us to construct the energy gap as a function of direction (everywhere, except for several "blank spots") once we know $\Delta_0 = \Delta_{\min}(\mathbf{n})$. A study of threshold phenomena for the absorption of ultrasound and of electromagnetic waves gives thus still another method to construct the energy gap.

In conclusion the authors express their gratitude to L. P. Gor'kov for drawing their attention to the problem considered here.

[1] Bardeen, Cooper, and Schrieffer, Phys. Rev. **108**, 1175 (1957).

[2] D. C. Mattis and J. Bardeen, Phys. Rev. **111**, 412 (1958).

[3] V. L. Pokrovskii, JETP **40**, 898 (1961), Soviet Phys. JETP **13**, 628 (1961).

[4] Abrikosov, Gor'kov, and Khalatnikov, JETP **35**, 265 (1958), Soviet Phys. JETP **8**, 182 (1959).

[5] V. L. Pokrovskii, JETP **40**, 143 (1961), Soviet Phys. JETP **13**, 100 (1961).

[6] P. L. Richards and M. Tinkham, Phys. Rev. **119**, 575 (1960).

[7] Bezuglyĭ, Galkin, and Korolyuk, JETP **39**, 7 (1960), Soviet Phys. JETP **12**, 4 (1961).

[8] V. L. Pokrovskii and V. A. Toponogov, JETP **40**, 1112 (1961), Soviet Phys. JETP **13**, 785 (1961).

Translated by D. ter Haar
313

INTERACTION OF CHARGED-PARTICLE BEAMS WITH LOW-FREQUENCY PLASMA OSCILLATIONS

A. I. AKHIEZER, A. B. KITSENKO, and K. N. STEPANOV

Physico-Technical Institute, Academy of Sciences, Ukrainian S.S.R.

Submitted to JETP editor January 27, 1961

J. Exptl. Theoret. Phys. (U.S.S.R.) **40**, 1866-1870 (June, 1961)

The interaction of a charged-particle beam with the low-frequency oscillations of a plasma (magnetoacoustic and Alfvén waves) is analyzed in the absence of collisions. It is shown that if the thermal velocity spread of the particles in the beam is sufficiently small this interaction can cause the plasma-beam system to become unstable.

1. As is well known, a charged-particle beam passing through a plasma can excite electromagnetic oscillations in the plasma.[1,2] These can be high-frequency oscillations, due to the electrons alone, and/or low-frequency oscillations, in which both the electrons and ions participate. In general, excitation of oscillations is associated with a plasma instability. Hence, to clarify the stability conditions in a plasma it is important to investigate the interaction of charged-particle beams with all the waves that can propagate in the plasma. In the present paper we investigate the interaction of a compensated beam of charged particles with low-frequency plasma oscillations (primarily the magnetoacoustic waves) in the presence of a fixed magnetic field parallel to the direction of motion of the beam.*

If the plasma is dilute so that the oscillation frequency ω is much higher than the collision frequency $1/\tau$ the kinetic equation must be used to analyze the plasma oscillations. If, however, $\omega\tau \ll 1$, the plasma can be treated as a hydrodynamic system. We consider the case $\omega\tau \gg 1$, which is of greatest interest.

2. The general dispersion equation for plasma oscillations in an external magnetic field, with an arbitrary particle velocity distribution, can be written in the form

$$An^4 + Bn^2 + C = 0, \tag{1}$$

where $n = kc/\omega$, $\mathbf{k}$ is the wave vector and the quantities A, B and C are expressed in terms of the components of the dielectric tensor ϵ_{ij}.

We assume that the following conditions are satisfied:

$$\omega \ll \omega_{Hi}, \qquad kv_i \ll \omega_{Hi}, \qquad kv_0 \ll \omega_{Hi}, \tag{2}$$

where ω_{Hi} is the ion gyromagnetic frequency, $v_i = (T_i/M)^{1/2}$ is the mean thermal velocity of the ions (T_i is the ion temperature and M is the ion mass), and $\mathbf{v}_0$ is the beam velocity. In this case, as an approximation the general dispersion equation (1) can be separated into two equations

$$(kc/\omega)^2 \cos^2\theta - \varepsilon_{11} = 0, \tag{3}$$

$$(kc/\omega)^2 - \varepsilon_{22} - \varepsilon_{23}^2/\varepsilon_{33} = 0, \tag{4}$$

which describe respectively the Alfvén and magnetoacoustic waves (the 3 axis is along the external magnetic field $\mathbf{H}_0$, the wave vector $\mathbf{k}$ lies in the 1-3 plane and θ is the angle between $\mathbf{k}$ and $\mathbf{H}_0$).

We assume that the equilibrium velocity distributions of the plasma electrons and ions are Maxwellian with characteristic temperatures T_e and T_i; the velocity distribution of the particles in the beam is assumed to be

$$f_{e,i} = n_0' \left(\frac{m_{e,i}}{2\pi T'_{e,i}}\right)^{3/2} \exp\left\{-\frac{m_{e,i}(\mathbf{v}-\mathbf{v}_0)^2}{2T'_{e,i}}\right\} \tag{5}$$

(n_0' is the number density of the beam particles, T_e' and T_i' are the temperatures of the electrons and ions in the beam, $m_e = m$, $m_i = M$). In this case the components of the tensor ϵ_{ij} are given by[9]

*The excitation of acoustic oscillations that result from the motion of the plasma electrons relative to the ions in a highly nonisothermal plasma with no magnetic field has been studied by Gordeev[3] (cf. also references 4 and 5). The same problem, but with a magnetic field, has been investigated by Bernstein and Kulsrud[6] for the case in which the Alfvén velocity is large compared with the acoustic velocity. Analyses of the excitation of magnetohydrodynamic waves in which the thermal motion of the plasma particles is neglected have been carried out by a number of authors.[5,7,8]

$$\varepsilon_{11} = 1 + \sum_{\alpha} \frac{\Omega_\alpha^2 (\omega - k_\parallel v_{0\alpha})^2}{\omega_{H\alpha}^2 \omega^2},$$

$$\varepsilon_{22} = \varepsilon_{11} + \sum_{\alpha} \frac{\Omega_\alpha^2 k^2 v_\alpha^2}{\omega_{H\alpha}^2 \omega^2} \, 2i \sqrt{\pi} \sin^2\theta z_\alpha w(z_\alpha),$$

$$\varepsilon_{33} = 1 + \sum_{\alpha} \frac{\Omega_\alpha^2}{k_\parallel^2 v_\alpha^2} (1 + i \sqrt{\pi} z_\alpha w(z_\alpha)),$$

$$\varepsilon_{23} = -\sum_{\alpha} \frac{\Omega_\alpha^2}{\omega \omega_{H\alpha}} \sqrt{\pi} \operatorname{tg}\theta z_\alpha w(z_\alpha), \qquad (6)^*$$

where

$$w(z_\alpha) = e^{-z_\alpha^2}\left(\pm 1 + \frac{2i}{\sqrt{\pi}} \int_0^{z_\alpha} e^{t^2} dt\right), \qquad z_\alpha = \frac{\omega - k_\parallel v_{0\alpha}}{\sqrt{2} k_\parallel v_\alpha},$$

$$\Omega_\alpha^2 = 4\pi e^2 n_{0\alpha}/m_\alpha, \qquad v_\alpha^2 = T_\alpha/m_\alpha,$$

$$\omega_{H\alpha} = e_\alpha H_0/m_\alpha c, \qquad k_\parallel = k\cos\theta$$

(the upper sign is taken in the expression for $w(z_\alpha)$ when $k_\parallel > 0$ and the lower sign is taken when $k_\parallel < 0$; the subscript α indicates the kind of particle for both the plasma and beam).

3. Using Eq. (6) and the dispersion equation (3), we find the following expression for the frequency of the Alfvén wave as modified by the presence of the beam:†

$$\omega = k_\parallel \frac{v_0 \Omega_i'^2 \pm [(\Omega_i^2 + \Omega_i'^2) c^2 \omega_{Hi}^2 - \Omega_i^2 \Omega_i'^2 v_0^2]^{1/2}}{\Omega_i^2 + \Omega_i'^2}. \qquad (7)$$

We see that the plasma-beam system is unstable against the excitation of Alfvén waves if the following condition is satisfied‡

$$v_0^2 > V_A^2 + V_A'^2, \qquad (8)$$

where $V_A = H_0/\sqrt{4\pi n_0 M}$, $V_A' = H_0/\sqrt{4\pi n_0' M}$.

It follows from Eq. (8) that Alfvén waves cannot be excited at sufficiently low beam densities. However, this result has been obtained neglecting the coupling between the Alfvén waves and the magnetoacoustic waves. When this coupling is taken into account it is found that an instability also arises at densities for which the relation in (8) is not satisfied. In this case the growth factor for $V_A \gtrsim v_i$ is found to be at least $(\omega_{Hi}/\omega)^2$ times smaller than the growth factor for the magnetoacoustic waves. For this reason we shall not investigate this question in any greater detail.

4. We now consider the interaction of the beam with the magnetoacoustic waves, assuming that the beam density is small compared with the plasma density. If $kv_i \ll \omega \ll kv_e$, in the absence of the beam, the solution of the dispersion equation (4) is[9]

$$\omega_\pm = kV_\pm,$$

$$V_\pm^2 = \tfrac{1}{2}\{V_A^2 + s^2 \pm [(V_A^2 + s^2)^2 - 4V_A^2 s^2 \cos^2\theta]^{1/2}\}, \qquad (9)$$

where $s = (T_e/M)^{1/2}$. We note that when $V_A \sim s$ the quantities $V_\pm$ are also of order s. In this case the condition $\omega \gg kv_i$ is satisfied only for a highly nonisothermal plasma ($T_e \gg T_i$); when $T_e \lesssim T_i$ the magnetoacoustic waves are strongly damped.

In addition to assuming $kv_i \ll \omega \ll kv_e$ we assume that the condition $|\omega - k_\parallel v_0| \gg kv_e'$ is satisfied; this means that the thermal spread of the electrons in the beam is small. With these assumptions the solution of the dispersion equation can be written in the form

$$\omega = k_\parallel v_0 + \varepsilon, \qquad (10)$$

where $|\epsilon| \ll |k_\parallel v_0|$. It follows from Eqs. (4) and (6) that

$$\varepsilon = (M/m)^{1/3}\varepsilon_0$$

$$= \pm k_\parallel v_0 \left[\frac{n_0' M (v_0^2\cos^2\theta - V_A^2) s^2 \cos^2\theta}{n_0 m (v_0^2\cos^2\theta - V_+^2)(v_0^2\cos^2\theta - V_-^2)}\right]^{1/3} (1 + i\eta), \qquad (11)$$

$$\eta = \pm \sqrt{\frac{\pi}{8}} \frac{v_0}{v_e}\left(\frac{2s^2}{v_0^2}\sin^2\theta + \frac{V_A^2 - v_0^2\cos^2\theta}{s^2}\right) \qquad (12)$$

(the upper sign in (12) corresponds to $k_\parallel < 0$ and the lower sign to $k_\parallel > 0$).

The quantity ϵ is given by Eq. (11) if the thermal motion of the electrons in the beam can be neglected. If $V_A \sim s$ it is legitimate to neglect this motion if the inequality $n_0 T_e' \ll n_0' T_e$ is satisfied. Furthermore, the condition $|\epsilon| \ll k_\parallel v_0$ must be satisfied. Thus, when $V_A \sim s$, Eq. (11) is valid when $T_e'/T_e \ll n_0'/n_0 \ll m/M$.

We see that the plasma-beam system is unstable against the excitation of magnetoacoustic waves for the conditions being considered here. If the velocity v_0 does not lie in the interval $s < v_0 < V_A$ the instability arises even if the quantity η ($|\eta| \ll 1$) is neglected. Even when v_0 lies within the interval $s < v_0 < V_A$, however, the imaginary part of ϵ is proportional to η.

The frequency increment ϵ, given by (11), becomes infinite when $v_0 \cos\theta \to V_\pm$. In this case Eq. (11) does not apply and must be replaced by the expression

$$\frac{\varepsilon}{\omega_\pm} \equiv \left(\frac{M}{m}\right)^{1/3} \frac{\varepsilon_0}{\omega_\pm} = \frac{-1 + i\sqrt{3}}{2^{4/3}} \left|\frac{n_0' M \cos^2\theta s^2 (V_\pm^2 - V_A^2)}{n_0 m V_\pm^2 (V_+^2 - V_-^2)}\right|^{1/3}. \qquad (13)$$

Thus, for the strongest interaction (resonance), i.e., $V_\pm = v_0\cos\theta$, the growth factor for the oscillations is proportional to $(n_0'/n_0)^{1/3}$ rather than $(n_0'/n_0)^{1/2}$.

---

*tg = tan.

†Hereinafter quantities pertaining to the beam are denoted by primes.

‡The condition (8) is given by Dokuchaev[7] (cf. also reference 9).

5. The solutions in (10) — (13) for the dispersion equation (4) apply for a highly nonisothermal plasma. When $|\omega - k_{\|}v_0| \gg kv'_e$, however, Eq. (4) admits of a solution of the form (10) when $T_e \lesssim T_i$, too. In this case, if the thermal motion of the beam electrons is neglected ($|\omega - k_{\|}v_0| \gg kv'_e$) the following expression is obtained for ϵ:

$$\varepsilon \equiv \left(\frac{M}{m}\right)^{1/2} \varepsilon_0 = \pm \frac{\Omega'_e [n^2 - \varepsilon_{22}^{(0)}]^{1/2}}{[\varepsilon_{33}^{(0)} (n^2 - \varepsilon_{22}^{(0)}) - \varepsilon_{23}^{(0)2}]^{1/2}}, \qquad (14)$$

where the $\epsilon_{ij}^{(0)}$ are the components of the plasma dielectric tensor in the absence of the beam for $\omega = k_{\|}v_0$.

Since $\epsilon_{ij}^{(0)}$ has a nonvanishing imaginary part, it follows from (14) that an instability arises for $T_e \lesssim T_i$ in which the characteristic oscillations of the plasma are highly damped. The growth factor Im ϵ is proportional to $(n'_0/n_0)^{1/2}$ in this case. In order of magnitude terms Im $\epsilon \sim$ Re $\epsilon \sim (n'_0 M/n_0 m)^{1/2}$ for $v_0 \sim v_i \sim s \sim V_A$. This estimate holds, obviously, if the condition $kv'_e \ll |\epsilon| \ll |k_{\|}v_0|$ is satisfied, i.e., when $T'_e/T_e \ll n'_0/n_0 \ll m/M$. If $T_e \gg T_i$, Eq. (14) goes over to Eq. (11).

6. If the inequality $kv'_i \ll |\omega - k_{\|}v_0| \ll kv'_e$ holds, the thermal motion of the electrons in the beam must be taken into account. In this case the solution of (4) is of the form

$$\omega = k_{\|}v_0 + \varepsilon_0, \qquad |\varepsilon_0| \ll |k_{\|}v_0|, \qquad (15)$$

where ϵ_0 is given by Eq. (14). As a rough approximation, we have Im $\epsilon_0 \sim$ Re $\epsilon_0 \sim (n'_0/n_0)^{1/2} kv_i$ for $T_e \sim T_i$ and $v_0 \sim s \sim V_A$. In this case Eq. (15) applies if the inequalities $T'_i/T \ll n'_0/n_0 \ll MT'_e/mT_e$ are satisfied.

If $k_{\|}v_0$ is close to the characteristic frequency of the magnetoacoustic waves in a nonisothermal plasma $kV_{\pm}$, then

$$\omega = kV_{\pm} + \varepsilon_0, \qquad |k(v_0 \cos\theta - V_{\pm})| \ll |\varepsilon_0|, \qquad (16)$$

where ϵ_0 is given by Eq. (13). As a rough approximation $\epsilon_0 \sim (n'_0/n_0)^{1/3} kV_{\pm}$ when $v_0 \sim s \sim V_A$. The expression in Eq. (16) applies if $T'_i/T_i \ll (n'_0/n_0)^{2/3} \ll MT'_e/mT_e$ (it is assumed that $v_0 \sim s \sim V_A$).

7. The preceding expressions are valid if the temperature of the ions in the beam is low enough so that $|\omega - k_{\|}v_0| \gg kv'$. Since ϵ is proportional to the small parameter $(n'_0/n_0)^{1/2}$, the inequality indicated above is not satisfied for sufficiently small values of n'_0/n_0. In this case the solution of (4) is of the form

$$\omega = \omega_{\pm} + i\gamma_{\pm}, \qquad (17)$$

where $\omega_{\pm}$ is given by Eq. (9)

$$\gamma_{\pm} = -\frac{\sqrt{\pi}\omega_{\pm} \sin^2\theta (\xi_e + \xi'_e + \xi'_i)}{4\zeta_{\pm} |\cos^2\theta - \zeta_{\pm}| (\zeta_+ - \zeta_-)}, \qquad \zeta_{\pm} = \left(\frac{V_{\pm}}{s}\right)^2. \qquad (18)$$

Here, the quantity ξ_e ($\xi_e > 0$) determines the Cerenkov damping of the magnetoacoustic waves:

$$\xi_e = |(2\cos^2\theta - \zeta_{\perp})^2 + \zeta_{\|}^2| \omega \sqrt{2} |k_{\|}| v_e. \qquad (19)$$

The quantities ξ'_e and ξ'_i determine the damping (or growth) of the magnetoacoustic waves due to the Cerenkov absorption (or emission) of these waves by the electrons and ions of the beam:

$$\xi'_e = \frac{n'_0 s^2}{n_0 s'^2} \left\{\left[\frac{2s'^2}{s^2}(\cos^2\theta - \zeta_{\pm}) + \zeta_{\pm}\right]^2 + \zeta_{\pm}^2\right\} \frac{\omega_{\pm} - k_{\|}v_0}{\sqrt{2}|k_{\|}|v'_e} \times \exp\left\{-\left(\frac{\omega_{\pm} - k_{\|}v_0}{\sqrt{2}k_{\|}v'_e}\right)^2\right\}, \qquad (20)$$

$$\xi'_i = \frac{n'_0 s^2}{n_0 v'^2_i} \left\{\left[\frac{2v'^2_i}{s^2}(\cos^2\theta - \zeta_{\pm}) - \zeta_{\pm}\right]^2 + \zeta_{\pm}^2\right\} \frac{\omega_{\pm} - k_{\|}v_0}{\sqrt{2}|k_{\|}|v'_i} \times \exp\left\{-\left(\frac{\omega_{\pm} - k_{\|}v_0}{\sqrt{2}k_{\|}v'_i}\right)^2\right\}. \qquad (21)$$

Equations (17) — (21) show that a low-density beam with large thermal spreads in the ion and electron velocities will in general not excite magnetoacoustic oscillations in a plasma.

[1] A. I. Akhiezer and Ya. B. Faĭnberg, Doklady Akad. Nauk SSSR **68**, 555 (1949); JETP **21**, 1262 (1951).

[2] D. Bohm and E. P. Gross, Phys. Rev. **75**, 1851 (1949), ibid. **75**, 1864 (1949).

[3] G. V. Gordeev, JETP **27**, 19, 24 (1954).

[4] L. M. Kovrizhnykh, JETP **37**, 1692 (1959), Soviet Phys. JETP **10**, 1198 (1960).

[5] M. S. Kovner, JETP **40**, 527 (1961), Soviet Phys. JETP **13**, 369 (1961).

[6] I. B. Bernstein and R. M. Kulsrud, Phys. Fluids **3**, 937 (1960).

[7] V. P. Dokuchaev, JETP **39**, 413 (1960), Soviet Phys. JETP **12**, 292 (1961).

[8] K. N. Stepanov and A. B. Kitsenko, J. Tech. Phys. (U.S.S.R.) **31**, 167 (1961), Soviet Phys.-Tech. Phys. **6**, 120 (1961).

[9] K. N. Stepanov, Ukr. Phys. Journ. **6**, 678 (1959).

Translated by H. Lashinsky
314

Letters to the Editor

ASYMMETRY OF THE BETA RADIATION OF Co^{60} NUCLEI POLARIZED IN A COBALT-IRON ALLOY

B. N. SAMOĬLOV, V. V. SKLYAREVSKII, V. D. GOROBCHENKO, and E. P. STEPANOV

Submitted to JETP editor April 3, 1961

J. Exptl. Theoret. Phys. (U.S.S.R.) 40, 1871-1874 (June, 1961)

WE reported earlier[1] on the results of investigating the asymmetry of beta radiation from Co^{60} nuclei polarized in Permendur (a ferromagnetic alloy containing 50% Co and 50% Fe). From the experimentally determined sign of the asymmetry we established that the effective magnetic field at the cobalt nuclei is directed oppositely to the external, magnetizing field. Hanna and his co-workers arrived at similar conclusions[2] as a result of investigating by the Mössbauer method the hyperfine splitting of levels of the Fe^{57} nucleus in metallic iron and of measuring the dependence of this splitting on the added external field. Dash and co-workers[3] showed by an indirect method that the effective field at Co^{57} nuclei in iron has the same direction as the field at Fe^{57} nuclei, i.e., opposite to the domain field. This letter presents the final results of our investigations of asymmetry of the beta radiation of Co^{60} nuclei polarized in Permendur.

The orientation was effected by the ferromagnetic method.[4] The sample was cooled by bringing it into thermal contact with an adiabatically demagnetized block of potassium chrome alum. To magnetize it, a small (~ 1000 oe) magnetic field created by coils placed inside the helium Dewar was applied. The sample, in the form of a thin plate ($3 \times 1.5 \times 0.01$ mm), was positioned in such a way that its plane made an angle of 30° with the direction of the magnetic field. The beta radiation was counted in the same direction. Such a placement of the sample satisfied at the same time two requirements: a small thickness along the direction of emission of the recorded beta radiation and a small angle between the polarization axis of the nuclei* and the direction in which the counting is performed (the maximum asymmetry value corresponds to the zero value of this angle). A diagram of the low-temperature part of the apparatus is presented in Fig. 1. The beta radiation was registered by a disc of scintillating plastic (diameter 9 mm, thickness 1.5 mm). Scintillations were led from the scintillator via a methyl metacrylate light pipe (~ 1000 mm long) to the photocathode of a FEU-13 multiplier tube. Another multiplier with a 40×40-mm NaI(Tl) crystal recorded the gamma radiation of the sample in a direction perpendicular to the axis of polarization. The remaining devices employed to record radiation and measure the temperature of the salt, as well as the experimental procedure, were the same as in our previous experiments.[5]

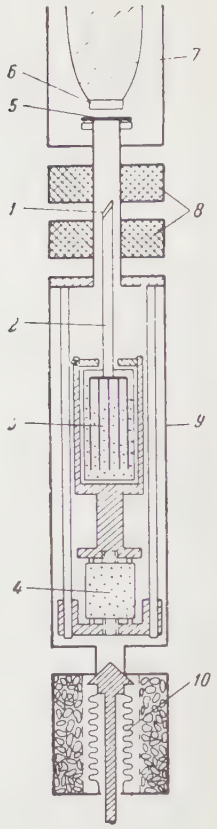

FIG. 1. Diagram of the apparatus: 1 – sample; 2 – cold conductor; 3 – cooling salt with contact plates; 4 – insulating salt; 5 – aluminum foil (thickness 25 μ); 6 – scintillator; 7 – light pipe; 8 – coils for magnetizing the sample; 9 – vacuum jacket; 10 – adsorption pump.

Figure 2 represents the results of one of the experiments. Every fifteen minutes the direction of the magnetizing field was reversed, and after thirty minutes the sample was warmed up to the temperature of the surrounding bath. It is evident that reversal of the field has no effect on the anisotropy of the gamma radiation, but that it does reverse the direction of preferred emission of electrons. Quantitatively, the anisotropy of the gamma radiation and the asymmetry of the beta radiation may be described by the parameters

$$\varepsilon_\gamma = N_\gamma(\pi/2)/N_\gamma^0 - 1, \quad \varepsilon_\beta = [N_\beta(0) - N_\beta(\pi)]/N_\beta^0,$$

where $N_\gamma(\theta)$ and $N_\beta(\theta)$ are the intensities of the gamma and beta radiation of the oriented nuclei at

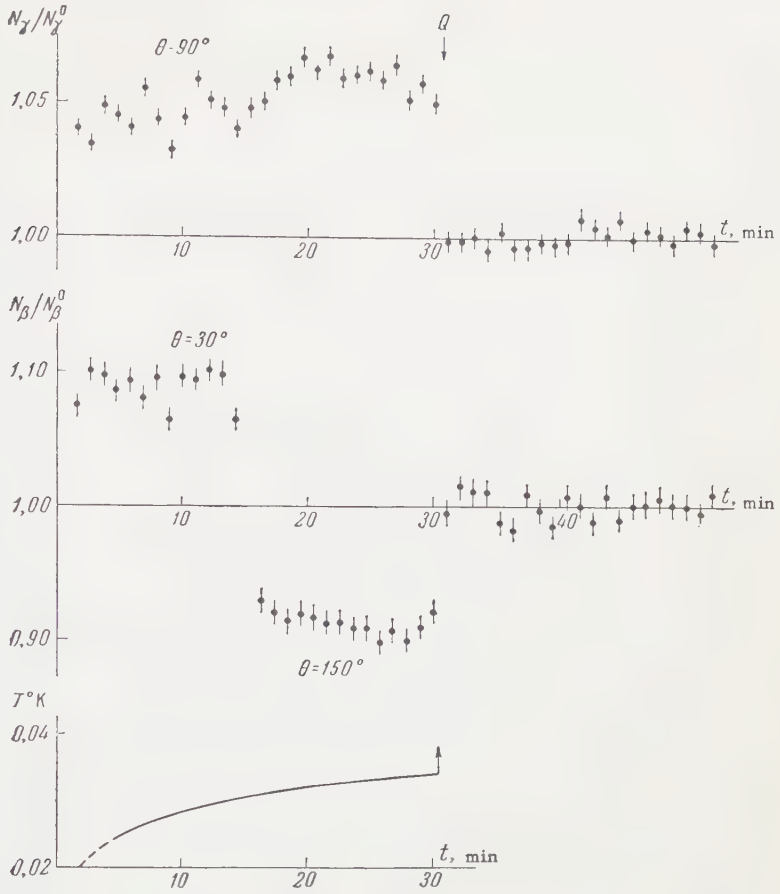

FIG. 2. Intensities of gamma and beta radiation of of the sample as a function of time. Below is shown the dependence of the salt temperature on time; the arrow marks the moment at which artificial warming of the salt begins.

an angle θ to the direction of the magnetizing field, and N_γ^0 and N_β^0 are the radiation intensities of the warmed-up sample. ϵ_γ and ϵ_β can be expressed in terms of the decay characteristics of the nucleus and the degree of orientation. For not very low temperatures in the case of Co^{60} decay, we can restrict ourselves to the first terms in the expansions of ϵ_γ and ϵ_β in powers of $\mu H/IkT$, writing the approximate equalities

$$\varepsilon_\gamma \cong \tfrac{13}{14}\left(\frac{\mu H}{IkT}\right)^2, \qquad \varepsilon_\beta \cong -\tfrac{2}{3}(I+1)\frac{v}{c}\left(\frac{\mu H}{IkT}\right),$$

where μ is the magnetic moment, I is the spin of the Co^{60} nucleus, H is the effective field at the nucleus, and v is the electron velocity.

Measurement of beta asymmetry obviously allows us to determine not only the magnitude but also the sign of the product μH, and if the sign of one of the factors is known the sign of the other can be determined. The sign of the magnetic moment of Co^{60} is known, allowing us to determine the sign of the effective field at the nucleus. Taking into account corrections for the imperfect coincidence between the directions of polarization and counting of beta radiation, as well as for the gamma background in the beta count, and adopting an average v/c value for the recorded part of the spectrum of ~ 0.6, we obtained for the effective field strength at the nucleus the value $H = -2 \times 10^5$ oe; this agrees with the magnitude $|H| = 2.8 \times 10^5$ obtained from ϵ_γ and with the value $|H| = 2.5 \times 10^5$ reported by us earlier.[6]

The experimentally obtained negative sign of the effective magnetic field at the cobalt nuclei can be explained by assuming that the contact interaction between the nucleus and the polarized inner s electrons determines the principal contribution to the field.† However Goodings and Heine[7] and also Freeman and Watson[8] have shown that, for the case of the free atom or ion electron configuration, such a mechanism cannot explain the large size of the negative field found at the nuclei in metal. The latter authors presented the interesting results of calculations of the dependence of the effective field at the nucleus on the position of the maximum of the density distribution of 3d electrons in the atom. They also suggested that the magnitude of the effective magnetic field at the nuclei of ferromagnetic atoms would apparently be explained if allowance were made for the real distribution of 3d electrons in the metal.

The authors sincerely thank E. K. Zavoĭskii and L. V. Groshev for their constant attention to the work, V. N. Agureev, N. V. Razzhivin and I. B.

Filippov for their help in preparing the apparatus and carrying out the experiments, and also N. E. Yukovich, V. A. Drozdov and V. D. Sheffer for furnishing the liquid helium.

*The axis of polarization of the nuclei, in our opinion, lay in the plane of the sample because of the considerable difference between longitudinal and transverse demagnetizing factors of the thin plate.

†This mechanism was also considered in Marshall's work,[9] but his calculations did not lead to the correct sign for the resulting field.

[1] Samoĭlov, Sklyarevsky, and Stepanov, Proc. of the VIIth Int. Conf. on Low Temp. Phys., Univ. of Toronto, Canada, 1960, Univ. of Toronto Press, 1961, pp. 171-173.

[2] Hanna, Heberle, Perlow, Preston, and Vincent, Phys. Rev. Lett. **4**, 513 (1960).

[3] Dash, Taylor, Craig, Nagle, Cochron, and Keller, Phys. Rev. Lett. **5**, 152 (1960).

[4] N. E. Alekseevskii and I. F. Shchegolev, Получение ориентированных ядер и их исследование, (The Obtaining of Oriented Nuclei and Their Investigation), Report, Inst. Phys. Prob., U.S.S.R. Acad. Sci., 1954. G. R. Khutsishvili, JETP **29**, 984 (1955), Soviet Phys. JETP **2**, 744 (1956). Grace, Johnson, Kurti, Scurlock, and Taylor, Comm. Conf. de Physique des basses Températures, 263, Paris, 1955.

[5] Samoĭlov, Sklyarevskii, and Stepanov, JETP **38**, 359 (1960), Soviet Phys. JETP **11**, 261 (1960).

[6] Samoĭlov, Sklyarevskii, and Stepanov, JETP **36**, 1366 (1959), Soviet Phys. JETP **9**, 972 (1959).

[7] D. A. Goodings and V. Heine, Phys. Rev. Lett. **5**, 370 (1960).

[8] A. J. Freeman and R. E. Watson, Phys. Rev. Lett. **5**, 498 (1960).

[9] W. Marshall, Phys. Rev. **110**, 1280 (1958).

Translated by Mrs. J. D. Ullman
315

TEMPERATURE DEPENDENCE OF HYPERFINE SPLITTING OF Dy^{161} *LEVELS IN PARAMAGNETIC DYSPROSIUM OXIDE*

V. V. SKLYAREVSKII, B. N. SAMOĬLOV, and E. P. STEPANOV

Submitted to JETP editor April 3, 1961

J. Exptl. Theoret. Phys. (U.S.S.R.) **40**, 1874-1876 (June, 1961)

WE have investigated spectra of the resonant absorption of Dy^{161} gamma rays of energies 26 and 75 kev. The source used was $Gd_2^{160}O_3$ (97% Gd^{160}) in which Gd^{161} is formed by irradiation in a reactor and then goes over ($\tau_{1/2}$ = 3.7 min) to Tb^{161} ($\tau_{1/2}$ = 7.15 days). The Dy^{161} gamma rays are emitted upon beta decay of the Tb^{161}. The compound $Dy_2^{161}O_3$ (90% Dy^{161}) was used as the absorber.

The dependence of the intensity of the gamma rays passing through the absorber on the rate of motion of the absorber toward the stationary source was measured. The absorber was set in motion by a mechanical system that converts (by means of a suitably shaped cam) rotary motion into reciprocating motion with constant speed. Different rates were obtained by changing the rate of rotation of the cam. The gamma rays were registered by a scintillation spectrometer using a crystal of NaI(Tl).

For the 26-kev gamma rays it turned out that the magnitude of the resonance absorption depended weakly on the temperature. This allowed the measurement of spectra at a series of temperatures: 80, 300, 400, 510, 640, and 840°K. In all cases the $Dy_2^{161}O_3$ absorber had a thickness of 15 mg/cm^2. Thicker absorbers gave a larger effect, but poorer resolution.

Figure 1 shows three of the spectral measurements. It can be seen that in all cases five almost equidistant peaks appear (besides the fundamental one at $v = 0$). Such a spectrum indicates that one of the levels of Dy^{161} between which the 26-kev gamma transition occurs ($5/2^- \rightarrow 5/2^+$) is split into six magnetic sublevels, such that the magnitude of the splitting is approximately the same for emitting and absorbing nuclei, but the splitting of the other level is significantly less and apparently is responsible for the width of the peaks. These splittings are caused by the interaction of the nuclear magnetic moment of Dy^{161} with the magnetic field produced at the nucleus by the electron shell.

The observed equal separation of the hfs (hyperfine splitting) levels is apparently associated

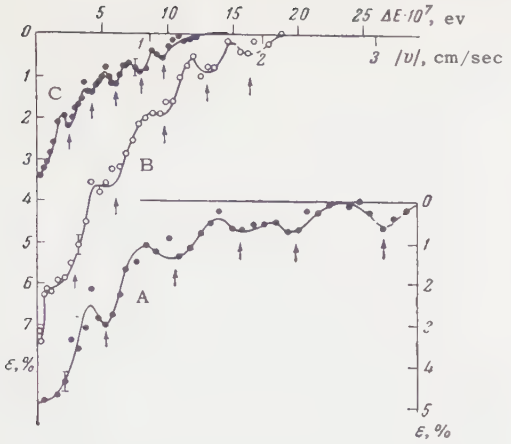

FIG. 1. Resonance absorption spectra of Dy^{161} gamma rays with energy of 26 kev at different temperatures: A – 80°K, B – 300°K, C – 640°K (temperature of source and absorber the same). On the ordinate axis the quantity $\varepsilon = [N(|v|) - N(v = \infty)]/N(v = \infty)$ is plotted in percent; $N(|v|)$ is the count intensity of gamma rays passing through the absorber moving at the rate $|v|$. On the abscissa axis (the same for all three curves) $\Delta E = (|v|/c)E_\gamma$ is plotted, as well as $|v|$.

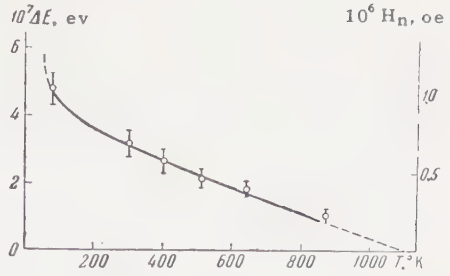

FIG. 2. The dependence of $\Delta E = \mu H_n/I$ and H_n on T. The values of ΔE were found from the mean separation between the peaks of the curves in Fig. 1, and H_n was determined from ΔE, with the assumption that the observed ΔE belongs to the ground level of Dy^{161}, for which μ is known.

with the presence of a quadrupole interaction between the electron shells of the Dy atoms and the internal electric field, leading to a removal of the degeneracy in J_z. This interaction is caused by the characteristics of the Gd_2O_3 and Dy_2O_3 lattices: the atoms of Gd or Dy are located at the centers of slightly distorted cubes in all corners of which, except the two on the diagonal, lie O atoms. Besides the spectra of $\epsilon(|v|)$ at T = 300°K, a spectrum was measured with separate registration of $\epsilon(+v)$ and $\epsilon(-v)$. In this spectrum there also appeared five peaks on each side of the central one, but the center of symmetry was shifted relative to v = 0 by a small amount corresponding to $\Delta E \approx 4 \times 10^{-8}$ ev. This asymmetry is caused by the different disposition of the levels of the emitting and absorbing nuclei on account of the different crystalline lattices of the source and absorber.

From Figs. 1 and 2 it is seen that $\Delta E = \mu H_n/I$ (the hfs of Dy^{161}) and consequently H_n (the magnetic field at the nucleus) depend significantly on the temperature.

This dependence of H_n on temperature is determined by the temperature dependence of the relaxation time τ_{rel} of the spin of the electron shell that creates the field at the nucleus. It is known that in such strong paramagnetic substances as Gd_2O_3 and Dy_2O_3 the time τ_{rel} is very short and decreases with increasing T. For a sufficiently small τ_{rel}, when $\tau_{rel} \ll \tau_{prec}$, where $\tau_{prec} = \hbar/\Delta E_0$ is the time of precession of the nuclear spin in the field of the electrons, the mean values of H_n and ΔE are equal to zero. For τ_{rel} sufficiently large $\Delta E = \Delta E_0$. In intermediate cases, which, evidently, correspond to the temperature region we have investigated, $\Delta E < \Delta E_0$ and decreases with increasing T.

Evidently, measurements of curves of $\Delta E(T)$ make it possible to obtain the dependence $\tau_{rel}(T)$. For this, our results need to be augmented by measurements in the low-temperature region. From the curve $\Delta E(T)$ obtained we estimate $\tau_{rel} \sim 10^{-10}$ sec.

In the spectrum of the resonance absorption of Dy^{161} gamma rays of energy 75 kev (transition $3/2 \rightarrow 5/2$) the hfs $\Delta E^{75} \approx \mu H_n/I \approx 27 \times 10^{-7}$ ev is six times greater than $\Delta E^{25}(80°K) = 4.8 \times 10^{-7}$ ev. From this it follows that the observed ΔE^{75} is created by a splitting of the 75 kev levels. From a comparison of the values we have measured for $\Delta E^{75}(80°K)$ and $\Delta E^{25}(80°K)$ with the known quantity $\mu^0 = 0.37$ n.m.,[1] we find that the magnetic moment of the Dy^{161} 75 kev levels is $\mu^{75} \approx 1.3$ n.m., which is in agreement with the shell model.[2]

The 26-kev gamma radiation of Dy^{161} is one of those rare cases in which the study of resonant absorption is possible even at high temperatures of the order of 1000°K. As Yu. Kagan (private communication) has shown, one can expect such an unusually weak dependence of the resonance absorption on temperature for lattices in which the atoms differ greatly in mass. In this case, the usual Debye temperature no longer characterizes the phenomenon, and it should be replaced by a much higher "effective" Debye temperature.

The Mössbauer effect in Dy^{161} has been investigated by Ofer et al.,[3] who obtained the spectrum for the 26-kev gamma rays at T = 300°K, also with Gd_2O_3 and Dy_2O_3 as source and absorber. Our spectrum at T = 300°K agrees with Ofer's results as far as the half-widths and magnitude of the effect is concerned. However, they did not notice the peaks we found, apparently on account

of using an absorber of unseparated Dy_2O_3.

The authors deeply thank E. K. Zavoĭskii, L. V. Groshev, D. P. Grechukhin, Yu. M. Kagan, S. T. Belyaev, and D. F. Zaretskii for numerous discussions, I. B. Filippov, K. P. Aleshin, G. P. Mel'nikov for taking part in the experiment, and V. S. Zolotarev for the gift of the separated isotopes.

[1] J. G. Park, Proc. Roy. Soc. (London) **A245**, 118 (1958).

[2] J. N. L. Gauvin, Nuclear Phys. **8**, 213 (1958).

[3] Ofer, Avivi, Bauminger, Marinov, and Cohen, Phys. Rev. **120**, 406 (1960).

Translated by L. M. Matarrese
316

PARAMAGNETIC RESONANCE IN METALLIC ALUMINUM

A. A. GALKIN and V. P. NABEREZHNYKH

Physico-Technical Institute of Low Temperatures, Academy of Sciences, Ukrainian S.S.R.

Submitted to JETP editor April 12, 1961

J. Exptl. Theoret. Phys. (U.S.S.R.) **40**, 1876-1877 (June, 1961)

A number of experimental and theoretical papers[1-9] have been devoted to paramagnetic resonance in the conduction electrons of a metal. However, most of the investigations have been made on alkali metals where the electron resonance line is sufficiently narrow, due to the weak spin-orbit interaction. The difficulty of observing paramagnetic resonance in "classical" metals, in which the spin-orbit interaction is strong, is increased because impurities can lead to a sharp reduction in the spin relaxation time and thus to a broadening of the absorption curve.

In this note we describe experiments on the observation of electron paramagnetic absorption in single crystal aluminum with a residual resistance of 6.7×10^{-5},* corresponding to an electron mean free path $\sim 2 \times 10^{-2}$ cm.

The specimen, in the form of a 10 mm diameter disc of thickness ~ 3 mm, was electropolished and served as the base of a cylindrical resonance cavity in which H_{011} mode oscillations were excited. The perfection of the surfaces was such that at T = 4.2° K several cyclotron resonance oscillations were fairly clearly observed.

The dependence of absorption on magnetic field was studied with a high sensitivity spectrometer, working at a frequency of 3.6×10^{10} cps in the temperature range 300 — 4.2° K.

A broad symmetrical line was visible at temperatures of 300 and 77° K. The intensity of the line depended weakly on temperature, indicating the electronic character of the absorption. At hydrogen temperatures the absorption line has pronounced asymmetry which increases somewhat as the temperature is reduced to 4.2° K.

Figure 1 shows the dependence of the derivative of the surface impedance, dR/dH, on magnetic field H at T = 4.2° K. The results of the investigation refer to a specimen in which the fourfold axis was perpendicular to the surface of the specimen. The line width, determined at the half height of the derivative, does not change over the interval 20 — 4° K and equals 140 oe, corresponding to a spin relaxation time $\tau_{sp} \approx 5 \times 10^{-10}$ sec.

One can deduce from the fact that the line width is weakly dependent on temperature, while according to B. I. Aleksandrov's measurements an appreciable change in the dc resistance of aluminum is still observed, that the spin relaxation time is determined by impurities with strong spin-orbit coupling. This deduction is also confirmed by measurements on aluminum with a large impurity content, for which the value $\tau_{sp} \approx 5 \times 10^{-11}$ sec was found.

The absence of anisotropy in the line width and g-factor (equal to 2.06) can also be explained by

the strong line broadening produced by impurities.

The shape of the absorption line, which has been studied very thoroughly by other authors,[5] is not understood. It was shown for the alkali metals that the positive part of the derivative dR/dH is considerably larger than the negative.

Examination of the shape of the absorption curve shows that for aluminum and copper the negative part of the derivative is considerably greater than the positive. This can be explained formally by particles with opposite sign of spin taking part in the paramagnetic resonance. It seems likely that Dyson's theory[6] is not fully applicable to our case, since $\mu H \lesssim kT$ and τ_{sp} is of the same order of magnitude as the collision time.

Since the electron mean free path is greater than the radius of the electron orbit in the magnetic field, a dependence of the signal strength on the inclination of the magnetic field relative to the specimen surface is observed in the experiments. The change in signal amplitude is in qualitative agreement with the theory of Azbel', Gerasimenko, and Lifshitz.[7]

*We are grateful to B. I. Aleksandrov for providing the initial specimen, prepared in his laboratory.

[1] Griswold, Kip, and Kittel, Phys. Rev. **88**, 951 (1952).

[2] Kip, Griswold, and Portis, Phys. Rev. **92**, 544 (1953).

[3] T. R. Carver and C. P. Slichter, Phys. Rev. **92**, 212 (1953).

[4] G. Feher and A. F. Kip, Phys. Rev. **95**, 1343 (1954).

[5] G. Feher and A. F. Kip, Phys. Rev. **98**, 337 (1955).

[6] F. J. Dyson, Phys. Rev. **98**, 349 (1955).

[7] Azbel', Gerasimenko, and Lifshitz, JETP **32**, 1212 (1957), Soviet Phys. JETP **5**, 986 (1957); JETP **35**, 691 (1958), Soviet Phys. JETP **8**, 480 (1959).

[8] M. S. Khaĭkin, JETP **39**, 899 (1960), Soviet Phys. JETP **12**, 623 (1961).

Translated by R. Berman
317

SMALL-ANGLE SCATTERING OF 0.8- AND 2.8-Mev NEUTRONS

Yu. A. ALEKSANDROV, G. V. ANIKIN, and A. S. SOLDATOV

Submitted to JETP editor April 15, 1961

J. Exptl. Theoret. Phys. (U.S.S.R.) **40**, 1878-1879 (June, 1961)

WHEN studying the scattering of neutrons with an average energy of about 2 Mev in the region of angles smaller than 8 — 10°, we discovered, besides Schwinger scattering,[1] an additional contribution to the scattering cross section of U and Pu nuclei.[2,3] In this work we have tried to establish the energy dependence of the indicated effect in the angle interval of 3 to 25°. The work was carried out with a fast-neutron reactor. Measurements were made in two energy intervals with average energies of 0.8 and 2.8 Mev. The neutrons, with an average energy of 0.8 Mev, were separated out of a broad spectrum of reactor neutrons by radiotechnical collimation of the recoil protons.[4] The measurements at an average energy of 2.8 Mev were made with a threshold detector (as was done in references 2 and 3). The performance of the collimation system used for the measurements is presented in Fig. 1.

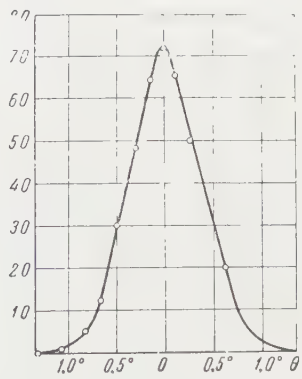

FIG. 1

Measurements were made in the 3 — 8° interval both to the left and to the right of the neutron beam; agreement of the two measurement results was observed. Figures 2 and 3 present the results of the measurements. The quantity $\gamma^2 \cot^2(\theta/2)$, which is the cross section for Schwinger scattering, was computed from the experimental points; $\gamma = \frac{1}{2}\mu_n(\hbar/mc)(ze^2/\hbar c)$, $\mu_n = 1.91$. As is evident from the graphs, the results of the measurements for neutrons of about 0.8 Mev agree with the theory of Schwinger scattering within the limits of error. At an energy of ~ 2.8 Mev, as was also reported in

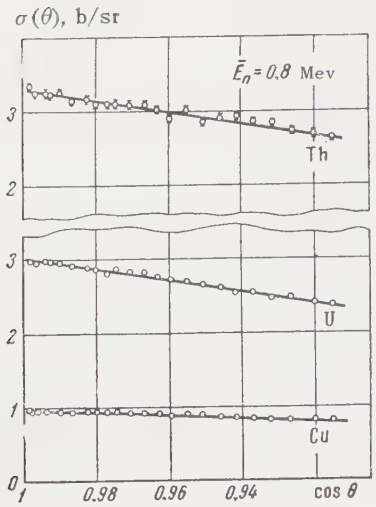

FIG. 2

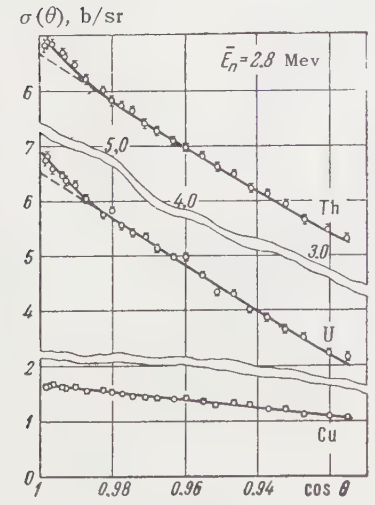

FIG. 3

references 2 and 3, a sharp increase in the scattering cross section of U and Th nuclei is observed in the region of angles smaller than 10°, in spite of allowances made for Schwinger scattering.

It must be observed that the detected phenomenon has not yet been satisfactorily explained.[5]

The authors are grateful to Professors A. I. Leĭpunskii and I. I. Bondarenko for their attention to the work.

[1] J. Schwinger, Phys. Rev. **73**, 407 (1948).

[2] Yu. A. Aleksandrov, JETP **33**, 294 (1957), Soviet Phys. JETP **6**, 228L (1958).

[3] Yu. A. Aleksandrov, Сб. Ядерные реакции при малых и средних энергиях (Collection: Nuclear Reactions at Low and Medium Energies), Acad. Sci. Press, 1958, p. 206.

[4] Anikin, Aleksandrov, and Soldatov, Report at Symposium on Physics Research with Neutrons Produced in Reactors, Vienna, 1960 (in press).

[5] V. M. Koprov and L. N. Usachev, Proceedings of the Conference on Nuclear Reactions at Low and Medium Energies, Moscow, July 1960, in press.

[6] V. M. Agranovich and D. D. Odintsov, ibid.

Translated by Mrs. J. D. Ullman
318

PRODUCTION OF NEGATIVE-TEMPERATURE STATES IN P-N JUNCTIONS OF DEGENERATE SEMICONDUCTORS

N. G. BASOV, O. N. KROKHIN, and Yu. M. POPOV

P. N. Lebedev Physics Institute, Academy of Sciences, U.S.S.R.

Submitted to JETP editor April 18, 1961

J. Exptl. Theoret. Phys. (U.S.S.R.) **40**, 1879-1880 (June, 1961)

IF a p-n junction in a semiconductor is biased in the forward direction, then there will be a decrease in the potential barrier due to space charge in the p-n junction, and the concentration of minority carriers near the junction will increase. The concentration of these carriers reaches a maximum once the potential barrier is completely removed by the applied field. This maximum value is about equal to the concentration of the carriers in a region of the crystal where they are the majority carriers (we assume the p-n junction to be abrupt). A negative temperature can arise in a junction only when the Fermi quasi-levels corresponding to the non-equilibrium concentrations of electrons and holes satisfy the relation[1]

$$\mu_e + \mu_p > \Delta, \qquad (1)$$

where μ_e and μ_p are the Fermi quasi-levels for electrons and holes, and Δ is the width of the forbidden band. If the p-n junction is now biased in the forward direction, the Fermi quasi-level of the minority carriers near the junction will be close to the Fermi level in that part of the crystal where these carriers are the majority ones. From equation (1) it then follows that in this case in at least some part of the p-n junction the carriers must be degenerate.

Semiconductors with such p-n junctions are tunnel diodes;[2] however, this mechanism for obtaining negative temperatures corresponds to the diffusion, rather than the tunnel, part of the voltage-current characteristic of the tunnel diode.

If the p-n junction is in a strongly degenerate semiconductor, negative temperatures can arise even before the potential barrier is completely destroyed so that quantitative estimates can be obtained with the aid of the theory of the diffusion of current through a p-n junction.

It can be easily shown that the minimum value of the external voltage at which a negative temperature can occur is given by*

$$U_{min} = \Delta/e \qquad (2)$$

where $-e$ is the electron charge. The current density I (of the electronic component, for example) is, in order of magnitude,

$$I \approx -(eDn_p/L)\exp(eU/kT), \qquad (3)$$

where D is the diffusion coefficient, L is the diffusion length, and n_p is the electron density in the p part of the semiconductor. From formula (3) it can be shown that the current density decreases with increasing degeneracy and decreasing sample temperature. A steady state with negative temperature can thus be obtained. However, the absorption coefficient for radiation in the semiconductor becomes negative at fairly high ($\sim 10^{15}$ cm^{-3}) nonequilibrium concentrations of the minority carriers,[3] and as a consequence it is impossible to work at very low current densities.

The negative temperature occurs in a thin layer near the p-n junction, the thickness of the layer being about a diffusion length. In a degenerate semiconductor the high density of the majority carriers surrounding the region of negative temperature can, apparently, serve as reflecting surfaces, i.e., a "resonating cavity" is formed.

It should be noted that lower current densities can be used if the semiconductors forming the p-n junction have forbidden bands of different widths.

Pankove[4] has observed recombination radiation from p-n junctions in degenerate semiconductors. In a negative temperature state, the concentration of current carriers is lower than in the state having negative absorption coefficient, so that to observe a negative temperature state one should look for changes in the voltage-current characteristic when the sample is illuminated with light of suitable frequency.

*In the case of indirect transitions[3] at low temperatures, the quantity Δ in formula (2) should be replaced by $\Delta - \varepsilon$, where ε is the energy of the radiated phonon.

[1] Basov, Krokhin, and Popov, Usp. Fiz. Nauk **72**, 161 (1960), Soviet Phys.-Uspekhi **3**, 702 (1961).

[2] L. Esaki, Phys. Rev. **109**, 603 (1958); I. I. Ivanchik, Физика твердого тела **3**, 103 (1961), Soviet Phys. Solid State **3**, 75 (1961).

[3] Basov, Krokhin, and Popov, JETP **40**, 1203 (1961), Soviet Phys. JETP **13**, 845 (1961).

[4] J. I. Pankove, Phys. Rev. Lett. **4**, 20 (1960).

Translated by R. Krotkov
319

RAREFACTION SHOCK WAVES IN IRON AND STEEL

A. G. IVANOV and S. A. NOVIKOV

Submitted to JETP editor April 25, 1961

J. Exptl. Theoret. Phys. (U.S.S.R.) **40**, 1880-1882 (June, 1961)

IN the case of a medium with a Poisson adiabat some part of which has a curvature of sign other than the usual one ($\partial^2 p/\partial V^2 < 0$), a rarefaction jump must be introduced in order to construct the rarefaction wave in this region of pressures, whereas a compression jump is impossible.[1] The kink in the shock-compressibility curve in iron at an ($\alpha \rightarrow \gamma$) phase-transition pressure of 132,000 atm, noted by Bancroft,[2] is a limiting case of such an anomalous part of the Poisson adiabat.* That a rarefaction jump can in principle be produced in iron was pointed out by Drummond.[3] It is obvious that when rarefaction shock waves interact, destructive stresses will be reached in a very narrow zone, determined by the width of the front of these waves, and this should lead to the appearance of fractures with much smoother surface than in the case when simple rarefaction waves interact.

We have investigated fracture phenomena in cylindrical specimens of steel on whose surfaces explosive charges were detonated. The diameter of the charge was equal to approximately half its length and to the diameter of the specimen. In all cases where the specimens were damaged, fractures were produced near the contact with the charge, in the form of cores of regular geometric shape with smooth surfaces (Fig. 1a and b). In experiments with steel specimens made in the form of rectangular and triangular right prisms, the lower part of each core, as in experiments with cylindrical specimens, was in the form of a

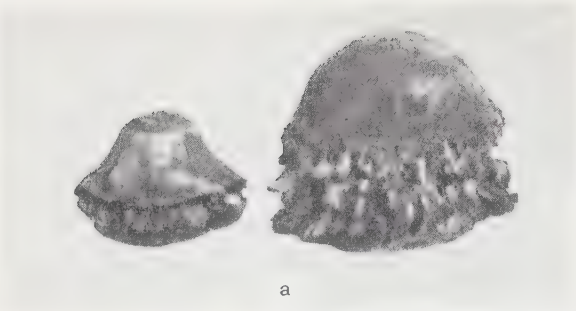

a

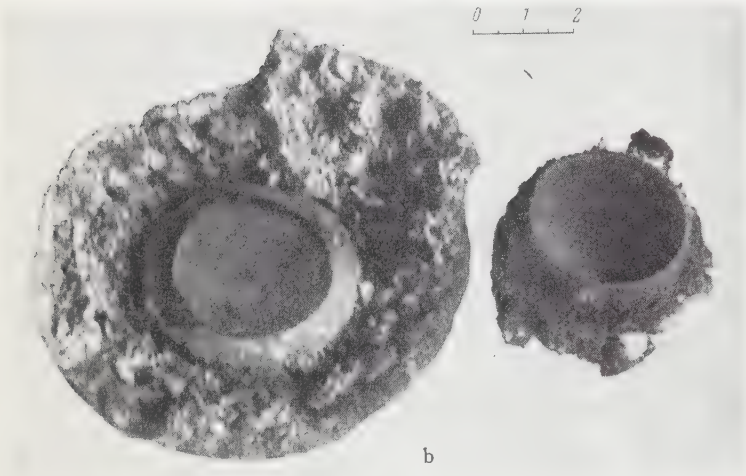

b

Fractures in the form of cores, obtained in experiments with cylindrical specimens of "Z" steel. Charge of TG 50/50 alloy, 65 mm high. a – "Full" cores. Specimens were 100 mm high and 80 mm in diameter (left) or 120 mm in diameter (right). The base of the cores was in contact with the explosive; b – cut cores. The height of specimen 60 mm, diameter 120 mm. 1 – Cut surface of lower core, 2 – cut surface of upper core (base of upper core was in contact with the explosive).

convex spherical surface, while the lateral surface was similar to that of a rectangular and triangular pyramid. Fractures in the form of cores bounded by a convex spherical surface (Fig. 1a) are formed in experiments with specimens whose heights exceed a certain value for the given charge. As the original height of the specimen is reduced below this value, a new phenomenon is observed: the lower part of the core appears to be cut off in a plane perpendicular to its axis. In the remaining part, the cut cores do not differ at all from the cores with spherical surface ("full" cores). The cut surface is much smoother than the lateral surface of the core. It has the finish produced by a fine cut on a lathe. A second core with a cut (Fig. 1b) is produced in the lower part of the specimen, instead of the usual rear fracture. It should be noted that the "full" cores had approximately half the height of the point where the cut appeared in the specimen. It follows therefore that the spherical core surface is formed some distance behind the front of the compression wave propagating in the specimen.

Similar experiments were also made with copper, brass, and aluminum. None however disclosed fracture phenomena similar to those described above.

The very fact of formation of smooth fractures in steel, the adiabat of which has an anomalous bend at the phase-transition point, enables us to relate the appearance of such fractures with the existence of rarefaction shock waves. From this point of view, the most obvious explanation can be offered for the appearance of cut cores. The cut is produced at the place where the rarefaction jumps meet; one of these jumps occurs in the specimen following the compression shock wave due to the explosion, and the other is produced when this compression wave is reflected from the free surface of the base of the specimen. Calculations carried out by the method of characteristics in the two-dimensional case, using the experimental shock adiabat of iron,[2] are in satisfactory agreement with experiment. On the basis of these experimental data it is natural to attribute the formation of the lateral surface of the core to the interaction between the rarefaction jump in the lateral unloading wave in the specimen and the rarefaction jump that follows the compression wave. Since these jumps collide at a certain angle, it is clear that the zone in which destructive stresses are reached will be broader than in normal collision of the jumps, and consequently the fracture surface will be less smooth than in normal collision. This is in good agreement with experiment.

The mechanism of formation of the spherical surface of the core is still not perfectly clear. The experimental data point to the existence of a con-

nection between the formation of this surface and the rarefaction jump propagating in the specimen behind the front of the compression shock wave.

In the opinion of the authors, these fracture phenomena serve as an experimental proof of the existence of rarefaction shock waves in substances that experience a polymorphic transition under shock loading.

The authors are grateful to Yu. I. Tarasov for participating in the discussion of the results and for his calculations of the collision between rarefaction jumps, and also to Academician Ya. B. Zel'dovich and Professor L. V. Al'tshuler for interest in the work and for valuable hints.

*Since the iron is not greatly heated by shock compression in the pressure interval under consideration,[2] it can be assumed that the expansion of the iron from the compressed state will follow a curve which differs only slightly from the shock adiabat.

[1] Ya. B. Zel'dovich, Теория ударных волн и введение в газодинамику (Theory of Shock Waves and Introduction to Gas Dynamics), AN SSSR, 1946.

[2] Bancroft, Peterson, and Minshall, J. Appl. Phys. **27**, 291 (1956).

[3] W. E. Drummond, J. Appl. Phys. **28**, 999 (1957).

Translated by J. G. Adashko
320

RECOMBINATION RADIATION FROM INDIUM ANTIMONIDE UNDER AVALANCHE BREAKDOWN

N. G. BASOV, B. D. OSIPOV, and A. N. KHVOSHCHEV

P. N. Lebedev Physics Institute, Academy of Sciences, U.S.S.R.

Submitted to JETP editor April 27, 1961

J. Exptl. Theoret. Phys. (U.S.S.R.) **40**, 1882 (June, 1961)

A number of investigations of the behavior of indium antimonide crystals in strong electric fields have established that at field strengths of ~ 200 v/cm the carrier concentration starts to increase rapidly, owing to the impact ionization of valence band electrons (avalanche breakdown).[1-3]

We have observed infrared luminescence radiation from n type indium antimonide crystals with small impurity concentrations, when pulses with current densities of up to 100 amp/mm^2 were applied. At these current densities the resistance of the specimen was more than an order of magnitude smaller than the resistance at small currents (voltages), which can be ascribed to avalanche breakdown. To avoid heating the specimen, current pulses not more than 3 μsec long were used with repetition frequency 50 cps. The luminescent radiation was observed at a temperature of 78°K, and disappeared when the specimen was warmed up to 120 — 180°K. The rise and decay times of the light pulse did not exceed 1 μsec, so that the observed radiation was not associated with heating of the crystal lattice. The spectrum of the radiation, with a maximum at $\lambda = 5.3\mu$ and half-width 0.25μ, allows it to be assumed that it is recombination radiation.[4] The effective temperature at the maximum of the spectrum was evaluated by comparison with black body radiation, and was 500°K.

The authors are grateful to D. N. Nasledov and his co-workers for their interest in the work.

[1] M. Glicksman and M. C. Steele, Phys. Rev. 110, 1204 (1958).

[2] M. C. Steele and M. Glicksman, J. Phys. Chem. Solids **8**, 242 (1959).

[3] A. C. Prior, J. Electr. and Control **4**, 165 (1958).

[4] T. S. Moss, Optical Properties of Semiconductors, (Butterworth, London; Academic Press, New York, 1959).

Translated by K. F. Hulme
321

Author Index to Volume 13

References with L are Letters to the Editor

Analytic Subject Index to Volume 13

References with L are Letters to the Editor. Items are listed under the following categories:

Contents of Coming Issues

SOVIET PHYSICS JETP VOLUME 14, NUMBER 1 JANUARY, 1962

LETTERS TO THE EDITOR

SOVIET PHYSICS JETP VOLUME 14, NUMBER 2 FEBRUARY, 1962

LETTERS TO THE EDITOR

ERRATA

Vol	No.	Author	page	col	line	Reads	Should read
12	3	L. G. Moroz	416	r	4	$\ldots(4k^4 - k^2\mathbf{p}_\mu^2 \sin^2\vartheta +$	$\ldots(2k^4 - \frac{1}{2}k^2\mathbf{p}_\mu^2 \sin^2\vartheta +$
					5	$\ldots + \frac{1}{2}\mu^2 l_\mu^2 k^4 (F_N + 2l_N M)^2\},$	$\ldots + \frac{1}{2}\mu^2 l_\mu^2 k^2 (F_N + 2l_N M) \times [k^2 (F_N + 2l_N M) - 2l_N M\mathbf{p}_\mu^2 \sin^2\vartheta]\},$
					17	$\ldots(1 + 2l_N M^2) \pm$	$\ldots(1 + 2l_N M)^2 \pm$
					18	$\pm\frac{1}{2}[\frac{1}{4}k^2(1 + 2l_N M) + \ldots$	$\pm\frac{1}{2}[\frac{1}{4}k^4(1 + 2l_N M) + \ldots$
12	5	Grechukhin	957	Eq. (1)			Add factor C^{10}_{1020} to right-hand side of first equation
13	2	Denisov et al	289	Capt. Fig. 4		$\leq 6 \times 10^3$	$\geq 6 \times 10^3$
13	4	Zyryanov	752	Eq. (17)			Expression in curly brackets should read $\left\{\ln\frac{\Omega - (n' - n) - \sqrt{2}(n_0 - n')^{1/2} q_z + q_z^2/2}{\Omega - (n' - n) + \sqrt{2}(n_0 - n')^{1/2} q_z + q_z^2/2} \times \right.$ $\left. + \ln\frac{\Omega - (n' - n) + \sqrt{2}(n_0 - n)^{1/2} q_z - q_z^2/2}{\Omega - (n' - n) - \sqrt{2}(n_0 - n)^{1/2} q_z - q_z^2/2}\right\}$

SOVIET PHYSICS JOURNALS

Translations of the 1961 Originals—*Published in English by the American Institute of Physics with the cooperation of the National Science Foundation.*

Publication year July, 1961—June, 1962.

Soviet Physics—**JETP**

A translation, beginning with 1955 issues of *Zhurnal Eksperimental'noi i Teoreticheskoi Fiziki* of the USSR Academy of Sciences. Leading physics journal of Soviet Union. Similar to "The Physical Review" in quality and range of topics. Outstanding new work is most likely to appear in this journal.

Vols. 13 and 14 comprising twelve issues, approx. 4000 pp.
$75 domestic, $79 foreign
Libraries $50 domestic, $54 foreign. Single copies, $8*

Soviet Physics—**SOLID STATE**

A translation, beginning with 1959 issues of *Fizika Tverdogo Tela* of the USSR Academy of Sciences. Offers results of theoretical and experimental investigations in the physics of semiconductors, dielectrics, and on applied physics associated with these problems. Also publishes papers on electronic processes taking place in the interior and on the surface of solids.

Vol. 3 comprising twelve issues, approx. 3800 pp.
$70 domestic, $74 foreign
Libraries $45 domestic, $49 foreign. Single copies, $8*

Soviet Physics—**TECHNICAL PHYSICS**

A translation, beginning with 1956 issues of *Zhurnal Tekhnicheskoi Fiziki* of the USSR Academy of Sciences. Contains work on plasma physics and magnetohydrodynamics, aerodynamics, ion and electron optics, and radio physics. Also publishes articles in mathematical physics, the physics of accelerators, and molecular physics.

Vol. 6 comprising twelve issues, approx. 2000 pp.
$55 domestic, $59 foreign
Libraries $35 domestic, $39 foreign. Single copies, $8*

Soviet Physics—**ACOUSTICS**

A translation, beginning with 1955 issues of *Akusticheskii Zhurnal* of the USSR Academy of Sciences. Devoted principally to physical acoustics but includes electro-, bio-, and psychoacoustics. Mathematical and experimental work with emphasis on pure research.

Vol. 7 comprising four issues, approx. 500 pp.
$12 domestic, $14 foreign
(No library discounts.) Single copies, $4

Soviet Physics—**DOKLADY**

A translation, beginning with 1956 issues of the physics sections of *Doklady Akademii Nauk SSSR*, the proceedings of the USSR Academy of Sciences. All-science journal offering four-page reports of recent research in physics and borderline subjects.

Vol. 6 comprising twelve issues, approx. 1500 pp.
$35 domestic, $38 foreign
Libraries $25 domestic, $28 foreign*
Single copies Vols. 1 and 2, $5;
Vol. 3 and later issues, $7

Soviet Physics—**CRYSTALLOGRAPHY**

A translation, beginning with 1957 issues of the journal *Kristallografiya* of the USSR Academy of Sciences. Experimental and theoretical papers on crystal structure, lattice theory, diffraction studies, and other topics of interest to crystallographers, mineralogists, and metallurgists.

Vol. 6 comprising six issues, approx. 1000 pp.
$25 domestic, $27 foreign
Libraries $15 domestic, $17 foreign. Single copies, $5*

SOVIET ASTRONOMY—AJ

A translation, beginning with 1957 issues of *Astronomicheskii Zhurnal* of the USSR Academy of Sciences. Covers various problems of interest to astronomers and astrophysicists including solar activity, stellar studies, spectroscopic investigations of radio astronomy.

Vol. 5 comprising six issues, approx. 1100 pp.
$25 domestic, $27 foreign
Libraries $15 domestic, $17 foreign. Single copies, $5*

Soviet Physics—**USPEKHI**

A translation, beginning with September, 1958, issue of *Uspekhi Fizicheskikh Nauk* of the USSR Academy of Sciences. Offers reviews of recent developments comparable in scope and treatment to those carried in *Reviews of Modern Physics*. Also contains reports on scientific meetings within the Soviet Union, book reviews, and personalia.

Vol. 4 comprising six issues, approx. 1700 pp.
(Contents limited to material from Soviet sources)
$45 domestic, $48 foreign
Libraries $30 domestic, $33 foreign. Single copies, $9*

**For libraries of nonprofit academic institutions.*